Application of new observational method on deep excavation retaining wall design in London Clay

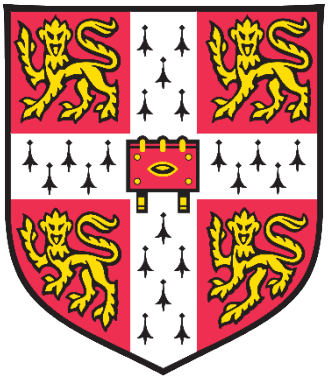

Ying Chen

Department of Engineering

University of Cambridge

This dissertation is submitted for the degree of

Doctor of Philosophy

Lucy Cavendish College

December 2018

Declaration

I hereby declare that except where specific reference is made to the works of others, the contents of this dissertation are original and have never been submitted in whole or in part for consideration for any degree, diploma or other qualification in this, or any other university. This dissertation is the results of my own work and includes nothing which is the outcome of work done in collaboration, except where specifically indicated in the text. This dissertation contains 72,000 words including appendices, footnotes, tables and equations and has 130 figures with pre-approved permission.

Ying Chen

December 2018

Acknowledgements

I would like to thank many people for making this thesis possible and supporting my doctoral degree studies in the past three years.

Firstly, I would like to thank my academic supervisor Dr Giovanna Biscontin for her support, guidance and useful suggestions throughout my research project. Also, I would like to thank my advisor Professor Kenichi Soga who granted me this opportunity at Cambridge in the first place and provided me with a unique perspective on the numerical finite element modelling for ground engineering problems.

My thanks must also go to several individuals from Arup Geotechnics who served as additional supervisors for my research:

Duncan Nicolson – who has been actively involved throughout in sorting out all administrative issues, ensuring my findings are disseminated in the industry through conferences and within Arup to promote the application of the observational method, and liaising with Crossrail and Arup to enable the collection of the Crossrail excavation case histories.

Brian Simpson – not only the inventor of one of the advanced soil constitutive model – BRICK, with border knowledge and experience in soil mechanics and ground engineering but also a patient teacher who shared with me the theory behind BRICK. Brian also reviewed my research numerical analysis results and asked intriguing questions that led to many enlightened discussions.

Anton Pillai and Qiu Xiang-bo from Arup numerical analysis team – for patiently teaching me how to use the LS-Dyna programme, allowing me access to the powerful analysis workstation at Arup, and providing me with access to the original Crossrail deep excavation 3D models.

I am grateful to have had the opportunity to study in an exciting and diverse Geotechnical and Environment research group. Thank you to my colleagues, Dr Yingyan Jin and others from the team.

I must also thank Duncan Nicholson and Ove Arup & Partners for their financial support.

Finally, thank you to my husband Yau Sing Hooi for his love and full support before, during and hopefully long after this Doctoral research course.

Application of new observational method on deep excavation retaining wall design in London Clay

by
Ying Chen

Abstract

Ground engineering in urban areas faces the great challenge of balancing the increasing demand for underground space against safety and asset protection while avoiding high construction costs. This study shows savings can be achieved on embedded retaining wall design for deep excavation in London Clay through the observational method, without compromising safety.

Despite the inherent benefits of the method and its acceptance by design codes, the application of the observational method for excavation design has been slow and inconsistent due to the lack of guidance, in addition to other difficulties.

This research aims to promote the application of the observational method in excavation design by proposing a new framework. The framework with four design approaches is established based on the review of historical excavation case histories and four Crossrail station excavations using the observational method. The term *Ab initio* is used for excavation design from the beginning of construction, covering Optimistic Approach A and Cautious Approach B. The term *Ipso-tempore* is introduced for excavation redesign after construction starts, comprising a newly defined Pro-active Approach C and the '*best-way-out*' or Reactive Approach D.

Back-analysis is critical in the observational method. The whole process of back analysis is examining monitoring systems (observations) and predictions by the numerical analysis with the adopted soil constitutive models. Three Crossrail excavation cases are back-analysed by the Mohr-Coulomb model using FEMs from Pseudo-FEM to 2D and 3D FEMs. The Crossrail Tottenham Court Road Station, Western Ticket Hall deep box excavation is also back-analysed by the BRICK model using the 3D FEM, representing the advanced soil model.

The above back-analysis results are presented including the calibrated most probable soil model parameters. The different results indicate the back-analysis is subject to the type of numerical analysis, the adopted soil constitutive model, also it needs to be tailored to the monitoring data used for comparison.

A reassessment of the TCR-WTH excavation design by Approach A is carried out using the semi-FEM with the Mohr-Coulomb model. The optimistic design with the calibrated most probable Mohr-Coulomb parameters shows over 30% saving in construction materials, which is supported by the contingency plan with the characteristic Mohr-Coulomb parameters if the excavation does not encounter the expected conditions.

Improvements of specifications for the instruments and monitoring data are recommended to provide more reliable monitoring data.

Contents

List of Figures

List of Tables

Nomenclature

Roman Symbols

A2 / A3	Sub-division of London Clay
B	total number of bricks OR width of the excavation OR sub-division of London Clay
$B_{(b)}$	component of the difference between current stain and brick “b”
C	sub-division of London Clay
D	component of stiffness matrix OR a material parameter controlling dilation/contraction toward the CSL in the critical state formulation of
e	void radio
G	Shear modulus
H_e	the maximum excavation depth
H_p	the retaining wall penetration depth
K	bulk modulus
k_0	coefficient of earth pressure at rest
k_a	coefficient of earth pressure at active
k_p	coefficient of earth pressure at passive
L	length of the excavation
$L_{(b)}$	string length for brick “b”
m	material parameter in the Viggiani (1992) equation for shear modulus
n	material parameter in the Viggiani (1992) equation for shear modulus
p	mean stress in three-dimensional space
q	an invariant measure of deviatoric stress
$R_{(b)}$	material proportion for brick “b”

S	area under the S-shape curve OR size of the yield surface in proportion to the history surface
s	mean normal stress in plane strain $s= (\sigma_x + \sigma_y)/2$
t	component of shear stress in $t= (\sigma_y - \sigma_x)/2$ or τ_{xy}
v	specific volume

Greek Symbols

β	over-consolidation parameter in the BRICK model
β^G	over-consolidation parameter for stiffness in the BRICK model
β^ϕ	over-consolidation parameter for strength in the BRICK model
γ	component of shear strain
δ	Increment displacement
δ_{vm}	the maximum vertical ground surface settlement
δ_{hm}	the maximum retaining wall horizontal displacement
ε	component of strain
θ	Lode angel
ι	elastic stiffness parameters
κ	slope of swelling line in ln ε_{vol} – p' space (the BRICK model parameter)
κ *	slope of swelling line in ln v– p' space (the BRICK model parameter)
λ*	slope of CSL in ln v – p' space (the BRICK model parameter)
μ (M_μ)	material parameters controlling Lode angle effects in the BRICK model
ν	Poisson's ratio
$\xi_{(b)}$	a string length correction variable that accounts for Lode angle effects in the BRICK model
ς	distance from the NCL
σ	component of stress
σ_1	major principal stress
σ_2	intermediate principal stress
σ_3	minor principal stress
τ	component of shear stress
χ^G	a measure of over-consolidation effects on stiffness in the BRICK model
χ^ϕ	a measure of over-consolidation effects on strength in the BRICK model

Statistical Terms

COV	coefficient of variation
n	number of data points used to generate a regression line
r	correlation coefficient

R^2	coefficient of determination
RD	relative deviation
SD (σ_χ)	standard deviation
SE	standard error in a regression
y_i	i^{th} observed y-value (response variable)
β	reliability index
μ_x	mean value
χ_{LS}	limit state value

Instrumentation & Monitoring Terms

A	the cross-sectional area: m^2
c_h	the coefficient of horizontal consolidation
d	Length of the longest drainage path
E	Young's modulus: kN/m^2
h_w	raised height of water column in a sandpipe
I	the relevant second moment of the cross-sectional area: m^4
IM	manually operated Inclinometer
IPI	automatically readout in-place Inclinometer
M_{xx}	bending moment in X-axis
M_{yy}	bending moment in Y-axis
MLVW	the multiple level vibrating wires (one type of piezometers)
SAA	Shape Accel Array
t_{50}	the time for 50 % dissipation of total excess pore-water pressures
T_{50}	The dimensionless time factor, $T_{50} = 0.196$ at the corresponding degree of the consolidation 50%
u	pore water pressure: kN/m^2
$u_{i,e}$	the initial pore pressure
$u_{i,d}$	the initial designed pore pressure
y	the distance from the gauge to the neutral axis
α_P	the coefficient of thermal expansion of the prop: $°C^{-1}$
β	degree of restraint of the prop in per cent %
Δf	change in the frequency of vibration: HZ
ΔP	change of axial strut load: kN
ΔT	change of temperature: °C
$\Delta\varepsilon$	change of strain in the wire, in microstrain: μm
$\Delta\varepsilon_P$	change of axial strain in microstrain: μm
ε_i	corrected indicated strains, in microstrain: μm

σ_a	total stress at active side: kN/m^2
σ_a'	effective stress at active side: kN/m^2
σ_p	total stress at active side: kN/m^2
σ_p'	effective stress at active side: kN/m^2
$4l^2m/EA$	a gauge factor, given by the strain gauge manufacturer
$\bar{B}$	overall pore pressure coefficient for a material (Skempton, 1954)

Laboratory testing & Soil property Terms

c'	effective cohesion
c_c	compression index
c_s	swelling index
c_r	recompression index
c_u	undrained shear strength
CPT	cone penetration test
E_u	undrained stiffness for soil
E_v'	vertical effective Stiffness for soil
f_1	empirical correlation factor dependent on the plasticity index ($c_u=f_1\times N_{60}$)
f_s	sleeve friction
G_s	specific gravity
I_L	liquid index of fine soil
I_p	plasticity index of fine soil
k_h	horizontal permeability
k_v	vertical permeability
N_{60}	SPT N value normalised for energy ratio of 60 per cent
OCR	over-consolidation ratio
P_L	plasticity limit
PSD	particle size distribution test
q_c	cone resistance
SBP	self-boring pressuremeter test
SPT	standard penetration test
$s_{u,\,CPT}$	undrained shear strength calculated from the in-situ CPT test
$s_{u,\,SBP}$	undrained shear strength by in-situ self-boring pressure test
$s_{u,\,SPT}$	undrained shear strength calculated from the in-situ SPT test blows N
$s_{u,100}$	undrained shear strength by U100 sample undrained triaxial test
W	moisture content (water content)
W_L	liquid limit of soil
ν'	Poisson's ratio

ρ_b	bulk density
ϕ'	angle of internal friction of soil (or the effective stress friction angle)
ϕ'_{cv}	angle of internal friction of soil under constant volume conditions (or the critical state friction angle)
ϕ'_f	angle of internal friction of soil with fissures
ϕ'_p	peak angle of internal friction of soil (or the peak friction angle)
ϕ'_r	residual angle of interface friction

Superscripts / Subscripts

0	initial OR reference value
1, 2,3	principle direction in stress and strain space
’	effective stress condition
A, B	sub-divisions of London Clay formation
e	excavation OR elastic component
p	plastic component
H / h	horizontal direction
i	increment or sub-increment number
max	maximum
min	minimum
r	direction in ‘r’ in polar coordinates
ref	reference value
t	tangent direction
s	secant direction OR shear
V/v	vertical direction
vol	volumetric
xyz	cartesian coordinates
Z	direction ‘z’ in Cartesian coordinates or polar
ult	Ultimate

Acronyms

1D	one-dimensional
2D	two-dimensional
3D	three-dimensional
ATD	a tunnel datum of ODN is used for the London Underground – where 100 m below the normal ordance datum is used as the reference level, and altitudes are written as meter above this reference level in m ATD.
BS	Crossrail Bond Street Station

CSL	critical state line
CEDS	civil engineering design standards – Crossrail internal document
CTC	contractors technical committee
FEM	finite element modelling
I&M	Instrumentation and monitoring
LC	London Clay
LIS-MS	Crossrail Liverpool Street Station, Moorgate Shaft
LMG	Lambeth Group
LU	London Underground
MG	Made Ground
mbgl	meter below ground level
NATM	New Austrian Tunnelling Method
NCL	normal consolidation line
OD	Ordnance Datum, defined as the mean sea level
PAD	Crossrail Paddington Station
PWP	porewater pressure
RTD	River Terrace Deposits
SCL	Sprayed Concrete Lining
TBM	Tunnel Boring Machine
TS	Thanet Sand
TCR-WTH	Crossrail Tottenham Court Road Station, Western Ticket Hall
UF	Upnor Formation
UCIMS	Underground construction information monitoring systems
WS-DSS	Crossrail Whitechapel Station, Durward Street Shaft

Chapter 1

Introduction

1.1 Background of the research

The demand for underground infrastructure has been growing worldwide in response to global urbanisation and the consequent growth of city developments, such as underground railways, subways, tunnels and utility tunnels. As demand increases, so does the infrastructure project complexity. This is due to increasingly crowded underground spaces and the multiple challenges in protecting existing structures.

Major infrastructure projects present unique opportunities to learn about these challenges. Examples of UK projects include Channel Tunnel Rail Link (CTRL) (Young and Ho, 1994; Powderham, 1994; Loveridge, 2001), the Jubilee Line Extension in London (Nishimura, 2005; Jardine, 2011), and the Heathrow Terminal 5 (Nishimura, 2005; Gasparre *et al.*, 2007). An example of an international project is the railway extensions of Mass Transit Railway in Hong Kong (Chan, 2003; Korff, 2012).

Crossrail, with a budget of £18 billion, is currently the largest infrastructure project in Europe. It involves the construction of 8 new underground stations, 2 new surface stations and more than 42 kilometres of tunnels across the Central London area. Large amounts of movement data were collected during the construction of the stations and tunnelling, and have been used effectively to protect existing infrastructure nearby.

This research will closely examine the Crossrail monitoring data to achieve a good engineering understanding of soil-structure interaction during excavations. A number of Crossrail station excavations used similar retaining structures, and an exceptional amount of data is available for study.

Monitoring data had been applied to optimise infrastructure design before the observational method was formulated by Peck (1969a). Since this method was introduced in the 9th Rankine lecture, savings of time and costs by using the observational method have been reported in historical case histories. Examples include the basement construction for a skyscraper building in Tokyo, Japan (Ikuta *et al.*, 1994), the cut and cover tunnel construction at three sites of the Channel Tunnel project (Powderham, 1994), the sheet-piled retaining wall to protect the power cables for the Channel Tunnel terminal at Folkestone (Young and Ho, 1994), and the open cut retaining structure for the Batheaston Swainswick Bypass (Nicholson *et al.*, 1998).

The observational method has been revisited on many occasions through a number of engineering projects. However, despite the obvious benefits to construction projects, the observational method has not been widely adopted. The reason is a combination of the absence of a code of practice for implementation, a misconception of the increased risk, and perhaps the increased fragmentation of the construction industry.

The observational method can generate a direct link between design and construction through back-analysis, evaluating the balance between safety and cost-effectiveness. The objective of this research is to investigate whether cost-effective designs can be achieved for excavations in London Clay by the observational method, without compromising safety.

1.2 Objectives of the research

In order to achieve the goal, the research has been divided into four areas to enable the investigation of cost-effective embedded retaining wall designs for excavations in over-consolidated London Clay by the observational method.

- establish the new observational method framework to provide guidance for practice and promote the application of the method;
- review instruments and monitoring data from the Crossrail project, and make suggestions on enhancements of monitoring data to provide reliable observations for the back-analysis;

- unify the way of deriving or calibrating the soil constitutive models related input parameters for a consistent back-analysis process;
- compare the back-analysis performance using different soil constitutive models and by different numerical analysis methods; and
- re-assess the existing excavation design by *Ab initio*[1] approach A of the new observational method framework to demonstrate possible cost advantages.

Two design approaches were defined in the original observational method by Peck (1969a), *Ab initio* and *best-way-out*. However, the design assumptions for the *Ab initio* approach by Peck, and later by Nicholson *et al.* (1999), created confusion when implementing the method. The best-way-out approach has been engaged only for difficult situations. Instead, the most widely used approach was a progressively modified design, although this concept was not previously defined. The inconsistencies in the implementation of the observational method justify the development of a new framework.

On the basis of the original observational method (Peck, 1969a), and findings from the review of excavation case histories, a new observational method framework is proposed. The refined approaches in the new framework will provide guidance for practice.

Observations are key elements in the back-analysis. Proper monitoring data review and correction of the data for accuracy and reliability are needed. A review of the instrumentations and their data from the Crossrail project show many details that affect the quality of observations. Some potential issues that affect the accuracy of monitoring data are discussed and error corrections are also recommended.

Back-analysis is a procedure for using field measurements in order to obtain input material parameters (Gioda & Maier 1980; Cividini *et al.* 1981). This procedure was firstly introduced in tunnelling engineering to establish a way to assess design parameters. Back-analysis is adopted in this research to study the Crossrail excavation case histories, and to calibrate the most probable design parameters for the London Clay units in relation to the soil constitutive models.

In the back-analysis of the Crossrail excavation case histories, two soil constitutive models are selected to model the over-consolidated London Clay:

[1] *Ab initio, a Latin term meaning "from the beginning".*

- the Mohr-Coulomb soil model is a linear elastic, perfectly plastic model, this model is widely used for retaining wall design in London Clay, and
- the BRICK soil model is one of the advanced soil models which can describe soil non-linear stiffness, and it was initially developed to simulate soil behaviour in London Clay. It has been applied in deep excavation and foundation design for many projects in London.

The performance of the back-analysis performance is found to be related to the complexity of the finite element numerical analysis model (FEMs). For instance, different results are obtained from different FEMs in the Crossrail excavation back-analyses including Pseudo-FREW, Plaxis 2D and LS-Dyna 3D. Hence, it is recommended that the calibrated most probable design parameters be presented in the context of the soil constitutive model and the analysis method. Examples of calibrating the most probable Mohr-Coulomb parameters for the London Clay divisions using inclinometer data with all three analysis methods are discussed in Chapter 5. The most probable BRICK parameters for the London Clay divisions are also calibrated using inclinometer data with LS-Dyna 3D and presented in Chapter 6.

Currently, the back-analysis is performed manually and engineering judgement is needed to ensure its quality. The following factors contribute to the poor performance of back-analysis: accuracy of the observations, as-built details (e.g. accurate excavation details) and other construction activities (e.g. grouting). More often, an increased number of iterations may be required for refined back-analysis results.

The ultimate use of the back-analysis will provide real-time analysis results during excavation, and the outcomes can be used to assist in construction decisions. For instance, more accurate trigger limits can be defined and updated based on real-time back-analysis results for construction control. If the real-time back-analysis is available and become part of the construction review process, the analysis results can be reviewed frequently and the opportunity for the observational method can also be identified at the early stage of the project.

The re-assessment of one Crossrail excavation case history by *Ab initio* Approach A of the new observational method framework indicates the potential savings in both construction materials costs as well as construction time.

1.3 Structure of the thesis

The thesis consists of eight chapters. Following the introductory section (Chapter 1), Chapter 2 presents a literature review on the observational method, including background, development and innovation of the method in the past decades. London Clay, as a typical heavily over-consolidated soil and its characteristic engineering features are reviewed. Review of the relevant subjects to the back-analysis is also carried out for the finite element numerical analysis methods, the BRICK soil constitutive model and the monitoring data.

Three Crossrail excavation case histories are introduced in Chapter 3, including their original design scheme, the numerical analysis, the as-built construction details and the collected observations with corrections for accuracy and reliability, if possible.

Chapter 4 describes the proposed new observational method framework with four design approaches and the corresponding operational procedures: *Ab initio* Optimistic Approach A, *Ab initio* Cautious Approach B, *Ipso tempore*[2] Proactive Approach C and *Ipso tempore* Reactive Approach D. A selection process is proposed for the different design approaches.

Chapter 5 presents the back-analysis of the Crossrail case histories with the Mohr-Coulomb soil model using inclinometer data. The back-analysis results from Pseudo-FE FREW, Plaxis 2D and LS-Dyna 3D are discussed. A supervised statistical regression method is proposed to derive the initial Mohr-Coulomb input parameters if the ground investigation data shows scatter. The representative values of the most probable Mohr-Coulomb model parameters for the London Clay divisions are summarised for the observational method design.

Chapter 6 presents the back-analysis of the Crossrail Tottenham Court Road Station – Western Ticket Hall (TCR-WTH) with the BRICK model. The initial BRICK parameters for the London Clay divisions are calibrated using the laboratory triaxial test data, and the representative most probable BRICK parameters are calibrated using inclinometer data through the back-analysis.

The re-assessment of the TCR-WTH deep box excavation design using *Ab initio* Optimistic Approach A is described in Chapter 7. The re-assessment is performed with the Mohr-Coulomb model in Pseudo-FE FREW. The optimistic design is developed with the calibrated most probable parameters from Chapter 5, and the contingency plan is prepared with the characteristic parameters which are used in the analysis of the original design. By thinning the retaining wall, it is shown that there are potential savings of over 30% in construction

[2] *Ipso tempore, a Latin term meaning "in the moment"*

material costs. There are also further potential savings in construction time if the contingency plan is not activated during construction.

Finally, the main findings of this research have been summarised in Chapter 8, and suggestions for future research work have also been recommended.

Chapter 2

Literature Review

This research is about the application of the new observational method on deep excavation design in London Clay, hereby, a literature review on the relevant subjects is summarised in this chapter. The review covers the observational method background and application in the excavation design, London Clay soil behaviours and subjects in relation to the back-analysis, like finite element method, soil constitutive models for over-consolidated clay soils, and monitoring in an excavation.

2.1 Observational method

2.1.1 Introduction

The observational method was first successfully applied in geotechnical engineering by Karl Terzaghi, and it had been formulated and developed as the 'learn-as-you-go' method (Terzaghi and Peck, 1967). The potential for savings in time and costs by applying the observational method on engineering projects without compromising safety has been reported since the early 1950s. In the 9th Rankine lecture, a formalised methodology and the name of 'Observational Method' were introduced by Peck (1969a), who provided a distinct and novel design approach in geotechnical engineering design to reduce costs of construction and manage risk.

After the 9th Rankine lecture, the observational method has been adopted and listed as one of acceptable design method to be used in several countries: the Ciria Report 185 by Nicholson *et al*. (1999) in the UK; guide to retaining wall design (HKGEO, 2000) in Hong Kong; guideline '*La méthode observationnelle pour le dimensionnement interactif des ouvrages*' by Allagnat (2005) in France; and '*Subsoil - Verification of the safety of earthworks and foundations - Supplementary rules to DIN EN 1997-1*' (DIN1054:2010-12) in Germany. The 7th edition of Eurocode as BS EN 1997-1 (2004) has also included the observational method as an alternative design approach by calculation.

A detailed review of the observational method in chronological order is presented in the following sections.

2.1.1.1 The 1940s – 1960s

In geotechnical engineering, many variables generate inevitable uncertainties, such as continuity of important strata and pressure conditions in the groundwater, even the structure uncertainties could be introduced during construction. Therefore, the results were more as working hypotheses, subject to verification or modification during construction. In order to deal with these uncertainties, two methods have been used in the past:

- adopt an excessive factor of safety; or
- make assumptions in accordance with general, average experience.

The first method was wasteful, but the second method involved much higher risks. A third approach proposed by Terzaghi through his project experience in the early 1940s, the "learn-as-you-go" method as a practical application. The statement of comparable clarity on the method was published in 1961 (Terzaghi, 1961). This experimental method advocated the following procedure:

- form a base design with the available information, identifying all possible differences between reality and assumptions;
- the results of calculations should be measurable in the field, such that a comparison between the measurement and the prediction can be followed, for instance, the displacement of the foundation or water pressure.
- on the basis of the above comparison, the gaps in knowledge will be closed gradually. If necessary the design is modified during construction.

2.1.1.2 The 9th Rankine Lecture (1969)

The term 'observational method' was introduced by Peck in the 9th Rankine Lecture in 1969. Two distinctive approaches to the implementation of the observational method were defined:

- "*Ab initio*" approach

The observational method will be adopted from the inception of the project. Peck recommended adopting the most probable conditions. Separately, a set of contingency measures would be developed to ensure the stability of the structure if required. Depending on the observed behaviours, inadequacies construction would either continue following the most probable behaviour or the pre-planned contingency measures would be implemented. This is an optimistic application of the observational method.

- "Best-way-out" approach

In contrast to *Ab initio*, the observational method will be adopted after the project has commenced, when an unexpected event occurred or whenever an unacceptable event (e.g. failure or accident, threatens) already took place. The observational method may offer a way of preventing failure, sometimes as the only satisfactory way out of these difficulties. This is a reactive use of the observational method to an adverse event.

The implementation of the observational method depends on the nature of the project. If the perceived failure mechanism of a project is brittle, the design cannot be altered during construction, or the physical phenomena governing the behaviour of the project cannot be measured, then the observational method cannot be used regardless of its potential savings.

Most observational method case histories in the early applications were demonstrated as the "Best-way-out" approach. However, from the point of view of safety, economy and time, the *Ab initio* approach will most likely offer a cost-effective design. The challenges in implementing the observational method *Ab initio* approach were considered in relation to design, observations, contract and management:

- Design

A failure to anticipate the unfavourable condition could be critical, as it means no appropriate contingency plan for the least favourable condition when it occurs in the field.

- Observations

It is equally important to have the right observations. The selection of the appropriate quantities to measure requires sufficient engineering experience and help from specialists, in order to ensure the physical phenomena governing the behaviour are best characterised. In

addition, the incompetence in the instrumentation & monitoring specification, installation, and data auditing could introduce the reduced reliability in the observations.

- Contract

Changes in design are a feature of the observational method which introduces complications in contractual relations. The possibility of a slow down in construction due to any changes may cause financial difficulties.

- Management

The secret of the successful application of the observational method is a collaborative project team with one individual with overall responsibility and authority.

2.1.1.3 The 1970s – 1990s

Since Peck's Rankine lecture, further study of the implementation of the observational method has been carried out. The application of the observational method was introduced to a wider range of ground engineering operations. For example, the observational method was recommended as one of the design principles for embankment dams (De Mello, 1977). In tunnel engineering, a six-step observational method for applying Peck's principles for use in tunnelling works was introduced by Wood (1987). The application of the observational method was also extended to hazardous waste site remedial treatment (Brown et al., 1990) and coastal engineering (Wood, 1995). The observational method was considered to be a suitable method for updating the probability of a given event in evaluating the calculated risk in geotechnical engineering (Whitman, 1984).

During the period of the 1970s and 1990s, a major development for the observational method was made in the progressive modified design, with the awareness of safety and the high certainty in the project performance.

In Peck's *Ab initio* approach, the 'most probable' design parameters with the most probable conditions were recommended for less conservative design, this avoided the unquantifiable judgement factors. Powderham (1994) proposed the progressive modified design as the new approach of observational method *Ab initio*. This approach would start with more probable parameters and 'more probable' design condition, design changes will be introduced incrementally towards the most probable design conditions.

For example, in a large excavation project, the modification to the design will be based on early observations, and the change can be applied in a small and well-controlled step. As more data became available as the excavation progressed, the trend would also begin to be clear.

Most likely, the modifications will be in the direction of saving costs rather than introducing contingency measures, which certainly makes the progressive modified design as a safer choice than Peck' *Ab initio* approach.

However, the progressive modification can only be successful in the project which has a long construction period, thus allowing sufficient time for reviewing the observations and making the modified design.

2.1.1.4 Ciria R185 (1999)

A symposium was held in January 1995 to discuss the observational method and its future development. Although the symposium was positive with regards to the application of the observational method, there was disagreement regarding its definition. Hence a further clarification on the definition was given in Ciria R185 "The Observational Method in ground engineering: principles and applications" (Nicholson *et al.*, 1999):

"*The Observational method in ground engineering is a continuous, managed, integrated, the process of design, construction control, monitoring and review that enables previously defined modifications to be incorporated during or after construction as appropriate. All these aspects have been demonstrably robust. The objective is to achieve greater overall economy without compromising safety.*"

The above definition has helped to clarify the overall objectives of the observational method, and point out that the operational process of the method was an integrated management process involving all associated parties.

In terms of the application of the observational method *Ab initio* approach, the progressive modification was preferred and named as "Cautious" *Ab initio* approach. For the serviceability limit state (SLS), a pre-defined design using characteristic parameters should be carried out. At the same time, a design using moderately conservative parameters should also be made available to ensure the safety of the ultimate limit state (ULS) design, in which analysis the most unfavourable conditions should be applied.

This progressive modification 'cautious' *Ab initio* approach enabled a design starting with characteristic parameters and then reverting to most probable parameters when the observations confirmed the overprediction by the characteristic parameters.

"Best-Way-Out" approach was excluded in the Ciria R185.

An operational framework for implementing the observational method was given in the Ciria R185, as shown in Figure 2. 1. The diagram showed the implementation of the

observational method was an integrated management process, involving all parties in a project: design, construction, quality control and clients.

A traffic light trigger system with corresponding trigger values was adopted in the Ciria R185, as shown in Figure 2. 2. It was to ensure a comfortable safety margin during the operational process.

- GREEN: construction is in a safe condition to be continuing.
- AMBER: continue with caution, prepare to implement contingency measures and increase the frequency of monitoring.
- RED: stop progress, do everything possible to slow movements and implement contingency measures.
- Emergency: evacuation, required under the health and safety construction regulation (CHSW, 1996).

In practice, a portion of the predictions was recommended (e.g. 75% to 95%) as trigger values. However, this was dependent on the engineers' experiences. In Ciria R185, the trigger values were linked with the predictions by the 'most probable' and the 'characteristic' designs.

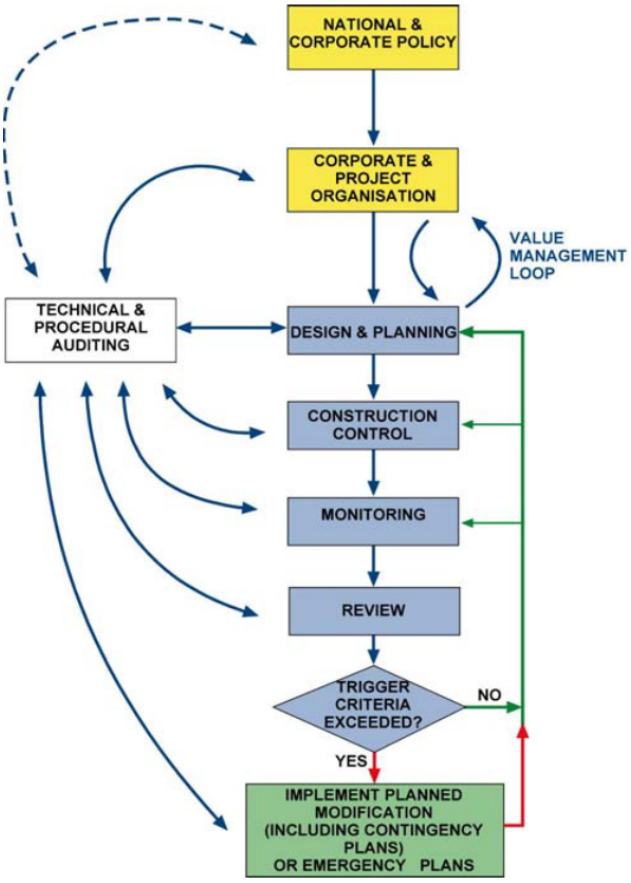

Figure 2. 1 Diagram of the operational process for the observational method Ciria R185 (Nicholson *et al.*, 1999)

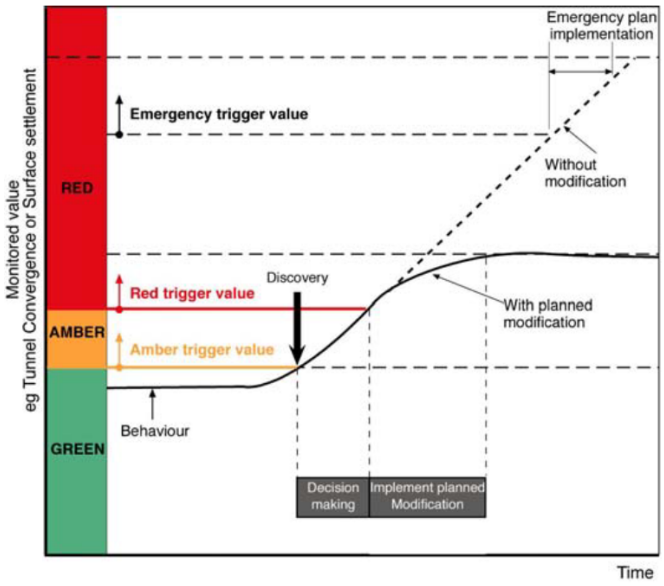

Figure 2. 2 Traffic light system for an incremental excavation process, (Patel *et al.*, 2007) after Ciria R185 (Nicholson *et al.*, 1999)

2.1.1.5 The 7th edition of Eurocode (2004)

Although the observational method was accepted as one of the design approaches in the 7th edition of Eurocode (BSI, 2004), the description of the implementation was very general. Firstly, the definition of the observational method was slightly different from Peck's version or the one given in Ciria R185. As a consequence, wide discussions and concerns on how to apply the observational method under the Eurocode have ensued (Nossan, 2006; Patel *et al.*, 2007; Spross, 2014).

In the 7th edition of Eurocode, the observational method was primarily aimed at the *Ab initio* approach, although it has not excluded the 'best-way-out' approach.

The 'acceptable limits of behaviour' was suggested for the observational method, when the 'characteristic parameters' or 'moderately conservative parameters' were adopted in the design and presented a lower cautious limit in design. However, it was not clear what should be used to determine the upper limit to represent the most likely behaviour. As a consequence of this point, it was not clear what trigger limits shall be defined for the planned contingency actions.

In this design code, no operational framework was described to manage the observational method within a contract, neither within the national policy nor project organisation.

2.1.2 Application of the observational method in excavation

The application of the observational method in the excavation construction was reviewed and summarised in Table 2.1. These excavation case histories demonstrated the successful application of the observational method achieving savings in costs and/or time. They were valuable case data for future excavations in similar ground conditions.

Review of these case histories has the following findings: 1) the progressively modified design filled the gap between *Ab initio* and 'Best-Way-Out' approaches defined by Peck; 2) 'Best-Way-Out' could be a proactive approach helping a project out of difficult situations, for example, overcoming various tight criteria of existing buildings protection; 3) the way of implementing the *Ab initio* approach has significantly changed since the original method by Peck. 4) the inconsistency in implementing of *Ab initio* approach led to confusions in design parameters and design conditions, which could have weakened the opportunities for the observational method *Ab initio* approach.

Table 2.1 Summary of observational method case history in excavation

Case history	**Reference**	**Description**	**Observational Method**
Harris Trust excavation support	Peck (1969a)	Soldier Pile Wall excavation, its support bracing system was designed using most probable prop force envelope values based on similar excavations in Chicago.	Peck's *Ab initio* approach
Minster Court excavation	Tse & Nicholson (1992)	To protect the nearby London Underground tunnel, the basement excavation in London Clay used a diaphragm wall with earth berm support. The berm geometry was progressively modified in response to the actual ground movement.	Ciria R185 *Ab initio* approach (Cautious *Ab initio*)
Channel Tunnel terminal at Folkestone	Young and Ho (1994)	The observational method was used to design major temporary works for the construction of a large reinforced soil structure adjacent to sensitive underground power cables.	Peck's *Ab initio* approach
CTRL[1] - Holywell & Castle Hill, north of Folkestone, UK	Powderham (1994)	Cut and cover construction at three sites: Castel Hill West, Sugarloaf Hill and Castel Hill East. To reduce the amount of temporary propping of the contiguous piled walls, the observational method was initiated at Castle Hill east and proceeded as a progressive modification application at Sugarloaf Hill and Castle Hill West.	Progressively modified design

[1] CTRL = Channel Tunnel Railway Link

Case history	Reference	Description	Observational Method
Tokyo basement for a high-rise building	Ikuta *et al.* (1994)	Top-down basement excavation using a diaphragm wall with permanent slabs as props, and temporary diagonal struts were designed initially but progressively verified as unnecessary and modified in construction.	Progressively modified design
Batheaston Swainswick Bypass	Nicholson *et al.* (1998)	To speed up the construction programme, an alternative construction sequence of bay excavations supporting by earth berm was proposed for the Batheaston bypass open cut excavation using a diaphragm wall to replace the initial excavation supporting with temporary props.	Ciria R185 *Ab initio* approach (Cautious *Ab initio*)
Limehouse Link	Glass and Powderham (1994)	The heavy temporary support works on for the Limehouse Link a major cut and cover highway tunnel construction	Progressively modified design
Mansion-house	Powderham (2002)	Mansion-house damage assessment and protection due to the accumulative effect of the tunnel excavation was being progressively modified and evaluated through phased construction, therefore the unnecessary protection option was avoided.	Peck's 'Best-Way-Out'
CWCS[2] Station - Headwalls	Travers and Yeow (2014)	The temporary earth berm supporting the headwall excavation was progressively modified during the station excavation in the dock so that the excavation was completed ahead of the plan and offered a spacious working area.	Progressively modified design
TCR-WTH[3]	Yeow *et al.* (2014)	The modification of omitting the lowest level of the temporary prop was made during construction for this bottom-up excavation in London Clay using diaphragm wall with temporary props.	Progressively modified design during construction (a new way of implementing OM)
LIS- MS[4]- North Wall	Farooq *et al.* (2015) Chen *et al.,* (2015)	To speed up the construction to meet the approaching TBM tunnels, the alternative design was proposed for this major top-down shaft construction. The modification was validated at three verification points and approved for implementation	Progressively modified design (Cautious Ab initio)
LIS-MS-East Wall	Chen *et al.* (2015)	London Underground tunnels nearby the East wall assessment due to the shaft excavation was being progressively evaluated through phased construction, therefore the unnecessary protection option was avoided and even the initial movement criteria was breached.	Peck's 'Best-Way-Out'

[2] CWCS = Canary Wharf Crossrail Station;
[3] TCR-WTH = Crossrail Tottenham Court Road Station, Western Ticket Hall;
[4] LIS-MS = Liverpool Street Station, Moorgate Shaft. The designer holds the view on the progressively modified design as the observational method applied in the Moorgate Shaft.

2.1.3 Constraints of implementing the observational method

Although some successful case histories have proven that savings of time and cost were possible (Glass and Powderham, 1994; Nicholson *et al.*, 1998; Powderham, 2002), concerns on the limitations and the proper application of the observational method have never ceased since its introduction to ground engineering. The uncertainties in the ground were believed as the major constraint of implementing the observational method.

The uncertainty of soil properties was recognized by Terzaghi (1936): "*A natural soil is never homogeneous. Its properties change from point to point, while our knowledge of these properties is limited to those few spots at which the samples have been collected.*"

The uncertainty in the structural properties and construction procedures was pointed out by Peck (1969a). A discussion of uncertainties and their relevance for the design of excavations were given by Bauduin (2003) and these uncertainties were classified in three sectors: the support system, ground properties and construction method (e.g. top-down and bottom-up).

The uncertainties were identified as knowledge-based epistemic and a random variable aleatory (Nossan, 2006). He thought it was possible to decrease the epistemic type uncertainties when more observations became available. With regard to the aleatory type uncertainties, the probabilistic analysis might be a solution offering a statistical result (Spross, 2014).

Other constraints of implementing the observational method were reviewed as per below.

2.1.3.1 Design parameters

Different terms were used to describe design parameters in the observational method over its development phases, such as 'most probable', 'more probable' and 'moderate conservative'. These definitions were unclear before the clarification given in Ciria R185.

In the current geotechnical design code in the UK, the 7th edition of Eurocode (BSI, 2004), the 'most probable' was used to describe the design parameters in the observational method. The statistical meaning of the 'most probable design parameters' referenced to Ciria R185 (Nicholson *et al.*, 1999): " *A set of parameters that represents the probabilistic mean of all possible sets of condition.*" However, the unclarity remained, was this 'mean' of all possible sets of laboratory and field data? It was not necessarily as 50% of the maximum value of the dataset. Or was this 'mean' as a set of parameters which can predict the most likely soil/structure performance among all possibility.

The same lack of unclarity was found in the probabilistic definition of the characteristic values in the 7th edition of Eurocode, section 2.4.5:

"The selection of characteristic soil parameters shall be based on derived results and derived values from laboratory and field tests, complemented by well-established experience. The characteristic value of a geotechnical parameter shall be selected as a cautious estimate of the value affecting the occurrence of the limit state."

" If statistical methods are used, the characteristic value should be derived such that the calculated probability of a worse value governing the occurrence of the limit state under consideration is not greater than 5%." (NOTE: In this respect, a cautious estimate of the mean value is a selection of the mean value of the limited set of geotechnical parameter values, with a confidence level of 95%; where local failure is concerned, a cautious estimate of the low value is a 5% fractile".)

It was debated that the statistical requirement in the 7th edition of Eurocode intended the probability of the limit state occurring to be limited to 5%, in the case of characteristic parameters for the ultimate limit states (ULS) calculation, but not the choice of the soil parameters only (Hardy, 2015).

Hence, it suggested that one possible way to comply with the Eurocode requirements was to derive a probabilistic distribution for each factor that would have affected the wall behaviour, and feeding them into a performance statistical model. By this way, the probability distribution of the total performance for the ULS design would be obtained. A conceptual diagram showing all potential elements that affected the retaining wall design is illustrated in Figure 2. 3.

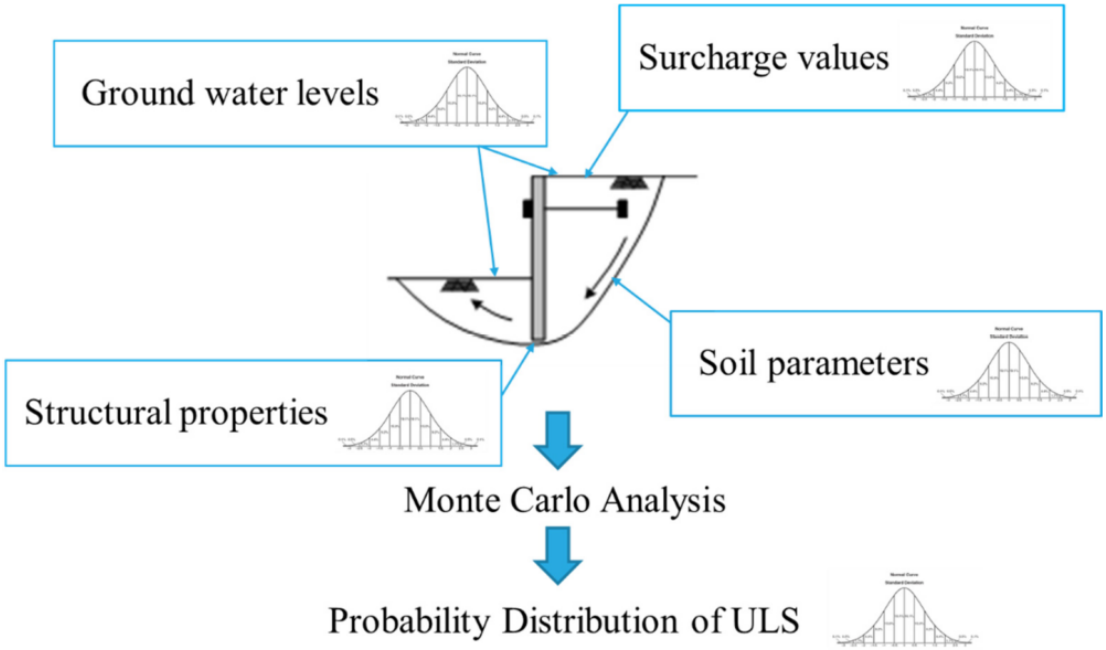

Figure 2. 3 Diagram of wall design satisfying Eurocode requirements for use of statistical analyses (Hardy, 2015)

Neither the lack of clarity in definitions of design parameters nor the complexity in using the statistical analysis has encouraged the users to derive the proper design parameters to develop the observational method optimistic design (e.g. *Ab initio* approach design) and prepare the appropriate contingency measures.

2.1.3.2 Observations (monitoring)

The importance of reliable field observations was emphasized since the beginning of the observational method. Peck (1969a) pointed out the monitoring data interpretation needs special care, sometimes the engineers' judgement would be essential to produce reliable data. For example, the toe movements of diaphragm walls have forced correction of inclinometer readings (Hwang *et al.*, 2007); the use of shape accel arrays measuring retaining wall deflection was required as the cross-reference checking to verify the data (Lipscombe *et al.*, 2012).

In the past decades, advancements in technology, telecommunication have provided access to a wider variety of instruments and enhanced applications in the monitoring industry: remote & automated data collection, and a collection of databases. However, fewer improvements were made regarding the data resolution, accuracy, precision and error control. The monitoring practice has a relatively low reputation in the construction industry, hence, an unnecessary safety factor has been commonly included in the prediction to cover the variances from the field observations.

2.1.3.3 Risk management

In the context of the observational method, it is essential to have a proper risk management strategy to ensure the safety of construction and reassure the stakeholders, in order that the chance of implementing the observational method can be promoted.

Owing to the nature of the observational method, the optimistic design would lead to a less conservative design, which could raise concerns about the increased risk. It was based on good practice experience, some guidance on mitigating the risk was proposed. For example, the tailored contingency measures, the good team management with clear work procedures (Powderham, 2002), and Ciria R185 recommended the risk assessment to manage risk. This risk assessment comprises four stages: hazard identification, risk assessment, risk reduction and risk control. In addition to the risk assessment, a traffic light trigger system was introduced as part of the construction operational process to manage risks (Nicholson *et al.*, 1999; Masurier *et al., 2006*).

Although efforts have been made to mitigate risk under the observational method, like the one introduced by Whitman (1984) to manage risk in geotechnical engineering, with increasing acceptance of this risk management concept in the industry over the years (Clayton, 2001), the confusion about risk management remained. For instance, the decision on trigger values was not uniform but relied upon the engineer's experience. The risk may be limited to an acceptable or agreed level, which was a very much individually perceived term rather than a quantifiable term.

2.1.3.4 Other constraints

Another constraint which presents preventing the implementation of the observational method is the human factor. For instance, 'Soft' key performance indicators (KPIs) – measuring the project team performance, human factors could have a significant impact on the success of the observational method (Masurier *et al.*, 2006). Nowadays, a construction project tends to be split into more fragments (e.g. more parties are getting involved), which also introduces the additional variable of human factors in using the observational method.

The introduction of the value engineering together with the observational method in the Limehouse Link construction showed success in achieving savings (Glass and Powderham, 1994). The compatibility of these two techniques and both having the same objective of achieving savings seemed to overcome the traditional contractual constraints in implementing the observational method. However, in most cases, the contractual constraint has always been a barrier.

2.1.4 Summary of the review of the observational method

The above literature review of the observational method suggested the following research topics. A new refined observational method framework would be necessary. Design parameters used in the observational method need to be clarified. A uniform way to derive design parameters for the observational method would be necessary to avoid confusion. Guidance on selecting the appropriate design approach of the observational method. Also, improvements in providing reliable observations will enhance the back-analysis performance, thus the observational method can optimise the design and aim for maximum savings

2.2 London Clay

This research focused on the Crossrail deep excavation case histories in the central London area. The typical soil stratigraphy in the London Basin was exposed in these excavations, hereby a literature review of the geology of London Clay was presented, including some of the crucial engineering features of this over-consolidated soil in relation to deep excavation.

2.2.1 Geology of London Basin

Since the early 19th century, the term 'London Basin' has been used to describe the sediments that make up the geology of London. The outcrop of Chalk defined the original limits of this basin. The British Geology Survey commenced the detailed geological mapping of the London Basin in 1861 and realised that the correlation of strata across and beneath London was not always straightforward.

In a recent overview of the Palaeogene depositional basin, the London Basin was verified as forming the middle and lower parts of the Thame Valley, extending eastwards offshore into the North Sea (Royse *et al.*, 2012).

A stratigraphic framework for the London Basin comprises four well-established major subdivisions, three of which extend into the Hampshire Basin: the Bracklesham Groups, the Thames Group and the Lambeth Group. In the central and eastern part of the London Basin and in East Anglia, the Lambeth Group is underlain by the oldest subdivision, comprising onshore components of the Montrose Group (Aldiss, 2012), as shown in Figure 2. 4.

The currently applied scheme for numbers of subdivisions and names of the Palaeogene groups in the London Basin was summarised in Table 2.2, following the recommendation of the stratigraphical framework for the Palaeogene successions of the London Basin, UK (Aldiss, 2012).

The upper Cretaceous Chalk (over 66 million years old) is present at subcrop through the London Basin and comes to the surface along its southern and northern margins.

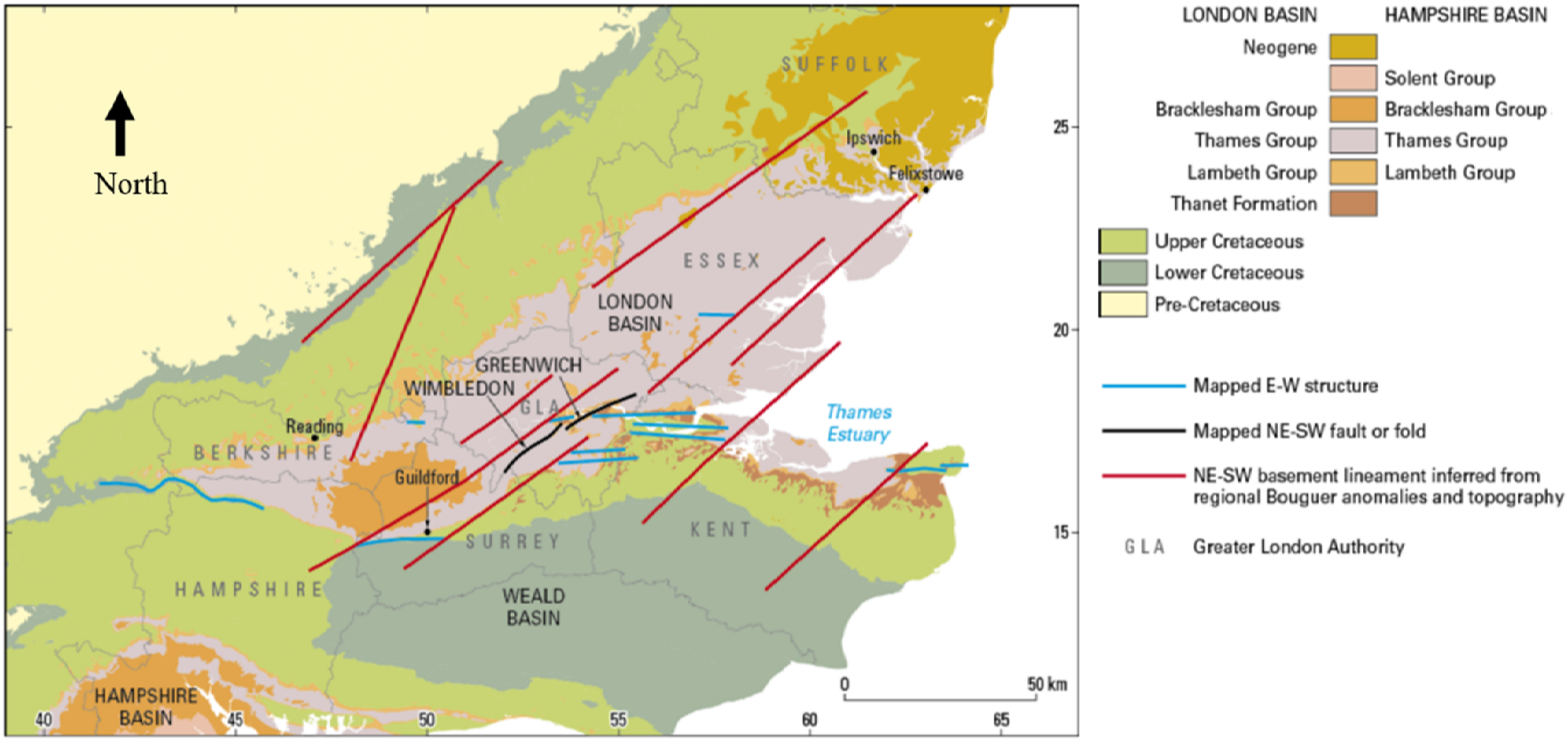

Figure 2. 4 Outercropt of geology strata in London Basin - selected structures controlling the London Basin (Aldiss, 2012)

Table 2.2 Stratigraphic hierarchy in the Palaeogene of the London Basin (Aldiss, 2012)

Group	**Formation**	**Members**
Bracklesham[2]	Camberley Sand	
	Windlesham	
	Bagshot	
Thames[3]	London Clay	Claygate; Sheppey; Aveley; Ockendon; Walton 5 Divisions: A to E by King (1981)
	Harwich	Swanscombe; Oldhaven; Blackheath; Wrabness; Orwell
Lambeth[4]	Woolwich Formation	*Woolwich Sands; Upper Shelly Clay; Striped Loams; Laminated Beds; Lower Shelly Clay;* Shorne
	Reading Formation	*Upper Mottled Clay; Lower Mottled Clay*
	Upnor	
Montrose[5]	Thanet[6]	Reculver Sand; Pegwell Silt; Kentish Sand; Stourmouth Silt; Base Bed
	Lista[7]	Ormesby Clay

Note:

1. In normal usage, unite names are terminated by the rank term at the head of the column, other than those shown in italic script, which is informal;
2. The Bracklesham Group was originally defined in the Hampshire Basin, its use was extended to the London Basin (King, 1981);
3. Thames Group was previously named as London Clay Group. It forms the greatest part of the Palaeogene outcrop in the London Basin, as defined by King (1981) and refined subdivision including Harwich Formation by Ellison (1994);
4. Lambeth Group crops out around the periphery of the London Basin, was defined by Ellison (1994) after the London Borough of Lambeth, in south-central London;
5. Montrose Group was defined by Deegan & Scull (1977);
6. Thanet Formation has previously named the Thanet Sand formation;
7. Ormesby Clay member was previously classified as a formation but now assigned to the Lista Formation (Aldiss, 2012).

As a major aquifer layer, the thickness of the Chalk preserved in the London Basin is between 170 and 210 m and generally thins from west to east. This succession within the London Basin is relatively thin compared to the completed Hampshire-Dieppe Basin (over 400 m) (Royse *et al.*, 2012).

Overlying the Chalk are the Palaeogene deposits (between 43 and 66 million years old), the Thanet Sand Formation, up to a maximum thickness of about 30 m. Above the Thanet Sand Formation lies the Lambeth Group between 20 and 30 m thick in London area with a highly variable lithology containing different proportions of sands, silts, clays and gravels. The Eocene sediments (between 58 and 51.5 million years old) of the Thames Group including Harwich and London Clay Formations are overlying the Lambeth Group. The Harwich Formation contains predominately sand and pebble beds up to 4 m thick. Approximately 90-130 m of the London Clay Formation, a sequence of grey to blue-grey when fresh, but weathering to brown at the surface, is above the Harwich Formation. Quaternary deposits are then encountered throughout the London Basin, including alluvium, peat, brickearth and river terrace deposits (Clements, 2010; Royse *et al.*, 2012; Aldiss, 2012; Aldiss *et al.*, 2014; Mathers *et al.*, 2014).

A generalised stratigraphic column to represent the typical vertical section at central London is presented in Figure 2. 5.

Evidence shows at least two extensive glaciations occurring in the Britain Isles during the Quaternary Period (from around 2.6 million years old to present), as indicated in Figure 2. 6. The Anglian Glaciation, the largest to affect Britain, occurred between 0.48 and 0.43 million years ago. The ice extended across two-thirds of Britain down to the Finchley area of north London. The second glaciation was during the Late Devensian period reducing a maximum ice sheet extent around 20,000 years ago (Lee, 2011; Royal Geographic Society, 2017). The huge amount of meltwater from the edge of the ice sheet could have caused powerful streams, for example, the ancient River Thames, to transport and deposit large amounts of sand and gravel, by forming the superficial layers just beneath the surface in London.

As the River Thames alternatively deposited and then cut down through the superficial layers, gravel terraces formed at slightly different elevations in the Thames Valley. Many parts of London are built on these various terraces (Royal Geographic Society, 2017).

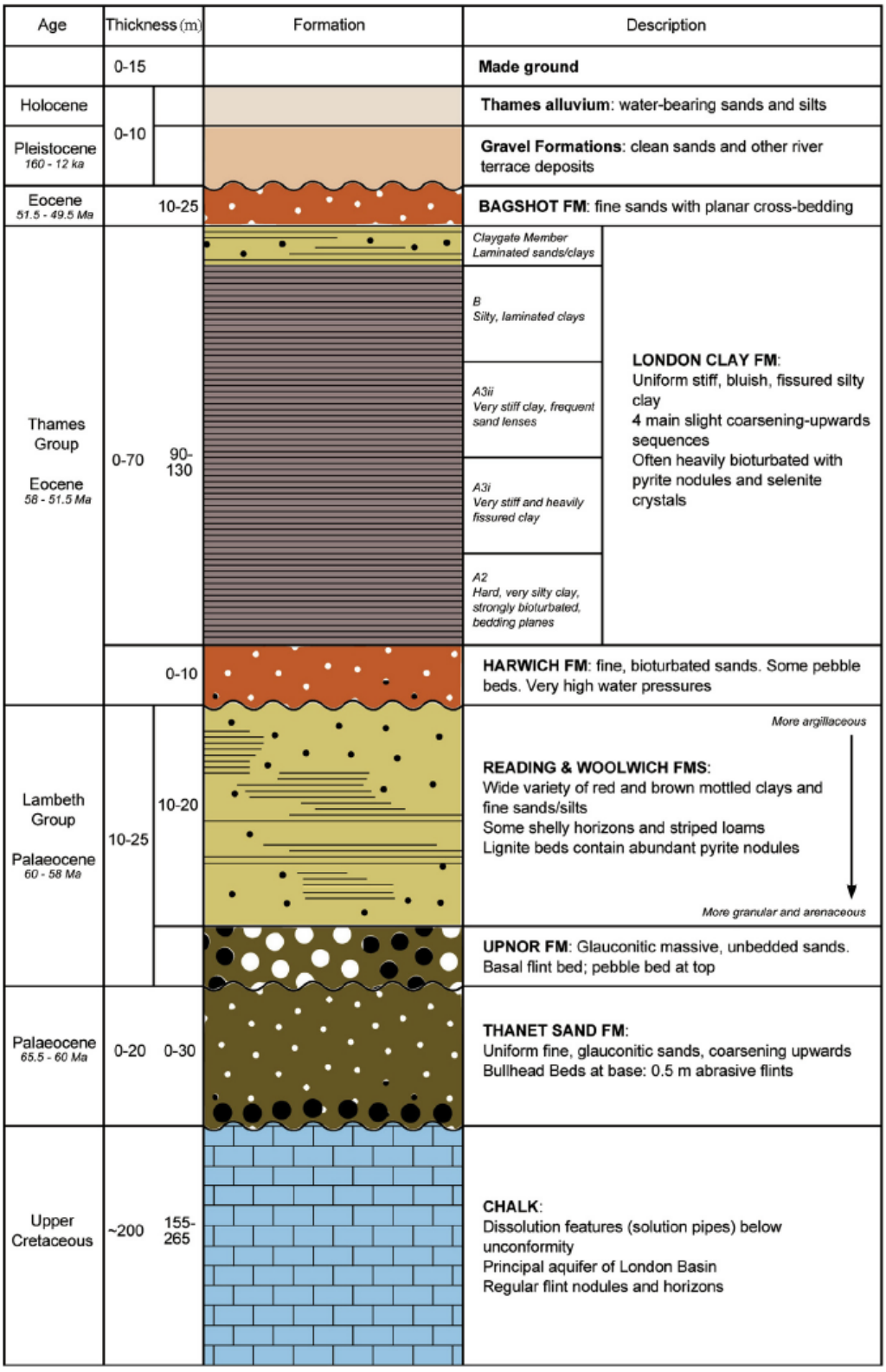

Figure 2. 5 Generalised central London stratigraphic column (Paul, 2016)

Note the thickness value at the left = range of borehole data for 6 units (made ground, drifts/alluvium, London Clay, Lambeth Group, Thanet Sand, Chalk); the thickness value at the right = typical strata thickness in the London Basin.

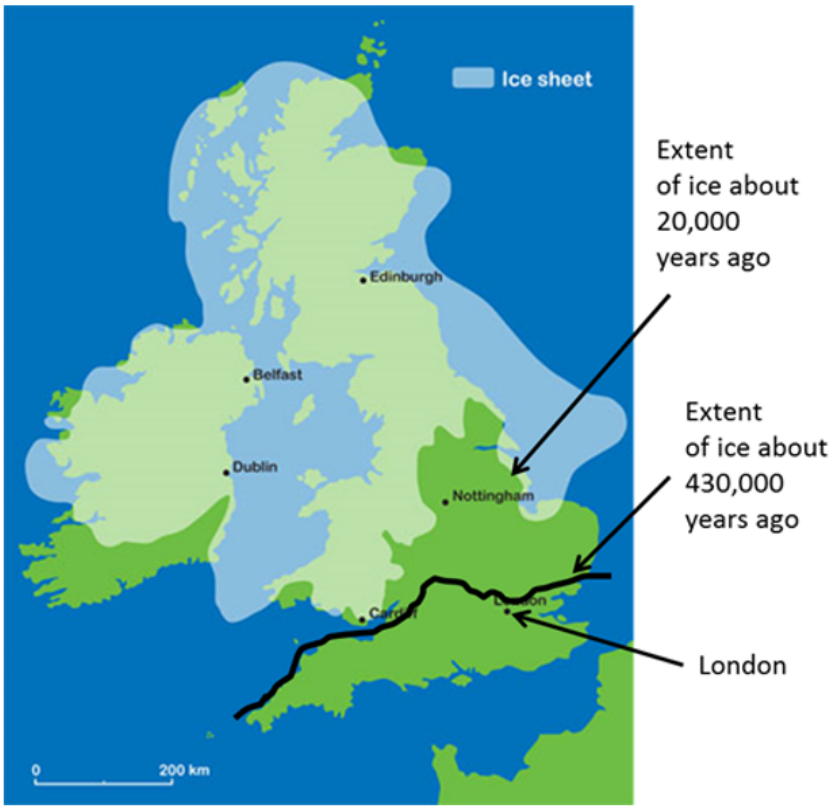

Reference: British Geology Survey, 2017; Royal Geographic Society, 2017

Figure 2. 6 The most recent British ice coverage with an indicative extent edge line of the previous ice sheet

2.2.2 London Clay engineering features

London Clay has been investigated for practical construction purpose and as major research material in the past decades. The London Clay Formation was probably the best known and characterised of all the Formations in the London Basin. Thanks to its relatively homogeneous nature, most of London underground development, such as tunnels, basements and foundations, were within the London Clay. This is also the case for the Crossrail project through the central London area. Hereby, the engineering features of this over-consolidated clay formation was reviewed and presented in this section.

The sedimentological history of a geological formation influences how the ground will respond to construction, thus influence the geotechnical risk of working within it (Royse *et al.*, 2012). A detailed profile of the geology and the engineering properties of the London Clay Formation were generated from the research, benefiting from a few large infrastructure projects in London, they have produced lots of quality ground investigations data.

The geology cross-section of the Crossrail eastbound tunnel alignment at the central London area was presented in Figure 2. 7. In the cross-section, the London Clay thickness is thicker in the west (e.g. at Royal Oak Portal & Paddington Station), and gradually thins towards the east (e.g. Farrington Station). The tunnelling works and station deep excavation are all within the London Clay Formation.

The key aspects of engineering features of London Clay in the excavation were highlighted below, including the stratigraphy.

- Small strain stiffness;
- Stress history;
- Stress path (strain history); and
- Stratigraphy;

These engineering features of the London Clay were reviewed in detail and they were believed to dominate the soil behaviour during the excavation. Other engineering features like soil anisotropy in strength and stiffness, soil structure & destructuration, stress localisation, the time-dependent effect of ageing and creep, could also have some effects on the excavation, but majorly affect consolidation and ground movements.

2.2.2.1 Stratigraphy

The London Clay Formation is predominantly a bioturbated clay with silt and sandy clay intervals. A combination of biostratigraphy and lithological variation, with the identification of marine flooding events, was used to define five sub-divisions (A to E) of London Clay (King, 1981; Royse *et al.*, 2012), as shown in Figure 2. 8. It has been found that the London Clay Formation was distributed consistently in both laterally and vertically throughout the London Basin.

The effects of stratigraphy on features of engineering behaviour are summarised by Hight *et al.* (2007):

"There are important differences in the behaviour between the lithological units. Units B2(a), A3 and A2 are clearly more structured than overlying units, having significant cohesive components of strength.

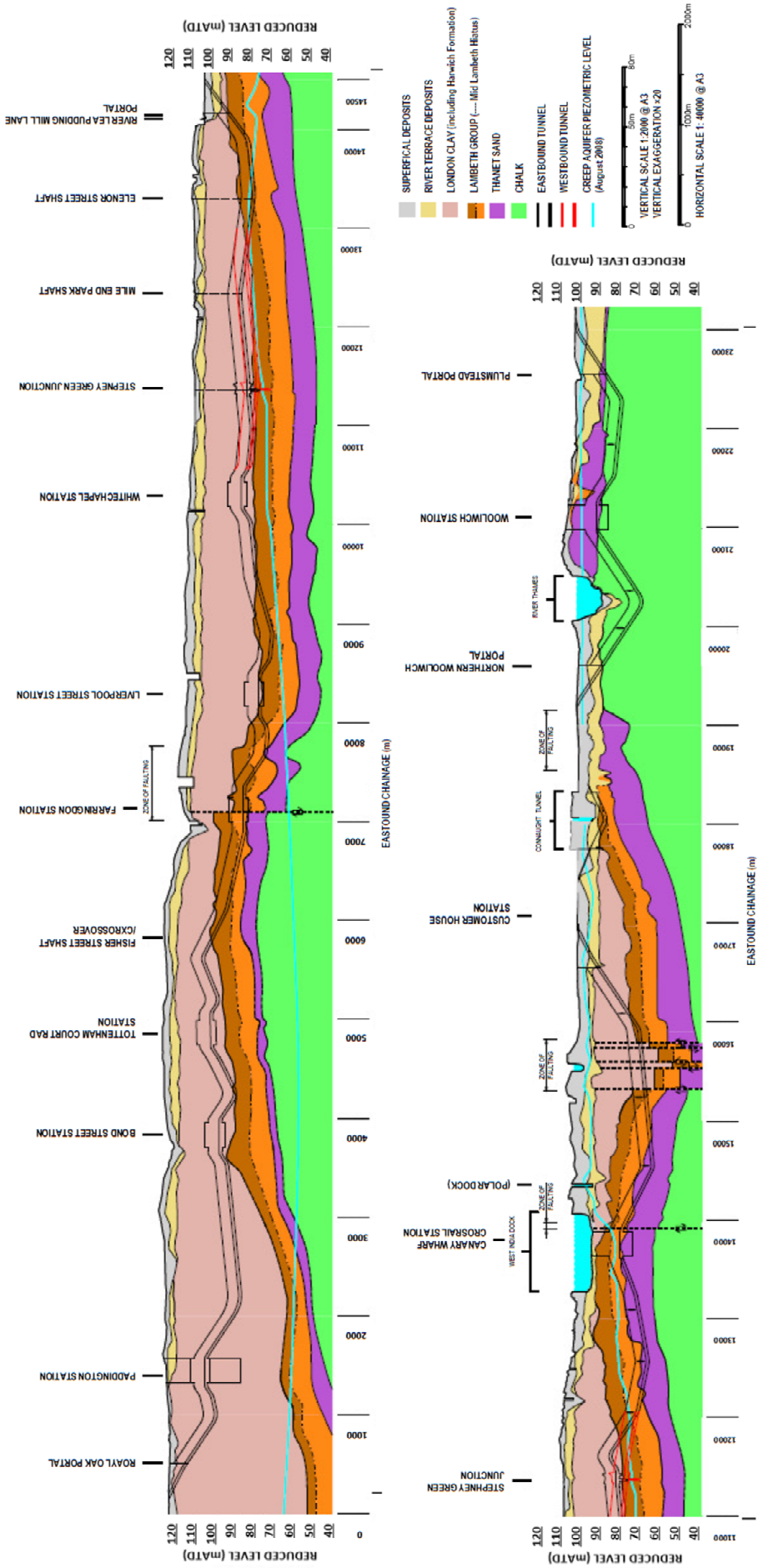

Figure 2. 7 Geotechnical and deep aquifer piezometric level profile (Crossrail, 2010)

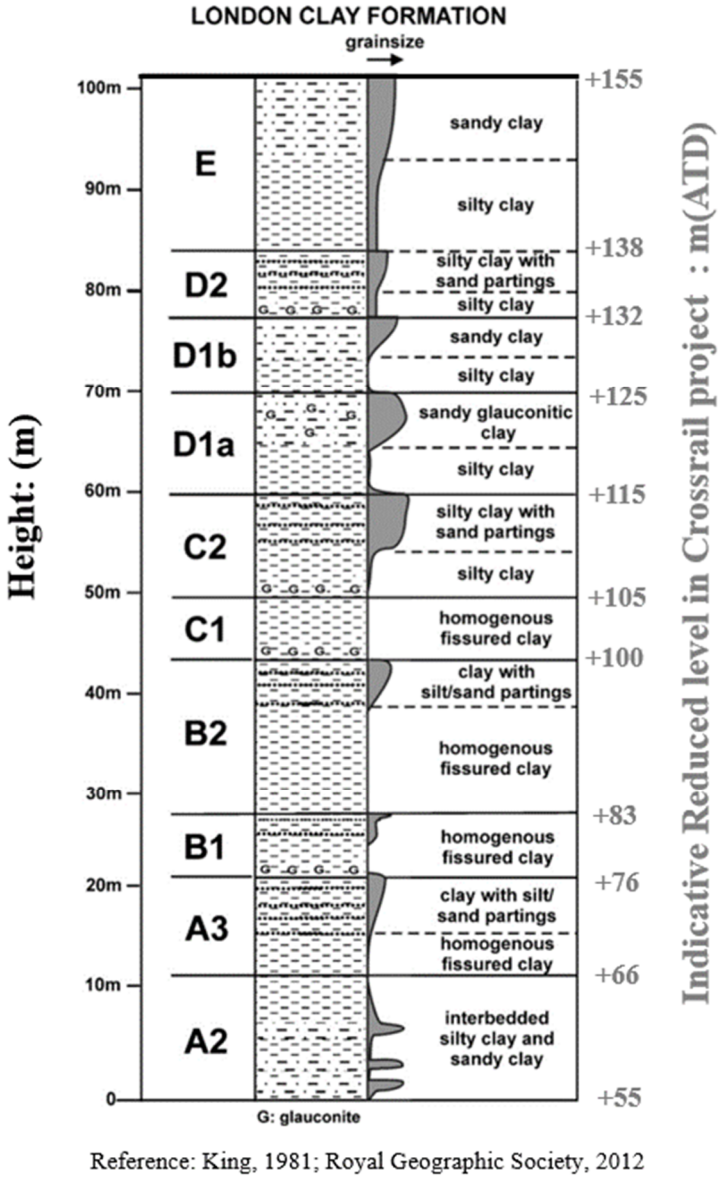

Figure 2. 8 Distribution of the blackearth Formation in London

Unit A2 is the most brittle but is non-fissured. Anisotropy increases with the depth of each unit and varies within units. Except for unit A2, there are no major differences between the modulus decay curves of the different unit. As the units appear to be of a consistent thickness, it is sufficient to establish the base of the London Clay at a site in order to anticipate the position of the lithological units within the profile."

The importance of permeability in the stratigraphic units is demonstrated in the study of long-term pore pressure changes around the Jubilee Line tunnels at St Jame's Park (Wongsaroj *et al.*, 2007). The major consolidation was found on either side of the tunnel. In principle, the rate of consolidation settlement depends on the permeability of the soil at the tunnel springing level. The finding on the permeability of the London Clay sub-divisions was consistent with

the hierarchies of permeability suggested by Hight *et al.* (2003), and Standing & Burland (2006):

$$k_{A2} > k_{A3ii(top)} > k_{A3i} \approx k_{A3ii(base)} > k_B \qquad (2 - 1)$$

Different combination of soils forms units of the London Clay, which have discontinuous distributions and present variable engineering properties from often highly permeable lithology to hard calcareous concretions at several levels (Royse *et al.*, 2012)

2.2.2.2 Small strain stiffness

Most soils present high stiffness at small strains which decrease as strains increase. This is widely known as the highly non-linear S-shaped stiffness curve like the one shown in Figure 2. 9. The character of small strain stiffness of soils was identified with improvement in soil laboratory testing techniques. The use of electrolytic levels enables accurate measurement of local axial strains of triaxial apparatus, resolves relative displacements to less than 1 μm over a range of 15 mm, corresponding to a strain of 6.67×10^{-5} (Jardine *et al.*, 1985).

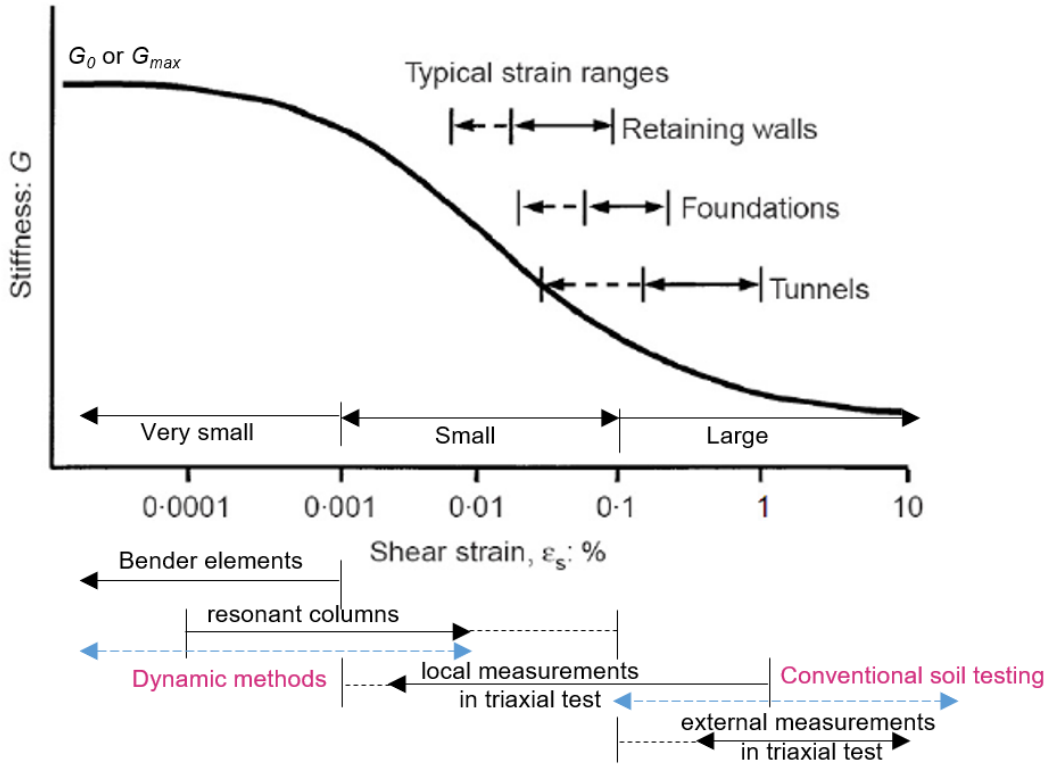

Figure 2. 9 Typical stiffness variation and strain ranges for different structures / approximate strain ranges in limits for reliable measurement of soil stiffness, redraw after (Mair, 1993) & (Atkinson, 2000)

Three regions were used to describe stiffness non-linearity: in the very small strain region ($< 1\times10^{-5}$), soil behaves as perfectly elastic material with strains being fully recoverable; in the

large strain region (>1×10^{-3}), the volumetric yield is developing towards the failure; in between, the shear stiffness decreases smoothly with increasing strain, as a combination of both elastic and plastic strains (Burland, 1989).

The very small strain region, as the linear elastic region, was identified below 3×10^{-5} in three tested soils: Bothkennar clay, London Clay and a high-porosity Chalk by Clayton and Heymann (2001), as shown in Figure 2. 10. For the London Clay soil samples, a rest period 6 to 12 days was allowed before shearing in the test, it was to mimic the effects of creep to an acceptable level.

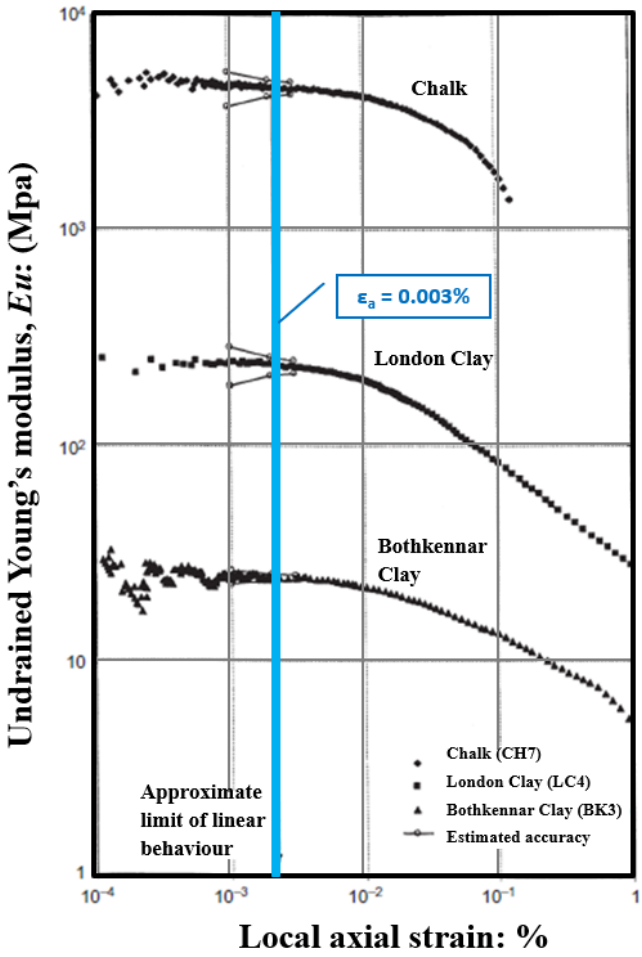

Figure 2. 10 Comparison of the stiffness: Chalk, London Clay & Bothkennar Clay (Clayton and Heymann, 2001)

The linear elastic region in stress space can grow in size as a result of over-consolidation or ageing effects (Vucetic and Dobry, 1991; Jardine, 1992). Figure 2. 11 shows a schematic diagram of kinematic sub-surface, where three characteristic zones (Zone 1, 2 & 3) within a bounding surface were defined by three sub-surfaces (Y1, 2 & 3). These sub-surfaces were defined by progressively larger stresses (Jardine, 1992). Three zones include:

- Linear elastic Zone 1: Y1 surface forms the boundary of the region where behaviour is perfectly linear elastic.
- Recoverable Zone 2: Y2 surface marks the limit to recoverable, but non-linear behaviour, this zone is between the Y1 and Y2 surfaces.
- Plastic Zone 3: Between Y2 and initial bounding surface Y3 (local boundary) is the area of irrecoverable plastic strain zone, where behaviour is transitional, and the plastic components of straining become progressively more important as the stress path approach to the Y3 surface. Naturally, the strain required to reach the Y3 surface depends on the relative position of the initial stress point and the direction of the probing stress path.

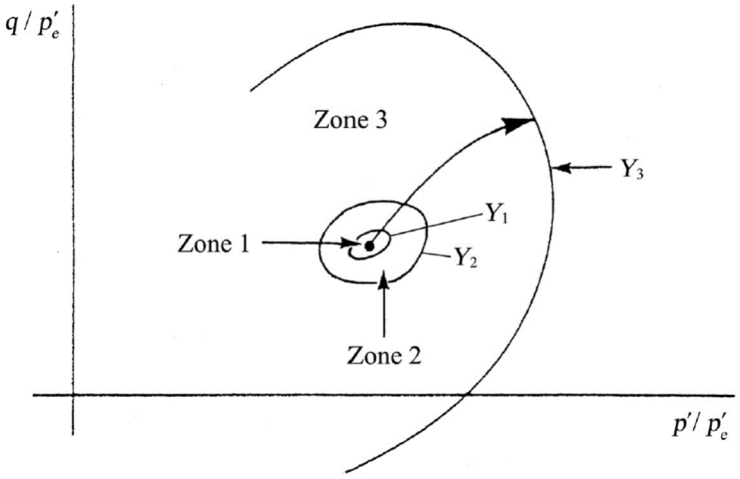

Figure 2. 11 Schematic diagrams of kinematic sub-surfaces, after (Jardine, 1992)

The experimental data demonstrated that the sub-surface could move, reposition and distort as the current stress point moves (Jardine, 1992). There were a few soil constitutive models that have been developed based on the sub-surfaces theory, such as the two-surface bubble model (Al-Tabbaa & Wood, 1989) and three-surface model (Stallebrass and Taylor, 1997).

The initial shear stiffness G_{max} or G_0 represents the elastic shear stiffness of the soil and it can be measured using bender element tests in the laboratory or geophysical testing in the field (Viggiani, 1992; Jovicic and Coop, 1998; Pennington, Nash and Lings, 2001).

From the previous construction projects in London, it was found that the shear strains governing the movements in the excavation, lied between the small strain region and large strain region: from 1×10^{-4} to 1×10^{-3} (Burland *et al.*, 1979). A strain of 1×10^{-3} (1mm per 1m) was thought to cause some typical damage (Simpson, 2010). Thus, the soil constitutive models that have better performance at strain range of 1×10^{-4} to 1×10^{-3} should be considered for the Crossrail deep excavation case history back-analysis.

2.2.2.3 Stress history

It has been acknowledged in soil mechanics that soil deformation has been significantly influenced by its stress history. The shear stiffness of overconsolidated clay was dependent upon its stress history, the semiempirical expression for G_{max} by Hardin and Black (1968, 1969) was an example:

$$G_{max} = CF(e)(OCR)^K p'^{1/2} \qquad (2 - 2)$$

C = constant, e.g. $3230^{1/2}$ or 1230 if G_{max} and p' are measured in psi.

$F(e)$ = a function of void ratio e, e.g. $F(e) = \frac{(2.973-e)^2}{(1+e)}$

OCR: overconsolidation ratio $OCR = \sigma'_{vmax}/\sigma'_v$ (maximum past vertical effective stress / current vertical effective stress)

K: coefficient associated with a plasticity index of soil

p': mean principal effective stress

It was based on laboratory testing data of reconstituted samples for superwhite kaolin, Viggiani and Atkinson (1995) proposed the equation for the very small strain shear modulus G_{max}:

$$\frac{G_{max}}{p_r} = A\left(\frac{p'}{p_r}\right)^n R_0^m \qquad (2 - 3)$$

Where R_0 is equivalent to OCR, p_r is a reference pressure (normally taken to be 1 kPa or atmospheric pressure), and A is non-dimensional soi parameter. The values for N and M are to be 0.76 and 0.25 for reconstituted London Clay.

The above equations indicated that the stiffness was in proportional to the effective stress p'. This pressure dependence was found to be true for both undisturbed and reconstituted samples, showing that G_{max} was unaffected by the soil structure and fabric. At small strains, the deformation was due to elastic deformation at points of contact between particles (Viggiani and Atkinson, 1995).

The complex stress history of the London Clay Formation, including multiple depositions, sedimentation and glaciation, has resulted in overconsolidated stress and G_{max}.

2.2.2.4 Stress path (Strain history)

The London Clay stiffness was studied further and the effect of 'recent stress history' or strain history was found to have a significant impact. The term 'recent stress history' was used by Atkinson (1990) to differentiate from the current path undertaken by the soil. The recent stress path could be the form of a change of direction in the stress path or an extended period of rest in shearing.

Richardson (1988) conducted triaxial compression tests using different stress paths, and found " *Soils behave in a stiffer manner if the direction in which they are being strained is changed."* Atkinson *et al.* (1990) explored further into the link between the degree of rotation in the stress path and the increase in shear stiffness. It was found that when the stress path direction changed, the soil strains initially remained in the original direction of movement, but showed a much stiffer response. Further exploration showed that if straining continued, the soil would eventually be strained in the new direction of straining.

Figure 2. 12 showed the testing results of the shear stiffness at different stress path rotation angles: the greater rotation in the stress path, the higher stiffness measured during the shearing. At small strains ($\leq 1 \times 10^{-4}$), the stiffness at the rotation $\theta = 180°$ test was approximately an order of magnitude larger than the corresponding stiffness at $\theta = 0°$ test. After strains over 5×10^{-3}, the differentiation from the rotation of the stress path has been minimised.

The 'recent stress history' effect was also observed in similar tests on kaolin samples (Stallebrass, 1990).

Clayton & Heymann (2001) found in undrained triaxial probes on undisturbed soft Bothkennar clay and London Clay samples that when the dissipation of creep strains was allowed, the measured initial stiffness was independent of the stress path rotation. Contrasting findings concerning the effects of recent stress history which might have been caused by different test procedures, and possibly different behaviours of the tested soils.

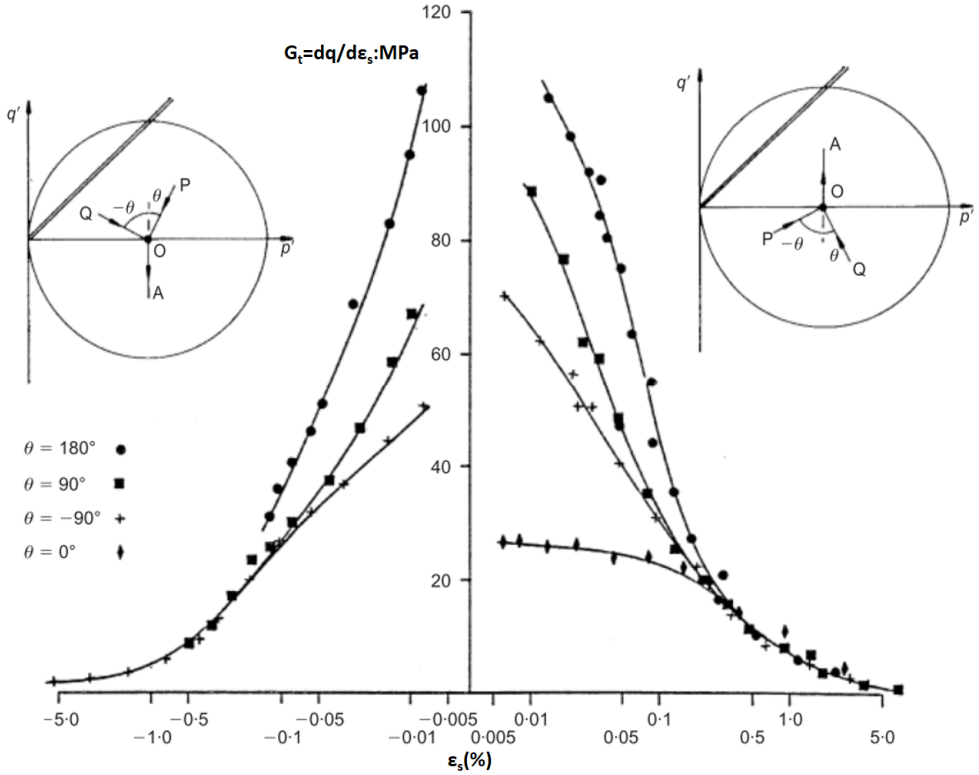

Figure 2. 12 Stiffness of reconstituted London Clay versus strain measured in constant p' test, (Atkinson, et al., 1990)

The influence of the approach path angle, creep time and approach path lengths were investigated further by Gasparre (2005). The undisturbed London Clay sample was taken to isotropic stress states followed by undrained stress probes in extension and compression. To investigate the approach path lengths, the approach paths were either short (within the Y2 locus, approximately ±10 kPa) or long (in the order of 100 kPa), and the creep was either allowed (rest under constant effective stress for a few days) or not (simple rest after a limited creep time of 3 hours) before the start of each stress probe. Where the creep was allowed, the results indicated that the stiffness was only influenced by the approach path angle if the path has been long enough to cause significant straining, (Gasparre, 2005; Gasparre et al., 2007b), as demonstrated in Figure 2. 13.

The exploration of the interaction between recent stress history, creep/ ageing periods and probing paths has shown that relatively short creep period can erase the effects of recent stress history within the original Y2 surface, but the approach path still matters if large enough strains are induced. It concluded that the strain history is more important than stress history (Gasparre, 2005)

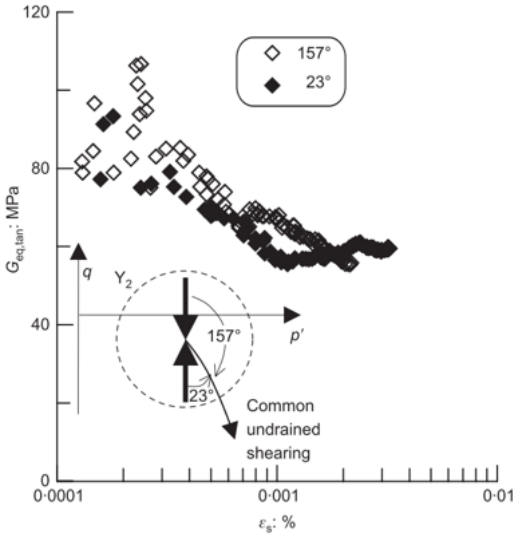

(a) Tangent stiffness for approach path within the Y2 surface, creep allowed

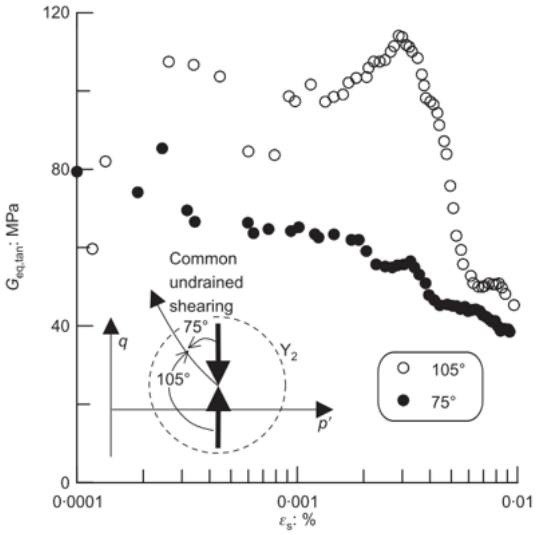

(b) Tangent stiffness for approach path within the Y2 surface, creep NOT allowed

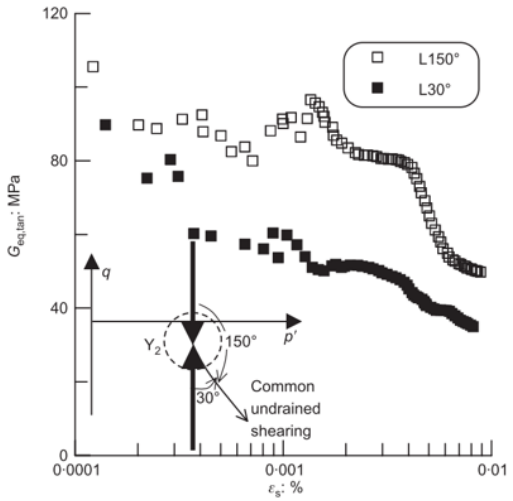

(c) Tangent stiffness for approach path above the Y2 surface, creep allowed

Figure 2. 13 Tangent stiffness decrease curves for different approach paths (Gasparre *et al.*, 2007b)

This recent strain history phenomenon is particularly relevant to deep excavations. At a point near the retaining structure where stresses are high, the soil-structure interaction will normally involve changes in stress paths, thus changes in stiffness. For the same volume loss in analysis, a better estimation of ground surface settlement induced by tunnel construction was achieved, when the previous geological stress history was taken into account for the tunnelling at St Jame's Park(Grammatikopoulou *et al.*, 2008).

2.2.2.5 Anisotropy in strength and stiffness

Anisotropy refers to any direction-dependent material property. Anisotropy effects have been described as 'inherent' and 'induced' based on the sources causing the effect. Inherent anisotropy results from soil particle shape and depositional processes, which is a physical characteristic and entirely independent of the applied stresses and strains (Casagrande & Carillo, 1944). Induced anisotropy is due to the strains associated with the applied stresses following deposition. Both sources coincide to make up the initial anisotropy and it is difficult to separate them (Yimsiri and Soga, 2001; Minh, 2006).

Early research on the shear strength anisotropy of London Clay was performed through samples prepared vertically, horizontally and sometimes diagonally oriented for triaxial and plane strain testing. A ratio of horizontal to the vertical undrained shear strength of clay was reported as s_{uH} / s_{uV} = 1.3 to 1.5 from several samples at variable locations (Ward, Samuels, & Butler, 1959). Other early studies showed no significant strength difference between vertically

and horizontally samples in terms of effective friction angle ϕ' and effective cohesion c' (Bishop, 1966; Agarwal, 1968).

Intensive laboratory experimental tests have been carried out in natural London Clay for the Heathrow Terminal 5 project (Hight *et al.*, 2007; Nishimura, *et al.*, 2007; Gasparre *et al.*, 2007a). Parallel studies aiming to characterise the shear strength anisotropy of London Clay were carried out using the hollow cylinder apparatus (HCA) and dynamic testing technique. The shear strength anisotropy was clearly shown in one of the results in Figure 2. 14. The ratio of normalised undrained shear strength s_u (normalised by s_u at $\alpha = 0°$) increases from 1.0 to above 1.5 at $\alpha = 90°$.

The study concluded that the effects of anisotropy can lead to up to 40% variation between maximum and minimum of peak stress ratio values. An increase in the degree of anisotropy with depth in London Clay was suggested based on testing profiles from samples taken 6 mbgl to 35 mbgl. The top 5 m layer of London Clay appeared much less anisotropic than layers below (Nishimura *et al.*, 2007).

Young's modulus measured in the laboratory specimen is controlled primarily by the effective stress in the direction of loading and due to the Poisson effect, it will also be influenced by the effective stress in the normal directions.

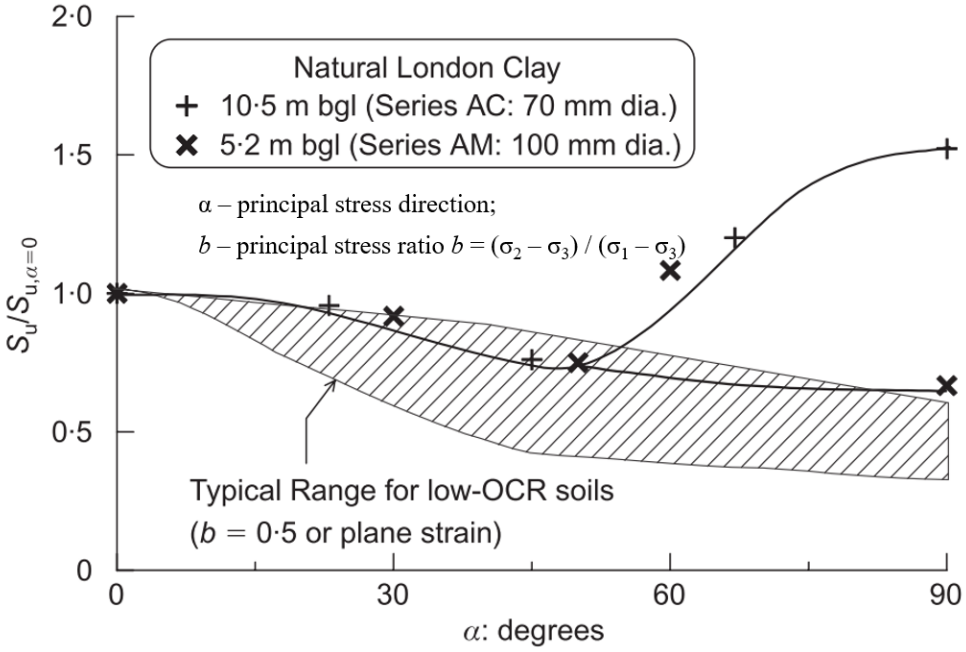

Figure 2. 14 Undrained shear strength anisotropy of natural London Clay (Nishimura *et al.,* 2007)

Shear modulus is controlled by the effective stresses acting in the plane of distortion. This means that in a transversely isotropic material, horizontal shear modulus G_h is a function of horizontal effective stress alone, whereas vertical shear modulus G_v is a function of both vertical

and horizontal effective stresses (Clayton, 2011). The tendency for London Clay to deform more easily in the vertical direction than in the horizontal is evidence of stiffness anisotropy (Wongsaroj, 2005; Gasparre, 2005; Gasparre A *et al.*, 2007b; Yimsiri and Soga, 2011).

A good example of the relevance of stiffness anisotropy is highlighted in isotropic compression tests: in the same stress path during loading and unloading process, the strain developed in the axial direction is almost 5 times larger than the one developed in the radial direction (Yimsiri, 2002).

The study of quantifying the stiffness anisotropy of London Clay can be traced back to 1960s. The horizontal to vertical undrained Young's modulus ratio of E_{uH}/E_{uV} = 1.1 to 2.0 from triaxial tests on samples taken from central London was reported by Ward, *et al.* (1959). A ratio of 2.0 for both drained and undrained triaxial and plane strain compression tests on samples from Barbican Art Centre, London, was reported by Atkinson (1975).

In general, natural specimens appear much more anisotropic than reconstituted samples, regardless of the consolidation conditions (Viggiani and Atkinson, 1995; Jovicic and Coop, 1998). Drained compression tests on London Clay showed a stable stiffness anisotropy ratio of E_h/E_v until the intermediate strain level (approximately Y2 yield point) (Yimsiri and Soga, 2011), as the displayed test results in Figure 2. 15.

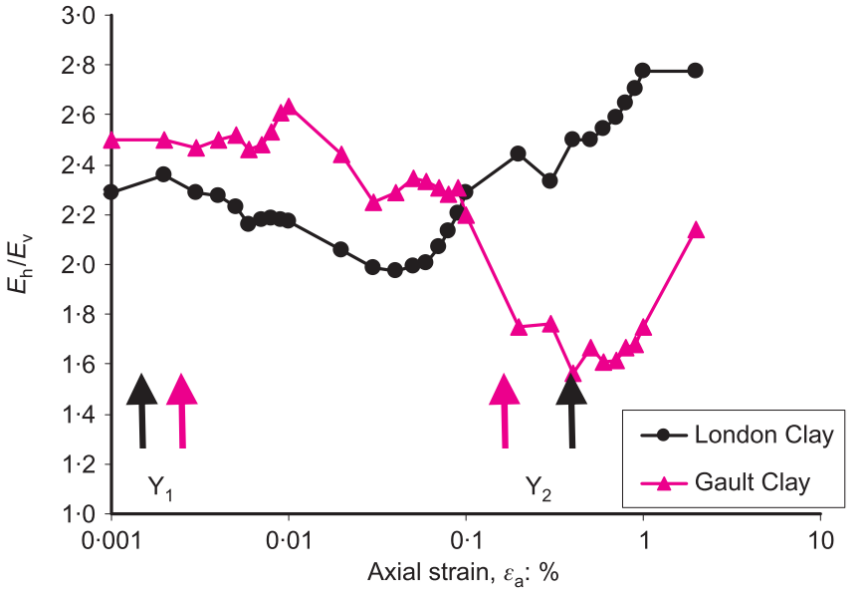

Figure 2. 15 Relationship between E_H / E_V versus axial strain ε_a for stiff clays (Yimsiri and Soga, 2011)

A summary of shear modulus G_{max} for London Clay from the literature was put together by Ellison (2012), as presented in Table 2. 3. The stiffness anisotropy of the London Clay can be interpreted as:

$$G_{HH} > G_{VH} \approx G_{HV} \quad (2 - 4)$$

$$\frac{\upsilon'_{vh}}{E'_{v}} = \frac{\upsilon'_{hv}}{E'_{h}} \quad (2 - 5)$$

$$G_{HH} = \frac{E'_{h}}{2(1+\upsilon'_{hh})} \quad (2 - 6)$$

Note: subscripts 'v' and 'h' represent the vertical and horizontal directions, G is shear modulus, E is Young's modulus and υ is Poisson ratio.

Table 2. 3 Ratio of shear modulus reported for natural London Clay, revised after (Yimsiri and Soga, 2002; Ellison, 2012)

Location	Reference	Testing method	Consolidation condition	G_{hh}/G_{vh}	G_{vh}/G_{hv}
Chattenden, Kent	(Powell and Butcher, 2003)	Down-hole and cross-hole wave velocity, cone seismic penetration test	In-situ	≈1.4	0.6 to 0.8
Heathrow Airport	(Simpson and Grose, 1996)	Bender element	In-situ & isotropic consolidation	≈1.54	≈1.0
Sizewell, Suffold	(Hight *et al.,* 1997)	Down-hole and cross-hole wave velocity, Bender element	In-situ	1.71 to 1.72	0.8 to 0.9
Heathrow Airport	(Jovicic and Coop, 1998)	Bender element	Isotropic consolidation	1.48 to 1.51	≈1.0
Crown Wharf and Kennington	(Yimsiri and Soga, 2001)	P and S wave transducers	Isotropic consolidation	1.6 to 1.8	n/a
Heathrow Terminal 5	(Hight *et al.,* 1997)	Down-hole and cross-hole wave velocity	In-situ	1.0 to 3.5	0.7 to 1.5
Heathrow Terminal 5	(Gasparre, 2005)	Triaxial, Bender element, torsional shear hollow cylinder	Anisotropic consolidation	1.8 to 2.1[1]	n/a
Heathrow Terminal 5	(Hight *et al.*, 2007)	Bender element	In-situ	~ 2.0[2]	n/a

Note 1. 1.8 for shallower depth, almost constant ratio of 2.0 over depth up to 30m; 2. the average value of 2.0 is based on the laboratory measurements.

Although the measured G_{VH} and G_{HV} were not absolutely equal, varying from 0.6 to about 1.0, it was logical to anticipate the symmetry of properties with regards to the vertical axis for a normal geotechnical problem. The assumption of cross-anisotropic elasticity may be applied to consider stiffness anisotropy in the deformation prediction (Gasparre, 2005).

The ordinary cross-anisotropic elastic (Love, 1944; Graham and Houlsby, 1983) matrix can be defined with five parameters, which can be measured using laboratory bender element tests (Lings *et al.*, 2000).

Efforts were made to include stiffness anisotropic effect into the soil constitutive models, such as anisoBRICK and anisoM3SKH models by Ellison (2012). However, the test of the King's Place excavation in London Clay using 3D LS-Dyna model showed negligibly predicted wall deflections between the BRICK and anisoBRICK, or between the M3SKH and anisoM3SKH, as shown in Figure 2. 16. Stiffness anisotropy effect on ground movement prediction induced by tunnel excavations was also reviewed for the Heathrow Trial Tunnel case using the BRICK models. A better-predicted ground surface settlement trough was obtained with the anisoBRICK model.

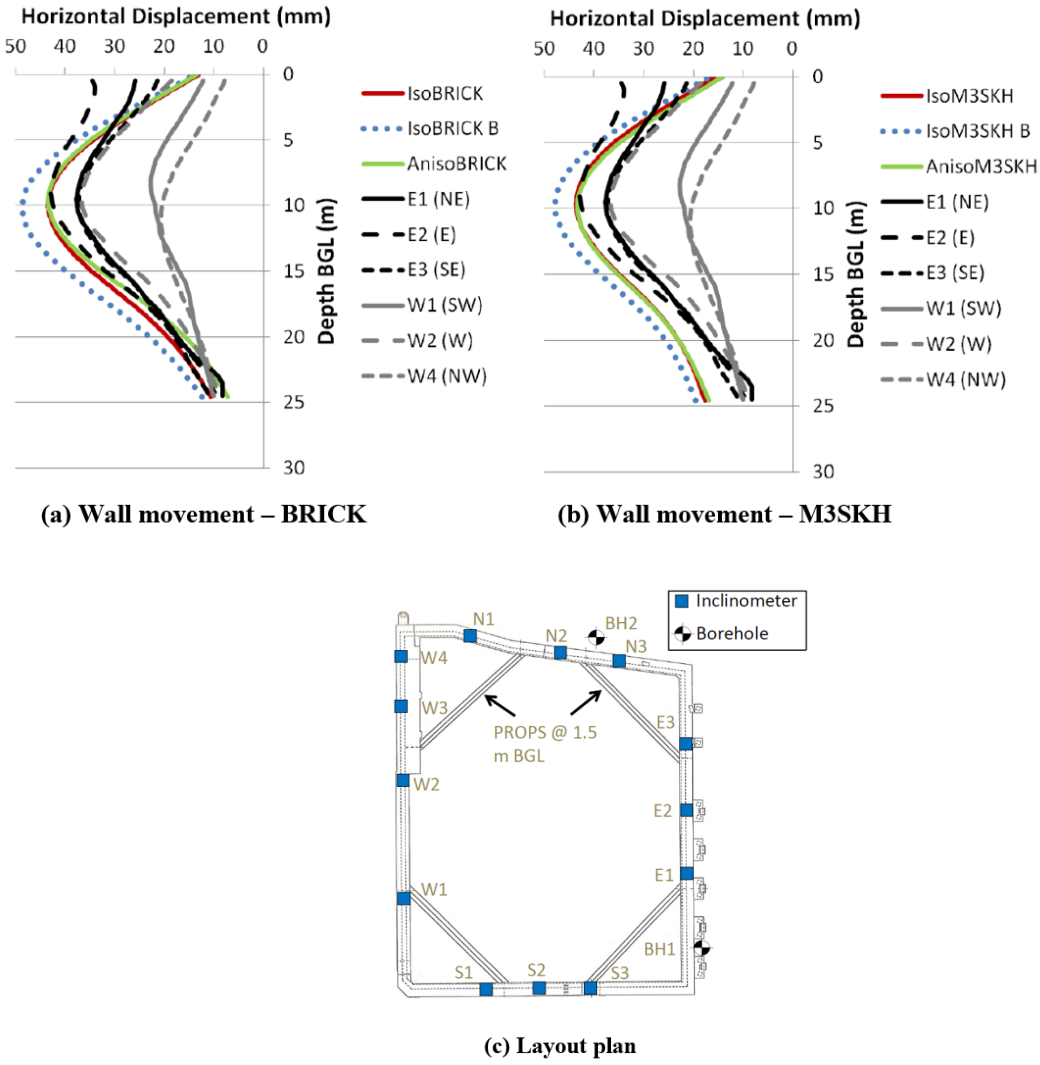

(a) Wall movement – BRICK **(b) Wall movement – M3SKH**

(c) Layout plan

Figure 2. 16 Wall deflection predictions from isotropic and anisotropic M3SKH & BRICK soil models for the King's Place excavation (Ellison, 2012)

2.2.3 Summary of the review of London Clay

The important geological information of the London Clay was reviewed and a better understanding of its engineering features in relation to excavation was achieved. This knowledge would be very useful for the back-analysis of the Crossrail deep excavations. For instance, selecting the appropriate soil constitutive models, and interpreting the back-analysis results.

Firstly, the London Clay Formations (A-E) were identified with variable properties, and therefore, they should be treated separately in each excavation case history. If possible the design parameters should be reviewed for each subdivision.

Besides the basic linear elastic-perfect plastic Mohr-Coulomb soil constitutive model which provides the reference results, the advanced soil models should be considered in the back-analysis to achieve better-predicted results.

Neither anisotropy nor stress history or stress path could dominate a ground problem by itself as the soil/structure interaction is a combination of characteristic soil engineering features. Hence, the selected advanced soil models need to be able to replicate some of these key engineering features of the London Clay.

For instance, the small strain stiffness, the stress history and the stress path can be accounted through a few pre-consolidation associated parameters (e.g. OCR). A series of the advanced soil models were reported with such capabilities, such as three surface kinematic hardening model (3SKH) (Stallebrass, 1990; Stallebrass and Taylor, 1997), the BRICK model (Simpson, 1992a; Clarke, 2009), the hardening small strain soil model (HS-Small) (Benz *et al.*, 2009), and MIT-E3 soil model (Whittle and Kavvadas, 1994). A further review of the soil models was conducted and as set out in section 2.4, the BRICK model was selected for the back-analysis research.

2.3 Finite element method

The numerical analysis became popular in excavation design in the urban area, because of the increasingly complex construction activities, together with the challenges associated with protecting existing adjacent structures. Hereby, the numerical analysis through finite element method (FEM) excluded the empirical methods or limit equilibrium methods as classified in Ciria C760 section 6.2 (Gaba *et al.*, 2017).

The choice of the FEM for excavation analysis depends on the geometry of excavation, the distribution of ground stratigraphy and the existing structures in the vicinity of the excavation. The irregular shape of geometry often leads to the need for more complex numerical analysis (e.g. 2D or 3D), particularly where sensitive adjacent structures are present.

In this research, the Crossrail excavation back-analysis case histories were reviewed, and FEMs applied in their designs were categorised into three types: semi-FEM (e.g. Oasys FREW, WAllAP); 2D FEM (e.g. Plaixs 2D, Oasys SAFE); and 3D FEM (e.g. Oasys LS-Dyna 3D, Plaxis 3D, ABAQUS, FLAC). A few analysis programs were selected for the back-analysis research and they were reviewed in detail below.

2.3.1 Semi-FEM (Pseudo-FREW)

2.3.1.1 Introduction

The simplest semi-FEM model by the Oasys© FREW program (Oasys, 2017) the retaining wall is modelled as a series of elastic beam elements joined at the nodes, as demonstrated in Figure 2. 17. The lowest node is either the base of the wall or at a prescribed rigid base in the ground beneath the wall. The soil at each side of the wall is connected at the nodes.

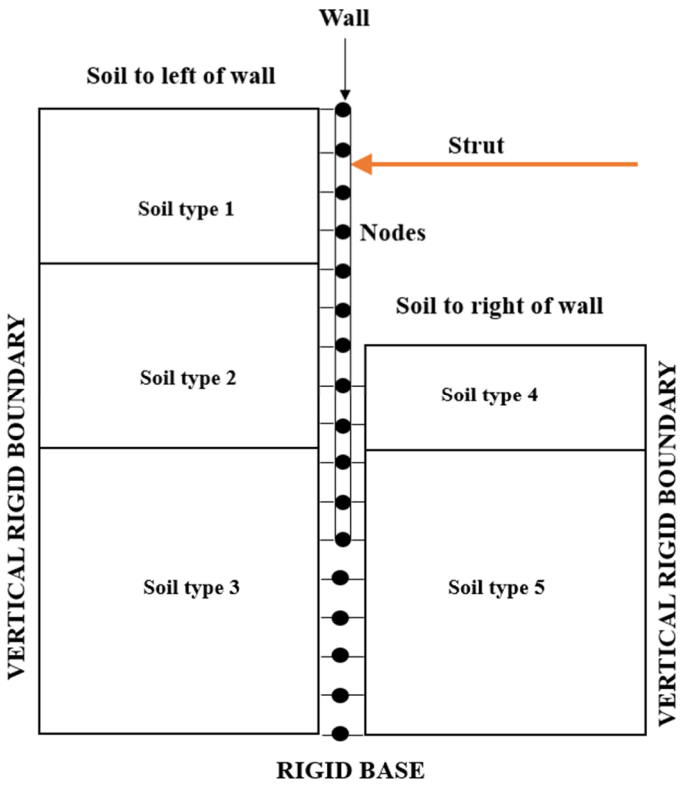

Figure 2. 17 Concept of Pseudo-FREW model (Oasys, 2017)

The analysis is carried out in steps corresponding to the proposed excavation stages.

- The initial stage is used to calculate the soil stress prior to the installation of the wall, displacements computed in this stage are set to zero.
- At each stage thereafter the incremental displacements, due to the change caused by that stage, are calculated and added to the existing displacements. The soil stresses, strut forces, wall bending moments and shear force are then determined.

The detailed calculation at each stage follows these steps:

1) The initial earth pressures and the out of balance nodal forces are calculated assuming no movement of the nodes;
2) The stiffness matrices representing the soil on either side of the wall and the wall itself are assembled;
3) The above matrices are combined, together with any stiffness representing the actions of struts or anchors, to form an overall stiffness matrix;
4) The incremental nodal displacements are calculated from the nodal forces acting on the overall stiffness matrix assuming linear elastic behaviour;
5) The earth pressures at each node are calculated by adding the changes in earth pressure, due to the current stage, to the initial earth pressures. The derivation of the changes in earth pressure involves multiplying the incremental nodal displacements by the soil stiffness matrices;
6) The earth pressures are compared with soil strength limitation criteria, conventionally taken as either the active or passive limits. If any strength criterion is infringed a set of nodal correction forces is calculated. These forces are used to restore earth pressures, which are consistent with the strength criteria and the consequent plastic deformation within the soil.
7) A new set of nodal forces is calculated by adding the nodal correction forces to this calculation in step (1);
8) Step (4) to (7) are repeated until convergence is achieved;
9) Total nodal displacements, earth pressures, strut forces and wall shear stresses and bending moments are calculated.

FREW is classified as the semi-FEM because the soil stiffness matrix is pre-calculated from the finite element analysis program Oasys SAFE (Oasys, 2014), and the generated flexibility coefficients stored in the Pseudo-FREW.

2.3.1.2 The basic SAFE model

In the SAFE model, a matrix of predetermined flexibility coefficients is used to represent the flexibility of the ground, the stiffness of the soil is then represented by inverting this flexibility matrix. Thus the predetermined coefficients can be generated.

Figure 2. 18 demonstrates the geometry and boundary conditions assumed for the mesh in the SAFEanalysis for the flexibility coefficient calculation. The mesh is divided into 101 elements in height, the length is 10 times the total mesh height. The unequal elements in length are divided, increasing in length away from the boundary AB.

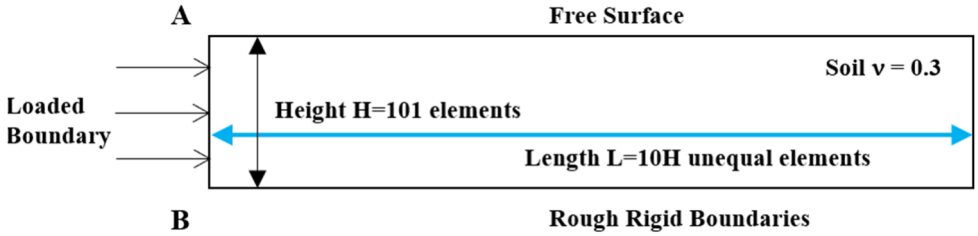

(a) Geometry of finite element model to derive the representative flexibility matrix for FREE model

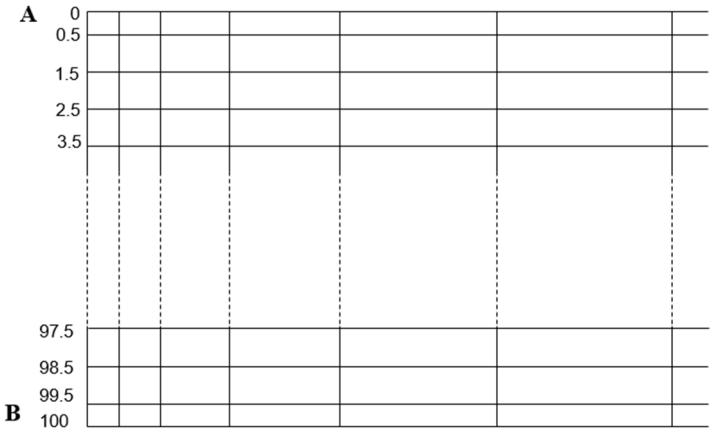

(b) Finite element mesh

Figure 2. 18 SAFE model for the FREW flexibility matrix

The model acts in-plane strain and the vertical free face AB represents the location of the retaining wall in FREW. The boundary AB is divided into 101 elements as shown. A unit force was applied to each element, the horizontal displacement at nodes in the middle of each element was then calculated. These displacements represent the flexibility coefficients and were stored as the flexibility matrix.

Two cases are considered: 1) the nodes on the line AB are free to move vertically, and 2) the nodes are fixed vertically. For each case, two sets of flexibility coefficients are stored within FREW. They apply for soils having either a constant Young's modulus (E) or Young's modulus

that increases linearly with depth from zero at the surface. The total horizontal displacement at all nodes due to any load combination can be estimated using the principle of superposition.

In many situations when props or struts are present, 'fixed' and 'free' give similar results. An exception is a cantilever situation where the fixed method will give fewer displacements because it models greater fixity between the soil and wall. Moreover, the fixed method is somewhat approximate because Poisson's ratio effects are not well modelled. For example, these effects in a complete elastic solution can cause outward movement of the wall when there is a shallow soil excavation.

In addition, the soil, on both sides of the wall, is represented as a linear elastic material. They are subject to active and passive limits.

2.3.1.3 Soil model and input parameters

The basic Mohr-Coulomb soil constitutive model is applied in the FREW. A minimum of five Mohr-Coulomb model parameters are required: soil stiffness either drained Young's modulus (E'), or undrained Young's modulus (E_u) depending on the drainage condition soil; soil strength as friction angle (ϕ') and cohesion (c') for drained soil or undrained shear strength (c_u) for undrained soil; Poisson's ratio (ν); soil density (ρ) and the earth pressure coefficient (K_0).

Other input parameters in the FREW model include surcharge loadings, strut properties, and modelling parameters, such as boundary limit, soil/wall friction and convergence limits. The sensitivity study found that there was less influence of these modelling parameters to the predictions and the default values in the FREW program were recommended.

The advantage of using Pseudo-FREW in the back analysis is the fast computation, it enables the automatic back-analysis under the probability analysis (Jin, 2018), which is significant progress for the near 'real-time' back-analysis. However, Pseudo-FREW analysis results are limited to the wall forces, deflections and struts load.

2.3.2 2D FEM (Plaxis 2D)

2.3.2.1 Introduction

PLAXIS is a finite-element analysis program which is developed specifically for the analysis of deformation, stability and flow in geotechnical engineering (PLAXIS, 2016).

Areas and surfaces in Plaxis 2D model are formed by 6-node or 15-node triangular elements. The program uses Gaussian integration within the area elements, while the integration

for the 6-node element is based on 3 sample points, and the integration for the 15-node element is based on 12 sample points. The local numbering, positioning of nodes and integration points of these two type of elements are shown in Figure 2. 19. For line element, one can formulate the numerical integration over areas.

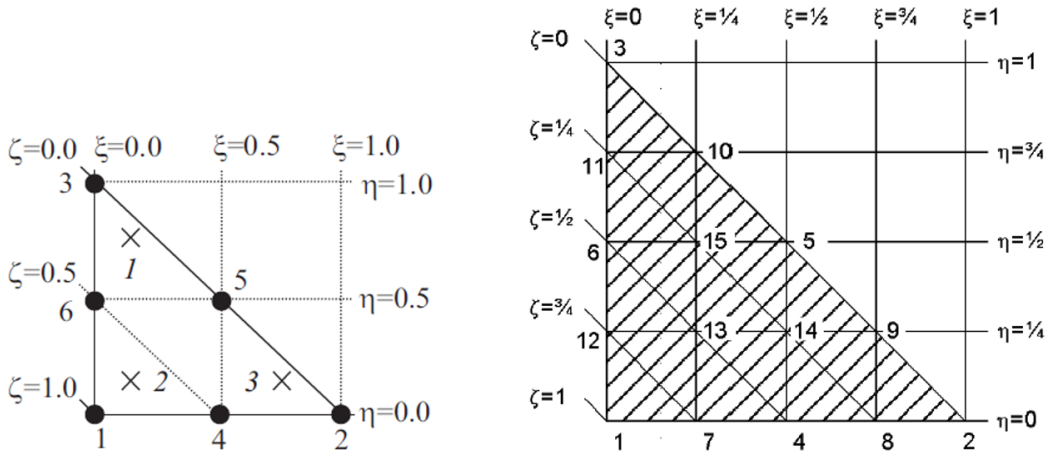

(a) 6-node **(b) 15-node**

Figure 2. 19 Triangular element for Plaxis 2D model (a) 6 integration points; (b) 15 integration points

The analysis is carried out after the element mesh generation. The initial stage is to calculate the soil stress prior to the installation of the wall and displacements in this stage are set to zero. The construction stages are thereafter calculated by the incremental displacements, due to the change caused by that stage, and added to the existing displacements. The soil strains, stresses, the resultant structural forces & movements (e.g. wall bending moment, shear force and deflections), and the accumulative ground displacement are then determined for each stage.

2.3.2.2 Soil model and input parameters

Except for the basic Mohr-Coulomb soil model, a number of soil constitutive models can be applied in the Plaxis 2D program, including soil models embedded in the program and user-specified soil models. This provides the choice to model the mechanical behaviour of soil at various degrees of accuracy, from linear isotropic elasticity to non-linear anisotropic plasticity.

For example, when assessing the undrained behaviour of clay in excavation, Lim et al (2010) used four soil models embedded in the Plaxis 2D program, including the modified Cam-clay model (MCC) (Roscoe and Burland, 1968); the Hardening soil model (HS) (Schanz et al., 1999); the Hardening soil model with small strain (HSsmall) (Benz et al., 2009; Obrzud, 2010; Likitlersuang et al., 2013); and the Mohr-Coulomb model (Coulomb, 1776; Juvinal & Marshek,

1991). Also, one user-defined model 'undrained clay model' by Hsieh *et al.* (2010) was used. It was concluded that none of these models accurately predicted ground settlements, and the simple Mohr-Coulomb model gave a good wall deflection prediction at the last excavation stage. It seemed each soil model was good at modelling one or a few soil behaviours, but none of the sophisticated constitutive models was capable of accurately modelling all soil behaviours.

The input soil parameters are in relation to the soil model applied in the analysis. The design associated information, like surcharge loadings, struts and groundwater should be input according to the design assumptions. Lastly, the Plaxis 2D modelling parameters, such as convergence criteria, are recommended to use the default values in the program.

Compared to the semi-FEM FREW modelling, the Plaxis 2D modelling provides flexibility in soil models, which will affect the level of accuracy in the soil stress-strain calculation, therefore resultant structural forces, deflections, and accumulative ground displacements will also change.

In addition, the Plaxis 2D program allows the assessment of the retaining wall by different types of element, such as the elastic plate element, the solid element and the geogrid element (PLAXIS, 2016b). The plate element is recommended for its simplest way of modelling and receiving the results (Sutti, 2015). Sometimes this way of modelling a piled-wall could affect the predicted results, as the real piled-wall is in three-dimension but the plate element modells the wall as a continuous wall with the equivalent stiffness.

In summary, the Plaxis 2D program achieves a good balance between the actual excavation problem and the rational finite element numerical analysis for the excavation design.

2.3.3 3D FEM (LS-Dyna 3D)

The 3D FEM reflects the actual three-dimension excavation problem and is likely to predict better structural performance. For example, the corner effect due to three-dimensional effect is well known, that the wall deflections are restrained near the corner position (Gourvenec et al., 2002; Zdravkovic et al., 2005; Finno et al., 2007; Lin and Woo, 2007).

One of the 3D FEM programs, LS-Dyna was applied to carry out the Crossrail excavation case histories back-analysis and a brief introduction of the LS-Dyna program and the sensitivity study for the LS-Dyna 3D model are presented below.

2.3.3.1 Introduction

LS-DYNA is one of the most flexible finite element analysis software It consists of a single executable file and is entirely command-line driven (LSTC, 2018). Oasys© integrated some advanced soil constitutive models into the LS-Dyna program to enable the soil mechanical calculation for geotechnical analysis (Oasys, 2010).

The database of the LS-Dyna model is organised in the keyword input file, where similar functions are grouped. For instance, 'NODE' and 'ELEMENT' are generated nodes and elements, 'PART' defines the type of element, element formulation for the grouped elements, hence nodal connectivities of these elements are determined, including solid, beam, shell, truss, spring, discrete dampers, lump mass and more choices. The given identity in 'PART' is also related to other groups included in the keyword file, like 'MAT' defining constitutive constants of materials; 'SECTION' defining the element formulation, integration rule, nodal thickness and sectional properties; 'HOURGLASS' defining nonphysical, zero-energy modes of deformation that produce zero strain and no stress. The additional sections are also available to define other conditions, such as 'LOAD' defining methods of loading: concentrated point loads, distributed pressures, and variety of thermal loadings; 'BOUNDARY' defining groundwater condition through the boundary, and 'CONTROL' resetting LS-Dyna default.

The quadratic 8-node hexahedron element is used as the solid element for civil engineering modelling in the LS-Dyna program, according to the LS-Dyna Civil Engineering Application Program (CEAP) (Oasys, 2010). This quadratic 8-node element is derived from 20-node hexahedrons, as shown in Figure 2. 20.

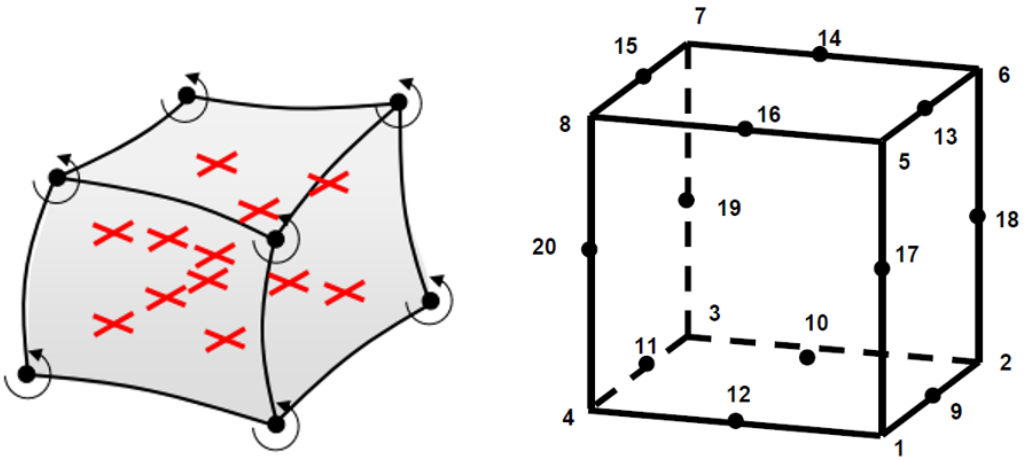

(a) Quadratic 8-node element **(b) 20-node hexahedrons**

Figure 2. 20 Quadratic 8-node hexahedron element (LSTC, 2018)

The default solid element is applied in the element formulation 1, the constant stress from under-integrated 1 point representing the solid element. The fully integrated or selective reduced (S/R) integrated solid element formulation 2 is applied to the solid element to avoid pressure locking during nearly incompressible flow, but it could lead to an excessively stiff response if the element shape is poor.

Element formulation 16 is applied for 10-noded tetrahedral structural shell element, allowing for an accurate representation of elementary deformation modes, such as stretching, bending and torsion.

Element formulation 2 is applied for 2-node Belyschko-Schwer beam element, which supports the nonsymmetric geometric stiffness contribution, to allow a plastic hinge formed and the hinge moment rotation behaviour follows the hysteresis algorithm. Otherwise, element formulation 1 is the default for the integrated beams.

Schroeder (2002) compared the shell element and the solid element in the Imperial College Finite Element Program (ICFEP). He summarised the shell element formulation was written in terms of structural forces rather than stresses so that the magnitudes of forces come as a direct result from the analyses. In the case of solid elements, structural forces have to be calculated from the stresses at element integration points through a data post process. Because the shell element allows rotational freedom, which can model the moment condition at the corner of the excavation problem, and receiving the results was simpler, the shell element was recommended to model the retaining wall in 3D FEM.

Dong *et al* (2015) studied the relative merits of using two types of elements to model the retaining wall in a 3D model by the ABAQUS program: a continuum solid element and an isoparametric shell element (e.g. 4 to 8 node quadrilaterals or 3 to 6 node triangular elements in any 3D orientation). The study showed the relative simplicity of using the shell element compared to the solid element, but the resultant wall deflections and the accumulative ground settlements increased. This was due to the inability of the shell element to consider the actual thickness of the wall, hence the downward shear stresses acting on the back of the wall was not accurately calculated. This conclusion was also supported by other research (Zdravkovic *et al.*, 2005).

Likewise, the LS-Dyna program provides a few options to model the retaining wall; the solid element and the shell element are two common choices. A sensitivity study was undertaken to investigate the effect of these two types of element and the installation impact, to the resultant wall forces, deflections and the accumulative ground displacements.

2.3.3.2 Sensitivity study of LS-Dyna 3D model

The sensitivity study used a generic excavation in London Clay to investigate the following modelling assumptions:

- Modelling the retaining wall by the solid element;
- Modelling a thin shear plane to limit the wall/soil friction;
- Modelling the retaining wall by the shell elements; and
- Modelling the retaining wall installation effects.

In modelling, the retaining wall is commonly installed as "wished-in-place", ignoring its installation impact. The last option in the sensitivity study was to assess the ground movements induced by the wall installation so that the loss of initial stresses, and the change in the earth pressure coefficient (K_o) prior to commencing the excavation process, can be investigated.

The generic excavation geometry for the LS-Dyna 3D model sensitivity study is shown in Figure 2. 21, a 30 m (B) × 60 m (L) × 15 m (H) excavation in London Clay.

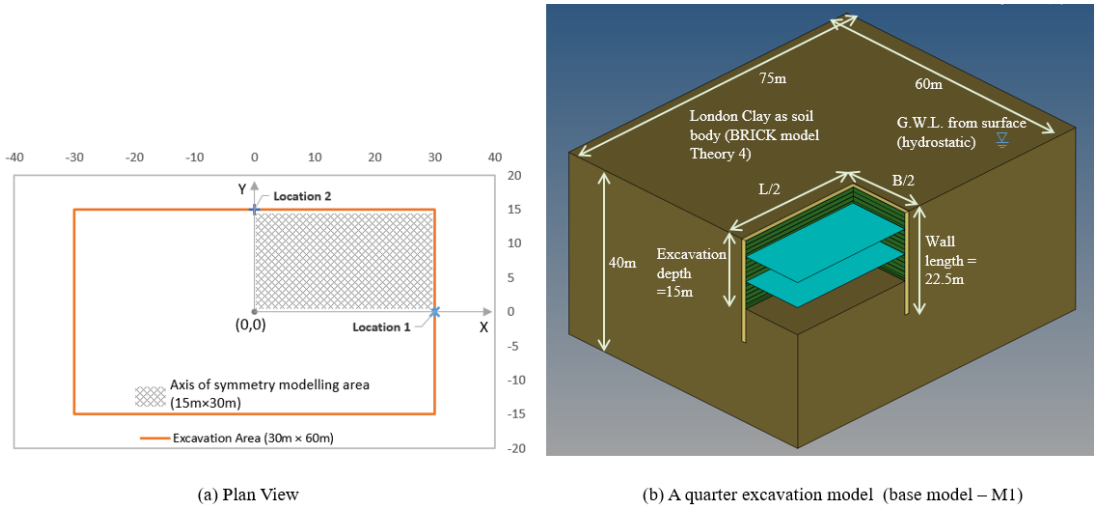

(a) Plan View

(b) A quarter excavation model (base model – M1)

Figure 2. 21 The generic excavation for LS-Dyna 3D model sensitivity study

Four models (M1 to M4) were tests, as described in Table 2. 4. The calculated wall forces (e.g. bending moment, shear force), wall lateral displacement (δ_x), and the accumulative ground settlement behind the wall (δ_z) were compared at two locations (as shown in Figure 2. 21) :

1) the centre of the width - location 1 at B/2; and
2) the centre of the length - location 2 at L/2.

The study showed a negligible difference in the resultant wall forces and wall deflections between M1 and M2, meaning the thin layer of shear planes would not change the wall performance. Though, M1 gave slightly smoother accumulative ground settlement profiles

immediately behind the wall, compared to M2 without the thin shear plane (Figure 2. 22 & Figure 2. 23).

Table 2. 4 Summary of LS-Dyna 3D model sensitivity study

Model	Description	Sketch
M1 (base model)	• 1.0 m diaphragm wall modelled by solid element with elastic concrete material; • 50 mm wide shear plane modelled using softer soil parameters • 2 level of props modelled by shell element[1]	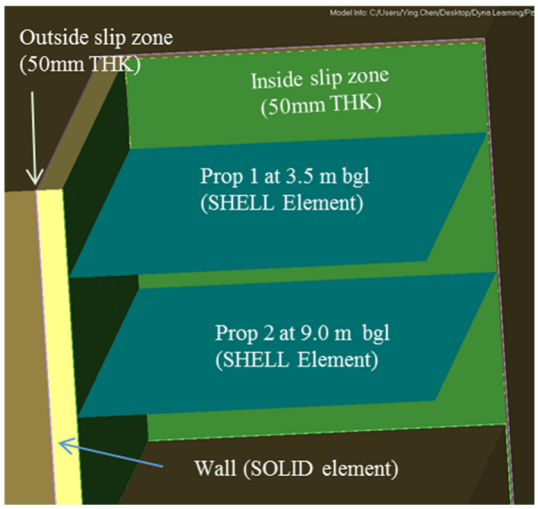
M2	As M1, but no shear plane (acting as slip zones)	
M3	• As M1, but the wall modelled by shell element	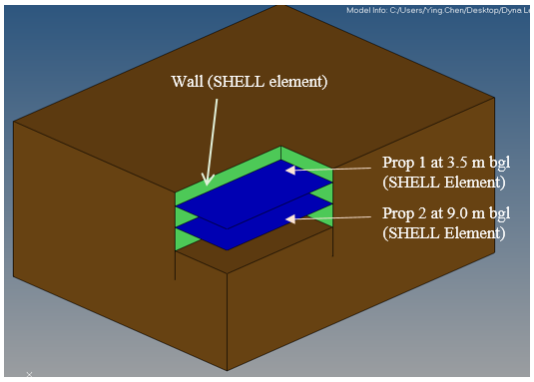
M4[2]	• As M3, including 14 pieces of diaphgram wall panels installed in the arranged sequence	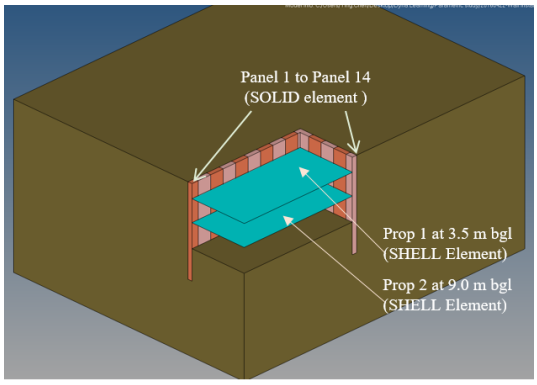

Note: the diaphragm wall panel installation followed a “hit and miss” basis, except for the last panels to close out the perimeter wall. The modelling method refers to Ng *et al.,* (1995) and Ng and Yan (1999).

Table 2. 5 Results of sensitivity study – the maximum wall deflections (δ_H),

Stage	Wall-in	Exc 4.0 m	Exc 9.5 m	Exc 15 m
$\delta_{H,max}$ at location 1 (B/2)				
M1 (mm)	0.03	12.76	16.14	25.90
M2/M1	1.00	1.01	1.01	1.00
M3/M1	-	1.18	1.15	1.12
*M4/M1	-	1.03	1.05	1.01
H_e /B	-	*1/7.5*	*1/3.2*	*1/2.0*
$\delta_{H,max}$ at location 2 (L/2)				
M1 (mm)	0.03	23.42	25.02	38.85
M2/M1	1.00	1.02	1.01	1.00
M3/M1	-	1.18	1.15	1.12
M4/M1	-	1.05	1.04	1.00
H_e /L	-	*1/15*	*1/6.3*	*1/4.0*

Note M1 / M 2 / M3, wall installed as 'wished-in-place' no installation effect. M4 has taken the installation sequence into account, for comparison purpose, the M4 results were zeroed at the beginning of the excavation works.

Table 2. 6 Results of sensitivity study – the maximum the wall bending moment

Stage	Wall-in*	Exc 4.0 m	Exc 9.5 m	Exc 15 m
BM_{MAX} at location 1 (B/2)				
M1 (kN.m/m)	1	377	1076	1395
M2/M1	1.00	1.03	1.00	1.00
M3/M1	*6.27*	0.68	0.91	0.92
M4/M1	*31.8*	0.95	0.89	1.00
H_e /B	-	*1/7.5*	*1/3.2*	*1/2.0*
BM_{MAX} at location 2 (L/2)				
M1 (kNm/m)	1	145	846	1123
M2/M1	1.00	1.02	1.00	1.00
M3/M1	*5.41*	3.12	1.41	1.39
M4/M1	*38.31*	1.00	0.89	1.01
H_e /L	-	*1/15*	*1/6.3*	*1/4.0*

Note: * the resultant wall bending moments at wall installation stage were negligible (< 40kNm/m).

Table 2. 7 Results of sensitivity study – the maximum the wall shear force

Stage	Wall-in*	Exc 4.0 m	Exc 9.5 m	Exc 15 m
SF_{MAX} at location 1 (B/2)				
M1 (kN/m)	1	108	492	942
M2/M1	1.00	1.02	1.00	1.00
M3/M1	*4.51*	4.28	1.77	1.57
M4/M1	*1.87*	0.97	0.90	0.92
SF_{MAX} at location 2 (L/2)				
M1 (kN/m)	1	91	443	856
M2/M1	1.00	1.01	1.00	1.00
M3/M1	*1.68*	2.57	1.89	1.33
M4/M1	*4.69*	1.08	0.84	0.92

Note: * the resultant wall shear forces at wall installation stage were negligible (< 5kN/m).

The wall modelled by the shell element (M3) was compared to the solid element (M1). The resultant maximum wall deflections by M3 were greater than M1 at each excavation stage, but the differential in the magnitudes was decreased with increasing excavation depth (H_e) (e.g. H_e = 4.0 m the ratio of $\delta_{H,max}$ by M3/M1=1.18, decreased to 1.12 at H_e = 15.0 m).

The significant difference was observed in the resultant wall forces between M3 and M1 models. The smaller BM_{MAX} at the location 1 (B/2) and the greater BM_{MAX} at the location 2 (L/2) by M3 were generated, and the tendency of underestimation and overestimation was magnified at the shallower excavation depth. However, the greater SF_{MAX} by M3 was predicted at both location 1 and 2, and the geometry shape seemed to induce this even higher difference in SF_{MAX} at location 1. Also, the tendency of overestimation was magnified at the shallower excavation depth.

In terms of the accumulative ground surface settlements behind the wall, an influence zone was identified extended about six times of the excavation depth behind the wall (Figure 2. 22 & Figure 2. 23), where the maximum settlement over the excavation depth ($\delta_{z,max}/H_e$) was less than 0.05%.

The much greater ground settlements from the model M3 were presented, showing the wall modelled by the shell element have less support to soils behind the wall, which agreed with the resultant greater wall forces.

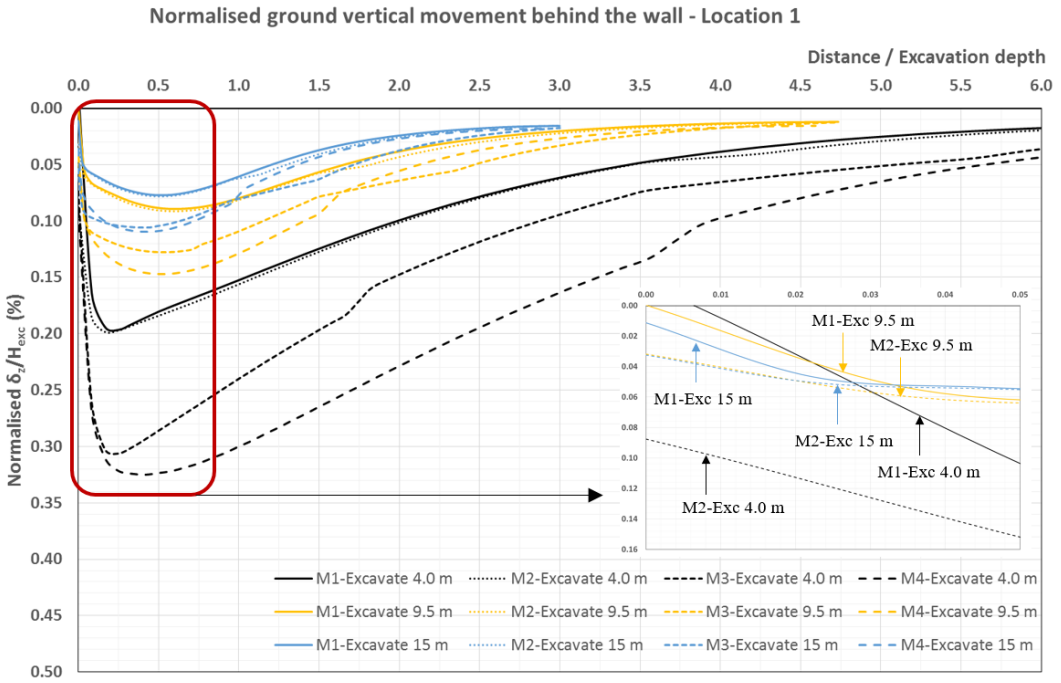

Figure 2. 22 Results of sensitivity study – normalised ground surface settlements at location 1 (B/2)

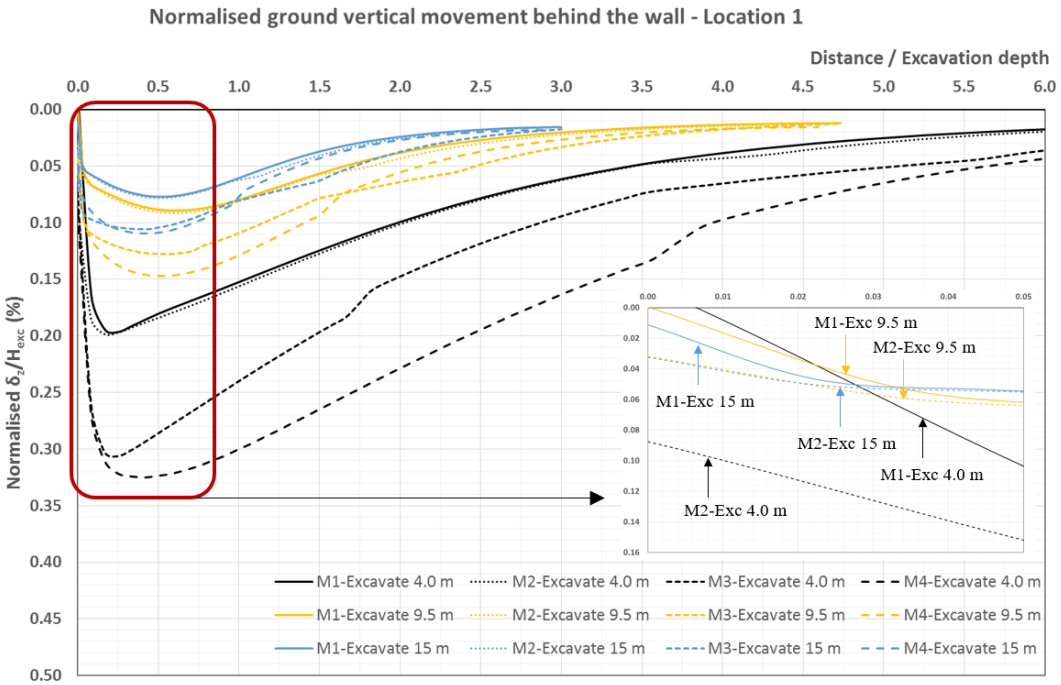

Figure 2. 23 Results of sensitivity study – normalised ground surface settlements at location 2 (L/2)

In model 4, the wall panels were modelled by the shell elements, and the wall installation sequence was simulated, following the modelling method of Ng and Yan (1999). The results from the model M4 were zeroed at the beginning of the excavation to enable the comparison with the other three models, as presented in summary tables (Table 2. 5 to Table 2. 7).

The negligible difference in the maximum wall forces and deflections was seen between the M4 and M1 models, while the installation induced wall forces and deflections were disregarded in the M4 results. This indicated that the wall modelled by the shell element (M3) may have overestimated the wall deflections and underestimated the wall bending moment, but if the wall installation impact was considered in the shell element model, the resultant difference would be minimised between the 'wished-in-place' solid element model (M1) and the 'installed' shell element model (M4).

However, the inevitable stress relaxation near the excavated trenches for the wall panels installation led to the greater ground surface settlements and the increased maximum settlement over the excavation depth ($\delta_{z,max}/H_e$) ratio within the influence zone.

The ground surface displacement contours in vertical (Z direction) and horizontal orientations (X and Y directions) at the completion of the wall installation are presented in Figure 2. 24. The maximum vertical displacement (settlement) was estimated as 8 mm and the maximum horizontal displacement was estimated as 5 mm, which were within the range of historical data for the diaphragm wall installation in London Clay presented in figure 6.7 & 6.9 in Ciria C760 section 6.2.1 (Gaba *et al.*, 2017).

As Ng and Yan (1999) concluded, the settlement bowl appeared behind the diaphragm wall with the maximum settlement presented at a distance of 20% of the trench depth (wall length). The settlement influence zone extended to a distance greater than 1.5 times the trench depth. In addition, three-dimensional corner effect was demonstrated in settlement contours (Figure 2. 24) and the settlement influence zone at the corner area was confined within one time the trench depth.

The model M4 showed the reduction of the initial horizontal earth pressures due to wall installation prior to the excavation, hence, the change of the earth pressure coefficient (K_o). This installation effect should be considered in the excavation back-analysis.

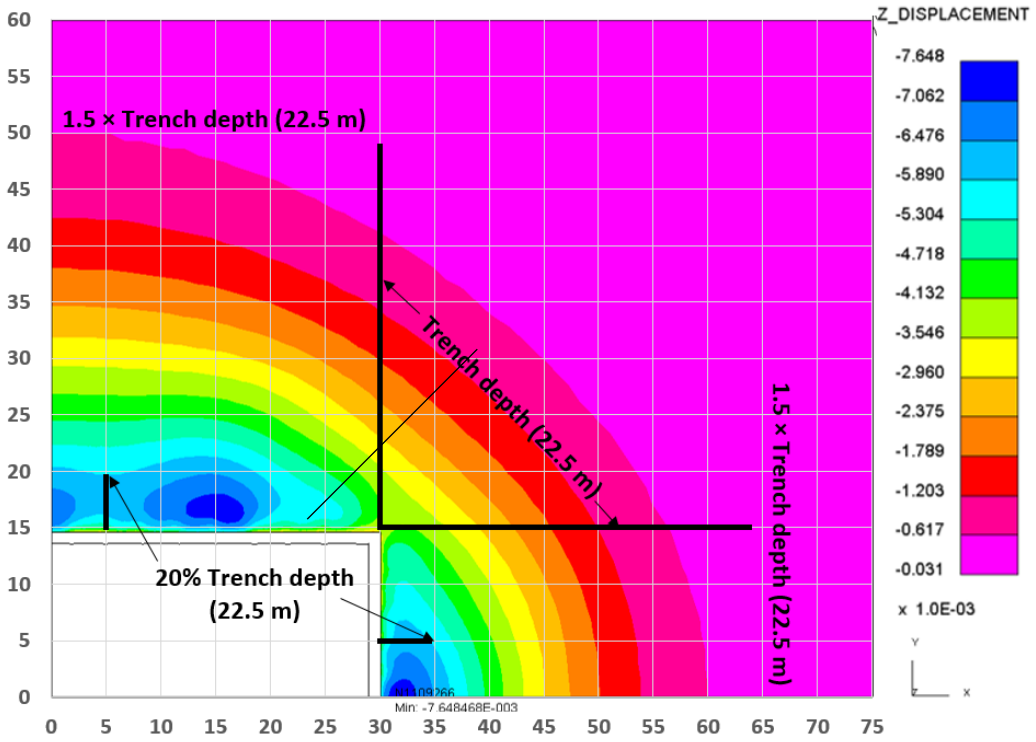

(a) Displacement contour in Z direction

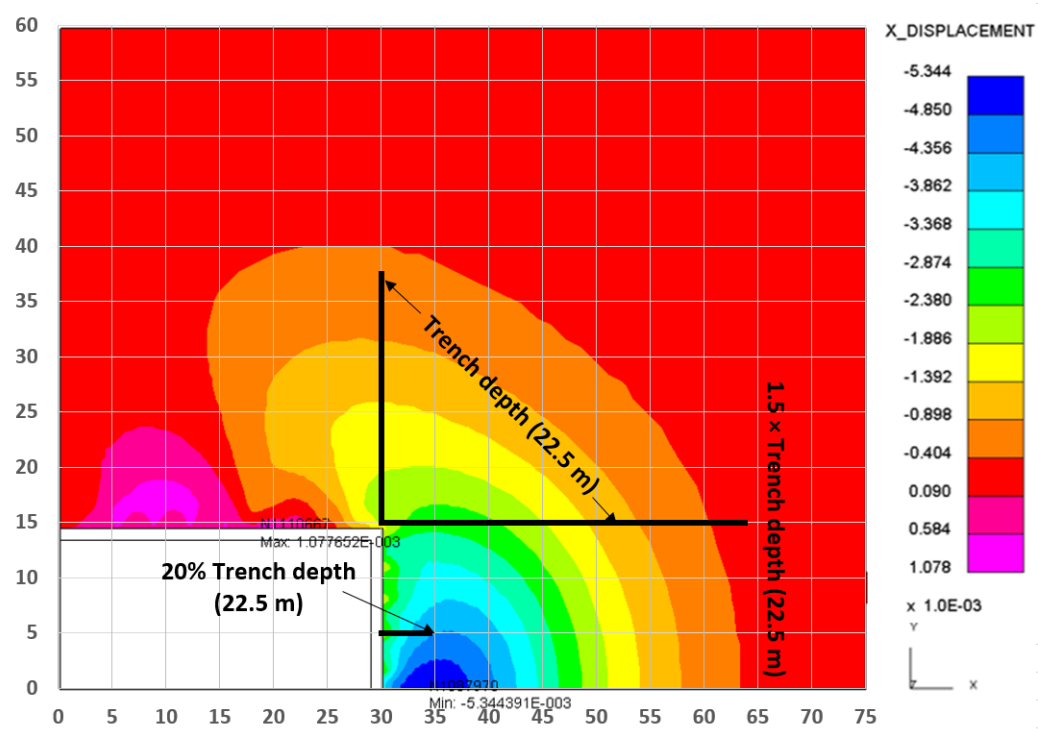

(b) Displacement contour in X direction

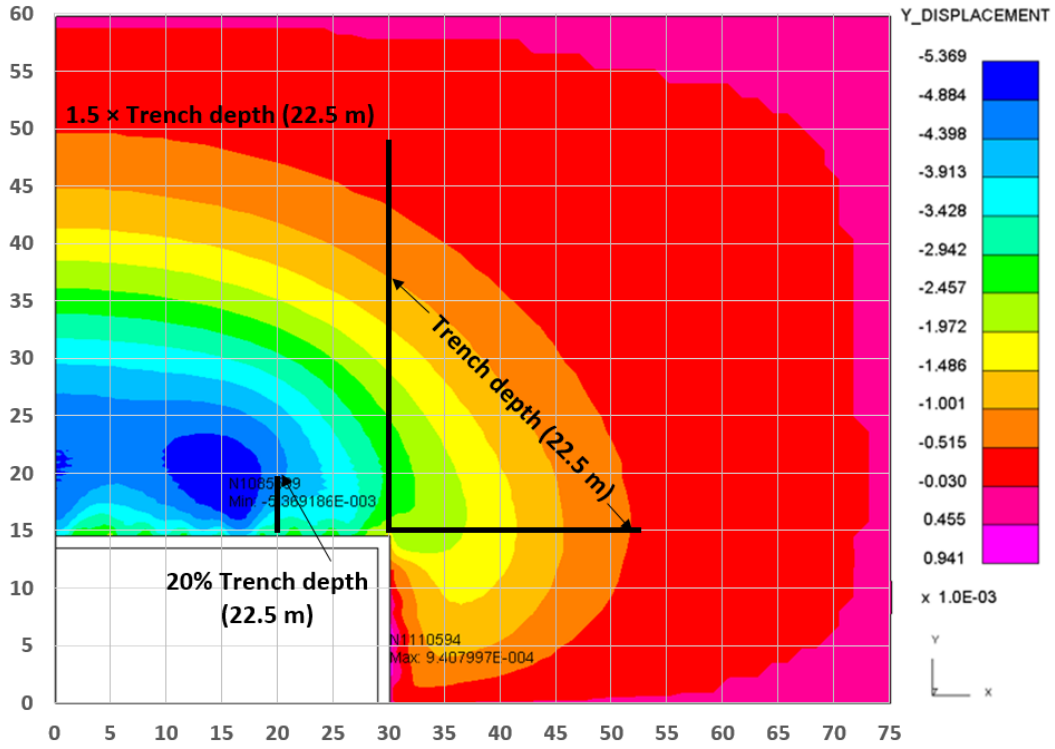

(c) Displacement contour in Y direction

Figure 2. 24 Results of sensitivity study – ground surface movement contours (mm) from M4 after diaphragm wall panel installation

2.3.4 Summary of the review of FEM

Three finite element analysis programs for excavation design were reviewed in this section and a better understanding of different types of FEMs and analysis programs was achieved. These FEM programs were applied in the back-analysis of the Crossrail deep excavation case histories, as described and presented in Chapter 5 and 6. The knowledge gained in this review has helped in interpreting the back-analysis results.

2.4 BRICK model

The engineering features of London Clay were reviewed in section 2.2 and it showed the need to apply the advanced soil model in order to better modelling this over-consolidated clay soil behaviours in the small strain range for the excavation problem.

Among plenty of choices of the soil constitutive models, the BRICK model was used for the back-analysis of the Crossrail deep excavations. It was based on the fact that the BRICK has been successfully applied in construction projects in the over-consolidated clay with promising predicted results, for instance, the Lion Yard excavation in Cambridge (Ng et al., 1998), the National Gallery extension in London (Long, 2001), and the Moorhouse

development in London (Yeow *et al.,* 2006). Meanwhile, the BRICK model was approved by the Crossrail project and applied in the asset protection and ground movement assessment due to the Crossrail tunnel boring machine (TBM) work and the deep excavations (Crossrail, 2007b).

A brief review of the BRICK model is presented below. The BRICK model parameters for the London Clay subdivisions and the model calibration will be discussed in detail in Chapter 6.

2.4.1 Introduction

A plane-strain (2D) version of the BRICK soil model was initially introduced by Simpson (1992a) to predict ground movements induced by d a typical geotechnical soil-structure interaction problem, for instance, a deep excavation. The model was based on the observation that the approach stress path affects soil stiffness (Richardson, 1988; Stallebrass, 1990), and the soil stiffness decreases with increasing shear strain.

Triaxial tests on the reconstituted specimens of London Clay were isotropically consolidated to 400 kPa before being repositioned to point A, B, C and D, then they were taken to the point O, as illustrated in Figure 2. 25 (Richardson, 1988). Figure 2. 25 show the tangent shear stiffness (G_t) on the path OX which was recorded and plotted against the corresponding shear strains.

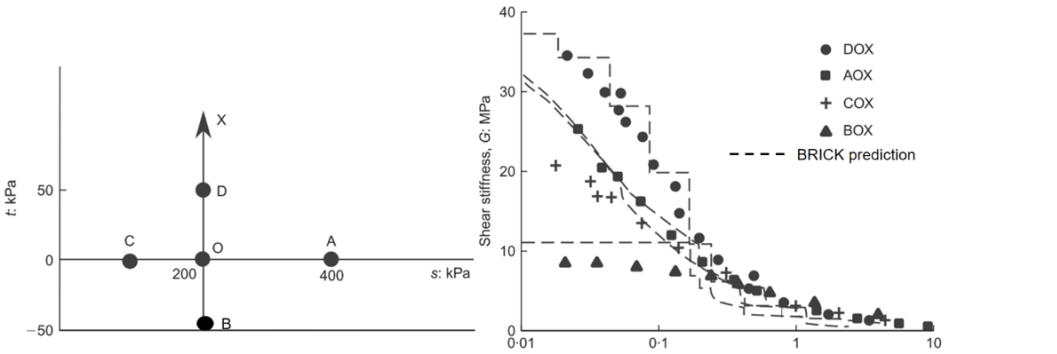

(a) Point along consolidation path **(b) Shear stiffness over shear strain curve G_t-γ(%)**

Figure 2. 25 Laboratory and BRICK replication of triaxial tests: (a) stress path; (b) shear stiffness over shear strain plot (Richardson, 1988; Ellison, 2012)

Using Richardson's data, the BRICK model used 10 pairs of string length $L_{(b)}$ and material proportions $R_{(b)}$ combination to fit path DOX, and well-replicated the different shear stiffness curves during shearing due to the change of the approach stress path. It also predicted the much

less resistance in the continuation straining direction which was previously followed (e.g. path BOX), than the reversed direction (e.g. path DOX).

This phenomenon of soil was explained by the BRICK model, using a physical analogue of a 'man' walking around a 'room' and pulling a series of 'bricks' behind him via strings of various lengths (Simpson, 1992a). The analogue of the 'man' dragging 'bricks' around a 'room' was visualised in Figure 2. 26. Some possible paths for the man and the strings were also illustrated.

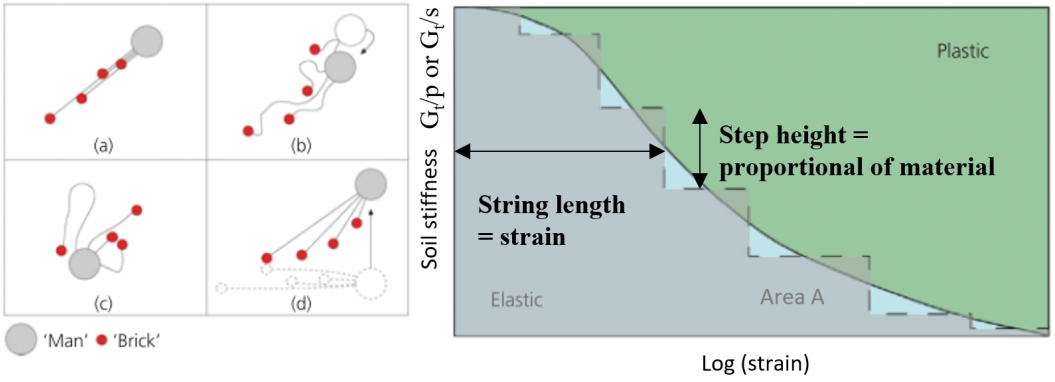

Figure 2. 26 Concept of BRICK soil model: (left) the analogue of a 'man' dragging 'bricks' in a 'room'; (right) non-linear soil stiffness curve. (Simpson, 1992a)

The room is the strain space defined by ([5]ε_{vol}, [6]γ) in the initial plane-strain BRICK model. The man represents the current strain state of the soil at one point, and each brick represents a fixed proportion of the material[7]($R_{(b)}$), the interactions between the man and these bricks are defined by variable strength of strings [8]($L_{(b)}$).

Movement of a brick means the development of plastic strain for the brick, and elastic strain is interpreted by the differential movement between the 'man' and the sum of the bricks' movement. Thus, when all strings are loose, as (b) in Figure 2. 26, the behaviour is entirely elastic for the 'man'; when all strings are taut and bricks lined up behind the man in the direction of the strain increment, as (a) in Figure 2. 26, the behaviour is plastic for the 'man'.

Additional assumptions were made to enable the stress-strain constitutive relations in the BRICK model:

- Elastic volumetric stiffness is in proportion to current mean effective normal stress [9](s'): $\delta_{s'} = s'\delta_{\varepsilon^e_{vol}}/\iota$ (2 - 7)

[5] ε_{vol} is volumetric strain, $\varepsilon_{vol} = (\varepsilon_x + \varepsilon_y)$ in plane-strain 2D BRICK model;
[6] γ is the shear strain, equivalent to the diameter of the Mohr's circle of strain, written as $((\varepsilon_x-\varepsilon_y)^2+\gamma_{xy}^2)^{1/2}$.
[7] $R_{(b)}$ are a matrix, expressed by G_t/s in per cent, referring to BRICK parameters in Table 2.8
[8] $L_{(b)}$ are a matrix, expressed by shear strain, referring to BRICK parameters in Table 2.8
[9] s is mean normal stress in plan strain 2D BRICK model, $s'=(\sigma'_x+\sigma'_y)/2$.

- Elastic shear stiffness is derived from elastic volumetric stiffness:

$$^{10}\delta_t = s'\delta_{\gamma^e}(1-2\nu)/\iota \qquad (2-8)$$

- Capacity for elastic straining increases as the mean normal effective stress increases, in a manner similar to the Cam-clay models (Roscoe and Burland, 1968), the plastic strain reduction is assumed as:

$$\delta_{\gamma^{P,red}} = \frac{t}{s'}\frac{\delta_{\varepsilon^e_{vol}}}{1-2\nu} \qquad (2-9)$$

during virgin compression: $\delta_{\varepsilon^{P,red}_{vol}} = \frac{\iota}{\lambda^*}\delta_{\varepsilon_{vol}}$ (2 - 10)

during swelling or recompression: $\delta_{\varepsilon^{P,red}_{vol}} = \frac{\iota}{\kappa^*}\delta_{\varepsilon_{vol}}$ (2 - 11)

Thus the capacity for elastic shear straining is increased due to volume changes as necessary to ensure radial straight line in s'-t space during monotonic strain paths.

- Increase in stiffness is proportional to pre-consolidation pressure, as proposed by Houlsby and Wroth (1991):

$$\frac{\delta_{s\prime}}{\delta_{\varepsilon^e_{vol}}} = \frac{s\prime}{\iota}\left[1+\beta(\varepsilon_{vol}-\varepsilon_{vol,0}-\lambda^*\ln\frac{s\prime}{s'_0}\right] \qquad (2-12)$$

$$\frac{\delta_t}{\delta_{\gamma^e}} = \frac{1-2\nu}{\iota}\left[1+\beta(\varepsilon_{vol}-\varepsilon_{vol,0}-\lambda^*\ln\frac{s\prime}{s'_0}\right] \qquad (2-13)$$

In total seven input parameters were proposed in the original plane strain BRICK model, as summarised in Table 2. 8.

Table 2. 8 Original BRICK model parameters (Simpson, 1992a)

Parameter	Description
λ^*	the slope of the isotropic normal compression line in ε_{vol} – ln *s'* space
κ^*	the slope of the isotropic swelling line in ε_{vol} – ln *s'* space
ι	parameter controlling the amount of stiffness in the model
ν	Poisson's ratio
β	parameter controlling the amount of strength and stiffness gained due to the state of over-consolidation
$L_{(b)}$	an array of initial string lengths corresponding to brick 'b'
$R_{(b)}$	the proportion of material, controlled by brick 'b; defined by G_t /*s*.

The parameter β will affect the area under the stiffness 'S' shaped curve (Figure 2. 26). The shearing resistance ϕ' is the resultant strength and can be interpreted by the area covered by the stiffness 'S' curve, Area = sinϕ'. In the later version, the β effect is split into β^G and β^ϕ, representing the gained stiffness and the gained strength from the over-consolidation. The β^G

[10] t is shear stress in plan strain 2D BRICK model, $t=(\sigma'_y-\sigma'_x)/2$ or $t=\tau_{xy}$; γ^e is the elastic strain.

will affect the initial value of the stiffness, and β^{ϕ} will affect the total area under the stiffness 's' curve, as demonstrated in Figure 2. 27.

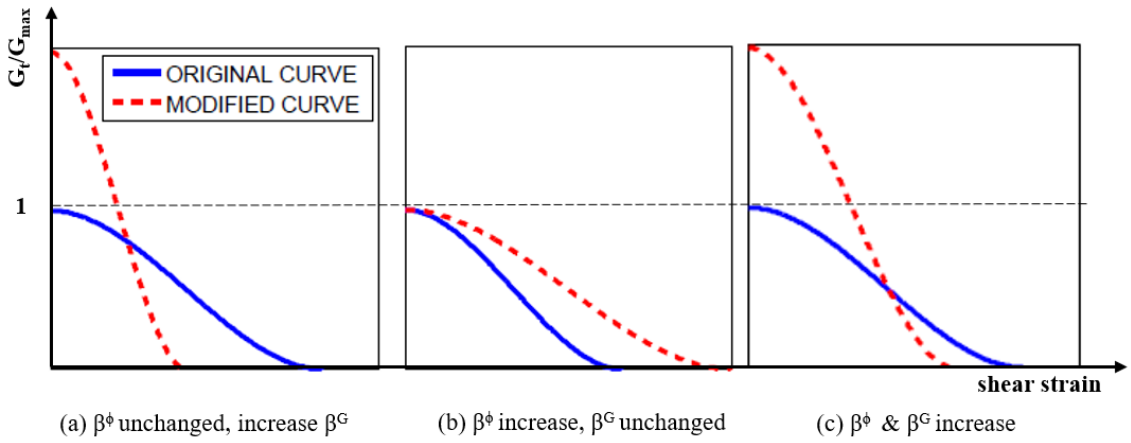

Figure 2. 27 Modification of a stiffness curve due to over-consolidation (Ellison, 2012)

The lode angle effect accounted for the observation that soils tend to fail sooner in extension than compression (Lade and Duncan, 1977). The Gudehus-Argyris surface (Argyris *et al.*, 1974) was introduced to the BRICK model by Ellison (2012) to consider the Lode angle effect. Its surface will be circular in the π-plane when $M_{\mu} = 1$ and convex whenever $M_{\mu} < 9/7$. A comparison of this surface with the Mohr-Coulomb hexagon shape surface was made for the case of $\phi' = 20^{\circ}$ in Figure 2. 28.

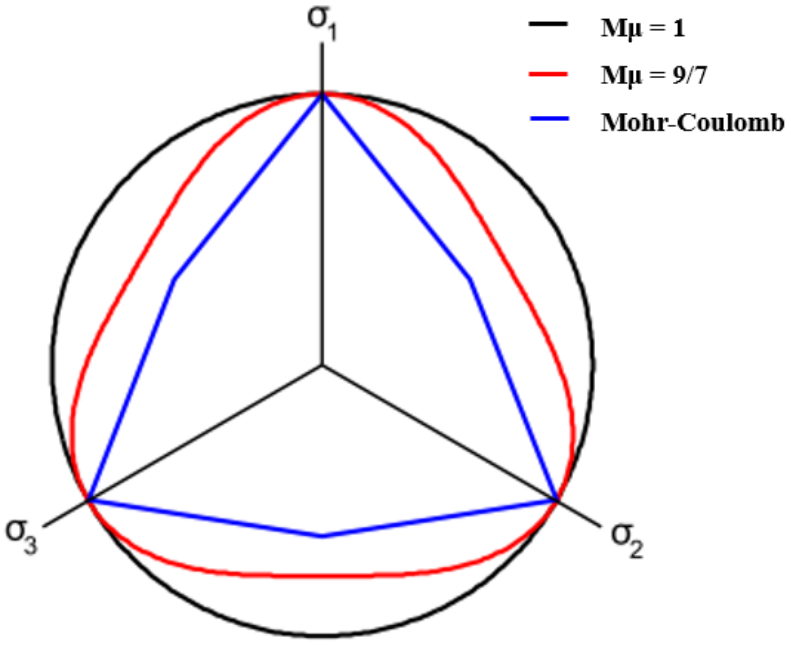

Figure 2. 28 The shape of the Gudehus-Argyris surface versus the Mohr-Coulomb surface in the π-plane when $\phi' = 20^{\circ}$ (Ellison *et al.*, 2012)

With the lode angle effect (M_μ), the string length reduction factor at failure was updated by:

$$X_{(b)} = 1/2\left[1 + M_\mu + (1 - M_\mu)\left(\frac{\gamma^r_{(b)}}{\gamma^q_{(b)}}\right)^3\right] \qquad (2 - 14)$$

Where M_μ varies from 1.0 for the triaxial compression to 9/7 for the triaxial extension. The ratio of $\gamma^r_{(b)} / \gamma^q_{(b)}$ indicates the string orientation in the π-plane.

The updated nine BRICK model parameters are presented in Table 2. 9.

Table 2. 9 BRICK model input parameter (Ellison, 2012)

Parameter	Description
λ^*	the slope of the isotropic normal compression line in ε_{vol}-ln (p') space[11]
κ^*	the slope of the isotropic swelling line in ε_{vol}-ln (p') space
ι	parameter controlling the amount of stiffness in the model
ν	Poisson's ratio on the normally consolidated line (NCL)
M_u	parameter controlling string length modifications due to Lode angle - constant in the Drucker-Prager modification (M_μ)
β^G	parameter controlling the amount of elastic stiffness gained due to the state of over-consolidation
β^ϕ	parameter controlling the amount of strength gained due to the state of over-consolidation
$L_{(b)}$	an array of initial string lengths for each brick 'b'
$R_{(b)}$	an array of material proportions for each brick 'b', defined by G_t /p', $\sum_{b=1}^{B} R_{(b)} = 1$ here B as total numbers of bricks, e.g. B =10.

2.4.2 Alternative advanced soil models

Besides the BRICK model, alternative advanced soil constitutive models were developed to model the cohesive soils and showed good performance in repeating the non-linear soil stiffness decrease with increasing shear strain. For instance, the hardening soil model (HS) by Schanz *et al* (1999), the three-surface kinematic hardening model (3SKH) by Grammatikopoulou (2004), the hardening soil with small strain model (HSS) by Benz (2007), the Hypoplastic model including stiffness anisotropy by Mašín (2014), and more proposed in literatures.

The 3SKH model and its modification (M3SKH model) were applied in the research and successfully repeated the laboratory triaxial testing conducted on soils samples from the London Clay, but neither of them was applied in the industrial excavation design in London Clay. The other advanced soil models shared negative experience in modelling the overconsolidated clay in real excavation projects, given the difficulty in deriving the required soil model parameters from the project-based ground investigations. As well as the derivation of the required factored

[11] p is mean normal stress in 3D BRICK model, $p' = (\sigma'_x + \sigma'_y + \sigma'z)/3$.

soil parameters under the design standard. For example, the factored soil strength parameters are required for the ULS analysis DA1C2 approach in the Eurocode 7th Edition.

Meanwhile, the imperfection was reported from all available soil models in modelling the over-consolidated clays. For example, Yeow and Coop (2015) reviewed and compared the BRICK model and the M3SKH model with regards to their applicability in modelling London Clay behaviour. They pointed out neither of these sophisticated soil models was capable of modelling two important aspects of soil behaviour in over-consolidated clay: 1) the anisotropy of small strain stiffness due to the natural microstructure; 2) the curtailment of strength arising either from the fissures or from strain localisation on new shear surfaces formed during loading.

The attempt to calibrate the HSsmall model parameters for the London Clay subunits was not successful, as the inconsistent model parameters were calibrated when the calibration used different triaxial testing data from the same London Clay unit. In the HSsmall model, this dilation angle was not recommended for the clay type soil, however, the significant sensitivity to the dilation angle value was observed during the HSsmall model calibration using the London Clay triaxial testing data, and the dilation did happen during the shearing in some of the London Clay soil samples.

In spite of the shortcomings in the BRICK model, but given limited choices, the BRICK model was applied in the Crossrail deep excavation case history back-analysis. The back-analysis results were compared with the results using the basic Mohr-Coulomb model, as presented in Chapter 6.

2.5 Monitoring data review

2.5.1 Response of soil/structure interaction in excavation

An excavation can cause the ground displacements and deformation of the retaining structures. The form and magnitude of the displacements depend on many factors, such as the ground geology, the groundwater conditions, the duration of the construction, the construction sequence, the shape of the excavation, the type and stiffness of the retaining structures including the bracing system, and the control of the workmanship.

Response of the soil/structure interaction in an excavation can be expressed and measured by displacements, structural forces, soil stresses and the groundwater pressures. Typical displacement in the excavation comprises the ground surface settlement trough behind the retaining wall, the wall deflection profile, and the heave at the surface of excavated soil if the

excavation was occurred in clay soils, as indicated by Hsieh and Ou (1998) in Figure 2. 29. These displacements will change with the depth of the progressed excavation and usage of the bracing system.

The empirical correlations between the ground surface settlements (δ_v), the retaining wall lateral movements (δ_h) and the excavation depth (H_e) were studied using historical data. Peck (1969b) found that lateral movements of sheet piles or soldier piles in clays strongly depend on the nature of the soil and the depth of excavation. This wall deflections are in relation to the ground settlements, resulting in an approximately equal volume ($\delta_{vm} \approx \delta_{hm}$).

Clough & O'Rourke (1990) updated the empirical correlations for δ_{vm}/H_e *and* δ_{hm}/H_e to include the excavations with other types of retaining walls, such as the stiffer walls: diaphragm walls, secant & tangent piled-walls, tie-back supports; and the softer walls: soil nail supports and grouted walls. It was based on case history data provided by Goldberg *et al.* (1976), the average δ_{hm}/H_e = 0.2% and δ_{vm}/H_e = 0.15% were recommended for the excavation in the stiff clay. No differential behaviours due to the stiffness of the bracing system were found in excavations in the stiff clay, thus the stiffness of the stiff clay was considered more influential in the soil/structure interaction.

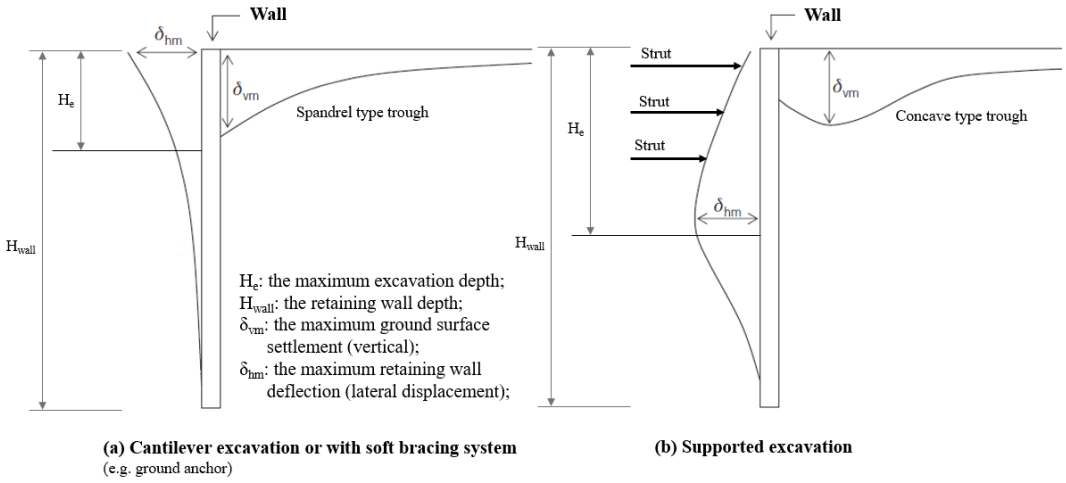

Figure 2. 29 Response of soil/structure interaction in excavation (Hsieh and Ou, 1998)

With more excavation case histories in stiff clays (e.g. London Clay), the state of practice on the evaluation of δ_{hm} & δ_{vm} induced by excavations with different supporting systems were summarised in Ciria C760 (Gaba *et al.*, 2017): fewer displacements occurred in practice due to 'high stiffness' in the top-down construction, either the stiffer walls or the stiffer bracing system, δ_{vm}/H_e = 0.08% was recommended, as shown in Figure 2. 30.

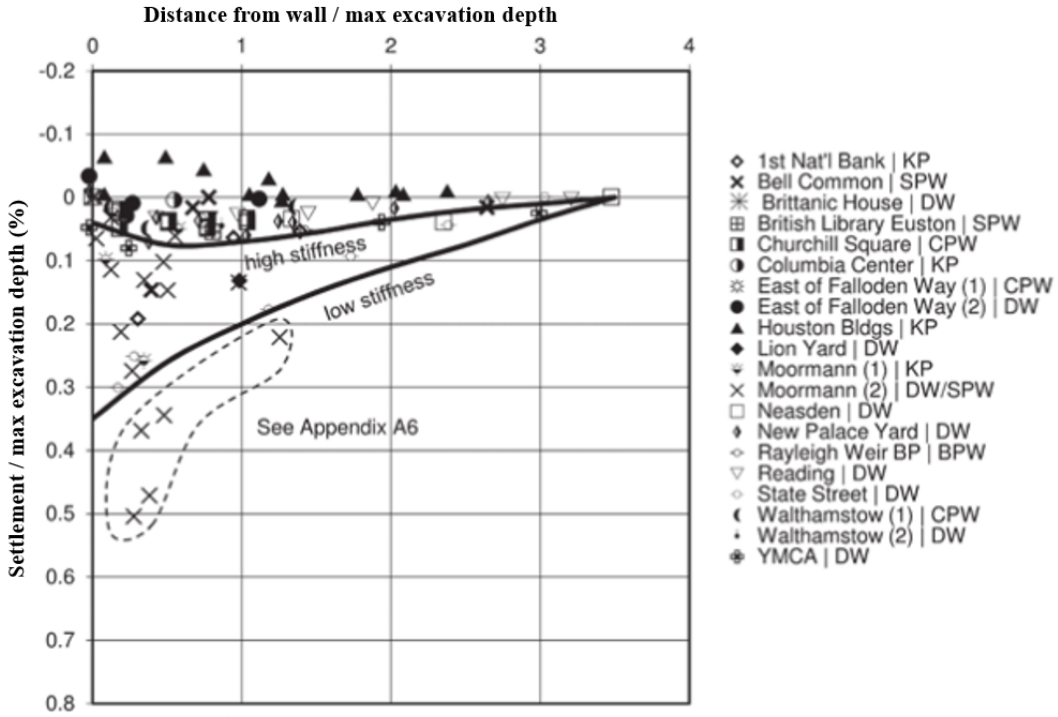

Figure 2. 30 Ground surface settlement due to excavation in stiff clay, Ciria C760 (Gaba *et al.*, 2017)

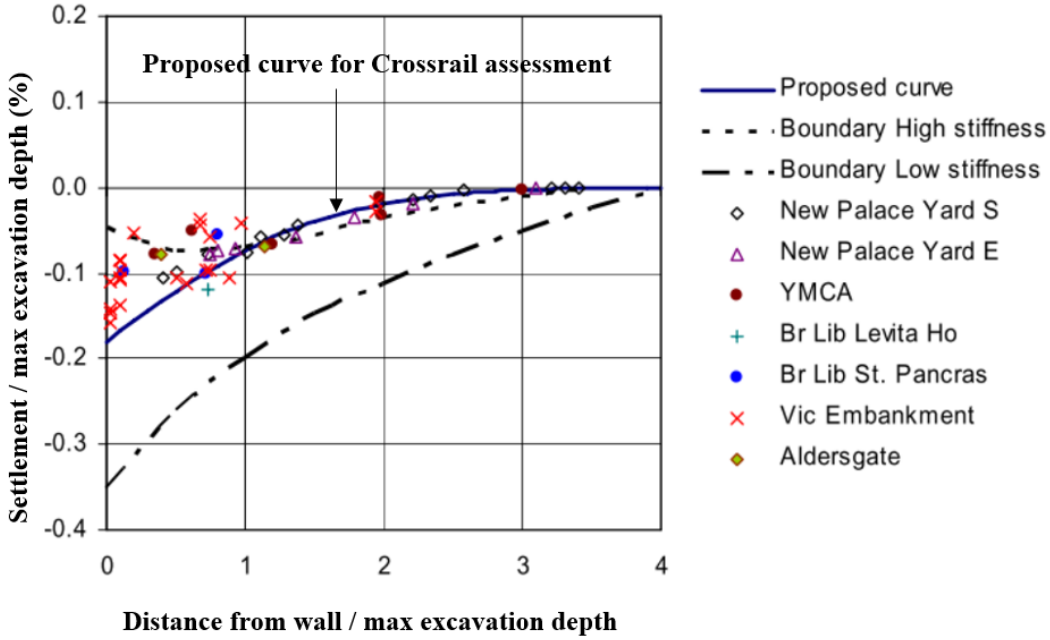

Figure 2. 31 Selected ground settlement Gaussian curve trough for the Crossrail assessment (Bologna, 2017)

Bologna (2017) studied ground settlements from the excavation case histories in the London Clay with the stiffer diaphragm walls. The data of these case histories showed some unconservative settlements within one time of the maximum excavation depth and presented a higher ratio of δ_{vm}/H_e = 0.18%, as presented in Figure 2. 31.

These empirical correlations provide a guide to estimate and review the measured δ_{vm} and δ_{hm} due to excavation in the stiff clay. The monitoring data review for the selected instruments is described in the following sections.

2.5.2 Inclinometers

It is still common for inclinometer data to be riddled with noise at best, and measurement bias at worst (Fowler and Meynink, 2013). The potential for error can be greater than the magnitude of real displacement, therefore, all measurements should be questioned and checked (Mikkelsen, 2003a).

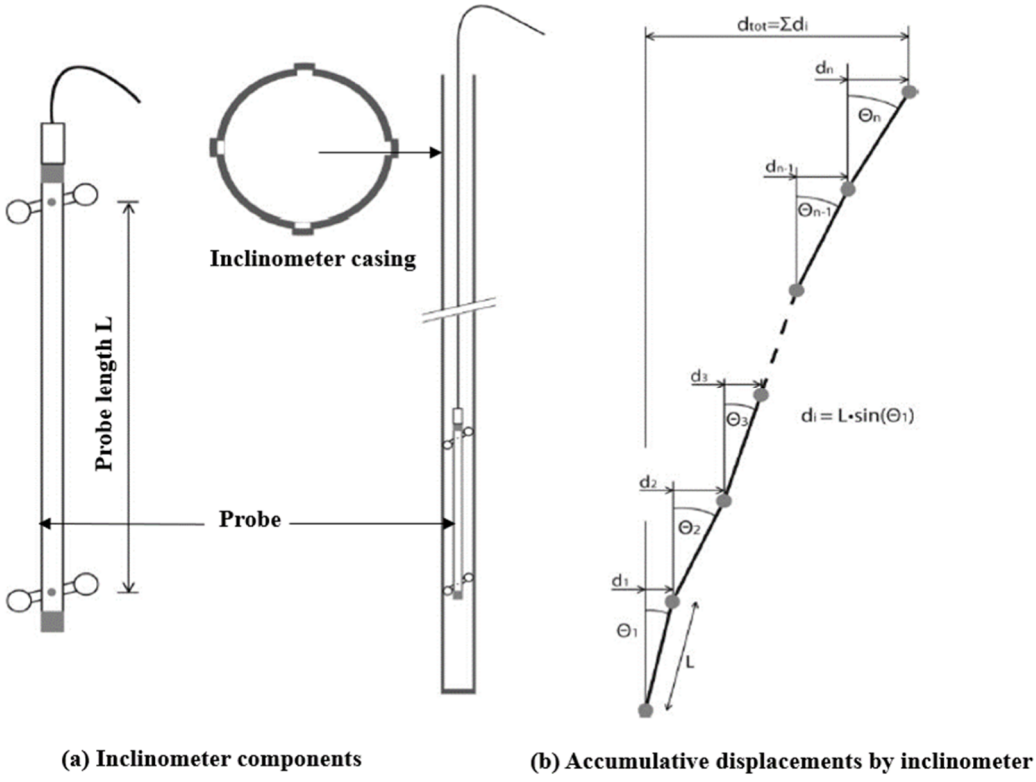

Figure 2. 32 Inclinometer probe, casing and deflection derivation diagram (Tann, 2014)

Firstly, the inclinometer as the monitoring instrument was reviewed, the inclinometer components were shown in Figure 2. 32. Tann (2014) compared five commercial inclinometer probes, mainly in two categories: inclinometer with manual operated sensors (IM) and in-place-

inclinometer (IPI). Different terms were used to describe the accuracy and precision of inclinometers, and values appeared inconsistent across the different manufacturers.

The following common factors were listed for attention:

- Resolution

Sensor resolution is the smallest change that can be reliably measured and it may differ from the resolution of the digital output. The resolution of the probe in degree as the probe measures the tilt angle and the resolution of the final output of the inclinometer (e.g. in millimetre) should be clearly specified.

- Sensor accuracy

It is given in ± value in percentage of the full-scale value for the calibrated sensor range. This information was provided in only one out of five probes studied.

- System accuracy

It is given in ± value (mm) of the final output for the specified length. This is the total system accuracy including errors introduced by the combined factors, such as a probe, casing, operator and operational environment.

- Repeatability

Repeatability indicates the precision of the inclinometer probe and this value varies in both the unit and test range from different manufacturers.

- Linearity

Linearity is an index between the calibration curve and the straightness of sensors. Only one inclinometer probe was given this value, in a percentage of the full-scale value for the calibrated sensor range.

- Sensitivity

It is used to describe the slope of the calibration curve, representing the mathematical relationship between the surveyed quantity and the system output (Kalantar-Zadeh, 2013). However, this value was not provided in any of the studied inclinometer probes.

2.5.2.1 Error diagnostics and corrections

Mikkelsen (2003a) suggested error diagnostics and correction procedures for inclinometer data assessment on the basis of systematic error, which is inherent in the sensor and/or in the system, but the random error is generally less significant and remains constant in variable surveys for the same probe.

The imperfection of instruments and external influences will cause inevitable random errors. For instance, noise in the data due to the digital output of the electric current. This noise could be further amplified due to temperature and interactions with the surrounding environment. The random error spreads around the real value and can likely not be avoided.

It was believed that one or a combination of the following factors caused the systematic errors of the inclinometer data: sensor bias shift, sensitivity drift, sensor alignment shift (e.g. rotation), depth positioning error, and casing inclination & curvature.

In the above factors, the depth positioning and casing inclination & curvature are associated with the installation. The quality of the installation can be improved through the specification and close supervision during installation.

For other factors, a guide to detect and correct the inclinometer errors was summarised below, on the basis of the case studies by Mikkelsen (2003a), Fowler and Meynink (2013), and Tann (2014).

- Bias-shift

It is also referred to as 'zero shift', a function of the inclinometer probe calibration. As one of the most common systematic error, bias shit can drift over time and result in the unusual cumulative displacements. This error can be detected and corrected by conducting a data bias check, as referred to as Cornforth's work (2005). Alternatively, the bias-shift check is a built-in function in most commercial inclinometer data processing software. Occasionally, the bias-shift can occur due to sensor warm-up, which is not a systematic error and will not be automatically detected and corrected in the data processing.

- Rotation

A small alignment change in the probe axis relative to the baseline setting, in combination with the installation imperfection, can cause a systematic rotation error. This rotation error varies for each probe. Corrections can be achieved using a trial and error procedure: the tolerance is calibrated for a probe, if the surveyed rotation exceeded the tolerance, it might be a sign of rotation error. As rotation error is not a routinely performed error correction, experts would be required to supervise the rotation error correction.

- Sensitivity drift

The sensitivity drift occurs very rarely and is difficult to identify. It can only be detected during factory calibration or regular calibration for long-term monitoring. For instance, in embankment slope displacement monitoring over decades and arranging probe calibration at regular intervals would be the ideal.

- Drift and hysteresis

Drift and hysteresis errors are time-related effects, and they can develop due to repeated cycles of operation or general ageing of sensors. Except for the frequent calibrations, there are no effective measures to correct these errors.

Moreover, the practice in the field also suggested extending inclinometers 3 to 6 meters into the ground below the rigid structural boundary, ensuring the fixity at the bottom of inclinometers (Mikkelsen, 2003a). Alternatively, the inclinometer data can be countercheck if reliable reference displacements at another position are available.

2.5.2.2 Shape Accel Arrays

The Shape accel arrays (SAA) is an alternative option to the inclinometer with advantages in data density and survey capacity. SAA also surveys the tilt angle and its data review can be referenced to inclinometer data error diagnostic and corrections.

An SAA is made of an array of rigid segments in 0.3 or 0.5 m lengths, joined by flexible 'knuckles'. Each segment contains three-dimension micro-electro-mechanical system accelerometers (MEMS) that measure tilt angle relative to gravity along the X, Y and Z axes. The assembled SAA segments allow bend angles between two segments to be calculated and thus the shape of the SAA can be determined (Measurand, 2013).

Unlike normal inclinometers, no grooved casing and guide wheels are needed for SAA. The SAA alignment orientation is ensured through the special design of 'anti-twist' joints (Levesque *et al.*, 2017). A number of shorter length SAA segments will lead to a higher density of data points, hence the shape of the surveyed profile will be more precise than normal inclinometers.

Segments of an SAA are assembled and calibrated in the laboratory and then rolled on a reel for delivery, as illustrated in Figure 2. 33. The installation of an SAA in the field needs an axial force to snag all joints straight from top to bottom, which is highly dependent on the operators and the installed casing conditions. For example, the reinstallation of SAAs due to straightness issue was reported in one of the Crossrail station excavation (Crossrail, 2014).

Measureand® Inc. is the only manufacturer of SAA in the market. The application of SAA in ground engineering is still in its early stages, and a good understanding of the instrument performance relies on more practical experience

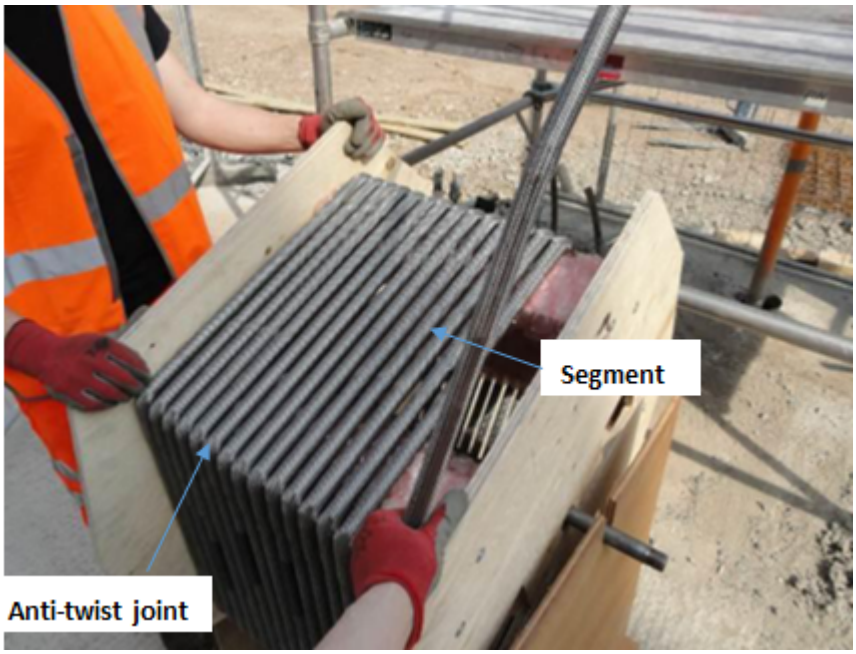

Figure 2. 33 Photography of an SAA on a real (Lipscombe *et al.*, 2012)

2.5.3 Extensometer

Heave, an upwards displacement, is observed at the surface of excavated soil when the excavation occurred in clays. Heave can be measured using an extensometer. It measures the distance between distinct points, with a series lined up points in the extensometer borehole the ground vertical movements profile will be formed.

Two common types of extensometers are in use: rod extensometer and magnetic extensometer, as demonstrated in Figure 2. 34.

The rod extensometer anchors a number of rods at distinct levels of a prepared hole surveying the vertical ground displacement during construction. The magnetic extensometer also called 'spider magnets', comprises a series of magnetic rings and a casing. These spring-loaded 'spider' legs extend outside of the casing into the ground when the springs are released. When a magnetic sensitive electrical reed switch is lowered into the casing, reading will be recorded when passing one of the magnetic rings, providing the relative distances between the magnets. The deepest magnet is the default fixed point so that the relative vertical displacements can be derived.

Data processing for extensometer is relatively simple and the potential errors are associated with installation and operation. For instance, extensometers that are installed within the excavated area, they are in a vulnerable position as they are exposed to construction activities.

Extra care and close supervision are needed to protect extensometers during the monitoring period.

The installation procedure could affect the extensometer reading. For example, the stiffness of the grout holding the magnets in-place matters for the settlement measurement. Wan *et al.,* (2014b) pointed out that the grout needs to be stiffer than the surrounding soil so that the magnet will capture the vertical displacement due to the surrounding soil movement, but the stiffer grout could potentially introduce an adverse effect, that the measured displacements are smaller than the actual movements.

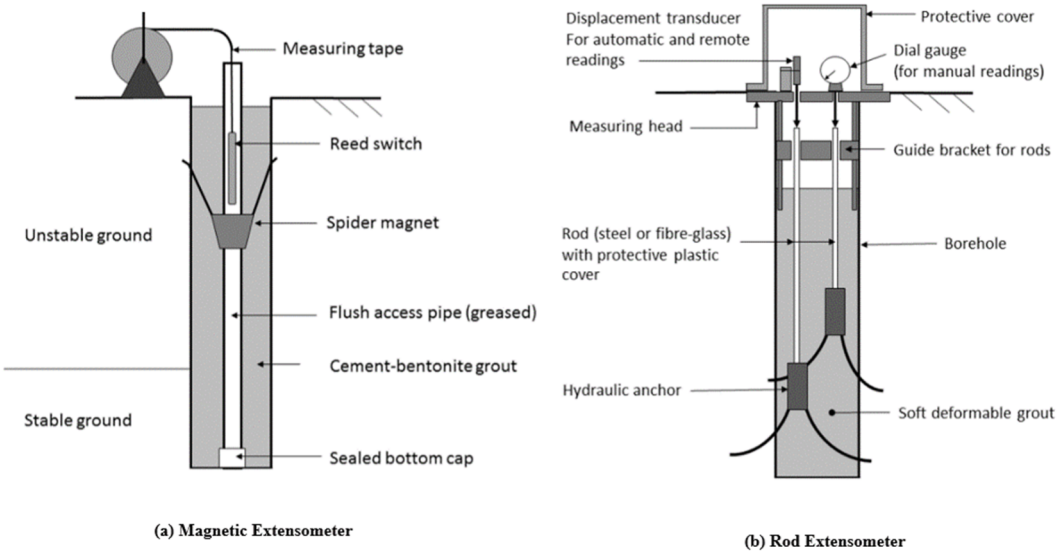

Figure 2. 34 The diagrams for extensometers (Geotechnical Observation, 2018)

2.5.4 Vibrating wire strain gauges

The vibrating wire strain gauges are used to measure the increment strain on the surface of structures, thus the stresses and the resultant forces of the structure can be calculated.

The mechanism of the vibrating wire strain gauge is based on Hooke's law, as given by Battern *et al*., (1999):

$$\Delta\varepsilon = \left(4l^2 \frac{m}{EA}\right) \times (\Delta f)^2 \qquad (2 - 15)$$

$\Delta\varepsilon$	change of strain in the wire, in microstrain: μm
Δf	change in the frequency of vibration
E	Young's modulus of material: kN/m^2
$4l^2m/EA$	A gauge factor, given by the manufacturer, in the unit of $\times 10^{-12}$ s^2 to give $\Delta\varepsilon$ in microstrain

The change of strain value is linked with the change in vibration frequency and the material properties of the strain gauge. With the measured strain (ε), the structural force can be calculated. For example, using strain gauge a steel prop axial force (F) can be calculated by $F/A = \sigma = \varepsilon \times E$, where A is the cross-section area of the prop, E is the steel stiffness and σ is the distributed stresses.

The potential sources for errors in vibrating wire strain gauge data are reviewed below with regard to the temporary prop monitoring.

2.5.4.1 Installation

The position of the monitoring point on a prop, where strain gauges are installed, can introduce some errors to strain gauge readings. The common practice includes at least two monitoring points in one prop, thus the prop axial force can be calculated and validated.

It was recommended to have the monitoring point away from the sectional joints (e.g. weld line), as the axial stress distribution may not be uniform at these joints (Batten *et al.*, 1999).

Furthermore, the non-uniform stress distribution may also occur at the end where the prop is connecting to the waling beam or the retaining wall. Using a quarter steel tubular prop numerical model, the stress distribution at the end was investigated by Batten *et al.,* (1999). An extreme loading case assumed that a point load was applied to the side of this quarter steel prop and the highly non-uniform stress distribution of axial stresses was observed at a distance of three times the prop diameter. This indicated the eccentric loading applied at the end of a prop can cause non-uniform stress distribution that extends to a length of three times of the prop diameters.

However, in the field, for the purpose of gauge protection and easy access during monitoring, it was preferable to have the monitoring point as close to the end as possible.

When a straight prop is connected to the waler beams or the walls at two ends, it may experience bending stress due to one or the combination of following factors: wall rotation, eccentric loadings and the locked-in self-weight. If the welded connections are present, the differential temperature across the prop could introduce the additional stresses at these welded locations. The numbers of strain gauges and their arrangement on the surface of the prop determine if these potential bending stresses can be captured, thus the prop axial force can be accurately calculated through strain gauges data. This effect was investigated by Batten *et al.* (1999) and Richards *et al.* (2001).

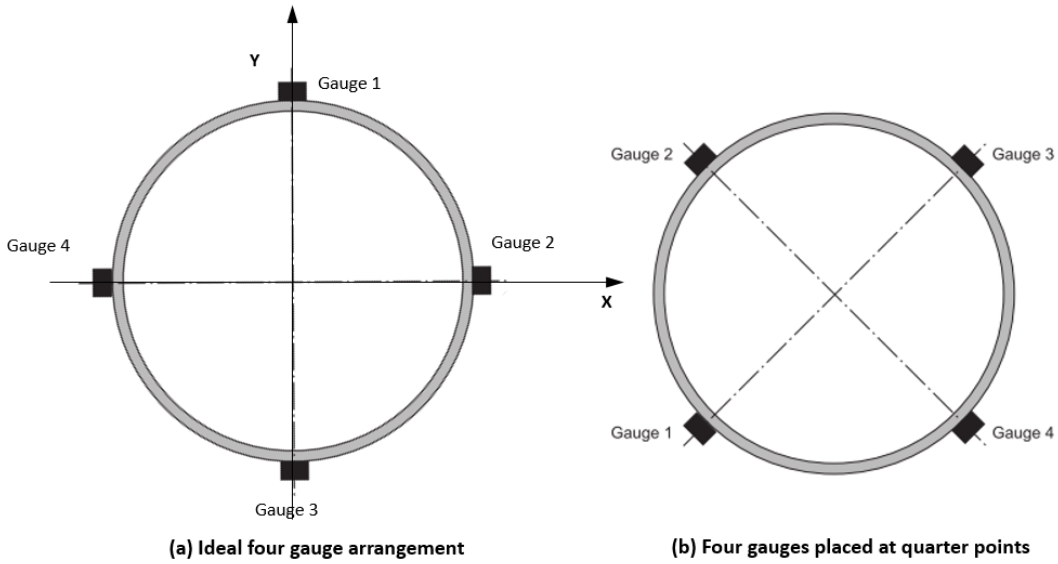

Figure 2. 35 Four strain gauge arrangements (Richards *et al.*, 2001)

Battern *et al.* (1999) studied one to six gauges placed on the circumference of a steel tubular prop and concluded that a minimum of three gauges would be required with one gauge fixed at the top (12 o'clock position), in order to measure the prop axial force involved in the potential bending stresses. However, it was not practical to space three gauges evenly, instead, four gauges were recommended by placing them at the top, the bottom and sides of a prop (Figure 2. 35). By this arrangement, the average of four strain gauges readings would cancel out the bending stress and give the true axial prop force:

$$F = AE\left(\frac{\varepsilon_1+\varepsilon_2+\varepsilon_3+\varepsilon_4}{4}\right) \quad (2 - 16)$$

Sometime, four gauges will be placed at quarterly points of the circumference of the prop to avoid the damage from construction activities, as shown in Figure 2. 35. The prop axial force will be calculated by the following equations:

$$\sigma = E\varepsilon = \frac{My}{I} \pm \frac{F}{A} \quad (2 - 17)$$

$$M_{XX} = \frac{EI}{y}\frac{(\varepsilon_1-\varepsilon_3)}{2} \quad (2 - 18)$$

$$M_{YY} = \frac{EI}{y}\frac{(\varepsilon_2-\varepsilon_4)}{2} \quad (2 - 19)$$

ε_i	strains measured at the corresponding location, in microstrain: μm
I	the relevant second moment of the cross-sectional area: m^4
A	the cross-sectional area of the prop
E	Young's modulus of the steel prop in kN/m^2
y	the distance from the gauge to the neutral axis
F	axial prop force in kN

M_{XX} Bending moment in X-axis along the prop axial in kNm

M_{YY} Bending moment in Y-axis perpendicular to the prop axial in kNm

2.5.4.2 Baseline

The baseline (or reference) reading is the value against which all future measurements will be compared with. For strain gauges monitoring the prop axial force, the baseline reading should be taken when the prop is in position but not loaded yet. An incorrect prop force is likely calculated if the baseline reading is taken after the prop has been partially loaded, for instance, the loading from the prop self-weight.

It was recommended to establish the baseline by taking a number of readings over a short period (e.g. in minutes) (Batten *et al.*, 1999) so that thermal effect would be eliminated and the influence of external construction activities minimised.

Besides the standard gauge calibration in the laboratory prior to the installation in the field, a small scale load test on the prop was recommended to ensure these installed strain gauges work properly (Simpson, 2017).

2.5.4.3 Thermal effect

Thermal expansion of a steel prop is expected when the temperature increases. If a steel prop is restrained at the ends, the thermal expansion of the prop would introduce a change in prop axial force, with a magnitude in relation to the wall stiffness and the efficiency of the supporting system, including waler beams, props, and their connections.

The change of axial strain due to the thermal expansion can be calculated by:

$$\Delta\varepsilon_P = \alpha_P \Delta T \qquad (2 - 20)$$

$\Delta\varepsilon_P$ change of axial strain in microstrain: μm

ΔT change of temperature: °C

α_P the coefficient of thermal expansion of the prop: $°C^{-1}$

Then, the prop thermal force can be calculated with the equation given below, as listed in Ciria C580 (Gaba *et al.*, 2003):

$$\Delta P = AE\alpha_P \Delta T(\frac{\beta}{100}) \qquad (2 - 21)$$

ΔP change of axial strut load: kN

A the cross-sectional area of the steel prop: m^2

E Young's modulus of the steel prop: kN/m^2

β percentage degree of restraint of the prop $\beta = \Delta\varepsilon_d/\Delta\varepsilon_a$

A diagram illustrating a steel prop status is shown in Figure 2. 36, including the basic state, under the thermal expansion, and the combination of thermal expansion & restraint.

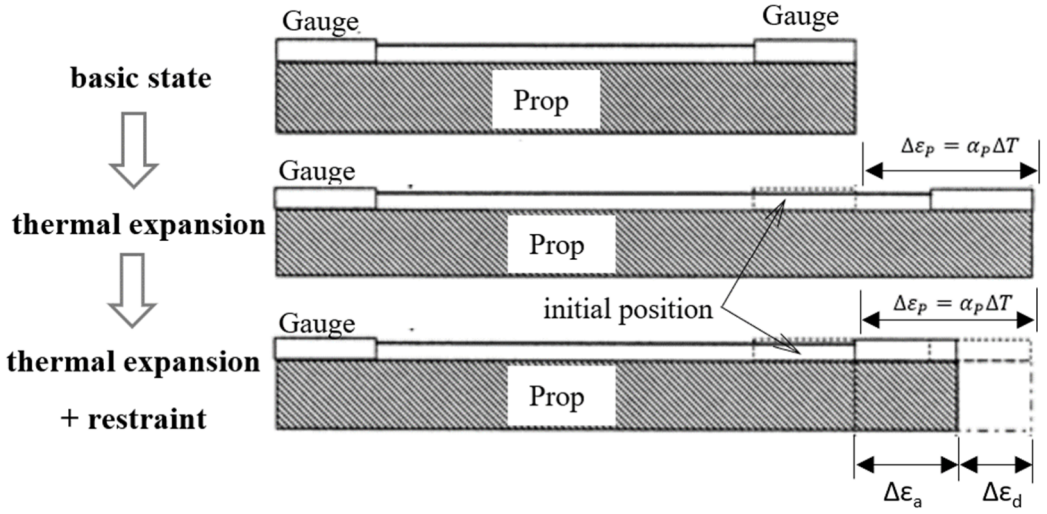

Figure 2. 36 Schematic diagrams of the relative strain on prop (Batten *et al.*, 1999)

In the diagrams, $\Delta\varepsilon_P$ is the thermal expansion of a prop without restraint, $\Delta\varepsilon_a$ is the actual strain increment, the measured strain, and $\Delta\varepsilon_d$ is the differential strain increment, which is determined by the restraint properties, such as the wall stiffness and the bracing system efficiency.

The factor β is given as $\beta = \Delta\varepsilon_d/\Delta\varepsilon_a$ assuming that the prop is perfectly placed perpendicular to the wall in the symmetric condition. Hence, β can represent the strains due to the restraint, and the thermal strut load can be identified. However, if the actual props are in an asymmetric condition, β will vary for each construction stage. Its value depends on the integrated supporting system efficiency and the corresponding temperature condition.

The differential temperature between the strain gauge and the steel prop is another factor in the thermal effect. The thermistor in the strain gauges measures the temperature of the gauge, this is in relation to a position where the gauge is installed on the surface of the steel prop, and with respect to the source of heat. For example, when a steel prop shows exposure to the sunlight, the top of the prop is directly exposed to sunlight, thus the most fluctuating temperature readings are recorded here; in contrast, the bottom of the prop is in the shadow with the lowest temperature readings of a daily cycle and a yearly cycle; and the sides of the prop are normally with steadier temperature readings, except for special cases in which the sunlight is projected from inclined angle.

A couple of mitigation measures are practised in the field to minimise the differential temperature between the strain gauge and the prop, for instance, using a steel plate to house strain gauges on the surface of the prop and painting the steel prop in white.

2.5.4.4 Other sources of errors

Reviewing the case histories, the prop axial force could also be affected by the following:

- accidental damage of gauges: 2 out of 29 gauges were damaged at Jubilee Line Extension (JLE) Canada Water Station; 1 out of 32 gauges were damaged at JLE Canary Wharf Station (Batten *et al.*, 1999). It was therefore recommended to have more than one monitoring point for each surveyed prop.
- the roughness of the wall or change of wall thickness at the joint where the prop connected could introduce a change in the prop axial force. A ± 5 % change in the prop axial force due to the wall thickness change was reported in JLE Canada Water Station (Batten *et al.*, 1999).
- vibration and other external impacts from construction activities may affect the gauge data as a random noise remains in the reading.

The previous case histories showed the significant impact of the thermal effect on the prop axial force, in addition to other possible sources of errors, but in most cases, the reality was that the calculated prop axial forces using the strain gauge data were far below the provided structural capacities. For the purpose of validating a design and compared to the defined trigger value as part of construction control, the strain gauge remains a useful instrument in providing the measurements to calculate the prop axial force. However, the accuracy of the calculated prop axial force was flagged as a concern.

2.5.5 Piezometers

There are two types of Piezometers and they are classified by the installation method (Dunnicliff, 1993): standpipe piezometer and vibrating wire diaphragm piezometer.

The conventional Casagrande type piezometer (Casagrande, 1949) is installed using a sand pocket. The piezometer is surrounded with the poured-in sand filter which allows a large amount of water flow through from the side and sealed by bentonite on the top, as illustrated in Figure 2. 37.

Later on, the diaphragm type sensor was implemented in piezometers. This new type of sensor only requires a small amount of water flow, thus a fully grouted installation method is applied.

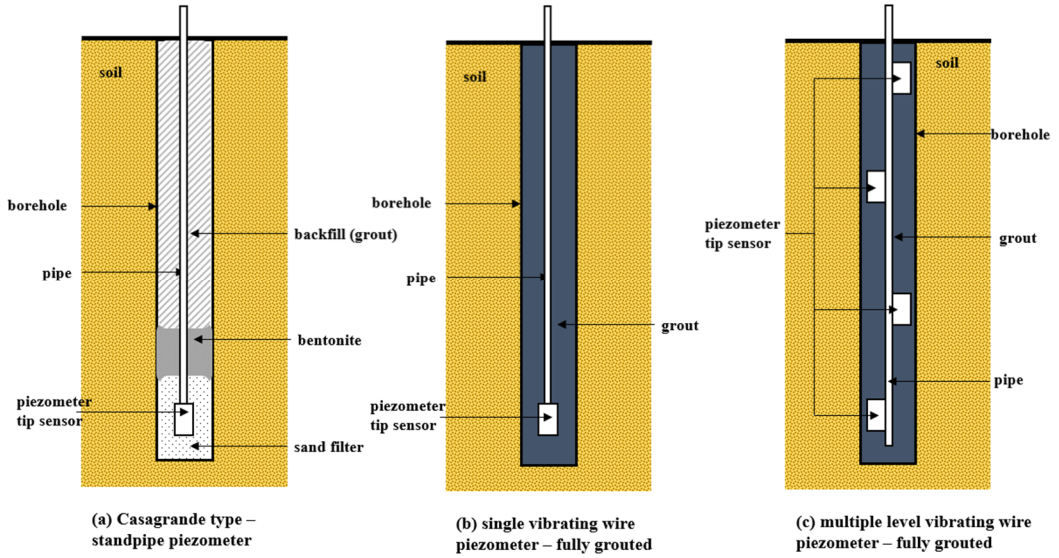

Figure 2. 37 Schematic sketches of piezometers

The earliest installation of a single vibrating wire diaphragm piezometer using the fully grouted method in the field was reported by McKenna (1995). A number of researches were carried out to investigate the fully grouted method in relation to practical issues, including Mikkelsen and Green (2003b), Dunnicliff (2008), Contreras *et al.* (2012). Good performance of the fully grouted piezometer was considered to be associated with the appropriate water /cement ratio of the grout, as this ratio relates to the grout unconfined strength, the grout permeability, and pumpability. The advantage of fully grouted installation was it's a straightforward backfilling with fast installation, and also the opportunity to establish the vertical groundwater pressure profile through one borehole using a multi-level piezometer (Mikkelsen and Green, 2003b).

Wan and Standing (2014a) reported the use of multiple levels of vibrating wire (MLVW) diaphragm type piezometers. These MLVW piezometers were installed using the fully grouted method. The ratio between the grout permeability and the surrounding soil was investigated by Marefat *et al*. (2017): for the higher ratio (e.g. >1000), a hydrostatic short-circuit between the piezometer and the aquifer was observed, but for smaller ratios (e.g. 10) smooth and dampened response was observed.

2.5.5.1 Installation

Piezometer installation comprises two steps: sensor preparation and piezometer borehole installation. Firstly the piezometer tip sensor and porous filters need to be de-aired by boiling in water. The 'zero' baseline reading is established in the field at ground level before assembly in the piezometer borehole. Future readings can then be referenced to this 'zero' point under atmospheric pressure (Wan and Standing, 2014b).

After the piezometer sensor preparation, they are assembled in a PVC pipe which is also used for backfilling the borehole, pumping grout into the borehole through the pipe. The pipe is lowered down into the borehole and the borehole is backfilled according to the specifications. Electronic pressure transducers are combined with the piezometer to provide readouts automatically.

A smaller piezometer borehole usually means faster and more effective drilling with less disturbance to the ground.

2.5.5.2 Data interpretation

A good set of piezometer data should be able to clearly indicate the three-stage of groundwater pore water pressure change:

1) the immediate measurement at the post-installation stage;
2) equilibration stage; and
3) steady-state stage.

At the post-installation stage, a significant negative excess pore water pressure or a sudden change of pore pressure could be recorded. It is a result of a combination of factors: borehole drilling procedures caused stress relief in the surrounding soils; the chemical processes during the grout hardening would require some amount of water from the surrounding soil; in addition, the horizontal permeability determines the speed of flow into the piezometer borehole.

The equilibration is the stage between the post-installation stage and the steady-state stage. For London Clay, accounting for the slightly different permeabilities in different units, this period was suggested to be about one month (30 days) by Wan & Standing (2014b), based on their research of monitoring groundwater pressure in London Clay at variable levels using MLVW piezometers. The example is given by one of these piezometers, HP32, and its monitoring results are presented in Figure 2. 38. The grout used in the this MLVW piezometers is made of water, cement, and bentonite in the ratio of 2 (W):1 (C):0.5 (B), this is to ensure a

suitable grout strength and permeability for the groundwater pore pressures monitoring in London Clay soil.

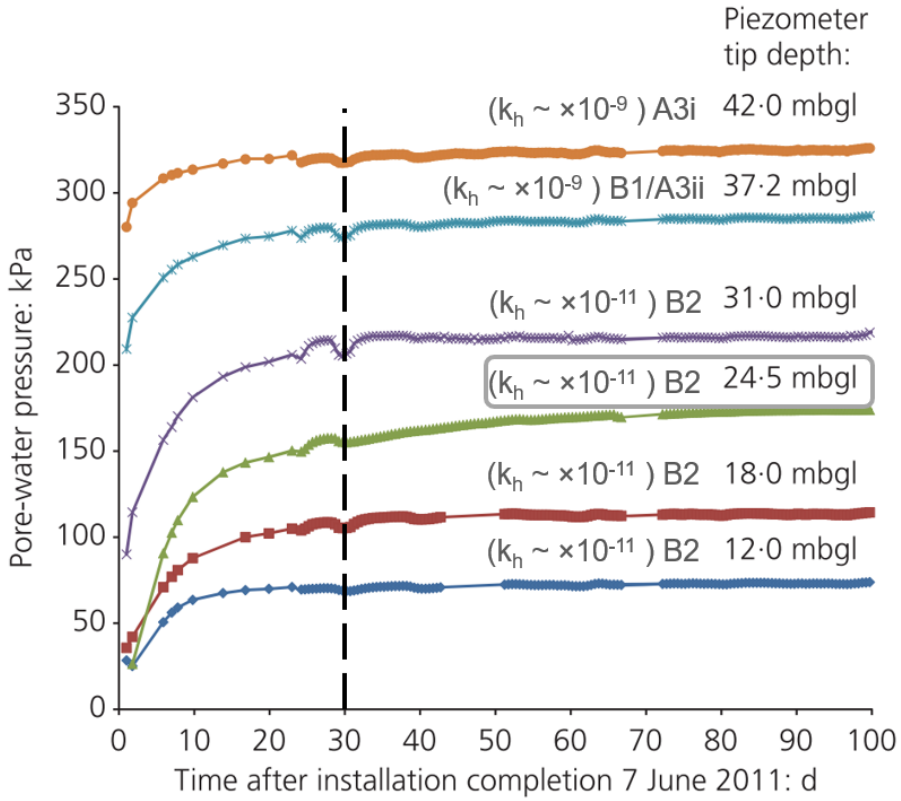

Figure 2. 38 Pore pressure measurements from piezometers in fully grouted borehole HP32(Wan and Standing, 2014a)

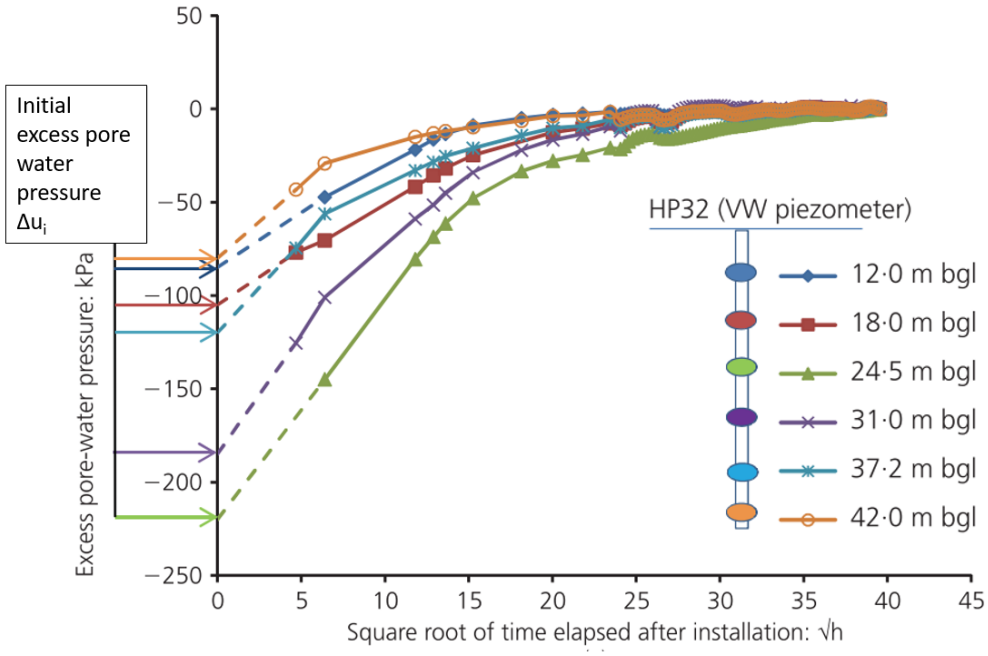

Figure 2. 39 Dissipation of excess pore-water pressures plotted against the rooted elapsed time from piezometers in fully grouted borehole HP32 (Wan and Standing, 2014a)

A steady-state stage is when the steady pressure is reached. Depending on the groundwater inflow, ground stratigraphy, and soil' permeabilities, the value could be as close to the hydrostatic water pressure if there is no water inflow.

Approaching to the steady-state, Wan & Standing (2014a) suggested a linear response for the first 50% of excess pore pressure dissipation. Figure 2. 39 shows the processed HP32 data, the measurements are compared with the steady-state water pressure value and plotted against the square root of the elapsed time (unit: $\sqrt{hour}$). The indicative initial water pressure can be estimated by extrapolating the early straight-line back to time = 0.

2.5.5.3 Source of errors

The performance of piezometers is dependent on the good installation. In the conventional installation method using a sand pocket, the connectivity between a few sealed layers could be established during installation and results in the poor performance. This connectivity problem is minimised in the MLVW piezometers by using the fully grouted installation method, although there is a possibility that inter-connectivity between sensors is channelled through cables where small continuous voids may not be fully grouted (Wan and Standing, 2014a). Meanwhile, the water content in the grout may influence the piezometer readings in a short period, immediately after the piezometer installation if the grout has not fully set or hydration is not complete. In addition, obstructions in the ground, such as claystone, can also influence the piezometer readings.

2.5.6 Summary of the review of monitoring data

A series of monitoring instruments were selected to be reviewed in this section and knowledge of the data error diagnostic and corrections provided a good understanding of the relevant monitoring data review, which was an integrated process. Reliable monitoring data is dependent on the data acquisition and adequate data processing, including review, error diagnostics and corrections if necessary.

The monitoring data of the Crossrail deep excavation case histories were reviewed and the corrections were attempted if possible, they are presented in Chapter 3, and further improvements on the instrumentations and monitoring were suggested as well.

Chapter 3

Case histories of Crossrail excavation

The observational method has been successfully applied in underground station excavations for the recently constructed Crossrail project in Central London, demonstrating that savings can be achieved in both time and cost. A study of the Crossrail excavation case histories was undertaken for a better understanding of the embedded retaining wall design in London Clay, as well as the application of the observational method. Back-analysing these Crossrail excavation case histories will provide valuable knowledge for future successful application of the observational method design in London Clay.

3.1 Introduction to the Crossrail project

The Crossrail project is currently the largest infrastructure project in Europe, with a budget of over £18 billion and is expected to be in operation in 2020. This new railway line stretches more than 100 km, comprising of over 42 km of tunnels across the central London area, while the overground railway line extends to the outskirts of the city. Eight out of ten newly constructed stations are underground. Five excavation case histories were collected from the Crossrail project for this research, as summarised in Table 3. 1.

Table 3. 1 Summary of collected Crossrail excavation case histories

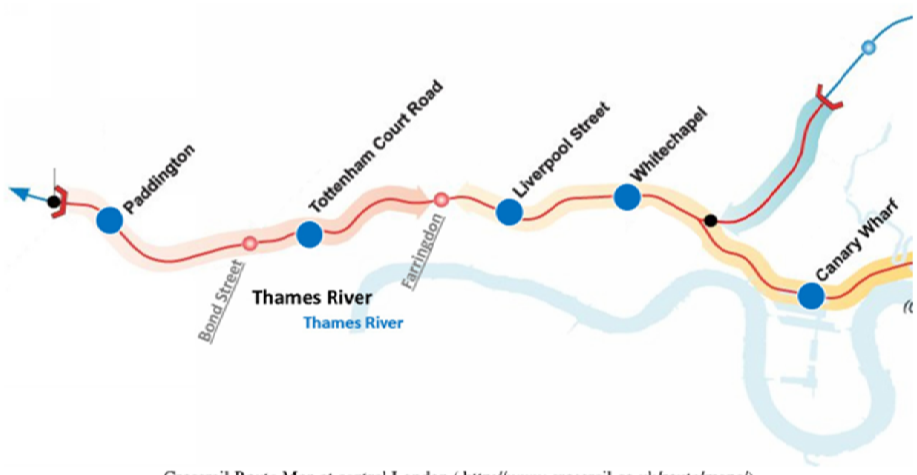

Crossrail Route Map at central London (http://www.crossrail.co.uk/route/maps/)

Case	Description	General Information			Remark	Numerical Analysis
1	Paddington Station box	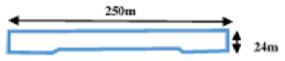	Retaining wall Max. Excavation depth Excavated soil	1.0m to 1.2m thickness diaphragm wall 25m London Clay		PLAXIS (2D) LS-DYNA(3D) – Asset protection only
2	Tottenham Court Road – Western Ticket Hall	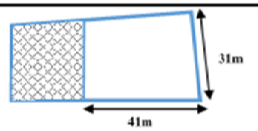	Retaining wall Max. Excavation depth Excavated soil	1.0m thickness diaphragm wall 30m London Clay	The observational method was implemented after construction has started. Saving of £75,000 and 4 weeks achieved. (Yeow, 2014)	FREW (*Oasys®*) PLAXIS (2D) LS-DYNA (3D) – Asset protection only
3	Liverpool Street Station – Moorgate Shaft	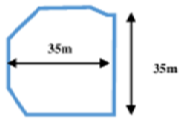	Retaining wall Max. Excavation depth Excavated soil	1.2m thickness diaphragm wall 40m London Clay and Lambeth Group	The observational method was implemented after the retaining wall installation but prior to excavation works. Programme saving has been achieved. (Farooq *et al.*, 2015)	PLAXIS (2D) FLAC (3D) LS-DYNA (3D) – Asset protection only
4	Whitechapel Station – Durward Street Shaft		Retaining wall Max. Excavation depth Excavated soil	1.0m thickness diaphragm wall 32m London Clay and Lambeth Group	The observational method was implemented after construction has started. Programme saving has been achieved. (Mills, 2016)	PLAXIS (2D) LS-DYNA (3D)
5	Canary Wharf Crossrail Station box		Retaining wall Max. Excavation depth Excavated soil	1.2m diameter Giken pile wall with tied anchor pile 27m Lambeth Group	The observational method was implemented after construction has started. Savings of cost and time has been achieved. (Yeow *et al.*, 2012)	PLAXIS (2D) LS-DYNA (3D)

Three Crossrail excavation case histories will be introduced in the following sections including a description of the original design, the as-built construction, instrumentation and a review of the monitoring data. They are listed as Tottenham Court Road station, Western Ticket Hall (TCR-WTH); Liverpool Street station, Moorgate Shaft (LIS-MS), and Paddington Station box (PAD).

Meanwhile, two other Crossrail excavation case histories - Whitechapel station, Durward Street Shaft (WS-DSS) and Canary Wharf Crossrail station box (CWCS) are included in the overview of the Crossrail project, but will not be discussed in the detailed back-analysis due to the lack of sufficient construction information and monitoring data (e.g. WS-DSS). In addition, the excavation of the CWCS box took place in the Lambeth Group, which is different from all other four case histories excavating in the London Clay.

The successful implementation of the observational method was reported in the construction of four Crossrail stations, from west to east London, listed as TCR-WTH, LIS-MS, WS-DSS and CWCS.

3.2 Tottenham Court Road Station, Western Ticket Hall

3.2.1 Introduction FREW model

The Crossrail Tottenham Court Road Station, Western Ticket Hall (TCR-WTH) is located in London's West End where Oxford Street crosses Tottenham Court Road. The TCR-WTH deep box excavation was constructed using the bottom-up construction method to minimise construction time. This decision was taken to facilitate the earliest possible construction of the base slab and preparatory sprayed concrete lining (SCL) tunnelling works in advance of the arrival of the Crossrail twin tunnel boring machines (TBMs).

The station design was conducted by an Arup/Atkins joint venture (AAJV), and the construction work was awarded to a BAM/Ferrovial/Kier joint venture (BFKJV). The temporary propping work supporting the TCR-WTH excavation was designed by Kier Engineering. Intensive monitoring work was commenced during the TCR-WTH construction by the Keller/Getec/itmsoil joint venture (KGiJV), including a few other monitoring sub-contractors for the installation of instruments and/or the acquisition of monitoring data acquisition. Due to the increased numbers of parties involved in the project, it was not easy to

engage all parties for information acquisitions. For example, in the back-analysis performed in 2012, the inclinometer data acquisition and review took two weeks, which accounted for half of the modified design time.

3.2.2 Original design

The TCR-WTH deep box excavation is almost rectangular in shape, measuring about 41 m × 31 m, with a maximum excavation depth of approximately 29.5 m. The original design adopted a 1.0 m thick diaphragm wall with 40 m depth from the ground level, with five levels of temporary props as retaining structures that support the excavation. The layout of the TCR-WTH site and cross-section A-A' are shown in Figure 3. 1.

The ground level is at +25.7 m in the ordnance datum (OD), which level also indicates the depth above the Crossrail tunnel alignment datum (± 0 at + 100 mOD), hence, this level is recorded as +125.7 mATD in the Crossrail project. It is to keep the consistency, in this thesis, levels from the Crossrail project are all recorded in this way.

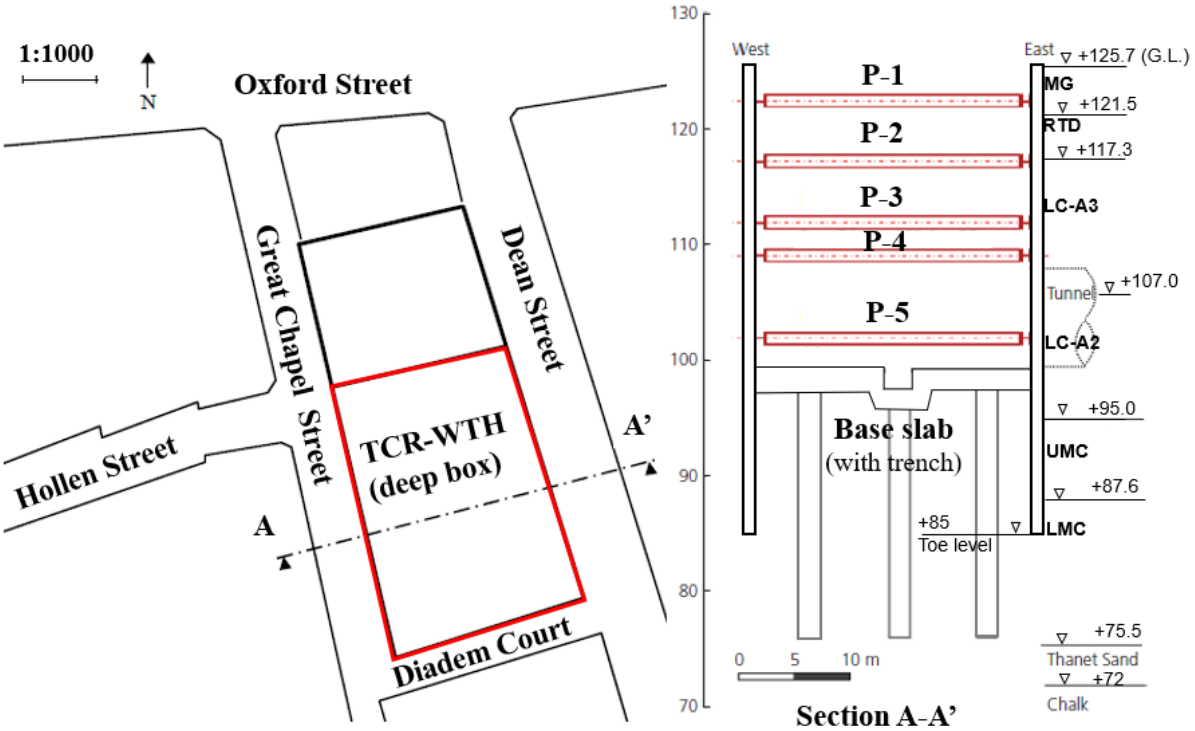

Figure 3. 1 TCR-WTH layout plan (Bologna, 2017) and section A-A' of the deep box (Yeow *et al.*, 2014)

The ground model adopted in the original design was based on the geotechnical design summary report (GDSR) for the Crossrail Tottenham Court Road station (Crossrail, 2010b), as shown in the Table 3. 2 and demonstrated in Figure 3. 1.

The geotechnical design parameters applied in the original design are summarised in Table 3. 2. It is based on the historical piezometric monitoring data, the pore water pressure design profile at the short term serviceability limit status analysis (SLS) was assumed as the under drained piezometric profile for the impermeable London Clay & Lambeth Group, and the drained hydrostatic profile for the lower aquifer, as shown in Figure 3. 2.

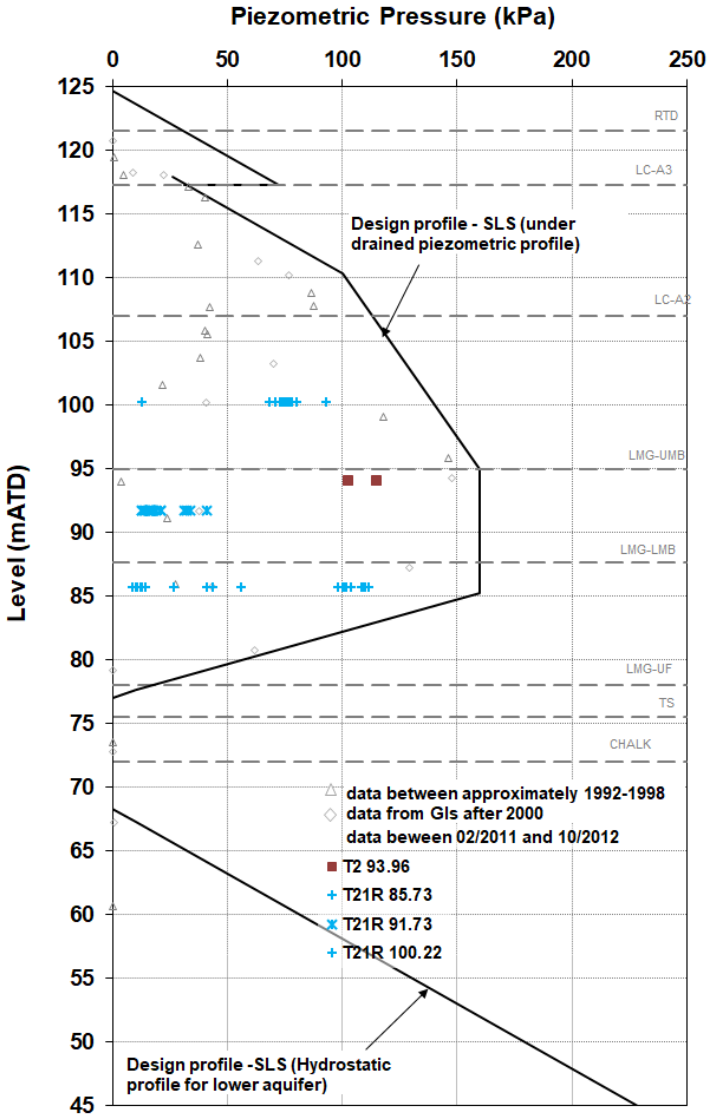

Figure 3. 2 Por water pressure design profile (SLS) for the TCR-WTH (Crossrail, 2010b)

Table 3. 2 Geotechnical design parameters for TCR-WTH original design (Crossrail, 2010b)

Stratum		Top (mATD)	Base (mATD)	γ (kN/m^2)	c_u (kN/m^2)	c' (kN/m^2)	ϕ'_{peak} (ϕ'_{cv}) (°)	$\phi'_{residual}$ (°)	ν' (ν_u)	K_0	E_{uv} - 0.1% strain (MN/m^2)	E_{uh} - 0.1% strain (MN/m^2)	E_v' - 0.1% strain (MN/m^2)	E_h' - 0.1% strain (MN/m^2)
MG		125.7	121.5	21	-	0	25	22	0.25	0.577	-	-	10	
RTD		121.5	117.3	20	-	0	40 (36)	36	0.25	0.357	-	-	75	
LC-A3		117.3	107	20	$80+8z_1$	10	20 (18)	15	0.15 (0.5)	*1.5 1.5-0.06z	$38+2z_1$	$76+3.9z_1$	$0.77E_u$	
LC-A2		107	95	20	$80+8z_1$	5	22 (20)	15	0.15 (0.5)	#1.0 (1.2)	$55+3.5z_2$	$109+7z_2$	$0.77E_u$	
Lambeth Group	UMC	95	87.6	21	250	10	26 (21)	15	0.15 (0.5)		$148+3.8z_3$		$0.77E_u$	
	LMC	87.6	78	21	250 $250+17.9z_4$	10	26 (21)	15	0.15 (0.5)		$175+7.5z_4$		$0.77E_u$	
	UF	78	75.5	21	-	0	31 (26)	22	0.2	1.0	$246+5.4z_5$		$0.8E_u$	
TS		75.5	72	19	-	0	36 (32)	32	0.2	1.0	-	-	200	

z1 = depth below 117.3 in m; z2 = depth below 107 mATD in m; z3 = depth below 95 mATD in m; z4 = depth below 87.6 mATD in m; z2 = depth below 78 mATD in m

* 1.5 above 115 mATD, 1.5-0.6z below 115 mATD, z = depth below 115 mATD in m;

1.2 above 95 mATD, drops to 1.0 at 83 mATD

Concrete C32/40 was required for the diaphgram wall, and the minimum required temporary prop stiffness EA = 180,000 kN/m

The original design was based on analyses carried out with Oasys FREW® and the Mohr-Coulomb soil model. The finite element program Plaxis® 2D was also employed in the original design to verify the design assumptions made in the FREW modelling (Yeow, *et al.* 2014). In addition, Oasys LS-Dyna® 3D finite element analyses using the BRICK soil constitutive model were carried out to better understand soil/structure interaction and the impacts of construction activities by AAJV. This LS-Dyna 3D model was then used to estimate ground movements due to the Crossrail tunnelling and excavation works for asset protection assessments (Crossrail, 2007b).

The TCR-WTH retaining structure design complied with the Crossrail civil engineering design standards (CEDS), a Eurocode-based design document, integrated with Ciria C580 (Gaba *et al.*, 2003). According to Clause 2.1 (1) P BSI (2004a), a geotechnical design needs to be verified that no relevant limit state is exceeded, hence, both the ultimate limit states (ULS) and serviceability limit states (SLS) analyses were carried out in the original design. The following major design requirements were applied in the original design for the TCR-WTH:

- A surcharge load not less than 75 kPa was applied at the ground level representing the existing building load;
- The mixed earth pressure calculation was assumed for the short-term ULS analysis - where total stresses (undrained) were calculated on the passive side, and effective stresses (drained) were calculated on the active side;
- A 0.5 m over-dig was included in the ULS analysis;
- A 0.5 m softening depth on the passive side below the excavation level was considered in the ULS analysis, as total stress calculation (undrained analysis) was performed.

3.2.3 As-built condition

A value engineering study before construction identified an opportunity for the observational method to be applied, which led to additional instrumentation being installed, which provided comprehensive real-time monitoring data. The collaboration between the client, contractor and designers enabled the adoption of the observational method, resulting in the elimination of the lowest level of temporary props. This successful implementation of the observational method led to a critical path programme saving of 4 weeks and a £715,000 reduction in cost (Yeow *et al.*, 2014).

The as-built construction conditions were verified from available site records, including the issued as-built drawings for the temporary and permanent works; the contractors' technical committee (CTC) meeting minutes, which detailed construction-related information and monitoring data either by week or by work shift; and the site photographs taken between April and October 2012, during the TCR-WTH deep box excavation.

The as-built construction sequence to the stage of casting the base slab for the TCR-WTH deep box is summarised in Table 3. 3. Although the prop installation is normally ahead of the subsequent excavation, these two activities are modelled together during the FREW analysis as the insignificant modelling result from the prop installation. In Table 3. 3, the actual construction dates of prop installation and the subsequent excavation are identified for cross-section A-A' and listed separately. In some instances, the excavation started before the completion of the prop installation (e.g. stage 5b).

Table 3. 3 Summary of construction sequence and the completion dates for TCR-WTH deep box section A-A', after (Yeow *et al.*, 2014; Chen *et al.*, 2015)

Stage		Description	Start	End
1		Excavate to +121.6 mATD	17/04/2012	09/05/2012
2	a	Installation P1 prop at +122.4 mATD	04/05/2012	17/05/2012
	b	Excavate to +116.4 mATD	27/05/2012	14/06/2012
3	a	Installation P2 prop at +117.2 mATD	17/06/2012	28/06/2012
	b	Excavate to +110.9 mATD	29/06/2012	17/07/2012
4	a	Installation P3 prop at +111.9 mATD	18/07/2012	27/07/2012
	b	Excavate to +108.3 mATD	27/07/2012	07/08/2012
5	a	Installation P4 at +109.1	07/08/2012	18/08/2012
	b	Excavate to +101.0mATD	12/08/2012	04/09/2012
6	*a*	*Installation P5 prop at +101.2 mATD*	*Planned in original design*	
	b	Excavate to +96.8 mATD (north half of the box)	05/09/2012	08/09/2012
	c	Excavate to +96.8 mATD (south half of the box) including a trench excavate to +95.4 mATD	22/09/2012	27/09/2012
7		Cast the base slab in 2.0 m thickness	28/09/2012	10/10/2012

Note:

1. Stage 6a was planned in the original design, but was eliminated in the as-built modified design;
2. The listed start and end dates for each construction stage are summarised for section A-A' during the TCR-WTH deep box construction, based on the available construction records and monitoring data. It is likely completion may have taken place in a ±2 days period at other locations.

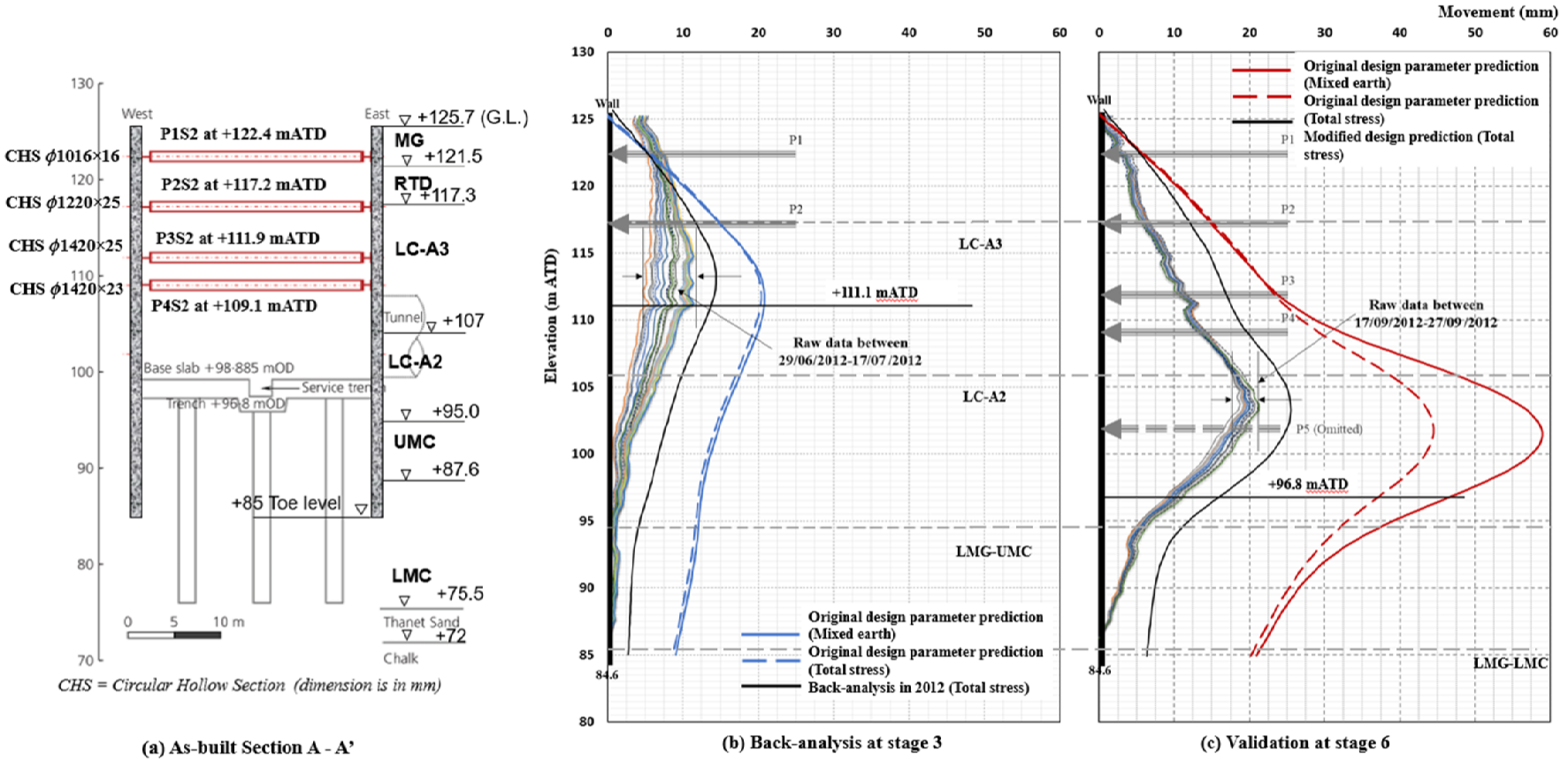

Figure 3. 3 TCR-WTH as-built configuration of modified design with supported back-analysis at stage 3 and predictions at stage 6

Evidence to support the implementation of the observational method with a modified design became available during stage 3 when the original predictions exceeded actual wall deflections by a factor of 2 based on the maximum uncorrected SAA-8003 data (Figure 3. 3).

The deep box excavation to the level of +111.1 mATD (stage 3) was back-analysed with FREW against inclinometer data (SAA-8003 raw data), and the predictions compared well with the measurements (Figure 3. 3). The design parameters were updated and applied to develop the modified design, which ultimately omitted the fifth (lowest) level of props. The new soil parameters predicted wall deflections in the final stage 6 of the modified design close to the measurements of SAAA8003 raw data, as shown in Figure 3. 3.

The back-analysis supported the use of total stress analysis, which predicted a better match with the deflection measurements. The mixed earth pressure approach overpredicted wall lateral displacements by a factor of about 3 in stage 6, as shown in Figure 3. 3.

A total of 46 props were installed, in different sizes of hollow circular sections or 'I' beam sections. Details of the four levels of props and the corresponding four waler beams are summarised in Table 3. 4.

Table 3. 4 Summary of as-installed temporary props during the TCR-WTH deep box construction (Crossrail, 2014c)

Level	Description	Size	Prop ID
Level – 1	Horizontal prop in East-West direction	CHS Ø1016×16t	P1S1, P1S2, P1S11, P1S12
Level – 1	Inclined Corner prop south end	CHS Ø1016×16t	P1S5, P1S6, P1S9, P1S10
Level – 1	Inclined Corner prop north end	2No.533×210×109UB	P1S3, P1S4, P1S7, P1S8
Level – 2	Horizontal prop in East-West direction	CHS Ø1220×25t	P2S1, P2S2, P2S11, P2S12
Level – 2	Inclined Corner prop south end	CHS Ø1420×23t	P2S5, P2S6, P2S9, P2S10
Level – 2	Inclined Corner prop north end	2No.533×210×109UB[1]	P2S3, P2S4, P2S7, P2S8
Level – 3	Horizontal prop in East-West direction	CHS Ø1420×25t	P3S1, P3S2
Level – 3	Horizontal prop in East-West direction	CHS Ø1220×25t	P3S11, P3S12
Level – 3	Inclined Corner prop south end	CHS Ø1520×30t	P3S5, P3S6, P3S9, P3S10

Level	Description	Size	Prop ID
Level – 3	Inclined Corner prop north end	2No.610×305×179UB	P3S3, P3S4, P3S7, P3S8
Level – 4	Horizontal prop in East-West direction	CHS Ø1420×23t	P4S1, P4S2
Level – 4	Inclined Corner prop	CHS Ø1420×40t	P4S3, P4S4, P4S5, P4S6, P4S7, P4S8, P4S9, P4S10
Level – 1	Waler beam	2No.686×254×170UB[2]	N/A
Level - 2	Waler beam	2No.914×419×343UB	N/A
Level - 3	Waler beam	2No.914×419×343UB[2]	N/A
Level - 4	Waler beam	2No.914×419×343UB	N/A

Note: CHS = circular hollow section, Ø = external diameter, t=thickness in mm, steel Young's Modulus = 200 GPa for grade S355 steel; UB =universal beam.

1. The corner props at the north end at level 2 are assumed based on the site photography, as no such props shown in the as-built drawing.
2. The part of waler beam at level 1 used 2No.533×210×109UB, and the part of waler beam at level 3 used 2No.914×305×201UB.

3.2.4 Monitoring system

A comprehensive monitoring system plan was designed for the TCR-WTH construction to assess the performance of the structure and control construction. This monitoring plan included inclinometers (shape accel arrays), strain gauges, piezometers and extensometers as shown in Figure 3. 4. Additional prisms were also installed at the capping beam level and the first level of props to cross-check the inclinometer readings. A couple of load cells to cross-check the strain gauge readings were initially requested but were not installed for unknown reasons. Levelling studs were installed along the roads surrounding the TCR-WTH box to monitor ground vertical displacements as a separate Crossrail ground movements and asset protection monitoring plan (Bologna, 2017). The layout of levelling studs was shown in Figure 3. 5.

3.2.4.1 Review of inclinometer data

In the TCR-WTH deep box excavation, traditional manual inclinometers were planned but replaced by Shape Accel Arrays (SAAs), which provided better resolution of the deformation profile (each segment is 0.5 m in length) with more frequent readings (every 15 minutes).

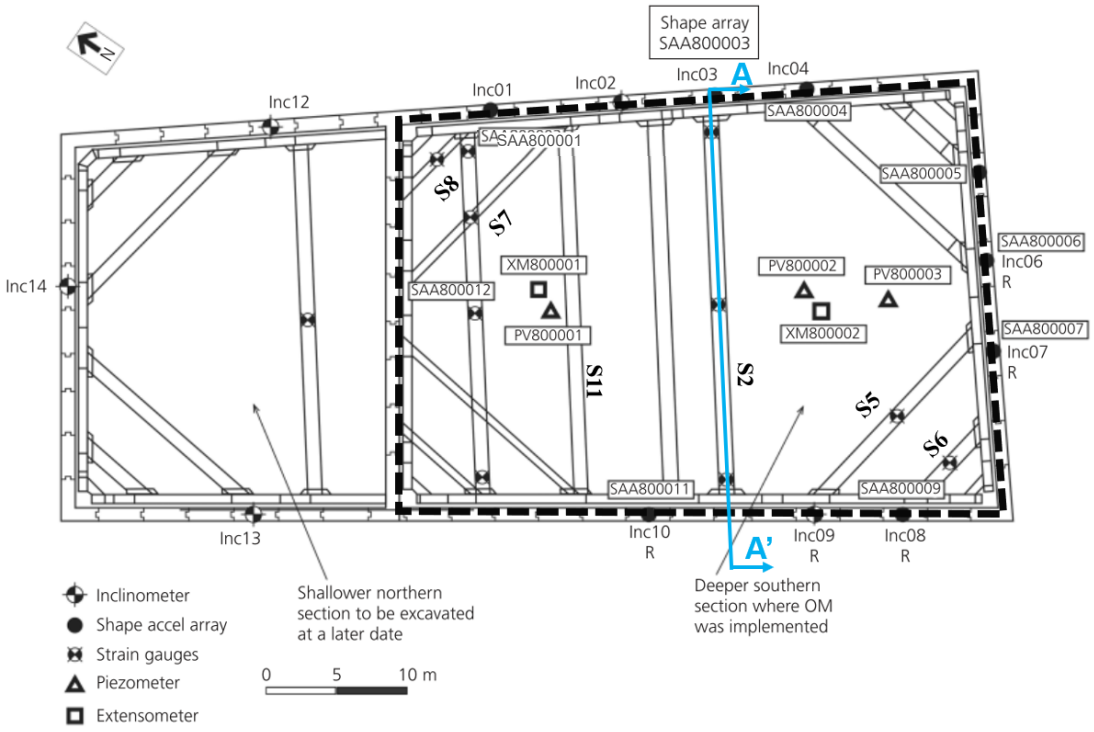

Figure 3. 4 TCR-WTH monitoring instrument layout plan (Yeow *et al*., 2014)

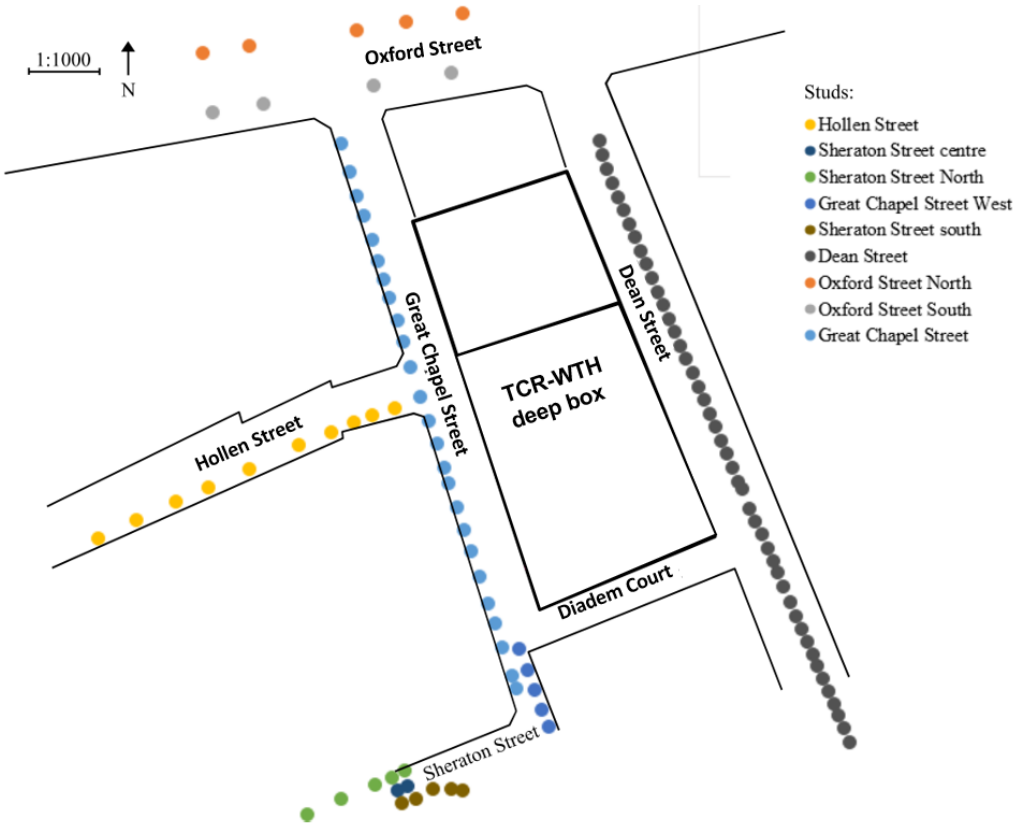

Figure 3. 5 Layout plan for the levelling studs at TCR-WTH (Bologna, 2017)

SAA-8003 located next to cross-section A-A' in the middle span of the deep box eastern side (Figure 3. 4), recorded the maximum wall lateral displacements during the excavation. Therefore, this set of data was reviewed, corrected using the prism data at the capping beam level (Figure 3. 6), and applied in the back-analysis for the modified design (Yeow *et al.*, 2014).

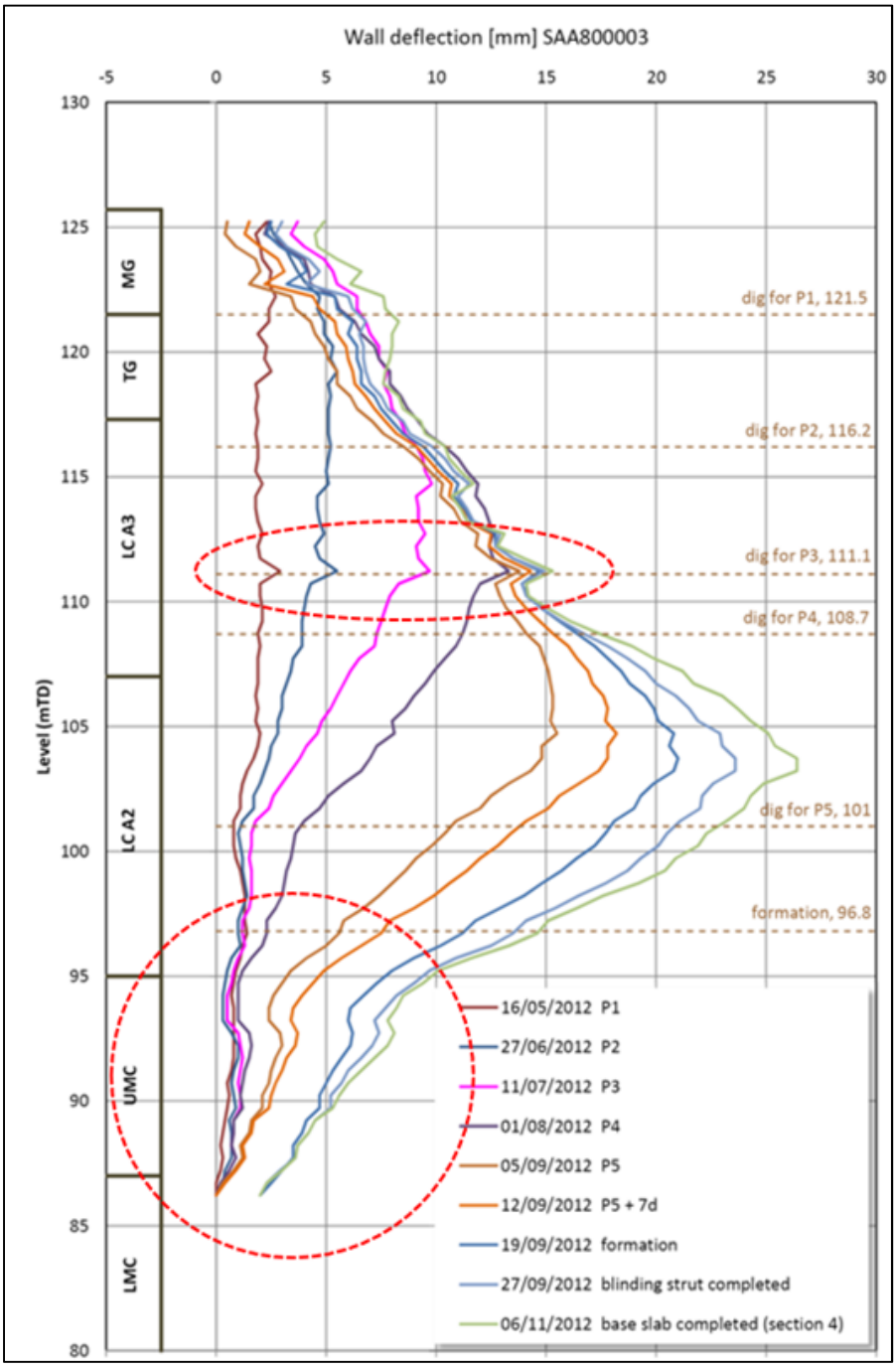

Figure 3. 6 Corrected SAA-8003 data in July 2013 (Lipscombe *et al.*, 2012)

SAA raw data acquisition was performed by the sub-monitoring contractor Geotechnical Observations Ltd. The raw data was reviewed for error diagnosis and correction if possible (Ridley, 2017). Review of SAA-8003 raw data raised the following issues:

- Anomalous displacements took place at the level of +111.0 mATD.
- A considerable displacement around +92.5 mATD developing from 1 mm on 15/6/2012 to 8 mm on 06/11/2012 – when the first excavation stage took place down to +121.6 mATD (15/6/2012). It was unlikely such a lateral displacement would then occur 29 m below the bottom of the excavation.
- The inflexion in the corrected data between + 90 and +95 mATD indicated a potential rotation error in SAA data.
- The lateral movements at the bottom of SAA-8003 (> 2 mm) at later excavation stages in the corrected data – which was against the fixity assumption at the bottom of the SAA.
- The increments in both X and Y directions from the bottom of SAA-8003 exceeded the random error of SAA data, which is given as $\pm (0.19 \times \sqrt{N})$ mm by Measurand (2013) (N is the number of segment counting from the bottom sensor).

The rotation error diagnostic was found to be the most significant correction to the raw data, compared to other potential errors, such as sensor bias shift or sensor depth positioning.

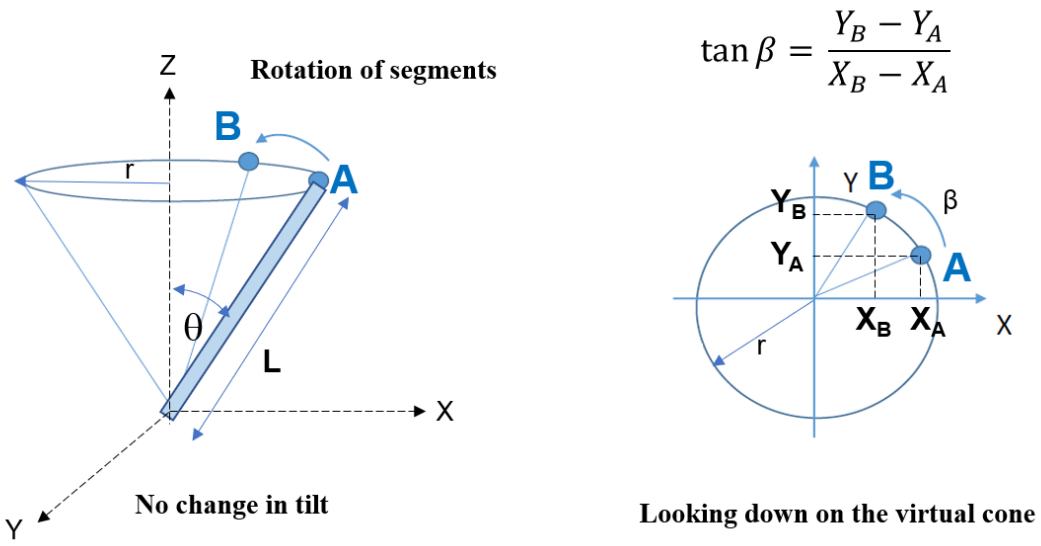

Figure 3. 7 Sketches for rotation error in SAA data (Measurand, 2014)

Rotation error in SAA data is illustrated in Figure 3. 7. For an SAA segment with a given tilt angle, a rotation from point A (X_A, Y_A) to point B (X_B, Y_B) will not change the measured title angle, however, the rotation will introduce apparent displacements in the X and Y directions and cause a change in the recorded deformations.

The SAA manual by Measurand (2013) recommends examining a large group of segments to identify the occurrence of this potential rotation error: showing similar displacements patterns with a positive increment along one axis accompanied to a negative increment in the perpendicular direction.

Reviewing SAA-8003 raw data, a similar pattern is observed in a group of segments near the bottom. This rotation error effect is also embedded in the measurements of the upper segments through cumulative displacement calculation.

Figure 3. 8 shows the rotation error diagnostic for SAA-8003 raw data, over a monitoring period of 600 days, each segment measurements in X and Y directions are compared against the reference readings (e.g. the baseline reading X_0, Y_0), the rotation angle is calculated by the incremental displacements: $\tan\beta = \Delta Y/\Delta X$. The pure rotation of SAA-8003 segment from the bottom (0 m) to the top (43 m) is mainly within ± 5 degrees, except for these white lines representing segments in a very small rotation (e.g. less than 0.35 degree as the resolution of the SAA measurement (Meaurand, 2014)).

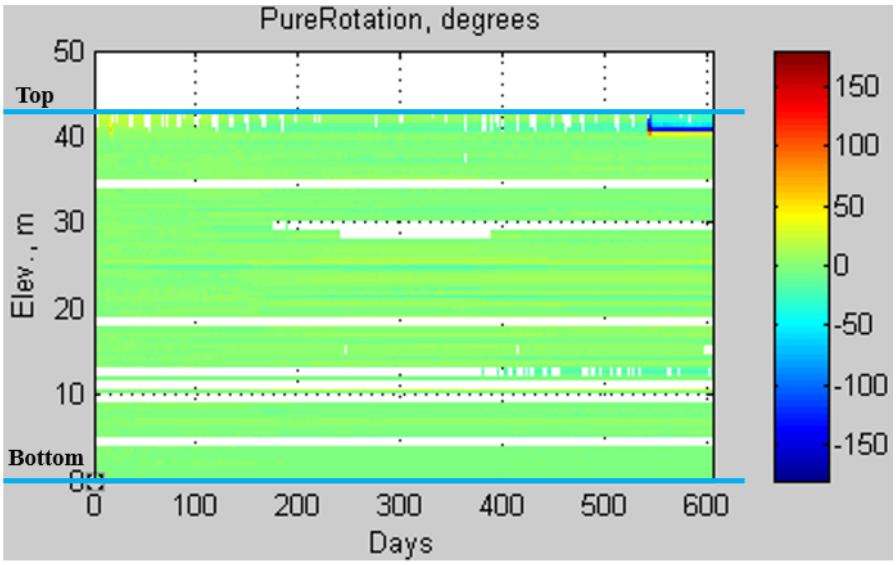

Figure 3. 8 SAA-8003 rotational error diagnostic – pure rotation

SAA-8003 was pre-aligned with the X-axis perpendicular to the retaining wall and the Y-axis parallel to the wall. As an example, the raw data shows apparent wall deformations in the X direction (Figure 3. 9) at 25 m above the bottom, decreasing in some phases over the 600-days monitoring period with the increase in Y measurements. After the anti-rotation correction by dismissing the increments from rotation, the displacement in the X direction slowly increases over the monitoring period, but a small displacement of ±2 mm seemed to have been developed in the Y direction from the correction (Figure 3. 9).

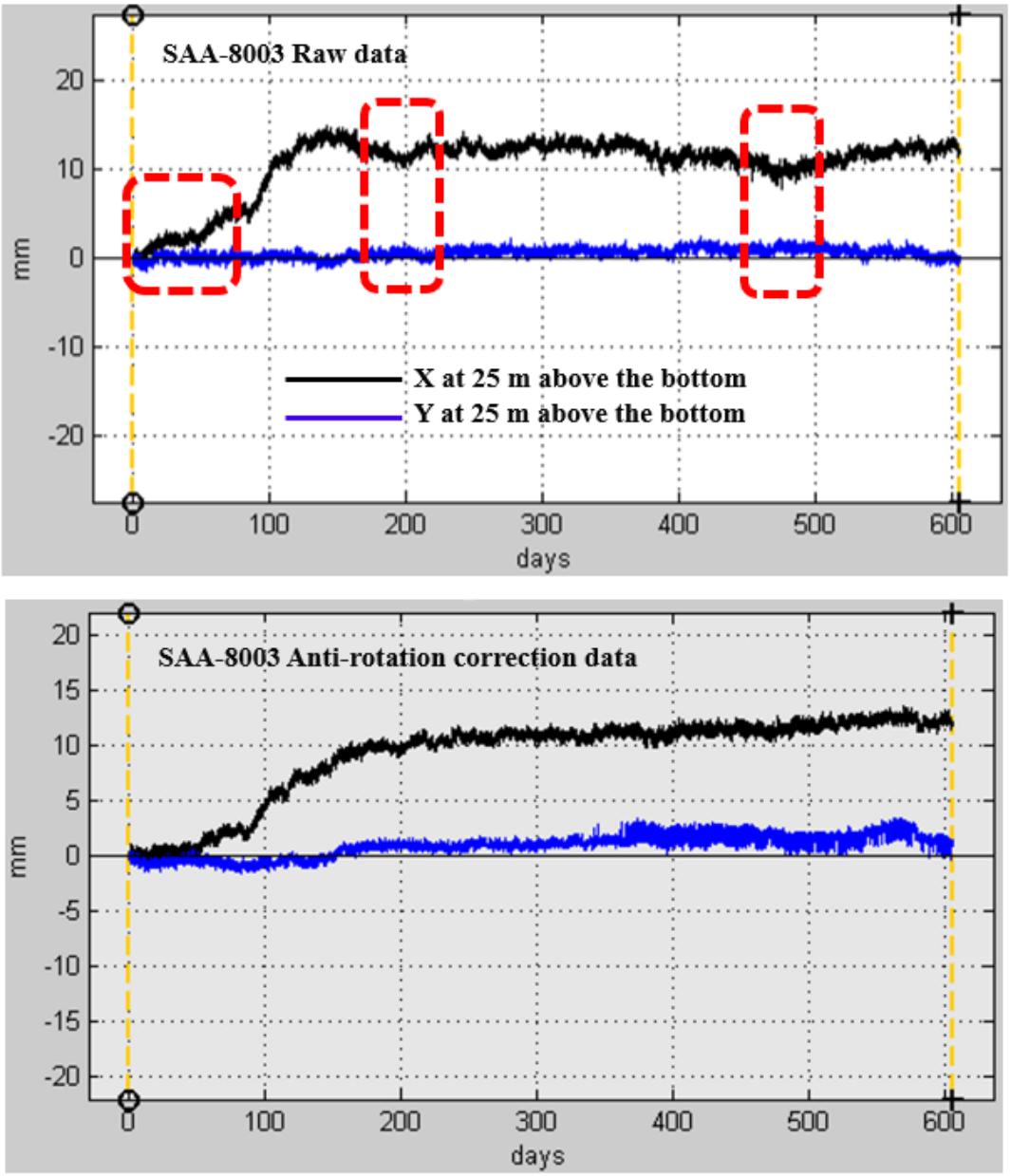

Figure 3. 9 SAA-8003 raw data versus anti-rotational corrected data

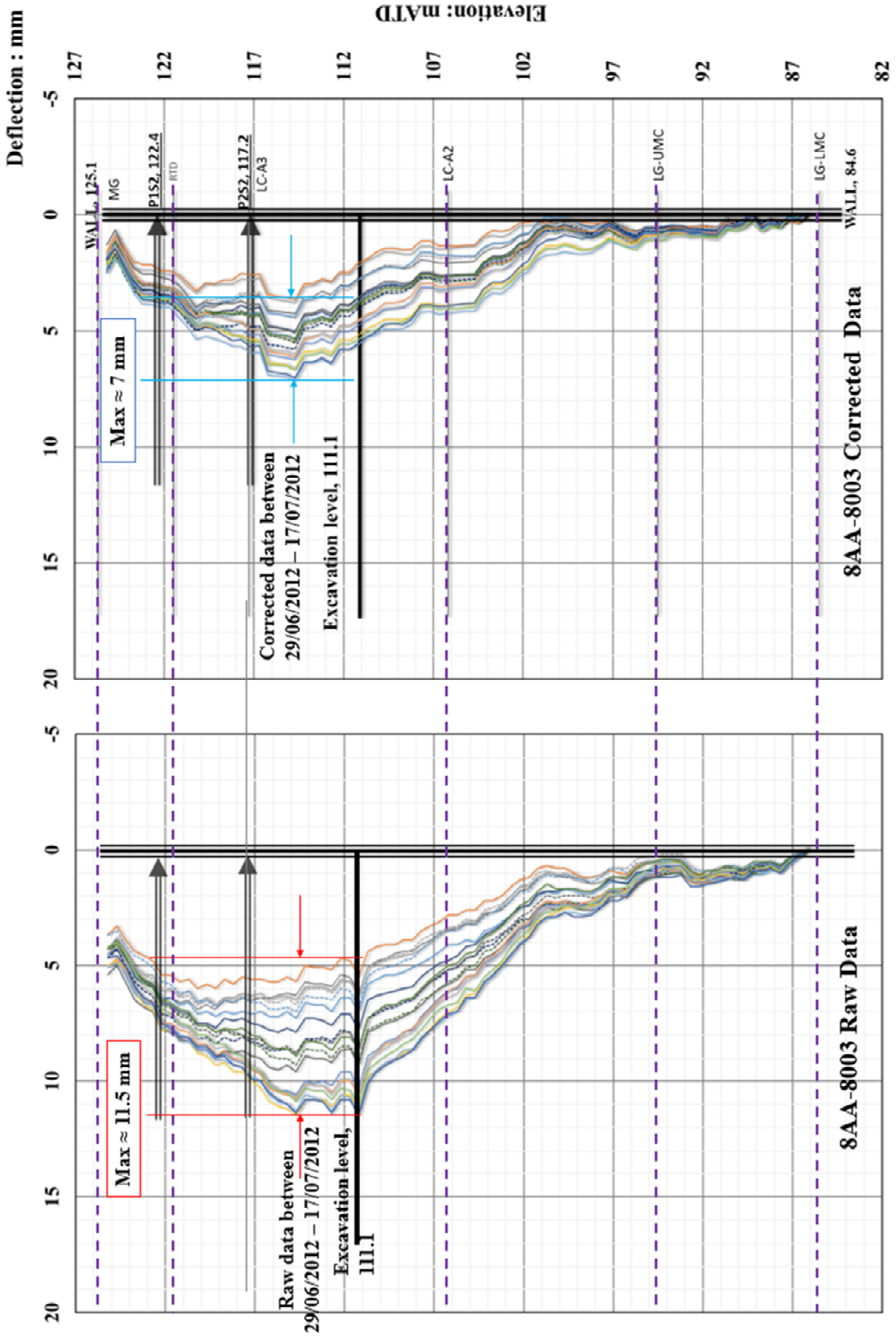

Figure 3. 10 SAA-8003 plot of wall deflection at excavation stage 3: raw data versus the corrected data

The anti-rotation correction changed the maximum wall deflection at each excavation stage and resulted in a significant change in the back-analysis. The comparison of SAA-8003 data at stage 3 is shown in Figure 3. 10, when the maximum wall deflection decreased from 11.5 mm in the raw data to 7 mm in the corrected data.

SAA-8003 data with anti-rotation correction is considered credible for the TCR-WTH box construction, based on the following findings in the corrected data: 1) a negligible (≤ 1.5 mm) wall deformations in the bottom 10 m agree with a fixity assumption at the bottom of the SAA; 2) the confined minimum increments (within 3 mm) at where the props were installed, agree with almost constant values of the strut axial force at corresponding levels.

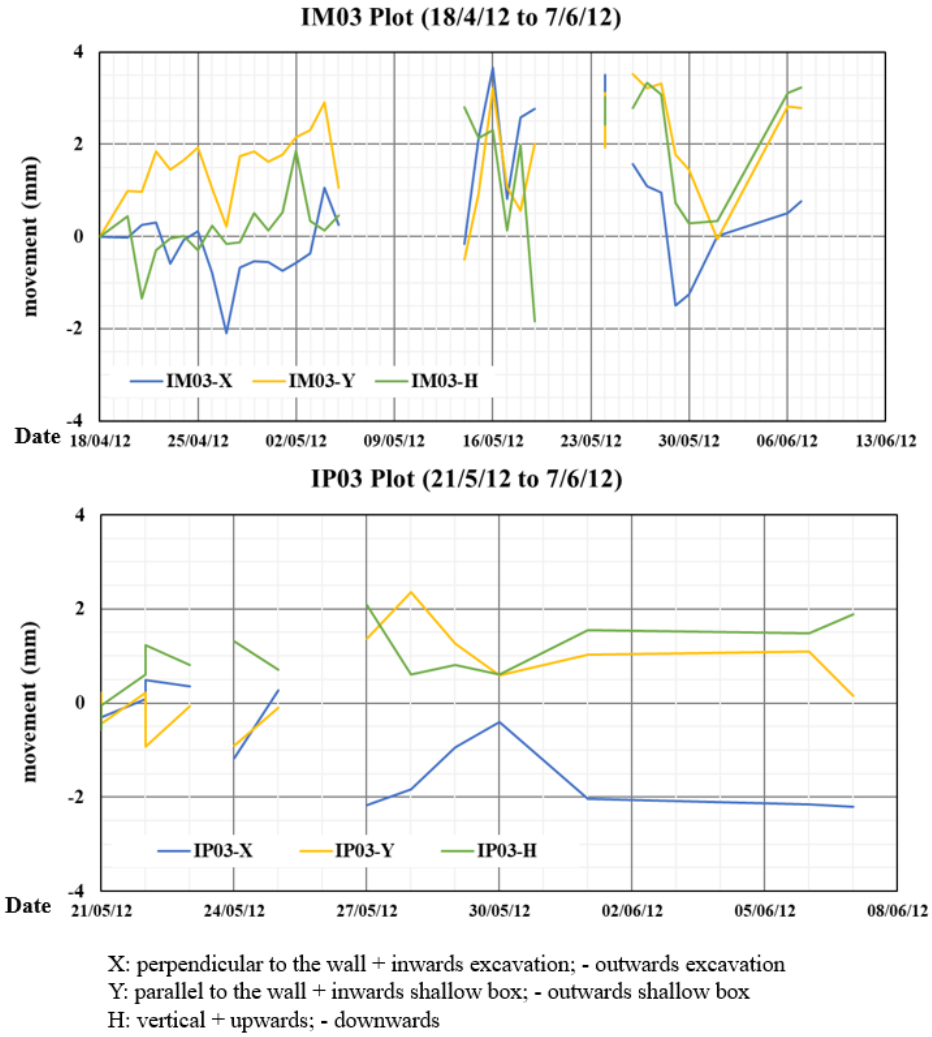

Figure 3. 11 Prism IM03 & IP103 plots over the surveyed period, reproduced after (Crossrail, 2013)

Two prisms (IM03 and IP 103) installed nearby SAA-8003 at the capping beam level (+125.6 mATD) and the 1st prop level (+123.4 mATD) could not be used to calibrate SAA-8003 data at the corresponding levels. This was due to the fact that over the two-month surveyed period between April and June in 2012, readings were taken at a varying frequencies (from daily to weekly), returned almost identical measurements in three directions (horizontal directions: X, Y, and vertical direction: H), as shown in Figure 3. 11. The measurements varied between -2 mm and 4 mm, but the recommended accuracy for the prism by the survey station was about ±2 mm (Hägglund Eriksson, 2014).

3.2.4.2 Review of strain gauge data

Six steel props from each level were selected for monitoring at the TCR-WTH, named as S2, S5, S6, S7, S8 and S11 (Figure 3. 4 & Table 3. 4), for instance, S2 referring to P1S2, P2S2, P3S2 and P4S2 at four levels; they were horizontal props and positioned next to SAA-8003 at the eastern side of the TCR-WTH deep box (Figure 3. 3).

The prop load or the strut axial forces were measured using vibrating wire strain gauges supplied by itmsoil®, installed and monitored by Getech®, with Campbell Scientific model CR1000 data loggers used to record hourly gauge readings.

Three monitoring points consisting of groups of four gauges were positioned at the two ends and the centre of the prop. The four gauges were attached on the surface of the circular prop at the 45° from vertical. This arrangement modified the original plan with gauges positioned at the top, bottom and sides of the prop, in order to eliminate the risk of damage from construction activities.

The prop load was calculated by averaging four strains readings:

$$P = AE\left(\frac{\varepsilon_1+\varepsilon_2+\varepsilon_3+\varepsilon_4}{4}\right) \qquad (3 - 1)$$

$$\Delta\varepsilon = \left(4l^2\frac{m}{EA}\right) \times (\Delta f)^2 \qquad (3 - 2)$$

$\Delta\varepsilon$	change of strain in the wire, in microstrain: μm
Δf	change in the frequency of vibration
E	Young's modulus of prop material: kN/m^2
$4l^2m/EA$	gauge factor, given by the manufacturer, in the unit of 10^{-12} s^2 to give $\Delta\varepsilon$ in microstrain
A	cross-sectional area of the prop

The calculated prop loads for P1S2 from three monitoring points, presented in Figure 3. 12, show the values below the Amber / Red trigger levels accounting for less than 1/3 of the structural capacity of the prop (CHS Ø1016×16t). In addition, thermal effects due to daily and seasonal temperature variations can be observed in the data.

In the post-installation stage, the calculated P1S2 prop loads from the east monitoring point (P_E) were almost twice these from the west (P_W) or the central (P_C) monitoring point. As a straight prop is supported at two ends only, this difference in the prop loads from different monitoring points seemed suspicious.

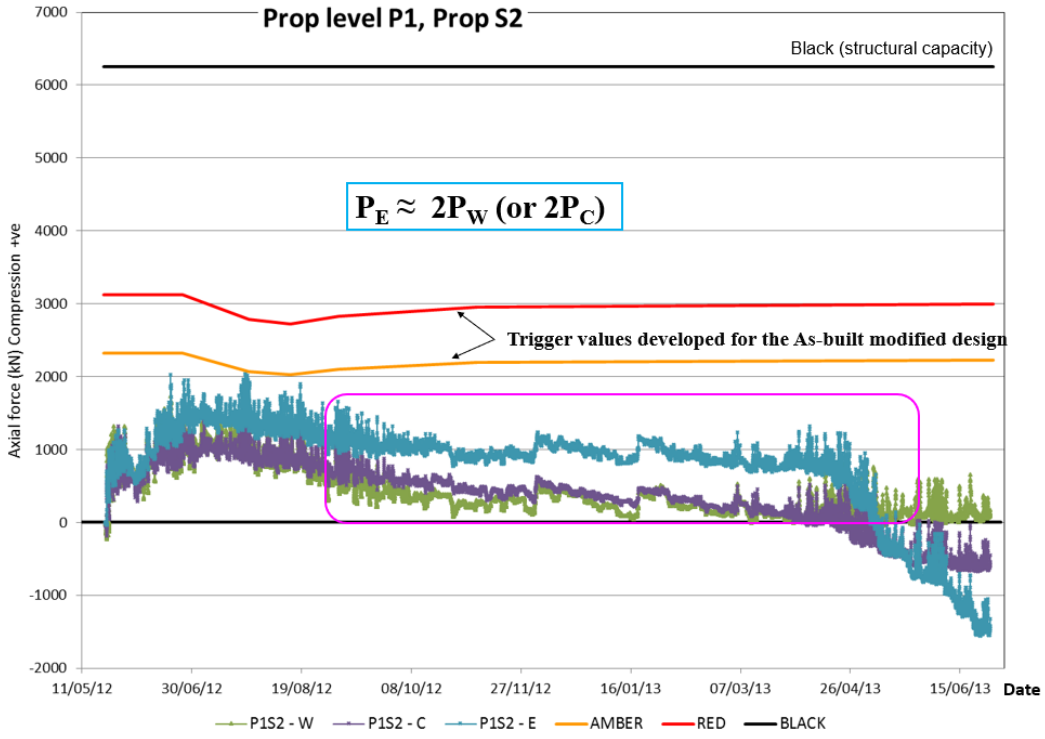

Figure 3. 12 Original P1S2 prop loads (Crossrail, 2013)

The site records suggested a number of reasons which may have caused the faulty interpretation of gauge data and the subsequent calculation of prop loads.

- The bending stress in both horizontal and vertical plane may have occurred in the props, due to the irregular shape of the deep box and the uneven surface of the diaphragm wall;
- Gauges may have been positioned close to the connections to the waler beams where the stress concentration and re-distribution were reported;

- The additional loading may have been introduced from the construction activities during the baseline reading establishment period, such as an uneven excavation sequence;
- The prop load calculation failed to consider the above additional bending stress, furthermore, the modified four gauges positions on the surface of the prop added further inaccuracy in the interpreted prop load.

Some of these circumstances can be seen in the TCR-WTH site photos (Figure 3. 13). It is highly likely biaxial bending stresses were introduced by a combination of one or multiple of factors as suggested by the development of both compressive and tensile strains from four gauges, as shown in Figure 3. 14.

Figure 3. 14 shows the gauge readings at the west monitoring point of P1S2. It is suspicious that the maximum compression (gauge 3) and the maximum tensile (gauge 4) were recorded at the adjacent gauges. Renumbering gauges without changing the strain readings will give a more rational strain development in the adjusted gauges as re-plot in Figure 3. 14.

The strain data for S2 props were reviewed with regards to gauge numbering, and the prop load calculation took the biaxial bending stresses into account, where the maximum strain measured the prop load can be calculated by:

$$\frac{P}{A} + \frac{My}{I} = \sigma_{max} = E\varepsilon_{max} \qquad (3 - 3)$$

$$\frac{P}{A} - \frac{My}{I} = \sigma_{min} = E\varepsilon_{min} \qquad (3 - 4)$$

σ	stress in kN/m^2
ε	strain in microstrain: μm
I	the relevant second moment of the cross-sectional area: m^4
E	Young's modulus of the steel prop kN/m^2
y	the distance to the neutral axis
M	Bending Moment (kNm) in X-axis or Y-axis

A linear increase along the radius direction of the tubular prop cross-section is assumed in order to interpolate the maximum and minimum strain values from four gauge readings, the re-calculated prop loads for P1S2 to P4S2 are presented in Figure 3. 15. The re-calculation results in increased prop loads.

Figure 3. 13 Site photos (a) uneven wall surface; (b) uneven excavation sequence; (c) monitoring point close to the welding sections

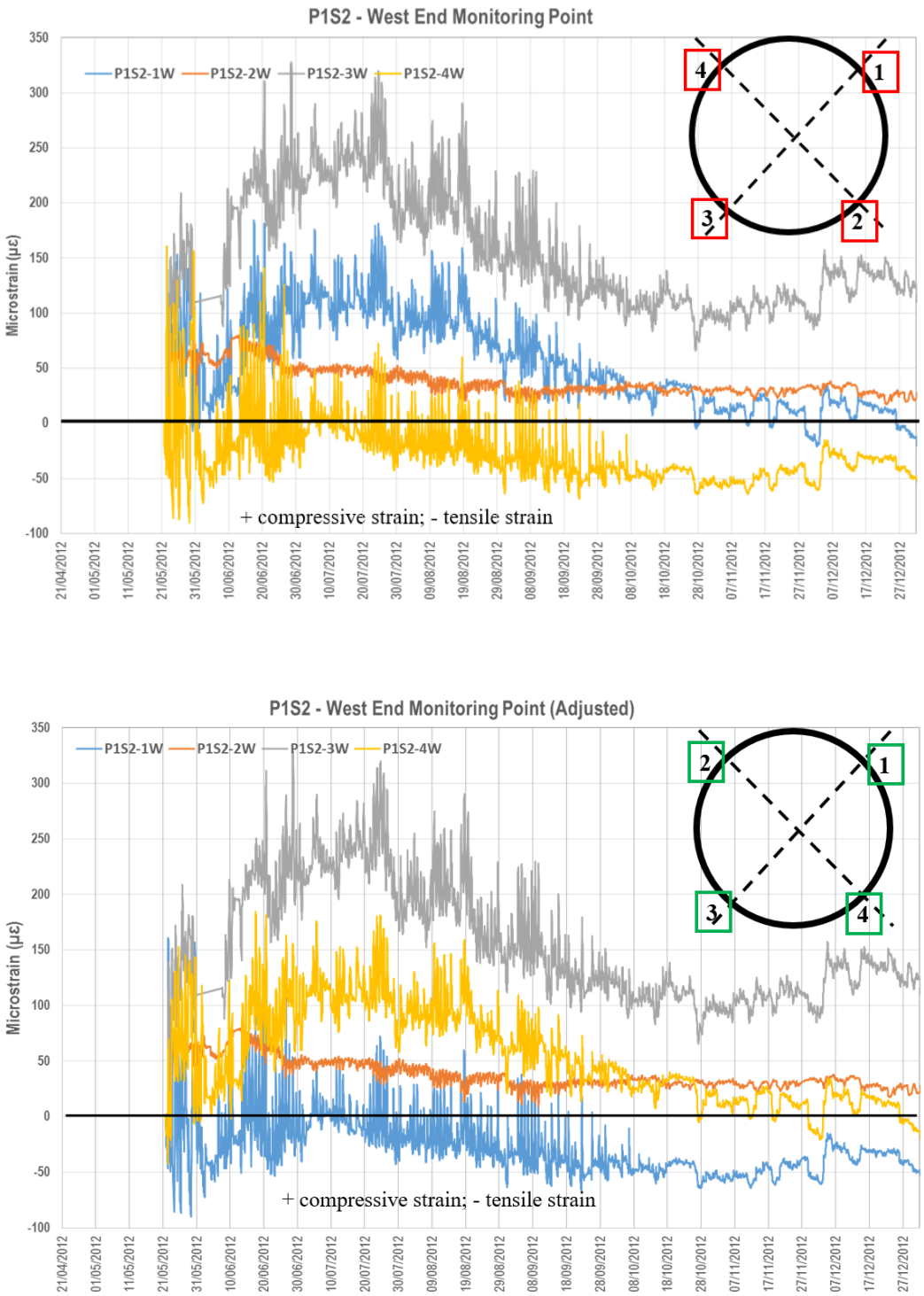

Figure 3. 14 Strain gauge data from the west monitoring point of P1S2: the raw strain data (top); the adjusted strain data (bottom)

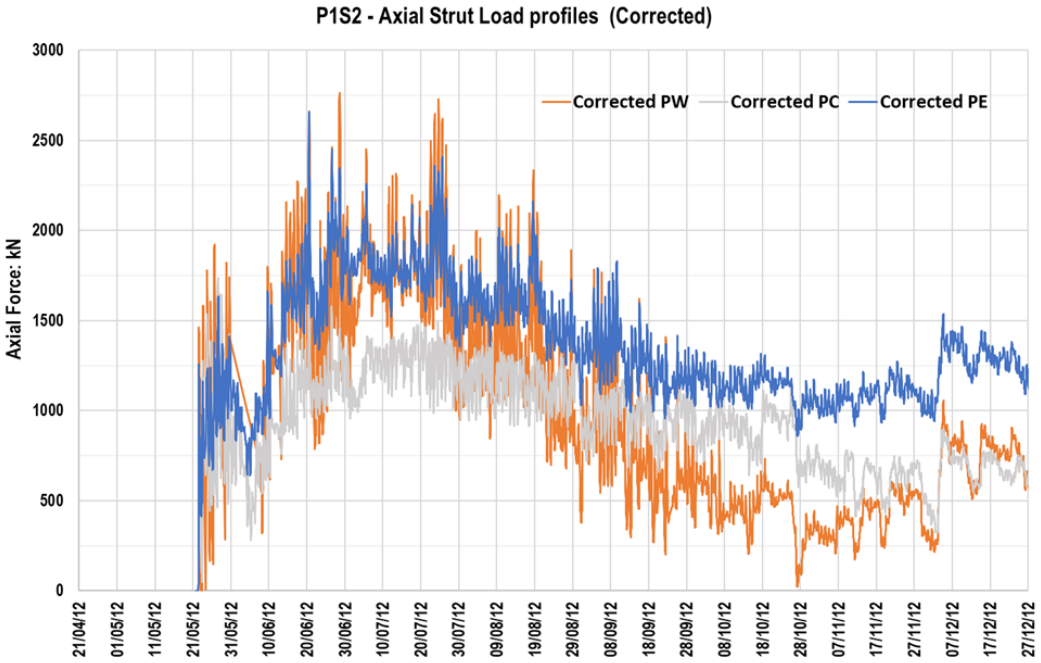
P1S2 - Axial Strut Load profiles (Corrected)
Corrected PW
Corrected PC
Corrected PE
Axial Force: kN
3000
2500
2000
1500
1000
500
0
21/04/12
01/05/12
11/05/12
21/05/12
31/05/12
10/06/12
20/06/12
30/06/12
10/07/12
20/07/12
30/07/12
09/08/12
19/08/12
29/08/12
08/09/12
18/09/12
28/09/12
08/10/12
18/10/12
28/10/12
07/11/12
17/11/12
27/11/12
07/12/12
17/12/12
27/12/12

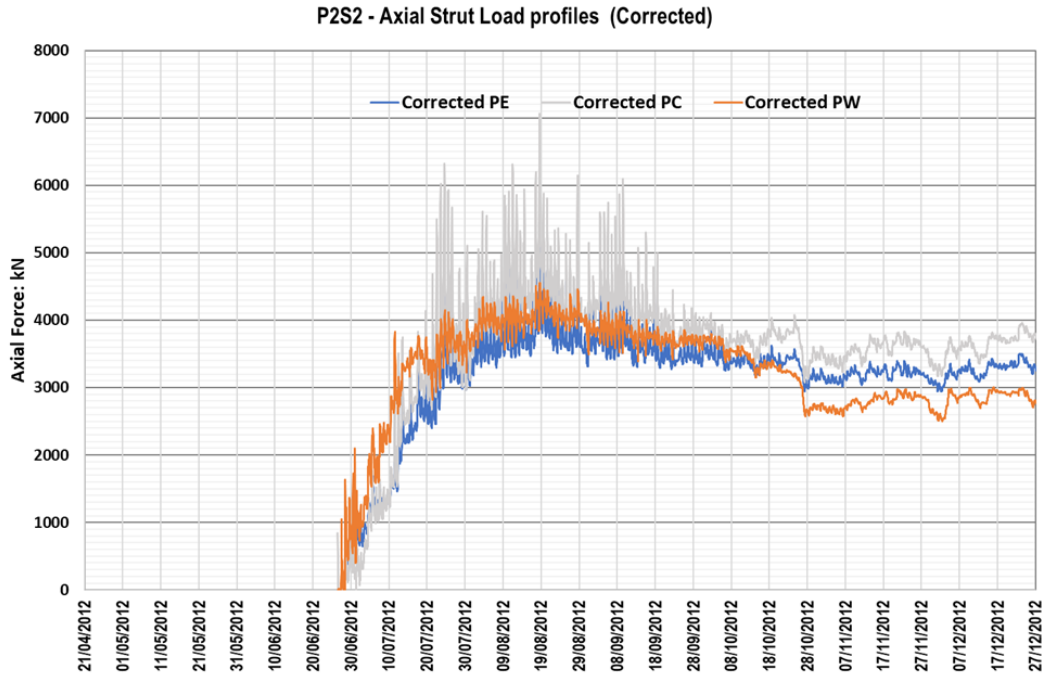
P2S2 - Axial Strut Load profiles (Corrected)
Corrected PE
Corrected PC
Corrected PW
Axial Force: kN
8000
7000
6000
5000
4000
3000
2000
1000
0
21/04/2012
01/05/2012
11/05/2012
21/05/2012
31/05/2012
10/06/2012
20/06/2012
30/06/2012
10/07/2012
20/07/2012
30/07/2012
09/08/2012
19/08/2012
29/08/2012
08/09/2012
18/09/2012
28/09/2012
08/10/2012
18/10/2012
28/10/2012
07/11/2012
17/11/2012
27/11/2012
07/12/2012
17/12/2012
27/12/2012

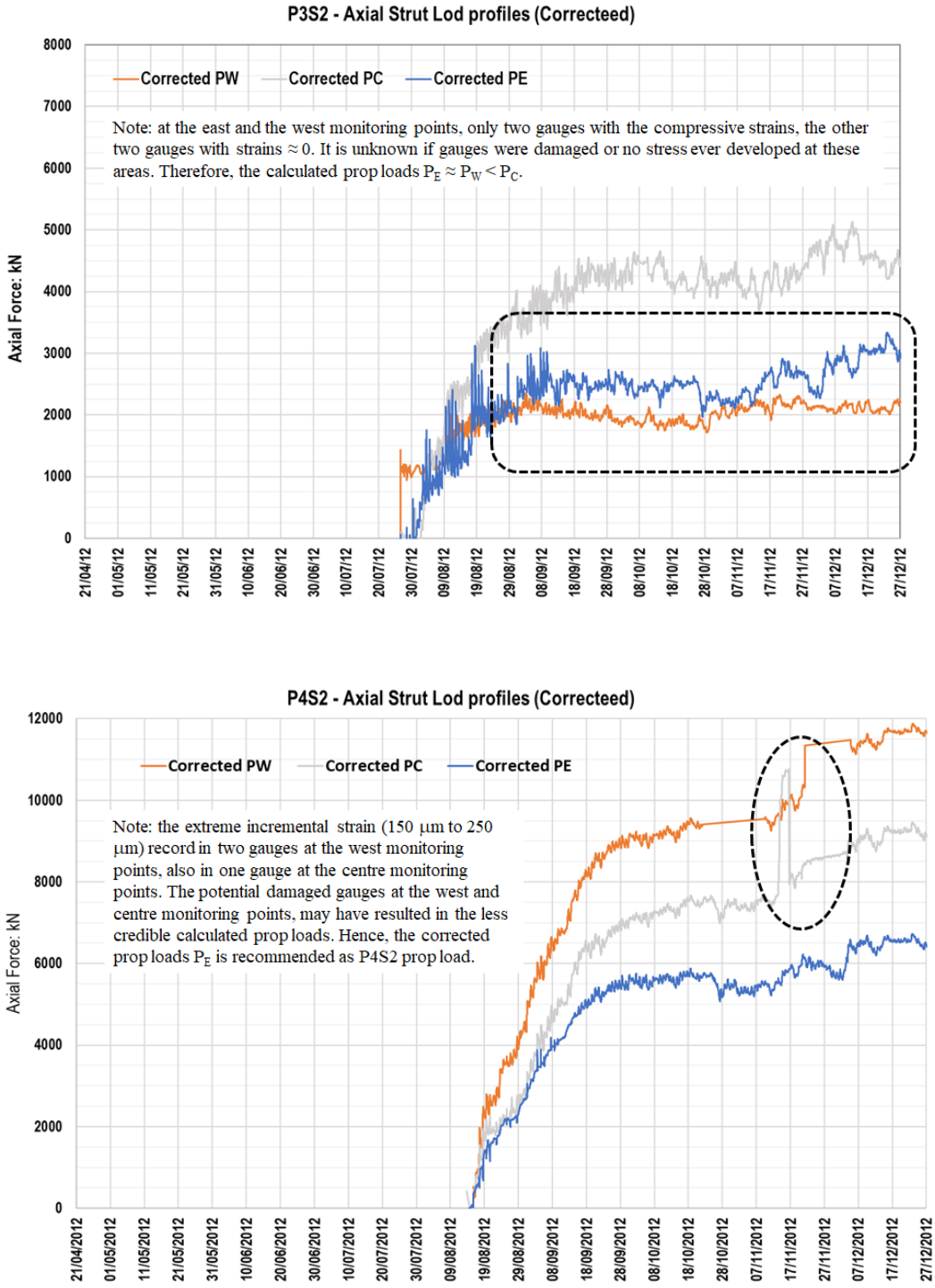

Figure 3. 15 The corrected prop loads for S2 props: P1S2, P2S2, P3S2, P4S2

Meanwhile, the damaged or deactivated gauges and the abnormal strains were identified. For instance, constant strain readings ($\varepsilon \approx 0$ μm) from gauges indicate these gauges might have been deactivated or damaged. If these strains were accounted in the prop load calculation, the smaller loads are expected (e.g. P2S3 in Figure 3. 15). Abnormal incremental strains ($\Delta\varepsilon \approx 150$ to 250μm) were found in a number of gauges' readings at the west and the centre monitoring points for P4S2. As a consequence, the sharp increase in prop loads was calculated for the west (P_W) and the centre (P_C) point (Figure 3. 15).

Although the difference in the re-calculated prop loads between the three monitoring points has decreased, the correction did not fully eliminate the difference.

A correction for thermal effects was attempted, but was not very successful, because of randomly missing data - from a couple of hourly readings to a few days' readings, and the extreme strains were recorded in the dataset.

3.2.4.3 Review of extensometer data

Two magnetic extensometers (XM80001/XM80002) were paired with two piezometers (PV80001/PV80002) and installed within the TCR-WTH deep box (Figure 3. 4). The vertical displacements at a series of levels were surveyed during excavation, as presented in Figure 3. 16.

In these plots, the upwards displacement is recorded as heave (+), and the downwards displacement is recorded as settlement (-). The weekly extensometer readings frequency is considered insufficient compared to the relatively fast excavation progress of the TCR-WTH deep box. The extreme incremental displacements are observed from the 2nd magnet of the XM80002 (from -10 mm to +5 mm), which could have affected the cumulative vertical displacements from the upper magnets.

It is difficult to correct the extensometer data after the instruments have been decommissioned, hence, no correction is made for the extensometer measurements. For future extensometer monitoring, it is recommended to include one or more cross-reference readings to verify the extensometer reading. For instance, surveying the top of the casing each time if the case is trimmed, will verify the repositioning of the casing.

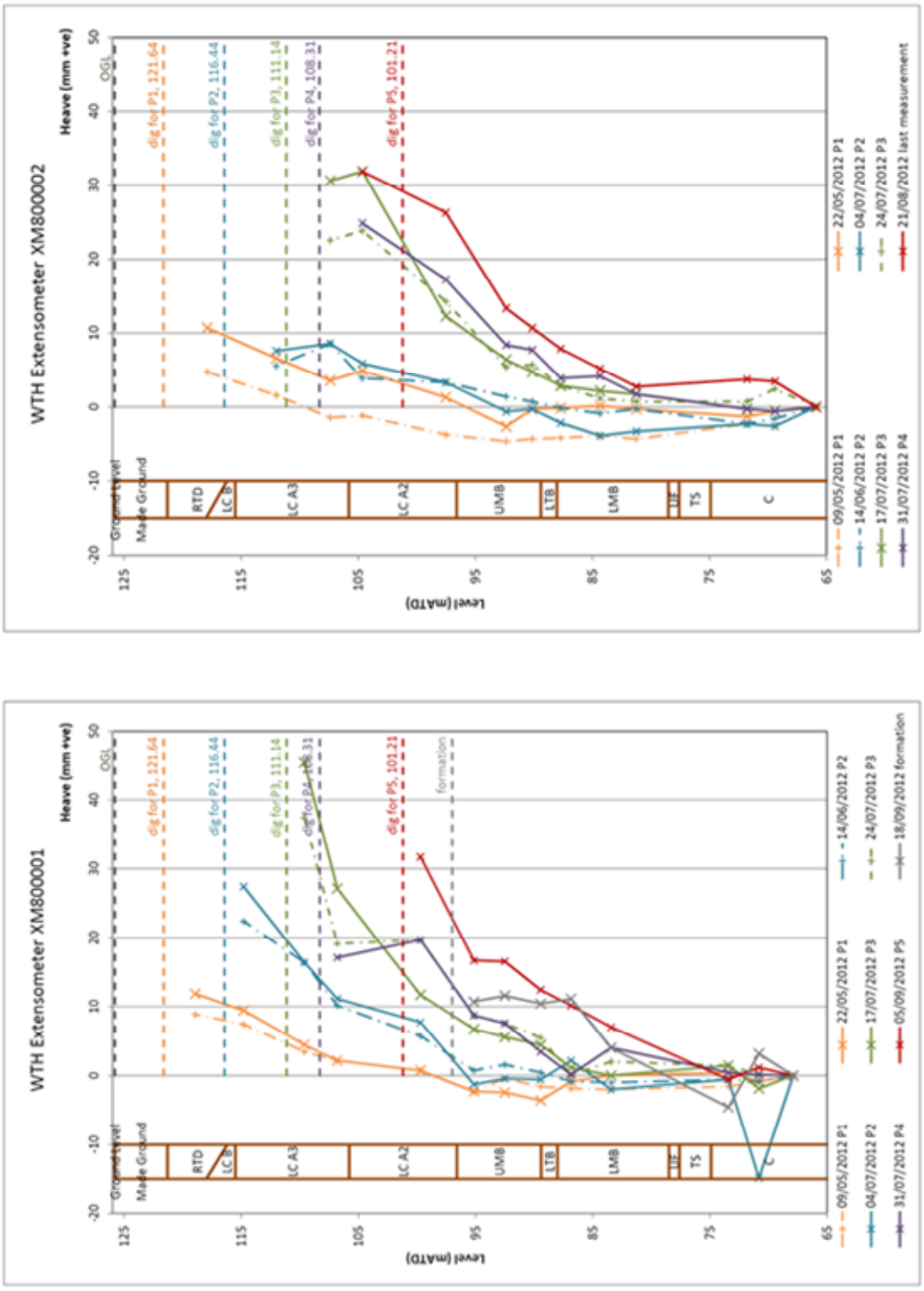

Figure 3. 16 Vertical displacements: XM8001 & XM8002 raw data (Crossrail, 2013)

3.2.4.4 Review of piezometer data

Three vibrating wire piezometers were installed inside the TCR-WTH deep box to monitor the change of pore-water pressure during excavation (Figure 3. 4). Two-levels vibrating wire piezometers PV80001 and PV80002 were installed using the fully grouted method, the single level piezometer PV8003 was not planned initially but installed as a supplement during excavation. The as-installed piezometer details are summarised in Table 3. 5. Readings from three piezometers are presented in Figure 3. 17.

Table 3. 5 Summary of as-installed piezometers for the TCR-WTH deep box excavation (Crossrail, 2012)

Piezometer	Coordination		Top (m ATD)	Depth (m)	Tip level (m ATD)	Installed date
	E	N				
PV80001A	79913.64	36031.64	124.74	29.2	95.54	13/03/2012 (fully grouted)
PV80001B				34.7	90.04	
PV80002A	79909.97	36042.97	125.97	30.5	95.47	09/03/2012 (fully grouted)
PV80002B				36.0	89.97	
PV80003	-	-	121.40	21.0	100.40	15/05/2012 (backfilled)

From the review of the monitored groundwater level from three piezometers (Figure 3. 17), it was found that the measured water levels from PV80003 were synchronized to the progressed excavated level. It is likely a connection to the surface water flow may have been established since the installation.

When piezometer is used to monitor the under drained groundwater pressure, like the one in London Clay & Lambeth Group at the TCR-WTH site, it is important to allow sufficient time for piezometers to reach the equilibrium pressure before other construction activities, such as excavation. A 30-day period is recommended as piezometers equilibrium time in London Clay by Wan and Standing (2014a).

However, it seemed PV80001 (A&B) and PV80002 (A&B) took more than 75 days reaching a stable water level (Figure 3. 17), while excavation forming the piling platform proceeded during the first 30-days and excavation continued afterwards. It was considered this prolonged 75 days piezometer pressure equilibrium time was due to the unloading excavation impact.

Moreover, PV80002B showed the erratic data from day 75 to day 160 days after the installation, including a 30-days (from day 109 to 139) interruption period without readings. A rising water level was recorded shortly after PV80002B reading was resumed, while the excavation was continuing. Following PV80002B, PV80002A also showed the rising water level, which indicated that an inner water flow connectivity might have been formed between these two sensors.

It was concluded that PV80002 (A&B) and PV8003 data were affected by poor installation, only PV80001 (A&B) data was considered suitable for further data processing. The processed PV80001 (A&B) data is presented in Figure 3. 18: 1) pore water pressure; and 2) the change of pore water pressure (excess pore water pressure: + suction).

Figure 3. 18 shows PV80001(A) at the level of +95.5 mATD with an approximate 187 kPa equilibrium pore water pressure at the stabilised water level. In addition, a decrease of 10 kPa in the equilibrium pore water pressure is observed in PV80001A (around day 90), which coincidentally took place during stage 2 excavation to level +116.2 mATD.

The change of pore water pressure compares the measured pore water pressure against the known or assumed initial in-situ pressure, the value zero indicates where equilibrium is reached. The change of pore water pressure for PV80001A&B was presented by changed pressure versus square root of time in hours in Figure 3. 18. As the initial pore pressure of 160 kPa (Figure 3. 2) was assumed for PV80001A at +90.04 mATD, a positive changed pressure of 37 kPa was derived at the stabilised water level, and no suction (negative changed pressure) was calculated at the final excavation stage. The same initial pore pressure of 160 kPa was assumed for PV80001B at +95.54 mATD, a small suction (-15 kPa) was derived at the final excavation stage.

Wan & Standing (2014a) recommended a linear response of pore water pressure dissipation during the first 50% of the equilibration period, in which the time unit is in square root of hours. An attempt to interpret the initial in-situ pore water pressure for PV80001A&B was made and derived 125 kPa for PV8001B at +95.54 mATD and 72.5 kPa for PV80001A at +90.04 mATD, as shown in Figure 3. 18.

The re-processed PV80001 (A&B) data by the updated ‘initial pore water pressure’ is presented in Figure 3. 19. With this correction, a constant 50 kPa pressure difference is shown between PV8001A & B; the decreasing in pressure matches with excavation progress.

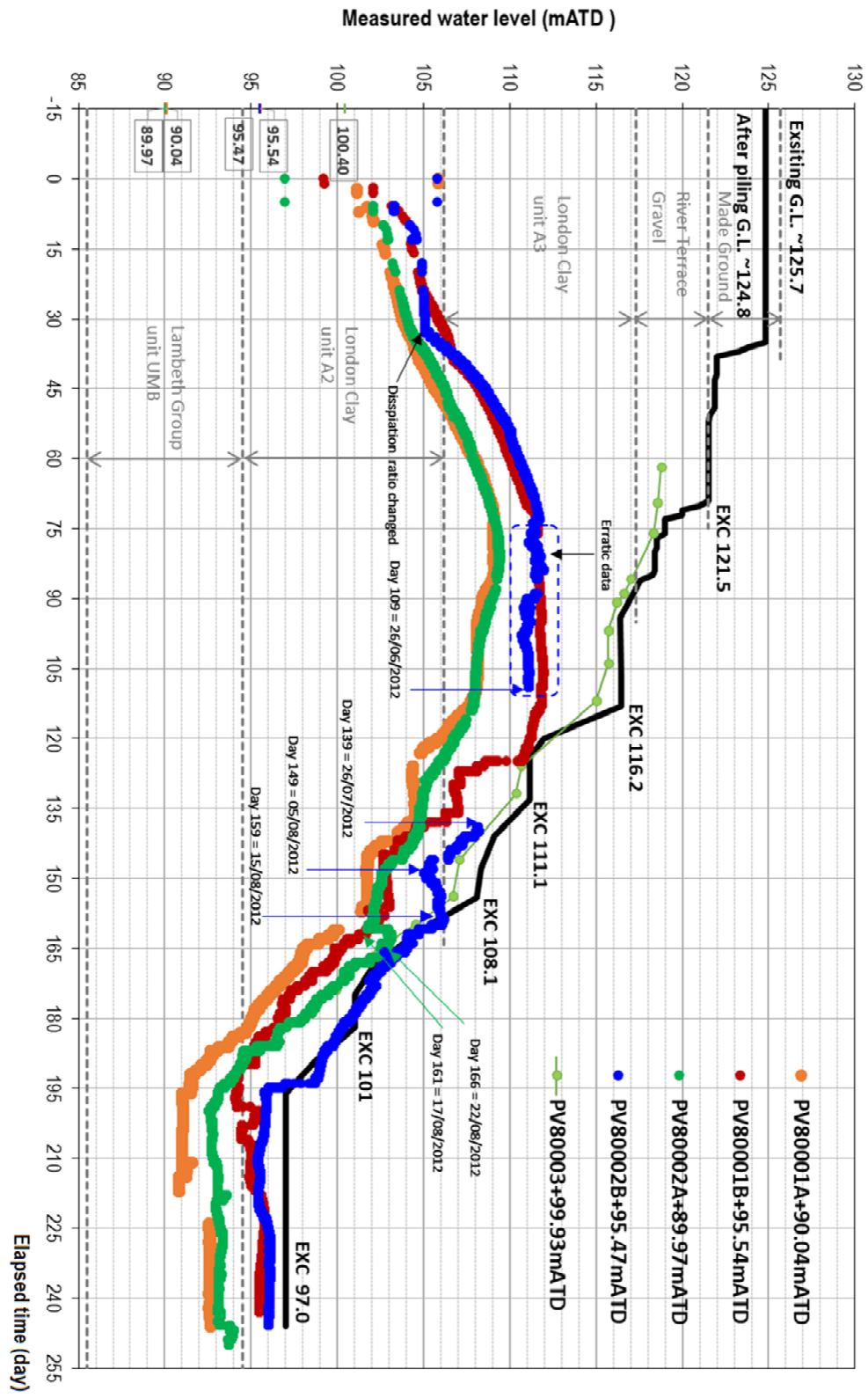

Figure 3. 17 Groundwater levels: PV80001, 80002 & 8003 (Crossrail, 2013)

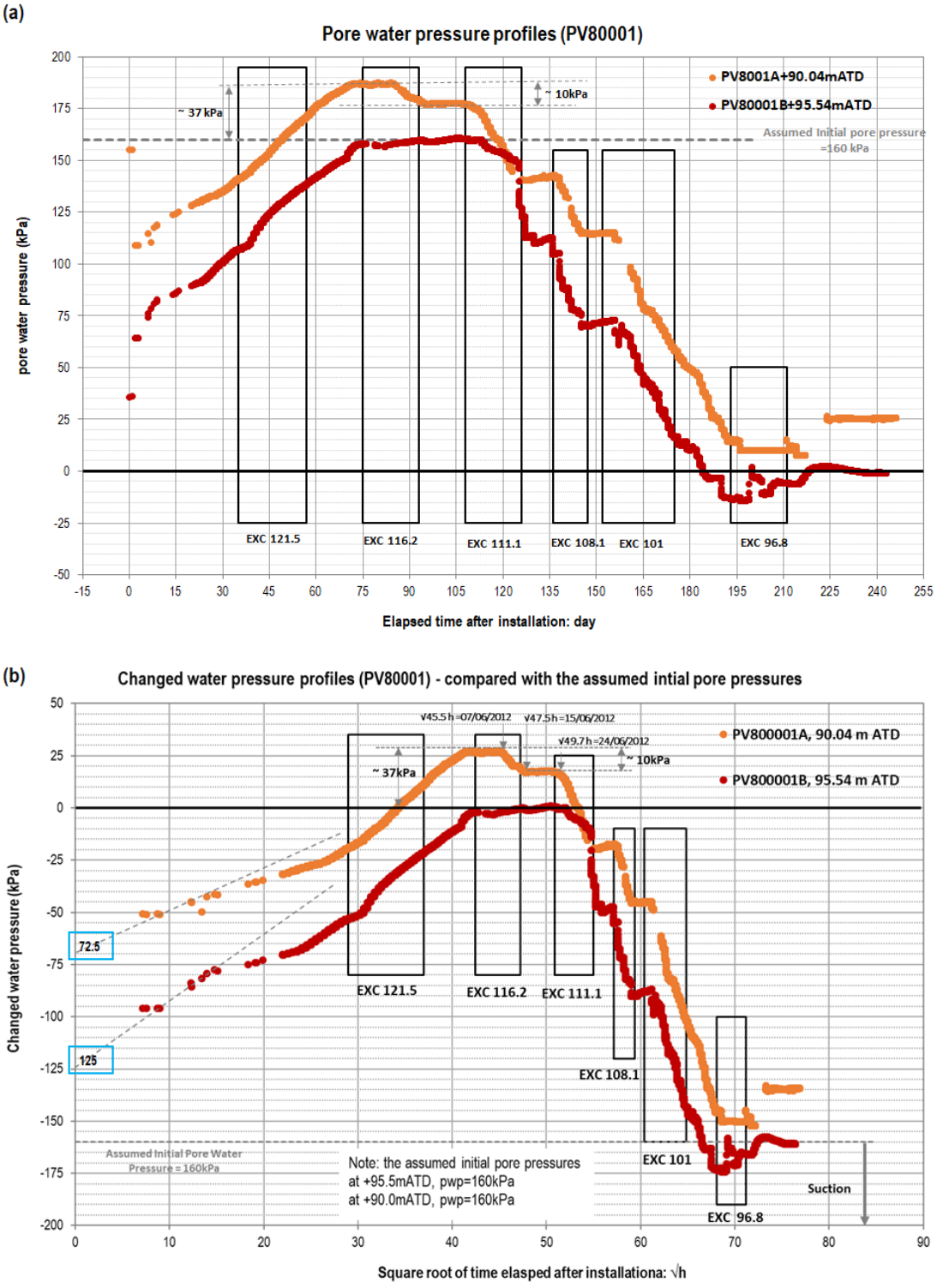

Figure 3. 18 PV80001 data (a) pore water pressure; (b) changed pore water pressure

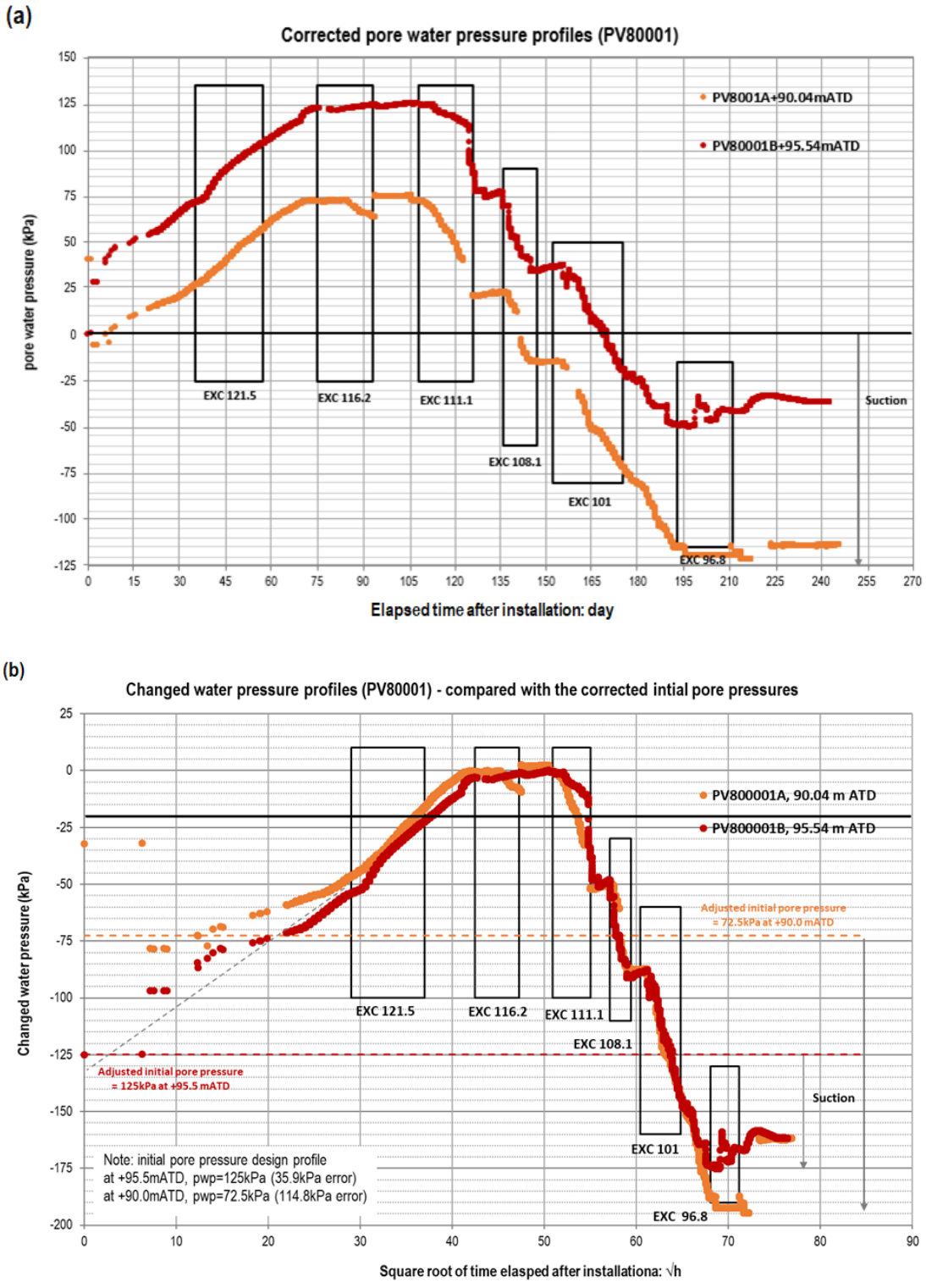

Figure 3. 19 PV80001 data (a) corrected pore water pressure; (b) corrected changed pore water pressure

In addition, a significant suction (negative changed pressure) over 125 kPa is also derived by re-processed PV80001B data. At the final excavation stage, this higher suction pressure beneath the excavation level would explain the relatively small vertical displacements measured by extensometers.

The suction induced by unloading excavation is reviewed with an empirical correlation by Skempton (1954), which recommended that the suction is in proportional to the total unloading stress:

$$\Delta u = \bar{B} \times \Delta\sigma_v \qquad (3 - 5)$$

Δu	suction, change of pore water pressure: kPa
$\Delta\sigma_v$	change of total stress for unloading: kPa
$\bar{B}$	the overall pore pressure coefficient, 0.73 for sandy-clay and a range of 0.50 to 0.62 for clay-gravel (Bishop, 1954).

The raw data of PV80001A and PV80001B calculated the $\bar{B}$ values of 0 and 0.05, whilst the re-processed data calculated the $\bar{B}$ values of 0.18 and 0.45. Although these $\bar{B}$ values from the re-processed data are lower than the recommendation for clay, it is an improvement compared to the raw data. The other factors, such as poor installation may have a built-in impact on the piezometer data, and without details of instrument calibration and installation, the further corrections are not possible (Wan, 2017).

3.2.4.5 Review of levelling studs' data

The levelling studs installed along Dean Street at a distance of 8.5 m to 9.0 m from the outline of the TCR-WTH box are shown in Figure 3. 5. The studs ID and readings over the monitoring period between 25/02/2012 (start) and 09/11/2012 (post-excavation period) are presented in Figure 3. 20. The baseline reading for the ground settlement was established over a two-month period. Vertical displacements gradually increased downwards (settlement records as -) with the excavation progress. The frequency of the readings varied from daily to weekly. The accuracy of the levelling studs is low, greater than ±1 mm, depending on digital levels and levelling stations applied (BRE, 1993). The accuracy of levelling studs in the filed is also subjected to external factors, such as climate, obstacles on the surveying route, and damage to the equipment. Particularly for excavations in urban areas, the congestion of the site inadvertently decreases the accuracy of precise levelling.

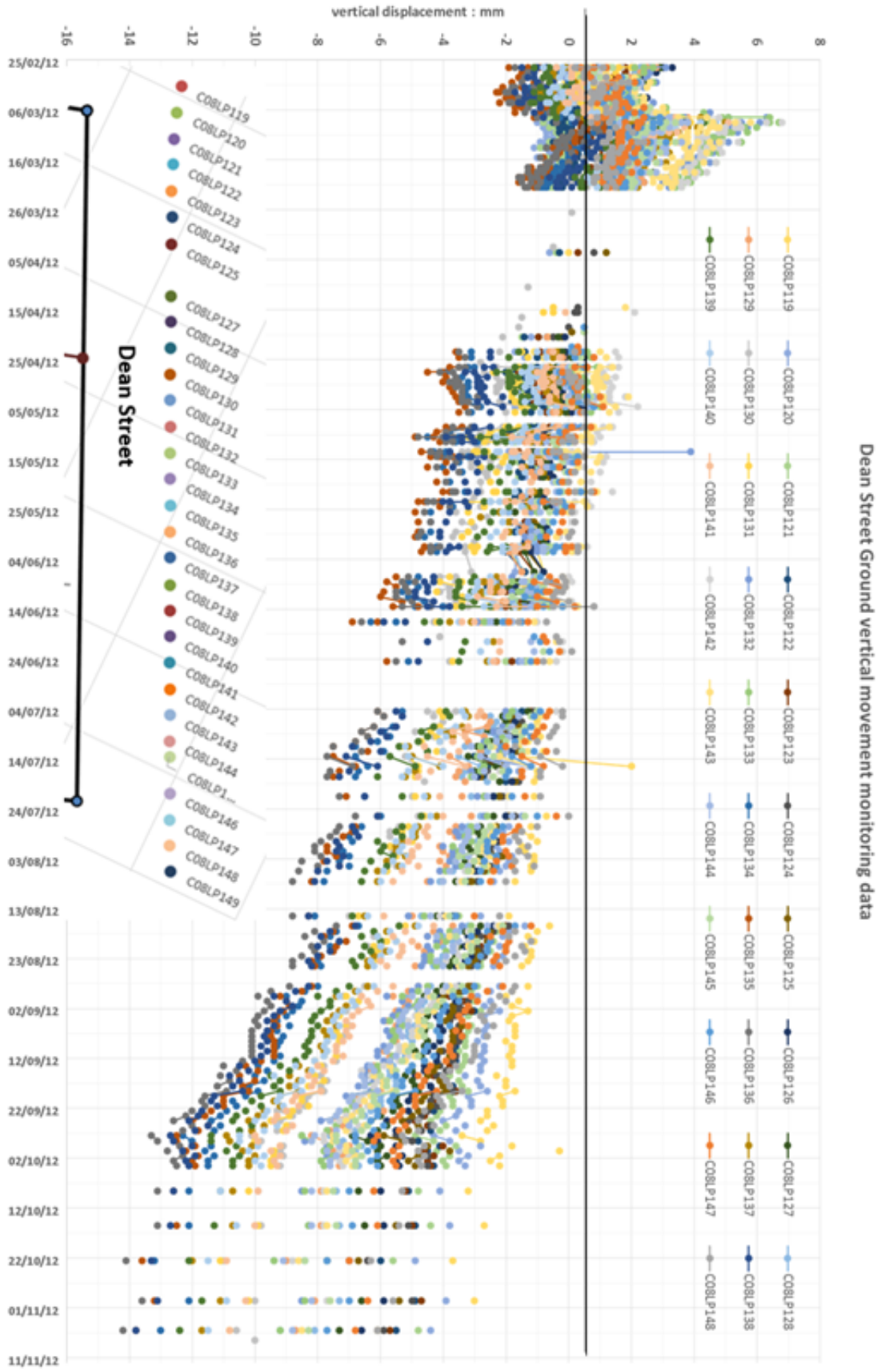

Figure 3. 20 Dean Street ground settlements between 25/02/2012 and 09/11/2012, reproduced from (Bologna, 2017)

3.3 Liverpool Street Station, Moorgate Shaft

3.3.1 Introduction

The Crossrail Liverpool Street station, Moorgate Shaft (LIS-MS) is located between Moorefields and Moorgate, at the western end of Finsbury Circus, as shown in Figure 3. 21. Below the ground level, this new shaft is surrounded by London Underground railway lines: Northern, Central, Metropolitan, Circle / Hammersmith & City lines, as demonstrated in the 3D model in Figure 3. 22. The top-down construction method was applied in this project, one of the deepest shafts for Crossrail, at one of the most constrained urban sites. Limitation of deformations to protect nearby assets, rather than strength, governed the design of the shaft.

The shaft design was carried out by Mott MacDonald and the construction work was awarded to a BAM/Nuttall/Kier joint venture (BNKJV). Intensive monitoring was performed during the shaft excavation and the TBMs tunnelling works.

3.3.2 Original design

The octagonal-shaped shaft is about 35 m by 35 m, with a maximum excavation depth of about 40 m from the ground level (+110 mATD), as shown in Figure 3. 21. The shaft is formed by a 1.2 m thick diaphragm wall with a depth of about 52 m. Lateral support is provided by a series of ring beams forming the top-down excavation sequence. In the East-West direction, two cross-walls act as props for the lower levels during excavation. The initial design included two levels of temporary props below the lowest ring beams (RBs), which were removed after the installation of the base slab.

The ground model used in the original design referenced the geotechnical design summary report (GDSR) for the Crossrail LIS (Crossrail, 2011b), and summarised in Table 3. 6. The geotechnical design parameters applied in the original design are summarised in Table 3. 6. The pore water pressure design profiles considered the under drained profile for the impermeable London Clay and Lambeth Group, and the drained hydrostatic profile for the lower aquifer. The proposed under drained pore water pressure design profile for the serviceability limit status analysis (SLS) is shown in Figure 3. 23.

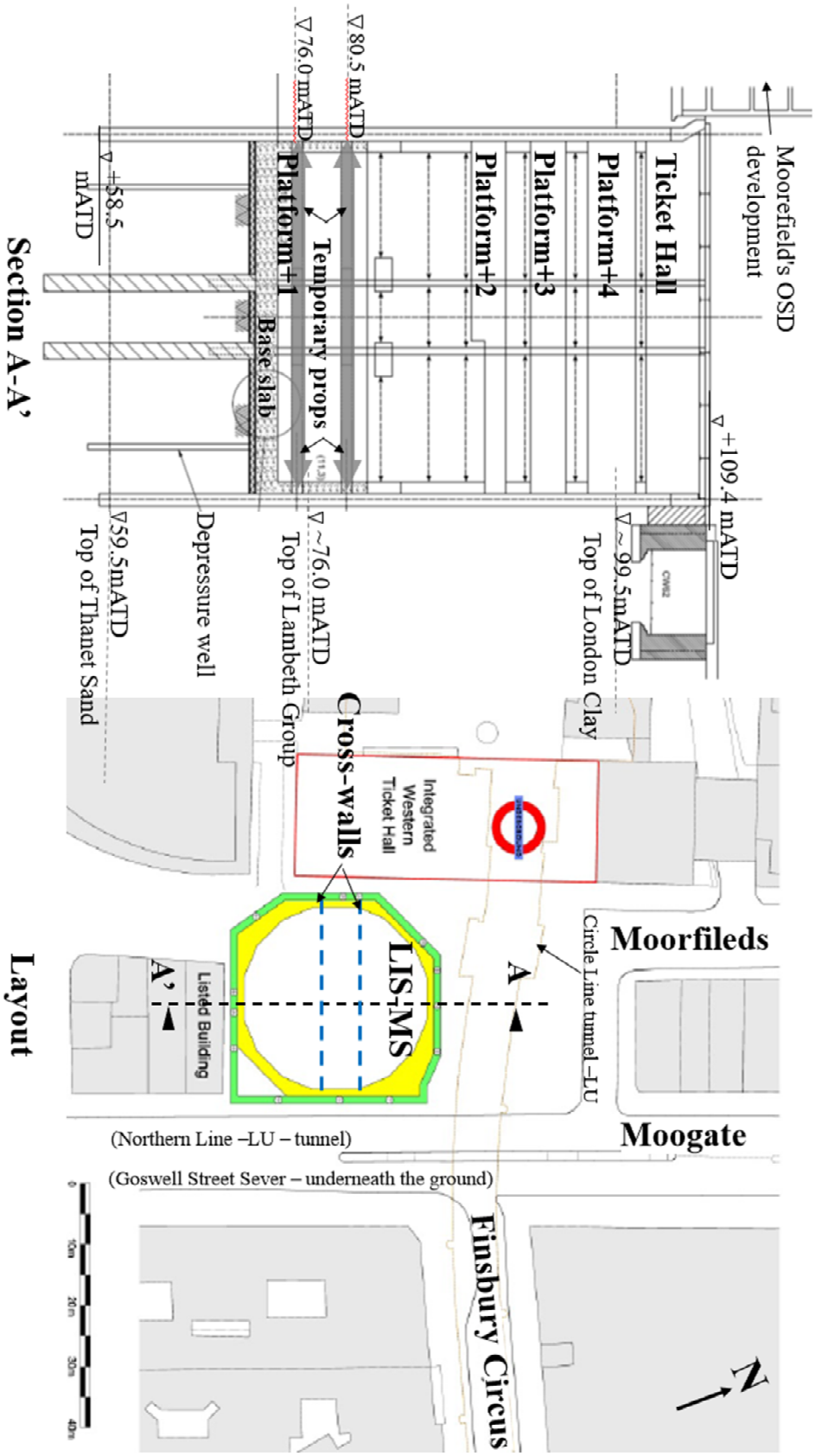

Figure 3. 21 LIS-MS layout plan and section A-A' (north-south), after (Farooq *et al.*, 2015)

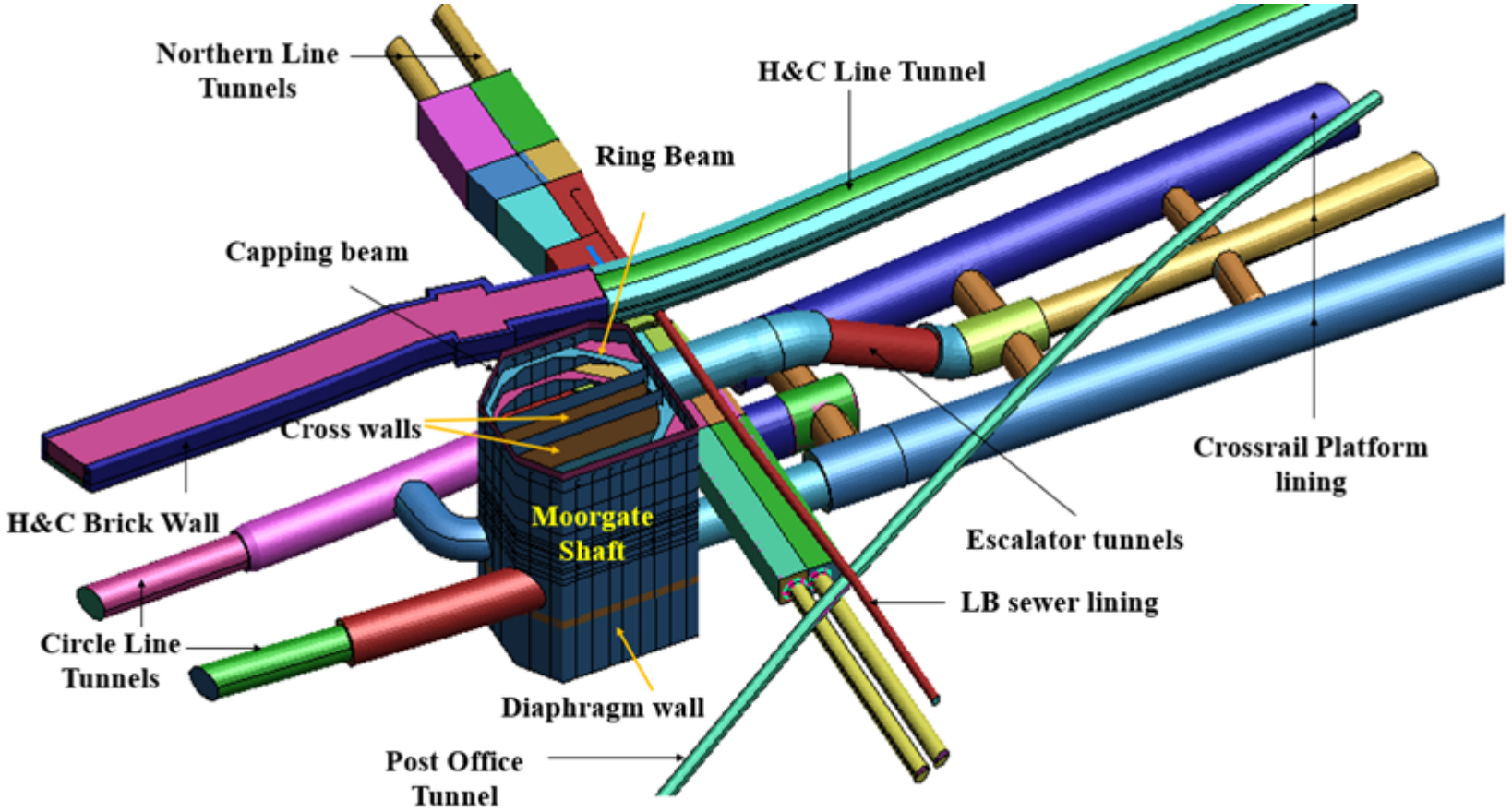

Figure 3. 22 LS-Dyna 3D model for LIS-MS (Chen *et al.*, 2018)

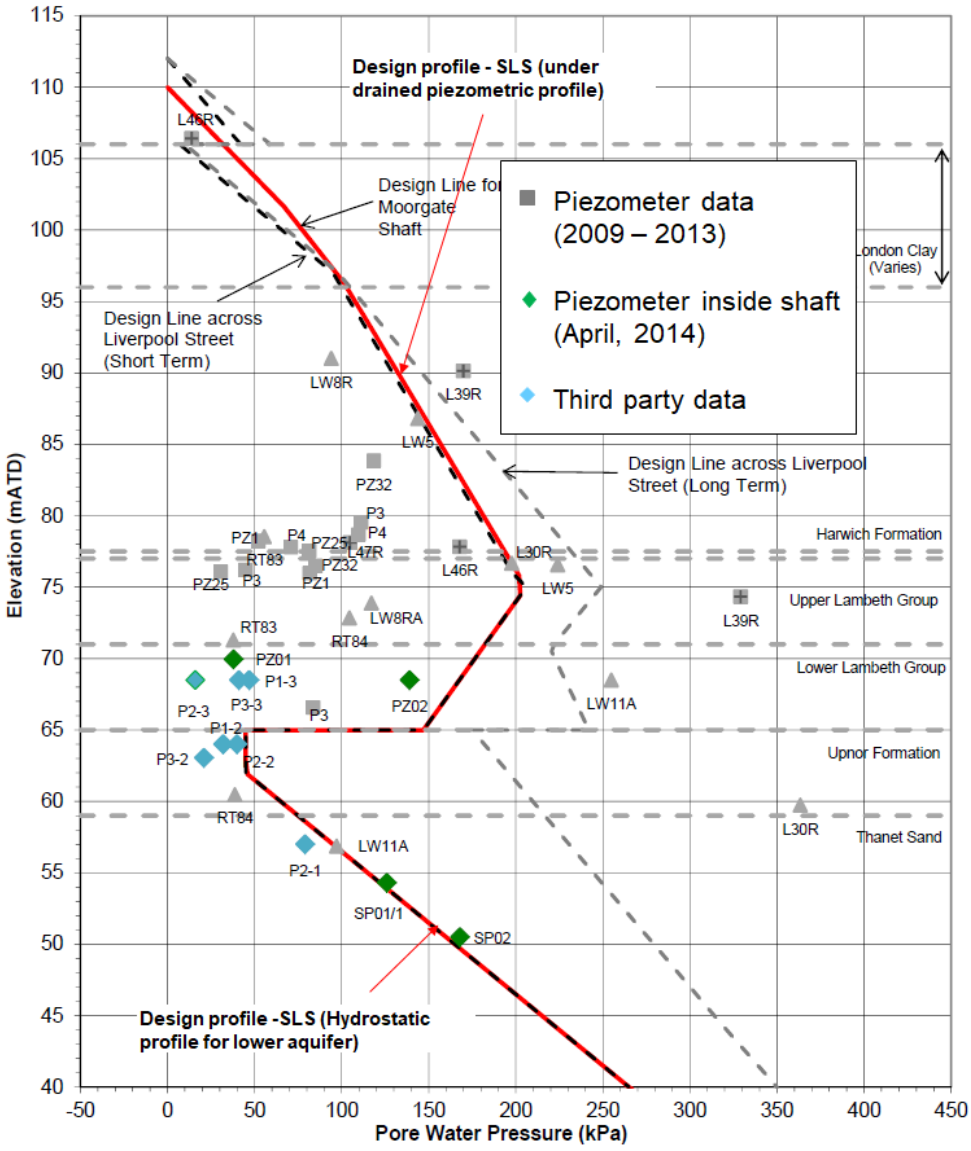

Figure 3. 23 Pore water pressure design profile for the LIS-MS design (Crossrail, 2014b)

The finite element numerical analysis with Plaxis 2D using the Mohr-Coulomb soil model was undertaken to develop the original design. In addition, an Oasys LS-Dyna® 3D finite element analysis using the BRICK soil constitutive model was also carried out to estimate ground movements for asset protection assessments due to the Crossrail tunnelling and the shaft excavation works (Crossrail, 2007b).

The LIS-MS shaft structure design complied with the CEDS, with the following major design requirements, as referred to in the GDSR (Crossrail, 2011b) for the LIS-MS:

- Mixed earth pressure analysis was assumed for the short-term ULS design - where total stress (undrained) were calculated at the passive side, and effective stresses (drained) were calculated at the active side;
- A 0.5 m over-dig was included in the ULS analysis;
- A 0.5 m softening depth on the passive side below the excavation level was considered in the ULS analysis when total stress (undrained) calculation was assumed.

3.3.3 As-built condition

The shaft was to be constructed on the footprint of 89-134 Moorgate, previously occupied by a 1970s' 6-storey concrete framed structure with a single-story basement. The building was founded on bored piles, mostly 900 mm diameter and approximately 34 m long. With the building demolished ahead of the LIS-MS construction, piles were left in the ground. Due to delayed site clearance work, it became critical to speed up the shaft construction to enable the twin TBMs to pass through the shaft on time.

The observational method was adopted to modify the original design in April 2013 prior to the start of shaft excavation. The re-analysis was conducted by FLAC® 3D analysis using an updated non-linear soil stiffness profile for over-consolidated clay, which was proposed by Jardine *et al.* (1986) and verified at three selected excavation stages. Several excavation stages were successfully combined and the lowest two levels of temporary propping were omitted with a significant saving in time of about 14 weeks (Farooq *et al.*, 2015).

The construction sequence for LIS-MS is summarised in Table 3. 7. The as-built dates at each construction stage refer to the north wall.

Table 3. 7 Summary of construction sequence and the as-built completion dates for LIS-MS north wall, after (Farooq *et al.*, 2015; Chen *et al.*, 2015)

Stage		Description	Start	End
1	a	Cast capping beam	-	-
	b	Excavate to +106.5 mATD	29/09/2013	02/11/2013
2	a	Cast RB 1 (1.0 m THK centre at +107.1 mATD	08/12/2013	16/12/2013
	b	Excavate to +100.3 mATD	21/12/2013	11/01/2014
3	a	Cast RB 2 (2.0m THK centre at + 101.4 mATD)	03/02/2014	-
	b	*Excavate to +97.8 mATD (combined with the next excavation)*		

Stage		Description	Start	End
4		Excacvate to +94.8 mATD	17/03/2014	12/04/2014
5	a	Cast RB 3 (2.25 m THK centre at + 96.7 mATD)	25/04/2014	-
	b	Excavate to +87.6 mATD	07/05/2014	18/05/2014
*6**	*a*	*Cast RB 4 (2.0 m THK centre at + 91.9 mATD) (combined with RB3 installation)*		
	b	*Excavate to +87.6 mATD (combined with the next excavation)*		
7	a	Cast RB 5 (2.13 m THK center at +88.6 mATD)	26/05/2014	-
	b	Excavate to +83.2 mATD	27/06/2014	02/07/2014
*8**	*a*	*Cast RB 6 (2.2 m THK centre at +86.5 mATD) (combined with RB5 installation)*		
	b	*Excavate to +83.2 mATD (combined with the previous excavation)*		
9		Cast RB 7 (2.2 m THK centre at +84.3 mATD)	12/07/2014	-
*10**	*a*	*Install temporary prop T13 at +80.5 mATD (omitted)*		
	b	Excavate to +79.1 mATD	01/08/2014	09/08/2014
11*	*a*	*Install temporary prop T23 at +76 mATD (omiited)*		
	b	Excavate to +71.3 mATD	22/08/2014	02/09/2014
12		Case the base slab in 2.0 m thickness	31/10/2014	-

Note:

1. * modified design in the as-built construction.
2. the as-built ring beams (RB) were assumed in 0.75 m width, but the actual width of RB varies depending on the location.

In the modified design, total stress calculation (undrained analysis) was assumed for fine-grained soils on both active and passive sides, based on the planned excavation period of shorter than 12 months. This assumption was confirmed in a couple of Crossrail excavations in London Clay by the time of the LIS-MS modified design. The modified design with the undrained analysis improved predictions for the north wall deflections at stage 4 (Table 3. 7), in the 1st verification (VP1), as shown in Figure 3. 24. The soil parameters were further updated in order to narrow the gap between the measurements and the predictions for the north wall deflections.

East wall movements were expected to be restrained by installing two cross walls (Figure 3. 21) to minimise the movements of the northern line tunnels at 5 m away from the east wall. However, in the 1st verification, the predicted east wall displacements were much less than the measurements and the projected east wall measurements at the next stages were breached the amber trigger values.

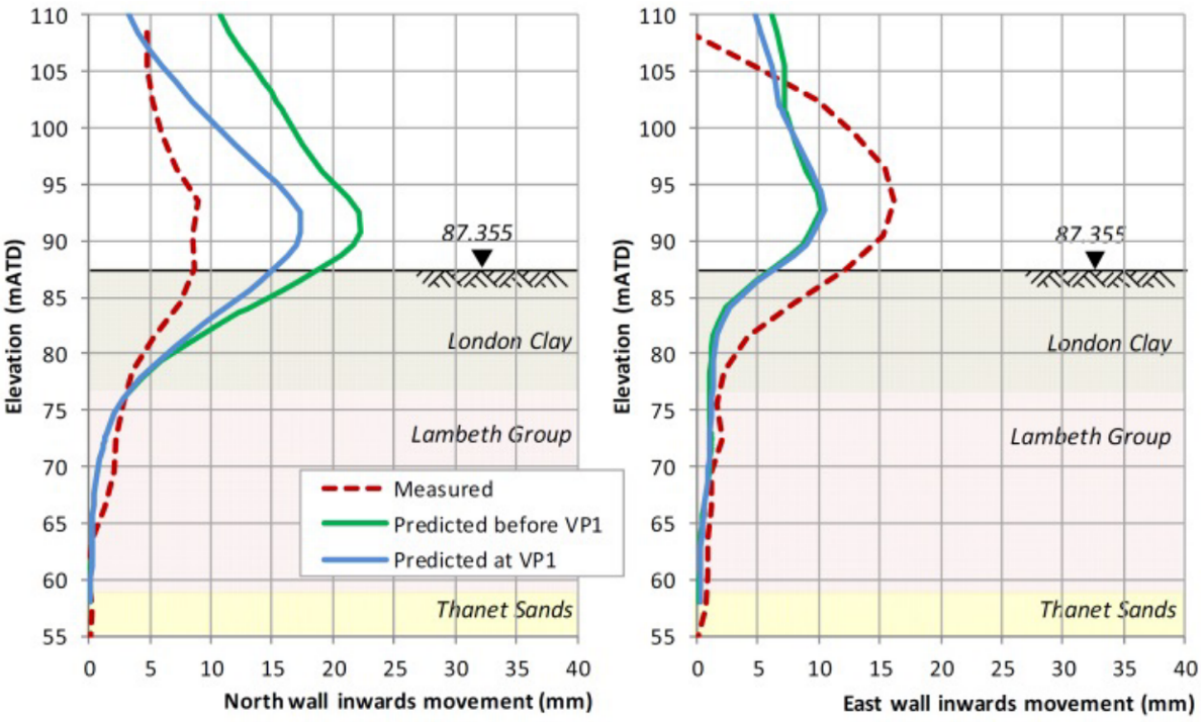

Note: excavation level used in verification followed the original design sequence, the actual excavated level was confirmed by construction records and summarised in Table 3.7

Figure 3. 24 Wall deflection at 1st verification for LIS-MS (Farooq *et al.*, 2015)

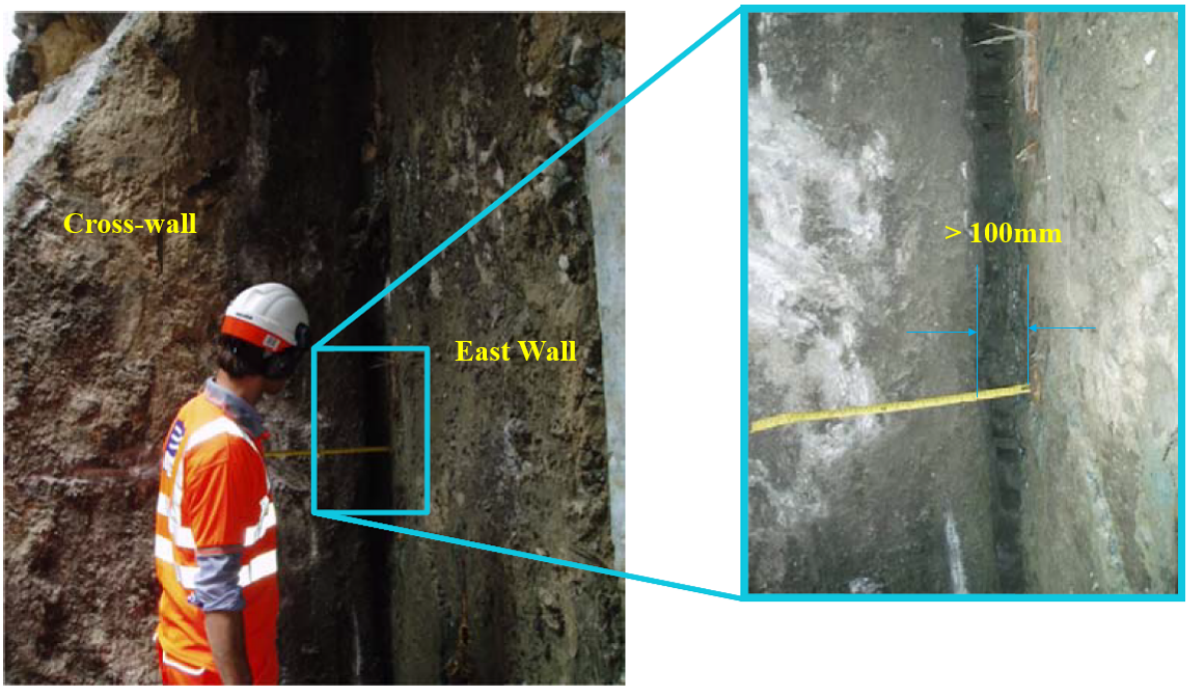

Figure 3. 25 Clay inclusion between cross-wall and the East wall (Crossrail, 2014b)

The weak support was revealed as the excavation progressed, that a layer of clay remained between two cross-walls and the east wall as shown by the photos in Figure 3. 25. This finding explained the weak lateral support to the east wall during excavation and the increased wall deflection measurements.

Application of the observational method in the LIS-MS excavations successfully modified the design and achieved savings in construction time. Meanwhile, the back-analysis identified the defect in construction and proposed the Approach D (best-way-out) solution for the east wall, such as re-installing the omitted props. None of these measures was needed by the end, as all movements stayed within the accepted limits, based on predictions with updated soil parameters.

3.3.4 Monitoring system

A comprehensive monitoring strategy was planned to assist in the verification of the modified design, as shown in Figure 3. 26. It included inclinometers in the diaphgram walls, vibrating wire piezometers monitoring water pressures in the Lambeth Group, extensometers measurements of ground heave inside the shaft, prisms and strain gauges installed in each ring beam. In addition, some standpipes monitoring groundwater level in the lower aquifer (Thanet Sand) were installed outside the shaft.

As the back-analysis of the LIS-MS excavation case was exclusively based on inclinometer data (wall deflections), only this information was considered in the review.

3.3.4.1 Review of inclinometer data

The in-place-inclinometers (IPI) with 3.0 m probe length were installed in the diaphragm wall panels for the LIS project. The IPIs were extended a few meters (> 3.0 m) below the wall toe level into the ground. The raw data of IE01 installed on the north wall diaphgram wall panel 01, was downloaded from the Crossrail monitoring database. The apparent cumulative displacements in the X direction, perpendicular to the wall, and the negligible cumulative displacements in the Y direction, parallel to the wall, are presented in Figure 3. 27. The data at 7:00 am representing the maximum reading of the day was presented in the plots, showing monitoring results over the period between 16/12/2013 and 18/11/2014.

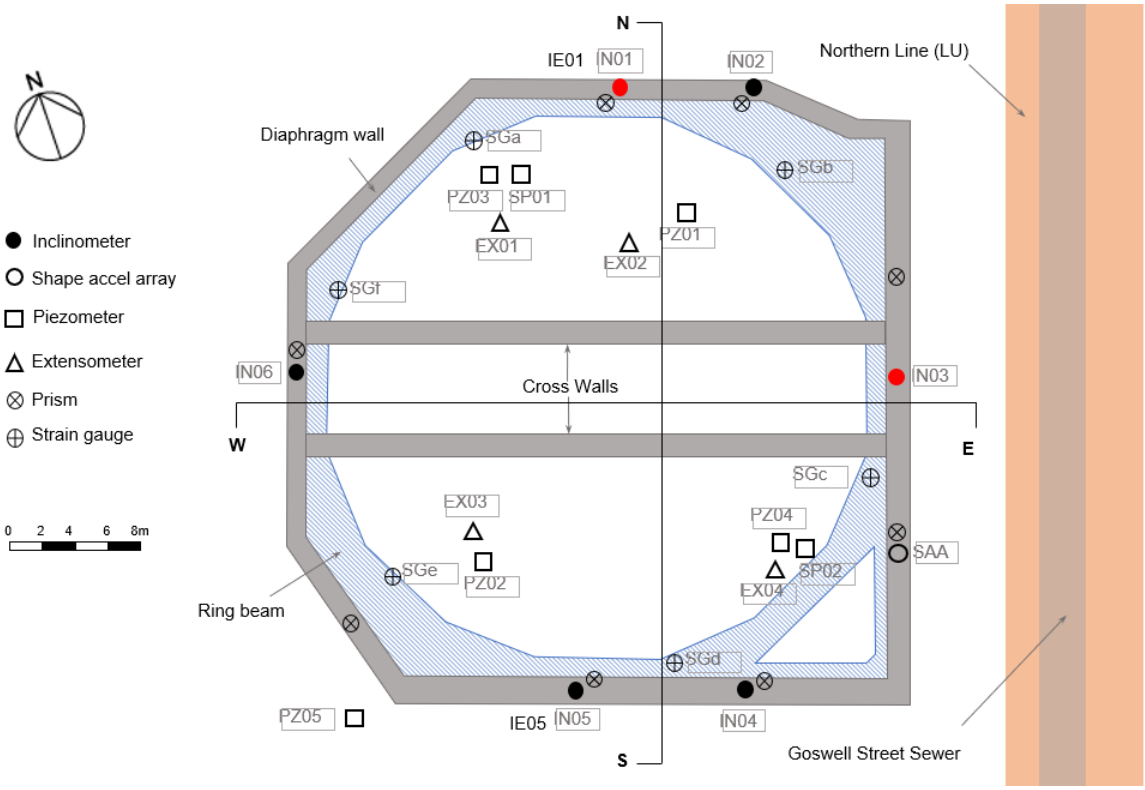

Figure 3. 26 LIS-MS monitoring instrument layout plan (Chen *et al.*, 2015)

The IE01 was extended a few meters below the wall toe level, the measurements from these extra a few monitoring points confirmed the fixity of IE01. The values of the measurements were less than 0.5 mm during the whole monitoring period (Figure 3. 27).

The good alignment of IE01 was indicated by the relative small Y displacements (within ±2 mm) before stage 7 (Table 3. 7). Whilst, the increased cumulative Y displacements (up to 4 mm) at the top was observed after stage 7, which might be related to the increased casing curvature of the inclinometer IE05 between +83 and +62 mATD.

Another 2 mm incremental displacement was recorded in the cumulative X displacement after the completion of the base slab (e.g. 18/11/2014), and it was considered that the time-dependent soil behaviour in clay (e.g. dissipation of pore water pressure) may play a role in this phenomena as there were no recorded other site activities during this period.

Temperature sensitivity of IE01 data is reviewed: the reading varied up to 1.5 mm in the top 15 m length of in a hot day, but this effect was diminished at the lower part of IE01.

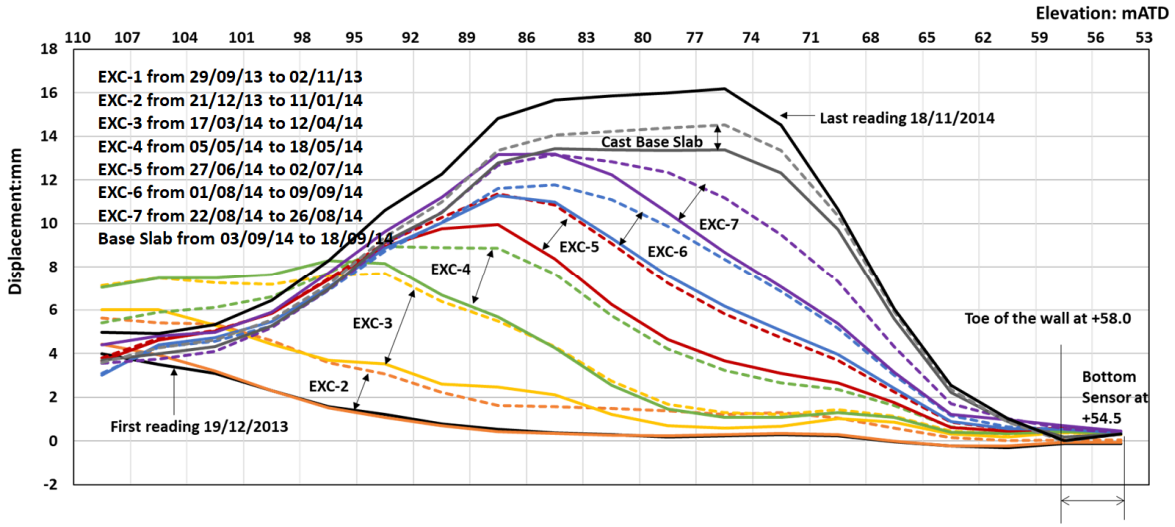

(a) IE01 X displacements - perpendicular to the wall

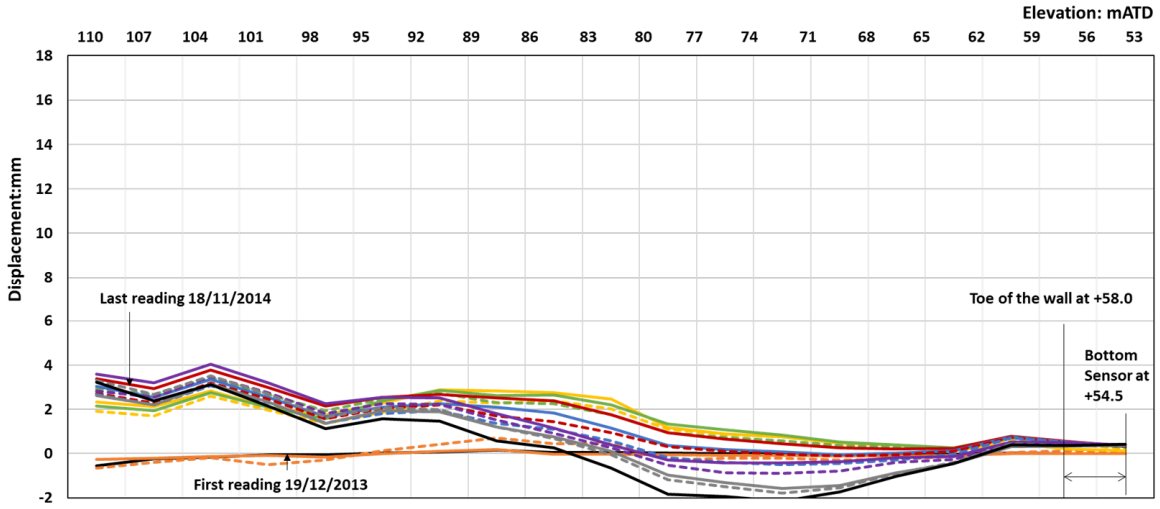

(b) IE01 Y displacements - along the wall

Figure 3. 27 IE01 raw data at 7:00 am: cumulative displacements

3.4 Paddington Station box

3.4.1 Introduction

The Crossrail Paddington station (PAD) is located underneath Eastbourne Terrace and Departures Road, adjacent to a Grade I listed building (MacMillan House) and the existing Network Railway Paddington Station. The box is about 263 m by 23.4 m (at central sections) to 24 m (at ends), as shown in Figure 3. 28. Contrary to other new Crossrail stations, the PAD box is constructed in open cut with the platform tunnels mined using tunnelling techniques.

The first Crossrail tunnel boring machine TBM was launched at the nearby Royal Oak Portal. It shortly passed through the PAD station box towards the east of London. Thus, the TBM drove passed the PAD during the installation of the perimeter diaphgram wall for the box.

The design was conducted by United Research Services (URS), and the construction work was awarded to a Costain/Skanska joint venture (CSJV). Intensive monitoring was undertaken during the TBM tunnelling works and PAD station box excavation

3.4.2 Original design

The PAD box excavation was supported with a 1.0 m (at ends) to 1.2 m (at central sections) thick diaphragm wall from the ground level at +123.6m ATD down to +85.5 mATD. The thinner wall (1.0 m) was used at ends over a length of 13 m to maximise the clearance between the running tunnels and the station box. As the diaphragm wall installation progressed, two TBM lined tunnels were built through the station box, then removed during the station excavation.

The station box was excavated with a 'top-down' construction sequence, in which one level of pre-stressed temporary props was installed between the roof and the concourse slab, and later replaced by the permanent intermediate slab, as indicated in section A-A', Figure 3. 28 (Scantlebury *et al.*, 2014; Chambers *et al.*, 2016; Chandegra and Kokkinou, 2016).

The geology of PAD station site is typical of a central London profile: a variable thickness of Quaternary deposits (Made Ground / Alluvium and River Terrace Deposits) overlay London Clay.

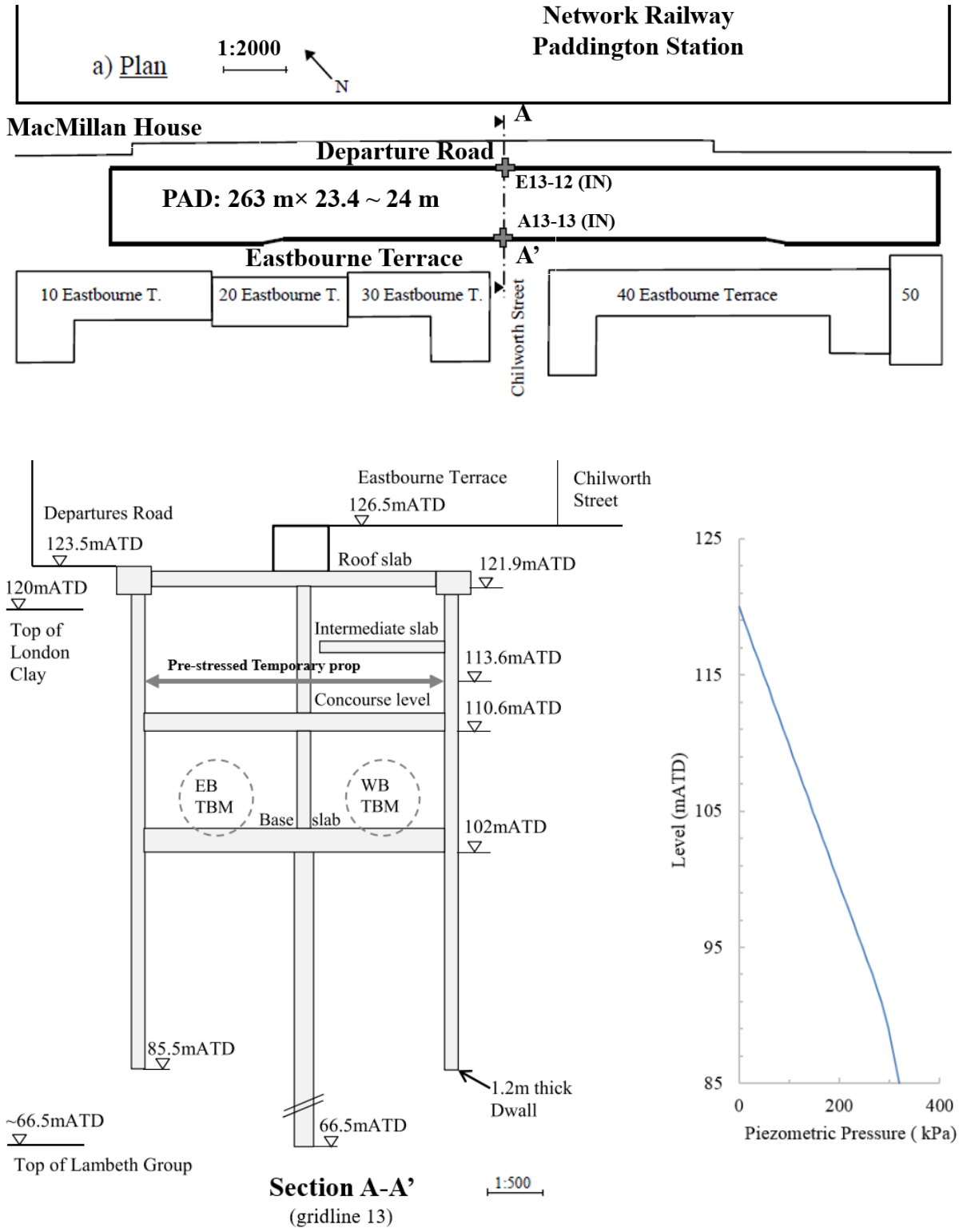

Figure 3. 28 Layout of the PAD and section A-A', (after Bologna, 2017)

The ground model and geotechnical design parameters applied in the design are summarised in Table 3. 8, referring to the geotechnical design summary report (GDSR) for the PAD (Crossrail, 2011a).

Table 3. 8 Geotechnical design parameters for PAD (Crossrail, 2011a)

Stratum	MG	RTD	London Clay	
			drained	undrained
Top (mATD)	124	123	121.5	
Base (mATD)	123	121.5	60	
γ (kN/m^2)	18	20	20	
c_u (kN/m^2)	-	-		85+5z
c' (kN/m^2)	0	0	0	-
ϕ'_{peak} (ϕ'_{cv}) (°)	25	38	*22 (20)	-
$\phi'_{residual}$ (°)	-	36	12	-
ν' (ν_u)	0.2	0.2	0.2	0.5
K_0	1-sinϕ'	1-sinϕ'	1.0	
E_{uh} - 1% strain (MN/m^2)	-	-	-	61.25+2.5z
E_h' - 1% strain (MN/m^2)	5	50	36.75+2.5z	-
E_{uh} - 0.05% strain (MN/m^2)	-	-	-	85+5.3z
E_h' - 0.05% strain (MN/m^2)	5	50	65+3.5z	-

z is m below +120 mATD.

* values are for intact material (3-D triaxial test), but for plane-strain analysis

ϕ' = 22+2 = 24 degree is applied for excavation

Concrete C32/40 was required for the diaphgram wall

Figure 3. 28 shows the applied pore water pressure design profile for the analysis (SLS): a hydrostatic pore water pressure profile starting from +120 mATD was assumed for London Clay, based on readings from ground investigations between 1992 and 1998; a reduction in pore water pressure was assumed for Lambeth Group due to the under drained impermeable soils below +90 mATD. In addition, a hydrostatic pore water pressure profile for the Lambeth Group starting at +60 to 62 mATD was also assumed but is not shown in the diagram of pore water pressure profile.

The numerical analysis with Plaxis 2D using the Mohr-Coulomb soil model was performed for the PAD box design. In addition, an Oasys LS-Dyna® 3D analysis using the BRICK soil constitutive model was also carried out for the ground movements and asset protection assessments due to the Crossrail tunnelling and the shaft excavation works (Crossrail, 2007b).

The PAD box design complied with the CEDS, with the following major design requirements, as referred to in the GDSR (Crossrail, 2011a) for PAD:

- Variable surcharge loads representing the existing building, fill material and possible future development, were applied in different analysis sections, as summarised in Table 3. 9;
- Mixed earth pressure analysis was assumed for the short-term ULS design - where total stress (undrained) were calculated for the passive side, and effective stresses (drained) were calculated for the active side;
- A 0.5 m over-dig was included in the ULS analysis;
- A 0.5 m softening depth on the passive side below the excavation level was considered in the ULS analysis, as total stress calculation (undrained analysis) was performed.

Table 3. 9 Summary of surcharge loads for PAD box design (Crossrail, 2011a)

Items	**Stories**	**Assumed surcharge value (kN/m^2)**	**Location**
Construction surcharge	-	20	All sections
Future development surcharge	-	75	Applicable sections
Traffic surcharge	-	*10 ~ 20*	*All sections*
Macmillian House Block A/B/C	2~5	100 at +120.0mATD	DR side
Macmillian House Block D	4	80 at +120.0mATD	DR side
Macmillian House Block E	6	120 at +120.0mATD	DR side
Hilton Hotel	6	120 at +120.0mATD	East end section, DR side
10 / 30 Eastbourne Terrace	6	90 at +123.0mATD	ETS side
20 Eastbourne Terrace	18	270 at +123.0mATD	ETS side
40-Eastbourne Terrace Block A	6	90 at +123.0mATD	ETS side
40-Eastbourne Terrace Block A	3	45 at +123.0mATD	ETS side
50-Eastbourne Terrace Block C	8	120 at +123.0mATD	ETS side
Eastbourne Terrace Bank	3	45 at +123.0mATD	East end section, ETS side
Royal Mail Building (London Street)	4	60 at +123.0mATD	n/a for excavation

Note: see Figure 3. 28 for building locations.

3.4.3 As-built conditions

The actual construction sequence of the PAD box is summarised in Table 3. 10. The completion dates at each stage were determined from records for the section A-A' (Figure 3. 28) in the table.

In total, 50 steel tubular props were installed: 42 horizontal MP500 props at a typical spacing of 6.11 m c/c along with the central box, and 2 MP250 props at each corner. Props

were connected to 900 mm by 600 mm fabricated plate girder as walers, and in turn connected to the diaphragm walls (Chambers *et al.*, 2016).

Table 3. 10 Summary of construction sequence and the completion dates for PAD station box section A-A', (Crossrail, 2016)

Stage		Description	Start	End
1 & 2		Existing condition	01/08/2012	
3	a	TBM – westbound tunnel (EBT)	15/9/2012	15/9/2012
	b	Diaphgram wall installation (EBT)	25/9/2012	15/10/2012
	c	TBM – eastbound tunnel (DR)	7/12/2012	7/12/2012
	d	Diaphgram wall installation (DR)	17/12/2012	20/12/2012
	e	Excavate to +123.0 mATD	-	-
	f	Install Plunge column	27/05/2012	14/06/2012
7		**Excavate to +121.s8mATD**	**26/3/2013**	**17/7/2013**
8		Cast Roof Slab at +122.68 mATD	6/8/2013	14/9/2013
9&10		Traffic at EBT return (20kPa surcharge and backfill to +126mATD)		
11	**a**	**Excavate to +116.1mATD**	**21/10/2013**	**21/11/2013**
	b	Cast Interchange slab (NA for section 12-13)	-	-
12		**Excavate to +113.6mATD**	**20/1/2014**	**24/1/2014**
13		Install prop at +114.5mATD with pre-load 700kN/m	14/2/2014	16/2/2014
14		**Excavate to concourse slab +110.9mATD**	**15/2/2014**	**18/2/2014**
15		Cast concourse slab a t+112.1mATD	3/4/2014	12/4/2014
16	a	Remove temporary prop	28/4/2014	17/5/2014
	b	Cast intermediate slab	7/6/2014	13/6/2014
		Excavate to mid-tunnel hold level (NA for section 12-13)		
17		**Excavate to base slab level +102.56mATD**	**15/8/2014**	**26/10/2014**
E1		Install contiguous wall at BLL box (NA for section 12-13)		
18a		Cast base slab	18/2/2015	25/3/2015
19		Install permanent plunge columns	8/9/2015	5/10/2015
20		Remove temp plunge column	27/11/2015	3/12/2015
		Last inclinometer reading	10/02/2016	

Note: The inclinometer data and the defined trigger values were provided at the highlighted stages only, referring to the inclinometer close-out monitoring report for the PAD (Crossrail, 2016).

3.4.4 Monitoring system

As indicated in the instrument layout plan in Figure 3. 29, the instrumentation for the PAD box included inclinometers, levelling studs on the ground and wall-mounted levelling studs on the existing buildings. The ground settlements by levelling studs were reported by Bologna (2017). Except for the inclinometer data, no other field monitoring data was available to review at the time of the back-analysis of the PAD box excavation.

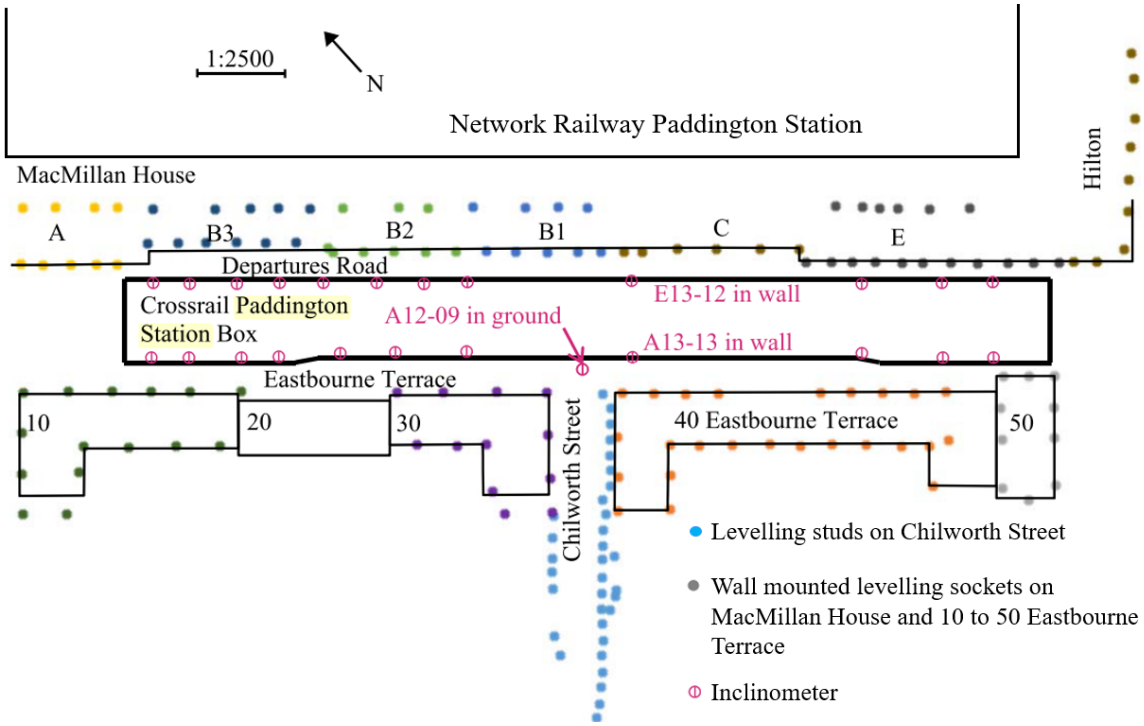

Figure 3. 29 PAD station box construction monitoring instrument layout plan (Bologna, 2017)

3.4.4.1 Review of inclinometer data

Approximately 42 inclinometers were installed between February 2012 and February 2013, in the diaphragm wall panels and in boreholes around the PAD box. The manually read inclinometer (IM) using itmsoil® probe was initially used monitoring the PAD box excavation, and two major changes were made to the inclinometer measurement since the installation (Crossrail, 2016):

- Itmsoil probes were replaced with Geokon® (GKN) probes – in April 2013.
- 21 IM inclinometers were replaced by automated in-place inclinometers (IPI) from January 2014 to February 2016.

The first change was due to significant technical issues resulting in erratic and unrealistic data. The second change replacing some IM inclinometers by automated IPIs was to minimise operational costs in terms of reduced manpower.

The baseline of the inclinometer data was recalculated at each change of equipment. However, the history of inclinometer equipment replacements has made a data review for the PAD case by a third party almost impossible. The measurements were interpreted by the monitoring contractor in "The final/close-out monitoring report for C405 inclinometers" (Crossrail, 2016). Results were given at a few selected key construction stages, for the multiple cross-sections between Eastbourne Terrace Street and Departure Road.

The following observations can be made from the interpreted inclinometer results:

- Uncertainty is introduced in diaphragm wall displacements by the lack of the fixity at the bottom of the inclinometer, and the inability to apply a drift correction to the results. For example, a typical IPI inclinometer is in 10 m length from the base slab level (+102.5 mATD) to a level of +92.5 mATD, but the fixity assumption was made for the inclinometer at the toe of diagram wall level, about +85.5 mATD.
- Some IPIs' showed significant drift through the monitoring period. Although it was uncertain, the rotation correction was applied with the assumption of fixity at the roof slab by the monitoring contractor during the final close-out interpretation.
- Excessive movements at the top of the wall were observed from many inclinometers installed in the diaphgram wall panels on the Eastbourne Terrace Street side. This was believed due to external construction activities, such as backfill enabling works, roof slab construction and the heavy plant traffic loads.
- A few inclinometers became inaccessible during construction or were subjected to disturbance. This resulted in unrecorded periods of deformation during construction activities.

3.5 Summary of Crossrail excavation case histories

Three excavation case histories from the Crossrail project were introduced, two of them showing a successful implementation of the observational method through different approaches. The proactively modified design using the observational method in the TCR-WTH case was a newly defined approach, whilst the cautious verified and executed modification

design in the LIS-MS was the Ab-initio approached recommended by Ciria R185. In addition, the adoption of the observational method also helped to resolve the issue of excessive movements on the east wall of LIS-MS due to the weak support from the defected cross-walls construction. This was a good example of using the 'best-way-out' observational method.

3.5.1 Preliminary finding

The monitoring data review in these case histories illustrates the variability in the quality of measurements depending on a number of factors, such as specifications, installation, instrument calibration, baseline reading, error diagnostic and correction. However, reliable observations are required for back-analysis to produce meaningful results and allow design modifications according to the observational method.

The monitoring data can be categorised based on the quality of data, as a combination of resolution, accuracy, frequency of data, simplicity and reliability of error diagnostic and correction.

- Primary: inclinometers;

Inclinometers are the most common and best-understood monitoring instruments. Due to a number of well-documented case histories, the confidence in the quality of the inclinometer data is high.

- Secondary: vibrating strain gauge or load cell; piezometers; extensometers; levelling studs; prisms

Prop loads measured by strain gauges or load cell are useful in bottom-up braced excavation case histories. Other field measurements, such as piezometers and extensometers, can be valuable to better understand the excavation processes in cohesive clay soils. Levelling studs and prisms are easy to install and can provide long-term monitoring data, but they are also vulnerable to damage on construction sites.

In addition, it requires advanced soil constitutive models (e.g. non-linear soil stress-strain correlations) and 3D modelling to better estimated the above ground response.

In later chapters, the primary monitoring data will be used for the back-analysis of Crossrail excavation case histories, while the secondary data will be used to validate the results.

The empirical correlation of the maximum wall deflections ($\delta_{H,\,Max}$) over the excavation depth (H_e) in London Clay ranges between 0.15% and 0.45%, as referred to in St. John *et al.*

(1992) and Ciria C760 (Gaba *et al.*, 2017). The inclinometer data from the Crossrail deep excavation case histories show a reduced ratio between 0.10% and 0.05% depending on the geometry of the excavation, as summarised in Table 3. 11. The maximum wall deflections at the corresponding excavation depths were plotted in Figure 3. 30.

Table 3. 11 Summary of the normalised maximum wall displacements in the Crossrail excavation case histories

Case history	As-built construction method	Width B (m)	Length L (m)	B/L	Inclinometer	$\delta_{H,Max}/H_e$ (average)
[1]PAD	Top-down + temporary prop	24	263	>10	IE13-12	0.10%
TCR-WTH	Bottom-up	31	41	1.3	SAA-8003	0.05%
LIS-MS	Top-down	35	35	1.0	IN01 (north) IN05 (south)	0.05%
[2]WS-DSS	Bottom-up with cantilever + slab rings	32	59	1.8	IN-3	0.08%

Note: 1. PAD inclinometer data were reviewed by the monitoring contractor (Crossrail, 2016); 2. WS-DSS inclinometer data refer to Mills, (2016).

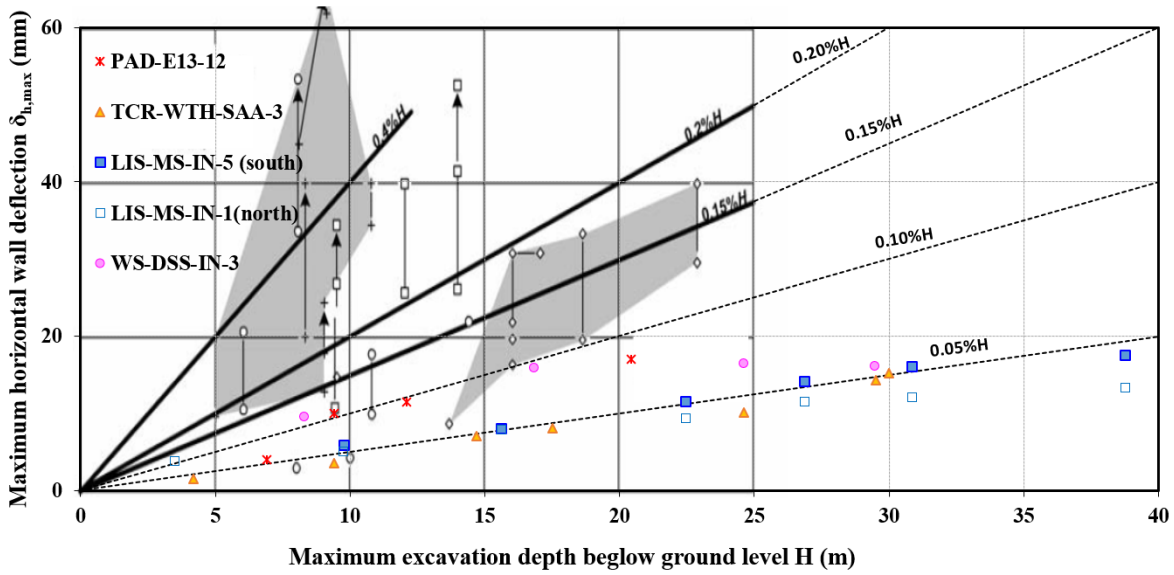

Note: 1. Paddington (PAD) station box inclinometer E13-12 data was reviewed by the monitoring contractor; 2. Whitechapel station – Durward Street shaft (WS-DSS) inclinometer IN-3 data refer to Mills (2016).

Figure 3. 30The maximum horizontal wall deflections from excavations in London Clay, after Ciria C760 (Gaba *et al.*, 2017)

The smaller ratio of $\delta_{H,\ Max}/H_e$ = 0.05% is more representative of cases in which three-dimensional effects are more prevalent for excavation length over width less than 2.0 (L/B < 2.0). For geometries resembling two-dimensional plane-strain excavation conditions (L/B ≥ 2.0), an increased ratio of $\delta_{H,\ Max}$ / H_e = 0.10% is observed.

3.5.2 Recommendation for instrumentation and monitoring

Confidence in the instruments' performance relies on the precise specification and the proper execution of the installation. Meanwhile, the reliability of the measurements depends on adequate data processing, good error diagnostics and corrections. Thus, the following recommendations were drawn from the monitoring data review, with the aim of providing some useful guidance:

- Specifications

Clear monitoring objectives help to guide the selection of instrumentations for deep excavation monitoring. A good understanding of the instruments, including measurement accuracy, resolution, operational range, monitoring performance, is the foundation of good specifications. An adequate data review procedure for error diagnostics and corrections also needs to be included.

Performance-based specifications will limit misunderstandings from different types of instruments. Practical issues should be taken into consideration in the specifications, for instance, easy and safe access to the instrument, and instrument protection measures. Early involvement of instrument experts helps to address these issues in the specifications.

- Installation

The installation needs to be enhanced in both specifications and execution. Installation is a crucial factor in obtaining quality measurements. In the case histories, there have been instances where wrong practices and poor installation have resulted in errors in the data.

- Data assessment

An adequate monitoring data review process should not be limited to error diagnosis and correction, but also include the study of the related information, such as the installation process, the establishment of the baseline reading, and the timeline construction activities. A complete review of the monitoring data will provide reliable observations for the back-analysis.

Error diagnostics is a key task in the data assessment, and the involvement of experts can speed up this process. Otherwise, training for engineers to do the monitoring data interpretation will be necessary.

- Data processing

The frequency of the field monitoring data readings has been increased by technological advances. The hourly to daily readings produce an extraordinary amount of data, which requires an efficient and reliable system to process the data, such as bespoke scripts or other alternative software.

- Alternative monitoring instruments

Innovations in technology have led to improvements in monitoring data with regards to accuracy, precision, and capacity to store and process a large amount of automated readout data. There are a few new instruments/technologies which have been applied in the excavation monitoring, as listed below, which could provide good alternatives to enhance the data quality in future:

- Fibre optic sensors (Schwamb *et al.*, 2014);
- Photogrammetry (Stanier *et al.*, 2016); and
- Laser Scanning (Fuentes, 2012)

- Communication & collaboration

Beyond the monitoring data, the management of the monitoring activities also affects the data quality. In the studied cases, quite a few monitoring contractors worked on site on different instruments. However, effective communication was not established between them, and field data was not cross-checked since an early stage. This poor practice resulted in failures in identifying errors at an early stage and/or applying contingency measures for additional monitoring.

Chapter 4

New Observational Method Framework

The excavation case histories of the observational method were reviewed in Chapter 2, while the new Crossrail excavation case histories were reviewed in Chapter 3. The review was to provide a better understanding of the design of embedded retaining walls in London Clay and the application of the observational method. A new framework with four approaches to classify the observational method is proposed in this chapter based on the review of the excavation case histories. The intention was to bring together previous work undertaken on the observational method in a logical and structured way and promote the method through this new framework. This chapter will describe the new observational method framework.

This new framework was developed as part of the update of guidance on embedded retaining wall design – Ciria C760 (Gaba *et al.*, 2017), with new terminologies for the four design approaches.

4.1 Development of the new observational method

In the recently constructed Crossrail project in Central London, the observational method was successfully applied in three out of four excavations which had used the observational method for optimisation, as summarised in Table 3.1. Savings in both time and cost were achieved in these three cases. The method was applied after the construction had started using the conventional design, as a progressive modification. However, this approach was not recognised

in the original observational method, neither *Ab initio* nor "Best-Way-Out" as defined by Peck (1969a).

In addition, in the observational method review in Chapter 2, the *Ab initio* approach proposed by Peck (1969a) is equally valid as the one put forward by Ciria Report R185 (Nicholson *et al.*, 1999), although they are quite different with regards to the balance between risk and opportunity of savings. Peck's *Ab initio* approach treats the application of the contingency measures as risk mitigation, whereas the cautious *Ab initio* approach by Nicholson *et al.* regards the application of modification as an opportunity. Being more cautious in its approach, the cautious *Ab initio* approach does not maximise potential savings.

If a retaining wall is constructed following a design by characteristic parameters, as the cautious *Ab initio* approach proposed, the wall embedment depth, thickness and reinforcement will be more onerous than if most probable parameters had been assumed as Peck's *Ab initio* approach. Once constructed, evidently, no change can be made on the wall. Therefore, savings can only be made by modifications to the excavation sequence and the supports to the wall. These savings may be significant, but can never match potential savings if most probable parameters and design conditions had been assumed from the start.

A new framework for the observational method with four design approaches was then proposed to overcome the apparent inconsistencies in the previous approaches. This new framework, with some new terminologies, was then introduced in Guidance on the design of embedded retaining walls, Ciria C760 (Gaba *et al.*, 2017), as presented in Figure 4. 1.

A new term '*Ipso tempore*' is used to cover the case in which the observational method is initiated after the construction has started. In this new framework, the observational method is divided into two broader categories and refined further into sub-categories:

- *Ab initio* - in which the application of the observational method is planned prior to the retaining wall installation.
    - Optimistically proactive Approach (A); and
    - Cautiously proactive Approach (B).
    - *Ipso tempore* - where the observational method is initiated after the retaining wall installation has been started.
    - Proactive Approach (C); and
    - Reactive Approach (D).

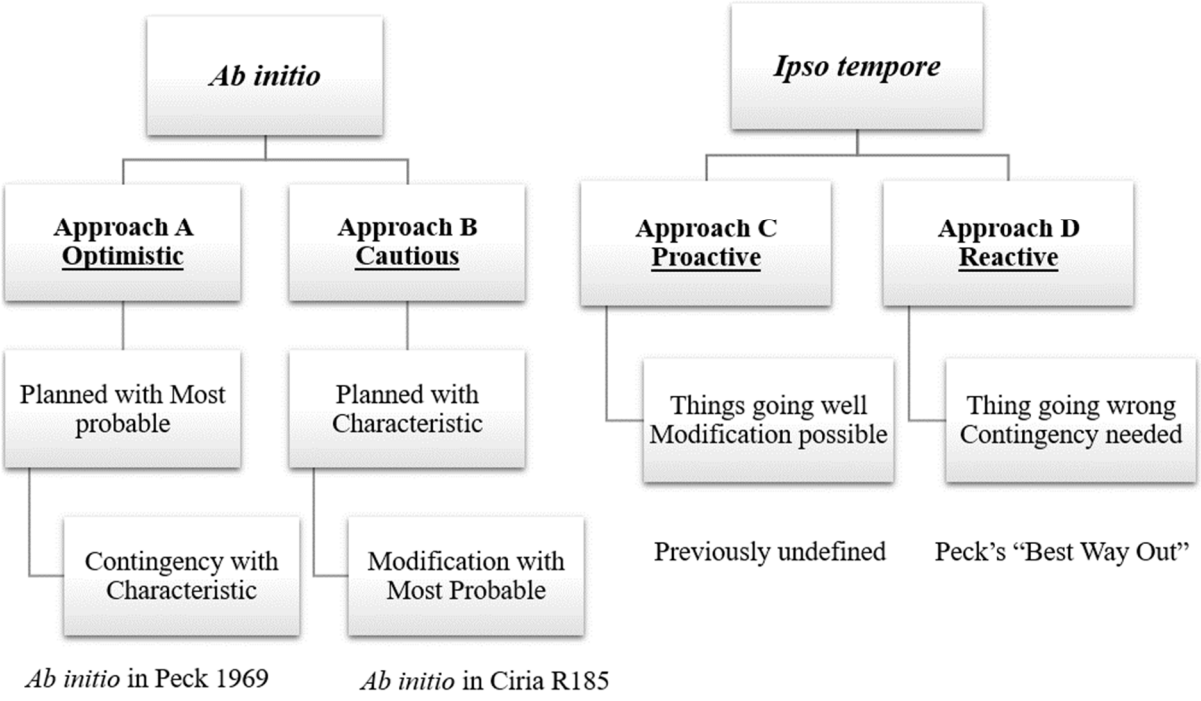

Figure 4. 1 The structure of the new observational method framework with four approaches, after (Chen *et al.*, 2015)

4.2 Design conditions and design parameters

The observational method is a performance-based design strategy, and the four approaches in the new framework are compliant with the standard design codes, for instance, Eurocode 7: Geotechnical design - BS EN1997-1 (EC7, 2004). The assessment of performance is a fundamental component of the observational method and can be carried out with any available methods, subject to their limitations: empirical to semi-empirical calculation, or numerical analysis. The predicted soil/structure response is compared with field observations, and action is triggered when a pre-set threshold is reached. The process is usually carried out by hand, but can also be automated for more rigorous updating.

For the consistency with existing codes, designs carried out under the new framework are based on either the characteristic or most probable approach. The former is applied to obtain a cautious estimate, in which characteristic design parameters and cautious design conditions are assumed. The latter assumes most probable design parameters and most probable design conditions, which parameters and conditions can be calibrated and verified through the back-analysis, hence, they could be updated as more available field observations become available.

4.2.1 Design conditions

Different terms have been used to describe designs and assumptions in the observational method. Distinctive names appear at different development stages, as summarised in the literature review in Chapter 2. For example, "most probable" and "most unfavourable" were cited in the original observational method (Peck, 1969a). Meanwhile, "moderately conservative" was cited in the progressively modified observational method (Powderham, 1994).

Two design conditions, 'characteristic' and 'most probable', are applied in the new observational method framework, based on the definitions given in Ciria R185 (Nicholson *et al.*, 1999), with some amendments:

- Characteristic condition

The cautious assumptions made under characteristic condition are to confine the risk of failure in a very small range of all the identified possible conditions. For example, a characteristic design for a retaining structure in London Clay may assume the drained behaviour and use effective stress analysis, as this is the most unfavourable condition for an overconsolidated clay, even if it is unlikely to occur during construction.

- Most Probable condition

These design assumptions are the most likely to actually occur in construction. Therefore, the most probable condition is suitable for evaluating performance-based design.

4.2.2 Design parameters

Similar to design conditions, different terminologies have been used to describe design parameters applied in the observational method at different development stages. Two types of design parameters, 'characteristic' and 'most probable', are adopted in the new observational method framework to maintain consistency with design conditions.

4.2.2.1 Characteristic parameters

Characteristic values of geotechnical parameters are defined in Clause 2.4.5.2 (2) of the Geotechnical design code BS EN1997-1 (EC7, 2004): "*A cautious estimate of the value affecting the occurrence of the limit state*". However, when this definition is applied in

interpreting values for soil design parameters, it is difficult to quantify. Moreover, experience-based engineering judgement will add further variation. An interpretation by Pohl (2011) pointed out the characteristic values of soil properties have to be determined in case of complex construction.

The characteristic values of soil parameters are selected from the ground investigation field and laboratory testing data, complemented by local information and experience. As Clause 2.4.5.2 (4) of EC7 states: "*geological and other background information, such as data from previous projects"*, and other relevant experiences listed in the Clause 2.4.5.2 of EC7. Simpson (2012) has further interpreted the definition of experience to include: "*Characteristic parameters required by EC7 are to be estimated, requiring a degree of human judgement, and they are to be cautious, not simple "best estimates", "most probable" or "statistically mean values". They are not simply the values measured in tests, and they are to take into account well-established experience as well test results made for the particular project."*

The review in chapter 3 showed that characteristic values of design parameters in a geotechnical analysis are a combination of considerations for the specific problem. As an example, Figure 4. 2 displays the undrained shear strength from ground investigations and the recommendations of characteristic values for retaining wall design and pile foundation design.

The volume of soil mobilised at the limit state behind a retaining wall is large enough to average out local variation in soil strength. Therefore, a cautious average value of soil strength from ground investigation data is regarded as appropriate as a characteristic value. For piled foundation, the volume of soil mobilised at the toe and along the shaft of the pile is localised. Therefore, the local soil strength will highly likely dominate the pile capacity. A more cautious estimated lower bound of soil strength or a local value may be required as a characteristic value.

Bauduin (2001) suggested the flowchart shown in Figure 4. 3 to derive characteristic values of design parameters, in accordance with Eurocode and German supplementary rules. The initial data filtering evaluates and corrects ground investigation data and also eliminates outliers. Characteristic values will then be interpreted from these filtered data through an assessment. This process will involve previous knowledge and project experience of the soil. For example, the following factors could affect the interpretation: numbers of tests, the statistical spread of results and variability of the subsoil. In the interpretation, the structure's mode of failure (e.g. retaining wall, piled foundation or shallow pad foundation) is an important factor to consider.

A statistical interpretation of characteristic values was attempted in Clause 2.4.5.2(11) of EC7: "*if statistical methods are used, the characteristic value should be calculated such that the calculated probability of a worse value governing the occurrence of the limit state under consideration is not greater than five per cent.*"

Due to the uncertainty of soil properties and the limited investigated area compared with the size of the construction site, in order to calculate the probability of failure, a probabilistic distribution of calculations is required. However, calculations of the probability of failure are extremely rare in practice. Attempts have been made to use a statistical approach to derive soil design parameters from the ground investigation data. Schneider (1997) suggested deducting half of a standard deviation from the mean value of the testing data and characteristic values were derived from the rest of the data. Foye *et al.* (2006) recommended the nominal procedure as an applicable statistical tool to determine the standard deviation: a) taking the mean of the sample (a regression line with depth) as a close representation of the population mean; b) drawing a trend line at where 80 % of data points will be above this trend line; c) the trend line can be determined by a value of 0.84 standard deviations below the mean line from a) and this trend line can be used as characteristic values. The derived characteristic values using the above two methods were found much closer to the mean of the testing data by Simpson (2012). Furthermore, these statistical 'characteristic values' of soil parameters do not represent "*the calculated probability of a worse value governing the occurrent of the limit state under the consideration*."

As the review of the observational method in Chapter 2 pointed out, when a statistical approach is used to derive design parameters, a probability distribution is required for all variables in the analysis. In addition to the input soil parameters for the constitutive model, other variables are also needed to consider, such as groundwater levels, surcharge load values and structural properties, as demonstrated in Figure 2.3. The probability distribution for any considered limit state can then be obtained, including the conditions leading to a 5% probability of failure.

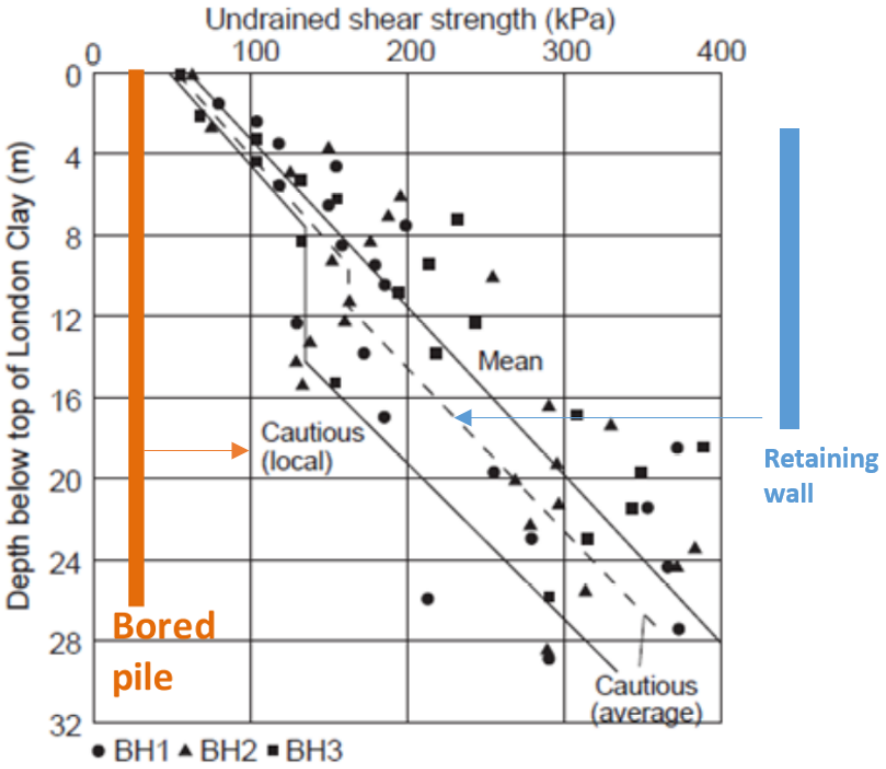

Figure 4. 2 Characteristic values of the undrained shear strength for London Clay under different geotechnical designs (Simpson, 2012)

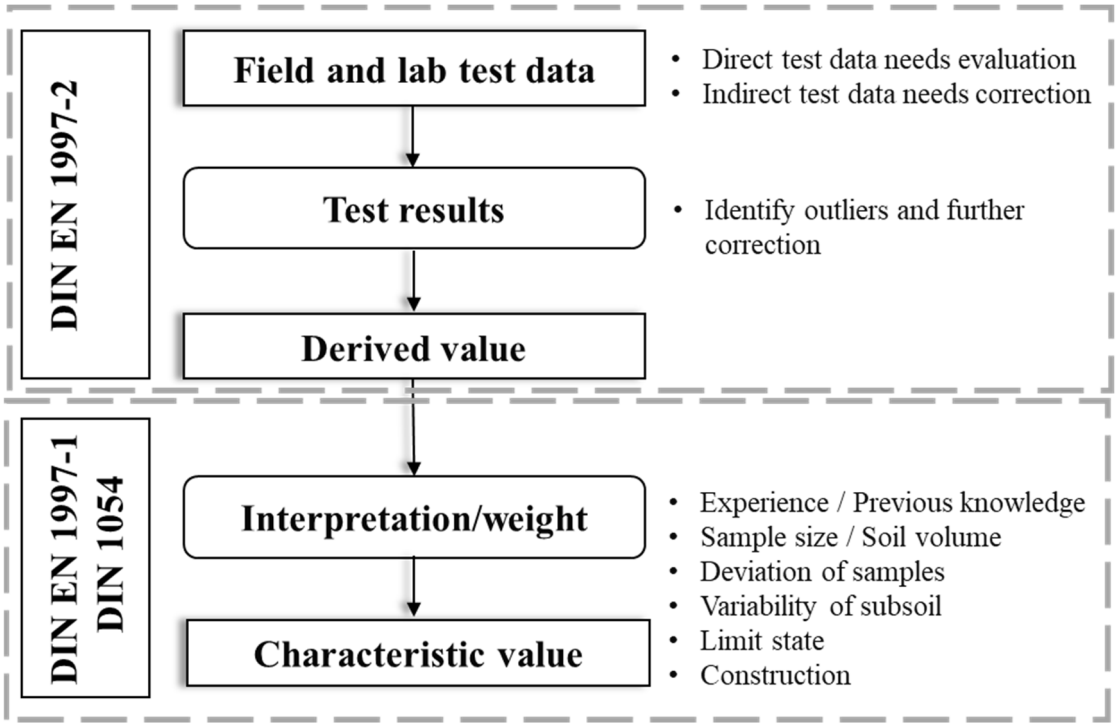

Figure 4. 3 Flowchart to assess characteristic values of soil properties (Pohl, 2011)

It is not a process fully appreciated the statistical meaning of the characteristic parameters, to derive characteristic values of soil parameters from ground investigations using the statistical approach. However, this approach can provide a way to derive the parameters based on the ground investigation data.

Given the definition of characteristic parameters can lead to very different interpretations of soil design parameters, in the absence of rigorous probabilistic analysis, values adopted in the original design of the Crossrail excavation case histories were regarded as the representative characteristic values in the back-analysis. However, a probabilistic analysis of the problem could be carried out to assess the probability of failure. In the absence of probabilistic analysis, the statistical approach to derive the representative characteristic values from ground investigation data is recommended, as it is a more impartial way to look at soil behaviours.

In addition, the experience-based correlations between soil parameters can be used to cross-check or derive the representative characteristic values. For example, Ciria C760 (Gaba *et al.*, 2017) recommended characteristic values of the undrained Young's modulus (E_u) for London Clay can be derived from the undrained shear strength (c_u): $E_u = 1000\ c_u$.

4.2.2.2 Most probable parameters

Most probable values of geotechnical parameters were defined in Ciria R185 (Nicholson *et al.*, 1999): *"A set of parameters that represents the probabilistic mean of all possible sets of conditions. It represents, in general terms, the design condition most likely to occur."* The statistical meaning of this definition is understood as that the most probable values need to ensure in a 50% probability of non-exceedance of the performance (e.g. serviceability limit state analysis). Thus, most probable values of the design parameters can be derived through a probabilistic analysis on all variables in the analysis.

In the absence of rigorous probabilistic analysis, the representative most probable values can be calibrated from the back-analysis, as field observations can be interpreted to represent the most likely to occur condition in the field. The term of calibration is normally used to describe the process of obtaining the initial input parameters for the soil constitutive models using the laboratory testing data. Hereby, the word 'calibration' is borrowed to describe the process of deriving the representative most probable values of the design parameters, meaning these values are changeable and subject to the outcome of the back-analysis.

The back-analysis of the Crossrail excavation case histories, as presented in Chapter 5 and Chapter 6, will demonstrate the process of calibrating the representative most probable values of the design parameters for London Clay subdivisions.

Chapter 5 will present the back-analysis using the base soil model - linear elastic and perfect plastic Mohr-Coulomb model. A statistical approach is developed to derive the initial input values from the ground investigation data. These initial inputs then enable the start of the iterative back-analysis process. By the end of this process, the calibrated values of parameters as the output of the back-analysis are regarded as the representative most probable values.

For comparison, Chapter 6 will present the back-analysis using one of the advanced soil constitutive models – the BRICK model. The initial input values of the BRICK model parameters will be calibrated using the relevant laboratory testing data, such as the anisotropic or isotropic triaxial tests, ensuring the non-linear stress-strain and the non-linear strain stiffness soil behaviours are replicated.

4.3 Design approaches

The four design approaches proposed for the new observational method framework are described in the following sections.

4.3.1 *Ab initio* Approach A – Optimistically proactive method

Ab initio Approach A is almost the same as the original *Ab initio* as defined by Peck (1969a). The assumption of the most probable condition is applied, and the design begins with the representative most probable values of design parameters to maximise the savings in construction materials.

The optimistic design is developed to comply with the agreed design standards, for instance, the Geotechnical design code BS EN1997-1 (EC7, 2004) in the UK, in which both the serviceability limit state (SLS) and the ultimate limit state (ULS) analysis are required to be satisfied. Meanwhile, an alternative contingency plan is also devised assuming characteristic conditions and using the representative characteristic values of the design parameters. This contingency plan needs to comply with the agreed design standards.

In the *Ab initio* Approach A, the relevant structural design, such as the reinforcement of the retaining wall are based on the conservative results of ULS analysis from both the optimistic

design and the contingency plan. Therefore, if the construction begins with the optimistic design and needs to be altered to the contingency plan, minimum changes in the wall construction will be required, but inevitably, additional supports will be required to ensure the stability of the wall.

As part of the construction control and risk management, a series of plan threshold performance values or triggers need to be defined for the following two key changes.

- Switching construction from the optimistic design to the contingency plan, (e.g. > Amber trigger);
- Switching construction from the contingency plan to the emergency plan (e.g. > Red trigger).

Due to an industry perceived difficulty in obtaining the representative most probable values of the design parameters, and lacking confidence in these values, *Ab initio* Approach A has not been a popular practice in excavation retaining structure design.

The Crossrail excavation case histories in London Clay offer a great opportunity to calibrate the representative most probable values for London Clay parameters and validate the most probable design conditions. Therefore, these calibrated values can be used in future excavations in London Clay to conduct the *Ab initio* Approach A design. An example of the re-assessment of one of the Crossrail excavation case history by Approach A is presented in Chapter 7.

For *Ab initio* Approach A, the back-analysis of the previous excavations at the pre-design stage is essential to provide representative most probable values of design parameters. Real-time back-analysis of the ongoing construction is recommended to validate the optimistic design and to assist in construction control.

4.3.1.1 Operation procedure

The initial operational procedure for the observational method was proposed by Nicholson *et al*. in Ciria Report R185 (1999), as reviewed in Chapter 2. An updated operational procedure for *Ab initio* Approach A is shown in Figure 4. 4.

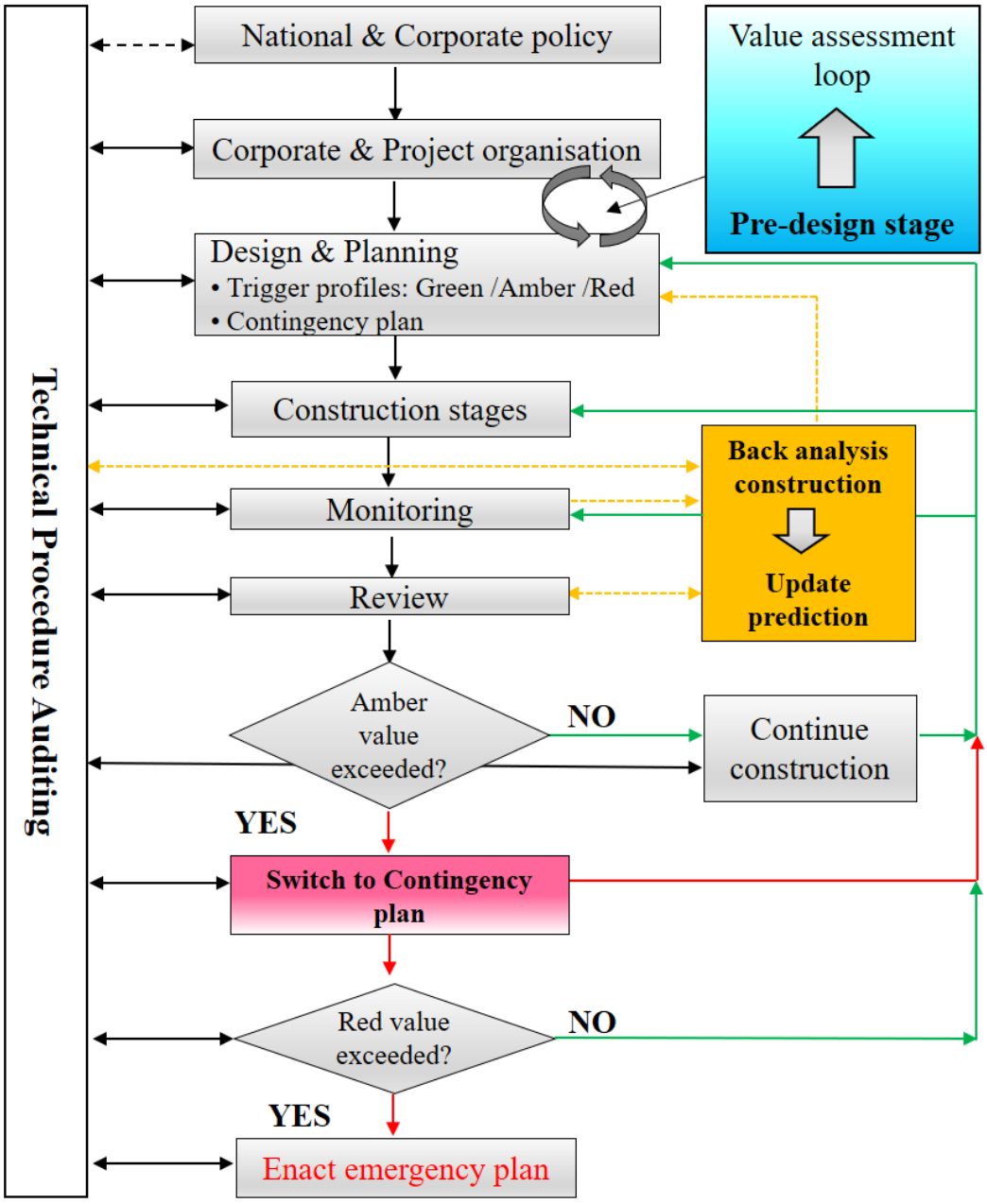

Figure 4. 4 Operational procedure for *Ab initio* Approach A, after (Nicholson *et al.*, 1999)

During construction, with the closely monitored field observations, regular review through the real-time back-analysis compares the present estimations and the planned triggers and feedbacks to construction control with regard to the validation of the most probable design conditions. This In accordance with the agreed design standards in a project, the relevant case

histories are back-analysed at the pre-design stage to provide support for the optimistic design. A cost comparison is also performed to assist in the selection of the appropriate design approach. If the *Ab initio* Approach A is selected for the excavation design, two sets of designs and associated construction sequences are prepared:

- Construction begins with the optimistic design using representative values of the most probable design parameters and most probable design conditions;
- An alternative construction for the contingency plan using representative characteristic values of the design parameters and characteristic design conditions.

real-time back-analysis also enables the project design team to proactively to look for opportunities to modify the optimistic design further in order to maximise cost-effectiveness.

However, if the defined Amber trigger values are breached, the construction will need to be altered to the prepared contingency plan. If the defined Red trigger values are breached, then it is necessary to halt construction immediately and activate an emergency plan.

4.3.2 *Ab initio* Approach B – Cautiously proactive method

Ab initio Approach B is closer to the *Ab initio* approach as defined by Nicolson *et al*. in Ciria Report R185 (1999). Instead of the most probable conditions, a cautious assumption of the characteristic conditions is applied in the starting design, which is based on representative characteristic values of the design parameters. Meanwhile, an alternative modification plan is developed using the representative most probable values of the design parameters and most probable design conditions. It is likely that less support will be required in the modification plan, resulting in an opportunity to omit props and shorten the construction time, which would achieve savings. In accordance with the agreed design standards, two corresponding construction sequences are developed.

It is clear that the material used in the wall construction cannot be optimised in *Ab initio* Approach B, as the wall is designed and constructed according to the cautious design. However, *Ab initio* Approach B allows the construction to be altered to the modification plan during construction when the favourable conditions have been confirmed.

As part of the construction control and risk management, a series of threshold performance values or triggers need to be defined for the following two key changes in construction by Approach B.

- Switching construction from the cautious design to the modification plan; (e.g. < Amber trigger);
- Reviewing construction and switching back to the cautious design (e.g. > Amber trigger).

As a cautious approach, the *Ab initio* Approach B has a slightly better success rate in excavation retaining structure design. For instance, the Batheaston Bypass excavation (Nicholson *et al.*, 1998), and the Crossrail Moorgate Shaft excavation (Chen *et al.*, 2015) have adopted this approach to optimise construction.

Ipso For *Ab initio* Approach B, the back-analysis of the on-going project is critical as it provides the calibrated most probable values of the design parameters to develop an enhanced modification plan.

4.3.2.1 Operation procedure

Approach B shares a similar operational procedure with Approach A, except that the construction control is proactively looking for an opportunity to implement the modification plan, as illustrated in the flowchart in Figure 4. 5.

If the *Ab initio* Approach B is selected for the excavation design, two sets of designs and associated construction sequences are prepared in accordance with the agreed design standards:

- A starting construction by the cautious design using representative characteristic values of design parameters and cautious design conditions;
- A modified construction by the modification plan using representative most probable values of the design parameters and most probable design conditions.

At the construction stage, the cautious design will be applied first, as the starting design. Incorporating inclinometer data and simulating actual as-built construction details, A regular back-analysis, incorporating inclinometer data and simulating actual as-built construction details, can confirm the time when the modification plan should be implemented. Otherwise, the construction will continue in line with the cautious design. If the defined red trigger values are breached, the construction will be stopped immediately and an emergency plan will be enacted.

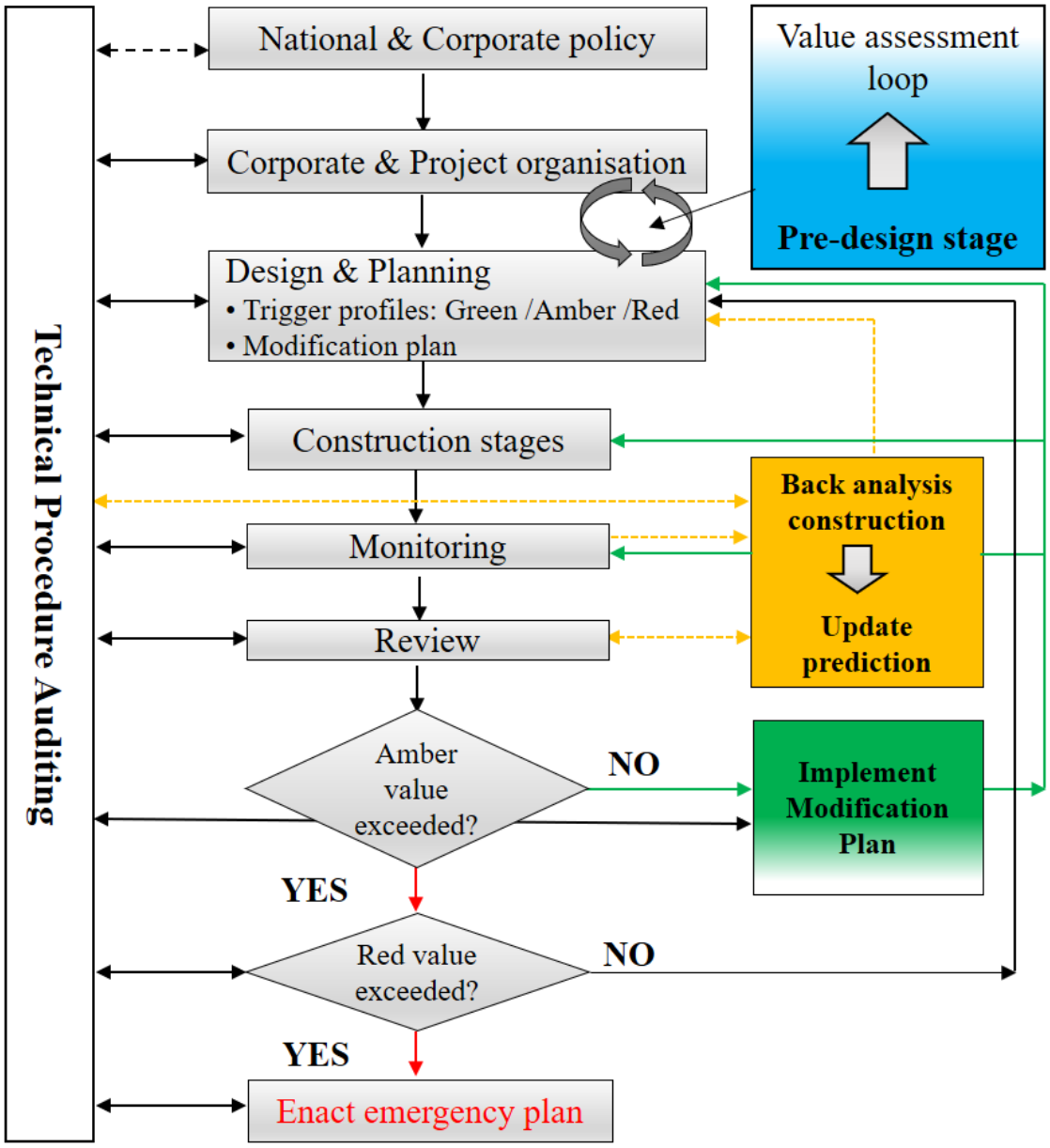

Figure 4. 5 Operational procedure for *Ab initio* Approach B, after (Nicholson *et al.*, 1999)

4.3.3 *tempore* Approach C – Proactive modification method

The *Ipso tempore* approaches differ from the *Ab initio* approaches as they are not planned from the beginning of a project, but rather they are adopted during construction, often after the retaining wall has been installed and excavation has occurred.

Ipso tempore Approach C is a newly defined approach in the new observational method framework. It represents a scenario, in which the observational method is implemented during construction, to proactively make improvements to the construction sequence.

The excavation design is carried out in accordance with the agreed design standards, and the cautious design conditions with representative characteristic values of the design parameters. This is akin to the starting design in the *Ab initio* Approach B. The significant difference is that there was no intention to implement the observational method when the excavation started, and therefore no alternative modification design was prepared. At a point in the construction stage, where field monitoring data indicates that the retaining wall is performing better than predicted, the project team can proactively decide to make changes to the construction sequence. The subsequent actions include a back-analysis to develop a suitable modification plan on the basis of the cautious design. The potential savings may be achieved by omitting unnecessary props and speeding up the excavation process.

A series of threshold performance values or triggers need to be defined for the construction by the cautious design, based on the predictions of serviceability limit state (SLS) analysis results. The representative most probable values of the design parameters will be calibrated through the back-analysis and applied to forward-predict the retaining wall performance at the next excavation stage. While prompt future actions include:

- Making an improvement to the current construction by the cautious design (e.g. Green triggers < field observations < Amber triggers);
- Switching construction from the cautious design to the newly developed modification plan (e.g. < Green triggers); and
- Reviewing construction and switching construction from the modification plan back to the cautious design (e.g. > Amber triggers).

In spite of not having been previously defined, *Ipso tempore* Approach C has been the most commonly adopted observational method in the past decade. For example, three case histories of Crossrail excavations successfully implemented Approach C to achieve the

significant savings: TCR-WTH deep box excavation (Yeow *et al.*, 2014; Chen *et al.*, 2015), WS-DSS shaft excavation (Mills, 2016; Chen *et al.*, 2018), and CWCS box excavation headwall design (Yeow *et al.*, 2012).

For *Ipso tempore* Approach C, the back-analysis of the early construction stages is the way of calibrating most probable values of the design parameters for the modification plan. The back-analysis case histories in similar ground conditions can also be used to calibrate the less accurate but representative values as the most probable design parameters to enable proactive modification.

4.3.3.1 Operation procedure

The operational procedure for the *Ipso tempore* approaches is shown in Figure 4. 6. Cost comparison will only be required when the opportunity for construction improvements appears.

The construction follows the initially developed sequences by the cautious design using representative characteristic values of the design parameters and cautious design conditions. When there is sufficient evidence that shows the retaining wall is performing better than the predictions by the cautious design, the project team can initiate a review to assess whether modifications may be beneficial and appropriate.

If *Ipso tempore* Approach C is adapted to modify the construction, the modification plan is developed using the calibrated most probable values of the design parameters. A corresponding new set of trigger values are defined based on the predictions from the serviceability limit state (SLS) analysis of the modification plan, which assists in the control of the modified construction sequences.

However, if the initial red trigger values defined by the cautious design, are breached, *Ipso tempore* Approach D may present an option prior to enacting the emergency action.

4.3.4 *Ipso tempore* Approach D – Reactive correction method

Ipso tempore Approach D is analogous to the "Best-Way-Out" originally proposed by Peck (1969a). As one of the *Ipso tempore* approaches, there is no intention to apply the observational method at the beginning of the project. However, when an unexpected event occurs, or when an unacceptable event is about to take place, the adoption of *Ipso tempore* Approach D can explore a way of preventing failure or ensuring safety.

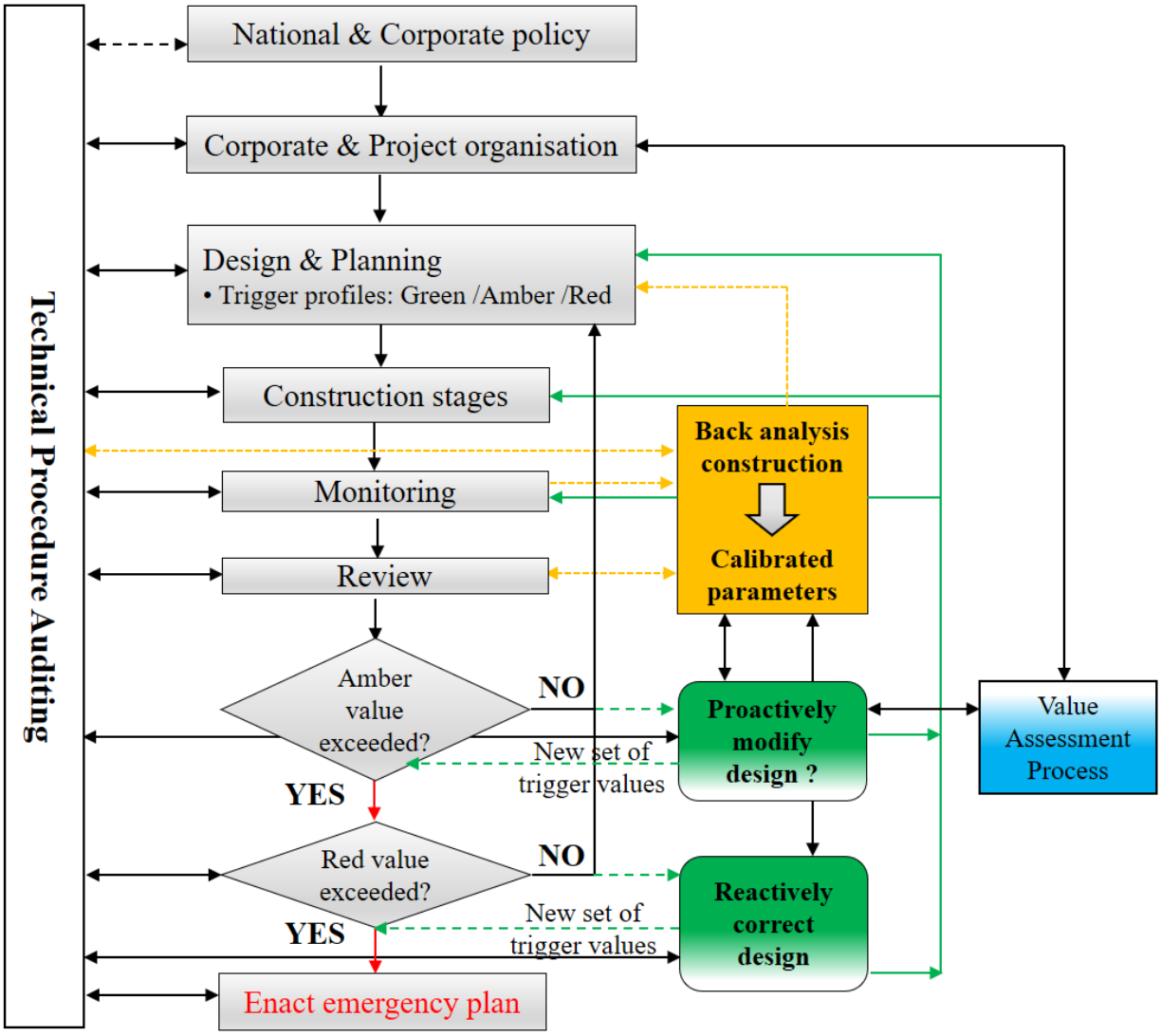

Figure 4. 6 Operational procedure for Approach C & D, after (Nicholson *et al.*, 1999)

The purpose of *Ipso tempore* Approach D, in contrast to Approach C, is to reactively to make corrections to ensure safety or stop potential hazard happening. Nowadays, Approach D is invoked in excavations mostly for performance concerns raised by tighter tolerance criteria for asset protection, especially for excavations in congested urban areas (e.g. the east wall of the LIS-MS shaft excavation, Chen *et al.*, 2015).

4.3.4.1 Operation procedure

According to the operational procedure for the *Ipso tempore* approaches (Figure 4. 6), once the defined plan threshold values (e.g. Red triggers) are breached in excavation, it is a joint decision by the project team whether or not to implement *Ipso tempore* Approach D.

In order to ensure the excavation construction safety and to meet the performance criteria, it is likely that additional supports to retaining walls or a revised construction sequences will be needed, for instance, to excavate with a berm for supplementary support.

4.3.5 Summary of the new observational method approaches

A summary of the four design approaches for the new observational method framework is given in Table 4. 1, showing the comparison between approaches regarding design, back-analysis, implementation objectives, and requirements of the instrumentation and monitoring system.

This new observational method framework was demonstrated through known excavation case histories from literature and industry practice, as summarised in Table 4. 2. It is clear that all case histories adopting the observational method can easily be categorised into the four design approaches under the new framework.

4.3.5.1 Flowchart for design approach selection

The choice between the conventional characteristic design method and the observational method will depend on a number of factors: the designers' awareness and knowledge of construction activities, such as the retaining structures and installation method (e.g. diaphgram wall, secant piled-wall, contiguous piled-wall); construction sequences (e.g. top-down and bottom-up); familiarity with the particular ground and groundwater conditions in the field, and confidence in the assumptions made for the *most probable* conditions.

Other factors beyond the design, such as project finance, contractual arrangements, construction management and the project teams' tolerance for risk, also play in the selection of the design method. As the impact of these factors on the design is indirect, they have been excluded from the discussion on the choice of the design method. A flowchart for the selection of the design approach for excavation is proposed in Figure 4. 7.

Table 4. 1 Summary of the *Ab initio* and *Ipso tempore* approaches in the new observational method framework

Approach		Ab initio (from the begining)		Ipso tempore (in the moment)	
		A (Peck's 69) Optimistically proactive	**B (Ciria C185) Cautiously proactive**	**C (Newly defined) Proactive to make modification**	**D (Peck's 69) Reactive to make corrections**
Design	OM implementation	Planned from project inception		Adopted during the construction	
	Back analysis (at pre-design stage)	Needed	Preferred	N/A	
	Starting design (condition & design parameters)	Most Probable	Characteristic	Characteristic	
	Alternative design (condition & design parameters)	Contingency Plan (Characteristic)	Modification Plan (Most Probable)	N/A	
	Back analysis (during construction)	Verify Most Probable design	Calibrated Most Probable design parameters		
		Update trigger values		Progressive modification of design & update trigger values	
	OM design objectives	Reduce wall size and depth	Reduces support	Reduces support	Increase support & Ensure safety
Value engineering	Saving in material	Maximise	Potential	Possible	Assurance of acceptable safety
	Saving in programme	Possible	Maximise	Potential	
	Minimum Requirement	Time and cost to implement OM ≤ the benefits achieved			
	Construction programme	Planned for OM		Amended when OM is applied	
I & M	Starting plan	Extensive	Standard	Standard	
	Starting frequency	High	Medium	Medium	
	Additional Instruments	Not needed	Needed	Needed when OM is applied	
	Increased frequency	Not needed	Needed	Needed when OM is applied	
Risk		Medium	Low	Medium	High

Notes:
1. The descriptive risk level is given to each design approach, showing the relative risk among four approaches
2. The recommendation on the instrument & monitoring frequency: High = hourly to daily; Medium = daily to weekly

Table 4. 2 Classification of the observational method in excavation case histories using the new observational method framework

Case history	**Reference**	**Observational Method**	**New Observational Method Approach**
Harris Trust excavation support	Peck (1969a)	Peck's *Ab initio* approach	*Ab initio* Optimistically proactive Approach A
Minster Court excavation	Tse & Nicholson (1992)	Ciria R185 *Ab initio* approach (Cautious *Ab initio*)	*Ab initio* Cautiously proactive Approach B
Channel Tunnel terminal at Folkestone	Young and Ho (1994)	Peck's *Ab initio*	*Ab initio* Optimistically proactive Approach A
CTRL - Holywell & Castle Hill, north of Folkestone, UK	Powderham (1994)	Progressively modified design	*Ipso tempore* Proactive modification Approach C
Tokyo basement for a high-rise building	Ikuta *et al.* (1994)	Progressively modified design	*Ab initio* Cautiously proactive Approach B
Batheaston Swainswick Bypass	Nicholson *et al.* (1999)	Ciria R185 *Ab initio* approach (Cautious *Ab initio*)	*Ab initio* Cautiously proactive Approach B
Limehouse Link	Glass and Powderham (1994)	Progressively modified design	*Ipso tempore* Proactive modification Approach C
Mansion-house	Powderham (2002)	Peck's 'Best-Way-Out'	*Ipso tempore* Reactive Approach D
CWCS Station - Headwalls	Travers and Yeow (2014)	Progressively modified design	*Ipso tempore* Proactive modification Approach C
TCR-WTH	Yeow *et al.* (2014)	Progressively modified design (Not a defined Ab initio approach)	*Ipso tempore* Proactive modification Approach C
LIS- MS-North Wall*	Farooq *et al.* (2015) Chen *et al.,* (2015)	Progressively modified design (Cautious Ab initio)	*Ab initio* Cautiously proactive Approach B
LIS-MS-East Wall	Chen *et al.* (2015)	Peck's 'Best-Way-Out'	*Ipso tempore* Reactive correction Approach D

Note: description of case histories refers to Table 2.1.

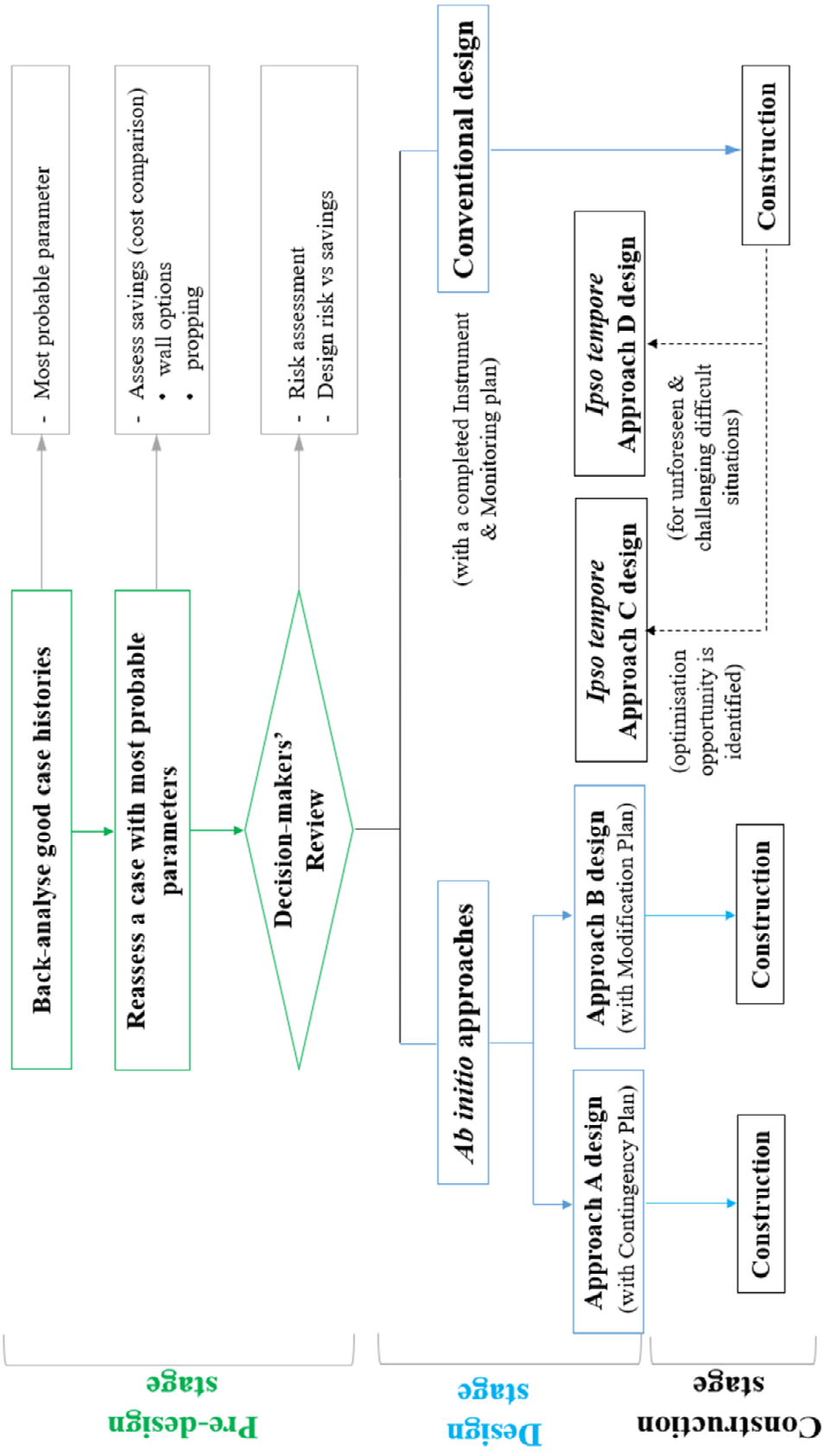

Figure 4. 7 Flow-chat for selection of design approach for deep excavations

The choice between *Ab initio* Approach A & B particularly depends on the designers' prevailing knowledge of the ground conditions. Therefore, a pre-design stage is suggested prior to the design stage. In this pre-design stage, designers can explore similar excavation case histories, back-analyse them and re-assesses one of the cases for a cost comparison. Thus, this information can be useful for decision-makers (e.g. clients, contractors and actively engaged third parties) in selecting an appropriate design method for a new excavation project.

The pre-design stage exercise provides the most probable design parameters to develop the optimistic design and preliminary evaluation of cost comparison. The assessment presents a direct comparison between potential risks and possible savings hence assisting the decision-makers in selecting the most advantageous design approach. Without this assessment, it would be reckless to adopt *Ab initio* Approach A for excavations in unfamiliar ground conditions, instead, the cautious *Ab initio* Approach B may be applicable.

If the conventional design method is selected to carry out the design, the opportunity to employ the *Ipso tempore* Approach C can be evaluated during the construction, when the condition is right for the implementation. The *Ipso tempore* Approach D can be useful when unforeseen events occur. All these choices rely on a suitable instrumentation and monitoring plan to provide reliable field observations for back-analysis.

4.3.5.2 Threshold values (triggers)

A series of the planed threshold values or triggers need to be defined for construction control. The choice of threshold values or triggers should be based on clear performance indicators. For example, asset protection is a major issue for excavation projects in urban areas. Therefore, either settlement at a monitored location away from the excavation boundary, or a proxy such as wall displacements, can be chosen as indicators. Appropriate threshold values should be selected based on an assessment of tolerable distortions, either empirically or by numerical simulation. Tighter asset protection criteria require strong and accurate predictive models to assess the performance. However, in many cases, trigger values are set stringently without clear performance analysis.

4.4 Back-analysis

The observational method relies on a reliable and consistent process to provide the most probable design parameters for the optimistic design. Back-analysis is a process of using the field measurements in order to obtain the input parameters (Miranda *et al.*, 2011). This process is adopted in the observational method new framework to calibrate the most probable design parameters.

Figure 4. 8 indicates there are four major elements to the back-analysis process: inputs, predictions, comparison and outputs. All four elements relate to the numerical analysis adopted in the back-analysis.

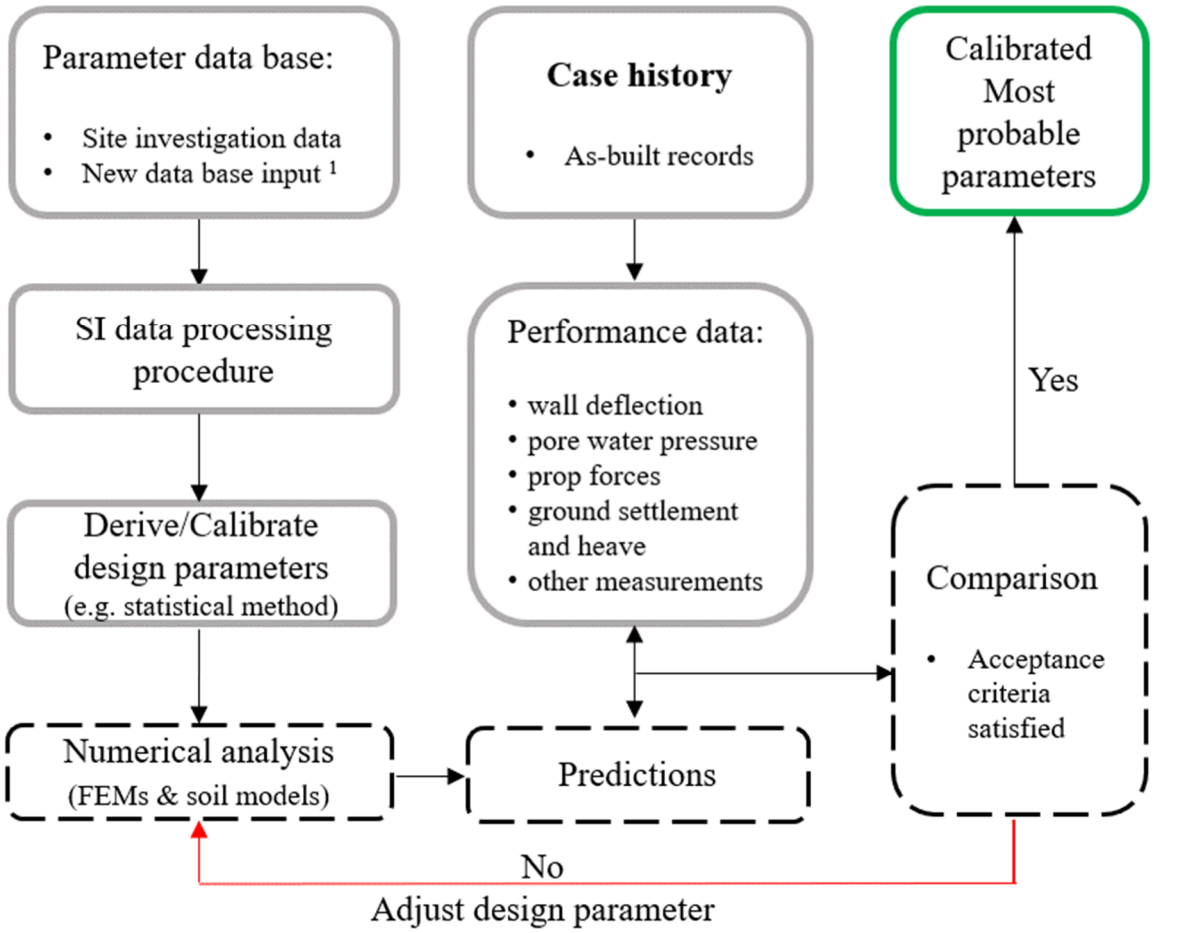

Figure 4. 8 Diagram of back-analysis process

4.4.1 Inputs

The input parameters in the back-analysis comprise the field observations (e.g. monitoring data, the as-built construction details) and input parameters for the numerical analysis. The first part is factual data, and their quality and reliability rely on a review process. The second part of inputs is defined by the soil constitutive models used in the numerical analysis and they may not be transferred across different models. The selection of material parameters is generally linked to site investigation data (e.g. laboratory and field testing data).

For example, the basic linear elastic and perfect plastic Mohr-Coulomb model requires a minimum of five model parameters: strength (ϕ', c' or c_u), stiffness (E' or E_u), Poisson's ratio (ν), and dilatancy angle (ψ). In addition, basic soil properties need to be provided, such as density (γ), earth pressure coefficient (K_0), soil/wall friction ratio. An example of deriving the Mohr-Coulomb model input parameters for London Clay is presented in Chapter 5.

An increased number of model parameters is required for advanced soil constitutive models to simulate complex soil behaviours. For instance, the BRICK model reviewed in Chapter 2, is able to simulate the non-linear soil stiffness with the strain and a few other features of London Clay's response. An example of the calibration of the BRICK model input parameters for London Clay is presented in Chapter 6.

4.4.1.1 Site investigation data

Ground investigation can only discover a small area of soils and uncertainty remained in the ground conditions, the site investigation data is a major and only reliable resource in deriving the values of input parameters. The quantity and quality of the site investigation determine the reliability of the data. The empirical relationships between different test results can be useful to crosscheck for quality. For instance, Stroud (1989) suggested the standard penetration test (SPT) blow-count N and the undrained shear strength (c_u) are correlated, $c_u=f_1\times N_{60}$. Where f_1 is related to the plasticity index (I_p) of the soil. With a typical I_p value between 30 to 50 in London Clay, $f_1 = 4.5$ is recommended.

4.4.1.2 As-built construction information

The back-analysis is performed to simulate the response of the ground and structural elements, like ground settlements, retaining wall deflections and temporary prop strut forces. These estimates are compared with the corresponding observations – levelling stud data, inclinometer data and strut forces from vibrating strain gauges installed on the temporary prop. Therefore, it is necessary to replicate the as-built construction details in the back-analysis to eliminate errors due to approximate design assumptions. For instance, the monitoring data selected for comparison needs to be extracted for the date at which the back-analysis is replicated. The actual structural properties of the supports (e.g. temporary props) should be confirmed from the as-built details.

Surcharge loads and other site activities can lead to unexpected responses, and they should be confirmed and included in the back-analysis. For example, in a few excavations, excessive ground movements due to ground compensation grouting work nearby were observed.

4.4.1.3 Field monitoring data

Monitoring data is collected during construction as a measure of construction control and risk management. In constructions by conventional designs, these observations are used to access the performance of the excavation to ensure construction safety. In many excavation projects by the conventional design, their observations show the predictions are as high as twice the measurements, hence monitoring data are often treated carelessly. The Crossrail case histories presented in Chapter 3 showed errors in the monitoring data, as well as methods to diagnose and correct these errors.

In the back-analysis, one of the priorities is to ensure the reliability of the monitoring data through a data review process.

4.4.2 Predictions

A more accurate predictive tool means fewer iterations are needed in the back-analysis. A good prediction depends largely on the soil constitutive model and its limitation to determine the tolerance in the comparison.

Simplifying assumptions are also made to enable modelling. 3D FEM can model accurately the actual excavation geometry and no compensation assumptions are required for

structural elements, leading to the best predictions. However, it takes a lot of efforts to set up the 3D FEM model and to adjust it to match the as-built construction details for the back-analysis. All of these factors should be taken into account in the selection of FEMs for the back-analysis.

The performance of the back-analysis using different FEMs is presented through Crossrail excavation case histories in Chapter 5.

4.4.3 Comparison

The comparison is the control step in the back-analysis process, in which predictions are compared with observations, and input values of the predictive model are adjusted until the two matches. The convergence criteria should be rational, covering all possible errors in the observations and predictive models, and practical for the back-analysis. A loose tolerance leads to most probable parameters that are less representative, but a tight tolerance can result in too many iterations for practical use.

A direct visual comparison was applied in this research, back-analysing the Crossrail excavations. A point-by-point visual comparison between predictions and observations was carried out for the selected ground/structure response profiles. Selecting allowable tolerance is based on combined considerations of the random errors in the field observations, modelling errors and construction safety. Through the comparison, the representative most probable values of the design parameters for different soil models are calibrated for different FEMs. The performance of FEMs and soil models in the excavation back-analysis is also illustrated in Chapter 5.

Alternatively, error functions and appropriate optimisation algorithm for a rigorous and unbiased back-analysis can be applied, such as a least-square minimisation approach and a maximum likelihood approach. More optimisation algorithms are also available for automated back-analysis, such as the classical optimisation algorithms: Simplex and Gradient-based method (steepest descent); artificial neural networks (ANN) (Jahangir and Jagath, 1998; Hashash *et al.*, 2003), genetic algorithms (GA) (Miranda *et al.*, 2011;Yazdani *et al.*, 2013) and evolutional strategies (ES) (Moreira *et al.*, 2013). Recently, the development of Bayesian search techniques enhance the automated back-analysis process, furthermore, they can perform the statistical analysis of the estimations (Tang and Kung, 2009; Gardoni *et al.*, 2009; Juang *et al.*, 2012; Cañavate-Grimal *et al.*, 2015; Jin, 2018).

4.4.4 Outputs

The output of the back analysis is the calibrated most probable values of the design parameters. The values from one case history can feed to other projects, as a starting input database. Examples of calibration of the representative values of the most probable parameters for the London Clay sub-units are presented in Chapter 5, which are based on the Mohr-Coulomb soil model and three different FEMs: semi-FE (FREW), 2D FE (Plaxis 2D) and 3D FE (LS-Dyna 3D). As a comparison, the representative values of the BRICK model most probable parameters for the London Clay sub-units are calibrated by 3D FE (LS-Dyna 3D) and presented in Chapter 6.

Chapter 5

Back-analysis Crossrail Excavations by the Mohr-Coulomb model

The importance of the back-analysis in the observational method was highlighted in Chapter 4, as the only way to calibrate the representative most probable values of the design parameters for the alternative optimistic design. The most relevant design conditions can be also validated in this process. Since design parameters are inherently linked to the soil constitutive model, the calibration of the most probable design parameters is also be subjected to the soil models.

Chapter 5 presents the back analysis of the Crossrail deep excavations using the Mohr-Coulomb soil constitutive model, and the back-analyses are performed by three different numerical finite element analysis methods (FEMs). Initial values of the design parameters are derived from the site investigation, laboratory and in-situ testing data, while the representative values of the most probable parameters are calibrated through back-analysis.

5.1 Numerical analysis method

Three types of FEMs were adopted in the original designs for assessing ground movements and developing the as-built modified design in the Crossrail excavation case histories, as summarised in Table 5.1, including Pseudo-FREW(or pseudo-FEM), 2D FEM and 3D FEM.

Table 5. 1 Summary of numerical analysis (software) for in the Crossrail excavation case histories

Numerical analysis	Semi-FEM	2D FEM	3D FEM
Analysis program	FREW[1] / WALLAP[2]	PLAXIS[3] / SAFE[4] / FLAC[5] / LS-DYNA[6] / ABAQUS[7]	PLAXIS[8] / FLAC[9] / LS-DYNA / ABAQUS
Soil Constitutive models	Mohr-Coulomb soil model	Mohr-Coulomb/ Hardening soil / Hardening soil small strain / Modified Cam Clay / Hypoplastic / other soil models	Mohr-Coulomb / Hardening soil / Hardening soil small strain / Modified Cam Clay / Hypoplastic / BRICK / Modified three-surface kinematic hardening model / other soil models
Predictions	• wall deflections • wall forces (bending moment and shear force); • strut loads	• wall deflections • wall forces (bending moment and shear force); • strut loads; • ground settlement profiles in the plan; • groundwater pressure vertical profile.	• wall deflection • wall forces (bending moment and shear force) • individual prop strut loads • ground movement profiles in space; • groundwater pressure vertical profile
Remarks	• fewer input parameters; • fast computation; • simplified modelling assumptions; • fewer predictions	• flexible in soil models choices; • relatively fast computation; • more predictions available than semi-FEM; • simplified modelling assumptions;	• flexible in soil model choices; • most predictions available; • more accurate modelling assumptions; • relatively longer computation and model preparation time.

Note: the listed above soil constitutive models are thought relevant to over-consolidated clay (e.g. London Clay), other soil constitutive models are avaiable in the analysis probrams

1. FREW version 19.0 and above (Oasys, 2017);
2. WALLAP version 6.0 (WALLAP, 2017) ;
3. PLAXIS 2D version 2016 (PLAXIS, 2016a);
4. SAFE version (Oasys, 2014);
5. FLAC version 8.0 (Damping, 2015);
6. LS-Dyna version 940 (Oasys, 2010);
7. ABAQUS version (Abaqus, 2010);
8. PLAXIS 3D version 2016 (Brinkgreve, Engin and Swolfs, 2016a);
9. FLAC 3D version 5.0 (Itasca, 2012).

Different approaches have varying abilities to accurately model excavation construction stages and predict all ground/structure responses. In general, the increased details are available from semi FEM to 2D FEM and 3D FEM, but less simplified assumptions are required. In practice, each technique is available through different commercial software packages, which also offer different constitutive soil models.

In the Crossrail excavations back-analyses by the Mohr-Coulomb model, all three types of FEMs were applied to investigate the impact on the calibrated most probable parameters. The same software used in the original design was adopted for the back-analysis to avoid introducing additional modelling errors. For instance, the original Crossrail TCR-WTH design was carried out with Pseudo-FREW (semi-FEM), Plaxis 2D (2D FEM), in addition to Ls-Dyna 3D (3D FEM) which was used for ground movement assessments.

5.1.1 Back-analysis by FEMs

A more detailed overview of the back-analysis process using the FEM with the Mohr-Coulomb model is presented in Figure 5. 1. The initial values of the Mohr-Coulomb input parameters are based on the design records, including site investigation data and historical case history data. Other required input parameters in the back-analysis model refer to the factual as-built construction records. The received monitoring data are reviewed and compared with the predictions.

In comparison, when the difference between predictions and observations exceeds the predetermined tolerance criteria, adjustments are made to the values of the Mohr-Coulomb input parameters. Other required input information is fixed. This iterative back-analysis process is repeated until the criteria are satisfied, providing the calibrated most probable design parameters for the Mohr-Coulomb constitutive model.

5.2 Pseudo-FREWback-analysis of the TCR-WTH

The original design of the Crossrail TCR-WTH excavation used the characteristic values of Mohr-Coulomb parameters and a mixed earth pressure approach for excavation analysis. During construction, a back-analysis of the retaining wall deflections was performed using the reported inclinometer data with FREW model, which led to the successful modified as-built design. A total earth pressure (undrained) analysis was considered as the appropriate design

assumption in the back-analysis, as the excavation period was less than 12 months and no significant change was observed from the surrounding groundwater pressure monitoring data.

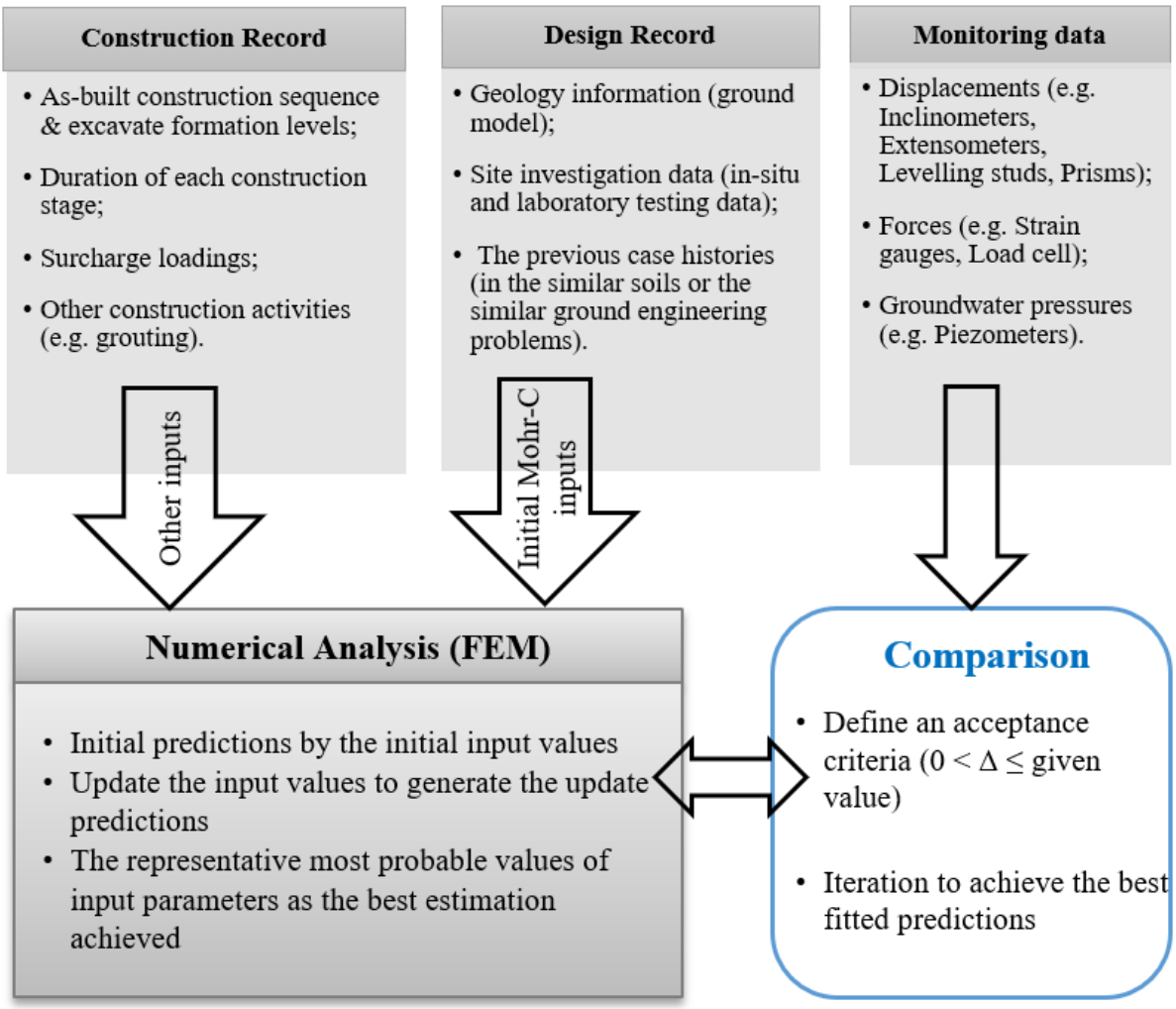

Figure 5. 1 The process of back-analysis using FEM with the Mohr-Coulomb soil model

However, a review of the inclinometer (SAAs) data resulted in significantly corrections, which reduced the maximum wall lateral movements from early excavation stage 3 (Table 3.3), as indicated in Figure 3.10. This necessitated another back-analysis using the retaining wall deflections from the corrected inclinometer data to update the representative values of the most probable Mohr-Coulomb parameters.

5.2.1 FREW model

The east diaphragm wall panel on section A-A'(Figure 3.1) was modelled in semi-FREW for the original design. This model was then used in the back-analysis of the as-built modified

design. The original FREW model was modified according to the as-built construction records, in details such as stratigraphy levels, wall & temporary struts' properties, the excavated levels at each stage. The model for the final excavation stage 6 is presented in Figure 5. 2.

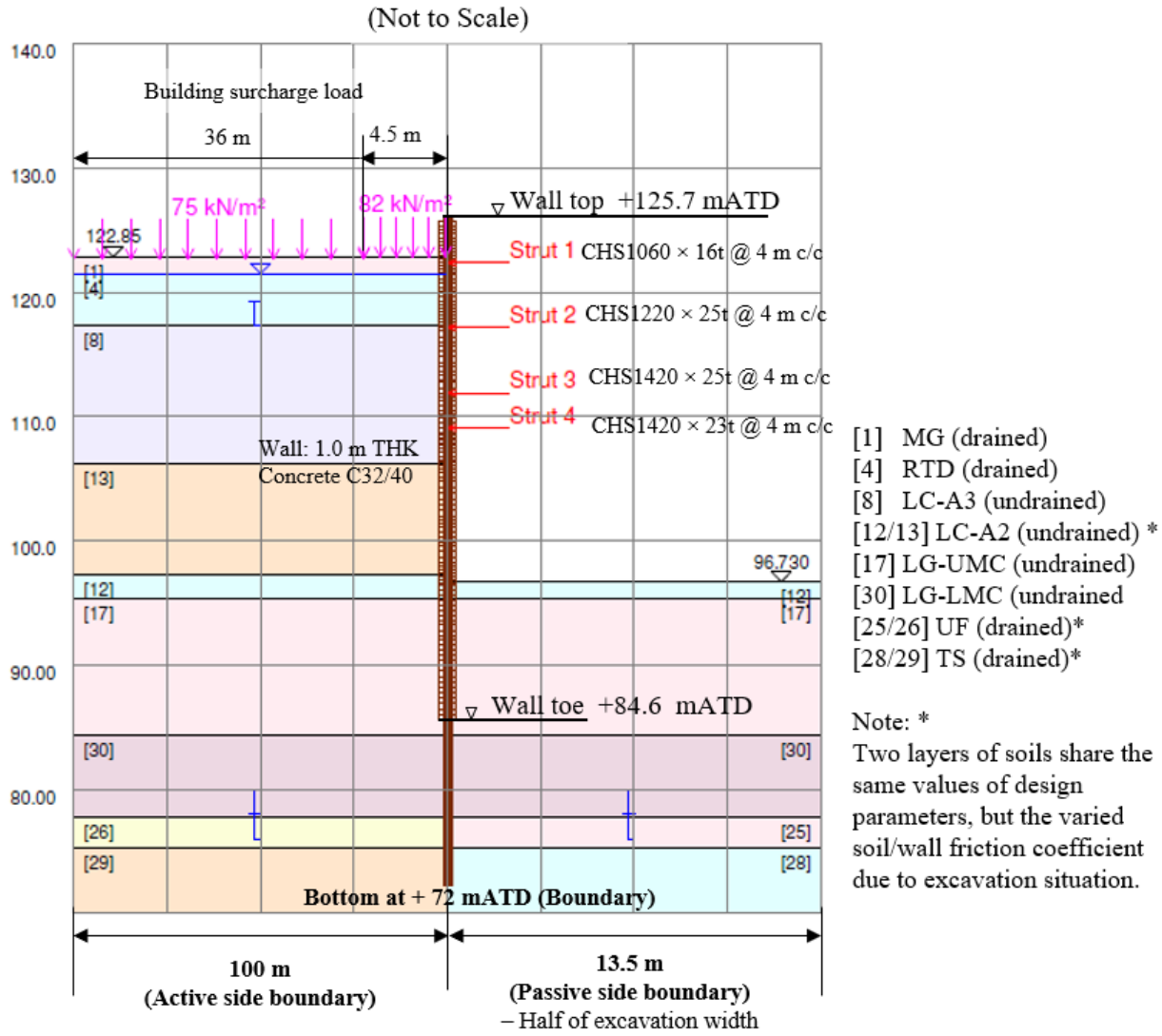

Figure 5. 2 FREW model for TCR-WTH deep box at final excavation stage 6

The passive side boundary was placed at half of the excavation width for section A-A', about 13.5 m. The active side boundary was three times larger than the maximum excavation depth (29.5 m), approximately 100 m. The boundary at the bottom was assumed in the Lambeth Group, about 12 m below the diaphragm wall toe level (+84.6 mATD for panel P50 diaphragm wall where the SAA-8003 was installed).

The surcharge load of the existing building, 75 kPa, was applied in section A-A' at the existing foundation level, about 3 m below the ground surface level. A traffic load combined

with the adjusted building surcharge loads, 82 kPa, was applied immediately next to the wall extending a distance of 4.5 m.

The structural properties were updated for the as-built specifications: grade C32/40 concrete with a Young's Modulus of $E_{concrete} = 33 \times 10^6$ kN/m^2; circular hollow section (CHS) steel temporary struts with a Young's Modulus of $E_{steel} = 200 \times 10^6$ kN/m^2 with final configurations shown in Figure 5. 2.

The design conditions assumed for the modified design are compared with the one in the original design, as summarised in Table 5. 2. Total stress analysis (undrained) on both active and passive sides of the excavation was carried out due to the relatively fast construction. For the first stage of the FREW analysis, in which a drained calculation was carried out to establish the initial stresses, the groundwater profile matched the pore-water pressure design profile for the TCR-WTH design (Figure 3.2).

Table 5. 2 Comparison of design conditions

FREW model	Original design assumptions	Modified design assumptions
Short-term excavation analysis	Mixed earth pressure	Total stress
Over-dig	0.5 m	na
Softening	80%	na

5.2.2 Initial values of the Mohr-Coulomb input parameters

Different values of the design parameters were applied in the original design and the modified design. Examples of the undrained shear strength (c_u) and the undrained soil stiffness (E_u) for over-consolidated London Clay and Lambeth Group are plotted against triaxial laboratory data in Figure 5. 3.

A lower bound of the undrained shear strength values from the triaxial testing data was derived as the representative characteristic strength in the original design. In the as-built modified design, values closer to the mean of the triaxial testing data was adopted for the c_u design parameters. However, it is unclear how these updated 'most probable' values were derived.

The undrained soil stiffness from the triaxial testing results at three shear strain levels (0.01%, 0.05% and 0.1%) are plotted in Figure 5. 3. The triaxial results at shear strain level of 0.05% were adopted as representative characteristic values in the original design. In the

modified design, the representative most probable values were derived based on empirical correlations: E_u/c_u =1000 for London Clay, and E_u/c_u =2000 for Lambeth Group (Yeow *et al.*, 2014). It is observed that the most probable E_u values match with the triaxial results at shear strain level of 0.05% in the LC-A3 division, but are slightly above the results at shear strain level of 0.05% in the LC-A2 division, whereas no connection between the two seems to exist in Lambeth Group.

It is important to avoid bias and personal influence in deriving the initial input parameters for the back-analysis. A statistical regression method is adopted for this work to minimise the influence of the operator on the results.

A linear regression using the least-square method provides the simplest description of a parameters' variability from the scattered data set. Quality of fit is indicated by the coefficient of determination R^2: the closer to 1.0, the better the fit. Judgment is also applied for interpretation, for instance, a negative undrained shear strength value is clearly impossible.

It is recommended to manually filtered the data set to eliminate outliers. The process may start using all available data for the target site, then gradually reduce the size of the data set to the most relevant data. Whether to include or exclude outliers will depend on the influence of these outliers. They can be identified by reviewing the geological description in the borehole logs, for example, if claystone or dense sand layers identified at locations where the unusual testing results are shown. Outliers may cause a significant impact on the derived regression, such as a sharp or flat gradient, unrealistic values at the top or the bottom of a stratum.

An example of deriving initial values of the undrained shear strength from scattered testing data for the TCR site is described below. The data comprises of the laboratory (e.g. triaxial test) and the in-situ field tests (e.g. standard penetration test SPT, cone penetration test CPT, and self-boring pressuremeter test SBP).

The available undrained shear strength testing data were from boreholes drilled in site investigations for the TCR site, as summarised in Table 5. 3 and shown in Figure 5. 4.

The undrained shear strength data from the triaxial tests were filtered and the supervised linear statistical regression method was applied to derive the initial values for the back-analysis, using:

a) all available data;
b) data from the boreholes within a 50 m distance to the TCR-WTH site;
c) data from the boreholes right next to the TCR-WTH deep box.

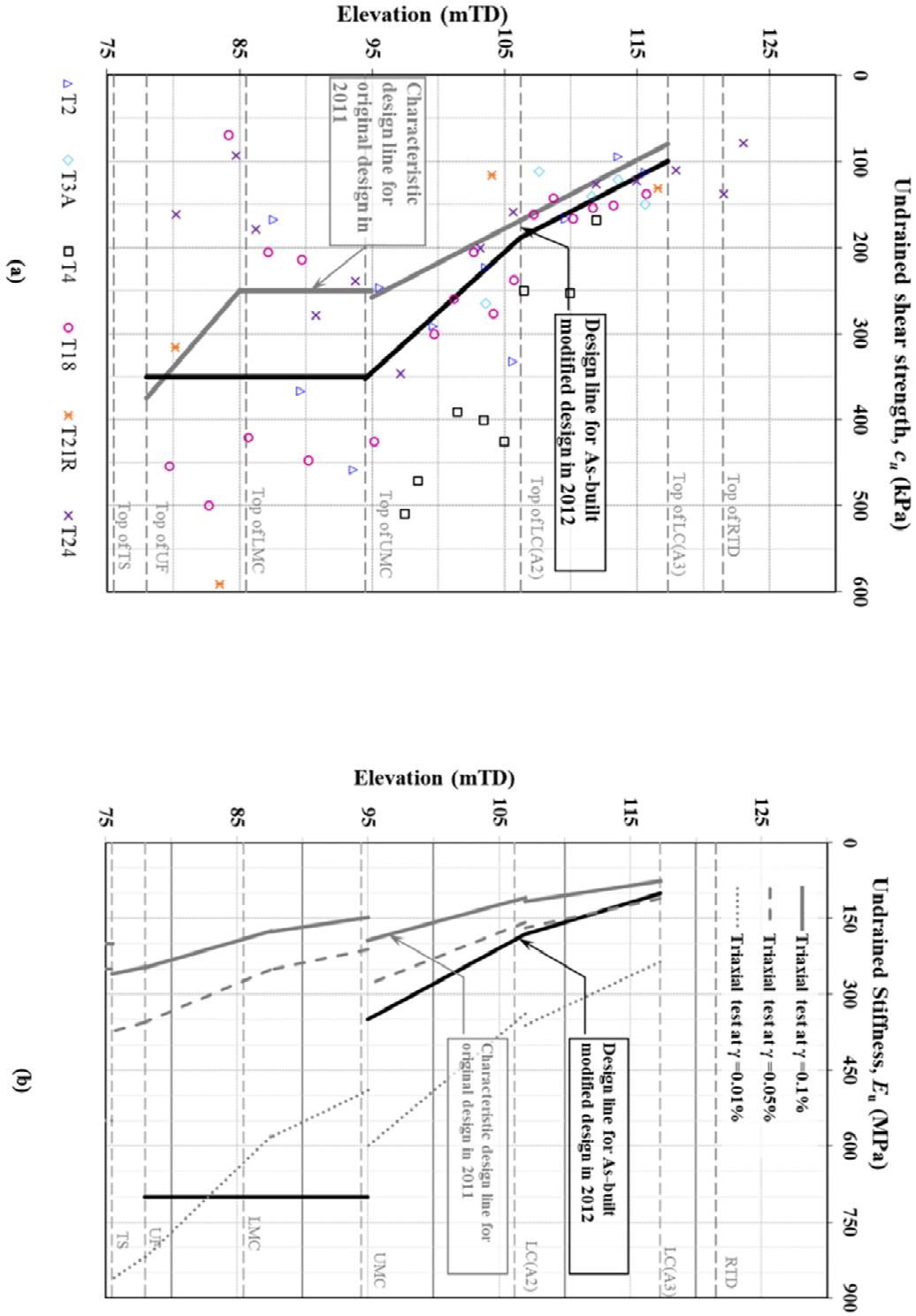

Figure 5. 3 Design values versus laboratory testing data (a) undrained shear strength; (b) undrained shear stiffness

Table 5. 3 Summary of boreholes used to derive the design values of the undrained shear strength

BH ID	Top (mATD)	Depth (m)	Base of LC (mATD)	Source	Log	Remark
T2	125.6	40.5	95.9	1992 GI	Yes	shallow box
T3A	125.7	25.0	n/a	1992 GI	Yes	shallow box
T4	125.5	40.2	94.5	1992 GI	Yes	deep box
T18	125.7	65.5	94.8	1992 GI	Yes	deep box
T19P*	125.8	n/a	n/a	2008 GI	No	Shallow box
T20*	125.7	n/a	n/a	2008 GI	No	Shallow box
T21R*	125.2	60.0	91.8	2008 GI	No	> 40 m distance
T24*	125.3	55.0	94.8	2008 GI	No	> 50 m distance

Note: * T19P to T24 by the 3rd party ground investigation, no borehole logs information was available to review.

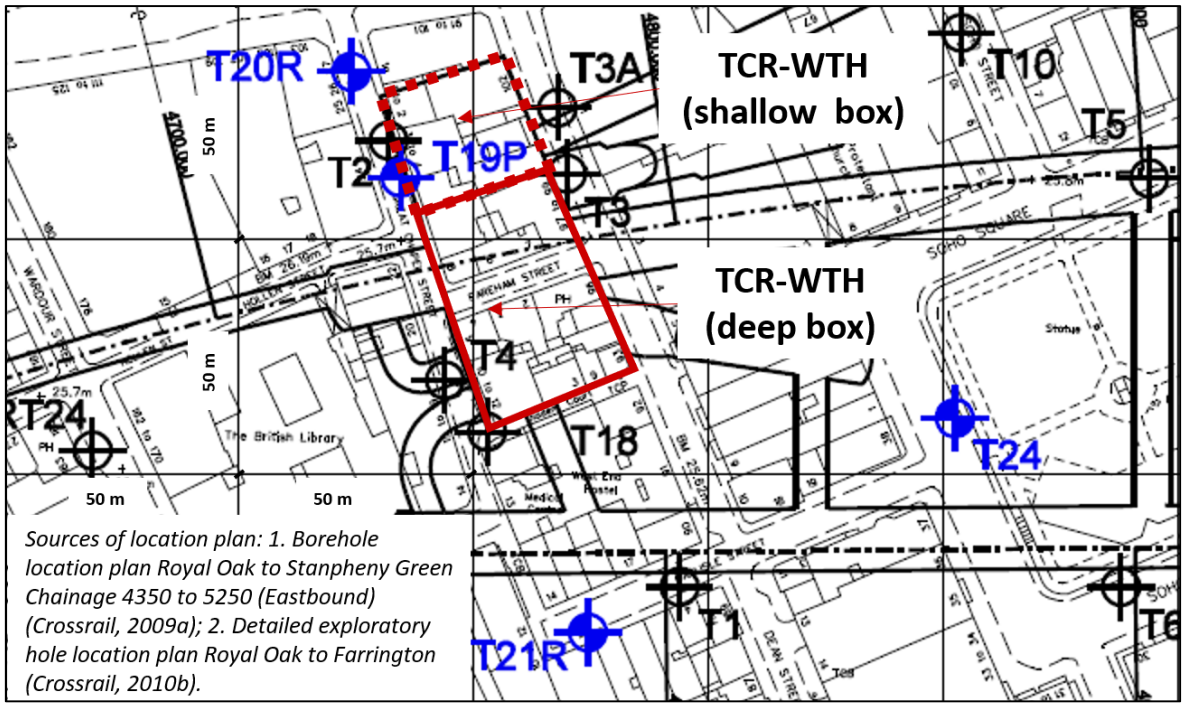

Figure 5. 4 Layout of boreholes nearby the TCR-WTH site

This process reduced the size of the data and focused on the data from boreholes closer to the back-analysed location, although fewer data may be less representative of the ground conditions.

The plots for each data set together with the corresponding linear regressions and the values of the coefficient of determination R^2 for the LC-A3 division are shown in Figure 5. 5. There were no outliers identified in these data sets, with the size of the data set narrowed down the higher fitness R^2 values were obtained. The regression of c_u=75+15.6z was obtained from

the 3rd data set, including the adjustment at the top to avoid the negative values. This regression was almost comparable with the mean value of the 3rd data set, c_u=176 kPa, and was adopted as the initial input undrained shear strength parameter in the back-analysis.

In addition, the field testing results were also reviewed to estimate undrained shear strength, based on an empirical correlation, $c_u = f_1 \times N_{60}$ (Stroud, 1989), N_{60} is the Standard Penetration Test (SPT) blow-count with energy correction. This correlation has been applied in a number of projects in clays and is recommended by Ciria C760 (Gaba *et al.*, 2017).

The SPT blow count N_{60} data was filtered and the supervised linear statistical regression method was applied to derive the design values of N_{60} and calculate the undrained shear strength c_u values, using:

a) all available data;
b) data as per above, excluding the outliers;
c) data from the boreholes within a 50 m distance to the TCR-WTH site;
d) data from the boreholes right next to the TCR-WTH deep box.

Plots of four data sets are shown in Figure 5. 6, including the derived linear regressions and the coefficient of determination R^2 values to indicate the fitness of regression in each data set. In general, the SPT N_{60} data shows less scatter compared to the undrained shear strength (c_u) data. However, the extreme values were spotted in the SPT N_{60} data set (e.g. N_{60} = 125 and 200 in Figure 5. 6), they resulted in a poorly fitted regression with an R^2 = 0.0107.

Some extreme values of the SPT N_{60} can be received from tests, which is often caused by a change of local geology. For example, N_{60} of 200 from borehole T18 in Figure 5. 6, the review of the borehole log T18 (Figure 5. 7) has revealed at about 11.3 m below the ground level, the mudstone was encountered. A total blow-count of 90 for 0 mm penetration SPT test result was interpreted as an equivalent N_{60} of 200. As the SPT N_{60} test is not from the LC-A3 layer, this data is treated as an outlier. Reviewing all boreholes' logs, in total two outliers were identified and excluded in the data set (b) in Figure 5. 6. This resulted in an improved fitted regression for the data set (b) with an R^2 = 0.1909.

The increased fitness R^2 values are obtained with the size of the data set further reduced in SPT N_{60} data set (c) and (d) in Figure 5. 6. The regression of N_{60} = 10.6 +2.2z with R^2 = 0.5809 from the data set (d) is taken to calculate the undrained shear strength (c_u) and compared with the derived regression for c_u from triaxial testing data in Figure 5. 8. A value of f_1 from 4.5 to 5.5 is recommended to derive $c_u = f_1 \times N_{60}$ for London Clay with a typical I_p of 30 to 50 (Stroud, 1989).

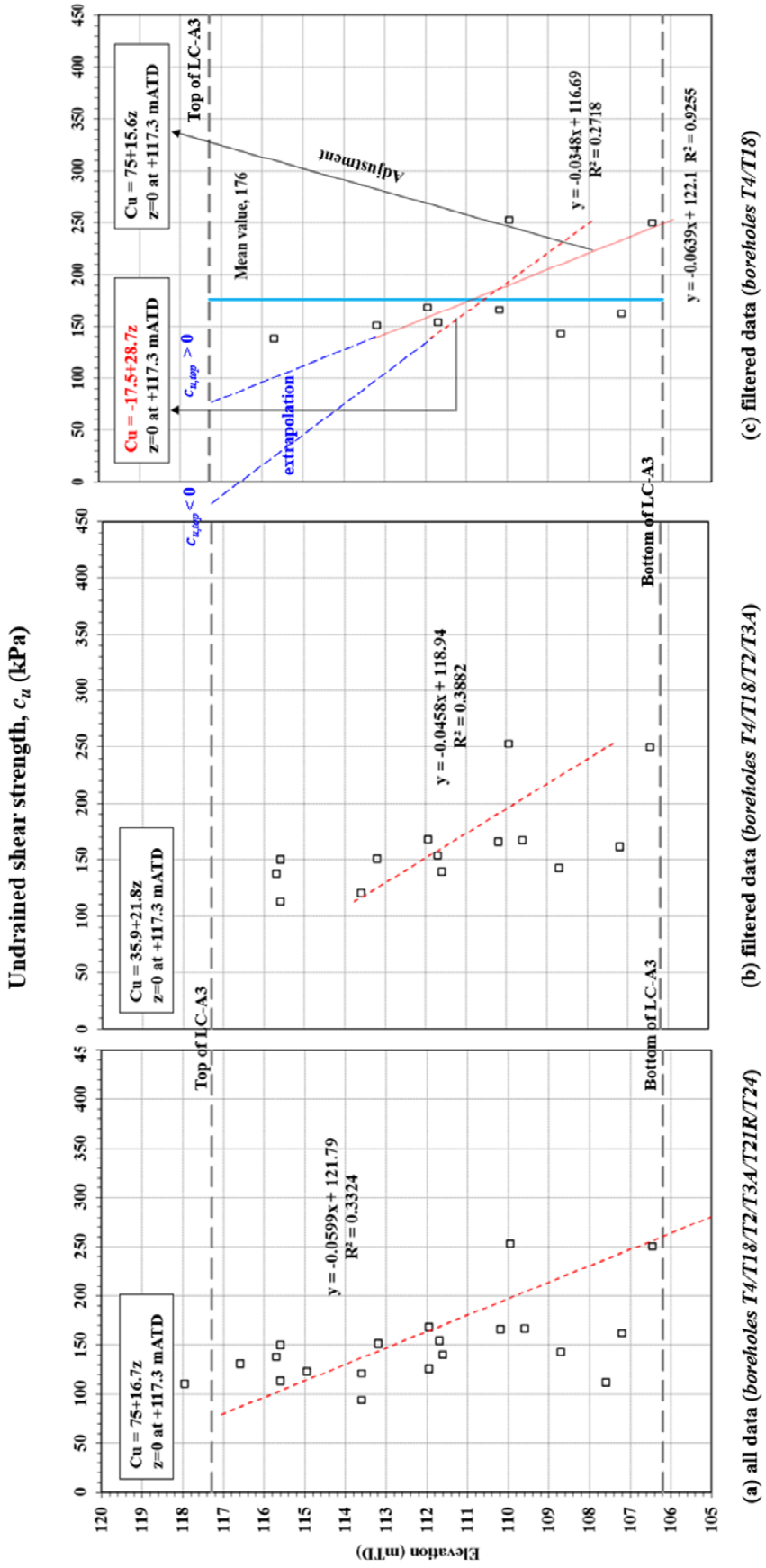

Figure 5. 5 Deriving the linear statistical regression of undrained shear strength (c_u) for LC-A3 division

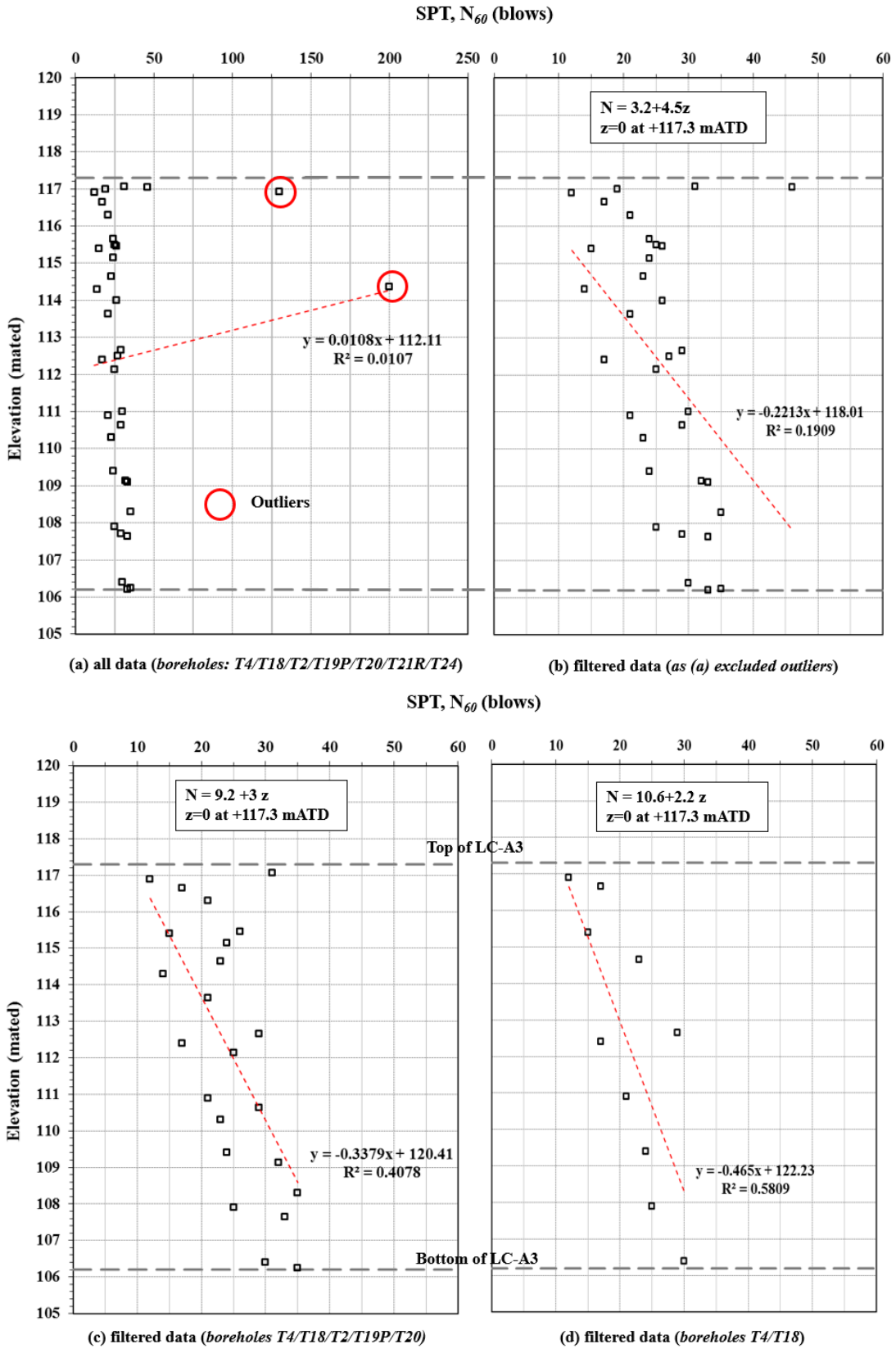

Figure 5. 6 Deriving the linear statistical regression of SPT N_{60} for LC-A3 division

These f_1 values lead to the lower calculated c_u values compared to triaxial testing data in the LC-A3 layer. Recent site investigations in London have suggested a higher f_1 factor may be adopted (White *et al.*, 2019). A factor of f_1 = 7.1 calculates a c_u line from SPT N_{60} in agreement with the regression for c_u from triaxial testing data.

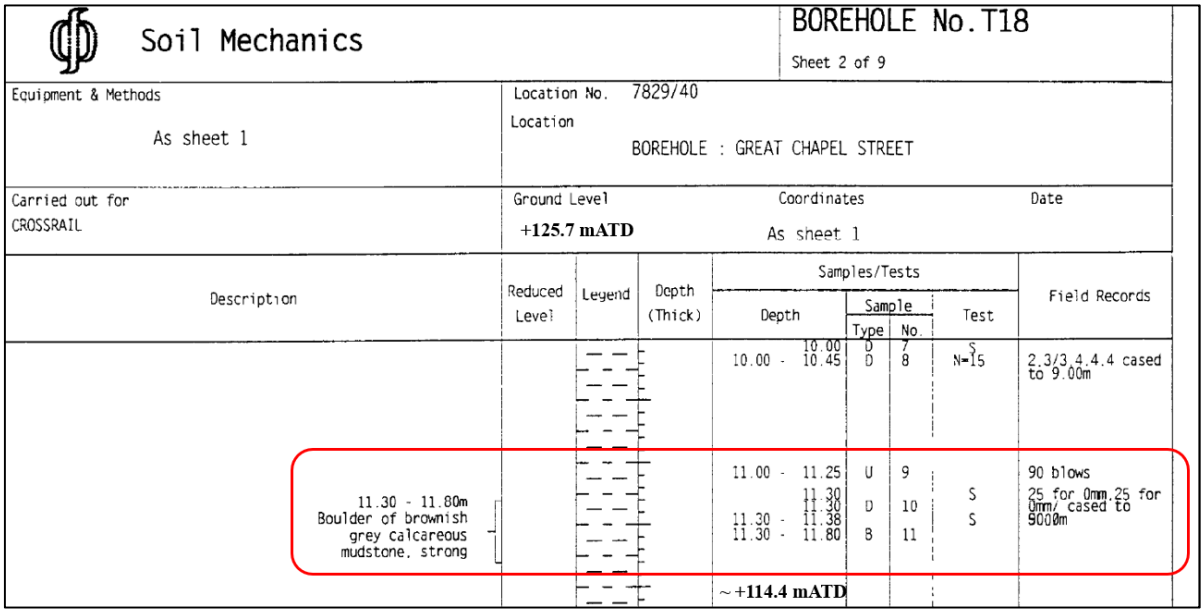
Soil Mechanics

BOREHOLE No.T18

Sheet 2 of 9

Equipment & Methods: As sheet 1

Location No. 7829/40

Location: BOREHOLE : GREAT CHAPEL STREET

Carried out for: CROSSRAIL

Ground Level: +125.7 mATD

Coordinates: As sheet 1

Date

Description	Reduced Level	Legend	Depth (Thick)	Samples/Tests: Depth	Sample Type	Sample No.	Test	Field Records
				10.00 - 10.45	D	7 8	S N=15	2,3/3,4,4,4 cased to 9.00m
11.30 - 11.80m Boulder of brownish grey calcareous mudstone, strong				11.00 - 11.25	U	9		90 blows
				11.30 - 11.38	D	10	S	25 for 0mm,25 for 0mm/ cased to 9000m
				11.30 - 11.80	B	11	S	
				~+114.4 mATD				

Figure 5. 7 Screenshot of the T18 borehole log

The initial values of the Mohr-Coulomb parameters for the TCR-WTH back-analysis by FREW model are summarised in Table 5.3, in which parameters with the updated values are highlighted and compared to the characteristic parameters for the original design (Table 3. 2).

The initial values of undrained soil stiffness (E_u) are calculated from empirical correlation, E_u = 1000 c_u for London Clay and E_u = 2000 c_u for Lambeth Group, which approach is adopted in the as-built modified TCR-WTH design. In addition, the top level of a few strata (e.g. LC-A2, LMG-UMC&LMC) are adjusted based on the construction records of diaphragm wall panels near section A-A'. Other required soil properties (e.g. density γ and Poisson's ratio ν) in the FREW model can be obtained from the ground investigation data for London Clay in the Crossrail project, which is included in Appendix A.

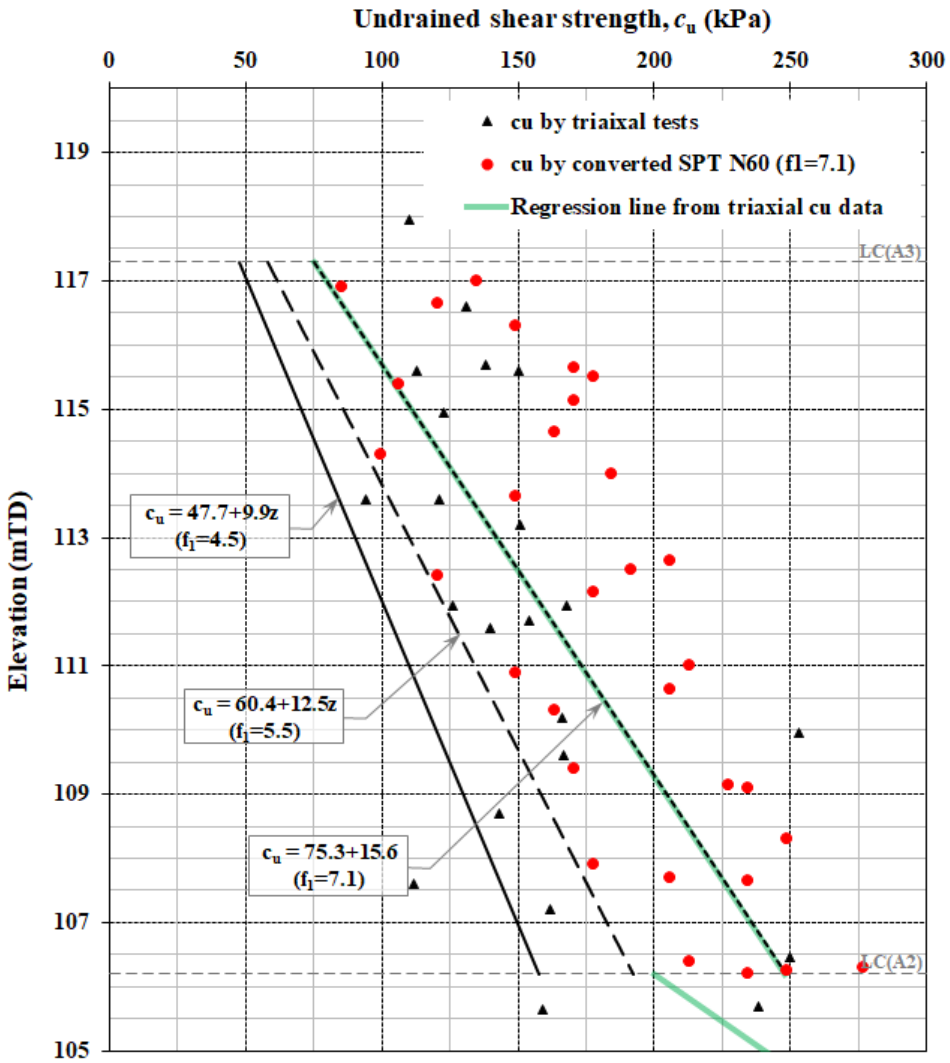

Figure 5. 8 Undrained shear strength for LC-A3 division at TCR-WTH site

5.2.3 Sensitivity and parametric study

There are eight layers of soils included in the FREW model for the TCR-WTH, in addition to structural properties and the modelling parameters; in total there are more than 40 input parameters are involved. In order to investigate the influence of these input parameter, a sensitivity study is carried out. In a series of trials, the soil stiffness (E_u or E') was found to have the most impact on the wall deflection estimation by FREW, which agreed with the conclusion from the probabilistic back-analysis using FREW by Jin (2018).

A parametric study of undrained soil stiffness (E_u) on the wall deflection estimation with FREW is presented in Figure 5. 9. It shows the stiffer London Clay and Lambeth Group stiffness are, the better-fitted wall deflections are predicted.

Table 5. 4 Geotechnical input parameters for TCR-WTH back-analysis

Stratum		Top (mATD)	Base (mATD)	γ (kN/m^2)	c_u (kN/m^2)	c' (kN/m^2)	ϕ'_{peak} (ϕ'_{cv}) (°)	$\phi'_{residual}$ (°)	ν' (ν_u)	K_0	$E_{uv} = E_{uh}$ (kN/m2)	$E_v' = E_h'$ (kN/m^2)
MG		125.7	121.5	21	-	0	25	22	0.25	0.577	-	10
RTD		121.5	117.3	20	-	0	40 (36)	36	0.25	0.357	-	75
LC-A3		117.3	*106.2*	20	*75+15.6z $_1$*	10	20 (18)	15	0.15 (0.5)	*1.0*	*1000 c_u*	0.77E_u
LC-A2		*106.2*	*94.5*	20	*200+17.5z $_2$*	5	22 (20)	15	0.15 (0.5)	*1.0*	*1000 c_u*	0.77E_u
Lambeth Group	UMC	*94.5*	*85.5*	21	*280+6.4z $_3$*	10	26 (21)	15	0.15 (0.5)	*1.0*	*2000 c_u*	0.77E_u
	LMC	*85.5*	78	21	*350*	10	26 (21)	15	0.15 (0.5)	*1.0*	*2000 c_u*	0.77E_u
	UF	78	75.5	21	-	0	31 (26)	22	0.2	1.0	-	196.8+4.32z_5
TS		75.5	72	19	-	0	36 (32)	32	0.2	1.0	-	200

z1 = depth below 117.3 in m; z2 = depth below 106.2 mATD in m; z3 = depth below 94.5 mATD in m; z4 = depth below 85.5 mATD in m; z5 = depth below 78 in m.

Concrete C32/40 was used in constructing the diaphgram wall, and the temporary prop stiffness EA should be calculated using the as-built configurations.

Italic values were updated as initial values for the back-analysis

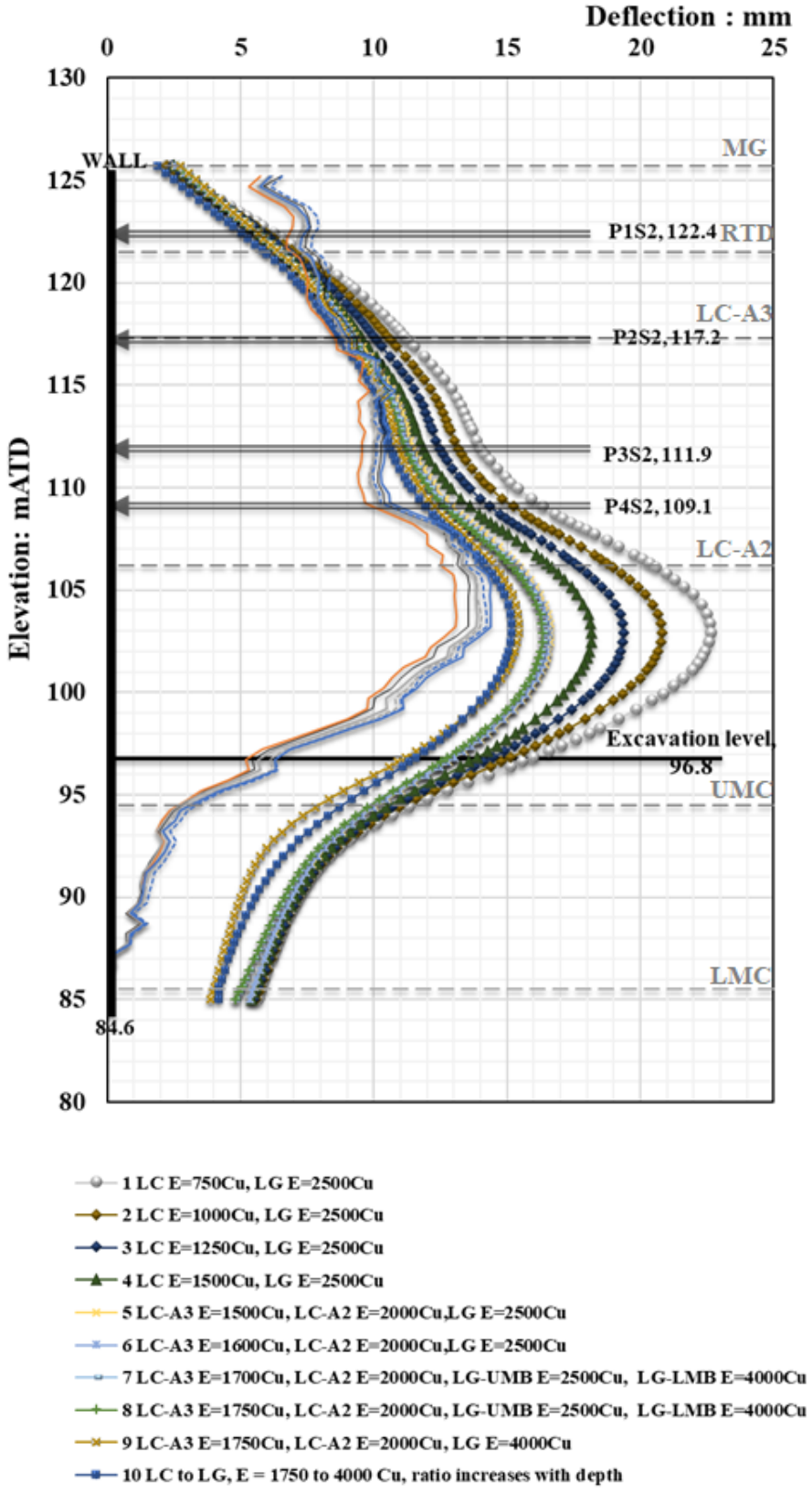

Figure 5. 9 Parametric studies of E_u in FREW model– wall deflections at stage 6 versus corrected SAA-8003 data (22/09/2012 to 27/09/2012 at 7 am)

Other input parameters were also tested in the FREW model and were observed to have some influences on the wall deflection estimations. They were discussed below.

- The lateral earth pressure coefficient at rest k_0

The lateral earth pressure coefficient at rest k_0 =1.0 is adopted for over-consolidated London Clay and Lambeth Group. The measured k_0 values range between 1.0 and 2.5, the higher values measured near the top of the stratum. A high k_0 value will introduce a large lateral earth pressure at rest status and cause excessive wall deflections at excavation stages.

Review of the diaphragm wall construction effect in Chapter 2 indicates the relaxation of the initial lateral earth pressures due to the diaphragm wall panel trench excavation, hence, a lower k_0 =1.0 is adopted.

- Total stress analysis (undrained) versus mix-earth pressure analysis

Total stress analysis (undrained) is applied in the as-built modified design and received a better-estimated wall deflection profile at excavation stage 6 (Figure 3.3), compared to the one predicted under mixed earth analysis design assumption. Mixed earth pressure analysis results in excessive wall deflections due to the combination of the additional pore-water pressure acted on the wall, and the less stiff drained stiffness ($E^{'}$). Where the drained stiffness (E') is related to the undrained stiffness (E_u) through Poisson's ratios, for instance, with a drained Poisson's ratio of ν'= 0.15 and an undrained Poisson's ratio of $\nu_u = 0.5$ for clay, $E' = 0.77\ E_u$ ($E' = (1+\nu')/(1+\nu_u)\ E_u$).

- Structural properties

In the original design, the reduced structural properties were assumed, such as conrete stiffness $E_{concrete}$ for the retaining wall and slabs, and temporary steel prop stiffness K (in the unit of kN/m/m). For the performance-based back-analysis using inclinometer data, it is considered the non-reduced structural properties should be used unless the construction records report the defects.

The propping system for the TCR-WTH deep box excavation comprises straight tubular steel struts and steel plate as waler beams at four levels. The efficiency of the integrated steel propping system is reported from 40% up to 90% in Ciria C760 (Gaba *et al.*, 2017); hence, a proportional reduction of the strut stiffness was assumed in the back-analysis with the FREW model. Due to the limitation of Pseudo-FREW, the fixed prop stiffness values with reduction were applied at all analysis stages, which were varied from stage to stage in the actual construction.

- Soil properties

Soil physical properties were found to vary in a very small range and caused negligible change on the wall deflection estimation with the FREW model.

5.2.4 Iterative back-analysis

In the back-analysis of the TCR-WTH deep box excavation by FREW, the iterative process is focused on updating the soil stiffness parameters, which is considered as the most influential parameter on the wall deflection estimation. The back-analysis uses the measured wall deflections by inclinometers. The difference between estimations and observations should be larger than 0 and smaller than the sum of maximum total errors:

$[0 \leq \Delta_i \leq \sum errors_{max}]$

Where $\sum errors_{max}$ is the maximum of total errors from instruments and modelling, and Δi is the difference between estimation and observation at the i^{th} iteration.

Underestimating wall deflections could lead to unsafe conditions. It is suggested to maintain estimates as close as possible to observations in the comparison, but no underestimations. This may lead to some conservative values calibrated as the representative values of the most probable parameters, but this slightly conservative approach is safer.

Errors include monitoring data accuracy and modelling error. For section A-A' back-analysis, SAA-8003 with 80 segments, each in 0.5 m length, has a maximum random error of $\pm (0.19 \times \sqrt{N})$ mm, or ± 1.71 mm at the top, based on the installation report (Crossrail, 2014a). Given the accuracy of SAAs and the additional error introduced by curvature in the casing, the maximum error for SAA-8003 is assumed to be 2.5 mm.

The FREW modelling error is difficult to determine. Conversations with Oasys FREW developers indicate that realistic retaining wall deflections can be obtained from the propped excavation analysis. However, unusual extra large deflections of the retaining wall during the cantilever excavation stage are reported. Moreover, the wall deflection at the bottom of the wall relates to the boundary setting, in which the last node at the bottom is the default zero point for deflection. Hence, deflections are unlikely to be zero at the bottom of the wall, if it is above the last node, due to the accumulated movement. The maximum FREW model error is hereby assumed to be same as the value of the SAA data error of 2.5 mm.

The adoption of a maximum of 5 mm as the total errors seems arbitrarily small enough for a practical ground engineering assessment, however, it is also aware that this tolerance

value is above 30% of the maximum wall lateral displacement, which has been introduced at the final excavation stage 6 (5 mm over the maximum of 15 mm). In the absence of a rigorous error function, a tolerance of $0 \leq \Delta_{max} < 5$ mm was applied for the point-to-point comparison in the manual back-analysis.

5.2.5 Results

FREW back-analysis for the TCR-WTH deep box in final excavation stage 6 was carried out. The wall deflection estimations from an iteration, which mostly met the tolerance criterion mostly, are presented in Figure 5. 10 against the corrected SAA-8003 data. The calibrated most probable parameters from stage 6 also predict matching wall deflections at an early excavation stage 3, and the difference between estimation and observation is within the given tolerance.

At the top of the wall between level 1 and level 2 props, the measured lateral displacements increased as the excavation progressed. For example, at P1S2 level (+122.4 mATD), the measured deflections increased from less than 3 mm at the beginning of stage 3 to 7.5 mm at the completion of stage 6. However, during this period, the measured P1S2 strut loads changed an average value of about 500 kN (Figure 5. 11), which is very unlikely to cause such a deflection (> 4.5 mm). It is likely the efficiency of the integrated steel propping system varied between excavation stages, but FREW was incapable of changing the prop stiffness at the different analysis stages. In the FREW model, once the strut was activated, strut force was steady with minimum changes in the resultant wall deflections at the corresponding level, as shown in Figure 5. 9 (e.g. estimated wall deflection ≈ 5 mm at P1S2 level at both stage 3 and stage 6).

Results of strut loads at four levels are presented in Figure 5. 11. They were obtained by applying the reduced prop stiffness: 85% for P1S2, 80% for P2S2 and 70% for P3S2 & P4S2. Compared to the estimate using the characteristic parameters, the back-analysis predictions show a better match with the reviewed strut loads calculated by strain gauges measurements. However, strut loads for P1S2, P2S2 were underestimated, while strut loads for P4S2 were overestimated.

It is difficult to draw the further conclusions from the examination of strut loads, as the actual strut loads are a combination of excavation lateral load and thermal expansion load, but the calculated strut loads from strain gauge do not separate loads from different sources.

5.2.6 Representative values of the most probable Mohr-Coulomb parameters for London Clay with FREW

Values of the sets of parameters for London Clay, which are calibrated from the TCR-WTH deep box final stage 6 FREW back-analysis, are regarded as the representative values of the most probable Mohr-Coulomb parameters with FREW. The undrained shear strength (c_u) values and the undrained soil stiffness (E_u) values of the Mohr-Coulomb input parameters for London Clay and Lambeth Group are summarised in Table 5. 5, including values used in the original design and the as-built modified design.

Table 5. 5 Summary of Undrained shear strength (c_u) and Undrained soil horizontal stiffness (E_{uh}) for London Clay and Lambeth Group at the TCR-WTH with FREW

Parameters	***Original design[2]***	***Modified design[3]***	***Initial values in back-analysis***	***Most Probable values of back-analysis***
LC-A3				
c_u (kN/m^2)	80+8z	100+8z	75+15.6z	75+15.6z
E_u (MN/m^2)	E_{uh}= 76+3.9z	$E_{uh} = 1000c_u$	$E_{uh} = 1000c_u$	$E_{uh} = 1750c_u$
LC-A2				
c_u (kN/m2)	162+8z	182.4+14z	200+17.5z	200+17.5z
E_u (MN/m2)	E_{uh}= 109+7.0z	$E_{uh} = 1000c_u$	$E_{uh} = 1000c_u$	$E_{uh} = 2000c_u$
LG-UMC				
c_u (kN/m^2)	250	350	280+6.4z	280+6.4z
E_u (MN/m^2)	$E_{uh} = 148+3.8z$	$E_{uh} = 2000c_u$	$E_{uh} = 2000c_u$	$E_{uh} = 4000c_u$
LG-LMC				
c_u (kN/m^2)	250+17.9z	350	350	350
E_u (MN/m^2)	$E_{uh} = 175+7.5z$	$E_{uh} = 2000c_u$	$E_{uh} = 2000c_u$	$E_{uh} = 4000c_u$

Note 1. z is the depth below the top of the stratum in meter; 2. Characteristic design parameters (Crossrail, 2010b); 3. Parameters applied in as-built modified design were back-analysed using the uncorrected SAA-8003 data by Yeow, *et al.,* (2014).

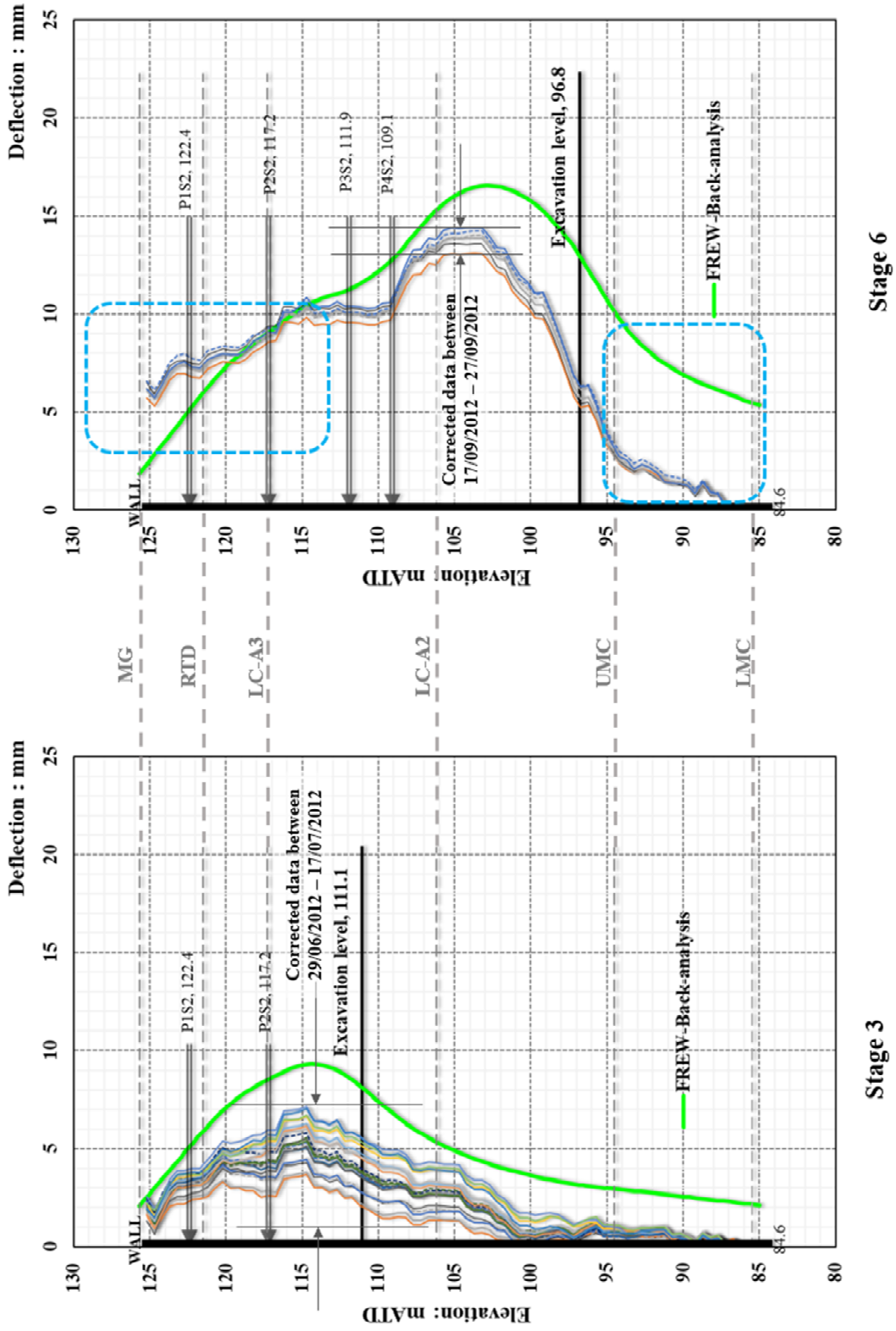

Figure 5. 10 FREW back-analysis result for TCR-WTH - wall deflections versus the corrected SAA-8003 data

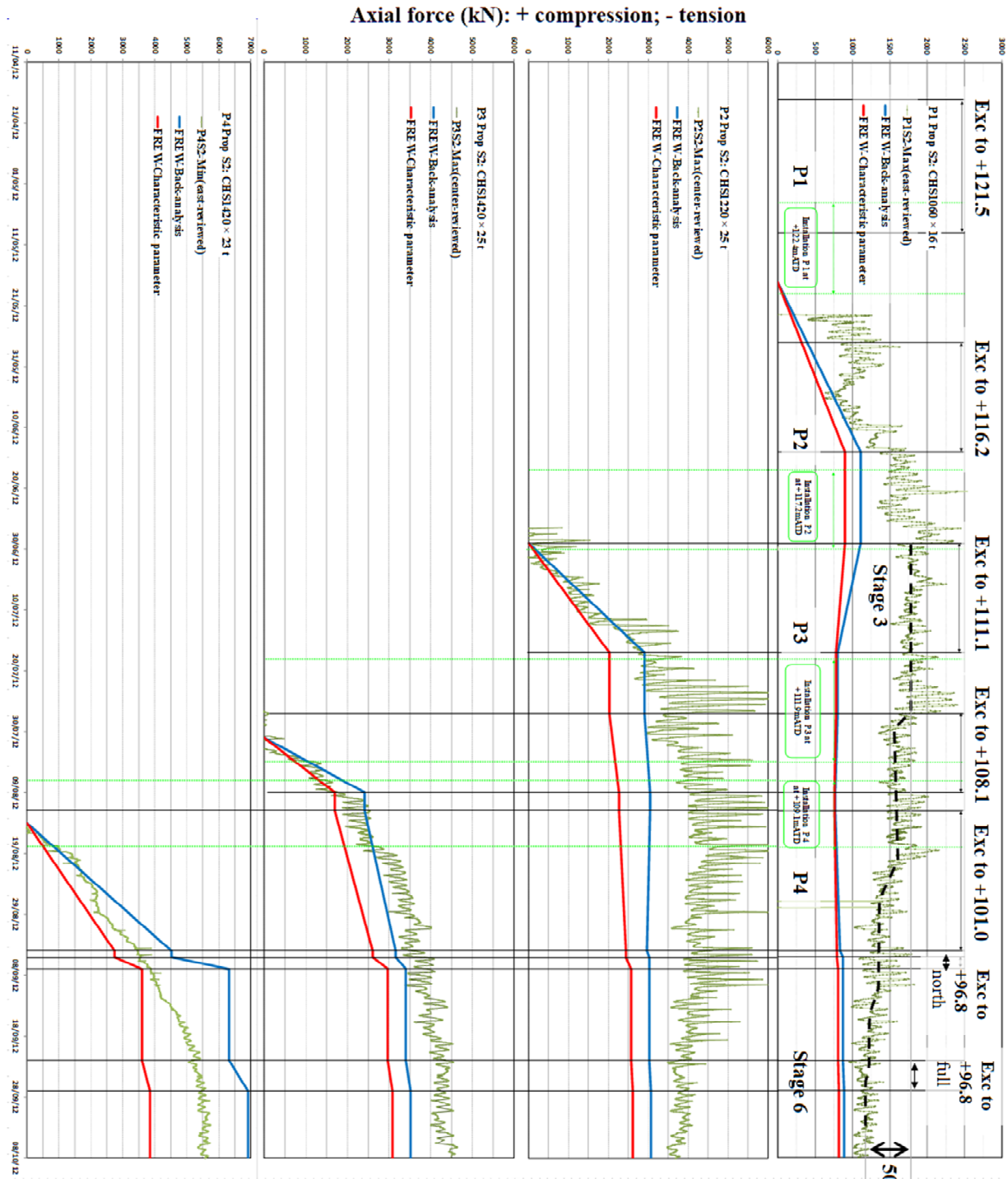

Figure 5. 11 FREW back-analysis result for TCR-WTH – strut loads versus the reviewed axial forces by strain gauge data (P1S2 to P4S2)

A general trend is observed that the increased soil undrained horizontal stiffness is required in order to obtain the wall deflection estimations that agree with inclinometer data. Despite that the undrained shear strength c_u design values have been changed in the different analyses (original design, modified design and the back-analysis), the empirical correlation between (c_u) and (E_{uh}) seems to be proven, but the ratio factor increases from around 1000 in the original design analysis up to 1750 for the LC-A3 from the back-analysis, and this ratio factor increases from around 700 to 2000 for the LC-A2, 700 to 4000 for the Lambeth sub-divisions.

The undrained soil stiffness E_u values adopted in the original design were based on triaxial test results at a strain level of 0.1% (Table 3.2). The calibrated most probable E_u values for London Clay are close to triaxial test results at a smaller strain level of 0.01%. A detailed discussion will be included in section 5.5.

5.2.7 Validation in LIS-MS shaft excavations

The calibrated representative values of the most probable Mohr-Coulomb parameters from the TCR-WTH case are tested in two other Crossrail excavations so that the representativeness of these most probable parameters for London Clay and Lambeth Group could be validated.

- Liverpool Street Station, Moorgate Shaft (LIS-MS): a typical three-dimensional excavation with the length over width L/B ≈1.0;
- Paddington Station Box excavation (PAD): a typical plane-strain excavation with the length over the width L/B ≈10.0.

The validation is undertaken using FREW for the LIS-MS and the PAD case histories, although neither was designed by FREW in the original designs.

5.2.7.1 LILS-MS shaft excavation

The Crossrail LIS-MS shaft excavation case history refers to section 3.3. In the validation, a FREW model is set up for the north diaphragm wall as shown in section A-A' (Figure 3.22), and the resultant wall deflections are compared with the measured data from inclinometer IE01 installed in the northern wall panel (Figure 3.27).

The FREW model is prepared according to the as-built conditions. The final excavation stage 11 in Table 3.7 is presented in Figure 5. 12. The passive side boundary is taken as half of the excavation width, about 16.2 m. An arbitrary 50 m is assumed for the active side boundary, considering the complex ground conditions beyond this distance, including the existing

tunnels, piled foundations of existing buildings and traffic loads on the road. The rigid boundary at the bottom is assumed in the Lambeth Group, about 10 m below the diaphragm wall toe level (+58 mATD the as-built diaphragm wall P01 where the IE01 was installed).

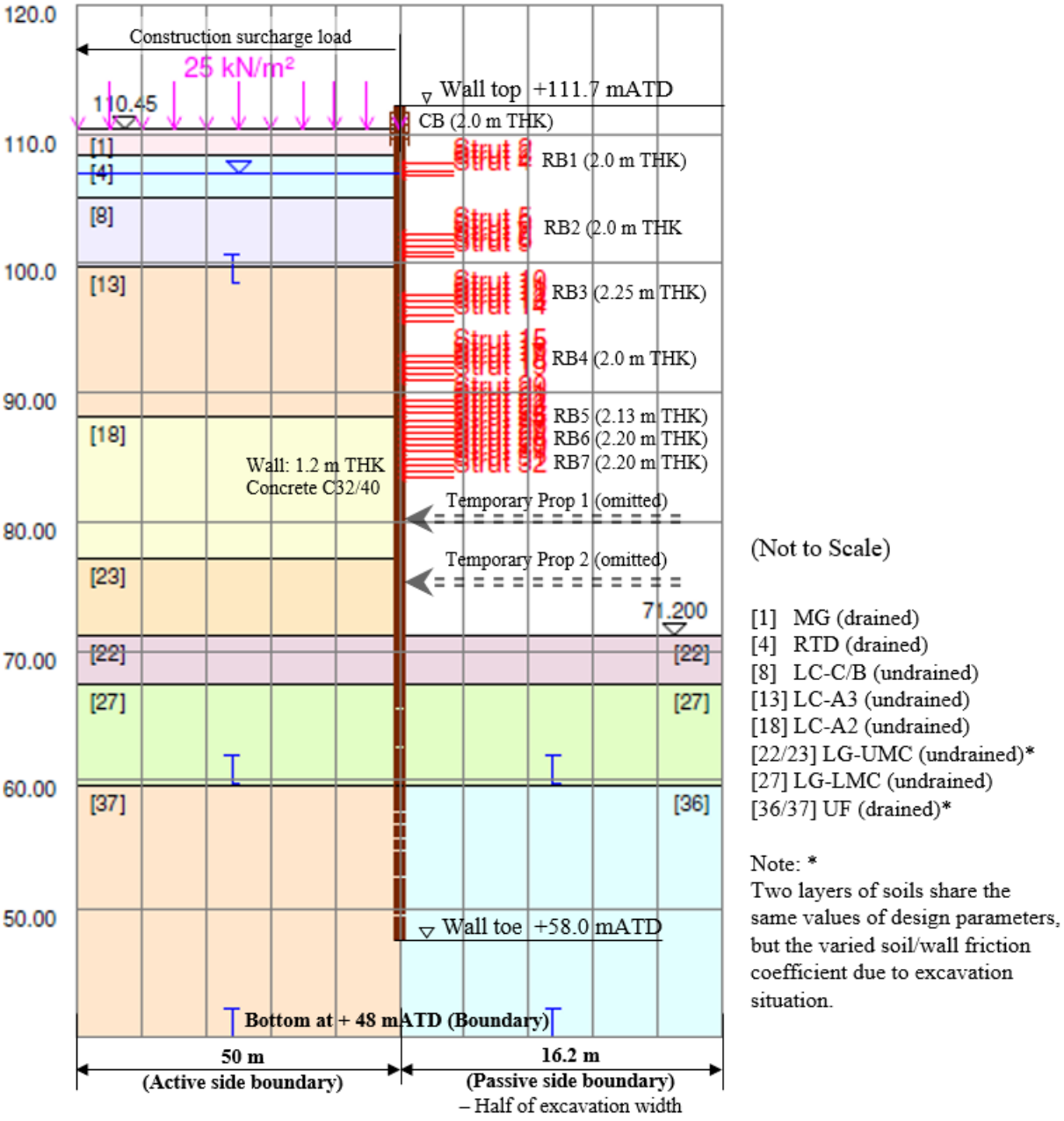

Figure 5. 12 FREW model for LIS-MS shaft excavation at final excavation stage 11

As no existing buildings are immediately behind the retaining wall, a 25 kN/m^2 surcharge pressure is assumed to represent the combined traffic and construction loads.

The as-built structural properties are applied in the FREW model. For instance, the grade C32/40 concrete with a Young's Modulus of $E_{concrete} = 33 \times 10^6$ kN/m^2 is used for the

diaphragm wall panels, capping beam and ring beams. The average thickness of the beams are indicated in Figure 5. 12, but the varying thickness or the manholes that cut through the beams are not considered due to the lack of sufficient details. The beams are modelled in the FREW model as struts, their stiffness values are calculated as, $E_{steel}A_{cross\text{-}section}/(B/2)$, in a unit of kN/m per meter.

Total stress analysis is assumed in the as-built design of the LIS-MS shaft excavation due to the relatively fast excavation (section 3.3.3), and this assumption is applied in the back-analysis with FREW. A drained analysis is applied in the first stage of analysis to establish the initial stresses with the groundwater profile shown in Figure 3.24.

The initial values of the input parameters in the FREW model are based on the design parameters for the original design in Table 3.6. Except for the undrained shear strength (c_u), the values are derived by the supervised linear statistic regression method, and the undrained soil stiffness (E_u) values are calculated by the calibrated correlations between c_u and E_u for London Clay and Lambeth Group from the TCR-WTH back-analysis with FREW.

In addition, the drained soil stiffness (E') is calculated from $E' = (1+\nu')/(1+\nu_u)\ E_u$ with the given $\nu' = 0.1$ and $\nu_u = 0.5$ for London the Clay and the Lambeth Group at the LIS site (Table 3.6). Correlations between the E' and SPT N_{60} by Stroud (1989) are used to updated the E' values for the granular soils: firstly, the SPT N_{60} design values are derived by the supervised linear statistic regression method; then the E' values are estimated from of case history data, for instance, if a foundation is found to have a working load of $q_{net}/q_{ult} \approx 0.1$, then E'/N_{60} for normally consolidated sands and gravels (e.g. River Terrace Deposits (RTD) is in the range of 1 to 2.5; or if a foundation is found to have a working load of $q_{net}/q_{ult} \approx 0.01$, then $E'/N_{60}$for overconsolidated sands and gravels (e.g. Thanet Sand (TS)) is in the range of 4.0 to 7.0.

The initial values of the input parameters in the validation of the LIS-MS shaft excavation are summarised in Table 5. 6. The updated values are highlighted. The London Clay division LC-B/C is not presented at the TCR-WITH site, therefore, its undrained soil stiffness in the validation test of the LIS-MS shaft excavation was initially set equal to the most probable value for the LC-A3, $E_u = 1750c_u$. The LIS-MS shaft excavation experiences larger strain over the layer of London Clay due to the increased excavation depth. The top-down excavation with the less stiff supports of the ring beams may also contribute to this larger stain. Hence, a reduced undrained soil stiffness, $E_u = 1600c_u$ was applied in the validation with FREW.

Table 5. 6 Geotechnical input parameters for LIS-MS validation test

Stratum		Top (mATD)	Base (mATD)	γ (kN/m^2)	c_u (kN/m^2)	c' (kN/m^2)	ϕ'_{peak} (ϕ'_{cv}) (°)	ν' (ν_u)	K_0	$E_{uv} = E_{uh}$ (kN/m2)	$E_v' = E_h'$ (kN/m^2)
MG		*113.8*	108.4	20	-	0	25	0.3	0.5	-	*12.5+5.5z*
RTD		108.4	105.4	20	-	0	38	0.3	0.5	-	*38+15.5z*
London Clay*	C/B	105.4	*100.0*	20	*105.6*	10	22	0.1	1.0	*1750 c_u* (*1600c_u*)	0.73E_u
	A3	*100.0*	88.0	20	*108+5.4z*	10	22	0.1	1.0	*1750 c_u* (*1600c_u*)	0.73E_u
	A2	88.0	77.2	20	*216+11z*	5	26	0.1	1.0	*2000 c_u*	0.73E_u
Lambeth Group	UMC	77.2	67.5	21	*364*	25	27	0.1	1.0	*4000 c_u* (*3000c_u*)	0.73E_u
	LMC	67.5	59.7	21	*383*	25	27	0.1	1.0	*4000 c_u*	0.73E_u
	UF	*59.7*	*52.0*	21	-	0	37	0.2	1.0	-	*612+7.3z*
TS		*52.0*	not proven	21	-	0	39	0.2	1.0	-	*708+8.3z*

z = depth below the top of the stratum in m.

Concrete C32/40 was used in constructing the diaphgram wall, and the ring beams stiffness EA should be calculated using the as-built configurations.

Italic values were updated as initial values for the validation test, the adjusted values in the bracket as the final values used in the validation test

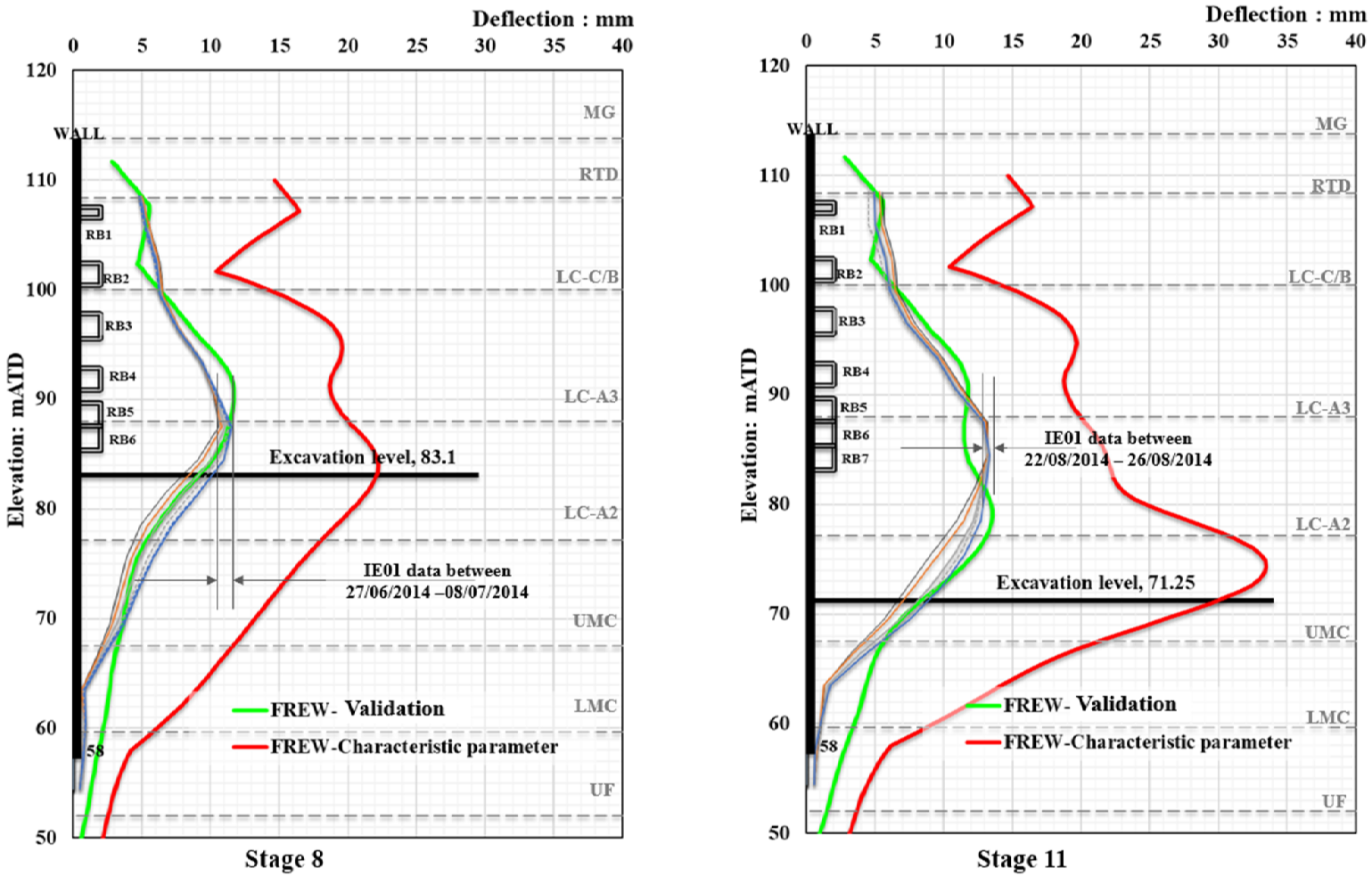

Figure 5. 13 FREW validation result of LIS-MS shaft excavation - wall deflections versus the IE01 data

Likewise, the LG-UMC layer also experiences larger strain as the excavation actually occurred within this stratum, which differs from the TCR-WTH case. Hence, a reduced E_u = $3000c_u$ is adopted for the LG-UMC.

In addition, the reduction of the strut stiffness for the lower levels of ring beams is considered, due to thickness change and breakout cut in beams. A proportional reduction ratio is applied: RB4 (70%), and RB5 to RB7 (50%).

The wall deflection estimations from validation with FREW are found close to the reviewed inclinometer data, at both early exacavation stage 8 and final excavation stage 11 (Figure 5. 13). Although, at a couple of positions, the underestimations are observed around the ring beam 2 level (RB2) and around the lower ring beams (RB4 to RB7).

Figure 5. 13 shows better performance of the wall deflection predictions from the validation than those by characteristic parameters. In the plot, the predictions have been re-zeroed at stage 1 (Table 3.7), when the inclinometer IE01 started recording during the installation of RB2.

In conclusion, the representative values of the most probable undrained soil stiffness (E_u) for London Clay were obtained by back-analysis of the TCR-WTH deep box excavation using FREW. Despite the change of construction method and depth of excavation, these values are applicable in predicting the wall performance for the LIS-MS shaft excavation by FREW as well.

5.2.7.2 PAD station box excavation

For a description of the Crossrail PAD station box excavation case history, please refer to section 3.4. As part of validating the representative values of the most probable parameters for London Clay, a FREW model is set up for the PAD box diaphragm wall constructed at Departure Road. The left side of section A-A' (Figure 3.29), and the resultant wall deflections are compared with the measured data by inclinometer E13-12 (Figure 3.27). The modelling of the diaphragm wall at Eastbourne Terrace Street, on the right side wall of section A-A', presents difficulties due to the enabling works (e.g. backfilling and traffic loads). Given the uncertainty in the inclinometer data (see section 3.4.4), the comparison of the wall deflections in the validation is rather indicative than quantitative.

The FREW model is prepared according to the as-built conditions and the final excavation stage 17 (Table 3.10) is presented in Figure 5. 14. The active side boundary is taken at 70 m approximately three and a half times the maximum excavation depth (20.5 m). The passive side boundary is placed at half of the excavation width (11.6 m). The boundary at the bottom is assumed in the London Clay, about 13 m below the diaphragm wall toe level (+85.5 mATD the as-built diaphragm wall panel N44 where the E13-12 was installed).

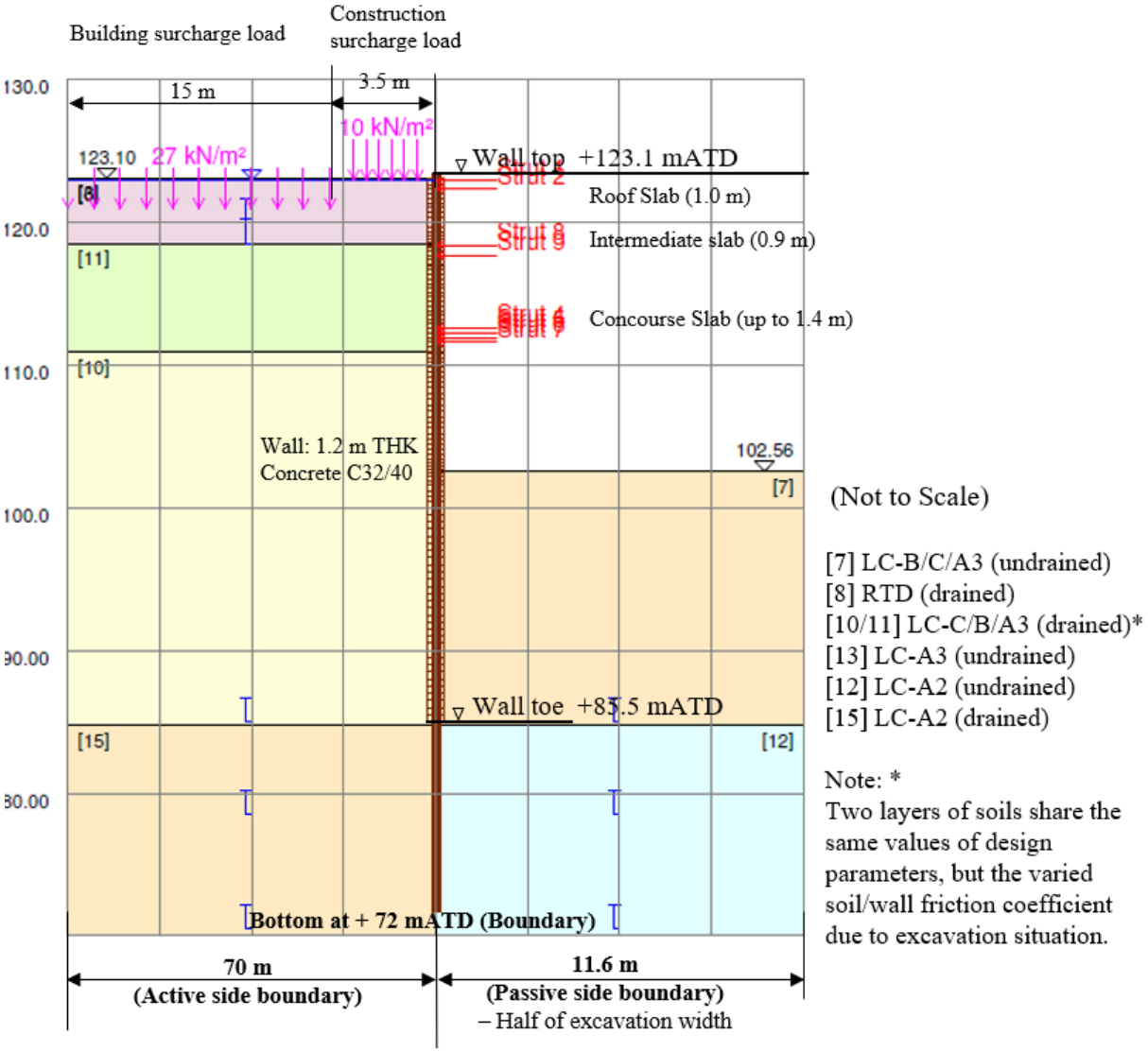

Figure 5. 14 FREW model for PAD station box excavation at final excavation stage 17

The surcharge loads of the existing building, 27 kPa, is applied at the existing foundation level, about 2 m below the ground surface level. A construction working load of 10 kPa is applied immediately next to the wall extending for a distance of 3.5 m.

The as-built structural properties are applied in the FREW analysis. For instance, the grade C32/40 concrete with a Young's Modulus of $E_{concrete} = 33 \times 10^6$ kN/m^2 is used for the diaphragm

wall panels and slabs. The thickness of the slabs is indicated in Figure 5. 14, but the manholes cut through slabs are not considered due to the lack of sufficient details. Slabs are modelled as struts in the FREW model and the strut stiffness is calculated by EA/(B/2 in a unit of kN/m per meter. In addition, one level of temporary steel tubular props (MP500) at 6.11 m c/c spacing was installed at +114.5 mATD and removed after the installation of the concourse slab.

Total stress analysis is assumed up to stage 15 (Table 3.10), accounting for a construction period of 12 months. A mixed earth pressure analysis is assumed for the subsequent to final excavation stages due to an 18 month construction period, including a 4-month preparation period for removing the tunnel linings in the station box prior to the final excavation. A close to hydrostatic pore-water pressure profile from the ground level (Figure 3.29) is adopted for the drained analysis in the FREW model.

The initial values of the input parameters in the FREW model are based on characteristic parameters (Table 3.8) for the original design with updates. The ground stratigraphy is updated to include the subdivisions of London Clay and levels are updated according to the diaphragm wall installation record. The undrained shear strength (c_u) values for these subdivisions are derived by the supervised linear statistic regression method, and the undrained soil stiffness (E_u) values are calculated by the calibrated correlations between c_u and E_u for London Clay and Lambeth Group from the TCR-WTH back-analysis with FREW.

The drained soil stiffness (E') is calculated from $E' = (1+\nu')/(1+\nu_u)\, E_u$ with the given ν'= 0.2 and ν_u = 0.5 for London the Clay and the Lambeth Group at the PAD site (Table 3.8). In addition, correlation between the E' and SPT N_{60} by Stroud (1989) is used to derive the E' values for the granular soils (e.g. MG & RTD): firstly, the SPT N_{60} design values are derived by the supervised linear statistic regression method, then the E' values are estimated from of case history data, if a foundation has a working load of $q_{net}/q_{ult} \approx 0.1$, E'/N_{60} for normally consolidated sands and gravels is in the range of 1 to 2.5.

The initial values of input parameters in the validation of the PAD station box excavation are summarised in Table 5. 7. The updated values are highlighted. The London Clay division LC-B/C is not presented at the TCR-WITH site, therefore, its undrained soil stiffness in the validation test of the PAD station box excavation was initially set equal to the most probable value for the LC-A3, $E_u = 1750c_u$, then reduced to $E_u = 1300c_u$ to account for shallower overlaid topsoils above London Clay and the plane-strain PAD station box analysis.

Table 5. 7 Geotechnical input parameters for PAD station box validation test

Stratum		Top (mATD)	Base (mATD)	γ (kN/m^2)	c_u (kN/m^2)	c' (kN/m^2)	ϕ'_{peak} (ϕ'_{cv}) (°)	$\phi'_{residual}$ (°)	ν' (ν_u)	K_0	$E_{uv} = E_{uh}$ (kN/m2)	$E_v' = E_h'$ (kN/m^2)
MG		*125.7*	123	18	-	0	25	-	0.2	1-sinϕ'	-	*40*
RTD		123	*118.5*	20	-	0	38	36	0.2	1-sinϕ'	-	*51.25*
London Clay	LC-A3	*118.5*	*85*	20	*100+4z*	0	22 (20)	12	0.2 (0.5)	1.0	*1750 c_u* *(1300c_u)*	0.7E_u
	LC-A2	*85*	*below 70*		*144+13z*	0			0.2 (0.5)	1.0	*2000 c_u*	0.7E_u

z = depth below the top of the stratum in m.

Concrete C32/40 was used in constructing the diaphgram wall, and the slabs' stiffness EA should be calculated using the as-built configurations.

Italic values were updated as initial values for the validation test, the adjusted values in the bracket as the final values used in the validation test

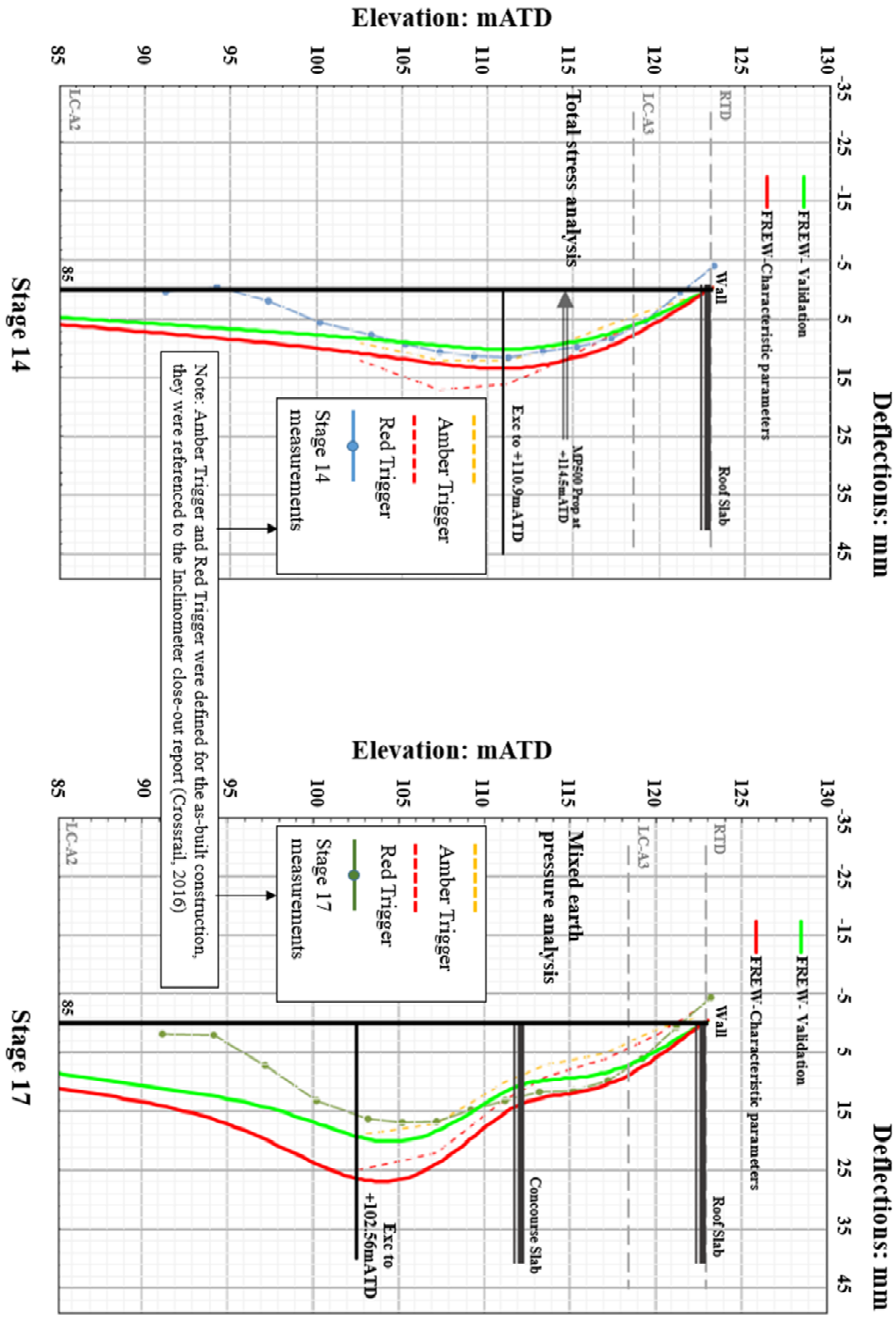

Figure 5. 15 FREW validation result of PAD station box excavation - wall deflections versus the E13-12 data

The wall deflection estimations from validation with FREW are presented in Figure 5. 15. These predictions capture the trend of the wall deflections at excavation stage 14 with the total stress analysis, and at the final excavation stage 17 with the mixed earth pressure analysis.

The difference between the validation and inclinometer data for the bottom 10 m of the wall is larger than 5 mm, this is due to the combination of uncertainty in the inclinometer data and FREW modelling error. E13-12 was installed at section A-A' (Figure 3. 28), its measurements indicate the bottom of the inclinometer is at 6 m above the wall toe level. This is insufficient to justify the fixity of the wall toe.

Meanwhile, the difference between the validation estimates and the predictions by characteristic parameters is found to be small (e.g. < 5 mm), in comparison with two other Crossrail excavations (TCR-WTH & LIS-MS). This might link to the distribution of London Clay being higher at the west of London (e.g. PAD), and lower towards the centre (e.g. TCR) and east of London (e.g. LIS).

In addition, at the PAD site, a layer of London Clay is over 55 m deep, hence the diaphragm wall is embedded in the London Clay and a 20 m deep excavation is proceeding mainly in the less stiff LC-C/B and LC-A3. For TCR-WTH and LIS-MS cases, the relatively thin layer of London Clay is just over 20 m, thus their diaphragm walls are embedded into the stiffer Lambeth Group, and their excavations are proceeding in the stiffer LC-A2, even in Lambeth Group (LIS-MS). Different wall performances in response to the different geology and excavation depth are therefore expected.

For the purpose of validation, the empirical correlation of the most probable undrained soil stiffness (E_u), E_u/c_u =2000 for the LC-A2 was calibrated in the back-analysis of the TCR-WTH deep box excavation, and it is applicable in predicting the wall performance for the PAD station box excavation with FREW.

5.3 2D FEM back-analysis of the TCR-WTH

Two-dimensional plane-strain finite element analysis is the most common FEM applied in the excavation design. All five Crossrail excavation case histories were performed Plaxis (2D) analysis for their original design.

5.3.1 Plaxis 2D model

The Crossrail TCR-WTH excavation case history is described in section 3.2. The Plaxis 2D model for the TCR-WTH deep box excavation design is modified according to section A-A' (Figure 3.1) and as-built construction records (Table 3.3). The Plaxis 2D model at the final excavation stage 6 is presented in Figure 5. 16.

This Plaxis (2D) model uses 15-noded-element, providing a fourth-order interpolation for displacements and twelve Gauss stress points (Brinkgreve *et. al.,* 2016a), a total of 3,170 elements generated for soils with the average element size of 2.83 m.

The structural items are modelled by 6-noded-elements, providing a second-order interpolation for displacements, while the numerical integration involves three Gauss points, which are compatible with the soil element type in Plaxis. For instance, diaphragm walls are modelled by isotropic linear elastic plate element and temporary props are modelled by a linear elastic node-to-node anchor.

The lateral boundary is placed at a distance of 100 m from the retaining walls, about three times the maximum excavation depth (29.5 m). A width of 27 m at the location of section A-A' (Figure 3.1) is adopted for two walls. The boundary at the bottom is assumed to be in the Thanet Sand at +50 mATD, about one and a half times the maximum excavation depth (29.5 m) below the deepest excavation level (+96.8 mATD). In addition, a 3 m × 1.4 m deep trench along the centre of the deep box is included in the Plaxis 2D model.

The as-built surcharge loads as described in the FREW back-analysis in section 5.2.1, are applied behind the walls on both sides in the Plaxis model. Grade C32/40 concrete with a Young's Modulus of $E_{concrete} = 33 \times 10^6$ kN/m^2 and configurations of the walls are used to calculated the isotropic linear plate parameters: EA=3.30×10^7 in kN/m; EI=2.75×10^6 in kNm^2/m; weight of plate is taken as 4 kN/m^3 (the concrete density of 24 kN/m^3 deduces an average soil density of 20 kN/m^3).

The circular hollow section (CHS) of steel temporary strut with a Young's Modulus of $E_{steel} = 200 \times 10^6$ kN/m^2 and the as-built sizes (Table 3.4) are used to calculate the strut stiffness, EA=8.97×10^6 (P1S2), 1.58×10^7 (P2S2), 1.61×10^7 (P3S2), 1.48×10^7 (P4S2), in kN at a spacing of 4 m.

The most probable design conditions for the as-built modified design are applied in Plaxis (2D) back-analysis, including total stress analysis assumption. In the Plaxis program, the drainage type A, Undrained (A) is selected to model the undrained soil behaviour. This

approach models the undrained behaviour using the effective stiffness (*E'*) and the effective strength (*c'* & ϕ') parameters (Brinkgreve *et. al.,* 2016b) to perform an effective stress analysis, generating excess pore pressures, which then allow to perform a consolidation analysis after the undrained calculation, but maybe inaccurate depending on the soil constitutive model and parameters. In this process, the undrained shear strength is the outcome of the constitutive model. Although the effective stiffness and strength parameters are required as Undrained (A) input parameters, in the back-analysis for the TCR-WTH excavation, the values of the undrained stiffness (E_u) and the undrained shear strength (c_u) are used for *E'* and *c'*.

A drained analysis is carried out at the initial stage of the Plaxis calculation to establish the initial stresses. The groundwater profile has used the same design profile (Figure 3,2) which was applied in the original design analysis.

The initial values of Mohr-Coulomb parameters (Table 5. 4) derived for the FREW analysis are applied to the Plaxis one as well.

A sensitivity analysis was undertaken to identify the most influential input parameters in the Plaxis model. Similarly to the FREW model, the soil stiffness parameters (E_u) is found to have the most impact on the wall deflection prediction.

In addition, the surcharge load conditions had some influence on the wall deflection predictions. However, the actual surcharge load condition is variable and its magnitude is hard to confirm. An onerous design assumption on the site of the surcharge loads is therefore adopted for the back-analysis.

The back-analysis of the TCR-WITH deep box excavation by the Plaxis 2D model also relied on the inclinometer data (SAA-8003) for comparison. Hence, the same criterion between the predictions and the observations (described in section 5.2.1) can be used: $0 \leq \Delta_{max} < 5$ mm. No adjustment for the Plaxis modelling error is made as there are fewer references available.

5.3.2 Results

The wall deflection predictions from the Plaixs 2D back-analysis for the TCR-WTH deep box excavation are presented in Figure 5. 17, showing better estimates than the FREW back-analysis predictions at the final stage 6, that are close to the corrected inclinometer data. The calibrated most probable parameters from stage 6 also predict matching wall deflections at an early excavation stage 3, the difference between Plaxis predictions and observation is less than the one between the FREW predictions and observations.

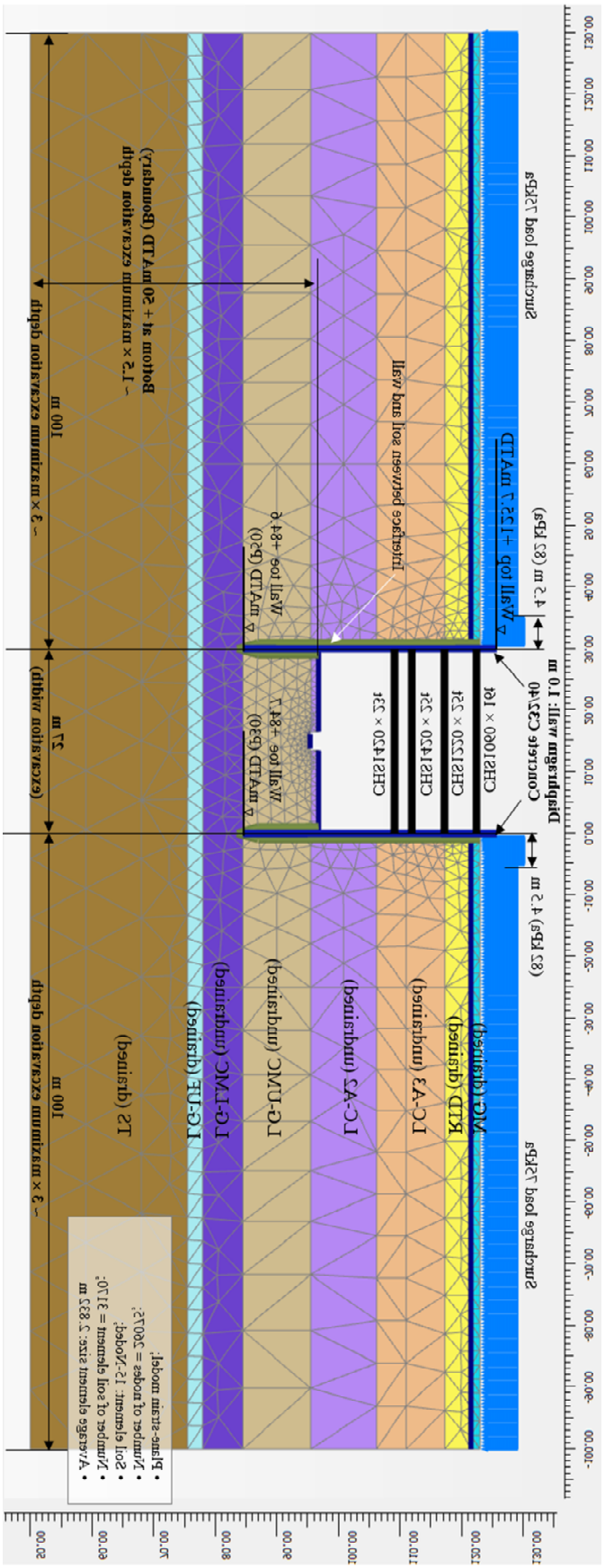

Figure 5. 16 Plaxis 2D model for TCR-WTH deep box excavation at final excavation stage 6

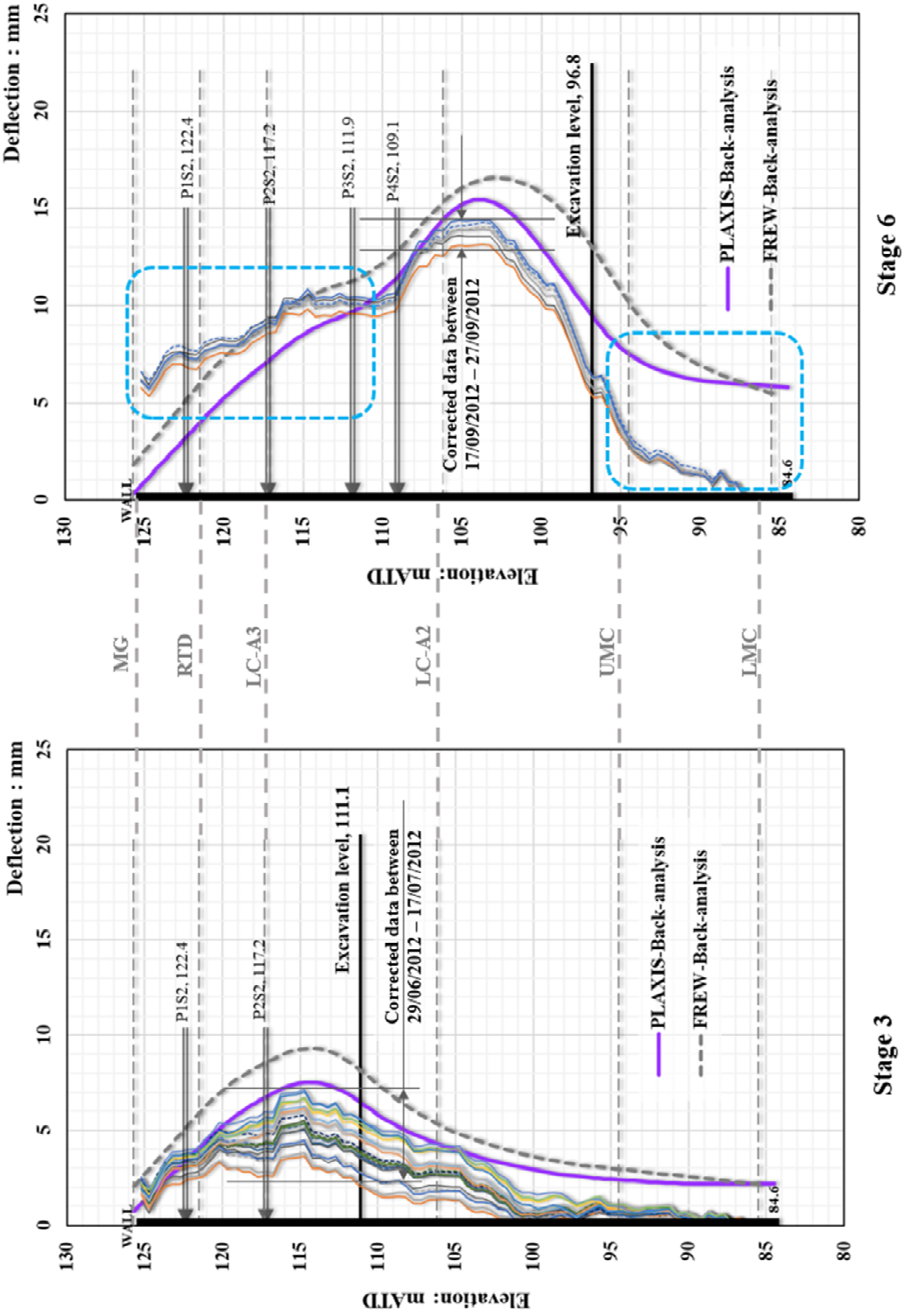

Figure 5. 17 Plaxis 2D back-analysis result for TCR-WTH - wall deflections versus the corrected SAA-8003 data

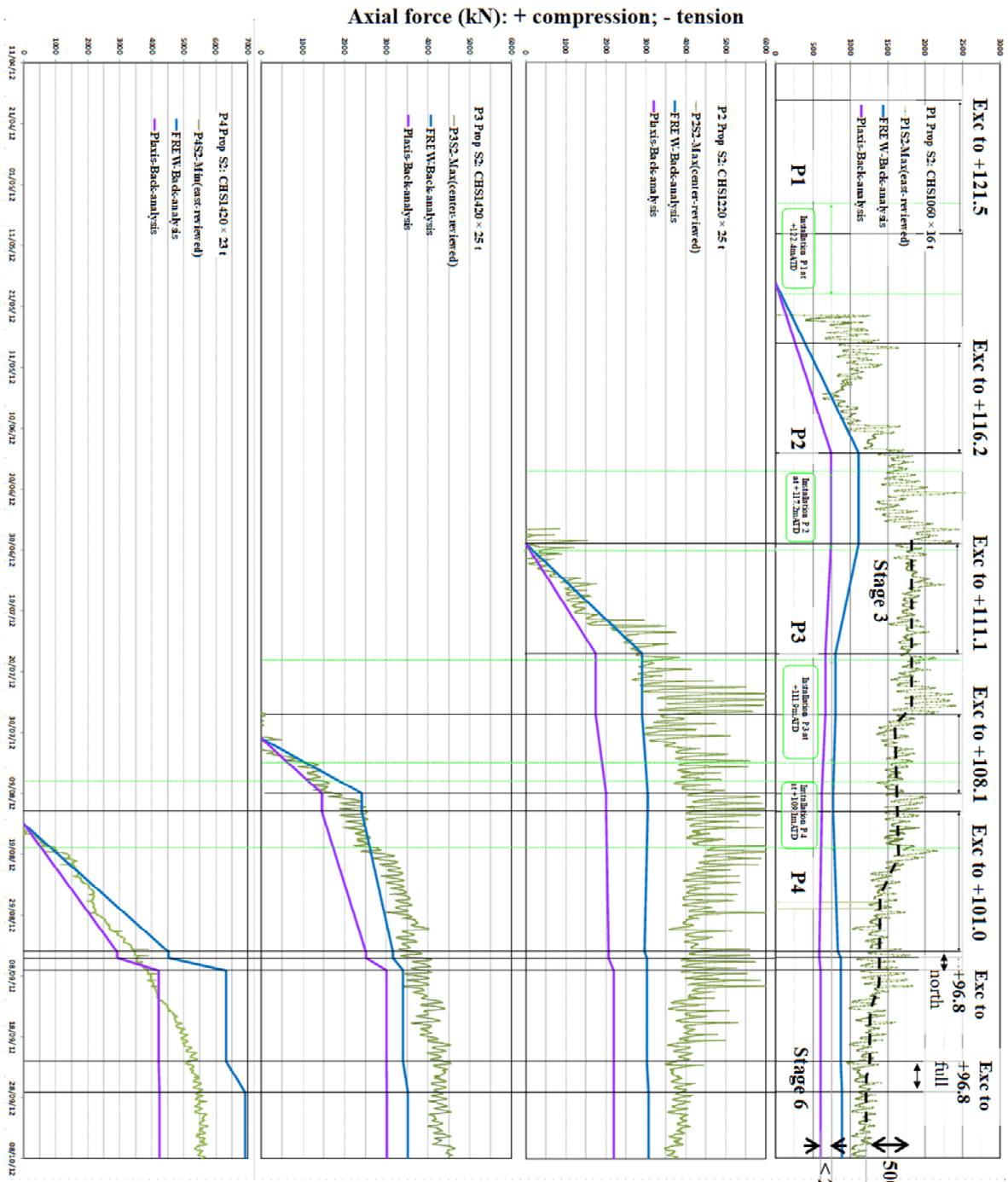

Figure 5. 18 Plaxis 2D back-analysis result for TCR-WTH – strut loads versus the reviewed axial forces by strain gauge data (P1S2 to P4S2)

The Plaxis 2D predictions are more accurate than FREW's. However, the Plaixs 2D underestimates deformation in the final excavation stage 6 from the top of the wall to below the level 3 props, while the FREW underestimation is up to the level 2 props.

As explained in the FREW back-analysis results (section 5.2.5), the increased displacement of the corrected SAA-8003 data at the P1S2 level from stage 3 to stage 6 is incongruence with the change in P1S2 strut loads during the same period. Meanwhile, like in the FREW model, the prop stiffness is fixed at different analysis stages in the Plaxis model. As far as the strut is activated, a steady strut force is generated, and the wall lateral displacement is fixed at the level the strut propped. For instance, a displacement of 7 mm at P2S2 level is estimated in the Plaxis 2D model at both stage 3 and 6 (Figure 5. 17). Over this period, the estimated strut force is maintained around 2000 kN in P2S2, with a small variation (< 250 kN).

It was likely the integrated steel propping system efficiency had changed between excavation stages. For the individual prop, its stiffness is related to this support system. This is beyond the capability of the plane-strain Plaxis 2D model.

Compared to the estimation by the FREW model, the Plaxis 2D model predicts more accurate strut loads for the lowest level prop P2S4 but underestimates strut loads for the other three levels of props: P2S2, P2S3 and P2S4.

Plaxis 2D back-analysis predictions of the strut loads at four levels are presented in Figure 5. 18. These results are based on the reduced prop stiffness in the Plaxis model: 85% for P1S2, 80% for P2S2 and 70% for P3S2 & P4S2.

In addition to the wall deflection predictions and strut forces, the Plaxis 2D model can provide more details, such as stresses, strains and cumulative movements. These results can provide useful information to assess retaining structure performance.

The maximum ground settlement at the final excavation stage 6 (22/9 to 27/09/2012) was measured by the levelling road studs installed along Dean Street at a distance of 8.5 ~ 9.0 m from the TCR-WTH deep box (Figure 3.5). It is approximate 12 mm after deducting the initial 2 mm settlement induced by the diaphragm wall installation (Figure 3.21). Whilst the Plaxis 2D back-analysis estimated 4 mm settlement at the same location over the same period. It seemed that the calibrated most probable Mohr-Coulomb parameters for London Clay using the inclinometer data, may not be representative for ground movement prediction. Or anisotropy of soil stiffness in vertical and horizontal directions for London Clay is significant and their most probable values need to be calibrated by different observations.

5.3.3 Representative values of the most probable Mohr-Coulomb parameters for London Clay with PLAXIS

The representative values of the most probable Mohr-Coulomb parameters for London Clay are calibrated from the Plaxis 2D back-analysis of the TCR-WTH case. The undrained shear strength (c_u) values and the undrained soil stiffness (E_u) values of the Mohr-Coulomb parameters are compared with those from the FREW analysis in Table 5. 8.

Despite a much less stiff LG-UMG (E_u/c_u = 2500) and a slightly less stiff LC-A3 (E_u/c_u = 1600) from the Plaxis 2D back-analysis, the Plaxis 2D predictions of the wall deflections are closer to the corrected SAA-8003 data (Figure 5. 17) than FREW's. In the LC-A3 layer, the less stiff LC-A3 (E_u/c_u = 1600) enables a more accurate wall deflection to be predicted at the early excavation stage 3. At the final excavation stage 6, the wall deflections are underestimated, due to change in the props' stiffness and possibly a further reduction in soil stiffness at the increased strain level. This is beyond the ability of the linear elastic and perfect plastic Mohr-Coulomb model.

Table 5. 8 Summary of Undrained shear strength (c_u) and Undrained soil horizontal stiffness (E_{uh}) for London Clay and Lambeth Group at the TCR-WTH (Plaxis 2D & FREW models)

Parameters	Initial values in back-analysis	Most Probable values of back-analysis (FREW)	Most Probable values of back-analysis (Plaxis 2D)
LC-A3			
c_u (kN/m^2)	75+15.6z	75+15.6z	75+15.6z
E_u (MN/m^2)	$E_{uh} = 1000c_u$	$E_{uh} = 1750c_u$	$\underline{E_{uh} = 1600c_u}$
LC-A2			
c_u (kN/m2)	200+17.5z	200+17.5z	200+17.5z
E_u (MN/m2)	$E_{uh} = 1000c_u$	$E_{uh} = 2000c_u$	$E_{uh} = 2000c_u$
LG-UMC			
c_u (kN/m^2)	280+6.4z	280+6.4z	280+6.4z
E_u (MN/m^2)	$E_{uh} = 2500c_u$	$E_{uh} = 4000c_u$	$\underline{E_{uh} = 2500c_u}$

LG-LMC			
c_u (kN/m^2)	350	350	350
E_u (MN/m^2)	$E_{uh} = 2500c_u$	$E_{uh} = 4000c_u$	$E_{uh} = 4000c_u$

Note: z is the depth below the top of the stratum in meter.

5.3.4 Validation in PAD station box excavations

The calibrated most probable values of the Mohr-Coulomb parameters for London Clay in the Plaxis model are tested in the Crossrail PAD station box excavation, as the PAD station box (263 m × ~ 24 m) is a typical plane-strain excavation case, in which the Plaxis 2D model is normally performing well. Given the uncertainty in the inclinometer data (see section 3.4.4), the comparison of the wall deflections in the validation is rather indicative than quantitative.

5.3.4.1 Plaxis 2D model

For a description of the Crossrail PAD station box excavation case history, please refer to section 3.4. A Plaxis 2D model for the Crossrail PAD station box excavation is prepared according to the as-built sequence (Table 3.10) for section A-A' (Figure 3.29). The approximation of the enabling works on Eastbourne Terrace Street is included: backfilling loads and traffic loads. The Plaxis 2D model for the PAD station box excavation at the final excavation stage 17 is presented in Figure 5. 19. This model uses the 15-noded-element generating a total of 6,303 elements for soils with the average element size of 1.67 m. The structural items are modelled with a 6-noded-elements: diaphragm walls are modelled by isotropic linear elastic plate element, as well as piles and slabs, temporary props are modelled by a linear elastic node-to-node anchor.

The lateral boundary is placed at a distance of 80m from the retaining wall, about three times the maximum excavation depth (20.5 m). Width of 23.4 m at the location of section A-A' (Figure 3.29) is adopted for two retaining walls. The boundary at the bottom is assumed in the Lambeth Group at +50 mATD, about two and a half times the maximum excavation depth (20.5 m) below the final excavation level (~ +102.5 mATD). This extended vertical boundary is to compensate for piles with the toe level at +66.5 mATD.

The as-built surcharge loads are adjusted referenced to the PAD station design surcharge loads (Table 3.9), and applied in the Plaxis model: at Departure Road, a 10 kPa working load

is applied over 5 m distance, and followed with the existing building surcharge load of 27 kPa applied over 15 m at +121 mATD (2 m below the ground level at the foundation level); at Eastbourne Terrace Street side, a distance of 7.5 m to 22.5 m from the wall, the existing building surcharge load of 27 kPa is applied at +121 mATD; above the roof slab, a 20 kPa traffic load is applied during the backfill enabling works and a 10 kPa working load is also included.

Grade C32/40 concrete with a Young's Modulus of $E_{concrete} = 33 \times 10^6$ kN/m^2 is used to calculate the isotropic linear plate parameters for structural items. For instance, the 1.2 m thick diaphragm wall plate parameters are EA=3.97×10^6 in kN/m, EI=4.75×10^6 in kNm^2/m and weight of the plate is taken as 4 kN/m^3. For 1.8 m diameter pile at 6.11 m c/c spacing, the plate parameters are EA=1.37×10^7 in kN/m, EI=2.78×10^6 in kNm^2/m and weight of the plate is taken as 5.4 kN/m^3. The steel temporary strut (MP500) with a Young's Modulus of $E_{steel} = 200 \times 10^6$ kN/m^2 is used to calculate the strut stiffness, EA=7.65×10^6 in kN at a spacing of 6.11 m.

The most probable design conditions are assumed in the Plaxis 2D back-analysis, which replicate the FREW analysis for the PAD station box excavation (see section 5.2.7.2). Total stress analysis is assumed up to stage 15 (Table 3.10), accounting for a shorter construction period, and a mixed earth pressure analysis is assumed for the subsequent excavation stage for the longer 18 month construction period. Following the TCR-WTH back-analysis by Plaxis 2D model, the total stress analysis uses the Undrained (A) method. The groundwater profile for the initial drained analysis stage is referenced to the design profile for the PAD station box original design (Figure 3.29).

The initial values of input parameters in the PAD station box validation with Plaxis are based on Table 5. 7, the inputs for the PAD validation test with FREW. Undrained shear strength (c_u) values are derived from the supervised linear regression method. For undrained soil stiffness (E_u) values, the calibrated most probable empirical correlations from the Plaxis 2D back-analysis for the TCR-WTH are applied: $E_u = 1600\ c_u$ for the LC-A3 division and $E_u = 2000\ c_u$ for the LC-A2 division and the Lambeth Group.

Inaccurate predictions of wall deflections for the diaphragm wall on Eastbourne Terrace Street are expected due to the approximation in modelling of the enabling works. The wall deflection predictions for the one at Departure Road are presented in Figure 5. 20. The Plaxis 2D analysis predicts well the wall deflections at stage 14 (by total stress analysis) and also captures the trend of wall deflections at stage 17 (by mixed earth pressure analysis).

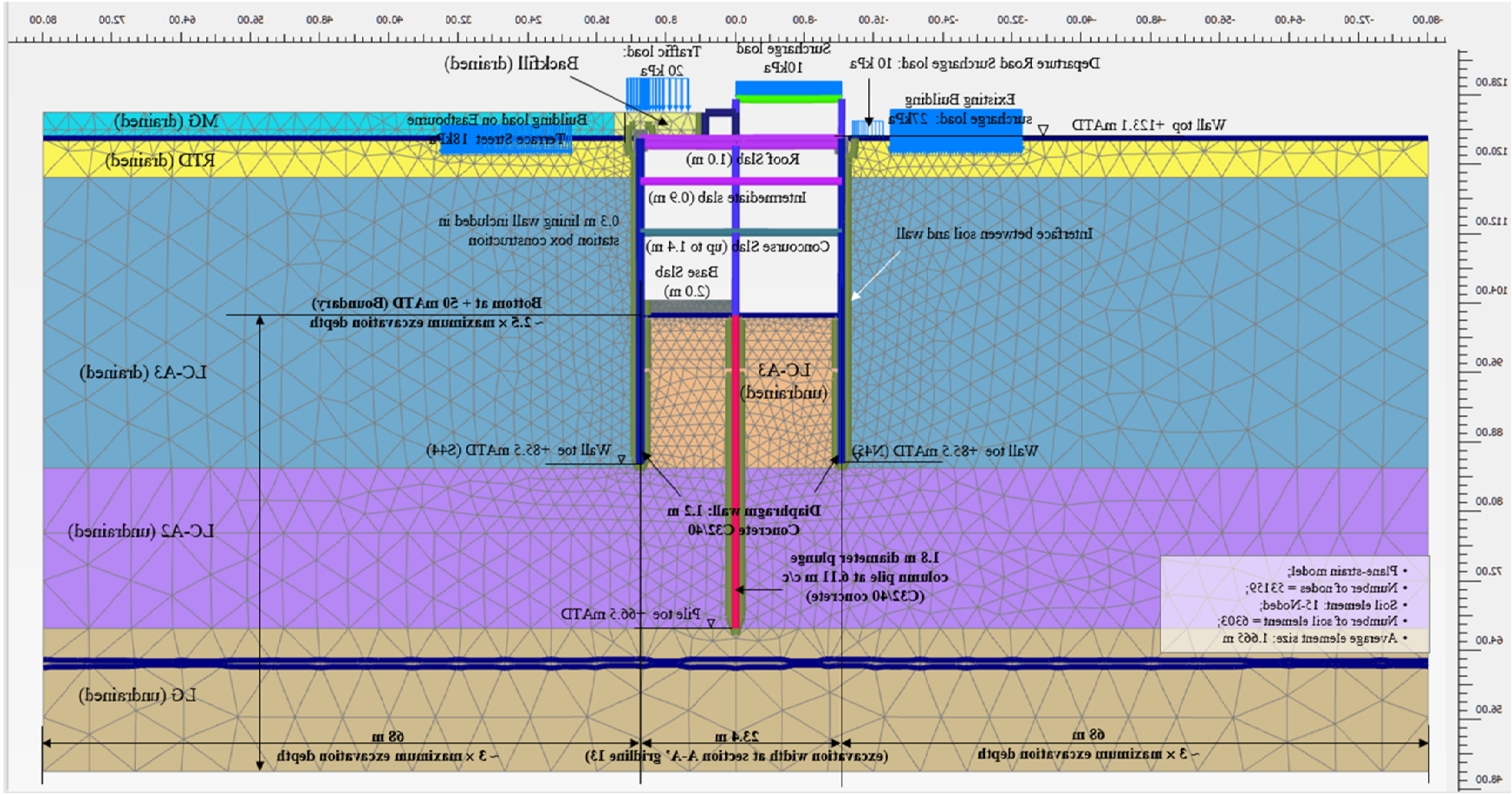

Figure 5. 19 PLAXIS 2D model for PAD station box excavation at final excavation stage 17

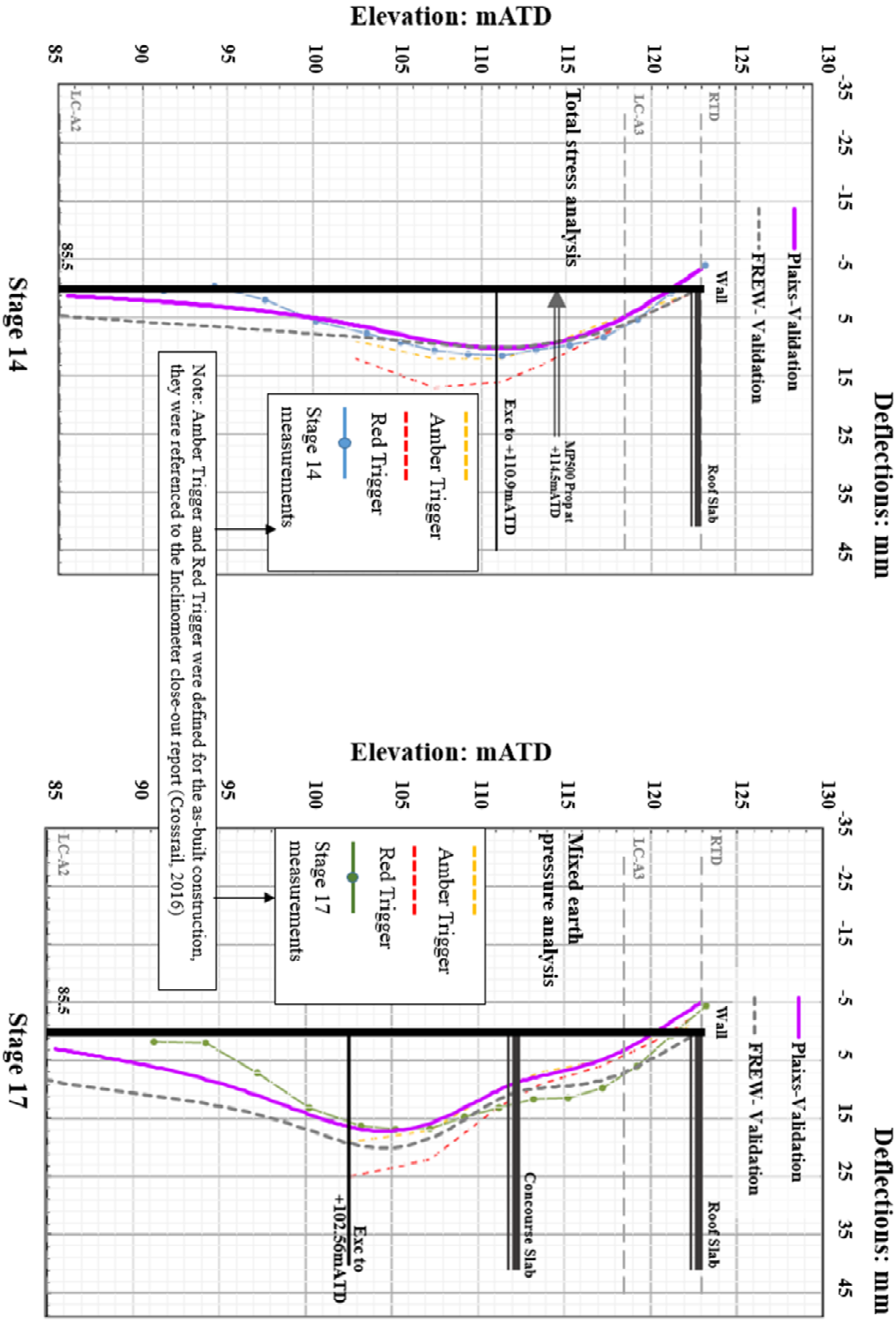

Figure 5. 20 Plaxis 2D validation result of PAD station box excavation - wall deflections versus the E13-12 data

Sensitivity analysis of the Plaxis 2D model was carried out to investigate the surcharge loads influence and it found a level of impact on the wall deflection predictions. The underestimated deflections in the upper part of the wall at stage 17 are considered one of the consequences. In addition, the mixed top-down and bottom-up construction sequence and the changed slab thickness are also considered to have some impact on wall deflections, but they are difficult to quantify due to the lack of insufficient details.

The difference between the Plaxis 2D validation and the FREW estimate is small at stage 14 but increases at stage 17. In general, the Plaxis 2D analysis shows the wall deflection predictions closer to the inclinometer data than the FREW's.

As a validation, empirical correlations of the most probable undrained soil stiffness (E_u) over undrained shear strength (c_u) were obtained by back-analysis of the TCR-WTH deep box excavation using Plaxis, they are applicable in predicting the wall performance for the PAD station box excavation by Plaxis 2D.

5.4 3D FEM back-analysis of the TCR-WTH

The actual excavation takes place in three-dimensional space, hence, the 3D FEM has an advantage in numerical modelling. For instance, a 3D model can simulate a process of excavation across the site, or install the individual structural items in an order. More information is available from a 3D model for comparison with observations, such as ground movements in both vertical and horizontal directions and wall deflections at multiple positions.

The original LS-Dyna 3D model for the TCR-WTH was prepared for the Crossrail ground movement assessment. The original LS-Dyna model was modified according to the as-built construction records (Table 3.3) for the back-analysis. The keyword file of the LS-Dyna 3D back-analysis (the final iteration) for the TCR-WTH case history is enclosed in Appendix B.

5.4.1 LS-Dyna 3D model

The LS-Dyna 3D model for the TCR-WTH excavation is presented in Figure 5. 21, showing a 267 m × 267 m × 55 m (deep) 3D model with a total of 1,276,198 solid elements with an average element size of 1.486 m. Additional elements are generated for structural items: 86,772 shell elements for the diaphragm wall; 215 shell elements for the capping beam and waler beams; and 54,134 beam elements for temporary props.

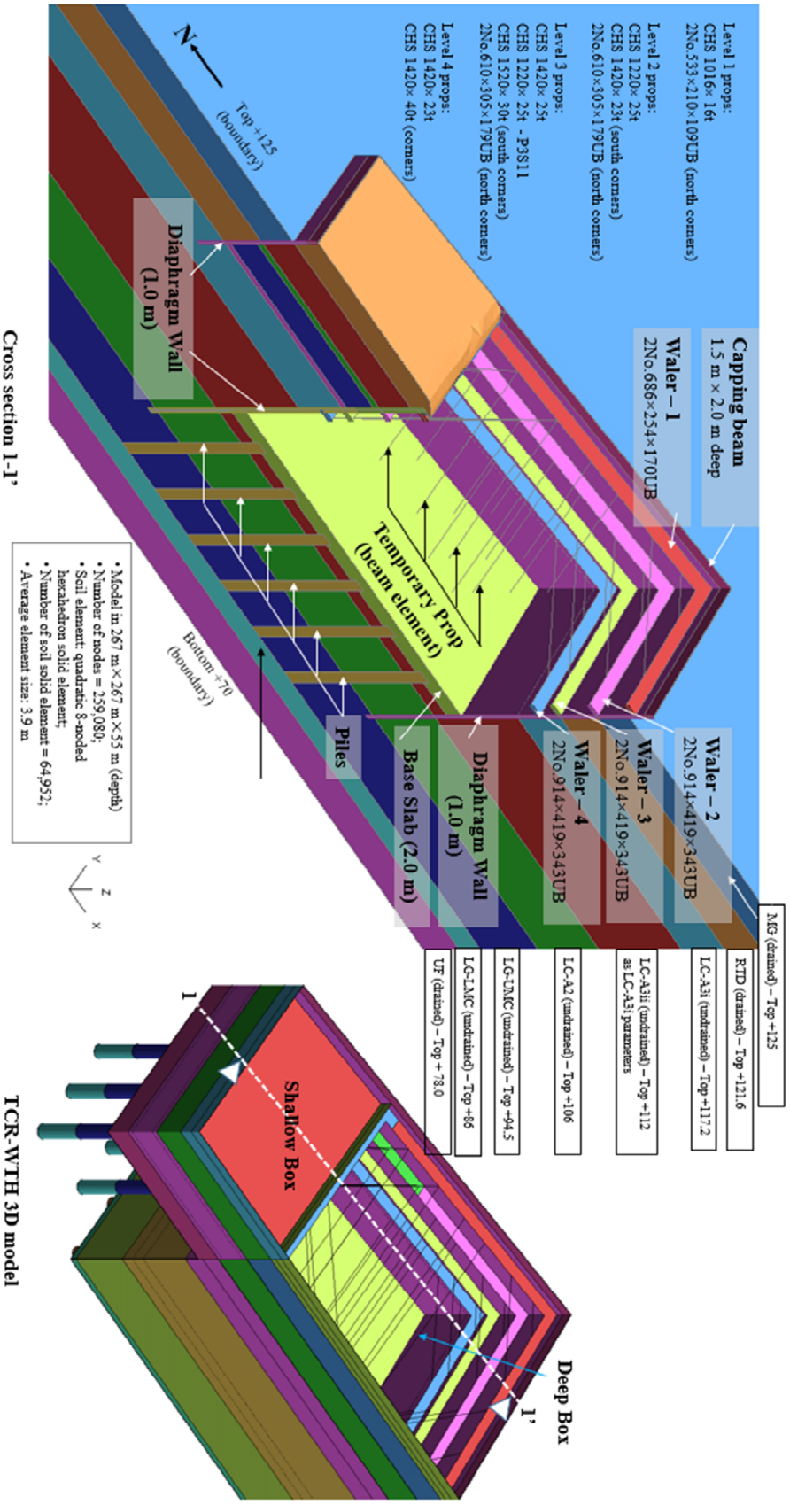

Figure 5. 21 LS-Dyna 3D model for TCR-WTH deep box excavation

Levels of stratigraphy are adapted to the solid elements mesh (Figure 5. 21), and they slightly differ from the ground models assumed in the FREW and the Plaxis 2D analyses. Other as-built structural properties are applied in the 3D model (see Appendix B).

In the 3D model, a quadratic 8-noded hexahedron element allowing nodal rotations (Oasys, 2010), is the default element type for the solid element and assigned to soil elements. Structural elements in LS-Dyna were discussed in Chapter 2. Accounting for the balance between accuracy and computation time, the following elements are selected to simulate the structural items in the LS-Dyna 3D model:

- Diaphragm wall by shell element and installed as wished-in-place;
- Capping beam and waler beam by shell element;
- Temporary props in CHS section or steel truss girder section by beam element; and
- Piles underneath the base slabs by solid element.

The boundary conditions are defined through nodes:

- Nodes at the bottom (Z=50): free rotation but restrained the displacement in all directions (X, Y, Z);
- Nodes at vertical boundaries: free rotation and allowing free movements in the Z direction.

Although the surcharge loads are known to have some effects on the wall deflections, no surcharge loads are applied in the LS-Dyna 3D model, because it is difficult to identify all surcharge loads for the 3D model covering an area of 267 m ×267 m. Additionally, some loads are not suitable for this static analysis, like the dynamic cyclic traffic loading. The surcharge loads impact on the predictions will be discussed in the interpretation of results.

The initial values of Mohr-Coulomb parameters (Table 5. 4) derived for the FREW analysis are applied in the LS-Dyna model as the initial inputs. The undrained soil stiffness E_u values are based on the calibrated most probable values from the Plaxis 2D back-analysis: E_u = 1600 c_u for the LC-A3, E_u = 2000 c_u for the LC-A2, E_u = 2500 c_u for LG-UMC and E_u = 4000 c_u for the LG-LMC.

An example of the Mohr-Coulomb soil material card for the LC-A3 in the LS-Dyna 'keyword' file is given in Table 5. 9. Each material is given a specific ID and defined by a minimum of three cards for the Mohr-Coulomb model: general Mohr-Coulomb parameters in card 1 (Line 1 & Line 2); constitutive calculation control card 2 (Line 3 & Line 4); additional parameters in card 3 (Line 5 & Line 6). Explanations for each input parameter and unit of the input values are included in the table.

Table 5. 9 Mohr-Coulomb input parameters for LC-A3 division in the TCR-WTH keyword file of the LS-Dyna model

Line1	MID	RO	GMOD	RNU	(BLANK)	PHI	CVAL	PSI
explaination	*material ID*	*mass density*	*Shear Modulus G*	*Poisson's ratio*	-	*friction angel*	*undrained shear strength* c_u	*Dilation angel*
unit	-	$kNm^3/10$	kN/m^2	-	-	*in radians*	kN/m^2	*radians*
Line 2	3	2.0	4.00E+04	0.2	0	0.001	75	0
Line 3	STR_LIM	NPLANES	ELASTIC	LCCPDR	LCCPT	LCCJDR	LCCJT	LCSFAC
explaination	*minimum shear stregnth of material*	*number of joint planes (Max=3)*	*1 = Elastic behaviour only*	*Loadcurve for dynamic relaxation*	*Loadcurve for transient*	*loadcurve for dynamic relaxation (joints)*	*locadcurve for transient (joints)*	*loadcurve for factor on strength vs time*
unit	-	-	-	-	-	-	-	-
Line 4	0.1	0	0	0	0	0	0	0
Line 5	GMODDP	GMODGR	LCGMEP	LCPHIEP	LCPSIEP	(BLANK)	CVALGR	ANISO
explaination	*reference depth for G*	*gradient of G (negative value)*	*Loadcurve of G versus plastic strain (override G)*	*Loadcurve of PHI versus plastic strain*	*Loadcurve of PSI versus plastic strain*	-	*gradient of* c_u *(negative value)*	*factor applied to elastic shear stiffness*
unit	*m*	kN/m^2	-	-	-	-	kN/m^2	-
Line 6	117.2	-8320	0	0	0	0	-15.6	0

* Shear modulus G rather than soil stiffness E is input in the LS-Dyna model. G=E/2(1+n): Eu=1600 cu = 1600 * 75 = 120 E+03 kPa, and G = 120E+03/2(1+0.5)=40E+03 kPa;

In addition, the 'BOUNDARY_PORE_FLUID_PART' in the keyword file defines the groundwater pore pressure, which is based on the groundwater design profile (Figure 3,2) of the original design. In this card, a suction limit of 100 kPa is given to the undrained calculation.

A sensitivity study for the LS-Dyna 3D modelling was undertaken as part of the literature review in Chapter 2. A couple of factors proved to be influential. For example, the type of elements selected to model the retaining wall, diaphragm wall: shell element versus solid element, whether to include the wall installation effect in the model, can affect the wall deflection prediction. It was found that when modelling assumptions were agreed and the fixed structural properties were applied in the LS-Dyna model, that the Mohr-Coulomb model parameters dominated the simulation, particular the soil stiffness values were found to have a significant impact on the wall deflection calculations

The LS-Dyna 3D model provides the predictions of deflection at any location of the wall, as well as strut forces for an individual temporary prop, and ground movements in any direction. The back-analysis of the wall deflections at the location where the SAA-8003 was installed are compared with the inclinometer data (SAA-8003) for consistency with FREW and Plaxis 2D back-analyses.

The tolerance between the predictions by LS-Dyna and observations is taken as that assumed in the FREW back-analysis (section 5.2.4): $0 \leq \Delta_{max} < 5$ mm. In general terms, more accurate predictions are obtained from 3D than 2D models, as the latter involves compensating modelling assumptions. An adjustment on the numerical modelling error was attempted for LS-Dyna, however, it was difficult to draw a conclusion as a couple of factors were found affecting wall deflection calculations, like the type of wall element and the surcharge loading conditions.

During the iterative back-analysis process, reduced soil stiffness values for the LC-A2 and LG-LMC divisions were required in order to match observations.

5.4.2 Results

The LS-Dyna 3D back-analysis results of the wall deflections at the location of SAA-8003 for the TCR-WTH deep box excavation, are presented in Figure 5. 22. The estimates agree well with the corrected SAA-8003 data at both the early excavation stage 3 and at the final excavation stage 6.

LS-Dyna underestimates deflections from the top of the wall to the level 3 props at the final excavation stage 6. Some incremental displacements are developed in predictions, for

instance, 7 mm deflection at P2S2 level is estimated at stage 3, which increases to 7.5 mm at stage 6 (Figure 5. 22). This is different from the FREW and Plaixs 2D analysis results. The latter two results are applied the reduced prop stiffness values and resulted in an almost fixed wall lateral displacement at levels where struts are propped. No reduction on prop stiffness is applied in the LS-Dyna model, instead, the as-built detail is modelled, including the capping beam, four levels of waler beams and a total of 46 steel props. The predicted incremental displacements at prop levels over the construction period match the corrected SAA-8003 data, only the incremental magnitudes are smaller than those in the measurements.

These incremental displacements are also reflected in the predicted strut loads, for instance, the predicted P1S2 strut load stabilised at 2000 kN at stage 3 and gradually increase to 3000 kN at stage 6 (Figure 5. 23).

A review of the predicted wall deflections in the LC-A3 at stage 3 and stage 6, it suggests a decreased soil stiffness with increasing strain, as the fixed stiffness value in the analysis calculates the matched deflections at stage 3, but underestimates at stage 6. A non-linear stiffness would be ideal to capture the response of LC-A3 soil, however, this is beyond the capability of the Mohr-Coulomb model.

Besides SAA-8003, which recorded the maximum wall deflections during the TCR-WTH deep box excavation, the wall deflection near the corner is monitored by SAA-8001 (Figure 3.4). The wall deflection predictions at this location are presented in Figure 5. 24, including the raw SAA-8001 data.

The difference in predictions by the initial values and the updated most probable values can be accounted for the increased structural stiffness at the corner, where the effect of the soil stiffness on the wall deflections is attenuated.

Unusual movements above the level 2 props are observed in the raw SSA-8001 data, a reduced displacement at the top of the wall and additional displacements at the level of +120 mATD at stage 6. The cause of these changes is unknown, but a possible explanation is that they are associated with construction activities in the vicinity of the location.

A few additional millimetres may be introduced by including actual surcharge load conditions in the LS-Dyna 3D model, but this is not expected to have a significant impact on the predictions according to the sensitivity study.

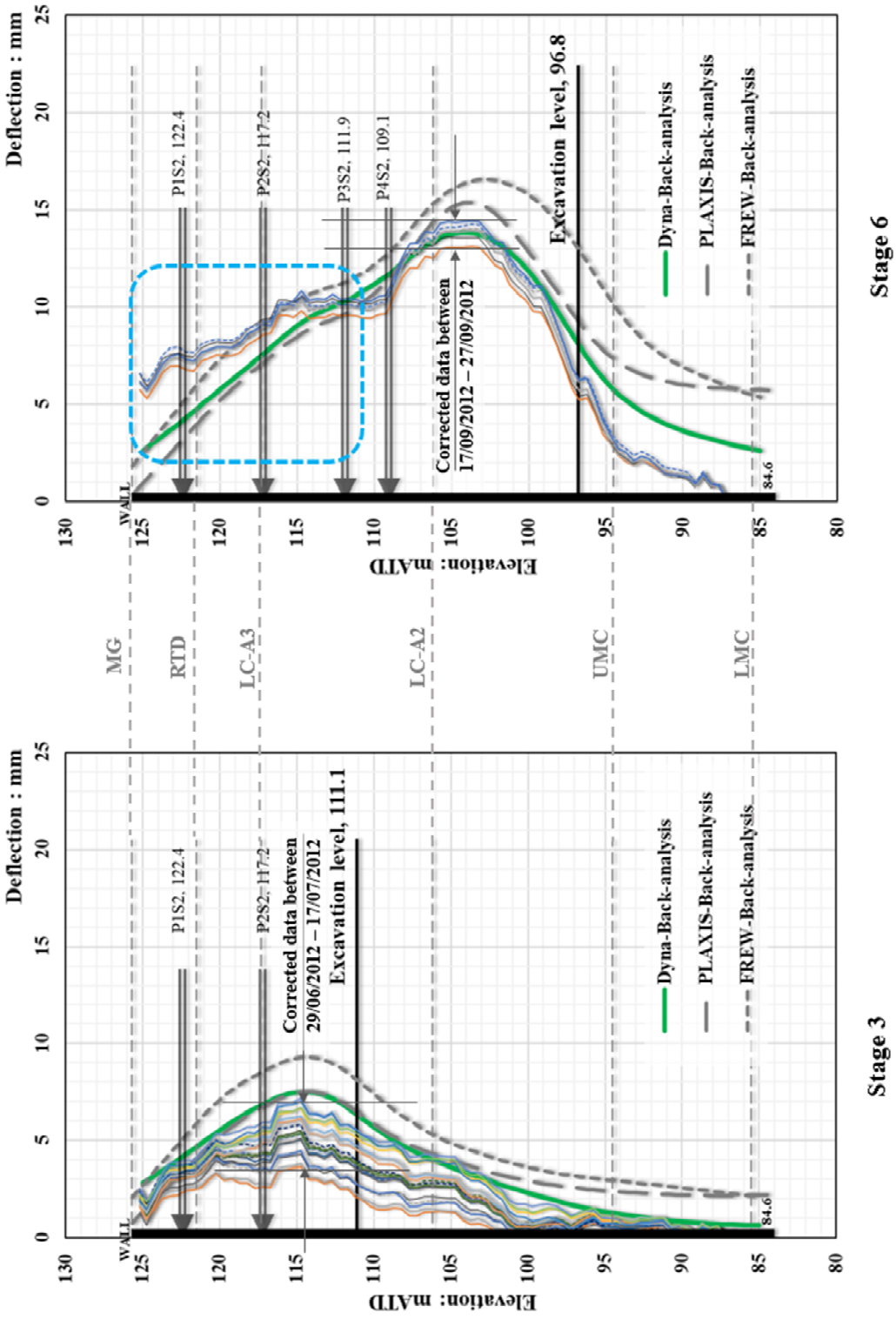

Figure 5. 22 LS-Dyna 3D back-analysis result for TCR-WTH - wall deflections versus the corrected SAA-8003 data

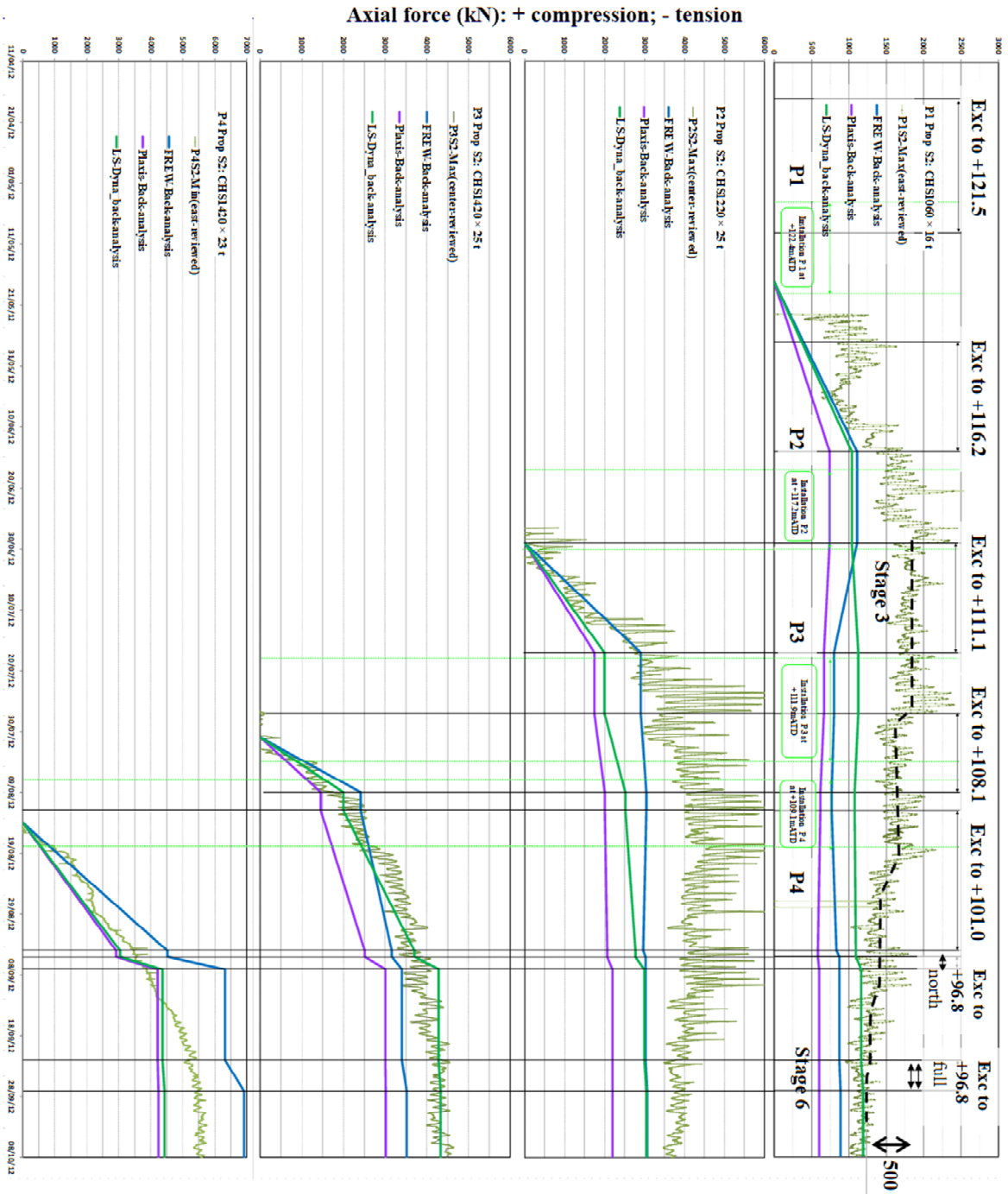

Figure 5. 23 LS-Dyna 3D back-analysis result (TCR-WTH) – strut loads versus the reviewed axial forces by strain gauge data (P1S2 to P4S2)

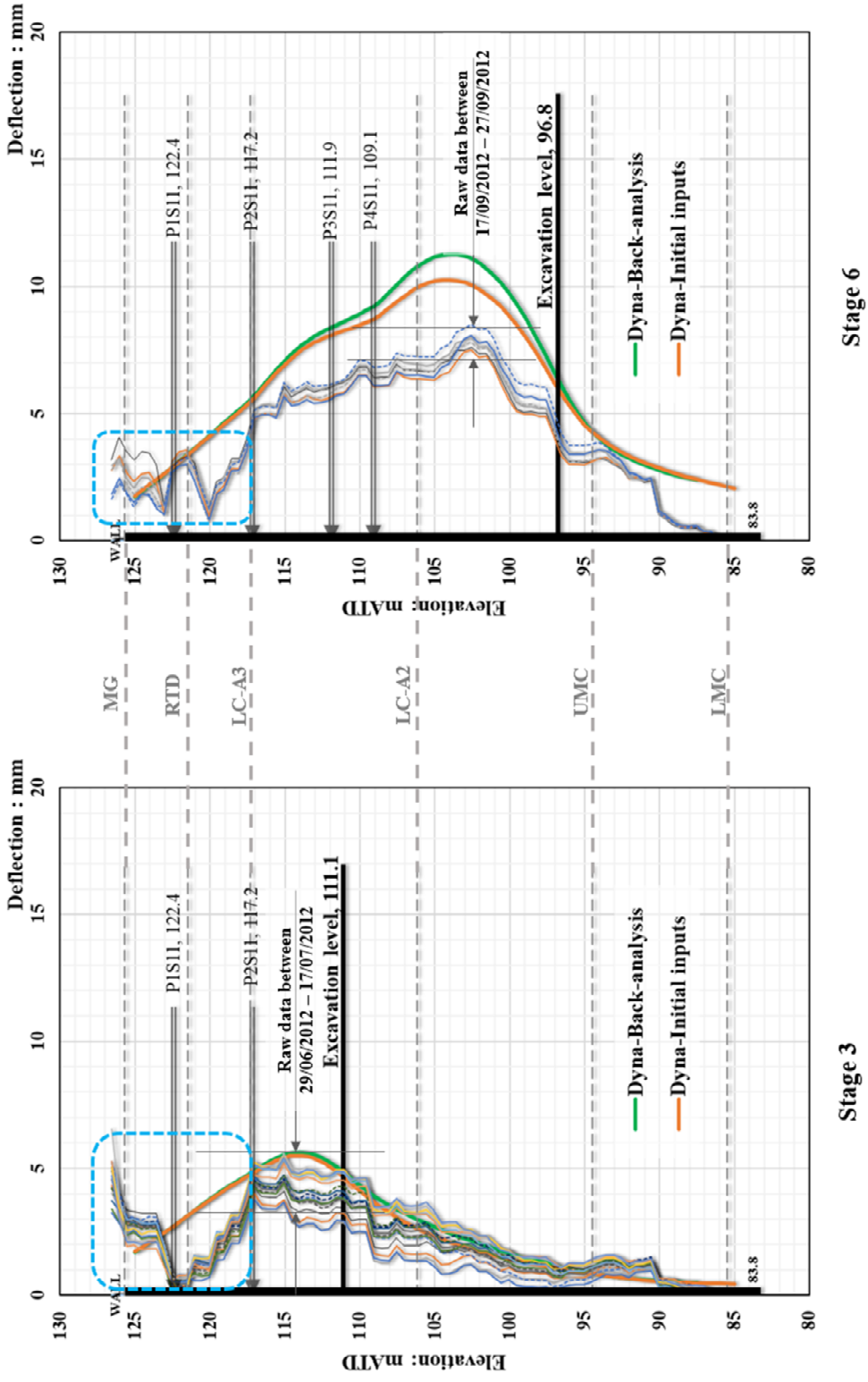

Figure 5. 24 LS-Dyna 3D back-analysis result (for TCR-WTH - wall deflections versus the corrected SAA-8001 data

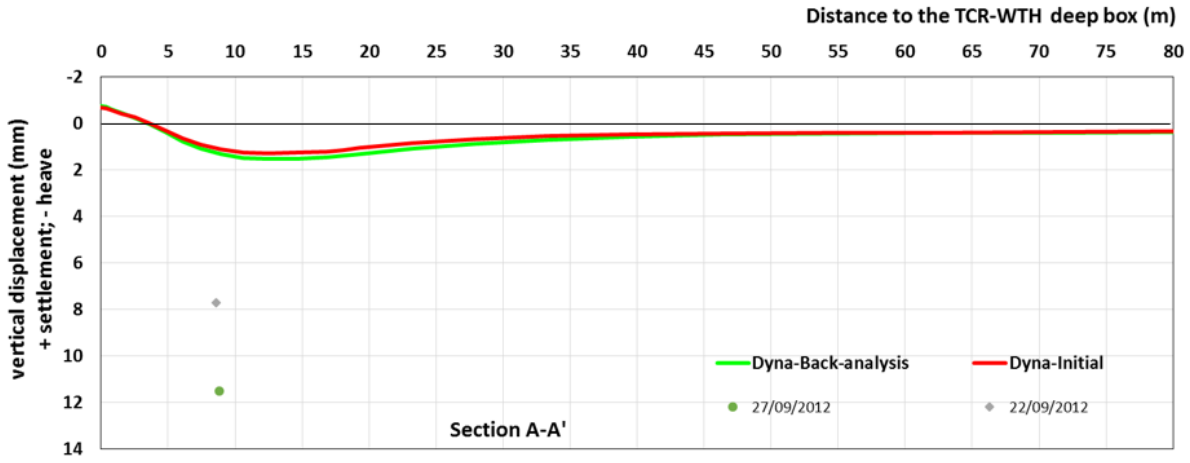

(a) Settlement behind the east diaphragm wall along the section A-A' at stage 6

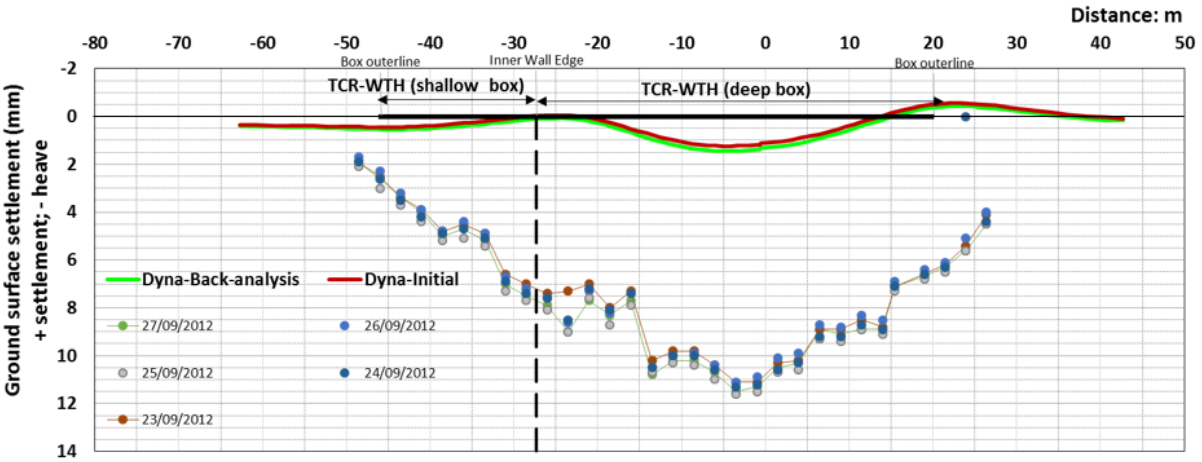

Note:
1. Dean Street Ground surface settlement was measured using levelling points, they were installed at 8.5 m to 9.0 m distance from the TCR-WTH box outer line;
2. The SAA-8003 location were marked as X = 0; and
3. Monitoring data along the Dean Street has been re-baselined referenced to the data on 19/04/2012 to exclude any settlements prior to the excavation works.

(b) Settlement along Dean Street at stage 6

Figure 5. 25 LS-Dyna 3D back-analysis result (TCR-WTH) – ground surface settlements at final excavation stage 6

The LS-Dyna 3D back-analysis predictions of the strut loads at four levels are presented in Figure 5. 23. For P1S2 and P2S2, the predicted stabilised loads are underestimated by up to 35%, and the differences are minimised after the installation of the 4th level of props. A good agreement in the predicted loads and the measurements is observed in P3S2. While the predicted strut load follows the trend of the measured force in P4S2 during the force establishment period, the predicted stabilised loads are underestimated by about 20%.

The ground surface settlement along Dean Street was monitored using levelling studs during the period between 25/02/2012 and 09/11/2012. The data were reviewed and compared with the predictions by the LS-Dyna model in Figure 5. 25. The predicted ground surface settlements at the final excavation stage 6 are presented in (a) perpendicular to Dean Street across SAA-8003; (b) along Dean Street. The monitoring data was re-baselined at the beginning of the excavation work (19/04/2012) to ensure the measurements and the predictions are comparable.

The difference in the predicted settlements by the initial values and the updated most probable values from the 4th iteration is negligible, but the difference between the predictions and the measurements is up to 12 mm by the final excavation stage 6. The limitation of the Mohr-Coulomb model is that it does not consider anisotropy of soil stiffness, and the potential impact of the wall installation not being included in the 3D model, are considered reasons for this significant differential settlement.

The other two predictions provided by LS-Dyna 3D using the Mohr-Coulomb model are the ground surface heaves and the groundwater pore pressures inside the excavated box. These will be discussed together with the results using the BRICK model in the next chapter.

5.4.3 Representative values of the most probable Mohr-Coulomb parameters for London Clay with LS-DYNA

The representative values of the most probable Mohr-Coulomb parameters for London Clay are calibrated using inclinometer data, from the LS-Dyna 3D back-analysis for the TCR-WTH deep box final excavation stage. The undrained shear strength (c_u) values and the undrained soil stiffness (E_u) values of the Mohr-Coulomb parameters for London Clay and Lambeth Group are compared with the most probable values calibrated by Plaxis 2D and FREW in Table 5. 10.

Table 5. 10 Summary of Undrained shear strength (c_u) and Undrained soil horizontal stiffness (E_{uh}) for London Clay and Lambeth Group at the TCR-WTH (LS-Dyna 3D & Plaxis 2D & FREW models)

Parameters	***Initial values in back-analysis (FREW & Plaxis)***	***Most Probable values of back-analysis (FREW)***	***Most Probable values of back-analysis (Plaxis 2D) & Initial values for LS-Dyna 3D***	***Most Probable values of back-analysis (LS-Dyna 3D)***
LC-A3				
c_u *(kN/m²)*	75+15.6z			
E_u *(MN/m²)*	$E_{uh} = 1000c_u$	$E_{uh} = 1750c_u$	$E_{uh} = 1600c_u$	$E_{uh} = 1600c_u$
LC-A2				
c_u *(kN/m2)*	200+17.5z			
E_u *(MN/m2)*	$E_{uh} = 1000c_u$	$E_{uh} = 2000c_u$	$E_{uh} = 2000c_u$	$\underline{E_{uh} = 1600c_u}$
LG-UMC				
c_u *(kN/m²)*	280+6.4z			
E_u *(MN/m²)*	$E_{uh} = 2500c_u$	$E_{uh} = 4000c_u$	$E_{uh} = 2500c_u$	$E_{uh} = 2500c_u$
LG-LMC				
c_u *(kN/m²)*	350			
E_u *(MN/m²)*	$E_{uh} = 2500c_u$	$E_{uh} = 4000c_u$	$E_{uh} = 4000c_u$	$\underline{E_{uh} = 2500c_u}$

Note: z is the depth below the top of the stratum in meter.

Despite a lower stiffness for LC-A3&LC-A2 (E_u/c_u = 1600) and LG-LMG (E_u/c_u = 2500), the LS-Dyna 3D analysis performs well in the wall deflections prediction, its estimates are closer to the measurements by the corrected SAA-8003 data (Figure 5. 22). In particular, the predictions for the lower part of the wall, based on the difference between the LS-Dyna predictions and observations are smaller, compared to differences between the Plaxis 2D predictions and observations, or differences between the FREW predictions and observations.

A less stiff LC-A2 enables better-matched wall deflection predictions at the early excavation stage 3. However, at the final excavation stage 6, the wall deflections for the upper part of the wall are underestimated, like the Plaxis 2D back-analysis. As the integrated propping system, including waler beams and individual props, had been modelled in the 3D model, the possible reasons for this underestimation are linked to the non-linear soil stiffness with increasing strain, or potentially contaminated monitoring data in the upper part of the wall at later excavation stages, like the impact of other construction activities (e.g. temporary gantry crane was operating on the capping beam during later excavation stages).

The 3D model shows competence in back-analysing retaining structure performance with respect to the wall deflection, strut loads supporting walls, and ground displacements assessment. Although the calibrated most probable soil horizontal stiffness (E_{uh}) values from LS-Dyna using inclinometer data are smaller than those calibrated from Plaxis 2D and FREW analyses, better-matched wall deflections are obtained from LS-Dyna back-analysis, as the 3D model accurately replicates the actual soil/structure interaction, including the geometry influence in excavation space.

Due to the difficulty in identifying the as-built construction details for each 3D model, time requirements, preparation of the adjusted 3D model, computational time and processing output results, no validation of the most probable Mohr-Coulomb parameters is undertaken in LS-Dyna for the other Crossrail excavations.

5.5 Summary of back-analysis by Mohr-Coulomb model

5.5.1 Representative most probable values of Mohr-Coulomb design parameters for London Clay

In the Crossrail excavation case histories back-analysis using inclinometer data, the undrained soil horizontal stiffness (E_{uh}) is identified as the most influential parameter of the Mohr-Coulomb model. The E_{uh} value is linked to the undrained shear strength (c_u) value through an empirical correlation. The supervised linear statistical regression method is recommended to determine c_u value for consistency. The recommended representative values of the most probable Mohr-Coulomb parameter, undrained soil horizontal stiffness E_{uh} for London Clay is written as E_{uh}/c_u for FREW, Plaxis 2D and LS-Dyna 3D and summarised in Table 5. 11.

These most probable E_{uh} values are calibrated in the back-analysis of Crossrail TCR-WTH deep box excavation through different FEMs: pseudo-FEM FREW, Plaxis 2D and LS-Dyna 3D. The validation of these most probable values is also undertaken in two other Crossrail excavations, the typical plane-strain excavation example of the PAD station box excavation and the LIS-MS shaft excavation.

Table 5. 11 Summary of the representative values of Mohr-Coulomb most probable Undrained soil stiffness (E_{uh}/c_u) for London Clay

FEM / Soils	**FREW**	**Plaxis 2D**	**LS-Dyna 3D**
London Clay (LC-A3)	1300 ~ 1750	1600	1600
London Clay (LC-A2)	2000	2000	1600
Lambeth Group*	*3000 ~ 4000*	*2500 ~ 4000*	*2500*

Note: 1. stiffness value is given as of E_{uh}/c_u correlation in kPa, in which c_u values are derived by the supervised statistical regression method; 2. correlations for the Lambeth Group are indicative, as the back-analysed Crossrail excavations barely involved excavation in this layer.

The undrained shear strength (c_u) values derived by the supervised statistical regression method at the TCR-WTH site are plotted against triaxial testing data and in-situ SPT testing data in Figure 5. 26. The representative values of the Mohr-Coulomb most probable undrained soil stiffness (E_{uh}) calibrated from the LS-Dyna 3D back-analysis for the TCR-WTH deep box final excavation stage are plotted against triaxial testing data in Figure 5. 26.

Figure 5. 26 shows these most probable stiffness values at the top of the LC-A3 division are closer to the triaxial results at a shear strain level of 0.05%. At the bottom of the LC-A3, the most probable stiffness values increase closer to the triaxial results at a shear strain level of 0.01%. In the LC-A2, the most probable stiffness values match with the triaxial results at a shear strain level of 0.01%.

No apparent correlation between the most probable stiffness values and the triaxial results is established for the Lambeth Group. As three back-analysed Crossrail case histories, their excavations barely reached into the Lambeth Group, therefore, the most probable stiffness values are less representative. A careful assessment will be required prior to applying the most probable stiffness values of the Lambeth Group in future excavation design.

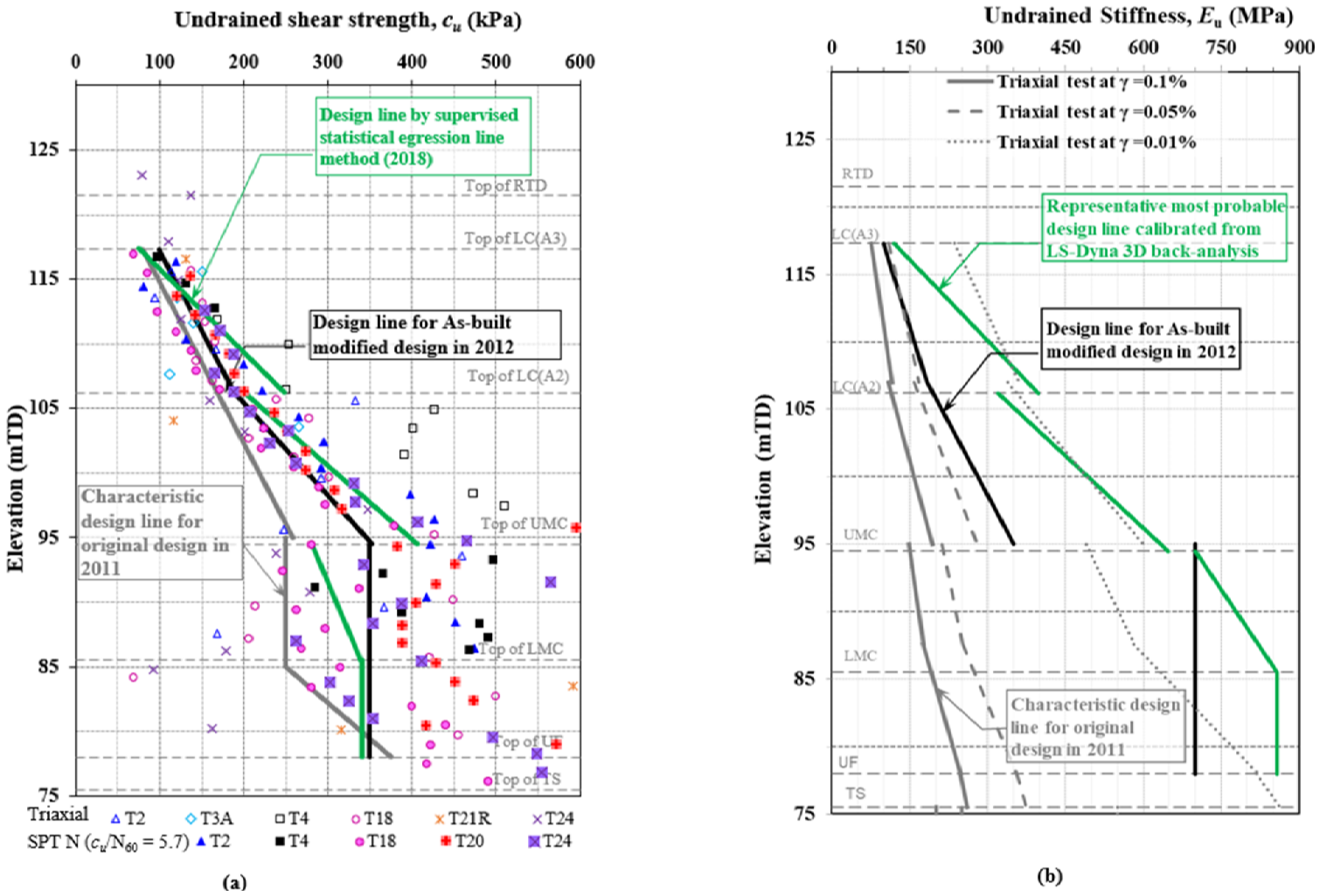

Figure 5. 26 Representative most probable values versus laboratory testing data (a) undrained shear strength; (b) undrained shear stiffness

Comparison between the most probable soil stiffness values and triaxial test data indicates that it is possible to derive the Mohr-Coulomb soil stiffness values from ground investigation testing data for a performance-based prediction. However, the quality of testing data needs to be ensured, in particular, results at very small strain levels (e.g. ≤ 0.01%), where the tested values from commercial laboratories can vary by up to 7 times (see Chapter 6).

5.5.2 Issues in the back-analysis

The back-analysis of the Crossrail TCR-WTH deep box excavation using the Mohr-Coulomb soil model was successfully conducted in three different FEMs. Some difficulties were found to remain in the process and can be detrimental to a successful back-analysis.

5.5.2.1 Reliable observations

Field monitoring data is the key in the back-analysis. The types of observations (e.g. wall deflection, strut loads, pore water pressures, and ground movements) and the quality of the data have a significant impact on the back-analysis performance.

Data review as a measure of error diagnostic and error correction is strongly recommended for each observation following the examples given in the Crossrail excavation case histories (Chapter 3).

If the back-analysis of the excavation or the observational method is envisaged at the beginning of a project, the instrumentation and monitoring (I&M) plan should take the needs of the back-analysis into consideration. For instance, type and number of instrumentation in order to capture the required observations for the back-analysis. Moreover, the accuracy of readings and the frequency of readings need to be clearly specified, as the quality and quantity of data are relevant to the back-analysis comparison. Ultimately, observations affect the calibrated most probable parameters.

5.5.2.2 Accurate predictions

The Mohr-Coulomb back-analyses using the inclinometer data in three different FEMs show different performance in predicting the wall deflections and temporary strut loads. Meanwhile, efforts to enable the back-analysis by different FEMs and obtain the predictions are also at different levels. From Pseud-FE FREW, Plaxis 2D to LS-Dyna 3D, amount of modelling details increase, in addition to the increased computational time.

Accuracy of predictions should be determined based on some basic factors: the needs of the back-analysis, the available observations, the known construction details, and understanding of the FEM for the back-analysis

5.5.2.3 Comparison

A rigorous back-analysis convergence criterion is necessary, especially for automated back-analysis. In current practice, engineering judgement in the back-analysis comparison is necessary due to the frequent unusual or exceptional results. Although, the judgement can be a bit bias and personal experience related and slow down the back-analysis process, however, if additional relaxation is allowed in the comparison, the calibrated most probable parameters will be less representative.

Chapter 6

Back-analysis TCR-WTH excavations by BRICK model

The back-analysis of the Crossrail excavations by the Mohr-Coulomb soil model is described in Chapter 5. However, the limitation of the Mohr-Coulomb model constrained further improvements of the back-analysis. The importance of the soil model in back-analysis performance is illustrated by applying an advanced soil model. This advanced soil model should be capable to simulate the non-linear soil stiffness decrease with increasing strains and other soil behaviours of an over-consolidated clay, like the London Clay as reviewed in Chapter 2.

The BRICK model as one of the advanced soil constitutive model was applied in the ground movement assessment for the Crossrail project (Crossrail, 2007b), and it was selected for the back-analysis. The procedure includes at least two steps: derive the initial values for the model parameters; calibrate the most probable model parameters in the back-analysis.

Chapter 6 presents the LS-Dyna 3D model back analysis of the Crossrail TCR-WTH deep box excavation using the BRICK soil constitutive model. The initial values of the BRICK model parameters for London Clay subdivisions are calibrated using the available triaxial testing data, while the representative values of the most probable model parameters are calibrated through the LS-Dyna 3D back-analysis using the inclinometer data.

6.1 BRICK parameters for London Clay

6.1.1 Representative characteristic values

The BRICK model requires non-linear soil stiffness values to be defined, in addition to parameters used for the Mohr-Coulomb analysis. Values are derived from testing data and summarised in Table 6. 1.

Table 6. 1 Original values of BRICK parameters for London Clay (Simpson, 1992b)

	London Clay	
String length $L_{(b)}$ *(shear strain)*	**$R_{(b)}$** (G_t /s')	**Soil property parameters**
0.000083	0.92	$\lambda^* = 0.1$,
0.00021	0.75	$\kappa^* = 0.02$,
0.00041	0.53	$\iota = 0.0041$,
0.00083	0.29	$\nu = 0.2$,
0.0022	0.13	$\beta = 4.0$.
0.0041	0.075	*implied* $\phi'_{crit} = 23.9°$
0.0082	0.044	
0.021	0.017	
0.41	0.0035	
0.08	0	

Using Richardson's (1988) triaxial testing data on the reconstituted London Clay samples, the initial string length $L_{(b)}$ and proportional material $R_{(b)}$ were chosen to fit the stiffness curve by the stress path DOX (Figure 2.25), which shows the highest shear stiffness values. Based on Viggiani's (1992) triaxial test data using bender elements, a maximum shear stiffness at very small strain is proportional to mean stress ($p^{0.83}$), and for normally consolidated clay $G_{max}/p \approx 146$. Assuming G_{max}/s' in the BRICK model is equivalent to G_{max}/p, with an assumed constant Poisson's ratio of $\nu = 0.2$, the parameter ι is calculated, $\iota=(1-2\nu)/(G_t/s')=(1-0.4)/146=0.0041$ (equation (2-8) in Chapter 2). The value of $\lambda^* = 0.1$ is taken from Schofield and Wroth (1968) allowing for the definition of consolidation and swelling used in the BRICK model in terms of volumetric strain. The value of $\kappa^*=0.04$ from Schofield and Wroth (1968) was applied and found to give rather high K_0, coefficient of earth pressure at rest, hence, an updated $\kappa^*=0.02$ was recommended based on BRCIK calibration of K_0 and Oedometer tests carried out for the British Library project (Simpson, 1992b). β is material constant, $\beta = 4$ in the BRICK model calculated a ratio of G_{max}/G_{nc}, which fits well with Viggiani's test data.

Values of the BRICK parameters for London Clay have been progressively reassessed. Pillai (1996) calibrated BRICK parameters using triaxial testing data from the Heathrow Express Link Project. The research project on sustainable construction of underground infrastructure (SCOUT) sponsored by the European Commission 6th framework programme calibrated BRICK parameters using the triaxial testing data from projects in central London (SCOUT, 2007). These parameters are summarised in Table 6. 2.

Table 6. 2 Updated BRICK parameters for London Clay

London Clay		
$R_{(b)}$ (G_t/G_{max})	**String length $L_{(b)}$** *(shear strain)* (Pillai, 1996)	**String length $L_{(b)}$** *(shear strain)* (SCOUT, 2007)
0.92	0.0000304	0.000030
0.75	0.0000608	0.000075
0.53	0.000101	0.00015
0.29	0.000121	0.00040
0.13	0.00082	0.00075
0.075	0.00171	0.0015
0.044	0.00352	0.0025
0.017	0.00969	0.0075
0.0035	0.0222	0.02
0	0.0646	0.06
Soil Property		
λ^*	0.1	0.1
κ^*	0.02	0.02
ι	0.0019	0.00175
ν	0.2	0.2
M_u	1.3	1.3
β^G	4.0	4.0
β^ϕ	4.0	4.0
	implied $\phi'_{crit} = 23.9°$	*implied $\phi'_{crit} = 24.2°$*

The progressive modification of the BRICK parameters for London Clay is illustrated through equivalent BRICK stiffness curves shown in Figure 6. 1, plotting the string length $L_{(b)}$ and the normalised tangent shear stiffness G_t/p'. The maximum shear stiffness G_{max} at a small strain level (strain < 0.01%) had increased significantly from Simpson (1992a) to SCOUT (2007). Compared to Pillai's (1996) BRICK parameters, SCOUT (2007) calibration had adjusted higher shear stiffness values in strain range between 0.01% and 0.04%.

More available triaxial data from different locations in London Basin, and from different subdivisions of London Clay may explain the change of modified BRICK parameters. Calibration of the BRICK parameters should be carried out for the different London Clay subdivisions. The local geology history, where testing samples are taken, should be carefully

studied to obtain a good assumption of pre-consolidation pressure and better interpret the testing results.

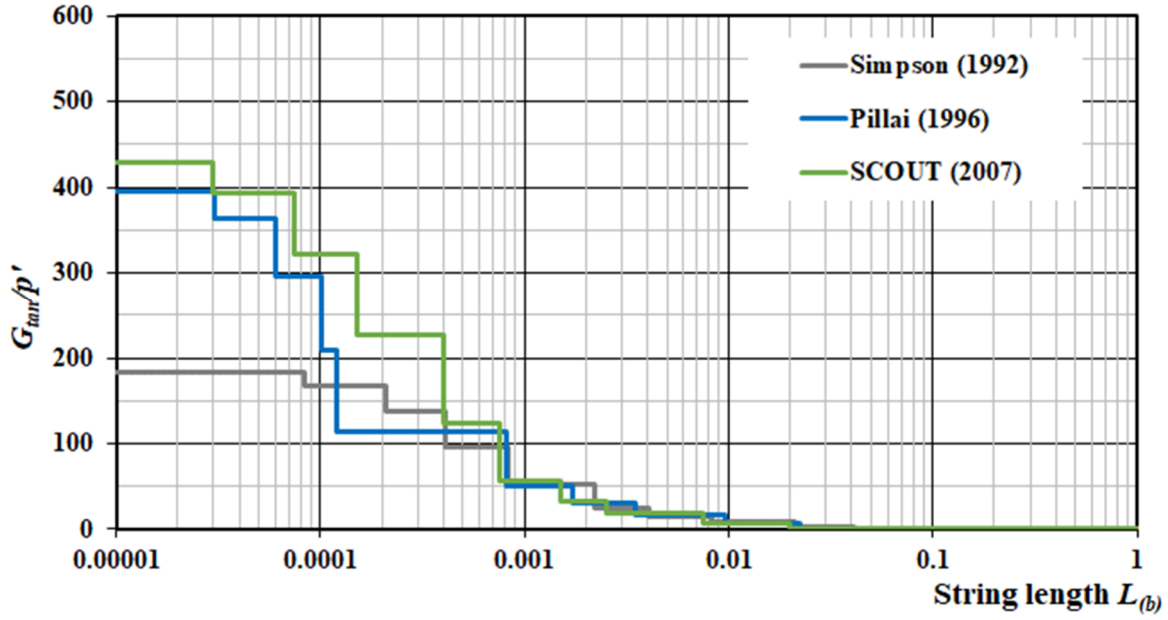

Figure 6. 1 Normalised shear stiffness of BRICK parameters for London Clay

6.1.2 Calibration BRICK parameters using laboratory testing data

In preparation for the TCR-WTH deep box excavation back-analysis, a calibration of BRICK parameters was undertaken using the available laboratory triaxial testing data from the Crossrail site investigations in between 1992 and 2006 (Crossrail, 2009a). These triaxial test results were grouped according to different London Clay subdivisions and used in the calibration. Variations in triaxial test results were observed, which are considered in relation to the quality of soil samples or the laboratory testing operations.

The BRICK parameters for the LC-A3 and LC-A2 subdivisions were calibrated using isotropically undrained consolidated triaxial (ICU) data from two boreholes: T9 located at about 200 m west of the TCR-WTH site, and B4 located at the Crossrail Bond Street station, about 1000 m east of the TCR-WTH site. The available test data was separated into compression tests and extension tests, as summarised in Table 6. 3.

Table 6. 3 Summary of isotopically undrained consolidated triaxial tests from borehole T9 and B4 (Crossrail, 2009a)

Filename	subdivision of LC	Ground level (mATD)	Top of LC (mATD)	Base of LC (mATD)	Sample depth (m)	Sample level (mATD)	Hight above LC base (m)	ϕ'_{peak} (°)	W (%)	W_L (%)	P_L (%)	I_P (%)	OCR
Borehole: T9													
xrt974c	A3ii	124.6	119.2	96.2	7.4	117.2	21.0	30.33	24	68	22	46	10.07
xrt912e	A3i				12.4	112.2	16.0	17.18	24	68	31	37	7.72
xrt914c	A3i				14.4	110.2	14.0	24.62	28	78	30	48	7.11
xrt916c	A2				16.4	108.2	12.0	25.71	22	66	31	35	6.25
xrt924c	A2				24.4	100.2	4.0	16.48	25	69	26	43	4.11
xrt926c	A2				26.4	98.2	2.0	37.54	-	-	-	-	3.96
Borehole: B4													
xrb4103c	A3ii	119.4	113.0	92.0	10.3	109.1	17.1	20.05	28	76	33	43	11.67
xrb413e	A3i				13.3	106.1	14.1	12.15	31	-	-	-	8.16
xrb4173c	A2				17.3	102.1	10.1	24.71	26	66	25	41	5.90
xrb4223c	A2				22.3	97.1	5.1	36.6	21	55	20	35	4.45
xrb4253c	A2				25.3	94.1	2.1	13.7	22	60	24	36	3.90

Note: 1 Borehole T9 and B4 were carried out in 1992 GI (Crossrail, 2009a); in the filename, c stands for compression test, e stands for extension test.

2 OCR values were calculated under assumption of a 170 m surcharge ice (γice = 10 kN/m3) above London Clay as pre-consolidation pressure.

6.1.2.1 London Clay Unit A3 (LC-A3)

Pillai's (1996) BRICK parameters were applied in the LS-Dyna 3D models to estimate ground movements for the Crossrail project (Crossrail, 2007a&b). Hence, calibration of the LC-A3 BRICK parameters for the CAR-WITH back-analysis began with this set of parameters.

Review of geology for the London Basin in Chapter 2 highlighted the importance of stress history in London Clay, an average surcharge of 200 m of ice (γ_{ice} = 10 kN/m^3) above London Clay was assumed as the pre-consolidation pressure.

During BRICK simulation of triaxial tests, the stiffness related parameters were found more responsive, like β^G & β^ϕ, parameters controlling the stiffness and the strength gained from over-consolidation. In addition, change of matrices by $L_{(b)}$ & $R_{(b)}$ and ι could also introduce some impacts on simulations. However, it was difficult to calibrate the sensitive parameter ι, which controls amounts of stiffness to be considered in the model, as the increment of ι needs to be 0.01% or even smaller. In terms of $L_{(b)}$ & $R_{(b)}$, their calibration will need more available accurate tests, with fewer tests the correlated matrics adjustment could end up a different combination for each replicated test. Therefore, calibration for the LC-A3 BRICK parameters is focused on β^G & β^ϕ.

Parameters β^ϕ was reduced gradually from 4.0 to 2.0 to achieve better-fitted stress path curves (p'- q) in the LC-A3 compression (Figure 6. 2) and extension (Figure 6. 3) tests. This change resulted in a negligible change on the shear stiffness curves (G_{sec}-$log\varepsilon_q$) in large strain range (>0.01%), however, it introduced much higher shear stiffness values in small strain range (0.0005% to 0.005%). The original β^ϕ value of 2.0 seemed to replicate better stress-strain curves (q-ε_q) in the compression tests but this was not shown in the extension tests.

Accuracy of the testing data was suspected, for example, the change of mean stress (p') was found small during shearing but a relatively high shear stress (q) was obtained in the compression test xrt974c: $\Delta p'$ = 25kPa and Δq = 150kPa; and in the extension test xrb413e: $\Delta p'$ = 75kPa and Δq = 200kPa. Both samples were taken from a shallow level: xrt974 sample from 7.4 m below ground level and xrb413 sample from 14.1 m below ground level. In addition, a sudden increase in shear stress was observed in the compression test of xrb4103c (plot of q-ε_q in Figure 6. 2), hence, BRICK simulations did not capture the trend of either the stress-strain curve (q-ε_q) or the shear stiffness curve (G_{sec}-$log\varepsilon_q$).

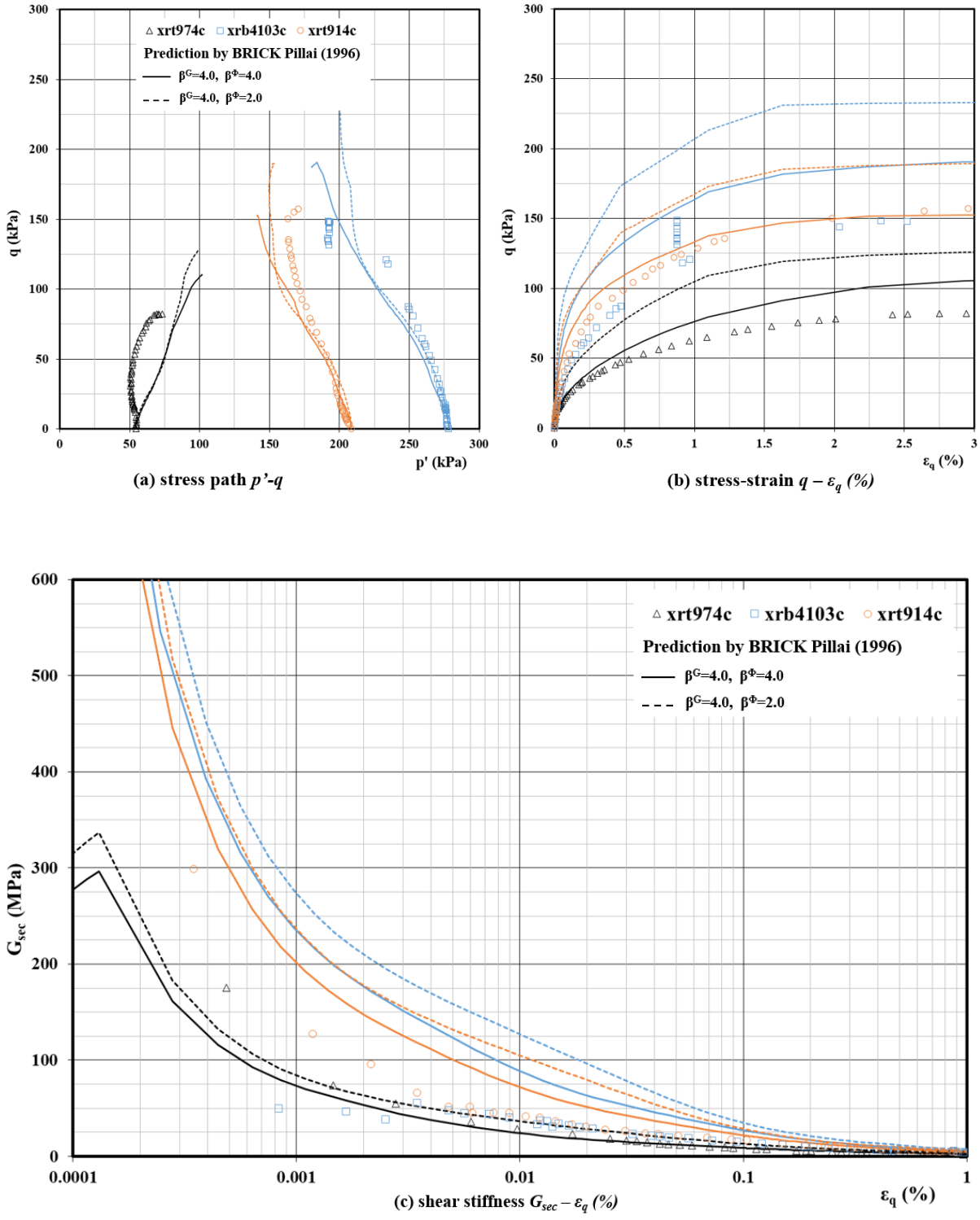

Figure 6. 2 Triaxial compression test results for LC-A3: lab test data versus BRICK simulation

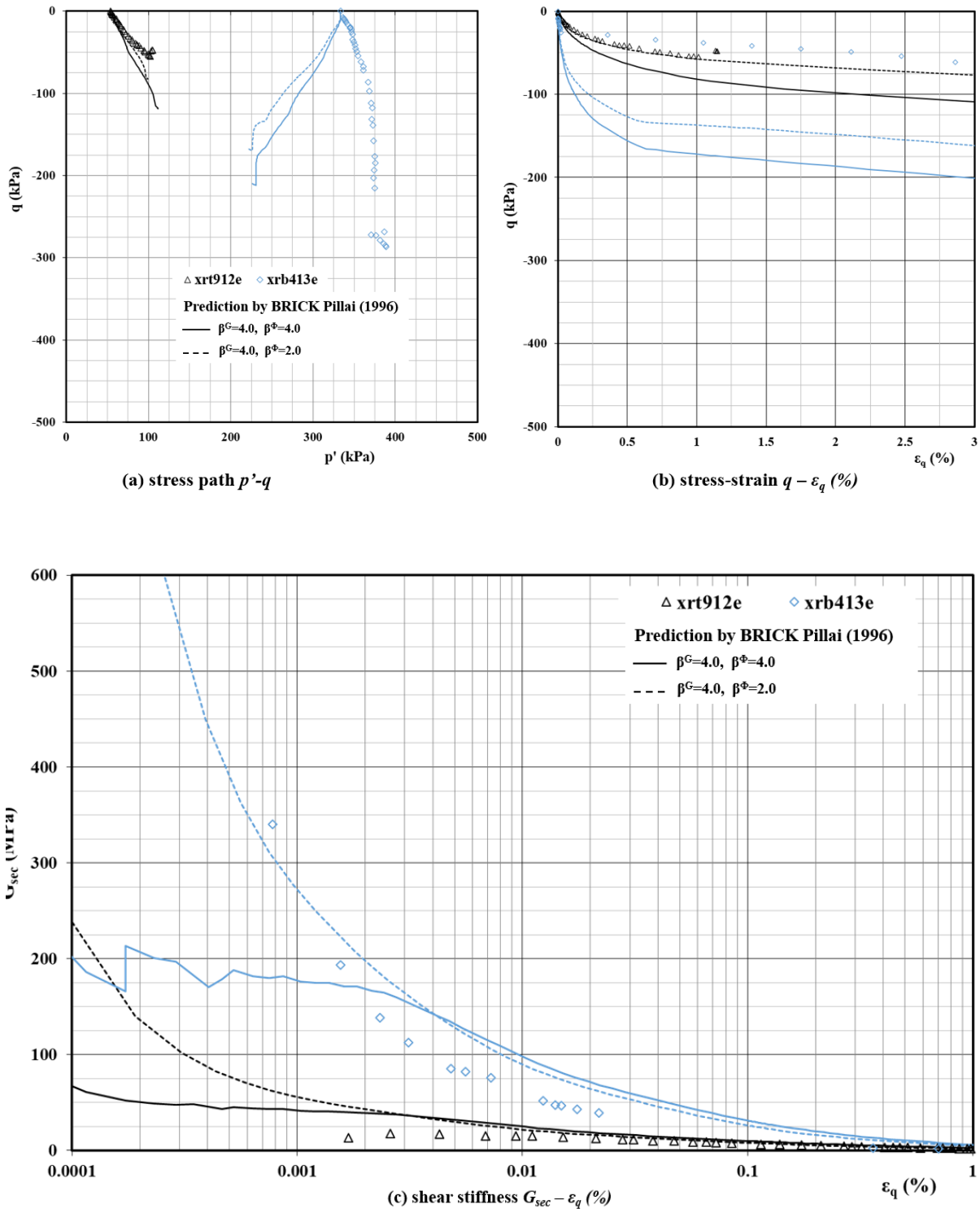

Figure 6. 3 Triaxial extension test results for LC-A3: lab test data versus BRICK simulation

Based on the above calibration using the limited number of triaxial data for the TCR-WTH site, the Pillai's (1996) BRICK parameters are considered applicable for the LC-A3 in the TCR-WTH deep box excavation back-analysis.

6.1.2.2 London Clay Unit A2 (LC-A2)

An assessment was also carried out for the LC-A2 division. No extension triaxial test was performed on soil samples from the LC-A2, instead, six CIU compression triaxial tests were selected for the calibration: three from borehole T9 and another three from borehole B4. The BRICK simulations and triaxial test results on borehole B4 soil samples are presented in Figure 6. 4. Figure 6. 5 shows the other three test results on borehole T9 soil samples and the BRICK simulations.

Two tests, xrt916c & xrb4253c with samples taken from 16 m and 25.3 m below ground level, were stopped at a strain level of less than 2% before reaching the maximum shear strength. Another two tests, xrt926c & xrb4223c with samples taken from 26 m and 22.3 m below ground level, showed a tendency to dilate during triaxial compression. The remaining two tests, xrt924c & xrb4173c with samples taken from 24 m and 17.3 m below ground level, displayed a tendency to contract during the compression shear. In addition, it was observed that the measured shear stiffness values varied between 100 MPa and 300 MPa at a small strain level of 0.001%, except for xrt924c, which shows a higher shear stiffness value of 650 MPa at this strain level.

Although, all six CIU tests were performed on soil samples from 16 m to 26 m below the ground level, BRICK simulations performed differently in all six compression tests. In the two tests on borehole B4 soil samples (xrb4173c & xrb4223c), simulations by Pillai's (1996) BRICK parameters replicated stress-strain curves (q-ε_q) but β^{ϕ} =2 seemed better predicted the shear stiffness curves (G_{sec}-$log\varepsilon_q$). For the test of xrb4253c on the deepest LC-A2 sample from borehole B4, with the smallest OCR (Table 6. 3), simulations with β^{ϕ} =2 replicated the shear stiffness curves (G_{sec}-$log\varepsilon_q$) before test stopped near strain of 2%, but performed poorly in stress-strain curves (q-ε_q) and stress path curves (p'- q).

In the tests on borehole T9 soil samples (xrt924c & xrt926c), neither β^{ϕ} =4.0 or β^{ϕ} =2.0 performed well in both the stress-strain curves (q-ε_q) and the shear stiffness curves (G_{sec}-$log\varepsilon_q$). However, simulations by SCOUT BRICK parameters with β^{ϕ} = 2.0 better matched with the

test of xrt924c in shear stiffness curve (G_{sec}-$log\varepsilon_q$) in strain range of 0.0005% and 0.001%. For the test of xrt916c on the shallower LC-A2 sample from borehole T9, none of the BRICK simulations matched the shear stiffness curves (G_{sec}-$log\varepsilon_q$) before the test stopped near strain of 2%.

Reviewing stress path curves (p'- q), BRICK simulations with a higher $\beta^{\phi} = 4.0$ achieved higher triaxial shear strength values in the LC-A2 tests, compared to those by $\beta^{\phi} = 2.0$.

It is hard to draw a conclusion on the above calibration for the LC-A2 division. As borehole T9 is nearer to the TCR-WTH site, triaxial tests on samples from T9 are possibly more representative for this site. SCOUT BRICK parameters with $\beta^{\phi} = 2.0$ were performed slightly better in tests from T9, therefore, this set is applied for the LC-A2 in the TCR-WTH deep box excavation back-analysis.

Table 6. 4 Recommended values of BRICK parameters for London Clay at TCR-WTH

	String length $L_{(b)}$ *(shear strain)*	
$R_{(b)}$ *(G_t/G_{max})*	**LC-A3** (Pillai, 1996)	**LC-A2** (revised SCOUT, 2007)
0.92	0.0000304	0.000030
0.75	0.0000608	0.000075
0.53	0.000101	0.00015
0.29	0.000121	0.00040
0.13	0.00082	0.00075
0.075	0.00171	0.0015
0.044	0.00352	0.0025
0.017	0.00969	0.0075
0.0035	0.0222	0.02
0	0.0646	0.06
Soil Property		
λ*	0.1	0.1
κ*	0.02	0.02
ι	0.019	0.00175
ν	0.2	0.2
M_u	1.3	1.3
β^G	4.0	4.0
β^{ϕ}	4.0	2.0

6.1.2.3 Summary of BRICK parameters for London Clay

A calibration process was considered necessary for any advanced soil constitutive model. Ideally, the model should be able to accurately replicate all three results of triaxial tests in the process: stress path (p'-q), stress-strain curve (q-ε_q) and a non-linear stiffness curve (G-ε_q). However, due to the limitation of the soil model, or disturbance in soil samples and poor testing quality, the outcomes of the simulations were variable.

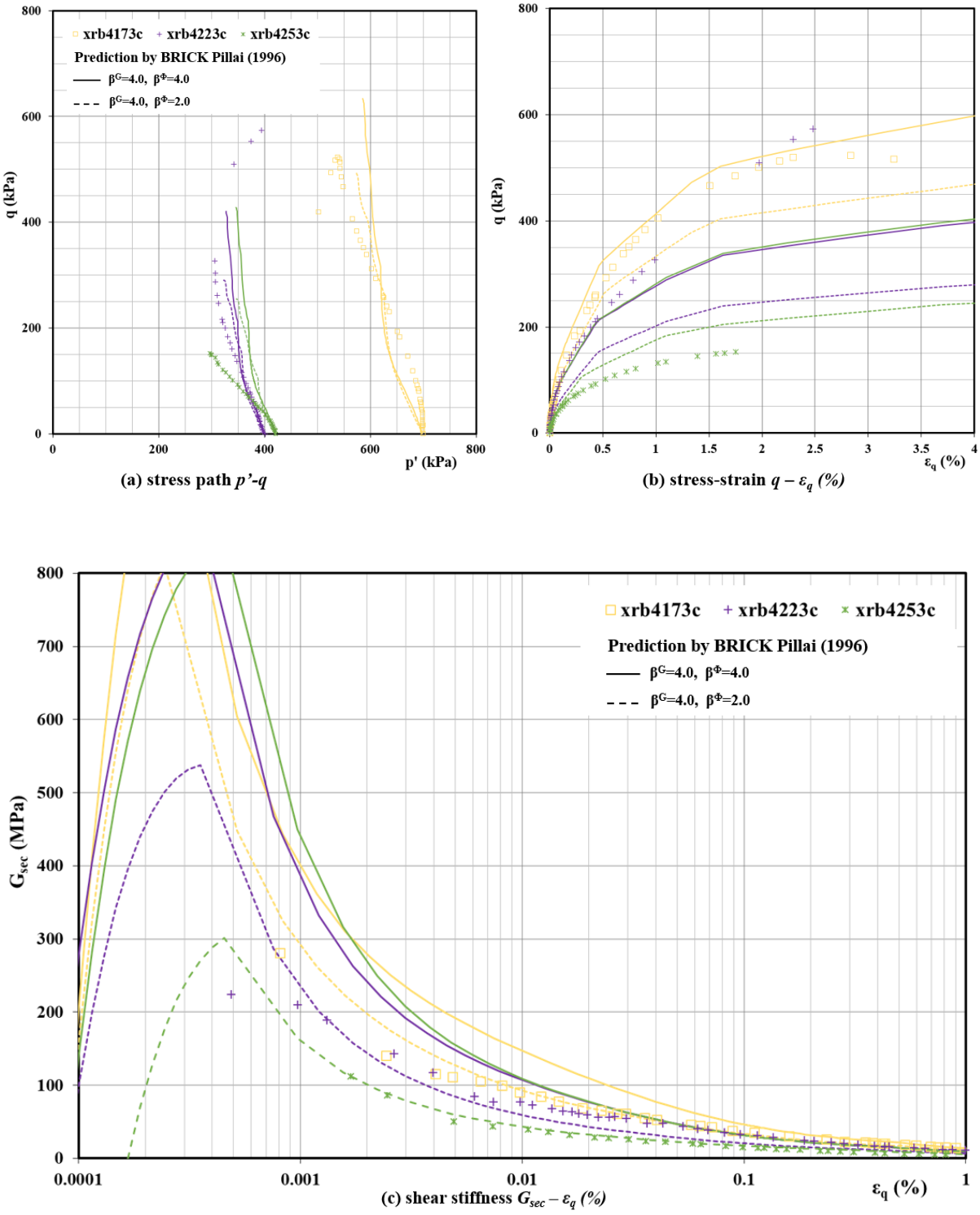

Figure 6. 4 Triaxial compression test results for LC-A2 (B4): test data versus BRICK simulation

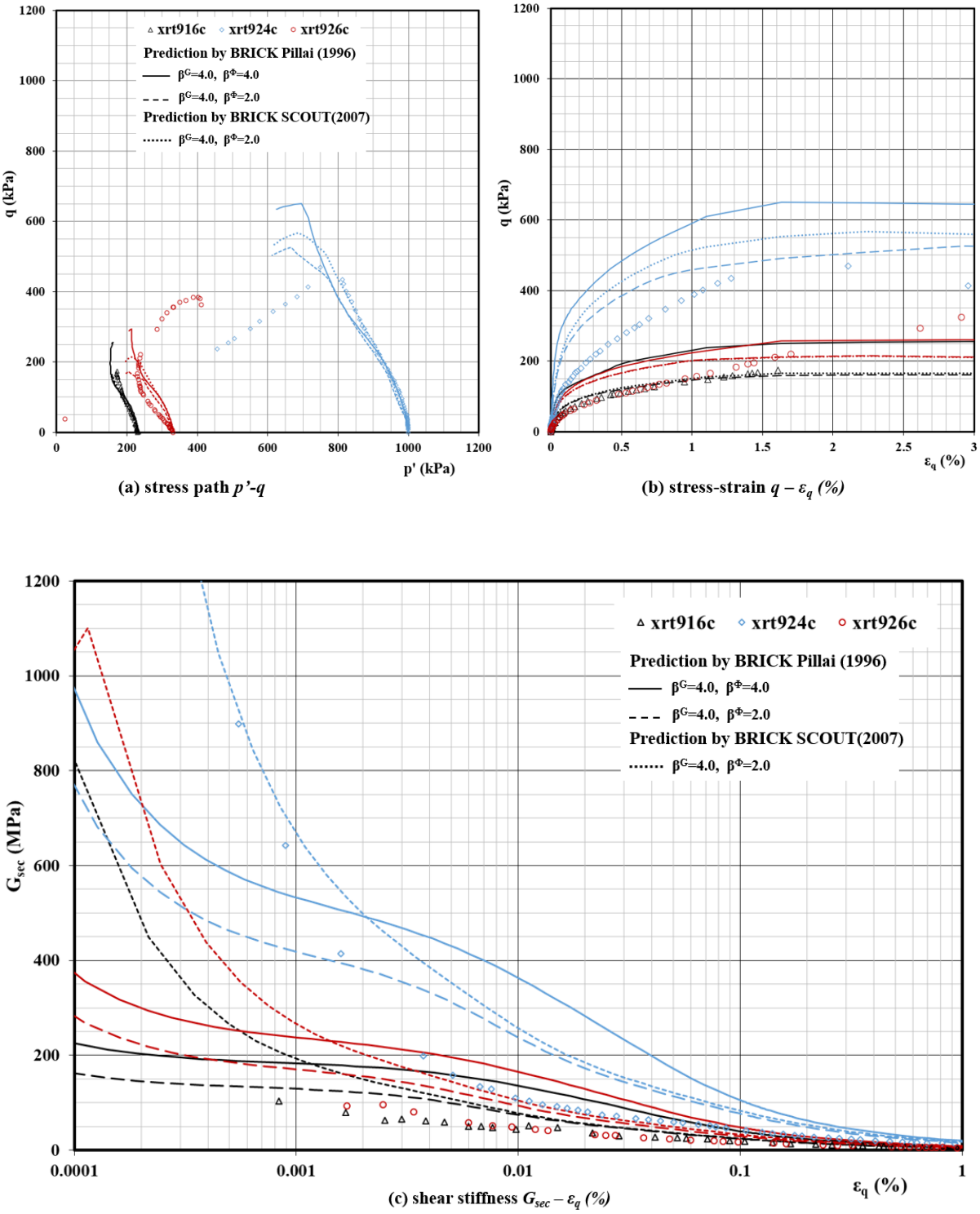

Figure 6. 5 Triaxial compression test results for LC-A2 (T9): test data versus BRICK simulation

In the BRICK simulation of triaxial tests in the LC-A3 and LC-A2 for the Crossrail TCR site, it was easier to replicate the non-linear soil shear stiffness curve, followed with the non-linear stress-strain curve. A good simulation of the stress path seemed the most difficult, due to the complex pre-consolidation stress history of London Clay.

Based on the limited BRICK simulation results, the BRICK parameters for the London Clay subdivisions, LC-A3 & LC-A2) are recommended for the back-analysis of TCR-WTH deep box excavation, as presented in Table 6. 4.

6.2 Back-analysis TCR-WTH deep box excavation (LS-Dyna)

6.2.1 LS-Dyna 3D model

The Crossrail TCR-WTH excavation case history was presented in section 3.2. The original LS-Dyna 3D model with the BRICK model for the TCR-WTH was prepared for the Crossrail ground movement assessment. This model was modified according to the as-built construction records (Table 3.3) for the back-analysis, as shown in Figure 5.21, the 3D model details were described in section 5.4.1.

The initial BRICK parameters for London Clay (Table 6. 4) were applied in the back-analysis with LS-Dyna model. An example of the BRICK soil material card for the LC-A3 in the LS-Dyna keyword file is presented in Table 6. 5. Each material is given a specific ID and defined by the minimum of three cards for the BRICK constitutive soil model: general BRICK parameters in card 1 (Line 1 & Line 2); constitutive calculation control card 2 (Line 3 & Line 4); and the additional anisotropy options' card 3 (Line 5 & Line 6). Explanations for each input parameter and unit of the input values are included in the table.

Due to the limited numbers of triaxial tests performed in soil samples from the Lambeth Group in the Crossrail ground investigations, in total 5 tests from boreholes distributed over a 20 km long railway alignment, no BRICK simulations for triaxial tests in the Lambeth Group was carried out, and the BRICK parameters for the LC-A2 were adopted for the Lambeth Group.

In addition, the 'BOUNDARY_PORE_FLUID_PART' in the keyword file defines the groundwater pore pressure, which adopted the design profile (Figure 3. 2) in the original design. In this card, a suction limit of 100 kPa is given to the undrained calculation. A high

suction limit of 1000 kPa is applied during back-analysis, allowing a maximum suction to develop during the undrained excavation phase.

The keyword file of the LS-Dyna 3D back-analysis by the BRICK model (at the final iteration) for the TCR-WTH case history is enclosed in Appendix B.

6.2.2 Iterative back-analysis

The LS-Dyna 3D back-analysis of the TCR-WTH deep box excavation using the BRICK constitutive model was undertaken, to allow direct comparison with the one using the Mohr-Coulomb model. Therefore, the tolerance between the wall deflection predictions by LS-Dyna and observations applied in the back-analysis using the Mohr-Coulomb model in section 5.4.1, is applied ($0 \leq \Delta_{max} < 5$ mm).

Results of back-analysing the final excavation stage 6 for the TCR-WTH deep box excavation are shown in Figure 6. 6, showing wall deflection predictions from four iterations with the BRICK model, predictions with the most probable Mohr-Coulomb parameters (LS-Dyna 3D), and the corrected inclinometer data SAA-8003.

The BRICK parameters and the suction limit assumed for the undrained clay soils have a significant impact on the wall deflection predictions. This is particularly true in soils below the 4th level of props (LC-A2 and LG-UMC).

The BRICK parameters for the LC-A3 and the LC-A2 in four iterations are summarised in Table 6. 6 and Table 6. 7. The BRICK parameters for the Lambeth Group followed those for LC-A2, except for the pre-consolidation pressure. Considering the Lambeth Group is formed in an even earlier geological period, a higher pre-consolidation pressure 3000 kPa is applied in the 4th iteration, instead of 2000 kPa used for London Clay.

The equivalent BRICK stiffness curves (G_t/p-$L_{(b)}$) for the LC-A3 & LC-A2 in the four iterations are displayed in Figure 6. 7 and Figure 6. 8. Both diagrams show clearly that increased shear stiffness values in strain range of 1e-5 and 2e-3 (equivalent from 0.001% to 0.2%) are required in order to obtain the better-fitted wall deflections. For example, in the LC-A3, the maximum shear stiffness (G_{max}) at a strain level of 1e-5 (equivalent 0.001%) is increased 25% from 400 MPa in the 1st iteration to 500 MPa in the 4th iteration. Besides, the shear stiffness distribution in a strain range of 1e-4 (0.01%) and 2e-3 (0.2%) is also increased in proportion.

Table 6. 5 BRICK input parameters for LC-A3 division in the TCR-WTH keyword file of the LS-Dyna model

Line1	MID	RO	RLAMDA	RKAPPA	RIOTA	RBETA1	RBETA2	RMU
explaination	*material ID*	*mass density ($kN/m^3/10$)*	λ^*	κ^*	ι	β^G	β^ϕ	*M_u (1.25 to 1.35)*
Line 2	3	2.0	0.1	0.01	0.00175	4	2	1.3
Line 3	RNU	RLCID	TOL	PGCL	SUB-INC	BLK	GRAV	THEORY
explaination	*Poisson's ratio*	*Loadcurve number referring to string-length $R_{(b)}$ - G/G_{max}*	*user defined tolerance for convergency checking*	*pre-consolidation ground level related to z=0 in the model*	*user defined strain increment size(default)*	*elastic bulk stiffness of the soil - contact stiffness only (kN/m^2)*	*gravitational aceleration (m/s)*	*stress calculation considered the stress history*
Line 4	0.2	1	0	317.2	5.00E-04	100000	9.807	4
Line 5	RVHHH	XSICRIT	ALPHA	RVH	RNU	ANISO_4	STRUSUB	BLANK
explaination	*Anisotropy ratio G_{vh}/G_{hh} (default = Isotropic behaviour)*	*Anisotropy parameter*	*Anisotropy parameter*	*Anisotropy ratio E_v/E_h*	*Anisotropy ratio N_{u2}/N_{u1}*	*Anisotropy parameter*	*strain for sybcycling*	
Line 6	0.5	0	0	0	0	0	0	0

* The reduced default elastic bulk stiffness of 100 kN/m2 was applied; Anisotropy options were not considered in the TCR-WTH back-analysis by the BRICK model.

THEORY = 4 - stress history of the soil is calculated prior to initialisation of the model and will take longer computational time;

THEORY = 104 - samilar to 4, except that during initialisation, reloading is performed to achieve the user-specified horiztoanl and vertical stress.

Loadcurve Card

Line 1	LCID	BLANK	BLANK	BLANK	BLANK	BLANK	BLANK	BLANK
Line 2	1	0	0	0	0	0	0	0
Line 3		3.00E-05		0.9200000				
Line 4		7.50E-05		0.7500000				
Line 5		1.50E-04		0.6000000				
Line 6		2.50E-04		0.5000000				
Line 7		5.00E-04		0.3500000				
Line 8		1.00E-03		0.2500000				
Line 9		1.50E-03		0.1500000				
Line 10		2.00E-03		0.0500000				
Line 11		3.30E-03		0.0100000				
Line 12		4.00E-02		0.0000000				
		$L_{(b)}$		$R_{(b)}$				

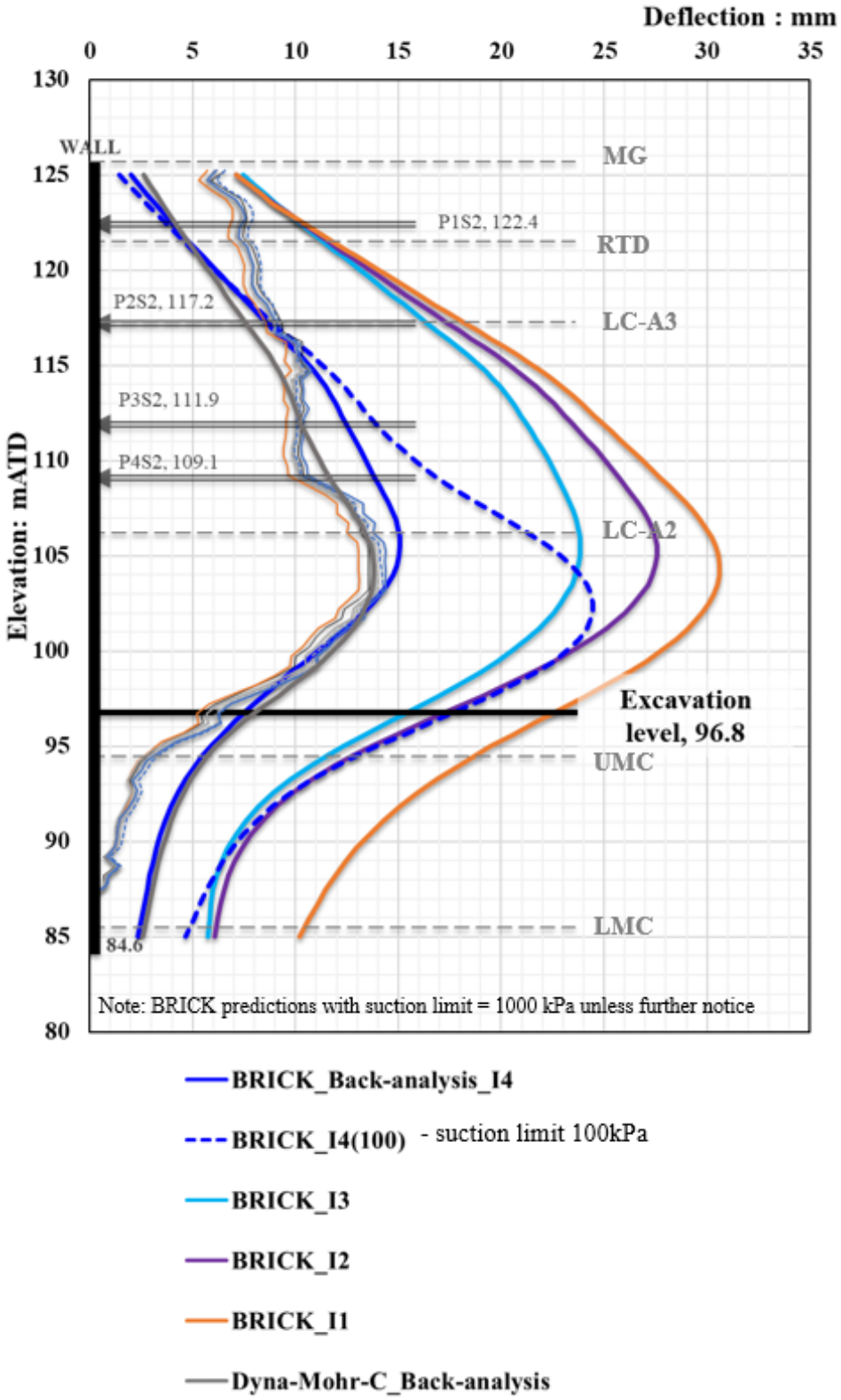

Figure 6. 6 BRICK back-analysis results – wall deflections at stage 6 versus corrected SAA-8003 data (22/09/2012 to 27/09/2012 at 7 am)

Table 6. 6 BRICK parameters for LC-A3 in back-analysis iterations

Iteration 1 (Pillai, 1996)		**Iteration 2** (revised SCOUT, 2007)		**Iteration 3**		**Iteration 4**	
$R_{(b)}$ G_t /G_{max}	String length $L_{(b)}$	$R_{(b)}$ G_t /G_{max}	String length $L_{(b)}$	$R_{(b)}$ G_t /G_{max}	String length $L_{(b)}$	$R_{(b)}$ G_t /G_{max}	String length $L_{(b)}$
0.92	0.0000304	0.92	0.0000304	0.92	0.0000304	0.92	0.0000304
0.75	0.0000608	0.75	0.0000750	0.75	0.0000750	0.75	0.0000750
0.53	0.0001010	0.53	0.0001500	0.53	0.0001500	0.60	0.0001500
0.29	0.0001210	0.29	0.0004000	0.29	0.0004000	0.50	0.0002500
0.13	0.0008200	0.13	0.0007500	0.13	0.0007500	0.35	0.0005000
0.075	0.0017100	0.075	0.0015000	0.075	0.0015000	0.25	0.0010000
0.044	0.0035200	0.044	0.0025000	0.044	0.0025000	0.15	0.0015000
0.017	0.0096900	0.017	0.0075000	0.017	0.0075000	0.05	0.0020000
0.0035	0.0222000	0.0035	0.0200000	0.0035	0.0200000	0.01	0.0330000
0	0.0646000	0	0.0600000	0	0.0600000	0	0.0400000
Soil Property							
λ*	0.1	0.1		0.1		0.1	
κ*	*0.02*	*0.02*		*0.01*		*0.01*	
I	*0.0019*	*0.00175*		*0.0015*		*0.0015*	
N	0.2	0.2		0.2		0.2	
M_u	1.3	1.3		1.3		1.3	
β^G	*4.0*	*4.0*		*4.0*		*5.0*	
β^ϕ	*4.0*	*2.0*		*4.0*		*5.0*	
implied ϕ'_{crit}	*23.9°*	*24.4°*		*28.1°*		*28.2°*	

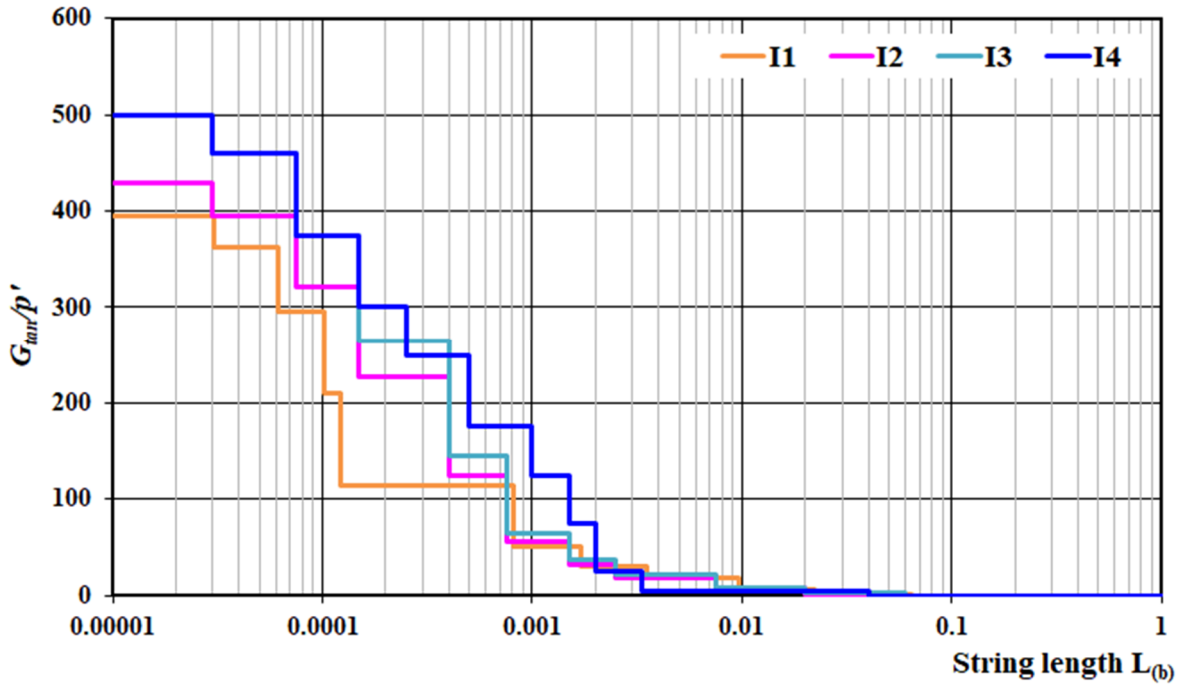

Figure 6. 7 Normalised shear stiffness of BRICK parameters for LC-A3 in back-analysis iterations

Table 6. 7 BRICK parameters for LC-A2 in back-analysis iterations

Iteration 1 (revised SCOUT, 2007)		**Iteration 2**		**Iteration 3**		**Iteration 4** (same as Iteration 3)	
$R_{(b)}$ G_t /G_{max}	String length $L_{(b)}$	$R_{(b)}$ G_t /G_{max}	String length $L_{(b)}$	$R_{(b)}$ G_t /G_{max}	String length $L_{(b)}$	$R_{(b)}$ G_t /G_{max}	String length $L_{(b)}$
0.92	0.0000304	0.92	0.0000304	0.92	0.0000304	0.92	0.0000304
0.75	0.0000750	0.75	0.0000750	0.75	0.0000750	0.75	0.0000750
0.53	0.0001500	0.55	0.0001500	0.60	0.0001500	0.60	0.0001500
0.29	0.0004000	0.30	0.0004000	0.50	0.0002500	0.50	0.0002500
0.13	0.0007500	0.17	0.0007500	0.35	0.0005000	0.35	0.0005000
0.075	0.0015000	0.095	0.0015000	0.25	0.0010000	0.25	0.0010000
0.044	0.0025000	0.044	0.0025000	0.15	0.0015000	0.15	0.0015000
0.017	0.0075000	0.017	0.0075000	0.05	0.0020000	0.05	0.0020000
0.0035	0.0200000	0.0035	0.0200000	0.01	0.0330000	0.01	0.0330000
0	0.0600000	0	0.0600000	0	0.0400000	0	0.0400000
Soil Property							
λ*	0.1	0.1		0.1		0.1	
κ*	*0.02*	*0.01*		*0.01*		*0.01*	
I	*0.00175*	*0.0015*		*0.0015*		*0.0015*	
N	0.2	0.2		0.2		0.2	
M_u	1.3	1.3		1.3		1.3	
β^G	*4.0*	*4.0*		*5.0*		*5.0*	
β^ϕ	*2.0*	*4.0*		*5.0*		*5.0*	
implied ϕ'_{crit}	*24.4°*	*28.1°*		*28.2°*		*28.2°*	

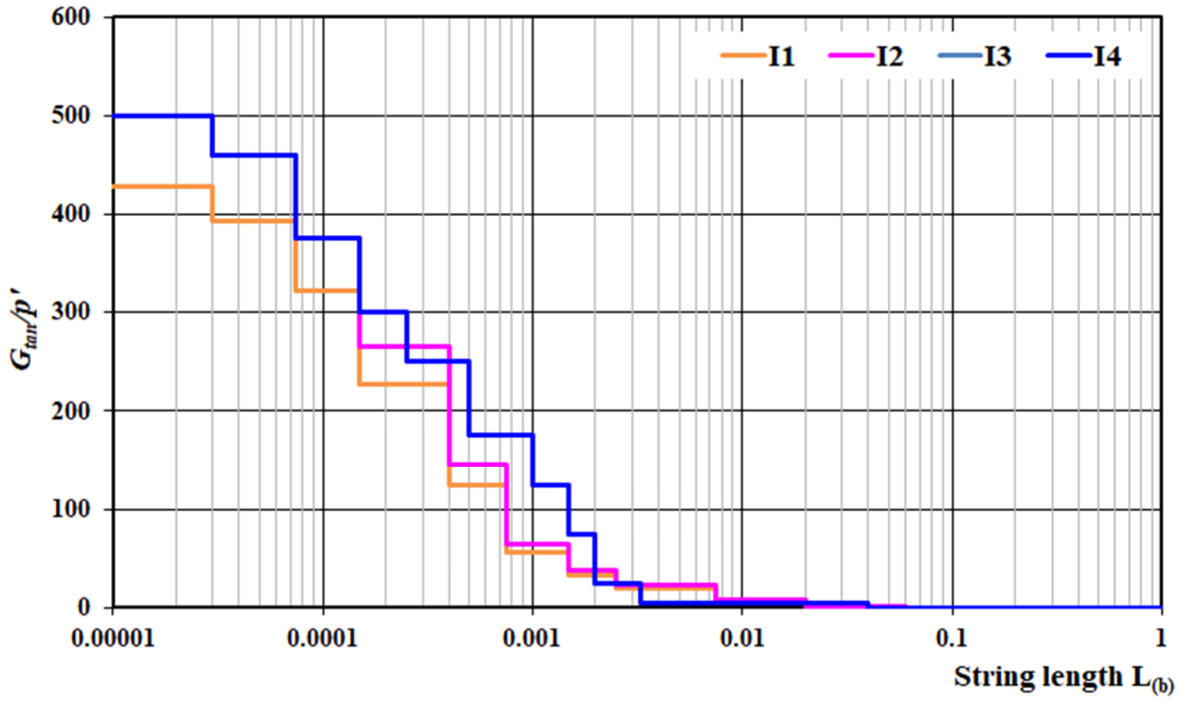

Figure 6. 8 Normalised shear stiffness of BRICK parameters for LC-A2 in back-analysis iterations

6.2.3 Results

6.2.3.1 Wall deflections

The LS-Dyna 3D back-analysis results of the wall deflections at the location of SAA-8003 for the TCR-WTH deep box excavation are presented in Figure 6. 9. The best-fitted wall deflections from the 4th iteration match with the corrected SAA-8003 data at the final excavation stage 6, but this set of BRICK parameters underestimates wall deflections at an early excavation stage 3. At the final stage 6, the groundwater condition seemed to have made an impact on the wall deflections, A suction limit of 100 kPa restricted the suction to be developed in the 3D model during undrained excavation, hence, lower effective stresses on the passive side of the wall resulted in larger wall deflections at stage6 (BRICK_I4(100) in Figure 6. 9). Whilst, a high suction limit of 1000 kPa did not restrict the maximum suction and led to higher effective stresses and smaller wall deflection (BRICK_Back-analysis_I4). However, the assumption of suction limit shows the negligible difference in the wall deflection predictions at the early excavation stage 3.

Updates of BRICK parameters are based on the back-analysis at the final excavation stage 6 when a medium to large incremental strain had been developed in the LC-A3, and a small to medium incremental strain had been developed in the LC-A2. However, when the excavation reached in the LC-A3 layer at stage 3, only a very small to negligible incremental strain was developed in soils below the excavation level (LC-A2 and Lambeth Group). BRICK parameters will need to be further calibrated for the corresponding strain range in order to accurately predicted wall deflections at stage 3.

Deformations in the upper part of the wall also exceed the BRICK predictions, but only the top of the wall above the level 2 props. Possible concerns about inclinometer data for the upper part of the wall were discussed in section 5.2.5.

No reduction on the prop stiffness was applied in the LS-Dyna 3D model, but BRICK model performed better in predicting wall lateral displacements at positions where props were installed. For instance, at the location of SAA-8003, BRICK parameters predicted 5.5 mm displacement at the 2nd props at stage 3(Figure 6. 9). This displacement increased to 9.0 mm in stage 6. The incremental displacement was comparable to the corrected SAA-8003 data over the same period.

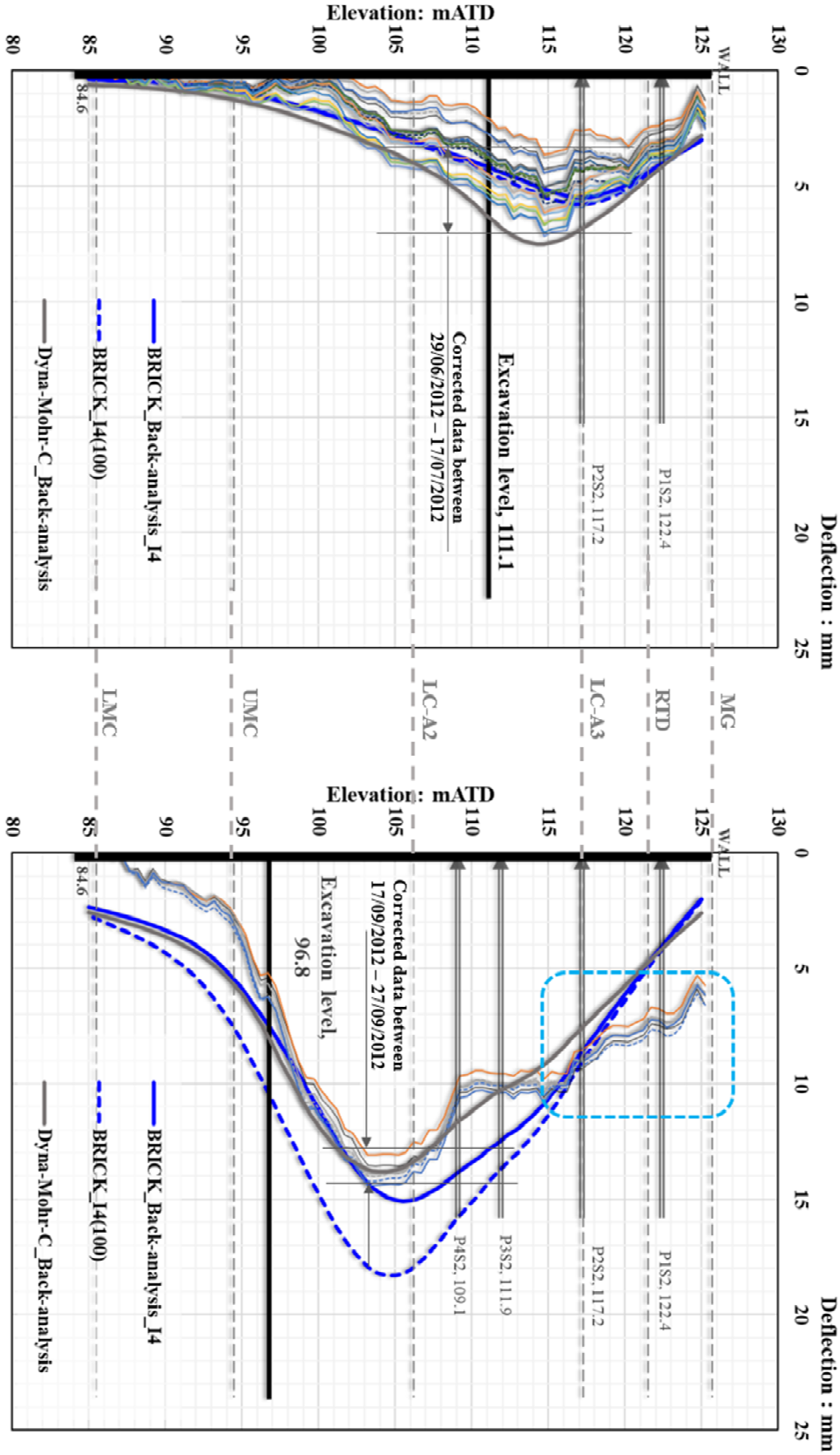

Note: predictions with suction limit = 1000 kPa except for BRICK_I4(100) with suction limit = 100kaPa

Figure 6. 9 LS-Dyna back-analysis result for TCR-WTH - wall deflections versus corrected SAA-8003 data

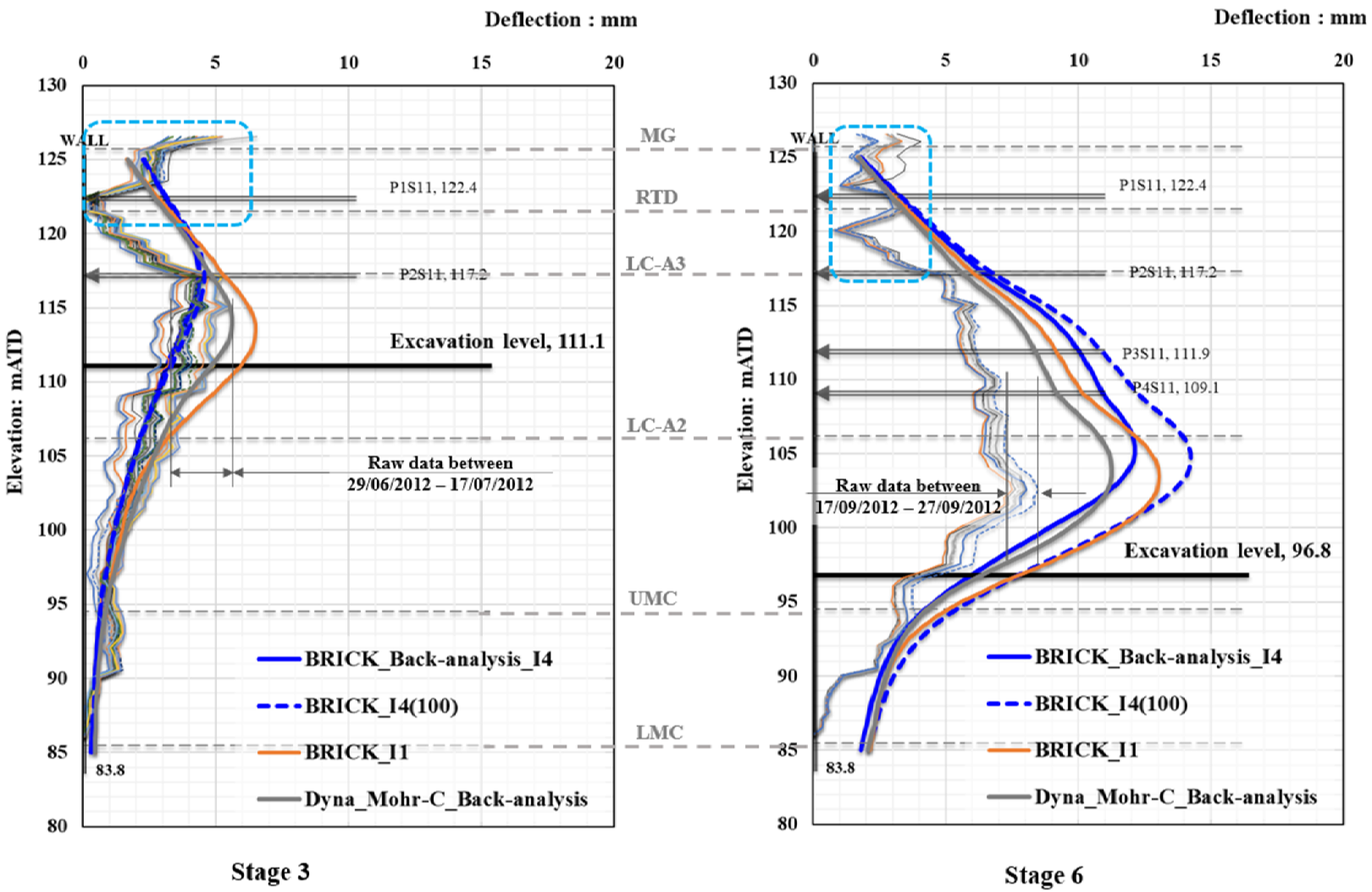

Note: predictions with suction limit = 1000 kPa except for BRICK_I4(100) with suction limit =100 kPa

Figure 6. 10 LS-Dyna back-analysis result for TCR-WTH - wall deflections versus raw SAA-8001 data

The improved performance can be linked to the as-built structural details incorporated in the 3D model and the advanced BRICK model that allows the soil stiffness to change with the increasing shear strain.

Figure 6. 10 presents the BRICK predictions of wall deflections at the location of SAA-8001. In this corner position, the differential wall deflections between different iterations are small (< 2 mm). Relaxation in the suction limit can reduce the maximum wall deflection (< 3mm), but on a smaller scale compared to those shown at the location of SAA-8003. This indicates that the soil stiffness has limited influence on the wall deflection at corners, and the structural stiffness determines the stress distribution, thus controlling the soil strains and thus the resultant wall deflections.

The unusual wall deflections above level 2 props in the raw data of SAA-8001 were discussed in section 5.4.2, and they were likely due to the corner effects. The 1st iteration overestimated the wall deflection at SAA-8001 at both early excavation stage 3 and the final excavation stage 6. The stiffened BRICK parameters in the 4th iteration (both suction limit of 100 kPa and 1000 kPa) slightly underestimated the wall deflections at stage 3, but the overestimation at stage 6 remained. The additional a few millimetres may be a consequence of the lack of information and accurate modelling of actual surcharge load conditions.

6.2.3.2 Strut loads

Predictions of the strut loads at four levels are presented in Figure 6. 11, showing the better-fitted strut loads from the 4th iteration of BRICK parameters with a suction limit of 1000 kPa. Although, strut loads in P1S2 and P2S2 are slightly underestimated before the final excavation stage 6, and the stabilised strut loads in P3S2 are overestimated by about 17% of measurements. As a comparison, less accurate predictions from the other three iterations with BRICK model and the most probable Mohr-Coulomb parameters are included. It indicates that the most probable BRICK parameters calibrated using the inclinometer data can also be applied in predicting the fitted strut loads.

6.2.3.3 Ground settlements

The ground surface settlements along Dean Street was monitored using levelling studs during the period between 25/02/2012 and 09/11/2012. The predicted settlements at the three

excavation stages are compared with the measurements in Figure 6. 12 (absolute settlements) and in Figure 6. 13 (normalised settlements by the excavation depth). The monitoring data was re-baselined at the beginning of the excavation work (19/04/2012) to ensure the measurements and the predictions are comparable.

The better performance by the BRICK model in predicting the ground settlement is illustrated in Figure 6. 12. A negligible difference is found in predictions from the 4th iteration with a suction limit of 100 kPa or 1000 kPa. Also, only small incremental settlements are developed between excavation stages in the 4th iteration predictions (< 2 mm). However, with the excavation progressing, the better-fitted settlement predictions are obtained from the 1st iteration with a suction limit of 1000 kPa.

The unexpected extra settlements occurred near the inner wall which separates the shallow box and the deep box, as highlighted in Figure 6. 12. The review of the as-built diaphragm wall record suggested the additional ground settlements might be associated with wall installation effects. The diaphragm wall installation records showed that panel P01 was installed on 30/08/2012 but the neighbouring panel P57 was installed on 14/12/2012, leaving a gap of 17 weeks as indicated in Figure 6. 14. This long installation period can cause stress redistribution and reduction in soil stresses surrounding the excavated trench for the wall panel. Review of wall installation impacts is discussed in Chapter 2.

The ground surface settlements perpendicular to Dean Street along section A-A' (Figure 3.1) across SAA-8003 are compared with the corresponding monitoring data, as shown in Figure 6. 13. Results are normalised by the excavation depth and the estimated maximum settlement trough is about 0.03% excavation depth at stage 6 from the 1st iteration of BRICK parameters with a suction limit of 1000 kPa, but the maximum measured settlement trough is approximate 0.038% excavation depth.

The measured maximum settlements at three excavation stages show an almost constant ratio to the corresponding excavation depths, like 0.035% (with ±0.01%) depending on the time of measuring. Predictions of BRICK iterations also show a steady ratio over different stages but in small magnitudes: around 0.015% from the 4th iteration and 0.030% from the 1st iteration. As a comparison, predictions of the Mohr-Coulomb back-analysis are normalised (Figure 6. 13) and show the smallest ratio of 0.005%.

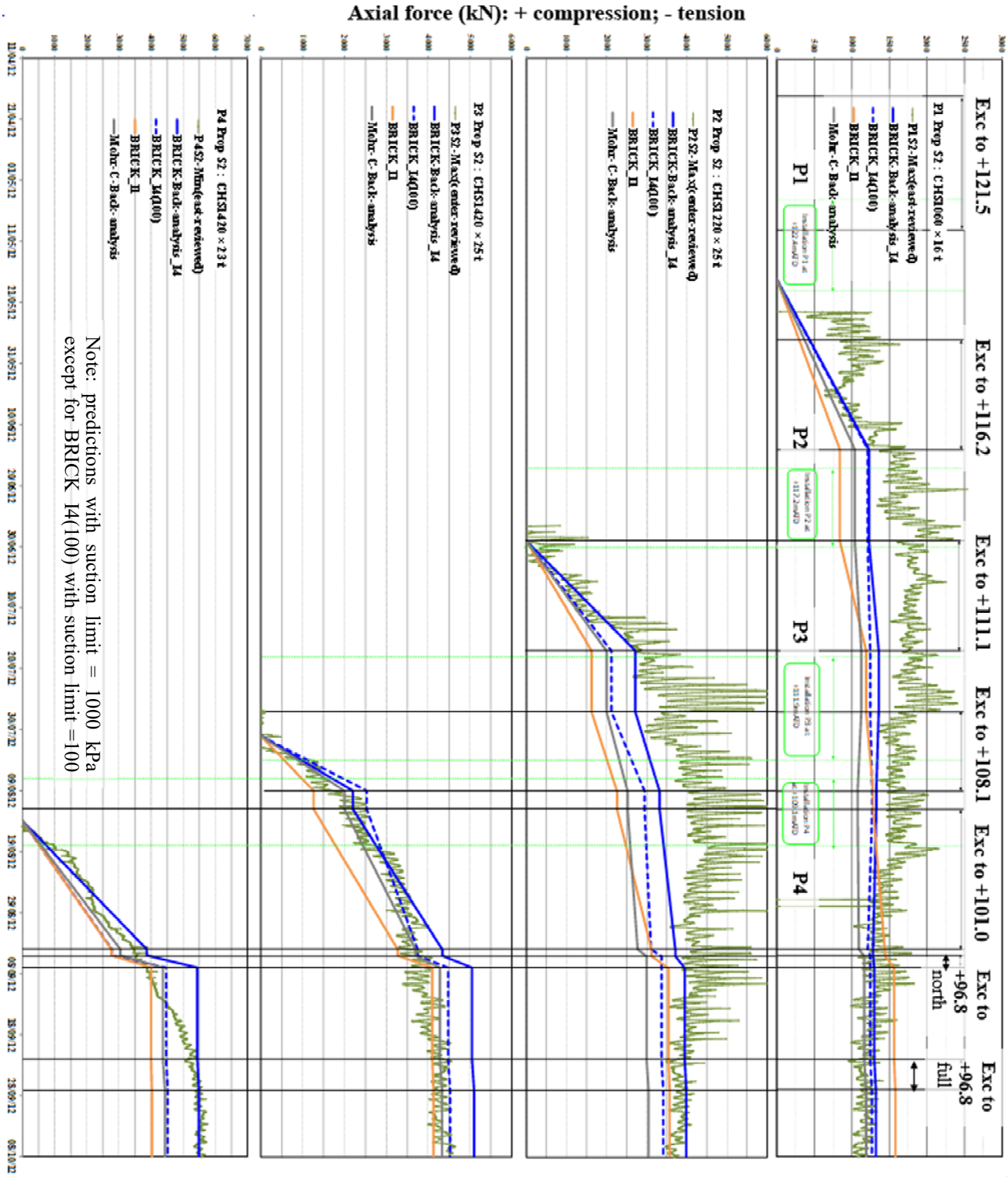

Note: predictions with suction limit = 1000 kPa except for BRICK_I4(100) with suction limit =100

Figure 6. 11 LS-Dyna back-analysis result for TCR-WTH – strut loads versus the reviewed axial forces by strain gauge data (P1S2 to P4S2)

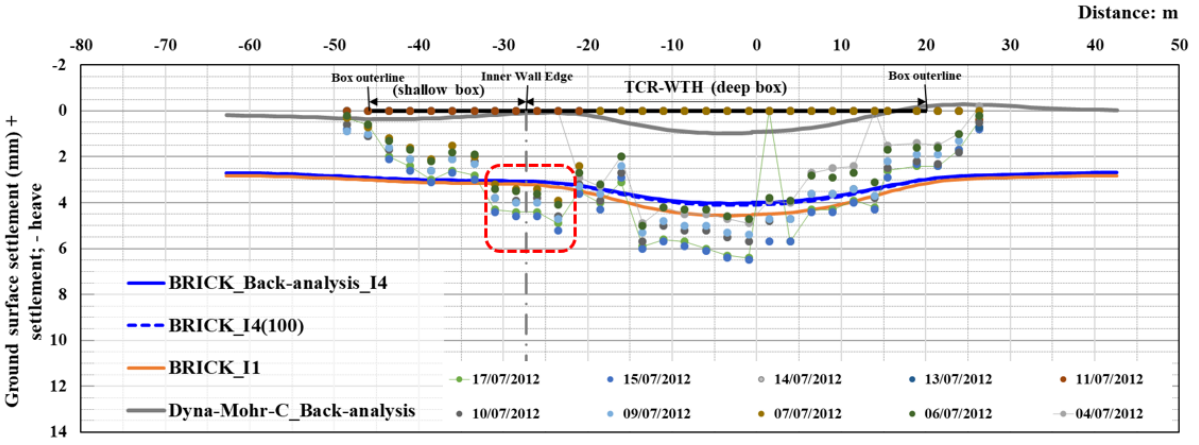

(a) Settlement along Dean Street at stage 3 (excavate to +111.1)

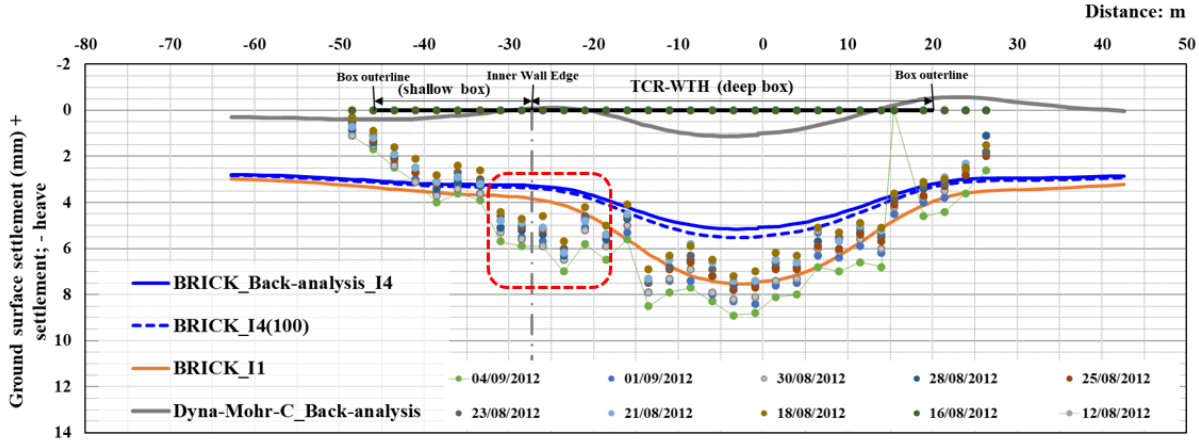

(b) Settlement along Dean Street at stage 5 (excavate to +101.0)

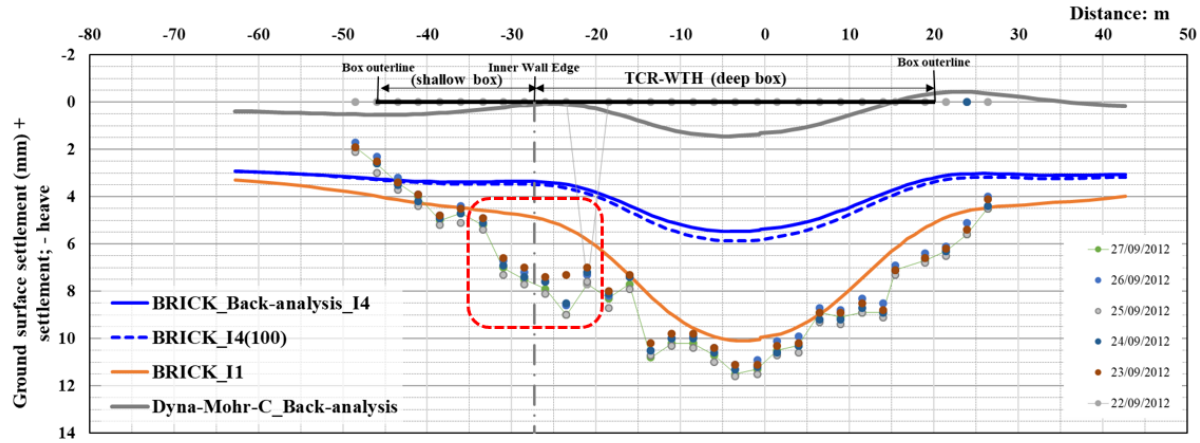

Note:
1. Dean Street Ground surface settlement was measured using levelling studs, they were installed at 8.5 m to 9.0 m distance from the TCR-WTH box outer line;
2. The SAA-8003 and Section A-A' was located at X = 0; and
3. Monitoring data along Dean Street has been re-baselined referenced to the data on 19/04/2012 so that the displacements prior to the first excavation could be excluded and compared with the LS-Dyna 3D model predictions.

(c) Settlement along Dean Street at stage 6 (excavate to +96.8)

Figure 6. 12 LS-Dyna 3D BRICK back-analysis result (TCR-WTH) – ground surface settlements along Dean Street: measurement versus estimations

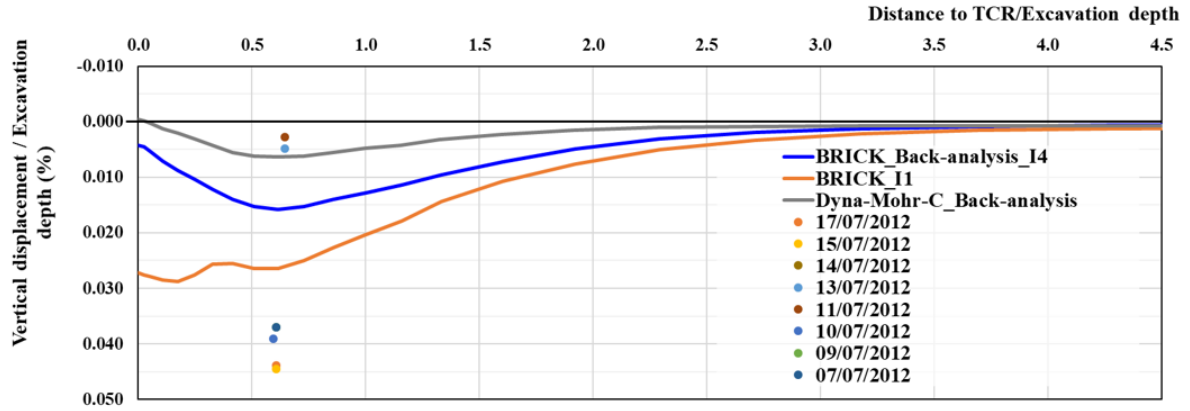

(a) Normalised settlement behind the east diaphragm wall along the section A-A' at stage 3 3 (excavate to +111.1)

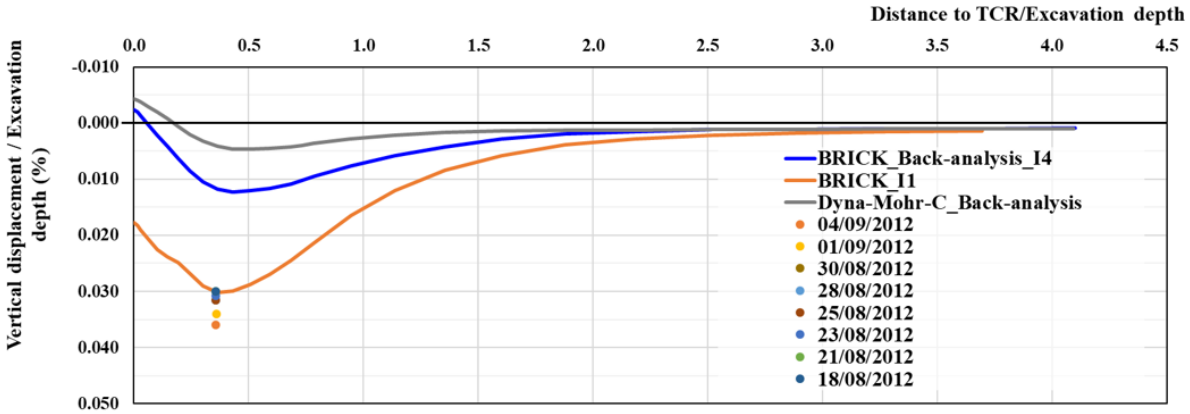

(b) Normalised settlement behind the east diaphragm wall along the section A-A' at stage 5 (excavate to +101.0)

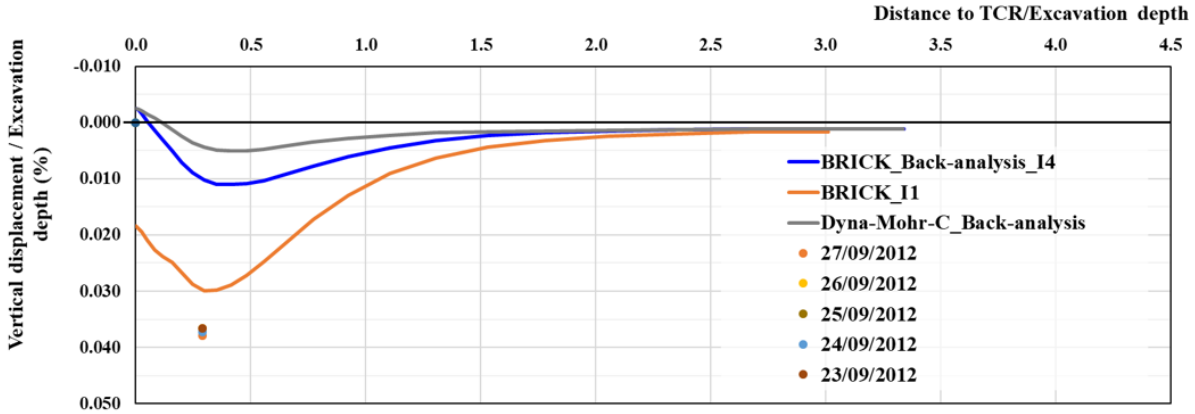

(c) Normalised settlement behind the east diaphragm wall along the section A-A' at stage 6 (excavate to +96.8)

Figure 6. 13 LS-Dyna 3D BRICK back-analysis result (TCR-WTH) – normalised ground surface settlements along the section A-A': measurement versus estimations

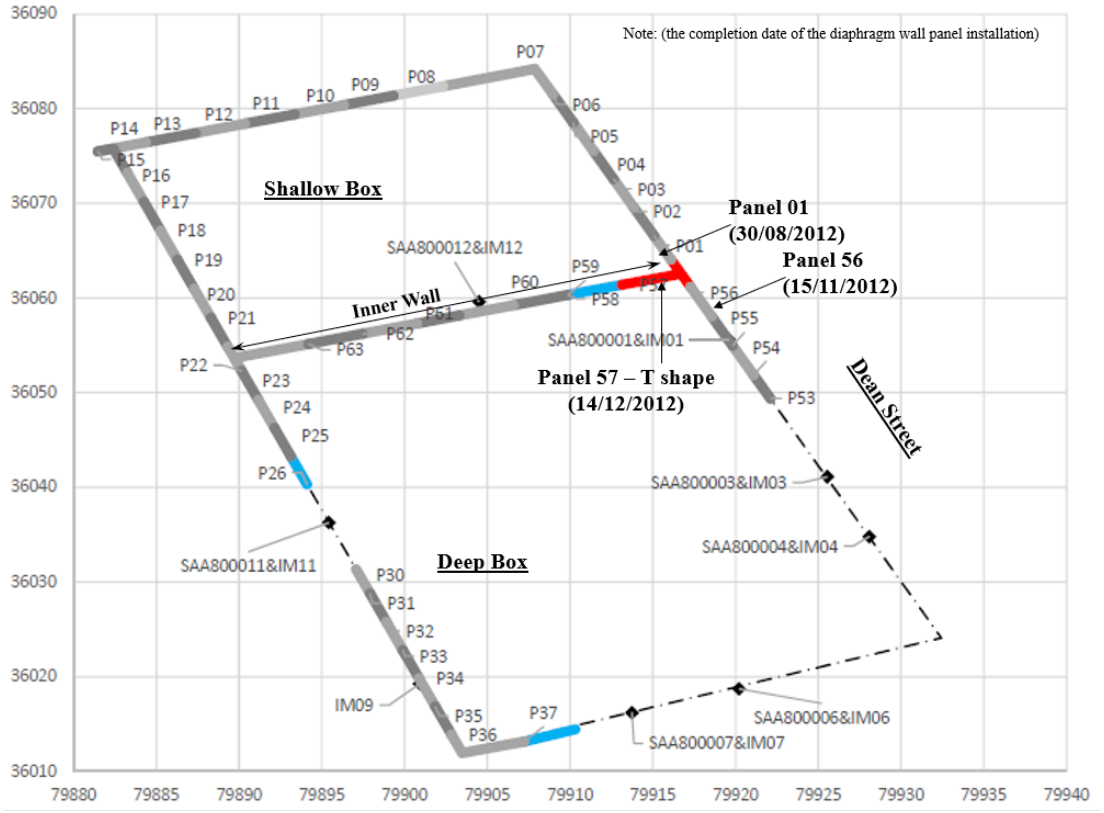

Figure 6. 14 TCR-WTH diaphragm wall construction record

The ground surface settlements induced by the excavation are concentrated in a distance of about 2.5 times the excavation depth, beyond which the settlement became insignificant (settlement < 0.005% excavation depth).

6.2.3.4 Groundwater pore pressures

The predicted pore water profiles by the LS-Dyna 3D back-analysis at the location of PV80001(Figure 3.4) are presented in Figure 6. 15, including the corrected PV80001 data at the corresponding excavation stages. The other two piezometers (PV8002 & PV8003) are not used due to the data quality issues, where were discussed in section 3.4.2.4. The predicted pore pressure profiles include results from:

1) Mohr-Coulomb analysis with the representative most probable soil stiffness values and a suction limit of 1000 kPa;
2) 1st iteration of BRICK analysis with parameters calibrated using triaxial test data and a suction limit of 1000 kPa;

3) 4th iteration of BRICK analysis with parameters derived from the back-analysis using inclinometer data (SAA-8003), and a suction limit of 1000 kPa; and
4) 4th iteration of BRICK analysis and a suction limit of 100 kPa.

None of LS-Dyna analyses accurately predicted groundwater developments during the undrained excavation phase for the TCR-WTH deep box construction. This might be due to the adopted design groundwater profile being a conservative assumption based on the long term monitoring data, but not necessarily reflecting the actual undrained groundwater conditions for the site over the excavation phase.

Review of PV80001 data showed the piezometer reached the equilibrium at about 75 days after the first reading (end of May 2012), when the excavation to the level of +116.2 mATD was about to start. Afterwards, with the excavation progressing, suction pressures were calculated at two sensors levels: +95.5 mATD and +90.0 mATD. It seems a linear correlation between the porewater pressure and the excavation depth is established at the position of PV80001, as shown in Figure 6. 15. A delayed porewater pressure drop is observed at both sensors, as PV80001 slowly reached the equilibrium at the excavation to level of +116.2 mATD stage 2.

The LS-Dyna BRICK predictions at PV80001A (+95.5 mATD) show a decrease of porewater pressure from a shallow excavation depth (e.g. excavation <5 m), and development of suction (negative pressure) when excavation depth is over 10 m. The maximum suction is over 400 kPa when the final excavation level is reached at +96.8 mATD. Figure 6. 16 also clearly shows a small suction limit can confine the suction development within the given range, see BRICK predictions from 4th iteration with a suction limit of 100 kPa. PV80001B was installed at a deeper level (+90.0 mATD) in the Lambeth Group. At this level, LS-Dyna BRICK predictions show decreases of porewater pressure at a later phase only when the excavation reached London Clay (e.g. excavation > 7.5 m). More steep decrease of porewater pressures is presented from the 1st iteration than those from the 4th iteration. However, the LS-Dyna Mohr-Coulomb predictions show a much smaller but smoother porewater pressure decrease at both PV80001A&B levels, and decrease rates are close to the measurements.

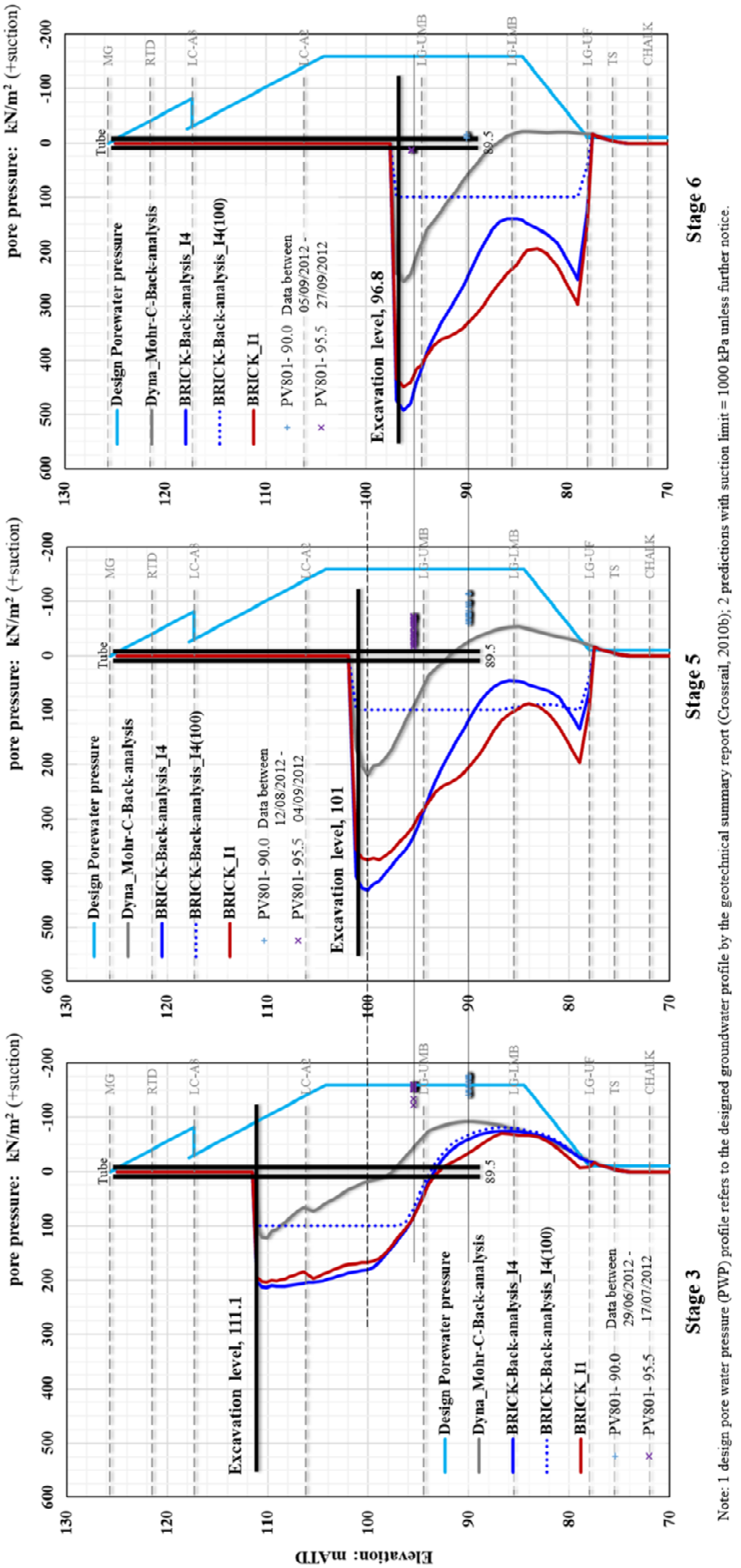

Figure 6. 15 LS-Dyna 3D BRICK back-analysis result (TCR-WTH) – pore water pressures versus raw piezometer data PV80001

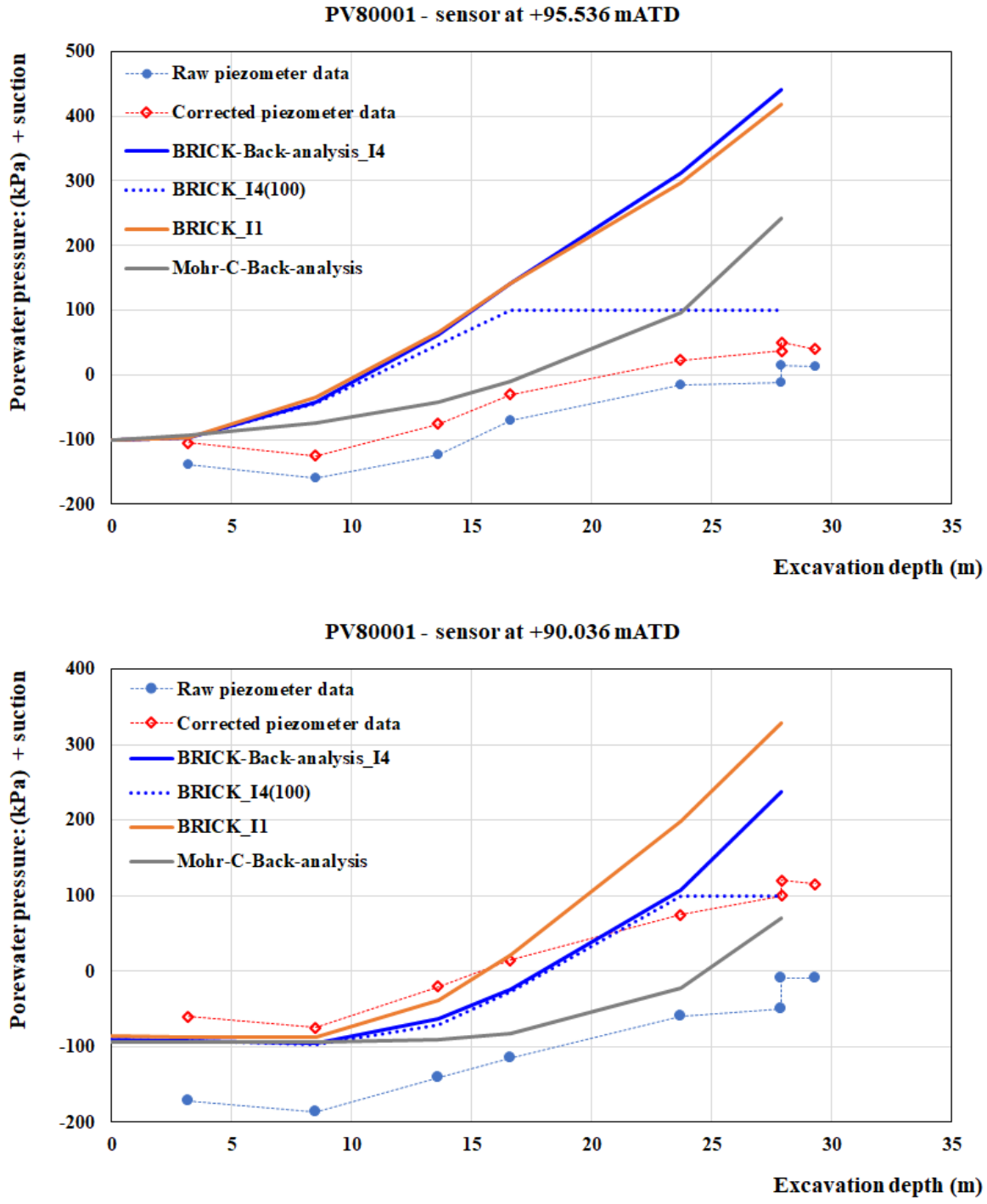

Figure 6. 16 Diagram of pore water pressures for PV80001: (a) sensor at +95.5 mATD; (b) sensor at +90.0 mATD

The BRICK model tends to predict a fast decrease of porewater pressure, as a consequence of the higher suction developed immediately beneath the excavated level. The suction limit effect is more severe in the BRICK model than in the Mohr-Coulomb model, as maximum suction developed in the Mohr-Coulomb model is only half of the one developed in the BRICK model. The consequence of the suction is illustrated clearly in the ground heave.

6.2.3.5 Ground heave

Two extensometers, XM80001 and XM80002, were paired with piezometers and installed inside the TCR-WTH deep box to monitor ground heave. Indicative locations of these extensometers are shown in Figure 3.4. Readings were taken between April and October in 2012 during the deep box excavation phase.

The predicted ground vertical displacements (heave) are compared with XM80001 data in Figure 6. 17, and XM80002 data in Figure 6. 18. The maximum heave is recorded and predicted immediately beneath the excavated level, and this heave gradually decreases with time.

At the location of XM80001, the maximum heave at stage 3 is measured as 45 mm on 17/7/2012, which is comparable with the estimation from the 4th iteration of BRICK parameters with a suction limit of 100 kPa. While a heave of 15 mm is predicted from the 4th iteration with a suction limit of 1000 kPa, due to higher suction being developed in the model. Less than 10 mm heave is predicted by the Mohr-Coulomb model with a suction limit of 1000 kPa, however, a constant and stiffer most probable stiffness is considered, which also control the Mohr-Coulomb analysis. The other two records on 4/7/2012 & 10/7/2012 at stage 3 show zigzag profiles and a significant settlement (10 mm) at the bottom of XM80001, their data quality is of concern.

All three records at stage 5 show record the similar heaves with the maximum heave of 30 mm immediately below the formation level of +101 mATD. The BRICK predictions with a suction limit of 1000 kPa are more accurate at this stage, the maximum heave is 35 mm from the 1st iteration or 28 mm from the 4th iteration, whilst the 4th iteration of BRICK predictions with a suction limit of 100 kPa show a maximum heave of 90 mm. Again, the Mohr-Coulomb model with a suction limit of 1000 kPa predicts the smallest heave at stage 5 with a maximum heave of less than 15 mm.

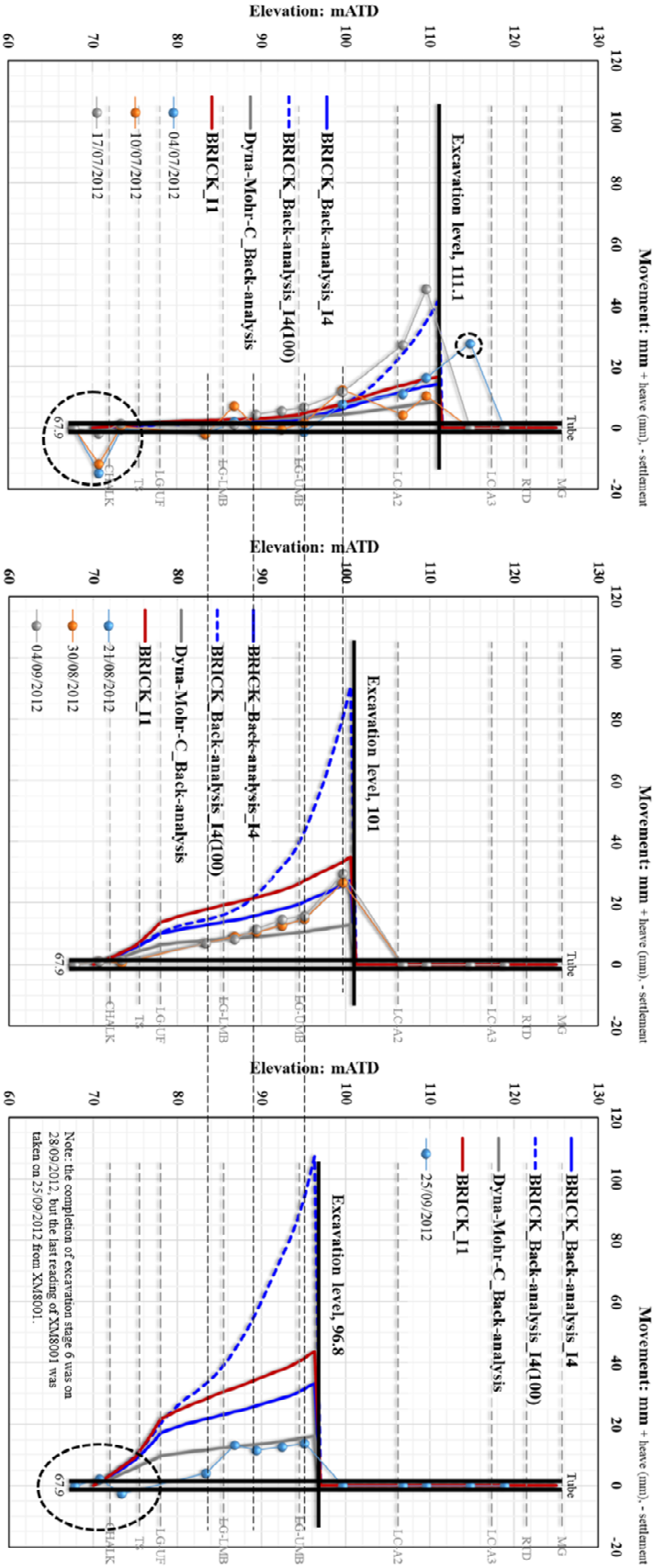

Note: predictions with suction limit = 1000 kPa except for BRICK_I4(100) with suction limit = 100 kPa

Figure 6. 17 LS-Dyna 3D BRICK back-analysis result (TCR-WTH) – ground heave versus raw extensometer data XM80001

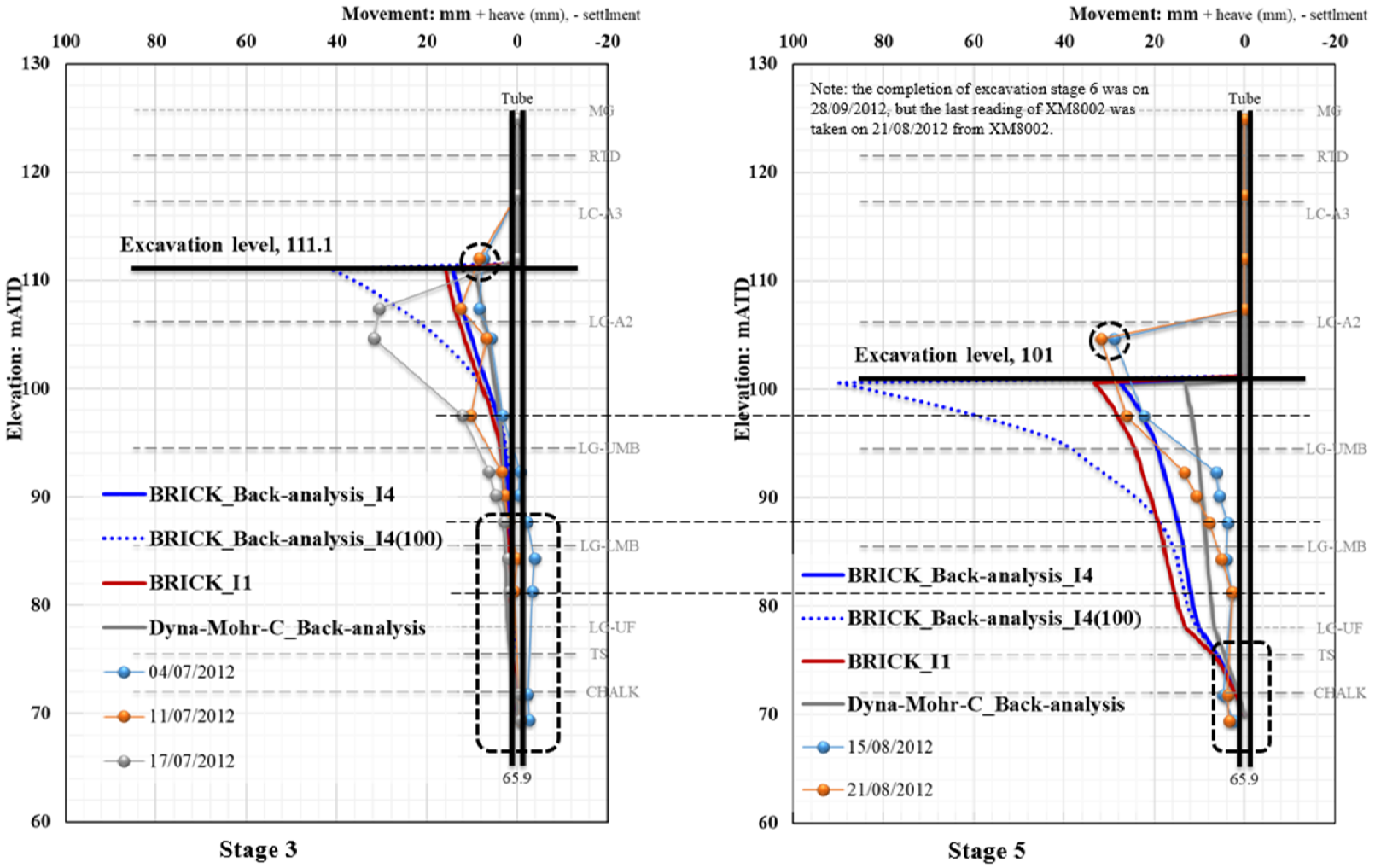

Note: predictions with suction limit = 1000 kPa except for BRICK_I4(100) with suction limit = 100 kPa

Figure 6. 18 LS-Dyna 3D BRICK back-analysis result (TCR-WTH) – ground heave versus raw extensometer data XM80002

Only one record on 25/9/2012 from XM80001 was provided for stage 6, showing less than 15 mm heave below the formation level +96.8 mATD. This record is likely taken before the completion of the excavation at this location and an increase in heave might have occurred but was not recorded. In addition, a settlement of a couple of millimetres was recorded near the bottom of XM80001, however, it is unclear whether the cumulated heave at the top is affected.

XM80002 monitoring was stopped in August 2012 before the completion of excavation stage 6, hence, Figure 6. 18 shows the predictions and the XM80002 data at excavation stage 3 and 5 only. Similar to XM80001, at shallow and early excavation stage 3, the 4th iteration of BRICK parameters with a suction limit of 100 kPa predicts the maximum heave in agreement with the measurement. However, when excavation is extended into the LC-A2 at stage 5, the BRICK predictions with a suction limit of 1000 kPa are more accurate. Unusual large settlements or heaves are observed at the bottom of the XM80002 at both stage 3 and 5, which is very likely related to the quality of the data.

In summary, up to ± 10 mm displacement variation was observed in the extensometer data, which caused some difficulty in interpreting the comparison of heave. In general, the BRICK model performs better in predicting the change of porewater pressure and heave in the undrained excavation phase than the Mohr-Coulomb model. A strong link between suction pressure and heave is observed in both field monitoring data and predictions: a smaller suction pressure accompanied by a larger heave at one excavation stage. However, the accurate predictions of suction and heave are depending on the actual groundwater pressure change and the associated non-linear soil stiffness. In contrast, the Mohr-Coulomb model can predict the matched wall deflection by stiffening soil stiffness, however, the will lead to smaller suction pressures and heave in the undrained excavation analysis.

6.3 Summary of back-analysis by BRICK model

6.3.1 Representative most probable values of the BRICK parameters for London Clay

Based on the LS-Dyna 3D back-analysis for the TCR-WTH deep box excavation using inclinometer data, the BRICK most probable parameters for London Clay are calibrated. The most probable BRICK parameters for London Clay are presented in Table 6. 8. It is

recommended that the Lambeth Group adopts the London Clay BRICK parameters. However, this might overestimate a wall deflection if excavation actually takes place near or within the Lambeth Group. Depending on the geology history and the specific project information, further calibration of BRICK parameters for the Lambeth Group divisions might be required.

Table 6. 8 Calibrated most probable BRICK parameters for London Clay with LS-Dyna 3D back-analysis

London Clay	
$R_{(b)}$ (G_t/G_{max})	**String length $L_{(b)}$** *(shear strain)*
0.92	0.0000304
0.75	0.000075
0.60	0.00015
0.50	0.0004
0.35	0.00075
0.25	0.0015
0.15	0.0025
0.05	0.0075
0.01	0.02
0	0.06
Soil Property	
λ*	0.1
κ*	0.02
ι	0.00175
ν	0.2
M_u	1.3
β^G	5.0
β^ϕ	5.0
	implied ϕ'_{crit} = 28.2°
Pre-consolidation pressure	*2000 kN/m²*

The undrained shear strength (c_u) values are derived from the triaxial compression test simulation using the calibrated most probable BRICK parameters. Based on the stress-strain (q-ε_q) curve, the undrained shear strength (c_u) is taken as half of the maximum shear stress (q) value, $c_u = q_{max}/2$ in kN/m^2. The undrained soil horizontal stiffness (E_{uh}) can also be derived from the stress-strain (q-ε_q) curve of triaxial test simulation, $E_{uh,\ secant} = 2(1+\nu)\ q/\varepsilon_q$, or $E_{uh,\ tangent} = 2(1+\nu)\ \Delta q/\Delta\varepsilon_q$ in kN/m^2.

The TCR-WTH ground model is adopted in a series of triaxial compression test simulations as illustrated in Figure 6. 19. The tests were prepared for a sample every 2.0 m from the top of the stratum, with a total of six tests in the LC-A3 division and six tests in the LC-A2 divisions.

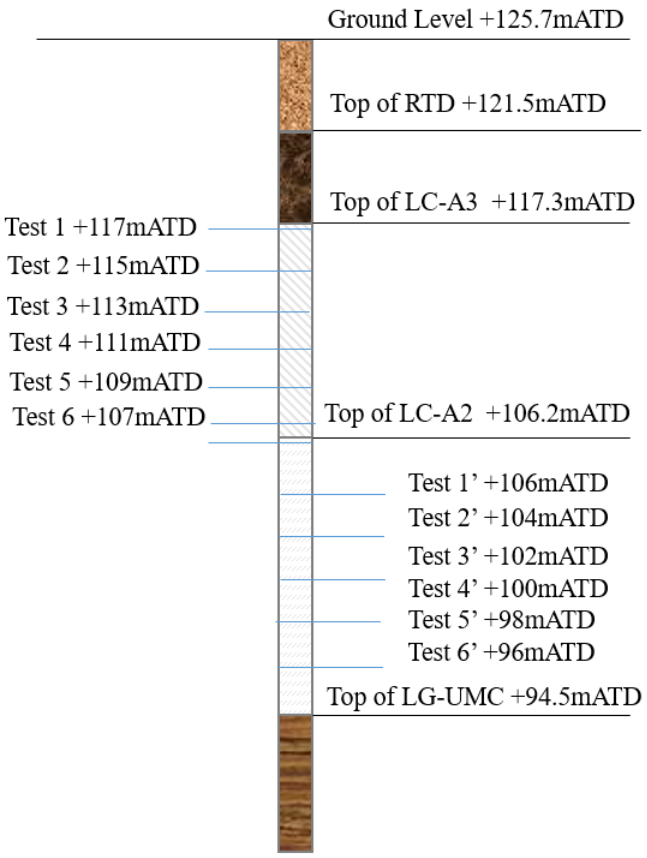

Figure 6. 19 Triaxial test simulations using the TCR ground model

Simulation results with the most probable BRICK parameters are prepared for: (a) the Mohr-Coulomb stress path[12] (*t-s'*); (b) stress-strain curve (q-ε_q); and (c) the normalised secant shear stiffness (G_s/p_0'-$log\varepsilon_q$). They are presented in Figure 6. 20 for the LC-A3 and Figure 6. 21 for the LC-A2.

Using the most probable BRICK parameters (Table 6. 8), the undrained shear strength (c_u) values are derived for the LC-A3, ranging from about 150 kPa near the top (test at +117 mATD) of the layer and linearly increased to 225 kPa near the bottom (test at +107 mATD). These c_u values are high compared to the Mohr-Coulomb most probable undrained shear strength (c_u) values and stay at an upper bound of triaxial test results for the LC-A3 (see Figure 6. 20).

The Mohr-Coulomb stress path (*t-s'*) curves are plotted for the LC-A3 in Figure 6. 20, indicating that derived soil strength with the most probable BRICK parameters can be

[12] The stress path curve uses *t-s'* plot, where shear stress $t = (\sigma_1 - \sigma_3)/2$ and mean stress $s' = (\sigma_1 + \sigma_3)/2$. This is different from the stress path *q-p'* curve provided in the triaxial compression test, where shear stress $q = (\sigma_1 - \sigma_3)$; mean stress $p' = (\sigma_1 + \sigma_2 + \sigma_3)/3$.

interpreted as combination of a friction angle of $\phi'_{peak} = 27.8°$ and an effective shear strength of c' = 30kPa, as the interpretation without effective shear strength of c' can lead to an unrealistic high friction angle of $\phi'_{peak} = 37.8°$. As a comparison, the characteristic soil strength of a friction angle $\phi'_{peak} = 20°$ is recommended. This is based on triaxial test results for the LC-A3 as shown in the diagram, three tests examples from the borehole T9 and B4 (xrt974c, xrb4123c and xrt914c).

The secant shear stiffness (G_{sec}) values are normalised by the initial mean effective stress (p'_0) and plotted against the shear strain (ε_q) in a log scale in the shear stiffness curves (G_s/p_0'-$log\varepsilon_q$). The normalised curves for the LC-A3 by the most probable BRICK parameters are way above the triaxial test results, but coincidentally, the derived normalised shear stiffness values do in agreeing with the field self-boring pressuremeter (SBP) test results undertaken in the LC-A3 (Crossrail, 2009a) in small strain range (< 0.02%)

BRICK simulations for the LC-A2 follow the trend of the LC-A3 results. The derived undrained shear strength (c_u) values linearly increase from 230 kPa at the top (test at +106 mATD) of the layer to 345 kPa near the bottom (test at +96 mATD). However, the derived c_u values for the LC-A2 are compatible with triaxial test results, slightly high at the top but slowly increasing with a small gradient and ending up low at the bottom. Whilst, the Mohr-Coulomb most probable undrained shear strength (c_u) values increase sharply from the top to the bottom with a higher value at the bottom (see Figure 6. 21).

The Mohr-Coulomb stress path (t-s') curves are plotted for the LC-A2 in Figure 6. 21, indicating that derived soil strength with the most probable BRICK parameters can be interpreted as a combination of a friction angle of $\phi'_{peak} = 30.5°$ and effective shear strength of c' = 40.5 kPa. Similarly to the LC-A3, the interpretation without effective shear strength of c' can lead to an unrealistic high friction angle of $\phi'_{peak} = 40.5°$ for the LC-A2. The recommended characteristic soil strength of a friction angle $\phi'_{peak} = 22°$ seems low based on three tests from borehole T9 (xrt916c, xrt924c and xrt926c).

The normalised secant shear stiffness (G_{sec}) values from the BRICK simulations for the LC-A2 are plotted against the shear strain (ε_q) in a log scale in the shear stiffness curves (G_s/p_0'-$log\varepsilon_q$) in Figure 6. 21. Again, the derived shear stiffness values are found to agree with the field self-boring pressuremeter (SBP) test results undertaken in the LC-A2 (Crossrail, 2009a) in small strain range (< 0.01%).

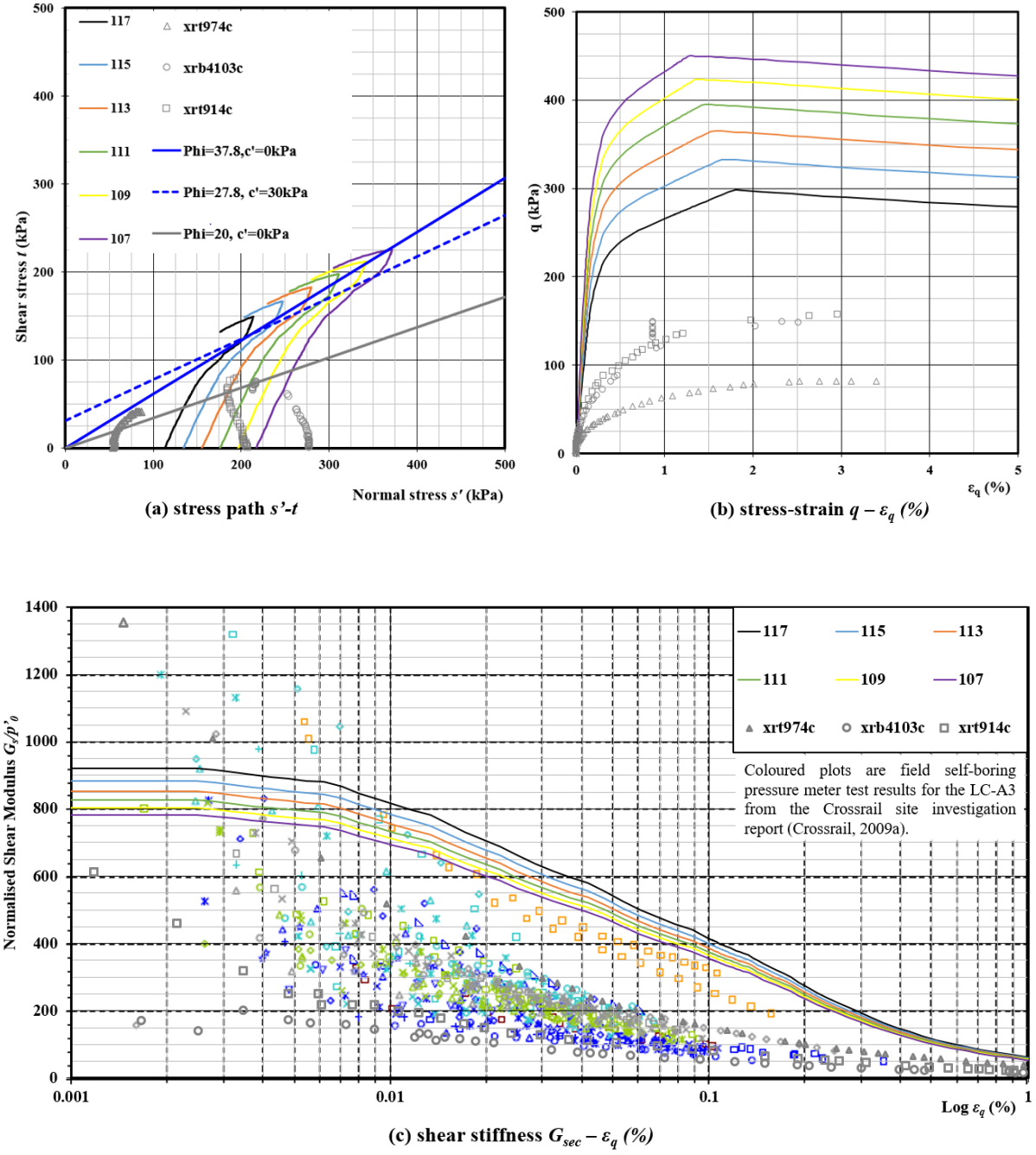

Figure 6. 20 Triaxial compression test results for LC-A3 by most probable BRICK parameters

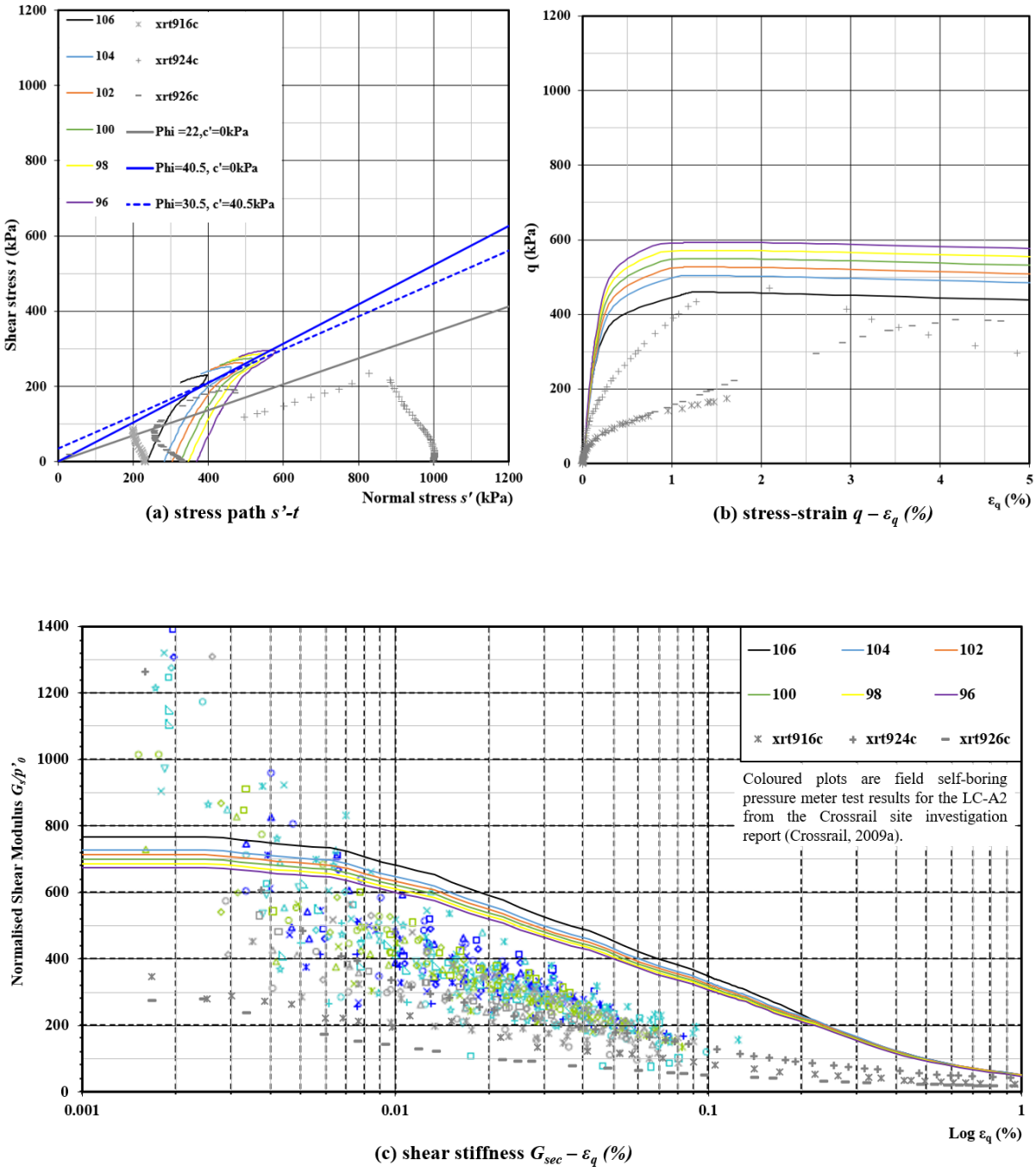

Figure 6. 21 Triaxial compression test results for LC-A2 by most probable BRICK parameters

A review of the BRICK simulations and ground investigation data, it indicates that the soils samples used for laboratory triaxial tests might have been disturbed, thus testing results are less representative of the in-situ soil conditions. Therefore, a gap is introduced between the initial BRICK parameters calibrated using triaxial data, and the most probable BRICK parameters derived from the back-analysis using inclinometer data.

Comparison of the undrained shear strength (c_u) is presented in Figure 6. 22. The most probable BRICK parameters tend to show the highest (c_u) values between different sets of (c_u) profiles derived for the LC-A3. However, for the LC-A2 the most probable Mohr-Coulomb (c_u) values derived by statistical regression method present the higher values. The undrained shear strength (c_u) values from both the Mohr-Coulomb and BRICK models are in the middle of triaxial test data of the Lambeth Group divisions, although these test data varies in a large range from 100 kPa to 600 kPa.

The undrained soil horizontal stiffness (E_{uh}) calibrated from the LS-Dyna 3D back-analysis for the TCR-WTH deep box final excavation stage with both the Mohr-Coulomb and BRICK models, is compared with triaxial test data at shear strain levels of 0.01%, 0.05% and 0.1% in Figure 6. 22. Incidentally, the undrained soil horizontal strength (E_{uh}) values by the most probable BRICK parameters at a strain level of 0.05% match well with the triaxial test results at strain level of 0.01%, with the exception of the LG-LMC layer. Also, a good match is observed in the most probable Mohr-Coulomb (E_{uh}) values and the triaxial test results at a strain level of 0.01% in the LC-A2. In addition, higher (E_{uh}) values by the most probable BRICK parameters at a strain level of 0.01% are expected, and these values in the LC-UMC layer are in perfect match with the most probable Mohr-Coulomb (E_{uh}) values. These undrained soil horizontal strength (E_{uh}) values explain the comparable performances of the Mohr-Coulomb and BRICK models in predicting wall deflections for the TCR-WTH deep box excavation using the LS-Dyna 3D model (Figure 6. 9 & Figure 6. 10).

Meanwhile, more details of the wall deflection predictions can be revealed with the understanding of these (E_{uh}) values: at an early excavation stage 3, the BRICK model is functioning with higher stiffness values (e.g. E_{uh} at strain of 0.01%) in London Clay, due to very small incremental strains developed in the undisturbed LC-A2 and not fully mobilised LC-A3, hence, the analysis presents a rigid wall with smaller wall deflections; however, the Mohr-Coulomb model uses the fixed (E_{uh}) values, which do not change with strains, and

predicts increased wall deflections because of the slightly low most probable (E_{uh}) values in the LC-A3 than the ones by the BRICK model.

For the final excavation stage 6, the BRICK model functions with medium to high stiffness values (e.g. E_{uh} at a strain of 0.05%) in London Clay, as medium to large incremental strains developed in the fully mobilised LC-A3 & LC-A2. Hence, the analysis estimates the slightly larger wall deflections; while the Mohr-Coulomb model uses the same (E_{uh}) values as stage 3, which are higher than the ones by the BRICK model at this stage, and predicts the smaller wall deflections.

However, in Lambeth Group, correlations between the most probable Mohr-Coulomb (E_{uh}) values, the most probable BRICK (E_{uh}) values and triaxial test data are only indicative, as three back-analysed Crossrail TCR-WTH deep box excavation barely reached in the Lambeth Group. These undrained soil horizontal stiffness (E_{uh}) values might decrease for excavations that occur in the Lambeth Group.

6.3.2 Comparison of Mohr-Coulomb and BRICK

Using 3D FEM, the linear elastic and plastic perfect Mohr-Coulomb model performs well in predicting the wall deflections for the Crossrail TCR-WTH deep box back-analysis. However, its' performance is poor in predicting strut loads and ground surface movements or ground heave, because the accurate predictions are related to non-linear soil stiffness as well as anisotropy in soil stiffness.

As a comparison, the BRICK model is capable of describing non-linear soil stiffness and shows a better performance in predicting wall deflections, strut loads, and ground movements including ground heave. The most probable BRICK parameters calibrated in the back-analysis using inclinometer data has managed to obtain fitted wall deflections, as well as matching strut loads and ground heave during the undrained excavation phase. Except for ground settlements, instead, the BRICK parameters calibrated using triaxial test data can result in fitted ground settlement profiles. The different performance in ground settlement predictions by the two sets of the BRICK parameters may be explained by anisotropy in soil stiffness. Further testing will be required to investigate the impact of soil stiffness anisotropy in ground movements.

Based on a comparison and discussion of the back-analysis results, it is concluded that a back-analysis can use either the Mohr-Coulomb model or another advanced soil model (e.g.

BRICK), depending on observations available for the back-analysis comparison. Review of instruments, installations, data acquisition, error diagnostics and correction, shows that inclinometers that consistently provide reliable data are the primary instruments, which have been utilised frequently in the back-analyses. However, when more accurate comparisons are required for the undrained excavation analysis, such as porewater pressures, heave and ground surface movements, data from the secondary instruments can be compared to more accurate predictions from the back-analysis with an advanced soil model.

6.3.3 Issues in the back-analysis

The LS-Dyna 3D back-analysis with the BRICK soil model also suffers similar issues as the Mohr-Coulomb model that was discussed in section 5.5.2: reliable observations, accurate predictions and comparison. In addition, it is difficult to calibrate the most probable BRICK. Firstly, the calibration of the initial BRICK parameters uses laboratory triaxial test data, which turns out not very successful due to the quality of tested soil samples and poorly operated testing procedure. Also potentially, there are the limitations of the BRICK model itself. During the back-analysis process, the BRICK parameters modification could be very sensitive and results in increased iterations.

In future calibrations of BRICK parameters, it might be worth using the field test data, like the self-boring pressuremeter test data. This will eliminate the inaccuracy of laboratory test results and capture the in-situ soil conditions for the performance-based back-analysis. Alternatively, the quality of the laboratory test data can be improved through the enhancement measures. For example, a better resolution in measuring strains can be provided by a triaxial bender element test. When better quality data for London Clay divisions are available, different sets of BRICK parameters for different divisions should be calibrated, including these sensitive parameters, like ι, κ, stiffness matrics by $L_{(b)}$ & $R_{(b)}$, β^G and β^ϕ.

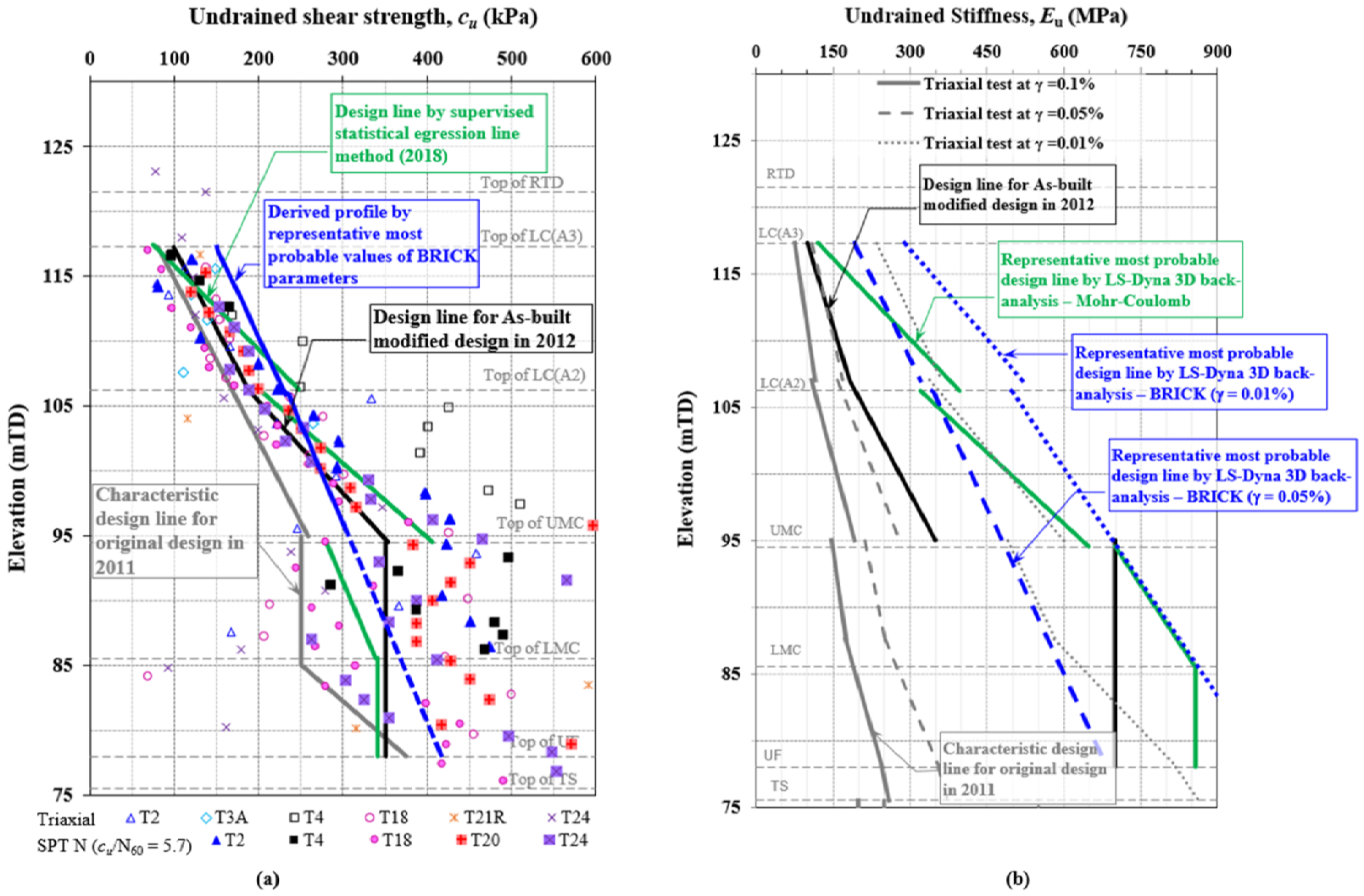

Figure 6. 22 Representative most probable values versus laboratory testing data (a) undrained shear strength; (b) undrained soil stiffness

Chapter 7

Re-assessment excavation design by Approach A

Since Peck (1969) formulated the observational method, most reported case histories of deep excavation have followed either *Ipso tempore* proactive Approach C, or *Ipso tempore* reactive Approach D (Best-Way-Out) in accordance with the new observation method framework proposed in Chapter 3. For instance, three examples have used the newly defined *Ipso tempore* proactive Approach C, including the Crossrail TCR-WTH deep box excavation (Yeow *et al.*, 2014); the Crossrail WS-DSS shaft excavation (Mills, 2016); and the Canary Wharf Crossrail Station box excavation (Yeow *et al.*, 2012). *Ipso tempore* Approach D was more often to rectify difficulties during construction, for instance, unforeseen geology in the Singapore Newton Station (Gaba and Mcgowan, 2017), uncertainties on structural properties during construction in the Crossrail LIS-MS East Wall (Chen *et al.*, 2015), and unexpected large ground movements during the retaining wall installation for the Victoria & Albert Museum excavation (ICE, 2015).

There were fewer published excavation case histories that were categorised as Peck's *Ab initio* approach. The review of these cases has identified most of them as *Ab initio* Cautious Approach B according to the new observational method framework. For example, the open-cut excavation design for the Batheaston Swainswick Bypass project (Nicholson *et al.*, 1998), where the observational method design was developed before installation of the retaining walls due to the program delays. During the bay-by-bay excavation, the field monitoring data confirmed the possibility for the implementation of the observational method design and the

construction switched to the pre-planned modification design resulting in a reduced schedule from the planned 15 months to the as-built 6 months.

An example of Approach A is Harris Trust excavation in Chicago, U.S.A (Peck, 1969). In this case, an empirical envelope of strut loads was summarised from the similar open-cut excavations in Chicago and this envelope was used to design the support bracing system for the excavation. The immediate insertion of the additional strut as the contingency plan was included under the condition of monitoring every strut axial force at all significant stages. It was revealed that the cost savings were rather small in this case, but the design provided positive assurance that no strut in the entire system became overloaded.

One objective of the new observational method is to promote the implementation of the *Ab initio* Optimistic Approach A and Cautious Approach B, in order to maximise savings in both construction materials and time.

In order to demonstrate the benefits from the implementation of *Ab initio* approaches, a re-assessment of the Crossrail TCR-WTH deep box excavation using *Ab initio* Optimistic Approach A was undertaken and presented in this chapter. A cost comparison was also drawn between different designs with regards to the construction costs and programme, showing maximised cost savings by Approach A.

7.1 Re-assessment of TCR-WTH excavation design

The Crossrail TCR-WTH deep box excavation is investigated in depth in this research. The representative most probable values of the soil model associated parameters for the London Clay are calibrated through the back-analysis using inclinometer data. Therefore, this case is selected for re-assessment by the observational method *Ab initio* Optimistic Approach A.

The Crossrail TCR-WTH deep box case history is reviewed in section 3.2.1, and the back-analysis with the Mohr-Coulomb model is discussed in Chapter 5. Although the back-analysis results from Plaxis 2D and LS-Dyna 3D are slightly better than FREW (Figure 5.22), the pseudo-FE FREW model shows the compatible performance. Given the simplicity of FREW modelling and it has been used in the original TCR-WTH design analysis, the re-assessment of Approach A design uses FREW.

In the re-assessment by Approach A, the optimistic design uses the most probable Mohr-Coulomb parameters for the London Clay divisions (LC-A3 & LC-A2), which are referred to Table 5.5, the calibrated values in the FREW back-analysis for the TCR-WTH deep box. In

addition, the contingency plan uses the characteristic Mohr-Coulomb parameters for the London Clay division, which are referenced to Table 3.2, the parameters applied in the original design of the TCR-WTH.

7.1.1 Approach A re-assessment design

In order to maintain the compatibility, the Approach A re-assessment for the TCR-WTH follows the same design requirements by Crossrail civil engineering design standards (CEDS), for instance, BSI (2004a) - Eurocode 7: Geotechnical Design. Under the EC7, each design needs to complete two analyses: serviceability limit state analysis (SLS) is to assess the performance of structures and to ensure it remains within the allowable thresholds, and ultimate limit state analysis (ULS) is to cover the worst credible design conditions.

The TCR-WTH deep box excavation re-assessment by Approach A comprises of the optimistic design and the contingency plan, design conditions for the two designs are summarised in Table 7. 1.

The optimistic design assumes a total stress analysis (undrained) during the short six-months excavation period, this undrained behaviour of the London Clay is widely reported during the fast excavation programme (e.g. less than twelve months) in previous excavations at central London. Whilst, a relative more conservative mixed-earth pressure analysis (effective stress analysis on the active side and total stress analysis on the passive side) is assumed for the contingency plan, which assumption is considered for a possible worst groundwater drainage condition within a slightly longer period (e.g. over twelve months).

A progressively developed groundwater drainage condition is assumed for the follow-up TCR-WTH deep box basement construction period. In the optimistic design, analysis is switched to mixed earth pressure for the basement construction phase, but an effective stress analysis is assumed for the contingency plan over the same phase.

This re-assessment is to investigate possible maximised savings, hereby, a minimum change to the original design is considered in the re-assessment, rather than a complete alternative scheme. A major change in diaphgram wall thickness is proposed from 1.0 m in the original design to 0.8 m in the Approach A re-assessment design. However, extra levels of temporary props might be required to enable the contingency plan with this thinner wall.

The construction sequence of the Approach A re-assessment design are presented in Table 7. 2, as a minimum change is made in the optimistic design, the construction sequence is also

following the original design and updated with the modified as-built sequence up to excavation stage 4 (Table 3.3).

Table 7. 1 Re-assessment design for the TCR-WTH deep box excavation by Approach A

Design	**Optimistic design**	**Contingency plan**
Analysis	FREW with the Mohr-Coulomb soil constitutive model	
Design parameters	Representative values of the most probable Mohr-Coulomb parameters (Table 5.5)	Representative values of the characteristic Mohr-Coulomb parameters (Table 3.2)
Design assumptions	Most probable conditions: • Total stress analysis during excavation (undrained) • Mixed earth pressure analysis during basement structure constructions.	Conservative conditions: • Mixed earth pressure analysis during excavation; • Effective stress analysis during basement structure constructions (drained)
Retaining wall	800mm (thickness) diaphragm wall (no change for the wall depth from +125.7 to +85.5 mATD)[1]	
Temporary propping[2]	4 levels of prop	6 levels of prop

Note:

1. In conjunction with the Crossrail TCR-WTH deep box original design reviewed in section 3.2.
2. The properties of the top four levels' temporary props are referenced to the as-built conditions for props (Table 3.4). The properties of the 4th level of props are assumed for the two additional levels of props in the contingency plan.

Table 7. 2 The proposed construction sequence for the TCR-WTH deep box excavation by Approach A re-assessment design

Optimistic design			**Contingency plan**		
Stage		**Description**	**Stage**		**Description**
1		Excavate to +121.6 mATD	**1**		Same as left
2	a	Installation P1 prop at +122.4 mATD	**2**	a	Same as left
	b	Excavate to +116.4 mATD		b	Same as left
3	a	Installation P2 prop at +117.2 mATD	**3**	a	Same as left
	b	Excavate to +110.9 mATD		b	Same as left
4	a	Installation P3 prop at +111.9 mATD	**4**	a	Same as left
	b	Excavate to +108.3 mATD		b	Same as left
5	a	Installation P4 at +109.1	**5**	a	Same as left
	b	Excavate to +100.0mATD		b	Excavate to +104.1mATD
	c	n/a		c	Installation P5 at +105.2mATD
	d	n/a		d	Excavate to +100.0 mATD
6		Excavate to +96.8 mATD including a trench along excavate to +95.4 mATD	**6**	a	Installation P6 at +101.1 mATD
				b	Excavate to +96.8 mATD including a trench along excavate to +95.4 mATD
Basement construction phase					
7		*Cast the base slab in 2.0 m thickness*	***7***		*Same as left*
8		*Cast Slab - 4*	***8***		*Same as left*
9		*Remove P4 prop*	***9***		*Remove P6 & P5 prop*
10		*Cast Slab -3 & Remove P3 prop*	***10***		*Cast Slab -3 & Remove P4 prop*
11		*Cast Slab -2 & Remove P2 prop*	***11***		*Cast Slab -2 & Remove P3 prop*
12		*Cast Slab -1 & Remove P1 prop*	***12***		*Cast Slab -1 & Remove P2 prop*
13		*Cast Slab - 0*	***13***		*Cast Slab 0 & Remove P1 prop*
14		*Long term groundwater and structural properties*	***14***		*Same as left*

Note: stage 1 to stage 4 referenced to the as-built TCR-WTH deep box construction sequence (Crossrail, 2013b).

7.1.2 Structure design – ULS analysis

ULS analyses of the Approach A re-assessment designs are carried out in accordance with the BSI (2004a), two design approaches (DA1C1 and DA1C2) of the ULS analysis are performed to obtain the maximum bending moment and shear force for the retaining wall reinforcement design. In approach DA1C1, partial factors are introduced on actions (loads) and the effect of actions (results) but no reduction on material strength (soil), but in approach DA1C2, partial factors are introduced on the material strength and action (variable loads) without reduction on the effect of actions. These partial factors used in DA1C1 and DA1C2 are extracted from Eurocode 7th Edition and summarized in Table 7. 3.

Table 7. 3 Partial factors for DA1C1 and DA1C2, BSI (2004a)

			Design Approach 1					
			Combination 1			Combination 2		
			A1	M1	R1	A2	M2	R2
Action	Permanent	Unfavorable	1.35	-	-	1.0	-	-
		Favorable	1.0	-	-	1.0	-	-
	Variable	Unfavorable	1.5	-	-	1.3	-	-
		Favorable	0	-	-	0	-	-
Soil	tanϕ’		-	1.0	-	-	1.25	-
	Effective cohesion		-	1.0	-	-	1.25	-
	Undrained strength		-	1.0	-	-	1.4	-
	Unconfined strength		-	1.0	-	-	1.4	-
	Weight density		-	1.0	-	-	1.0	-
Reaction	Resistance		-	-	1.4	-	-	1.0

Note: A = action, M = material strength, R = resistance

Outputs from the ULS calculations are applied in the diaphragm wall reinforcement design in accordance with the BSI (2014). Reinforcements of the Approach A re-assessment are summarised in Table 7. 4 for the main bars, and in Table 7. 5 for the shear links. The calculation takes accounts of the maximum bending moments and shear forces between the optimistic design and the contingency plan ULS analyses.

Table 7. 4 Main bars reinforcement for 800 mm diaphragm wall by Approach A design for TCR-WTH deep box

Elevation (mATD)	Maximum Bending Moment (kNm/m)		Main Bars	Capacity (kNm/m)
	Optimistic design	Contingency plan		
125 – 118.5	-450, 842	-169, 735	T: B32 @ 200 mm B: B40 @ 200 mm	-1084, 1640
118.5 – 115	-1167, 768	-510, 940	T: B40 @ 200 mm B: B40 @ 200 mm	-1637, 1637
115 -108.5	-2246, 1280	-1751, 1079	T: B50 @ 200 mm +B40 @ 200 mm B: B50 @ 200 mm	-3846, 2528
108.5 -94.0	-994, 1895	-1198, 1465	T: B50 @ 200 mm B: 2B40 @ 200 mm	-2512, 3030
94.0 – 85.0	-850, 10	-963, 90	T: B40 @ 200 mm B: B20 @ 200 mm	-1650, 696

Note: Maximum BM values were the greatest of 1.35 × DA1C1 and 1.0 × DA1C2. The capacity of the reinforcement was based on the *Oasys*® AdSec calculation for the typical diaphgram wall panel in 2.8 m width. T = top of the reinforcement cage, towards the soil; B = the bottom of the reinforcement cage, towards the excavation /basement.

Table 7. 5 Shear links for 800 mm diaphragm wall by Approach A design for TCR-WTH deep box

Elevation (mATD)	Maximum Shear Force (kN/m)		Shear Link	Capacity (kN/m)
	Optimistic design	Contingency plan		
125 – 118.5	-554, 486	-696, 451	B16 @ 250 mm c/c	-678, 678
118.5 – 115	-869,834	-820, 757	B20 @ 150 mm c/c	-1390, 1390
115 -108.5	-1766,1223	-1670, 1567	B25 @ 150 mm c/c	-2143, 2143
108.5 -94.0	-1332,1604	-1503, 1243	B25 @180 mm c/c	-1796, 1796
94.0 – 85.0	-267,128	-395, 378	B16 @ 250 mm c/c	-532, 532

Note: Maximum SF values were the greatest of 1.35 × DA1C1 and 1.0 × DA1C2. The requested shear resistance was checked against the concrete beam material shear capacities (concrete shear resistance and the reinforced concrete beam shear resistance). The listed capacity of the shear link was based on the calculation for the typical diaphgram wall panel in 2.8 m width.

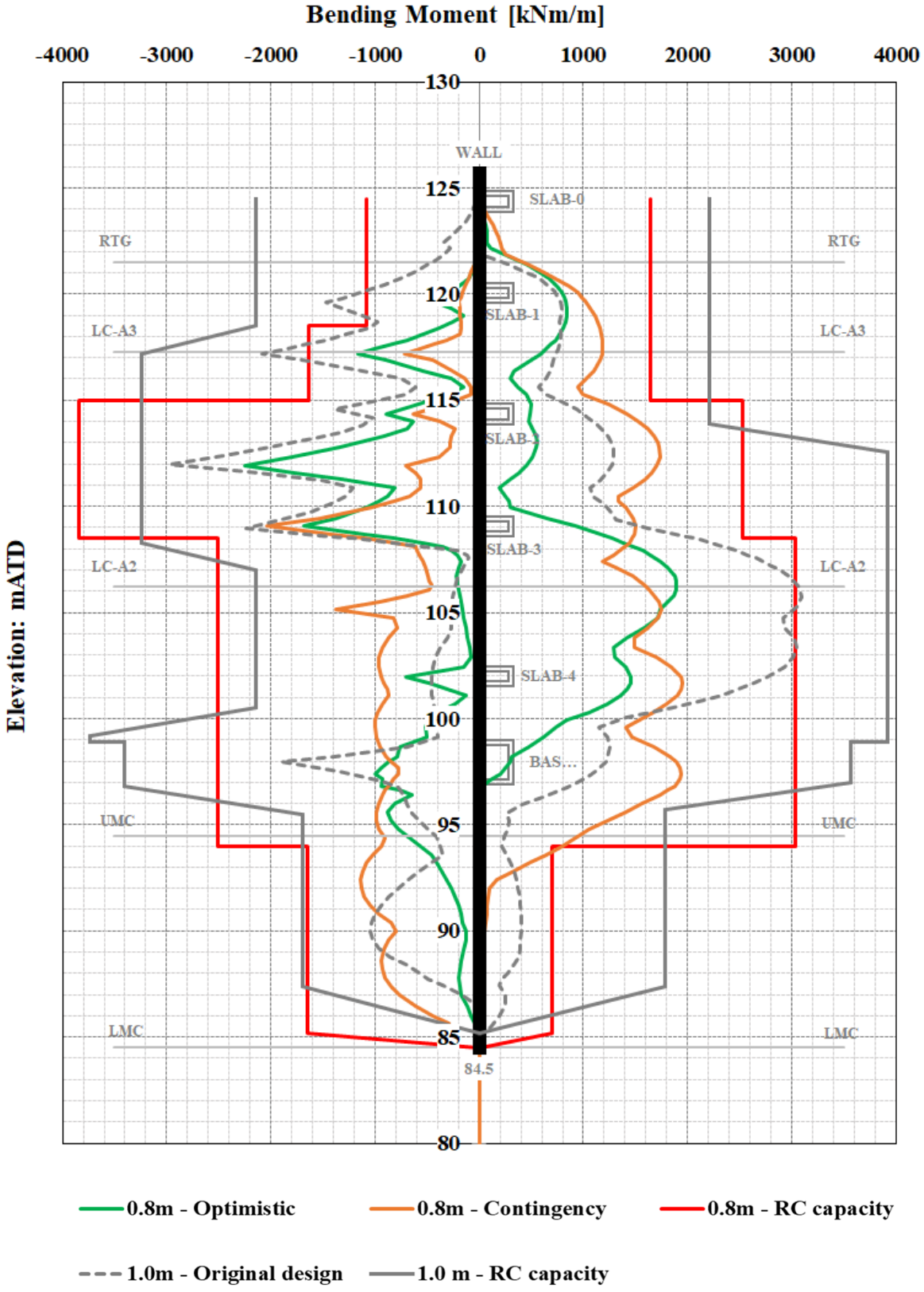

Figure 7. 1 Bending moment envelopes by Approach A design for TCR-WTH deep box

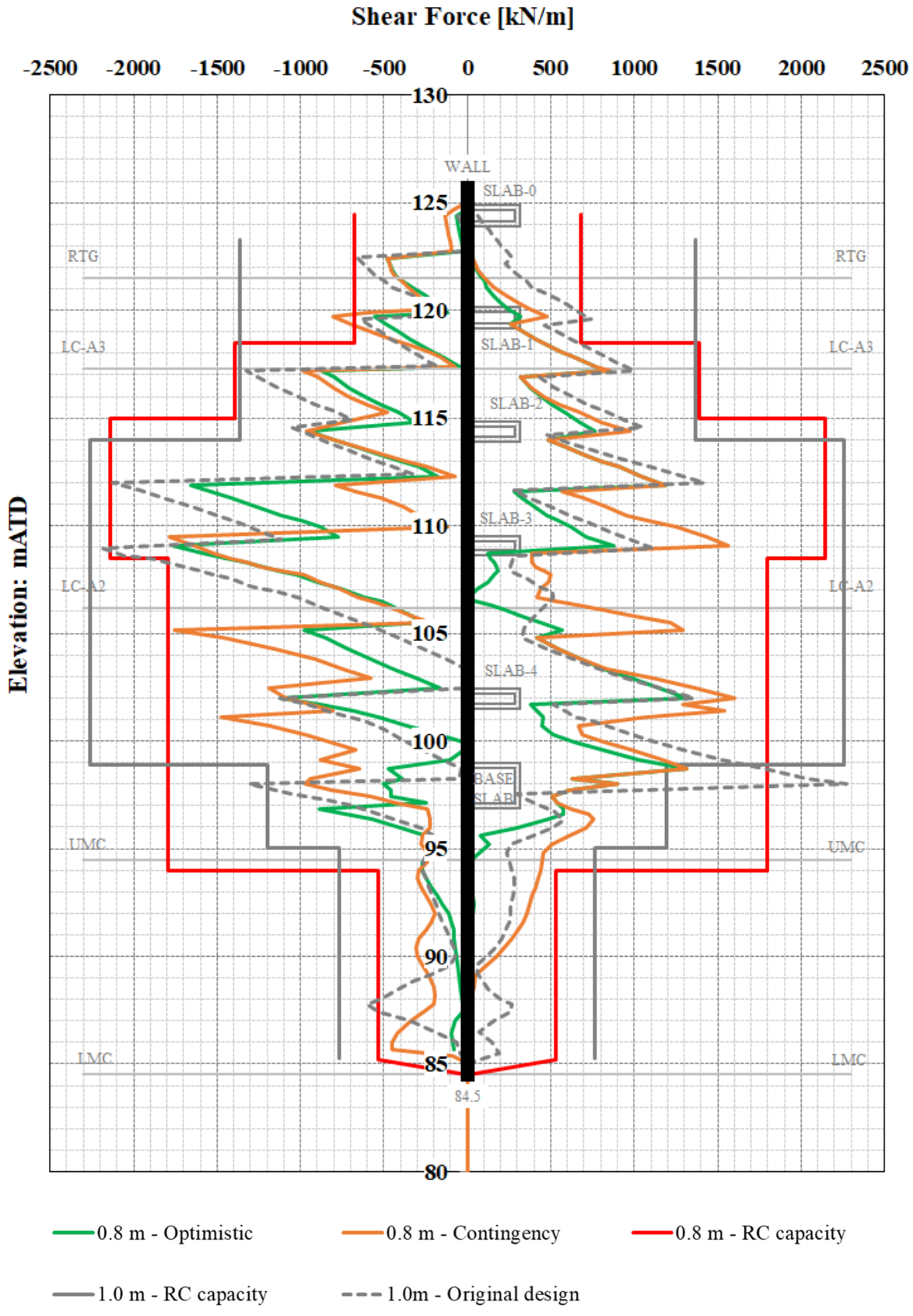

Figure 7. 2 Shear force envelope by Approach A design for TCR-WTH deep box

Bending moment envelope for 0.8 m thick walls by the Approach A re-assessment is within the calculated reinforcement capacity using *Oasys Adsec* (version 8.0), as illustrated in Figure 7. 1. Bending moment envelope for 1.0 m thick walls in the original design and the reinforcement capacity of the as-built 1.0 m walls are included for reference.

The shear force envelopes of the Approach A re-assessment are checked against the calculated shear force capacities, as presented in Figure 7. 2. The required shear links are designed in accordance with BSI (2014) to ensure sufficient shear resistance.

7.1.3 Performance check – SLS analysis

SLS analyses of the Approach A re-assessment designs are also carried out to obtain the performance-based predictions, such as wall deflection and strut loads. In the original design for the Crossrail TCR-WTH design, the SLS analysis estimated the wall deflections for the 1.0 m walls, which were assessed and approved with respect to the movement criterion induced by deep excavation (Crossrail, 2010b). Therefore, it is envisaged if the SLS analysis for the 0.8 m wall shows the estimated wall deflections not exceeding the ones for the 1.0 m wall in the original design, the re-assessment design is also satisfied the movement criterion.

In addition, the predicted wall deflections can be used to assist in decision making in the construction control process. A conceptual flowchart is proposed in Figure 7. 3, showing a step-by-step decision-making example. Firstly, a traffic light control system, including Green, Amber and Red trigger profiles, is defined using the SLS analyses results, which can be the predicted wall deflections at each excavation stage. At the number i construction stage, monitoring data are reviewed and the construction by the optimistic design is to be continued the ($i+1$) stage if no green triggers are breached. On the opposite, a back-analysis is carried out to confirm the most probable design assumptions & most probable parameters, and the construction is to be continued the ($i+1$) stage if no amber triggers are breached. In case amber triggers are breached, then the construction will need to switch to the sequence catered for the contingency plan. Lastly, the construction is stopped immediately and the emergency measures to be applied if red triggers are ever been breached.

Figure 7. 4 presents the predicted wall deflections at the selected construction stages, including deflections for the 0.8 m walls from the re-assessment SLS analyses, and deflections for the 1.0 m wall from the original design SLS analysis. The associated design parameters and design conditions used to obtain these wall deflections are summarised in Table 7. 6.

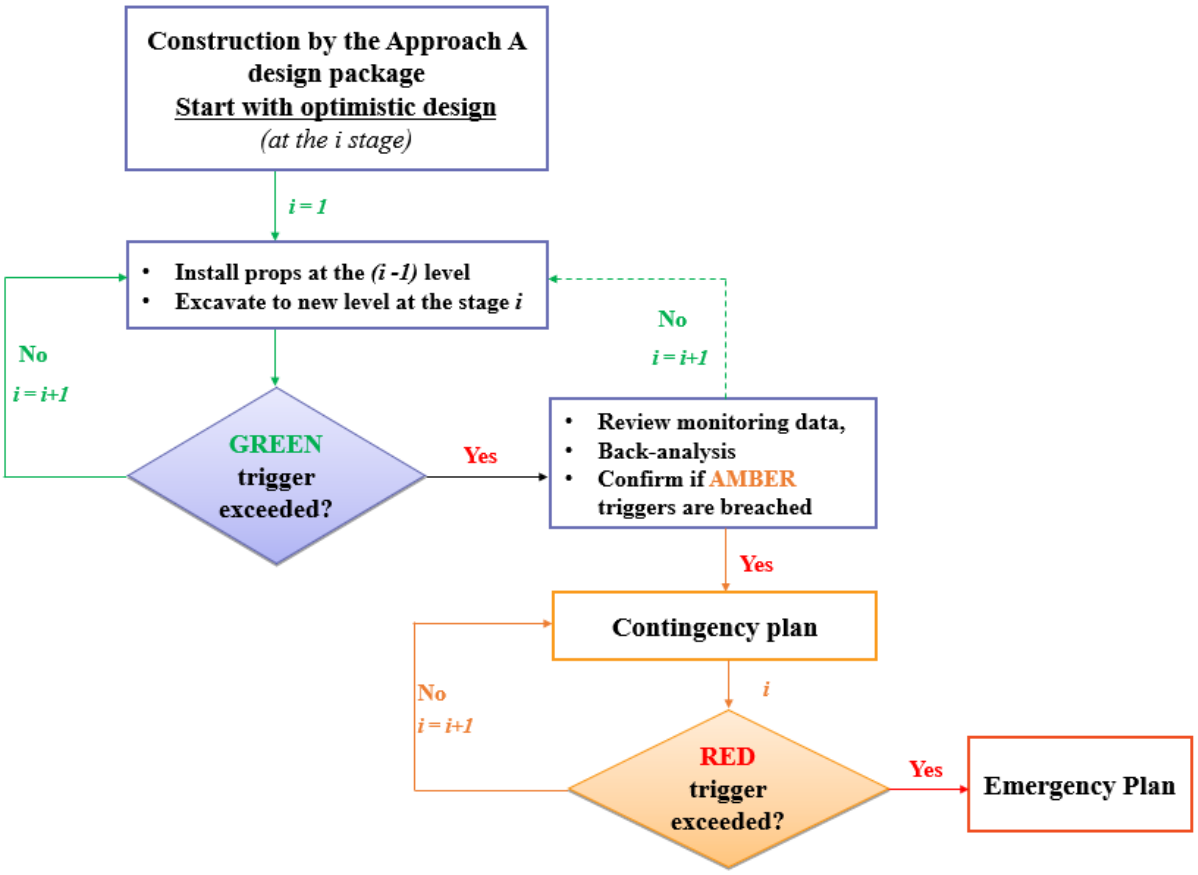

Figure 7. 3 Flowchart of decision making during construction by Approach A design

Table 7. 6 Summary of predicted wall deflection profiles by Approach A design

Design Scheme	Description	Temp props			Design parameters		Design conditions		Trigger level		
		4 levels	5 levels	6 levels	most probable	characteristic	total stress	mixed earth pressure	GREEN	AMBER	RED
0.8 m wall by Approach A	Optimistic design	√			√		√		√		
	n/a	√			√			√		√	
	n/a			√		√	√				√
	Contingency plan			√		√		√			
1.0 m wall scheme	As-built back-analysis	√			√		√				
	Red trigger for as-built		√			√	√				√
	Original design		√			√		√			

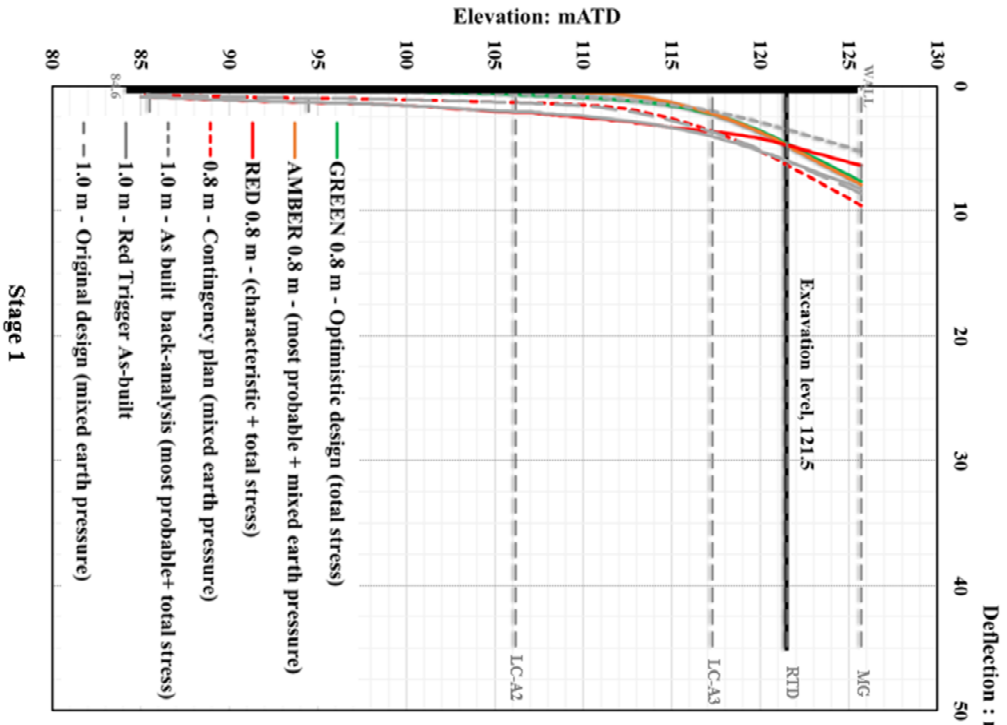
Stage 1
Elevation: mATD
Deflection : mm
Excavation level, 121.5
WALL
MG
RTD
LC-A3
LC-A2
GREEN 0.8 m - Optimistic design (total stress)
AMBER 0.8 m - (most probable + mixed earth pressure)
RED 0.8 m - (characteristic + total stress)
0.8 m - Contingency plan (mixed earth pressure)
1.0 m - As built back-analysis (most probable+ total stress)
1.0 m - Red Trigger As-built
1.0 m - Original design (mixed earth pressure)

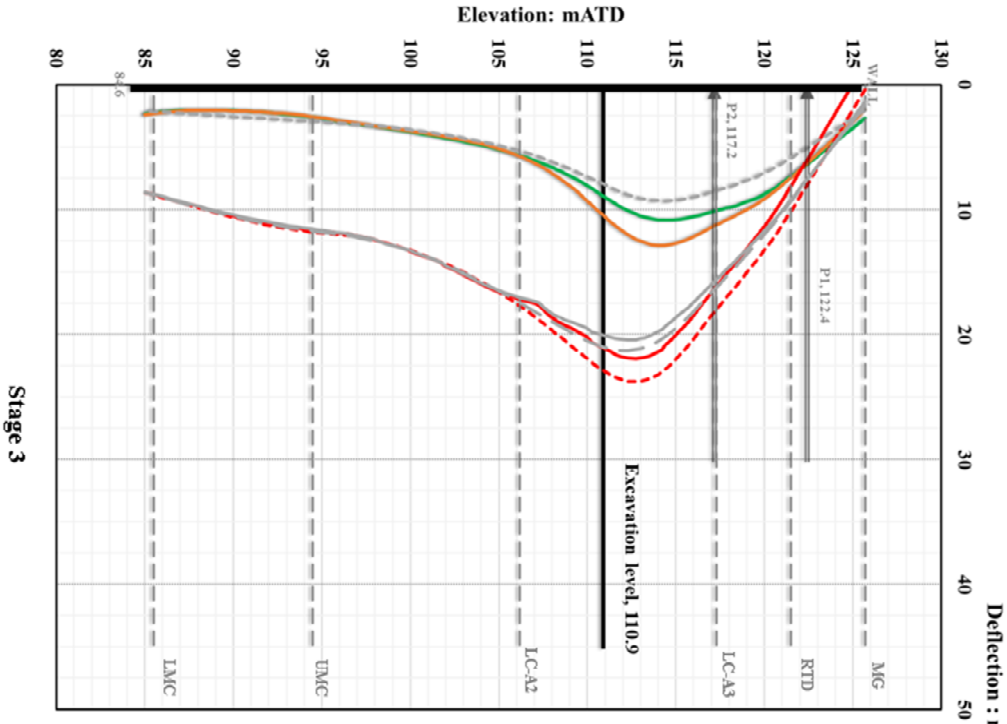
Stage 3
Elevation: mATD
Deflection : mm
Excavation level, 110.9
WALL
P2, 117.2
P1, 122.4
MG
RTD
LC-A3
LC-A2
UMC
LMC

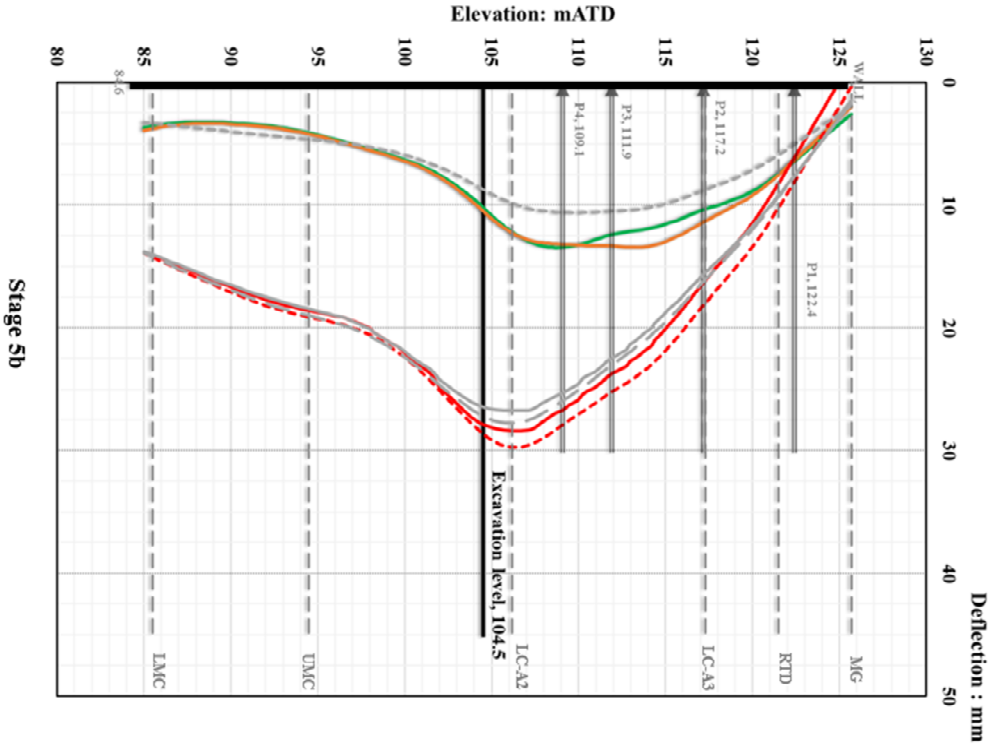
Elevation: mATD
Deflection : mm
Stage 5b
W.L.
P1, 122.4
P2, 117.2
P3, 111.9
P4, 109.1
Excavation level, 104.5
MG
RTD
LC-A3
LC-A2
UMC
LMC

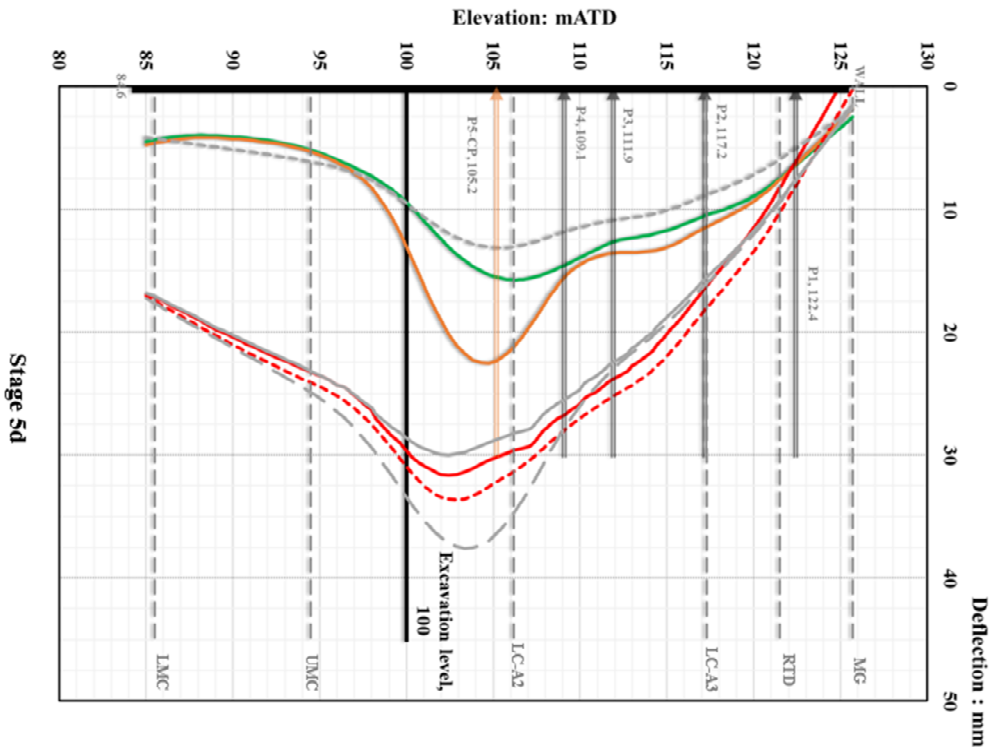
Elevation: mATD
Deflection : mm
Stage 5d
W.L.
P1, 122.4
P2, 117.2
P3, 111.9
P4, 109.1
P5-CP, 105.2
Excavation level, 100
MG
RTD
LC-A3
LC-A2
UMC
LMC

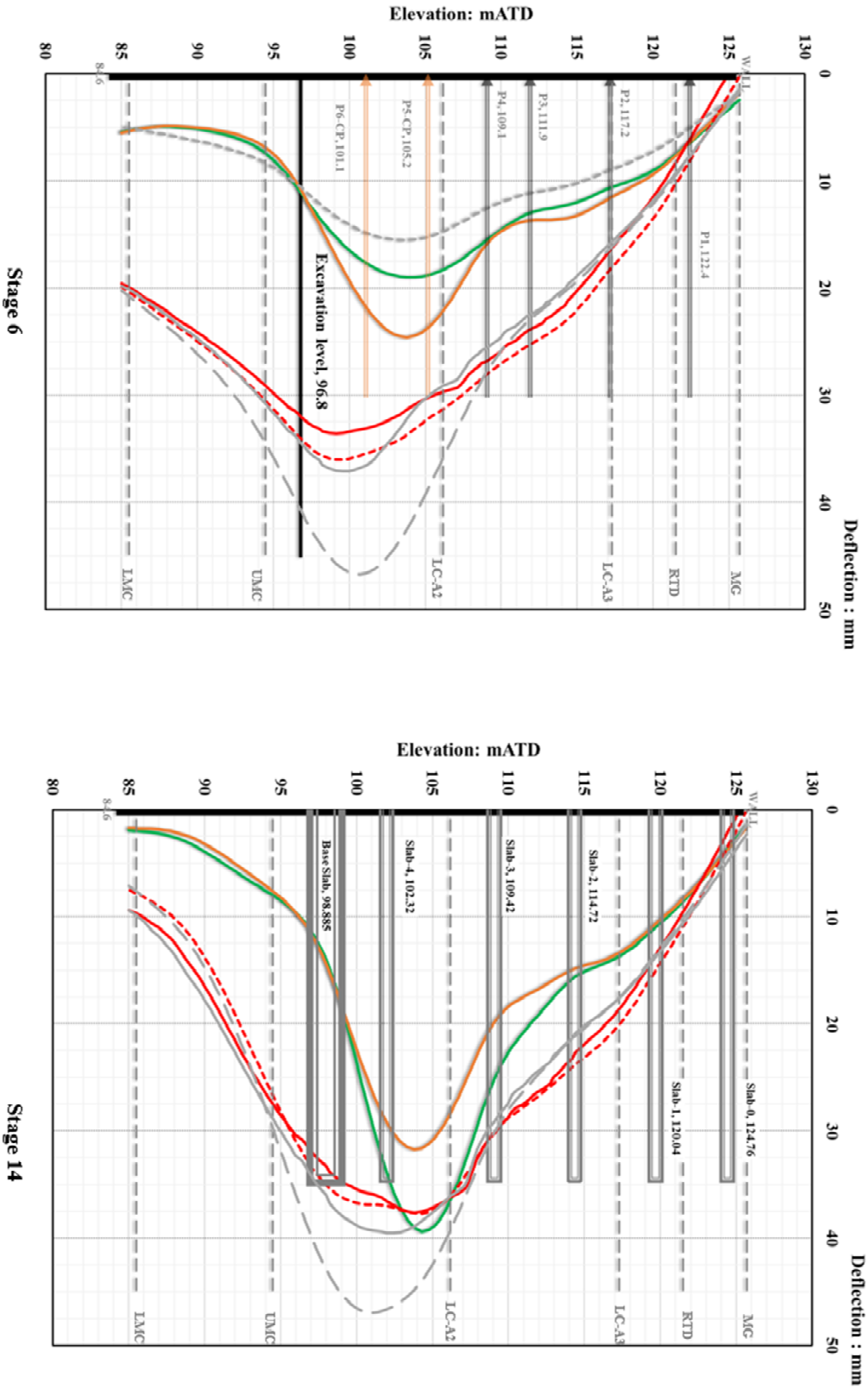

Figure 7. 4 Predicted SLS wall deflections by the Approach A design for TCR-WTH deep box

Based on the predicted wall deflection from SLS analyses of the re-assessment design by the Approach A. Green trigger profiles can be defined by predictions of the optimistic design SLS analysis. Amber trigger profiles are based on predictions of SLS analyses with the most probable parameters and a mixed earth pressure analysis assumption, which will give predictions less conservative but not the most onerous. Given the contingency plan SLS analyses use the characteristic parameters and assume a mixed earth pressure assumption, predictions are the most onerous. Red triggers are recommended to keep some margin for construction control and safety, hereby, predictions of SLS analyses with the characteristic parameters and total stress analysis assumption are chosen for red triggers.

If the contingency plan is activated, a separate set of green/amber/red triggers can be refined based on SLS analyses of the contingency plan, and trigger values can be defined by a proportion of the predicted wall deflections, for instance, 75% of predictions as the new green triggers, 90% of predictions as the new amber triggers, and 100% of predictions as the new red triggers.

Figure 7. 4 shows clearly, during the short six-month excavation phase, the derived green trigger profiles and amber trigger profiles for the 0.8 m walls do not exceed the as-built red trigger profiles applied for the 1.0 m walls, including the cantilever excavation stage 1. At an early excavation stage 3, the green trigger profile for the 0.8 m walls is very close to the back-analysed wall deflection profile for the 1.0 m walls, while the amber trigger profile for the 0.8 m walls follows the trend of the green trigger profile but in slightly higher magnitude. This trend is also observed in other excavation stages (stage 3, 5b, 5d and 6). During the long-term basement construction phase, the maximum green trigger for the 0.8 m walls increases from below 20 mm at stage 6 (end of excavation) to about 40 mm at stage 14 (end of basement construction). This significant increment is due to the design assumption of a mixed earth pressure analysis applied in the optimistic design SLS analysis for the long-term basement construction phase. In reality, in the less permeable overconsolidated London Clay, groundwater pressures on the active side will increase gradually, and a fully drained groundwater condition might take decades to reach, hence, such an increment of wall deflection developed in a couple of years is overestimated.

The red trigger profiles for the 0.8 m walls are based on predictions of SLS analyses close to the contingency plan. At stage 5b excavation with four levels of props, the red trigger profile for the 0.8 m walls is slightly above the as-built red trigger profile for the 1.0 m walls at excavation stage 5b, which is caused by the thinner wall in the re-assessment design. The

controlled increments in red trigger profiles for the 0.8 m walls are obtained with additional levels of props installed to support excavation at stage 5d and 6. The red trigger profile for the 0.8 m walls is controlled below the as-built red trigger profile for the 1.0 m walls at the final excavation stage 6.

In summary, comparisons of SLS analyses between the 0.8 m thick diaphgram wall of the re-assessment design and the 1.0 m thick diaphgram wall of the original design, show the re-assessment design does not introduce excessive displacements, and this design satisfies the Crossrail movement criterion for the TCR-WTH project.

7.2 Cost comparison

A cost comparison of different designs for the TCR-WTH deep box excavation is performed to investigate the possible cost impact of the Approach A. The cost estimation is based on the 2012 rate of construction materials in 2012 when the Crossrail TCR station was constructed, the TCR station Civils Cost Estimation Stage D Report (Crossrail, 2013c). Rate of the excavation programme (unit in £ per week) is interpreted from the achieved savings for the modified design of the TCR-WTH deep box excavation (Yeow *et al.*, 2014). A summary of the cost comparison of the four different designs is presented in Table 7. 7, including the original design as the base case, the as-built modified design, the Approach A re-assessment of the optimistic design and the contingency plan.

It is clear that concrete accounted for the major portion of the construction material costs in the TCR-WTH deep excavation, but the reinforcement (steel) of the wall has a negligible impact. The average diaphragm wall construction cost rates are given as proof, £711 m^2/m for the 1.0 m thick diaphgram wall versus the average of £438.5 m^2/m for the 0.8 m thick diaphgram wall.

In the as-built modified (Approach C) design, a significant volume of concrete has been used forming the 1.0 m thick diaphragm walls, hence, only 3% savings in material costs were achieved by omitting one level of temporary props. In contrast, the thinner 0.8 m diaphragm wall with four levels of temporary props proposed by the Approach A re-assessment, shows the saving in material costs could be up to 36%. Although the Approach A contingency plan will need two extra levels of temporary props and decrease the saving in material costs to about 30%.

Table 7. 7 Summary of cost comparison of different designs for the TCR-WTH deep box excavation

Design Scheme	**Original design**	**As-built modified design (Approach C)**	**Approach A design**	
			Optimistic design	**Contingency design**
Diaphgram wall thickness (Unit: mm)	1000	1000	800	800
Diaphgram wall construction rate (Unit: m^2 / m)(1)	£ 711	£711	£438	£438
Diaphgram wall volume (Unit: $m^2 \times m$)	6076 × 1.0		6076 × 0.8	
Diaphgram wall cost	£4.32 M	£4.32 M	£2.64 M	£2.64 M
Temporary prop rate (Unit: £ per level)	£ 140,000			
Levels of prop	5	4	4	6
Temporary prop cost	£0.7 M	£0.56 M	£0.56 M	£0.84 M
Sum: construction material cost	**£5.02 M**	**£4.88 M**	**£3.20 M**	**£3.48 M**
Saving to the original design	-	+3 %	+36 %	+31 %
Excavation programme (Unit: week)(2)	28	24	22(3)	30(3)
Programme rate (Unit: £ per week)	£143,750			
Time saving cost	-	+£0.575 M	+£ 0.863 M	-£0.288 M
Saving to the original design material cost	-	+11 %	+17 %	-6 %
Total savings to the original design	**-**	**14 %**	**53 %**	**25 %**

Note:

1) Diaphgram wall construction rate was provided as square meters per meter run vertically, including the concrete rate = £ 156.7 per m^3, steel rate = £1.6 per kg, guide wall rate = 399 per m run, soil excavation rate = £180.2 per m^3, and removal of obstructions rate = £505 per hour, referenced to the Crossrail TCR Civils Stage D Cost Report (Crossrail, 2013c).
2) The excavation programme listed in the above table accounted up to the completion of the excavation work but excluding the deep box basement construction.
3) The excavation programme for the Approach A design was estimated based on the as-built modified excavation programme for the TCR-WTH.
4) The total savings of each design was presented as a result of comparison with the cost of the original design, in per cent.
5) The value assessment accounted for the cost of the construction materials and excavation time only, the potential additional fees could be generated from the re-assessment by Approach A, additional monitoring data and data review to enable the quality back-analysis and administration fees. All these relevant fees could add ± 5% to the final savings.

The excavation programme (time) is another crucial financial factor in the construction project. It is based on the as-built modified TCR-WTH deep box excavation records and a time-related rate of the programme is interpreted. Extra levels of props will be needed in the Approach A contingency plan, which will result in a possible additional 2 weeks of construction time. The equivalent time cost for the extra two weeks is estimated about 6% of the excavation construction material costs by the original design. However, the Approach A optimistic design uses four levels of props, a total of 6 weeks of construction time is probably able to achieve, considering the well-prepared design and the pre-planned programme from the beginning of the project. The equivalent time cost is about 17 % of the excavation construction material costs by the original design.

The cost comparison shows that Approach A re-assessment maximises the possible savings in construction materials and in excavation time for the Crossrail TCR-WTH project. This Approach A design indicates an average saving of over 30% in construction material costs, in addition to the saving of construction time, but the Approach A design might end up with a compromised prolonged excavation time if the contingency plan is activated.

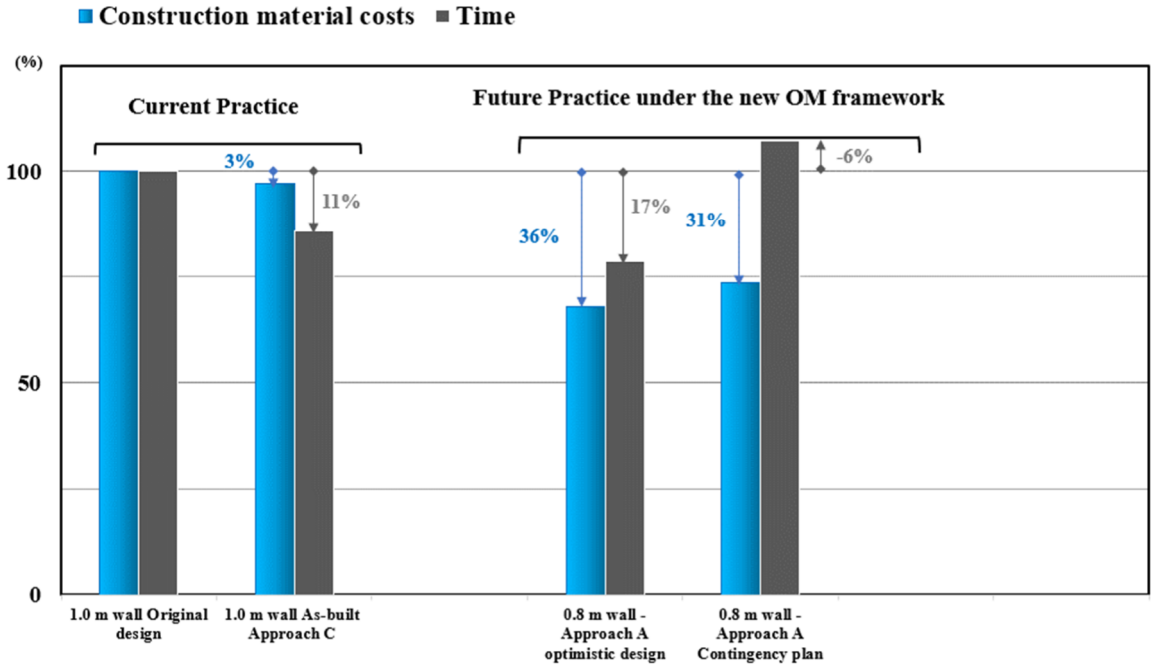

Figure 7. 5 Cost comparison of material costs and time costs by different designs for the TCR-WTH deep box excavation

This cost comparison has not considered the additional fees. For example, the administration fees (e.g. additional design and review) are subjected to the individual project arrangement, which is difficult to estimate.

Figure 7. 5 displays the cost comparison results in construction material costs and time costs. The as-built modified Approach C design represents the current best practice in the excavation. However, in order to achieve more cost-effective designs, Approach A under the new observational method framework would be a more attractive choice in future practices.

Chapter 8

Conclusions

8.1 Summary

The thesis establishes a new framework for the well-established observational method to provide practical guidance and promote the application of the method in deep excavation design.

Firstly, the literature review on the observational method and case histories identified several constraints that prevent the implementation of the method.

- Uncertainty in design parameters

Statistical terms like ‘most probable’ and ‘characteristic’ are used to describe methods of selecting design parameters for different analyses, however, the meaning of these terms in the Eurocode 7th Edition is hard to quantify when compared to their original statistical definitions.

- Accuracy and reliability of monitoring data

The successful application of the observational method relies on the most probable parameters which are calibrated from the back-analysis using field observations. Hence, the accuracy and reliability of the observations determine the performance of the back-analysis and the outcome of the calibrated most probable design parameters.

- Perception of risk

Uncertainty in construction projects can be managed through risk assessment and risk management (Nossan, 2006). The risk assessment comprises identifying the possible hazards, the potential damage and the possibility of these hazard occurring in the specific project. Although the management of risk for the observational method was proposed in the Ciria R185 (Nicholson *et al.*, 1999), including the tailored contingency plan and the traffic light trigger system to closely monitor the fieldwork, an acceptable level of risk is seldom easily agreed in a project.

- Increased fragmentation in the construction industry

Human factors have a significant impact on key performance indicators (KPIs) (Masurier *et al.*, 2006). As a consequence of the increased number of parties involved in the construction industry, additional barriers are also introduced in implementing the observational method.

The new observational method framework identifies four design approaches that clearly separates and rationalises the processes and their applications, including *Ab initio* Optimistic Approach A, *Ab initio* Cautious Approach B, *Ipso tempore* Proactive Approach C, *Ipso tempore* Reactive Approach D. Excavation case histories in which the observational method has been used, have been successfully categorised with this new framework.

The terminology of ‘characteristic’ and ‘most probable’ is retained in the new observational method framework to eliminate any confusion in identifying different sets of design parameters. An integrated probabilistic analysis would be required to support the statistical meaning of the design parameters, however, this is challenging and not practical for industrial design. Instead, the representative values of the characteristic design parameters are proposed to be derived (e.g. Mohr-Coulomb parameters) or calibrated using laboratory test data (e.g. BRICK parameters), and the representative values of the most probable design parameters are calibrated through back-analyses.

The literature review also covers the characteristic engineering features of London Clay in relation to the small strain range soil behaviours in a deep excavation. The knowledge of the soil behaviour has assisted in the selection of available soil constitutive models for the excavation analysis in London Clay. A better understanding of soil has also assisted in explanations of the analysis results for excavations in London Clay. The following characteristic engineering features of London Clay are discussed.

- Stratigraphy

The London Clay formation is a combination of biostratigraphy and lithological variations. King (1981) defined five divisions (A to E) from bottom to top of London Clay. The distribution of subdivisions is generally consistent laterally and vertically throughout the London Basin. However, discontinuity in the presence of some units and significantly different behaviour between these units (e.g. strength, stiffness, permeability) have caused uncertainty in the ground properties, hence, variations in the analysis results.

- Small strain stiffness

The strain range from 0.01% to 0.1% governs the movements in excavations (Burland, 1989). At a given very small strain level (e.g < 0.001%) the shear stiffness, G_{max} or G_o is considered as a constant. The shear stiffness G decreases non-linearly with increasing strain between the small and large strain range. Calibration of this degrading shear stiffness depends on laboratory and the in situ soil testing data from ground investigations. However, a gap has been found between laboratory tests and in situ field tests.

- Stress history and recent stress path

The shear stiffness of London Clay depends upon its stress history (Clayton and Heymann, 2001). In addition, soils behave differently if the direction in which they are strained changes (Atkinson *et al.*, 1990; Gasparre, 2005). This is particularly relevant to the analysis of excavations, where soil-structure interaction will introduce changes in stress paths, thus changes in the soil stiffness.

- Anisotropy

Anisotropy describes direction-dependent material properties. The anisotropy effects in soil strength and stiffness are reviewed for London Clay:

- Strength anisotropy

An increase in the degree of anisotropy with depth in London Clay is suggested by Nishimura *et al* (2007). Lower shear strength tends to occur when the principal stress direction $\alpha \approx 45°$ due to failure along pre-existing fissures, higher shear strength occurs at $\alpha \approx 90°$ (Nishimura *et al.*, 2007).

- Stiffness anisotropy

London Clay tends to deform more easily in the vertical direction of deposition than in the horizontal one (Wongsaroj, 2005; Gasparre, 2005; Gasparre *et al.*, 2007b; Yimsiri and Soga, 2011). The triaxial tests in London Clay using Bender elements showed strong

anisotropy at small strains, with E_H/E_V from 1.5 to 2.5 (Yimsiri and Soga, 2011), and G_{HH}/G_{VH} between 1.75 and 2.25 (Gasparre *et al.*, 2007).

The basic elastoplastic Mohr-Coulomb soil model was adopted to perform the back-analysis of the Crossrail excavation case histories. However, more accurate simulation of London Clay behaviour will need an advanced soil model. For instance, the BRICK model shows better performance in replicating triaxial tests on samples of the London Clay divisions, compared to another advanced soil model M3SKH (Ellison, 2012). As a comparison, the BRICK model was also applied in the back-analysis.

The initial input parameters in the back-analysis are either derived or calibrated from the available soil testing data, therefore, the quality of the testing data can affect the effectiveness of the iterative back-analysis process. For example, if the quality of testing data is poor and used to derive the initial input parameters in the back-analysis, more iterations may be needed to calibrate the most probable parameters, or the tolerance on the comparison of the back-analysis predictions and observations needs to be increased to reach the convergence of the analysis.

The back-analysis process was reviewed with respect to four important elements.

- Observations (monitoring data)

Observations are directly measured by data or indirectly interpreted calculations from the data. Depending on the accuracy and reliability of the data, observations are selected and applied in the back-analysis to compare with estimations from the analysis. The most probable soil models related parameters are then calibrated when the back-analysis meets the required convergence criterion.

A series of instruments used in monitoring the Crossrail project were reviewed, such as inclinometers, road levelling studs, extensometers, prisms with survey station, strain gauges, and piezometers. Review of these instruments and their measured data indicated that errors can be built into the data, and most of the errors can be eliminated through improved specifications for installation and data processing.

- Finite element numerical analysis method

More accurate predictions of soil/structure response depend on the numerical analysis method. Chapter 5 presents the Crossrail TCR-WTH deep box back-analysis with the Mohr-Coulomb model using three different levels of complexity in the numerical analysis, Pseudo-FE FREW, Plaxis 2D and LS-Dyna 3D, and different analysis results were then obtained. The pros and cons of each analysis are discussed in Chapter 5. For an excavation back-analysis, it

is suggested to consider the following factors in the selection of the appropriate analysis method, the agreed analysis method used in the original design, the appropriate soil constitutive model and the available observations with known accuracy for the back-analysis comparison.

- Soil constitutive model

The input design parameters in the numerical analysis are associated with the chosen soil constitutive model. The simple soil models require fewer input parameters, but their capacity is limited in predicting more soil/structure responses, and accuracy of the predictions is dependent on the chosen numerical analysis model. In contrast, the advanced soil models use more input parameters in order to accurately simulate complex soil behaviours and provide, in general, more accurate predictions. However, the calibration of the model related parameters for the advanced models is not easy, due to the availability of limited test data and the particular tests needed are not routine. For comparison, both the Mohr-Coulomb model and the BRICK model were selected for the back-analysis of the Crossrail excavations.

- Convergence criteria

A suitable convergence criterion for the back-analysis can improve the efficiency of this iterative process. The available optimisation algorithms were reviewed and it was found that the implementation of these methods was not easy due to the imperfection of actual construction. For example, additional construction activities can introduce excessive movements which will be recorded in the observations and lead to the poor performance of the back-analysis. In the Crossrail excavation back-analyses, engineering judgement is often required to interpret the analysis results.

A new observational method framework was proposed based on the thorough literature review, and the review of the Crossrail excavation case histories. The four design approaches under the new framework were discussed in respect to the applicable design parameters, design conditions and the operational procedures. A selection procedure was also proposed to assist in the selection of the appropriate design approach for an excavation project.

An example of the back-analysis using inclinometer data with the Mohr-Coulomb soil constitutive model was performed for the Crossrail TCR-WTH deep box excavation (Chapter 5). Results from the different numerical methods, Pseudo-FE FREW, Plaxis 2D and LS-Dyna 3D, were compared and discussed. The most probable Mohr-Coulomb parameters for the London Clay divisions were calibrated from the back-analysis and recommended in relation to the numerical analysis method. Validation of these parameters was performed in the other two Crossrail excavations, the plan-strain excavation example of the Paddington Station box

excavation, and 3D excavation (with length to width ratio <2.0) example of LIS-MS deep shaft excavation. In order to investigate the influence of the different soil models in the back-analysis, the BRICK model was applied in the back-analysis for the Crossrail TCR-WTH deep box excavation with LS-Dyna.

Finally, *Ab initio* Optimistic Approach A design was conducted to re-assess the Crossrail TCR-WTH deep box excavation. Cost comparison between the different designs showed the advantage of Approach A in the delivery of more cost-effective designs without compromising safety.

8.2 Main findings

8.2.1 New observational method framework

Previous excavations in which the observational method was used could be successfully categorised according to the new framework with four design approaches. This framework was accepted and included in the UK design code Ciria C760 (Gaba *et al.*, 2017), as a code of observational method practice providing alternative design options for the retaining structure design.

8.2.2 Most probable design parameters for London Clay

The most probable design parameters are required for the optimistic design in the observational method. Using inclinometer data, the back-analysis for the Crossrail excavations provided the calibrated representative values of the most probable Mohr-Coulomb parameters for the London Clay subdivisions (LC-A3 and LC-A2), and the calibrated representative values of the most probable BRICK parameters.

The most probable Mohr-Coulomb parameters are provided in relation to the numerical analysis method, as summarised in Table 6.2 (Pseudo-FE FREW), Table 6.5 (Plaixs 2D) and Table 6.7 (LS-Dyna 3D). It is recommended that undrained shear strength (c_u) values are derived from ground investigation data using the supervised statistical regression method, this is to maintain a level of consistency in the derivation of (c_u) values. The undrained soil horizontal stiffness (E_u) values are provided in empirical correlation with the undrained shear strength (c_u) values:

London Clay – A3 division (LC-A3):

E_u/c_u = 1600 ~ 1750 (Pseudo-FE FREW);

E_u/c_u = 1600 (Plaxis 2D);

E_u/c_u = 1600 (LS-Dyna 3D)

London Clay – A2 division (LC-A2):

E_u/c_u = 2000 (Pseudo-FE FREW);

E_u/c_u = 2000 (Plaxis 2D);

E_u/c_u = 1600 (LS-Dyna 3D)

The representative values of the most probable BRICK parameters for the London Clay are calibrated with LS-Dyna 3D and summarised in Table 6.10.

8.2.3 Gap between laboratory and in situ soil test data

The initial values of the model parameters for London Clay in the back-analysis were found to be conservative and they poorly predicted the wall deflections and other soil/ground responses. As these values were either derived from the ground investigation laboratory test data (Mohr-Coulomb model) or calibrated using laboratory triaxial test data (BRICK model), a concern is raised about the quality of laboratory test data. Coincidently, the calibrated representative values of the most probable model parameters were found in agreement with the field self-boring pressuremeter test.

The stress history and the recent stress path are proven to have a significant impact on the stiffness of overconsolidated London Clay. The laboratory soil tests were carried out on disturbed soil samples and were potentially also affected by the poor operation procedure (e.g. resolution of the test equipment). Therefore, laboratory test results might be less accurate and do not fully represent the soil in situ conditions, while the shear wave velocity and self-boring pressuremeter tests were performed in the field and their testing data can accurately reflect the in-situ soil conditions. Hence, the field test data might be more suitable to calibrate the model parameters for the performance-based back-analysis.

However, the initial values of the BRICK parameters did well in predicting the ground settlements with LS-Dyna 3D. Possibly, the anisotropy in soil stiffness is the reason for this performance.

8.2.4 Review monitoring data for the back-analysis

The importance of the observations in the back-analysis has been demonstrated and discussed in the Crossrail excavation case histories. The data review process including data acquisition, error diagnostic and error correction, is required in order to improve the accuracy and reliability of monitoring data. Enhancements in the specifications for the instrument installation and monitoring operation are also recommended.

Good understanding of instruments, monitoring data and the link to the construction and design analysis are the foundation for the enhanced specifications. For example, a unified terminology for different instruments will minimise misunderstandings around basic instrument information, like accuracy, resolution, precision and working conditions (range of measurement, temperature etc.). The cooperation between designers, monitoring contractors and clients at the early stage of the project might offer a way to resolve this issue.

Based on general accuracy and reliability in the data from the Crossrail project, the instruments are categorized as the primary instrument, inclinometer, and the secondary instruments including vibrating wire strain gauge, load cell, road levelling studs, vibrating wire piezometers, extensometers and the prisms with the survey station.

8.2.5 The smaller ratio of $\delta_{H,\,max}/H_e$ = 0.05% for the 3D excavation in London Clay with the stiff wall

The historical monitoring data from excavation in London Clay indicates that the maximum wall lateral displacements ($\delta_{H,\,Max}$) varies from 0.15% to 0.45% of the excavation depth (H_e) (St. John *et al.,* 1992; Gaba *et al.,* 2017), depending on the stiffness of the retaining structures. However, recent excavations in London Clay, like the Crossrail project, show much smaller wall movements during construction, due to the use of stiff retaining structures (e.g. diaphragm wall) and better-controlled excavation to meet the tighter movement criteria in urban areas.

Despite the variable thickness and length of diaphragm walls, and whether excavations were conducted with the top-down or bottom-up methods, the inclinometer data from the Crossrail project shows the maximum wall lateral displacement is about 0.05% of the excavation depth for a 3D excavation ($L/B \leq 2.0$). However, if the excavation involved a deep cantilever excavation stage earlier in the construction, this ratio can increase. For instance, in the Crossrail WS-DSS shaft excavation with the excavation length (L) over the width (B), $L/B < 2.0$, a ratio of $\delta_{H,\,max}/H_e$ = 0.08% is seen (Figure 3.30).

For a plane-strain excavation, the maximum wall lateral displacement increases. In the Crossrail PAD station box excavation, as an example, a higher ratio of $\delta_{H,\,max}/H_e = 0.10\%$ was observed on the central section of this over 260 m.

8.2.6 Cost-effective design by Approach A

Using the calibrated most probable Mohr-Coulomb parameters, the reassessment of the Crossrail TCR-WTH deep box excavation design by *Ab initio* Optimistic Approach A has been carried out. The cost comparison between the different designs for this excavation shows that the savings in construction material costs can be maximised. Potentially, time-saving is also possible if the contingency plan is not activated during construction.

8.2.7 Most probable design condition for excavation in London Clay

The excavation period for the Crossrail excavation case histories was found to vary between six months to twelve months. During this time, the back-analysis assumption of total stress analysis (undrained condition) tends to estimate the smaller wall deflections and agree with inclinometer data. However, when the excavation has proceeded for longer than a year or somehow was paused for more than a three-month period, a mixed-earth pressure analysis assumption (effective stress analysis on the active side and total stress analysis on the passive side), seems to perform better in the wall deflection prediction.

8.3 Suggestions for future research

This thesis explored some constraints in implementing the observational method. Work still needs to be done to improve the robustness of the back-analysis, so that more barriers can be removed to allow the implementation of the observational method. In addition, the application of the observational method could be extended to other soils. The research herein has also highlighted a few areas where improvements might be achieved.

- Back-analysis with the probabilistic approach

A probabilistic assessment of the numerical modelling results will enhance the robustness of the back-analysis. Jin (2018) presented an initial successful combination of the probabilistic analysis with Pseudo-FE FREW. The “supervised learning” uses a Monte-Carlo based probabilistic analysis to control the automated analysis with the FREW model, and results from a number of analyses are processed and presented with the statistical probability distribution

that indicates the confidence level of the outcomes from the back-analysis. In theory, there is no limit on the number of variables in this probabilistic analysis, but increasing the number of variables and therefore the complexity of the analysis, will greatly increase the computational time required to complete the analysis. However, if this probabilistic analysis can also work with other FEMs, such as Plaxis 2D and LSDyna 3D, the advantage of having the probabilistic analysis could lead to an automated and real-time back-analysis.

- A database of the excavation case histories

Developing a database of the excavation case histories is recommended. This will help to set up a standard procedure and standard criteria in collecting the required information for a good case history. Good quality case histories will enable the back-analysis and reassessment of the cases using the new observational method design approaches. Ultimately, this will promote the application of the observational method.

- Application of the observational method in other soils and other ground engineering design

Considering the potential benefits of the observational method, it is worthwhile to promote the application of the method into a broader range of practices. For instance, the application of the observational method could be extended to normally consolidated clay or even cohesionless soils. Meanwhile, the application of the observational method in other ground engineering has been reported before, such as tunnelling, embankment and ground improvement. Further study is required to develop suitable applications of the new observational method in these fields.

- Advanced soil constitutive model for over-consolidated soils

The review of the back-analysis for the Crossrail excavations with the Mohr-Coulomb and the BRICK models concluded that an advanced soil constitutive model is required to better describe the response of the overconsolidated soils, like London Clay. Although a better performing back-analysis is observed with the BRICK model than the Mohr-Coulomb model, in the back-analysis for the Crossrail excavations, some shortcomings of the BRICK model were also noted. For instance, in the simulation of triaxial tests, the BRICK model did not replicate the stress path curves very well. In addition, anisotropy in soil stiffness seems to affect the BRICK model in obtaining accurate predictions for both the wall deflections and the ground movements.

Alternatively, there are other advanced soil constitutive models available to model over-consolidated clay, such as the modified three-surface kinematic hardening model M3SKH (Grammatikopoulou, Zdravkovic and Potts, 2006), M3SKH with anisotropy (Ellison, 2012),

the hypoplastic model (Mašín, 2014), and the hardening soil model (Schanz *et al.* 1999). However, some of these advanced models are not accessible in available numerical analysis programs (e.g. Plaxis), and they may require careful calibration to derive the model related parameters.

Reference

Abaqus (2010) *Analysis user's manual. Vol I-IV*, *Pawtucket, USA*.

Addenbrooke, T. I., Puzrin, a. M. and Potts, D. M. (1997) 'The influence of pre-failure soil stiffness on the numerical analysis of tunnel construction', *Géotechnique*, 47(3), pp. 693–712. doi: 10.1680/geot.1997.47.3.693.

Agarwal, K.B. (1968) *The influence of size and orientation of sample on the undrained strength, London, PhD Thesis,* Imperial College, University of London, London, UK.

Aldiss, D., Burke, H., Chacksfield, B., Bingley, R. Teferle, N., Williams, S., Blackman, D. Burren, R. and Press N. (2014) Geological interpretation of current subsidence and uplift in the London area, UK, as shown by high precision satellite-based surveying, *Proceedings of the Geologists' Association*. The Geologists' Association. 125(1), pp. 1–13. doi: 10.1016/j.pgeola.2013.07.003.

Aldiss, D. T. (2012) *The stratigraphical framework for the Palaeogene successions of the London Basin, UK*. Available at: http://nora.nerc.ac.uk/17121/.

Allagnat, D. (2005) *La méthode observationnelle pour le dimensionnement interactif des ouvrages,* Presses de l'ecole nationale des Ponts et chaussees, Pairs. ISBN: 2-95978-409-8

Al-Tabbaa, A. & Wood, D. M. (1989) An experimentally based bubble model for clay. *Proceedings of International Symposium on Numerical methods in geomechanics*. NUMOG3, *Canada Elsevier* Applied Science, 91–99

Argyris, J.H., Faust, F., Szimat, J., Warnke, E.P., and William, K.J. (1974) Recent developments in the finite element analysis of prestressed concrete reactor vessels.

Nuclear Engineering and Design, pp.28

Arup & Partners (2007) *D18 – Report on Observational Method under the Framework of Eurocodes*, European Commission Sixth Framework Programme.

Atkinson, J. H. (1975) Anisotropic elastic deformations in laboratory tests on undisturbed London Clay, *Géotechnique*, 25(2), pp. 357-374. doi: 10.1680/geot.1975.25.2.357

Atkinson, J. H., Richardson, D. & Stabllebrass, S.E. (1990) Effect of stress history on the stiffness of overconsolidated soil, *Géotechnique*, 40(4), pp. 531-540. doi: 10.1680/geot.1990.40.4.531

Atkinson, J. H. (2000) Non-linear soil stiffness in routine design, *Géotechnique*, 50(5), pp. 487–508. doi: 10.1680/geot.2000.50.5.487.

Avgerinos, V. Ã., Potts, D. M. and Standing, J. R. (2016) The use of kinematic hardening models for predicting tunnelling-induced ground movements in London Clay, (2), pp. 106–120. doi: 10.1680/jgeot.15.P.035.

Batten, M., Powrie, W., Yu, H.T., Boorman, R., and Leiper, Q. (1999) Use of vibrating wire strain gauges to measure loads in tubular steel props supporting deep retaining walls, *Proceedings of the ICE - Geotechnical Engineering,* 137(11380), pp. 3–13.

Bauduin, C. (2001) Determination of characteristic values. Geotechnical Handbook – Volume 1: Fundamentals. Smoltczyk (Ed.). Berlin: Ernst & Sohn.

Bauduin, C. (2003) Uncertainties and their relevance for the design of deep excavations near existing structures, in *Proc. XIII ECSMGE Conf. 2003*, pp. 445–449.

Benz, T. (2007) *Small-Strain Stiffness of Soils and its Numerical Consequences*.

Benz,T., Vermeer, P.A. and Schwab, R. (2009) A small-strain overlay model, *International Journal for Numerical and Analytical Methods in Geomechanics*, 33(April 2008), pp. 25–44. doi: 10.1002/nag.701.

Bishop, A. W. (1954) The Use of Pore-Pressure Coefficients in Practice. *Géotechnique*, 4(4), pp. 148-152. doi: 10.1680/geot.1954.4.4.148.

Bishop, A. W. (1966) The Strength of Soils as Engineering Materials, *Géotechnique*, 16(2), pp. 91–130. doi: 10.1680/geot.1966.16.2.91.

Bologna, P. (2017) *Benchmarking empirical methods of prediction of ground movement for deep excavation*. *MSc. Dissertation,* University of Cambridge, Cambridge, UK.

Bond, A. J. (2011) 'A procedure for determining the characteristic value of a geotechnical parameter', in *Third International Symposium on Geotechnical Safety and Risk (ISGSR)*, pp. 419–426.

BRE (1993) *Monitoring building and ground movement by precise levelling*, Building

Research Establishment.

Brown, S., Lincoln, D., & Wallace, W. (1990) Application of Observational Method to Hazardous Waste Engineering. *Journal of Management in Engineering*, 6(4), 479-500.

Burland, J. B., B.Simpson and John, H. D. St. (1979) Movements around excavations in London Clay, in *The 7th European Conference on Soil Mechanics and Foundation Engineering*, pp. 13–29.

Burland, J. B. (1989) Ninth Laurits Bjerrum Memorial Lecture: "Small is beautiful" - the stiffness of soils at small strains, *Canadian Geotechnical Journal*, 26(4), pp. 499–516. doi: 10.1139/t89-064.

Burland, J. B. (1990) On the compressibility and shear strength of natural clays, *Géotechnique*, 40(3), pp. 329–378. doi: 10.1680/geot.1990.40.3.329.

Burland, J. B. and Standing, J. R. (2006) Unexpected tunnelling volume losses in the Westminster area, London, *Géotechnique*, 56(1), pp. 11–26. doi: 10.1680/geot.2006.56.1.11.

Brinkgreve, R. B. J., Engin, E. and Swolfs, W. M. (2016a) *PLAXIS 2016 3D Tutorial Manual 2016*, *Plaxis 2016*.

Brinkgreve, R. B. J., Engin, E. and Swolfs, W. M. (2016b) *PLAXIS 2D Reference Manual*, *Plaxis*.

British Geology Survey (2017), webpage visited on 5 October 2017. http://www.bgs.ac.uk/discoveringGeology/geologyOfBritain/iceAge/home.html?src=topNav

British Geographic Society (2017), webpage visited on 5 October 2017. http://www.rgs.org/OurWork/Schools/Teaching+resources/Key+Stage+3+resources/Glaciation+and+geological+timescales/London+-+its+geological+journey+and+heritage.htm

BSI (2004a) BS EN 1997-1: *Eurocode 7: Geotechnical design – Part 1: General rules and rules for buildings*. BSI (British Standard Institution), London, UK.

BSI (2004b) *UK National Annex to Eurocode 7: Geotechnical design Part 1: General rules*. BSI (British Standard Institution), London, UK.

BSI (2010) BS EN 1990:2002+A1: *Eurocode - Basis of structural design*. BSI (British Standard Institution), London, UK.

BSI (2014) BS EN 1992-1-1:2004 + A1:2014, *Eurocode 2: Design of concrete structures - Part 1 : General rules and rules for buildings*, *British Standard*. BIS (British Standard Institution), London, UK.

Calvello, M. (2002) *Inverse Analysis of a Supported Excavation through Chicago Glacial*

Clays. Evanston, Illinois.

Cañavate-Grimal, A., Falcó, A., Calderón, P. and Payá, I. (2015) On the use of stochastic spectral methods in deep excavation inverse problems, *Computers & Structures*, 159, pp. 41–60. doi: 10.1016/j.compstruc.2015.06.009.

Casagrande, A. & Carillo, N. (1944) Shear failure of anisotropic materials. *Journal of Boston Society of Civil Engineers*, 31, 74-87.

Casagrande, A. (1949) Soil Mechanics in the design and construction of the Logan Airport. *Journal of Boston Society of Civil Engineers*, 36(2), 192-221.

Chambers, P., Augarde, C., Reed, S. and Dobbins, A. (2016) Temporary propping at Crossrail Paddington station, *Geotechnical Research*, 3(1), pp. 3–16.

Chan, A.K.C. (2003) Observations for Excavations – A Reflection, Keynote Paper, *Proc. 23rd Annual Seminar*, HKIE Geot. Div.: 83-101.

Chandegra, M. and Kokkinou, A. (2016) 'Design of the Deep Cut and Cover Crossrail Paddington Station Using', *ICE publishing*.

Chen, Y., Nicolson P.D., Peter, I., Hardy, S., Liew, H.L., Farooq, I., and Biscontin, G. (2015) Application of the observational method on Crossrail project, *Proceedings of Crossrail: A Specialist Foundation Construction Lessons Learnt Conference, London,* UK. ICE (Institution of Civil Engineering) Publishing, pp. 63-72.

Chen, Y., Pillai, A.K., Nicolson, P.D., and Biscontin, G. (2018) Back analysis Crossrail deep excavations using three-dimensional finite element modelling, *Proceedings of 9th European Conference on Numerical Methods in Geotechnical Engineering, Porto,* Portugal.

CHSW (1996) *The Construction (Health, Safety and Welfare) Regulations 1996*.

Clarke, S. D. (2009) *Enhancement of the BRICK constitutive model to incorporate*. *PhD Thesis*, the University of Sheffield, Sheffield, UK. Available at: http://etheses.whiterose.ac.uk/id/eprint/158.

Cividini, A., Jurina, L., and Gioda, G. (1981) Some aspects of characterisation problems in geomechanics, *Rock Mechanics Mining Science & Geotechnics*, 18, pp. 487–503.

Clayton, C. R. I. (2001) *Managing geotechnical risk: Improving productivity in UK building and construction*, Department of the Environment, Transport and the Regions, Institution of Civil Engineers, Thomas Telford, London.

Clayton, C. R. I. and Heymann, G. (2001) Stiffness of geomaterials at very small strains, *Géotechnique*, 51(3), pp. 245–255. doi: 10.1680/geot.2001.51.3.245.

Clayton, C. R. I. (2011) Stiffness at small strain: research and practice, *Geotechnique*, 61(1),

pp. 5–37. doi: 10.1680/geot.2011.61.1.5.

Clements, D. (2010) *The Geology of London Introduction*. Geologist Association.

Clough, G. W. and O'Rourke, T. D. (1990) Construction induced movements of in situ walls', in *In Proceedings, Design and Performance of Earth Retaining Structures, ASCE Special Conference, Ithaca, New York*, pp. 439–470.

Coulomb, C.A. (1776) *Essai sur une application des regles des maximis et minimis a quelquels problemesde statique relatifs, a l'architecture. Memoires de mathematique et de physique. Presentes a l'Academie Royale des Sciences, Paris*. 7, pp. 343-382.

Contreras IA, Grosser AT and ver Strate RH. (2012) The use of the fully-grouted method for piezometer installation, Part 1 and Part 2. *Geotechnical Instrument News*, 30(2), pp. 20-25.

Cornforth, D. H. (2005) Landslides in Practice: Investigation, Analysis, and Remedial/ Preventative Options in Soils, John Wiley, New York.

Crossrail, 2007a. Settlement estimation procedure: Box Excavations & Shafts; internal references: 1D0101-G0G00-01004. London.

Crossrail, 2007b. Settlement estimation procedure: Phase 3 methodology for box excavations; internal references: 1D0101-G0G00-01019. London.

Crossrail, 2009a. Geotechnical Sectional Interpretative Report; Report 1&2: Royal Oak to Liverpool Street; internal references: 1D0101-G0G00-00549 to 551. London.

Crossrail, 2009b. Geotechnical Sectional Interpretative Report; Report 4: Isle of Dogs to Plumstead; internal references: 1D0101-C1G00-00520 to 522. London.

Crossrail, 2010a. Geotechnical Sectional Interpretative Report; Report 3: Liverpool Street to Pudding Mile Lane and Isle of Dogs; internal references: 1D0101-C1G00-00507 to 509. London.

Crossrail, 2010b. C134 – Tottenham Court Road Station, Geotechnical Design Report Part 2 Geotechnical Design Summary, internal references: C134-OVE-C2-RGN-N105-00003, revision 4.0. London.

Crossrail, 2011a. C130 – Paddington Station, Geotechnical Design Report Part 2 Geotechnical Design Summary, internal references: C130-SWN-C2-RGN-B071-500009. London.

Crossrail, 2011b. C138 – Liverpool Street Station, Geotechnical Design Report Part 2 Geotechnical Design Summary, internal references: C138-MMD-C2-RGN-C101-00008, revision 3.0. London.

Crossrail, 2011c. C40 – Whitechapel Station, Geotechnical Design Report Part 2

Geotechnical Design Summary, internal references: C140-HYD-C2-RGN-D061-00280, revision 4.0. London.

Crossrail, 2012a. C130 – Paddington Station, RIBA F - Geotechnical Design Report Part 2 Geotechnical Design Summary, internal references: C130-SWN-C2-RGN-B071-00004. London.

Crossrail, 2012b. C300/410 Western Tunnels & Caverns Project, Tottenham Court Road Western Ticket Hall, Instrumentation and Monitoring Proposals, internal reference: C300-BFK-C4-STP-CRT00_ST005-50008. London.

Crossrail, 2013a. Technical note for TCR-WTH box monitoring data; internal reference: C122-OVE-C4-RGN-N105-50003. London.

Crossrail, 2013b. Design package C122 Moorgate Shaft Permanent and Temporary works review - Dean Street Back-analysis to Level 5 report; internal reference: C122-OVE-C2-RGN-C101_OD017-50003. London.

Crossrail, 2013c. Tottenham Court Road Station, Civils Cost Estimation Stage D Report. October 2013, London

Crossrail, 2014a. C400/410 Western Tunnels & Caverns Project, Installation Report, Commissioning Report for the Installation of SAA (Shape Accel Array) In-Place-Inclinometers at Tottenham Court Road Western Ticket Hall South Box, internal reference: C300-BFK-C-STP-CRT00_ST005-50084, revision 4.0. London.

Crossrail, 2014b. C138 – Liverpool Street Station, C501 Moorgate Shaft – Verification Report, internal references: C138-MMD-C2-RGN-C101-50014, revision 4.0. London.

Crossrail, 2014c. C400/410 Western Tunnels & Caverns Project, Temporary Propping, general arrangement, southern box, Tottenham Court Road, Western Ticket Hall. August 2014, London

Crossrail, 2016. C405 Paddington Station, Final/Close-Out Monitoring Report for C405 Inclinometers, internal reference: C405-SKC-C2-LRC-B071_WS077-50041. London.

Damping, R. (2015) *FLAC 8 Basics*.

Darley, P., Carder, D.R., Ryley, M.D. and Hawkins, P.G. (1996) *Field evaluation of the TRL load cell pressuremeter*.

Darley, P., Carder, D. R. and Steele, D. P. (1999) *Field evaluation of the TRL load cell pressuremeter in Gault Clay*.

De Mello, V.F.B. (1977) Reflections on design decisions of practical significance to embankment dams: 17th Rankine Lecture, *Géotechnique*, 27 (3), pp281-355. doi: 10.1680/geot.1977.27.3.281.

Deegan, C.E. & Scull, B.J. (1977) *A standard lithostratigraphic nomenclature for the Central and Northern North Sea, Report No.77/25*, Institute of Geological Sciences, HMSO, London.

DIN 1054:2010-12 (2010) *Subsoil - Verification of the safety of earthworks and foundations - Supplementary rules to DIN EN 1997-1*, Safety of earthworks and foundations (Mirror Committee to CEN/TC 250/SC 7/PT1) at DIN.

Dong, Y. P., Burd, H., Houlsby, G. and Xu, Z.H. (2013) 3D FEM Modelling of a Deep Excavation Case History Considering Small-strain Stiffness of Soil and Thermal Shrinkage of Concrete, *7th International Conference on Case Histories in Geotechnical Engineering*, (3), p. # 3.28.b.

Dong, Y. (2014) *Advanced Finite Element Analysis of Deep Excavation Case Histories*, *Department of Engineering Science*. University of Oxford.

Dong, Y., Burd, H. J. and Houlsby, G. T. (2015) Finite element analysis of a deep excavation case history, *Géotechnique*, 66 (1), pp1-15. doi.org/10.1680/geot.14.P.234.

Dunnicliff, J. (1993) *Instrumentation for Monitoring Field Performance*. Wiley.

Dunnicliff, J. (2008) Geotechnical Instrument News – Discussion of 'The use of the fully-grouted method for piezometer installation' by Contreras *et al.* (2008). *Geotechnical News*, 26(2), pp. 38-40.

Dyvick, R. & Madshus, C. (1985) *Laboratory measurements of G_{max} using bender elements*, ASCE Convention, Detroit, Michigan.

Ellison, K. C. (2012) *Constitutive Modelling of a Heavily Overconsolidated Clay*. *PhD. Thesis*, University of Cambridge, Cambridge, UK.

Ellison, K. C., Simpson, B. and Soga, K. (2012) A strain space soil model with evolving stiffness anisotropy, *Géotechnique*, 62(7), pp. 627–641. doi: 10.1680/geot.10.P.095.

Ellison, R.A., Knox, R.W. O'B., Jolley, D.W. & King, C. (1994) A revision of the litho-stratigraphical classification of the early Palaeogene strata of the London Basin and East Anglia, *Proceedings of the Geologists' Association, Volume 105, Issue 3, pp 187-197*. http://doi.org/10.1016/S0016-7878(08)80118-6

Farooq, I., Place, D., Steele, B., Liew, H. and Victorino, S. (2015) An innovative verification process speeds construction of Crossrail's Moorgate shaft, *Geotechnics ICE*.

Fearnhead, N., Maniscalco, K., Standing, J.R. and Wan, M.S.P. (2014) Deep excavations: monitoring mechanisms of ground displacement, *Proceedings of the ICE - Geotechnical Engineering*, 167(2), pp. 117–129. doi: 10.1680/geng.13.00047.

Franzius, J. N., Potts, D. M. and Burland, J. B. (2005) The influence of soil anisotropy and K_0

on ground surface movements resulting from tunnel excavation, *Géotechnique*, 55(3), pp. 189–199. doi: 10.1680/geot.2005.55.3.189.

Finno, R. J., and Calvello, M. (2005) Supported Excavations: Observational Method and Inverse Modeling, *Journal of Geotechnical and Geoenvironmental Engineering.* 131(7), pp. 826–836. (ASCE)

Finno, R. J., Blackburn, J. T. and Roboski, J. F. (2007) Three-Dimensional effects for supported excavations in clay, *Journal of Geotechnical and Geoenvironmental Engineering*, 133(January), pp. 30–36. doi: 10.1061/(ASCE)1090-0241(2007)133:1(30).

Foye, K. C., Salgado, R. and Scott, B. (2006) Resistance Factors for Use in Shallow Foundation LRFD, *Journal of Geotechnical and Geoenvironmental Engineering*, 132(9), pp. 1208–1218. doi: 10.1061/(ASCE)1090-0241(2006)132:9(1208).

Fowler, M. and Meynink, P. S. (2013) Inclinometers - the good, the bad and the future, *Australian Centre for Geomechanics*, 41(December), pp. 21–24.

Fuentes, R., Pillai, A. and Devriendt, M. (2010) Short-term three-dimensional back-analysis of the One New Change basement in London, pp. 1–6. Available at: http://discovery.ucl.ac.uk/1318407/.

Fuentes, R. (2012) *Study of basement design, monitoring and back-analysis to lead to improved design methods*. *PhD. Thesis.* University of London, London, UK.

Gaba, A.R. (1990) *Jet grouting at Newton Station, 10th Southeast Asian Geotechnical Conference*, Taipei, Taiwan. pp 77-79.

Gaba, A.R., Simpson, B., Powrie, W. and Beadman, D.R. (2003) *Embedded retaining walls - guidance for design*. Report C580, *Proceedings of the ICE - Geotechnical Engineering* CIRIA, London. doi: 10.1680/geng.2003.156.1.13.

Gaba, A.R., Hardy, S., Doughty, L., Powrie, W. and Selemetas, D. (2017) *Guidance on embedded retaining wall design*. 1st edition, London: CIRIA. Available at: http://www.ciria.org.

Gaba, A.R. and Mcgowan, M. (2017) *The new CIRIA C760 Observational Method implementation framework and its potential application to projects in Singapore*.

Gardoni, P., Trejo, D., Vannucci, M. and Bhattacharjee, C. (2009) Probabilistic Models for Modulus of Elasticity of Self-Consolidated Concrete: Bayesian Approach', *Journal of Geotechnical and Geoenvironmental Engineering.* 135(4), pp. 295–306. (ASCE)

Gardoni, P., Reinschmidt, K. F. and Kumar, R. (2007) A Probabilistic Framework for Bayesian Adaptive Forecasting of Project Progress, *Computer-Aided Civil and*

Infrastructure Engineering, 22(3), pp. 182–196. doi: 10.1111/j.1467-8667.2007.00478.x.

Gasparre, A. (2005) *Advanced Laboratory*. *PhD. Thesis,* Imperial College, University of London, London, UK.

Gasparre, A. Nishimura, S. Minh, N.A. Coop, M.R. and Jardine, R.J. (2007a) The influence of structure on the behaviour of London Clay, *Géotechnique*, 57(1), pp. 19–31. doi: 10.1680/geot.2007.57.1.19.

Gasparre, A. Nishimura, S. Minh, N.A. Coop, M.R. and Jardine, R.J. (2007b) The stiffness of natural London clay, *Géotechnique*, 57(1), pp. 33–47. doi: 10.1680/geot.2007.57.1.33.

Gasparre, A. and Coop, M. R. (2008) Quantification of the effects of structure on the compression of a stiff clay, *Canadian Geotechnical Journal*, 45(9), pp. 1324–1334. doi: 10.1139/T08-052.

Gasparre, A., Hight, D.W., Coop, M.R. and Jardine, R.J. (2014) The laboratory measurement and interpretation of the small-strain stiffness of stiff clays, *Géotechnique*, 64(12), pp. 942–953. doi: 10.1680/geot.13. P.227.

Gens, A., Ledesma, A. and Alonso, E.E. (1996) Estimation of parameters in geotechnical back-analysis - II. Application to a tunnel excavation problem, *Computers and Geotechnics*, 18(1), pp. 29–46. doi: 10.1016/0266-352X (95)00022-3.

Gioda, G. & Maier, G. (1980) Direct search solution of an inverse problem in elastoplasticity: identification of cohesion, friction angle and in situ stress by pressure tunnels tests. *International Journal for Numerical Method in Engineering* (15), 1823-1848.

Glass, P. R. and Powderham, A. J. (1994) Application of the observational method at the Limehouse Link, *Géotechnique*, pp. 665–679. doi: 10.1680/geot.1994.44.4.665.

Goldberg, D.T., Jaworski, W.E., Gordon, M.D., 1976. Lateral support systems and underpinning: Volume 1, Design and construction, Federal Highway Administration Report FHWA RD-75-128.

Goh, A. T., Zhang, F., Liu, H.L., Zhang, W.G. and Zhou, D. (2016) Numerical analysis on strut responses due to one-strut failure for braced excavation in clays. doi: 10.1007/978-3-319-64861-3.

Gourvenec, S., Powrie, W. and De Moor, E. K. (2002) Three-dimensional effects in the construction of a long retaining wall, *Proceedings of the Institution of Civil Engineers-Geotechnical Engineering*, 155(January), pp. 163–173. doi: 10.1680/geng.2002.155.3.163.

Gouw, T. L. (2014) 'Common mistakes on the application of plaxis 2D in analyzing excavation problems', *International Journal of Applied Engineering Research*, 9(21), pp.

8291–8311.

Graham, J. and G.T. Houlsby (1983) Anisotropic elasticity of a natural clay, *Geotechnique*, 33(2), pp. 165–180.

Grammatikopoulou, A. (2004) Development, implementation and application of kinematic hardening models for overconsolidated clays. *PhD Thesis,* Imperial College, University of London, London, UK.

Grammatikopoulou, A., Zdravkovic, L. and Potts, D. M. (2006) General Formulation of Two Kinematic Hardening Constitutive Models with a Smooth Elastoplastic Transition, *International Journal of Geomechanics*, 6(5), pp. 291–302. doi: 10.1061/(ASCE)1532-3641(2006)6:5(291).

Grammatikopoulou, A., Zdravkovic, L. and Potts, D. M. (2008) The influence of previous stress history and stress path direction on the surface settlement trough induced by tunnelling, *Géotechnique*, 58(4), pp. 269–281. doi: 10.1680/geot.2008.58.4.269.

Hägglund Eriksson, M. (2014) *Accuracy and Precision Analysis of Total Station Measurements*. KTH Royal Institute of Technology, School of Architecture and the Built Environment. Available at: http://www.diva-portal.org/smash/record.jsf?pid=diva2%3A727374&dswid=-6931.

Hardin, B. O. and Black, W. L. (1968) Vibration Modulus of Normally Consolidated Clay, *Journal of Soil Mechanics & Foundations Div*, 94(SM 2), pp. 353–369. Available at: http://trid.trb.org/view.aspx?id=126917.

Hardin, B. O. and Black, W. L. (1969) Closure to Vibration Modulus of Normally Consolidated Clay, *Journal of Soil Mechanics & Foundations Div*, 95(SM 6), pp. 1531–1537. Available at: http://trid.trb.org/view.aspx?id=126917.

Hardy, S. (2015) Lies, damn lies, and statistics, *Anaesthesia*, 67(5), pp. 455–456. doi: 10.1111/j.1365-2044.2012.07133. x.

Hardy, S., Nicholson, D.P., Ingram, P., Gaba, A.R., Chen, Y. & Biscontin, G. (2017) New observational method framework and application, *Proceedings of the 19th International Conference on Soil Mechanics and Geotechnical Engineering*, *Seoul, Korea.* Tech Committee 207, pp1995–1998.

Hardy, S., Nicholson, D.P., Ingram, P., Gaba, A.R., Chen, Y. & Biscontin, G. (2018) New observational method framework for embedded walls, *Geotechnical Research*, 5(3):122-129. Doi.org/10.1680/jgere.18.00013

Hashash, Y. M., Marulanda, C., Ghaboussi, J. and Jung, S. (2003) Systematic update of a deep excavation model using field performance data. *Computers and Geotechnics*, 30,

pp. 477–488. doi: 10.1016/S0266-352X (03)00056-9.

Hight, D.W., Bennel, J.D., Chana, B., Davis, P.D., Jardine, R.J. & Porovic, E. (1997). Wave velocity and stiffness measurements of the crag and lower London tertiaries at Sizewell. *Géotechnique*, 47(3), pp. 451-474. doi: 10.1680/geot.1997.47.3.451

Hight, D. W., McMillan, F., Powell, J.J.M., Jardine, R.J. and Allenou, C.P. (2003) Some characteristics of London clay, in *Characterisation and engineering properties of natural soils*, pp. 851–907.

Hight, D. W., Gasparre, A., Nishimura, S., Minh, N.A., Jardine, R.J. and Copp, M.R. (2007) Characteristics of the London Clay from the Terminal 5 site at Heathrow Airport, *Géotechnique*, 57(1), pp. 3–18. doi: 10.1680/geot.2007.57.1.3.

HKGEO (2000) *Guide to retaining walls*, Geotechnical engineering office, Civil Engineering Department, The Government of the Hong Kong Special Administrative Region

Hommels, A., Molenkamp, F. and Heemink, A. W. (2005) Effectiveness of inverse modelling techniques applied in Geomechanics, in Patron (ed.) *Prediction, analysis and design in geomechanical applications. Bologna, Italy*. Bologna, pp. 49–56.

Houlsby, G. T. and Wroth, C. P. (1991) The variation of shear modulus of a clay with pressure and overconsolidation ratio, *1Soils and Foundations*, 31(3), pp. 138–143.

Houlsby, G. T. and Puzrin, A. M. (2001) Strain-based plasticity models for soils and the BRICK model as an example of the hyperplasticity approach, *Géotechnique*, 51(2), pp. 169–172. doi: 10.1680/geot.2001.51.2.169.

Houlsby, N. M. T. and Houlsby, G. T. (2013) Statistical fitting of undrained strength data, *Géotechnique*, 63(14), pp. 1253–1263. doi: 10.1680/geot.13.P.007.

Hsieh, P.G. and Ou, C.Y. (1998) Shape of ground surface settlement profiles caused by excavation, *Canadian Geotechnical Journal*, 35(6), pp. 1004–1017. doi: 10.1139/t98-056.

Hughes TJR and Hinton E, eds. (1986). Finite Element Methods for Plate and Shell Structures, two Volumes (Pineridge Press, Swansea, UK).

Hwang, R. N., Moh, Z. C. and Wang, C. H. (2007) Toe movements of diaphragm walls and correction of inclinometer readings, *Journal of GeoEngineering*, 2(2), pp. 61–71.

ICE Group (2015) Deep basement for Exhibition Road Building, Victoria and Albert Museum, London (Arup AL-A Wates Construction). *The 2015 Fleming Award competition, London.* Webpage visited on 22 April 2018. https://www.ice.org.uk/eventarchive/the-2015-fleming-award-competition

Ikuta, Y., Maruoka, M., Aoki, M. and Sato, E. (1994) Application of the observational

method to a deep basement excavated using the top-down method, *Géotechnique*, 44(4), pp. 655–679. doi: 10.1680/geot.1994.44.4.655.

Itmsoil (2018), webpage visited on 15 January 2018. http://soil.co.uk/products/strain-gauges/vibrating-wire-spot-weldable-strain-gauge/

Itasca (2012) *Fast Lagrangian Analysis of Continua in 3 Dimensions*.

Iwan, W. D. and Yoder, P. J. (1983) Computational aspects of strain-space plasticity, *Engineering Mechanics*, 109(1), pp. 231–243.

Jahangir, M. and Jagath, J. (1998) Application of artificial neural network and genetic algorithm in flow and transport simulations, *Advances in Water Resources*, 22(2), pp. 145–158. doi: 10.1016/S0309-1708(98)00002-5.

Jardine, R. J., Potts, D.M., Fourie, A.B. and Burland, J.B. (1986) Studies of the influence of non-linear stress-strain characteristics in soil-structure interaction, *Géotechnique*, 36(3), pp. 377–396. doi: 10.1680/geot.1986.36.3.377.

Jardine, R. J., Symes, N. J. and Burland, J. B. (1985) Discussion: The measurement of soil stiffness in the triaxial apparatus, *Géotechnique*, 35(3), pp. 378–382. doi: 10.1680/geot.1985.35.3.378.

Jardine, R. J. (1992) Some observations on the Kinematic nature of soil stiffness, *Soils and Foundations1*, 32(2), pp. 111–124.

Jardine, R. J. (2011) Characterization of mudrocks: a practical application of advanced laboratory testing, *Journal of Zhejiang University SCIENCE*, 12(1), pp. 1–14. doi: 10.1631/jzus.A1000420.

Jin, Y.Y. (2018) *Supervised Learning for Back Analysis of Excavations in the Observational Method. PhD. Thesis*, University of Cambridge.

Jovičić, V. and Coop, M. R. (1998) The measurement of stiffness anisotropy in clays with bender element tests in the triaxial apparatus, *Geotechnical Testing Journal*, 2(1).

Jovičić, V., Coop, M. and Simpson, B. (2006) Interpretation and modelling of deformation characteristics of a stiff North Sea clay, *Canadian Geotechnical Journal*, 43(4), pp. 341–354. doi: 10.1139/t06-007.

Juang, C. H., Luo, Z., Atamturktur, S. and Huang, H.W. (2012) Bayesian updating of soil parameters for braced excavations using field observations, *Journal of Geotechnical and Geoenvironmental Engineering*, 139(March), p. 495. doi: 10.1061/(ASCE)GT.1943-5606.0000782.

Juvinal, Robert C. & Marshek, Kurt. Fundamentals of machine component design. 2nd Edition. 1991, pp. 217, ISBN 0-471-62281-8

Korff, M. (2012) *Response of piled buildings to the construction of deep excavations PhD. Thesis*, University of Cambridge, Cambridge, UK.

King, C. (1981). The stratigraphy of the London Clay and associated deposits. *Tertiary Research Special Paper, No. 6. Rotter- dam*, Backhuys.

Lade, P.V. and Duncan, J.M. (1977). Elastoplastic stress-strain theory for cohesionless soil. *ASCE Journal of the Geotechnical Engineering Division, 101, pp. 1037– 1053.*

Ledesma, A., Gens, A. and Alonso, E. E. (1996) Estimation of parameters in geotechnical back-analysis I. Maximum likelihood approach, *Computers and Geotechnics*, 18(1), pp. 1–27. doi: 10.1016/0266-352X(95)00021-2.

Lee, J. R. (2011) Cool Britannia - from Milankovich wobbles to Ice Ages Cenozoic Ice Ages, a global perspective What causes Ice Ages? *Mercian Geologist*, 17(4), pp. 274–279.

Lehane, B. M. and Simpson, B. (2000) Modelling glacial till under triaxial conditions using a BRICK soil model, *Canadian Geotechnical Journal*, 37(5), pp. 1078–1088. doi: 10.1139/t00-032.

Leroueil, S. (1996) Compressibility of clays: fundamental and practical aspects, *Journal of Geotechnical Engineering*, 122(7), pp. 534–543. doi: 10.1061/(ASCE)0733-9410(1996)122:7(534).

Levasseur, S., Malecot, Y., Boulon, M., and Flavigny, E. (2008) Soil parameter identification using a genetic algorithm, *International Journal for Numerical and Analytical Methods in Geomechanics*, 32(March 2007), pp. 189–213. doi: 10.1002/nag.

Levasseur, S., Malecot, Y., Boulon, M., and Flavigny, E. (2009) Statistical inverse analysis based on genetic algorithm and principal component analysis: Method and developments using synthetic data, (February), pp. 1485–1511. doi: 10.1002/nag

Levesque, C., Danisch, L. and Patterson, T. (2017) Performance of a new installation method for SAA instrumented flexures, in *Proceedings of the 19th International Conference on Soil Mechanics and Geotechnical Engineering*, pp. 1903–1906.

Lings, M., Pennington, D. and Nash, D. F. T. (2000) Anisotropic stiffness parameters and their measurement in a stiff natural clay, *Géotechnique*, 50(2), pp. 109–125. doi: 10.1680/ssc.41080.0027.

Lipscombe, R., Carter, C., Perkins, O., Guerrero, S. and Thurlow, P. (2012) The Use of Shape Accel Arrays (SAAs) for Measuring Retaining Wall Deflection, *ICE*, pp. 1–15.

Likitlersuang, S., Surarak, C., Balasubramania, A., Oh, E., Syeung Ryull, K. and Wanatowski, D. (2013) Duncan-Chang - Parameters for Hyperbolic Stress Strain Behaviour of Soft Bangkok Clay, *Proc. 18th International Conference on Soil*

Mechanics and Geotechnical Engineering, 2-7 September 2013, Paris, pp. 381–384.

Lim, A. and Ou, C. Y. (2017) Stress paths in deep excavations under undrained conditions and its influence on deformation analysis, *Tunnelling and Underground Space Technology*, 63, pp. 118–132. doi: 10.1016/j.tust.2016.12.013.

Lim, A., Ou, C. Y. and Hsieh, P. G. (2010) Evaluation of clay constitutive models for analysis of deep excavation under undrained conditions, *Journal of GeoEngineering*, 5(1), pp. 9–20.

Lin, D. G. and Woo, S. M. (2007) Three dimensional analyses of deep excavation in Taipei 101 construction project, *Journal of GeoEngineering*, 2(1), pp. 29–42.

Livermore Software Technology Corporation (LSTC) (2018) *LS-DYNA Keyword User's Manual R11 Volume I/II/III*.

Love, A. (1944) *A treatise on the mathematical theory of elasticity*. 4th edition. Dover Publications Inc.

Long, M. A (2001) A case history of a deep basement in London Clay. *Computers and Geotechnics* 28(6-7), pp. 397-423.

Loveridge, F. (2001) Evaluation of prop loads at Channel Tunnel Rail Link Contract 430 - Ashford tunnels, *Ground Engineering*, (August), pp. 38–42.

Mair, R. J. (1993) Developments in geotechnical engineering research: application to tunnels and deep excavations, in *Unwin Memorial Lecture 1992*. Civil Engineering, pp. 27–41.

Mair, R. J. and Taylor, R. N. (1997) Bored tunnelling in the urban environment, *Proceedings of the 14th International Conference on Soil Mechanics and Foundation Engineering*. Balkema, pp. 2353–2362.

Machan, G. and Bennett, V. (2008) Use of inclinometers for geotechnical instrumentation on transportation projects, *Transportation Research*, (October).

Mašín, D. (2014) Clay hypoplasticity model including stiffness anisotropy, *Géotechnique*, 64(3), pp. 232–238. doi: 10.1680/geot.13. P.065.

Masurier, J. Le, Blockley, D. and Wood, D. M. (2006) An observational model for managing risk, *Proceedings of the ICE - Civil Engineering*, 159(6), pp. 35–40. doi: 10.1680/cien.2006.159.6.35.

Marefat, V., Duhaime, F., Robert, P.C. and Borgne, V.L. (2017) Fully grouted piezometers in a soft Champlain clay deposit Part I: Piezometer installation, *Geotechnical News*, 35(3), pp. 35–38.

Mathers, S. J., Burke, H.F., Terrington, R.L., Thorpe, S., Dearden, R.A., Williamson, J.P. and

Ford, J.R. (2014) A geological model of London and the Thames Valley, southeast England, *Proceedings of the Geologists' Association*. The Geologists' Association. 125(4), pp. 373–382. doi: 10.1016/j.pgeola.2014.09.001.

Mayne, P. W. and Kulhawy, F. H. (1982) K0 - OCR relationships in soil, *Journal of the Geotechnical Engineering Division (1982)*, 108(6), pp. 851–872. Available at: http://cedb.asce.org/cgi/WWWdisplay.cgi?34280.

Measurand (2013) *ShapeAccelArray manual*.

Measurand (2014) *SAA anti-rotational note*.

Measurand (2017) *Measurand software manuals: SAAView*.

Mikkelsen, P. E. (2003a) Advances in Inclinometer data analysis, in *Symposium on Field Measurements in Geomechanics, FMGM2003, Oslo, Norway, September*.

Mikkelsen, P. E. and Green, G. E. (2003b) Piezometers in fully Grouted Boreholes, *Field Measurements in Geomechanics*, 1, pp. 1–10.

Mills, C. (2016) Project in focus - Crossrail, Whitechapel Station, *Proceedings of the Basement and Underground Structures Conference*.

Minh, N. A. (2006) *An investigation of the anisotropic stress-strain-strength characteristics of an Eocene clay*. Imperial College London.

Miranda, T., Dias, D., Eclaircy-Caudron, S., Gomes Correia, A. and Costa, L. (2011) Back analysis of geomechanical parameters by optimisation of a 3D model of an underground structure, *Tunnelling and Underground Space Technology*, 26(6), pp. 659–673. doi: 10.1016/j.tust.2011.05.010.

Mitchell, J. K. (1960) Components of pore water pressure and their engineering significance, *Clays and Clay Minerals*, 9(1), pp. 162–184. doi: 10.1346/CCMN.1960.0090109.

Moreira, N., Miranda, T., Pinheiro, M., Fernandes, P., Dias, D., Costa, L. and Sena-Cruz, J. (2013) Back analysis of geomechanical parameters in underground works using an Evolution Strategy algorithm, *Tunnelling and Underground Space Technology*, 33, pp. 143–158. doi: 10.1016/j.tust.2012.08.011.

Ng, C. W., Lings, M.L., Simpson, B. and Nash, D.F.T. (1995) An approximate analysis of the three-dimensional effects of diaphragm wall installation, *Géotechnique*, 45(3), pp. 497–507. doi: 10.1680/geot.1995.45.3.497.

Ng, C. W. W. and Yan, R. W. M. (1999) Three-dimensional modelling of a diaphragm wall construction sequence, *Géotechnique*, 49(6), pp. 825–834. doi: 10.1680/geot.1999.49.6.825.

Ng, C. W., Simpson, B., Lings, M.L., and Nash, D.F.T. (1998) Numerical analysis of a

multipropped excavation in stiff clay. *Canadian Geotechnical Journal*, 25(1), pp. 115–130. doi: 10.1139/t97-074.

Nicholson, D., Cunningham G., Armstrong, A. and Boothman, J. (1998) Value achieved using the Observational Method on the retained cutting at the Batheaston/Swainswick Bypass, in *The Value of Geotechnics in Construction*, pp. 123–146.

Nicholson, D. Tse C. and Penny C. (1999) *The Observational Method in ground engineering: principles and applications*. Insitution of Civil Engineers (ICE). Caria, London, UK, Report R185.

Niemunis, A. and Herle, I. (1997) Hypoplastic model for cohesionless soils with elastic strain range, *Mechanics of Cohesive-Frictional Materials*, 2(4), pp. 279–299. doi: 10.1002/(SICI)1099-1484(199710)2:4<279:AID-CFM29>3.0.CO;2-8.

Nishimura, S., Jardine, R. J. and Minh, N. a. (2007) Shear strength anisotropy of natural London Clay, *Géotechnique*, 57(1), pp. 49–62. doi: 10.1680/geot.2007.57.1.49.

Nossan, A. S. (2006) Observations on the Observational Method, *XIII Danube-European Conference on Geotechnical Engineering*, pp. 171–178. Available at: http://bib.irb.hr/datoteka/270297.Observations_on_the_OM.pdf (Accessed: 01/12/2013).

Oasys (2008) GEO Suite for Windows, Oasys Ltd, Newcastle

Oasys (2010) *CEAP-Keyword appendix (Civil Engineering Application Program) based on LS-Dyna Version 940*.

Oasys (2014) *Safe 19.1 Manual*. Oasys Ltd.

Oasys (2017) *Frew 19.3 Help Guide*. Oasys Ltd.

Obrzud, R. F. (2010) On the use of the Hardening Soil Small Strain model in geotechnical practice, *Numerics in Geotechnics and Structures*, p. 16.

Osman, A., Yeow, Y. and Bolton, M. (2004) Estimation of undrained settlement of shallow foundations on London clay, *International conference on structural and foundation failures*, pp. 443–454. Available at: http://publications.eng.cam.ac.uk/327221/.

Ou, C.-Y., Chiou, D.-C. and Wu, T.-S. (1996) Three-dimensional finite element analysis of deep excavation, *J. Geotech. Engrg.*, 122(May), pp. 337–345.

Pantelidou, H. and Simpson, B. (2007) Geotechnical variation of London Clay across central London, *Géotechnique*, 57(1), pp. 101–112. doi: 10.1680/geot.2007.57.1.101.

Pantelidou, H. and Simpson, B. (2007) Geotechnical variation of London Clay across central London, *Géotechnique*, 57(1), pp. 101–112. doi: 10.1680/geot.2007.57.1.101.

Patel, D., Nicholson, D., Huybrechts, N. and Maertens, J. (2007) The Observational Method in Geotechnics, *Proceedings of the 14th ECSMGE: Madrid, Spain*, pp. 365–370.

Paul, J. D. (2016) Hing-resolution geological maps of central London, UK - Comparisons with the London Underground, *Geoscience Frontiers*. Elsevier Ltd, 7(2), pp. 273–286. doi: 10.1016/j.gsf.2015.05.004.

Peck, R. B. (1969a) Advantages and Limitations of the Observational Method in applied soil mechanics, *Géotechnique*, 19(2), pp. 171–187. doi: 10.1680/geot.1969.19.2.171.

Peck, R. B. (1969b) Deep excavations and tunnelling in soft ground, in *Proceedings of the 7th International Conference on Soil Mechanics and Foundation Engineering, State-of-the-Art-Volume, Mexico City*, p. 1969.

Pennington, D. S., Nash, D. F. T. and Lings, M. L. (2001) Horizontally mounted Bender Elements for measuring anisotropic shear Moduli in Triaxial clay specimens', *Geotechnical Testing Journal*, 24(2), pp. 133–144. doi: 10.1520/GTJ11333J.

Pillai, K.A. (1996) *Review of the BRICK model of soil behaviour, MSc. Dissertation,* Imperial College, University of London.

Pillai, K.A., Fuentes, R., Ferreira, P. and Swain, A. (2011) Back-analysis of a basement with a raft foundation in over-consolidated stiff clay, *Proceedings of 15th European Conference on Soil Mechanics and Geotechnical Engineering, Athens, Greece*. Available at: http://discovery.ucl.ac.uk/1323408/

PLAXIS (2016a) *PLAXIS General*.

PLAXIS (2016b) *PLAXIS 2016 2D Material Models Manual*.

Powderham, A. J. (1994) An overview of the observational method: development in cut and cover and bored tunnelling projects, *Géotechnique*, 44(4), pp. 619–636. doi: 10.1680/geot.1994.44.4.619.

Powderham, A. (2002) The observational method-learning from projects, *Proceedings of the ICE, Geotechnical Engineering, Vol.115, Issue*, 115(1), pp. 1–10.

Powderham, A. J. (2004) The Observational Method – Learning from Projects', in *Fifth International Conference on Case Histories in Geotechnical Engineering*, pp. 1–10.

Powrie, W. and Batten, M. (2000) Comparison of measured and calculated temporary-prop loads at Canada Water Station, *Géotechnique*, 50(2), pp. 127–140. doi: 10.1680/geot.2000.50.2.127.

Pohl, C. (2011) Determination of characteristic soil values by statistical methods, *International Symposium on Geotechnical Safety and Risk (ISGSR)*, pp. 427–434.

Preene, M., Roberts, T. and Powrie, W. (2016) *Groundwater control: design and practice, second edition*. Second Edi. London: CIRIA.

Richardson, D. (1988) *Investigations of threshold effects in soil deformations*, *City Research*

Online - City University London. doi: 10.1016/j.cpr.2010.02.004.

Richards, D. J., Holmes, G. and Beadman, D. R. (2001) Measurement of temporary prop loads at Mayfair car park, *Geotechnical Engineering*, 149(4), pp. 269–269. doi: 10.1680/geng.149.4.269.48652.

Roscoe, K. H. & Burland, J. B. (1968) On the generalised stress– strain behaviour of 'wet' clay. In Engineering plasticity (eds Heyman, J. & Leckie, F. A.), pp. 535–609. Cambridge: Cam- bridge

Royse, K. R., Freitas, M.D., Burgess, W.G., Cosgrove, J., Ghail, R., Gibbard, P., King, C., Lawrence, U., Mortimore, R.N., Owen, H. and Skipper, J. (2012) Geology of London, UK, *Proceedings of the Geologists Association*. The Geologists' Association. 123(1), pp. 22–45. doi: 10.1016/j.pgeola.2011.07.005.

R.Scantlebury, G.Brennan and M.Raiss (2014) Design of the new Crossrail station, Paddington, London', *The Structural Engineer*, January, pp. 12–18.

Ridley, A.M. (2017) Personal Communication.

Schanz, T., Vermeer, A. and Bonnier, P. (1999) The hardening soil model: formulation and verification, in *Beyond 2000 in computational geotechnics 10 years of PLAXIS International proceedings of the International Symposium beyond 2000 in Computational Geotechnics Amsterdam The Netherlands 1820 March 1999*, p. 281.

Shohet, D. C. (1995) Prediction of in Situ Horizontal Stresses in Clay Soils From the Measurement of Undrained Shear Strength, Plasticity Index and Vertical Effective Stress., *Proceedings of the ICE - Geotechnical Engineering*, 113(4), pp. 206–214. doi: 10.1680/igeng.1995.28016.

Schneider, H. R. (1997) Definition and determination of characteristic soil properties. Contribution to discussion session 2.3, *Proceedings of the 14th International Conference on Soil Mechanics and Foundation Engineering*. Hamburg, Balkema, pp. 2271–2274.

Schroeder, F.C. (2002) *The influence of bores piles on existing tunnels*. *PhD Thesis,* Imperial College, University of London, London, UK.

Schwamb, T., Soga, K., Mair, R.J., Elshafie, M.Z.E.B., Sutherden, R., Boquet, C. and Greenwood, J. (2014) Fibre optic monitoring of a deep circular excavation, *Proceedings of the ICE - Geotechnical Engineering*, 167(2), pp. 144–154. doi: 10.1680/geng.13.00036.

SCOUT. (2007) D18 Report on Observational Method under the Framework of Eurocodes. European Commission Sixth Framework Programme. Project no: 516290. Report ref no: SB. DTTAP-NOT-6.045. Arup Geotechnics.

Simeoni, L., Polo, F.D., Caloni, G. and Pezzetti, G. (2011) Field performance of fully grouted piezometers, in *Proc. of the 8th International Symposium on Field Measurements in Geomechanics*. Available at: http://www.geologimarche.it/wp-content/uploads/2013/11/GT11-S03_Simeoni.FMGM11.fullygrouted.pdf.

Simpson, B. (1992a) Development and application of a new soil model for prediction of ground movements, *Peter Wroth Memorial Conference, Oxford*. pp. 628–643

Simpson, B. (1992b) Retaining structures: displacement and design, *Géotechnique*, 42(4), pp. 541–576. doi: 10.1680/geot.1992.42.4.541.

Simpson, B., J.H., A. and V., J. (1996) The influence of anisotropy on calculations of ground settlements above tunnels, *Proc. Int. Symp. Geotechnical aspects of underground construction in soft ground, City University of London*, 2(1996), pp. 591–594.

Simpson B. (1999) Engineering needs, in *the Second International Symposium on the Pre-failure deformation characteristics of Geomaterials*.

Simpson, B. (2010) Engineering in stiff sedimentary clays, *Géotechnique*, 60(12), pp. 903–911. doi: 10.1680/geot.07.KP.002.

Simpson, B. (2012) Eurocode 7- fundamental issues and some implications for users, *Proceedings of the Nordic Geotechnical Meeting 2012*.

Simpson, B. (2017) Personal Communication.

Skempton, A.W. (1954) The Pore Pressure Coefficients A and B. *Géotechnique*, 4(4), pp.143-147. doi: 10.1680/geot.1954.4.4.143.

Sorensen, K., Baudet, B. and Simpson, B. (2007) Influence of structure on the time-dependent behaviour of a stiff sedimentary clay, *Geotechnique*, 57(1), pp. 113–124. doi: 10.1680/geot.2007.57.9.783.

Spross, J. (2014) A Critical Review of the Observational Method, *KTH Royal Institute of Technology*.

Stallebrass, S. E. (1990) *Modelling the effect of recent stress history on the deformation of overconsolidated soils*, *PhD. Thesis,* City University of London, London, UK. doi: 10.1016/j.cpr.2010.02.004.

Stallebrass, S. E. and Taylor, R. N. (1997) The development and evaluation of a constitutive model for the prediction of ground movements in overconsolidatcd clay', *Geotechnique*, 47(2), pp. 235–253.

Stanier, S. A., Blaber, J., Take, W.A. and White, D.J. (2016) Improved image-based deformation measurement for geotechnical applications, *Canadian Geotechnical Journal*, 53(5), pp. 727–739. doi: 10.1139/cgj-2015-0253.

Stroud, M. A. (1989) Standard penetration test - its application and interpretation, in *Penetration testing in the UK*. London: Thomas Telford, pp. 29–49.

Svoboda, T. and Mašín, D. (2008) Impact of a constitutive model on inverse analysis of a NATM tunnel in stiff clays, *Underground Facilities for Better Environment and Safety*, pp. 627–636.

Tang, Y.G. and Kung, G. T.C. (2009) Application of nonlinear optimization technique to back analyses of deep excavation, *Computers and Geotechnics*, 36(1), pp. 276–290.

Tann, L. von der (2014) *Uncertainties in subsoil horizontal deformation monitoring*, *Msc. Dissertation*, University College London.

Tatsuoka, F. (2001) Impacts on geotechnical engineering of several recent findings from laboratory stress-strain tests on geomaterials, *Geotechnics for roads, rail tracks and earth structures*, pp. 69–140. doi: 10.1017/CBO9781107415324.004.

Terzaghi, K. (1936) Relationship between soil mechanics and foundation engineering, *Proceeding of 1st International Conference Soil Mechanics and Foundation Engineering*, Graduate School of Engineering, Harvard University, pp 13-18.

Terzaghi, K. (1961) Past and future of applied soil mechanics, *Journal of the Boston Society of Civil Engineers*, 48(2), 110-139.

Terzaghi, K. & Peck, R.B. (1967) *Soil mechanics in Engineering Practice, 1st Edition*. John Wiley, New York.

Ti, K. S. (2009) A Review of Basic Soil Constitutive Models for Geotechnical Application, *Electronic Journal of Geotechnical Engineering*, 14. Available at: http://ejge.com/2009/Ppr0985/Ppr0985ar.pdf.

Tse, C. & Nicholson, D.P (1992) Design, Construction and Monitoring of the basement diaphragm wall at Minster Court, London. *Proceedings of the Conference on Retaining Structures, Cambridge,* ICE (Institution of Civil Engineers) Publishing, London, pp.323-332

Vahdati, P., Levasseur, S., Mattsson, H. and Knutsson, S. (2013) Inverse Mohr-Coulomb soil parameter identification of an earth and rockfill dam by genetic algorithm optimization, *Electronic Journal of Geotechnical Engineering*, 18 X, pp. 5419–5440.

Verruijt, A. (2001) *Soil mechanics*. Delft University of Technology. doi: 10.1038/143865a0.

Viggiani, G. (1992) *Small strain stiffness of fine grained soils*. City University of London. doi: 10.1016/j.cpr.2010.02.004.

Viggiani, G. (1992) *Small strain stiffness of fine-grained soils, PhD. Thesis*, City University of London, London, UK. doi: 10.1016/j.cpr.2010.02.004.

Viggiani, G. and Atkinson, J. H. (1995) Stiffness of fine-grained soil at very small strains, *Géotechnique*, 45(2), pp. 249–265. doi: 10.1680/geot.1995.45.2.249.

Vucetic. M. and Dobry, R. (1991) Effect of soil plasticity on cyclic response, Journal of Geotechnical Engineering, ASCE, Vol. 117, No. 1, pp. 89-107.

WALLAP (2017) *WALLAP version 6.0*.

Ward, W/H., Samuels, S.G. and Butler, M.E. (1959) Further studies of the properties of London Clay, *Géotechnique*, 9(2), pp. 33-58. doi: 10.1680/geot.1959.9.2.33.

Wehrens, R. and Buydens, L. M. C. (2006) Classical and Nonclassical Optimization Methods, *Encyclopedia of Analytical Chemistry*. doi: 10.1002/9780470027318.a5203.

White, F., Ingram, P., Nicholson, D.P. and Stroud, M. (2019) An update of the SPT-cu relationship proposed by M. Stroud in 1974. *Proceedings of the XVII European Conference on Soil Mechanics and Geotechnical Engineering*, *Reykjavik, Iceland*, 2019.

Whitman, R. V. (1984) Evaluating calculated risk in Geotechnical Engineering, *Journal of Geotechnical Engineering,* 110(2), pp. 143–188.

Whittle, A. J. and Kavvadas, M. J. (1994) Formulation of MIT-E3 constitutive model for overconsolidated clays, *Journal of Geotechnical Engineering*, 120(1), pp. 173–198. doi: 10.1061/(ASCE)0733-9410(1994)120:1(173).

Wan, M. S. P. and Standing, J. R. (2014a) Lessons learnt from installation of field instrumentation, *Proceedings of the ICE - Geotechnical Engineering*, 167(5), pp. 491–506. doi: 10.1680/geng.13.00054.

Wan, M. S. P. and Standing, J. R. (2014b) Field measurement by fully grouted vibrating wire piezometers, *Proceedings of the ICE - Geotechnical Engineering*, 167(6), pp. 547–564. doi: 10.1680/geng.13.00153.

Wood M.A. (1987) To NATM or not to NATM (Critical appraisal of New Austrain Tunnelling Method), Geocolloquium, Salzburg, October 1986, Felsbau V5, N1, 26-30.

Wongsaroj, J. (2005) *Three-dimensional finite element analysis of short-term and long-term ground response to open face tunnelling in stiff clay*, *PhD. Thesis,* Cambridge University.

Wongsaroj, J., Soga, K. and Mair, R. J. (2007) Modelling of long-term ground response to tunnelling under St James's Park, London, *Géotechnique*, 57(1), pp. 75–90. doi: 10.1680/geot.2007.57.1.75.

Wan, M.S.P. (2017). Personal Communication.

Yazdani, M., Daryabari, A., Farshi, A. and Talatahari, S. (2013) Application of Taguchi Method and Genetic Algorithm for calibration of soil constitutive models, *Journal of*

Applied Mathematics.

Yeow, H. (1994) *Loads on struts in excavations*, *Geotechnical Engineering*. London.

Yeow, H. C., Nicholson, D. P., and Simpson, B., (2006) Comparison and feasibility of three dimensional finite element modelling of deep excavations using non-linear soil models. *Proceedings of the international conference on numerical simulation of construction processes in Geotechnical Engineering for Urban Environment, 23-24 March 2006, Bochum, Germany,* pp. 467-474.

Yeow, HC. and Feltham, I. (2008) Case histories back analyses for the application of the Observational Method under Eurocodes for the SCOUT project, *Proceedings of the 6th international conference on case histories in Geotechnical Engineering, Arlington*, VA, pp. 1–13.

Yeow, H.C., Nicholson, D. P., Bryant, C., and Westbury, M. (2012) Achieving more for less at Canary Wharf Crossrail station, London, *Proceedings of the Civil Engineering Special Issue,* Vol. 165 (CE5), pp. 50–57. doi: 10.1680/cien.11.00039.

Yeow, H.C., Nicholson, D.P., Man, C.L., Ringer, A., Glass, P. and Black, M. (2014) Application of observational method at Crossrail Tottenham Court Road station, *Geotechnical Engineering*, Vol.167(GE2), pp. 182–193.

Yeow, H.C. and Coop, M. R. (2015) The Constitutive Modelling of London Clay, *Geotechnical Engineering*, XXXIII (2), pp. 81–87. doi: 10.1007/s13398-014-0173-7.2.

Yoder, P. J. (1980) *A strain-space plasticity theory and numerical implementation*. Pasadena, California.

Yimsiri, S. and Soga, K. (2001) Effects of Soil Fabric on Undrained Behavior of Sands, *International Conferences on Recent Advances in Geotechnical Earthquake Engineering and Soil Dynamics*, p. Paper 5.

Yimsiri, S. (2002) *Pre-failure deformation characteristics of soil: anisotropy and soil fabric. PhD. Thesis*, University of Cambridge, Cambridge, UK.

Yimsiri, S. and Soga, K. (2011) Cross-anisotropic elastic parameters of two natural stiff clays, *Géotechnique*, 61(9), pp. 809–814. doi: 10.1680/geot.9.P.072.

Young, D. K. and Ho, E. W. L. (1994) The observational approach to design of a sheet-piled retaining wall, *Géotechnique*, 44(4), pp. 637–654. doi: 10.1680/geot.1994.44.4.637.

Zdravkovic, L. and Jardine, R. J. (1997) Some anisotropic stiffness characteristics of a silt under general stress conditions, *Géotechnique*, 47(3), pp. 407–437. doi: 10.1680/geot.1997.47.3.407.

Zdravkovic, L., Potts, D. M. and John, H. D. S. (2005) Modelling of a 3D excavation in finite element analysis, *Géotechnique*, 55(7), pp. 497–513. doi: 10.1680/geot.2005.55.7.497.

Appendix A London Clay soil properties

The soil properties of the London Clay subdivisions for the Crossrail project were summarised in the Crossrail Geotechnical interpretative reports (Crossrail, 2009a). They were based on multiple site investigations in between 1992 and 2006. The soil properties comprise results from the laboratory classification tests, triaxial drained and undrained tests, 1D compression and swelling tests, permeability tests, and some field testing data.

Table A.1 presented the relevant soil properties for the London Clay divisions A3 and A2, these properties were linked to the back-analysis of the Crossrail deep excavation case histories.

Table A. 1 Soil properties for the London Clay subdivision LC-A3 & LC-A2

Parameters	**Unit**	**Unit A3**	**Unit A2**	**Remarks**
Classification				
Particle size < 0.002 mm < 0.06 mm < 2 mm < 60 mm	%	 43 to 74 84 to 100 100 100	 26 to 65 50 to 100 100 100	Test of the particle size distribution (PSD): identify grain size and categorise soil: clay, silt, sand, gravel and cobbles
Density bulk (ρ_b) Gs	 kN/m^3 -	 19.0 to 22.0 2.65	 19.0 to 22.0	Specific gravity G_s= mass of soil grain/mass of the equal volume of water
w p_L w_L	%	20 to 36 21 to 34 55 to 84	16 to 31 17 to 33 46 to 88	Atterberg limits vary vertically along with the London Clay profile, with respect to the height above the base of London Clay.
I_P I_L Plasticity chart	%	33 to 53 -0.3 to 0.2 CH to CV	23 to 57 -0.4 to 0.2 CI to CV	Plasticity chart classification (PI vs LL) indicates the plasticity of soil in clay (C) or silt (M): low, intermediate, high, very high and extremely high.
In situ field test				
SPT N CPT - q_c CPT- f_s	blow MN/m^2 MN/m^2	14+1.1z 2 to 9 0.1 to 0.4	14+1.1z - -	SPT N is converted design line from the interpretative report. z = 0 at top of LC, increase downwards. No CPT penetrated into the LC-A2 unit.
Undrained shear strength				

Parameters	Unit	Unit A3	Unit A2	Remarks
$S_{u,100}$ $S_{u,SBP}$ $S_{u,SPT}$ $S_{u,CPT}$	kN/m^2	75+5.5z 80 to 550 80 + 6.3z 50 to 400	75+ 5.5z 200 to 480 80+6.3z	$S_{u,100}$ design line from triaxial test results by U100 samples. z = 0 at top of LC; $S_{u,SBP}$ increase with depth; $S_{u,SPT}$ is converted from S_u/ N =5.7; $S_{u,CPT}$ is converted from N_k = 20, $S_{u,CPT}=q_{net}/N_k$.
Drained shear strength				
c'$_P$	kN/m^2	39.5 (C) 35.0 - 90.5 (B) (58.4) 4.0 – 47.0 (A3) (25.0) 9.5 – 72.5 (A2) (44.7)		Effective cohesion at peak (average value), from shear box testing data.
c'	kN/m^2	0 - 15 (C) 0 - 25 (B) 0 - 60 (A3) 0 – 75 (A2)		Effective cohesion c' varies with mean effective stress, from triaxial testing data.
ϕ'$_p$ ϕ'$_r$ ϕ' ϕ'f	∘	19.5 (C) 16.0 – 22.0 (B) (19.4) 18.0 – 26.5 (A3) (23.0) 20.0 – 28.5 (A2) (24.0) 13.4 (C) 11.6 (B) 11.9 (A3) 13.8 (A2) 20 (C / B / A3) 23 (A2) 20 (C/ B / A3/ A2)		Effective angle of shearing resistance at peak (average value), from shear box testing data. Residual friction angles are from the best-fit line to all the data, assuming c'= 0 kN/m^2, from shear box testing data. Effective angle of shearing resistance, from triaxial testing data. Fissure strength, from triaxial testing data.

Parameters	Unit	Unit A3	Unit A2	Remarks
ϕ'_{cv}		-		Critical state effective angle of shearing resistance, a value between the peak and the residual angles.
Large strain stiffness				
E'_v	MN/m^2	15 +1.1 z 12.6+1.0z	15+1.1z 12.6+1.0z	$E'_v/S_{u,100}$ = 200 (Stroud, 1989), $S_{u,100}$ = design line; E'_v/ SPT N = 0.9 (Stroud, 1989) at a load level of 10% of ultimate capacity (q_{net}/q_{ult}=0.1).
Small strain stiffness (strain dependent stiffness)				
E_u/p'_0 (ε_a=0.01%)		250 to 1500 (C / B/ A3) 400 to 1650 (A2) 400 to 1000 (C/ B/ A3) 500 to 1500 (A2)		Triaxial compression Triaixal extension
E_u/p'_0 (ε_s=0.01%)		750 to 2500 (C/B/ A3) 1000 to 2000 (A2)		Self-boring pressurementer testing data
Stiffness from 1D compression and swelling tests (corresponding stress ranges)				
c_c		0.386 (A3) (12-20 MPa)		Compression index;
c_s		0.12 (C) (150–400 kPa) 0.10 (B) (125-250 kPa) 0.102 (A3) (200-400 kPa) 0.081 (A2) (200-400 kPa)		Swelling index
c_r		0.035 (B) (180-255 kPa) 0.032 (A3) (150-250 kPa)		Recompression index.

Parameters	Unit	Unit A3	Unit A2	Remarks
		0.028 (A2) (430 –600 kPa)		
Permeability				
k_v k_h	m/s	10^{-12} to 10^{-9} 10^{-11} to 10^{-9}	10^{-12} to 10^{-10} 10^{-10} to 10^{-6}	The vertical permeability is based oedometer test, and the horizontal permeability is based on variable head tests.
In-situ horizontal stress coefficient – K_0				
K_0	1.0 1.5	K_0 design value for Crossrail, it has been determined by various methods (Mayne and Kulhawy, 1982, Shohet, 1995) and in situ self-boring testing data (Darley *et al.*, 1996, Darley *et al.*, 1999). For the section of Farrington Station to Liverpool Street Station only.		

Appendix B LS-Dyna 3D back-analysis for TCR-WTH input 'key' files

The LS-Dyna 3D model is executed by the computer commend lines in a 'key' file. The keyword files for the TCR-WTH deep box back-analysis at the last iteration were presented in Appendix B, including the additional boundary control files to enable the 3D modelling. Following are the listed keyword files:

1. Mohr-C.key;
2. Initial_Stresses_V2.txt;
3. Dewater.txt;
4. BRICK_I4.key; and
5. ne.k.txt – this was the generated finite element mesh for the TCR-WTH, including nodes, elements (solid/beam/shell) and boundary nodes. It was due to the size of files, over 5001662 numbers of nodes and the consequent elements, this file was excluded in Appendix B.

Mohr-C.key

```
*KEYWORD 200000000
$>
$> Primer14.0 created on: Fri Oct 20 09:48:35 2017
$> LS-DYNA version: R9.0
$>
$> model title: TCR_WTH_deep box (South box)_Mohr-Coulomb model
$>
$
$Stage 1- Initalisation
$
$CONSTRUCTION SEQUENCE
$ 1 - Initialisation with under-drained pwp profile
$ 2 - Construct DWalls & capping beam & wish in place 1.8mDIA piles
$ 3 - S/Box: Ex1 to 121.6mATD
$ 4 - S/Box: Install P1 at 122.4mATD and Ex2 to 115.975mATD
$ 5 - S/Box: Install P2 at 118.7mATD (corner) and 117.2mATD and Exc3 to 111.1mATD
$ 6 - S/Box: Install P3 at 112.0mATD and Exc4 to 107.84mATD
$ 7 - S/Box: Install P4 at 109.1mATD and Exc5 to 101.2mATD
$ 8 - S/Box: (INSTALL P5 AT 102.0MATD - NOT APPLIED) Exc6 to 97.0mATD
$
$ 9 - S/Box: Excavate to +96.3mATD(bottom of the base slab), and construct Base slab (S/Box: top level 98.27mATD)
$10 - S/Box: (Install Level -5 raking props and remove horizontal propping at P5 - NOT APPLIED)
$11 - S/Box: Remove P4
$12 - S/Box: (Remove raking props at Level -5 - NOT APPLIED) Install slab Level -3 at 109.1mATD
$13 - S/Box: Remove P3
$14 - S/Box: Install slab Level -2 at 114.4mATD and Level -4 at 102.0mATD
$
$15 - N/Box: Ex1 to 121.6mATD
$16 - S/Box: Remove P2 at 118.7mATD (corner) and install horizontal P2 at 117.2mATD
$17 - N/Box: Install P1 at 122.4mATD and Ex2 to +116.4mATD
$18 - N/Box: Cut down dividing DWall to 113.87mATD, install P2 at 117.2mATD and Ex3 to 112.7mATD
$19 - N/Box: Excavate to +112.0mATD (bottom of the base slab), and construct Level -2 slab at +114.4mATD(S/Box), Base slab (N/Box: top level 113.8mATD)
$20 - Remove P2
$21 - Install slab Level -1 at 119.7mATD
$22 - Remove P1
$23 - Install roof slab Level 0 at 125.0mATD
$
$
$ ASSUMPTIONS
$ South base slab = 1.97m (top at +98.27 and bottom at +96.3) and North base slab = 1.8m (top at +113.87 and bottom at +112)
$ 3D model is based on the As-built record
$ Temporaray propping is confirmed as the As-built information (4 levels of props for the S/Box)
$ Levels are as rounded to 1dp or nearest whole number to simplify the mesh
$ THE EXISTING BUILDINGS AND TUNNELS AROUND AND UNDER THIS SITE HAVE NOT BEEN MODELLED. NO SURCHARGES HAVE BEEN APPLIED - TBC ?
$ The top of the perimeter capping beam has been assumed to be at ground level, 125.0mATD.
$ No capping beam on the dividing wall.
$ Capping beam modelled as a 1m wide and 1.5m high continuous element, with isotropic stiffness.
$ No installation effects considered
$ Young's modulus of the 1m thick diaphragm wall: Ey = Ez = 33 GPa and Ex= 5.6 GPa (in-plane axis), mu=0.2
$ No lining walls modelled
$ Internal slabs modelled as 700mm thick continuous shell elements without internal openings (50% stiffness of structural concrete),
```



```
assumed weightless
$ Bottom slabs modelled as solid elements.
$ Top slab level is at +124.4mATD
$ Temporary props modelled as beam elements; thrust blocks as nodal restraints.
$ Waling beams are to be modelled as shell elements with appropriate stiffness.
$ 50mm slip elements adjacent to the perimeter walls and around the piles account for the disturbance effects during installation of structural elements
$ Undrained conditions during construction have been modelled with unlimited suction.
$ Long term drained conditions have not been modelled.
$
$ GENERAL COMMENTS
$ Mohr-Coloumb Model parametes are applied for all soil strategraphy
$
$
$ =============
$ INCLUDE cards
$ =============
$
*INCLUDE
C:\Analysis\TCR\INC\ne.k
$
*INCLUDE
C:\Analysis\TCR\INC\Initial_Stresses_V2.txt
$
*INCLUDE
C:\Analysis\TCR\INC\Dewater.txt
$
$
$ =============
$ CONTROL cards
$ =============
$
*CONTROL_OUTPUT
         1         3         0         0       0.0         0
         0         0
*CONTROL PORE FLUID
$water table at 120.0mOD
         2       0.0     120.0       1.0      10.0 2200000.0
         1       1.0
       0.0       0.0       0.0       0.0       0.0       0.0
       0.0       0.0
*CONTROL_SOLID
         1         0         0         0         0       0.0
         0
*CONTROL_STAGED_CONSTRUCTION
$               STGS      STGE      GRAV      FACT
       0.0         1         9      10.0    1.0E-6         0
         0         0
*CONTROL TIMESTEP
       0.0       0.8         0       0.0   -2.5E-4       111
         0         0
$
$
$ ==============
$ DATABASE cards
$ ==============
$
*DATABASE RCFORC
    5.0E-4         0         0         0
*DATABASE BINARY_D3PLOT
       0.5         0         0         0         0
*DATABASE BINARY_D3THDT
    5.0E-4         0
*DATABASE_EXTENT BINARY
$additional history variables (PWP is Solid Extra 2)
         1         0         0         1         0         0
         0         0
         0         1         0         0         0         0
```

```
          0         0
          0         0       0.0         0         0         0
          0         0         0
*DATABASE FORMAT
          0         1
$
$
$ ====================
$ MAT (Material) cards
$ ====================
$
*MAT MOHR COULOMB
$Mohr-Coulomb material - Made Ground(Drained) - phi=27, E'=46000
$top @ +125mATD, bottom at +121.6mATD
$      MID        RO      GMOD       RNU     BLANK       PHI
CVAL       PSI
          1       2.0   18400.0      0.25              0.4712
          1.0E-3       0.0
$    Blank   NPLANES     BLANK    LCCPDR     LCCPT    LCCJDR
LCCJT    LCSFAC
          0         0                   0         0         0
          0         0
$   GMODDP    GMODGR    LCGMEP   LCPHIEP   LCPSIEP    LCGMST
CVALGR     ANISO
      125.0       0.0         0         0         0       0.0
      0.0       0.0
$
*MAT MOHR COULOMB
$Mohr-Coulomb material - River Terrace Deposits - phi=42,E'=101000
$top @ +121.6mATD, bottom at +117.2mATD
$      MID        RO      GMOD       RNU     BLANK       PHI
CVAL       PSI
          2       2.1   40400.0      0.25               0.733
          1.0E-3       0.0
$    Blank   NPLANES     BLANK    LCCPDR     LCCPT    LCCJDR
LCCJT    LCSFAC
          0         0                   0         0         0
          0         0
$   GMODDP    GMODGR    LCGMEP   LCPHIEP   LCPSIEP    LCGMST
CVALGR     ANISO
      121.6       0.0         0         0         0       0.0
      0.0       0.0
$
*MAT MOHR COULOMB
$Mohr-Coulmb material - London Clay Layer A3i(Drained),phi'=22, E'=
92400+17500*Z
$top @ +117.2mATD, bottom at +112mATD
$      MID        RO      GMOD       RNU     BLANK       PHI
CVAL       PSI
          3       2.0   40200.0      0.15               0.384
          1.0E-3       0.0
$    Blank   NPLANES     BLANK    LCCPDR     LCCPT    LCCJDR
LCCJT    LCSFAC
          0         0                   0         0         0
          0         0
$   GMODDP    GMODGR    LCGMEP   LCPHIEP   LCPSIEP    LCGMST
CVALGR     ANISO
      117.2   -7596.5         0         0         0       0.0
      0.0       0.0
$
*MAT MOHR COULOMB
$Mohr-Coulmb material - London Clay Layer A3ii(Drained),phi'=22,
E'183000+17500*Z
$top @ +112mATD, bottom at +106mATD
$      MID        RO      GMOD       RNU     BLANK       PHI
CVAL       PSI
          4       2.0   79700.0      0.15               0.384
          1.0E-3       0.0
$    Blank   NPLANES     BLANK    LCCPDR     LCCPT    LCCJDR
LCCJT    LCSFAC
          0         0                   0         0         0
          0         0
```



```
$   GMODDP    GMODGR    LCGMEP   LCPHIEP   LCPSIEP    LCGMST
CVALGR     ANISO
      112.0   -7596.5         0         0         0       0.0
      0.0       0.0
$
*MAT MOHR COULOMB
$Mohr-Coulmb material - London Clay Layer A2(Drained),phi'=24, E'=
323000+141000*Z
$top @ +106ATD, bottom at +94.5mATD
$      MID        RO      GMOD       RNU     BLANK       PHI
CVAL       PSI
          5       2.1  141000.0      0.15               0.4189
          1.0E-3       0.0
$    Blank   NPLANES     BLANK    LCCPDR     LCCPT    LCCJDR
LCCJT    LCSFAC
          0         0                   0         0         0
          0         0
$   GMODDP    GMODGR    LCGMEP   LCPHIEP   LCPSIEP    LCGMST
CVALGR     ANISO
      106.0  -10530.4         0         0         0       0.0
      0.0       0.0
$
*MAT MOHR COULOMB
$Mohr-Coulmb material - Lambeth Group Layer UMB(Drained),phi'=28,c'=
10, E'=539000+11200*Z
$top @ +94.5ATD, bottom at +86mATD
$      MID        RO      GMOD       RNU     BLANK       PHI
CVAL       PSI
          6       2.1  234000.0      0.15               0.4887
          10.0       0.0
$    Blank   NPLANES     BLANK    LCCPDR     LCCPT    LCCJDR
LCCJT    LCSFAC
          0         0                   0         0         0
          0         0
$   GMODDP    GMODGR    LCGMEP   LCPHIEP   LCPSIEP    LCGMST
CVALGR     ANISO
       94.5   -4870.0         0         0         0       0.0
       0.0       0.0
$
*MAT MOHR COULOMB
$Mohr-Coulmb material - Lambeth Group Layer LMB(Drained),phi'=28,c'=
10, E'=674000
$top @ +86ATD, bottom at +78mATD
$      MID        RO      GMOD       RNU     BLANK       PHI
CVAL       PSI
          7       2.1  293000.0      0.15               0.4887
          10.0       0.0
$    Blank   NPLANES     BLANK    LCCPDR     LCCPT    LCCJDR
LCCJT    LCSFAC
          0         0                   0         0         0
          0         0
$   GMODDP    GMODGR    LCGMEP   LCPHIEP   LCPSIEP    LCGMST
CVALGR     ANISO
       86.0       0.0         0         0         0       0.0
       0.0       0.0
$
*MAT MOHR COULOMB
$Mohr-Coulmb material - Lambeth Group Layer UF(Drained),phi'=33, E'=
196800+4320
$top @ +86ATD, bottom at +78mATD
$      MID        RO      GMOD       RNU     BLANK       PHI
CVAL       PSI
          8       2.1   82000.0       0.2               0.576
          0.0       0.0
$    Blank   NPLANES     BLANK    LCCPDR     LCCPT    LCCJDR
LCCJT    LCSFAC
          0         0                   0         0         0
          0         0
$   GMODDP    GMODGR    LCGMEP   LCPHIEP   LCPSIEP    LCGMST
CVALGR     ANISO
       78.0   -1800.0         0         0         0       0.0
       0.0       0.0
```

```
$
*MAT_MOHR_COULOMB
$
$Mohr-Coulmb material - Lambeth Group Layer UF(Drained),phi'=33, E'=
196800+4320
$top @ +75ATD, bottom at +70mATD
$      MID        RO      GMOD       RNU     BLANK       PHI
CVAL       PSI
         9       1.9   83300.0       0.2              0.6632
         1.0E-3       0.0
$    Blank   NPLANES     BLANK    LCCPDR     LCCPT    LCCJDR
LCCJT    LCSFAC
         0         0                   0         0         0
         0         0
$   GMODDP    GMODGR    LCGMEP   LCPHIEP   LCPSIEP    LCGMST
CVALGR     ANISO
       75.0       0.0         0         0         0       0.0
       0.0       0.0
*MAT ELASTIC
$Concrete (Bearing Piles & solid base slab)
         10       2.4     2.8E7       0.2       0.0       0.0
         0.0
$
*MAT ORTHOTROPIC ELASTIC
$Linear Elastic - D-wall
$      MID        RO         EA         EB         EC      PRBA
PRCA       PRCB
         11       2.4 6600000.0     3.3E7     3.3E7       0.2
         0.2       0.2
$       GAB        GBC        GCA       AOPT         G      SIGF
    1.32E7    1.32E7 2600000.0       3.0    1000.0       1.0
         0.0       0.0       0.0       0.0       0.0       0.0
         0       0.0
         0.0       0.0       1.0       0.0       0.0       0.0
         0.0       0.0
$
*MAT ELASTIC
$Capping beam
         12       2.4     3.3E7       0.2       0.0       0.0
         0.0
$
*MAT_MOHR_COULOMB
$Slip_MG (Drained), phi=27, E'=46000
$Reduce strength to tan.phi'/ 2 (in Rads)
$      MID        RO      GMOD       RNU     BLANK       PHI
CVAL       PSI
         13       2.0   18400.0      0.25              0.2495
         1.0E-3       0.0
$    Blank   NPLANES     BLANK    LCCPDR     LCCPT    LCCJDR
LCCJT    LCSFAC
         0         0                   0         0         0
         0         0
$   GMODDP    GMODGR    LCGMEP   LCPHIEP   LCPSIEP    LCGMST
CVALGR     ANISO
       0.0       0.0         0         0         0       0.0
       0.0       0.0
$
*MAT_MOHR_COULOMB
$Slip_RTD (Drained), phi=42,E'=101000
$Reduce strength to tan.phi'/ 2 (in Rads)
$      MID        RO      GMOD       RNU     BLANK       PHI
CVAL       PSI
         14       2.1   40400.0      0.25               0.423
         1.0E-3       0.0
$    Blank   NPLANES     BLANK    LCCPDR     LCCPT    LCCJDR
LCCJT    LCSFAC
         0         0                   0         0         0
         0         0
$   GMODDP    GMODGR    LCGMEP   LCPHIEP   LCPSIEP    LCGMST
CVALGR     ANISO
       0.0       0.0         0         0         0       0.0
       0.0       0.0
```



```
$
*MAT MOHR COULOMB
$Slip LC A3i (Undrained) Cu= 75+15.6, Eu=1600 Cu
$Reduce strength to 0.5Cu
$Strata 5m thick, top @ 117mATD
$      MID        RO      GMOD       RNU     BLANK       PHI
CVAL       PSI
         15       2.0   20000.0       0.2              1.0E-3
         37.5       0.0
$    Blank   NPLANES     BLANK    LCCPDR     LCCPT    LCCJDR
LCCJT    LCSFAC
         0         0                   0         0         0
         0         0
$   GMODDP    GMODGR    LCGMEP   LCPHIEP   LCPSIEP    LCGMST
CVALGR     ANISO
      117.2   -4426.7         0         0         0       0.0
      -8.3       0.0
$
*MAT MOHR COULOMB
$Slip LC A3ii (Undrained), Cu= 156.1+15.6, Eu=1600 Cu
$Reduce strength to 0.5Cu
$Strata 6m thick, top @ 112mATD
$      MID        RO      GMOD       RNU     BLANK       PHI
CVAL       PSI
         16       2.0   43000.0       0.2              1.0E-3
         80.66       0.0
$    Blank   NPLANES     BLANK    LCCPDR     LCCPT    LCCJDR
LCCJT    LCSFAC
         0         0                   0         0         0
         0         0
$   GMODDP    GMODGR    LCGMEP   LCPHIEP   LCPSIEP    LCGMST
CVALGR     ANISO
      112.0   -4426.7         0         0         0       0.0
      -8.3       0.0
$
*MAT MOHR COULOMB
$Slip LC A2 (Undrained), Cu= 200+17.5, Eu=2000 Cu
$Reduce strength to 0.5Cu
$Strata 12m thick, top @ 106mATD
$      MID        RO      GMOD       RNU     BLANK       PHI
CVAL       PSI
         17       2.1   70000.0       0.2              1.0E-3
         105.0       0.0
$    Blank   NPLANES     BLANK    LCCPDR     LCCPT    LCCJDR
LCCJT    LCSFAC
         0         0                   0         0         0
         0         0
$   GMODDP    GMODGR    LCGMEP   LCPHIEP   LCPSIEP    LCGMST
CVALGR     ANISO
      106.0   -5766.7         0         0         0       0.0
      -8.65       0.0
$
*MAT MOHR COULOMB
$Slip LG UMB (Undrained),Cu= 280+6.4Pa, Eu=2500 Cu
$Reduce strength to 0.5Cu
$      MID        RO      GMOD       RNU     BLANK       PHI
CVAL       PSI
         18       2.1  117000.0       0.2              1.0E-3
         140.0       0.0
$    Blank   NPLANES     BLANK    LCCPDR     LCCPT    LCCJDR
LCCJT    LCSFAC
         0         0                   0         0         0
         0         0
$   GMODDP    GMODGR    LCGMEP   LCPHIEP   LCPSIEP    LCGMST
CVALGR     ANISO
       94.5   -2666.7         0         0         0       0.0
       -3.2       0.0
$
*MAT MOHR COULOMB
$Slip LG LMB (Undrained), Cu= 350kPa, Eu=2500 Cu
$Reduce strength to 0.5Cu
$      MID        RO      GMOD       RNU     BLANK       PHI
```

```
CVAL       PSI
        19       2.1  146000.0       0.2              1.0E-3
        175.0         0.0
$    Blank   NPLANES     BLANK    LCCPDR     LCCPT    LCCJDR
LCCJT    LCSFAC
         0         0                  0         0         0
         0         0
$   GMODDP    GMODGR    LCGMEP   LCPHIEP   LCPSIEP    LCGMST
CVALGR     ANISO
       0.0       0.0         0         0         0       0.0
       0.0       0.0
$
*MAT MOHR COULOMB
$Slip LG UF (Drained), E'=196800, Phi'=33 deg
$Reduce strength to tan.phi'/ 2 (in Rads)
$      MID        RO      GMOD       RNU     BLANK       PHI
CVAL       PSI
        20       2.0   82000.0       0.2               0.314
        1.0E-2       0.0
$    Blank   NPLANES     BLANK    LCCPDR     LCCPT    LCCJDR
LCCJT    LCSFAC
         0         0                  0         0         0
         0         0
$   GMODDP    GMODGR    LCGMEP   LCPHIEP   LCPSIEP    LCGMST
CVALGR     ANISO
      78.0   -1800.0         0         0         0       0.0
       0.0       0.0
$
*MAT ELASTIC
$Steel (Wailing beam 2No.UB686*254*170kg/m, P1 level)
        21    0.3335    1.07E8       0.2       0.0       0.0
        0.0
$
*MAT ELASTIC
$Steel (Girder Props 2NoUB533*210*109kg/m, P1 level)
        22    0.2139     2.1E8       0.2       0.0       0.0
        0.0
$
*MAT ELASTIC
$Concrete slabs- weightless and 50% stiffness of concrete (28e6 kPa)
        23       2.4     1.4E7       0.2       0.0       0.0
        0.0
$
*MAT ELASTIC
$Steel (CHS 1220, t=25, P2-horizontal)
        24    0.7228     2.1E8       0.2       0.0       0.0
        0.0
$
*MAT ELASTIC
$Steel (CHS 1067, t=16, P1)
        25    0.4068     2.1E8       0.2       0.0       0.0
        0.0
$
*MAT ELASTIC
$Steel (Wailing beam 2No.UB914*419*343kg/m, P2/P3/P4 level)
        26     0.673    1.76E8       0.2       0.0       0.0
        0.0
$
*MAT ELASTIC
$Steel (CHS 1420, T=23, P2-Corner)
        27    0.7773     2.1E8       0.2       0.0       0.0
        0.0
$
*MAT ELASTIC
$Steel (NONE)
        28      1.35     2.1E8       0.2       0.0       0.0
        0.0
$
*MAT ELASTIC
$Steel (Girder Props 2NoUB610*305*179kg/m, P2/P3level)
        29    0.3512     2.1E8       0.2       0.0       0.0
        0.0
```



```
$
*MAT ELASTIC
$Steel (NONE)
        30    0.7228     2.1E8       0.2       0.0       0.0
        0.0
$
*MAT ELASTIC
$Steel (CHS 1520, t=30, P3-Corner)
        31    1.0814     2.1E8       0.2       0.0       0.0
        0.0
$
*MAT ELASTIC
$Steel (CHS 1420, t=25, P3-Horizontal near the shallow box)
        32    0.8437     2.1E8       0.2       0.0       0.0
        0.0
$
*MAT ELASTIC
$Steel (CHS 1420, t=40, P4-Corner)
        33    1.3354     2.1E8       0.2       0.0       0.0
        0.0
$
$
$
$ =============
$ SECTION cards
$ =============
$
*SECTION BEAM
$Grade S355 CHS Props-1016 DIA, 16mm thickness
$P1 horizontal + corner props
$      SID    ELFORM      SHRF   QR/IRID       CST     SCOOR
NSM
         6         1       0.0       2.0       1.0       0.0
         0.0
$      TS1       TS2       TT1       TT2
     1.067     1.067     1.035     1.035       0.0       0.0
$
$
$ Steel props - 2No.UB 533*210*109kg/m, P1 level
$ P1 girder props at corners next to north box
         8         2       0.0       2.0       1.0       0.0
         0.0
$         a       iss       itt       irr        sa       ist
(Resultant beam)
   1.39E-2  6.682E-4  2.943E-5   1.78E-6       0.0       0.0
$
$
$Grade S355 CHS Props-1220 DIA, 25mm thickness
$P2 horizontal props
$      SID    ELFORM      SHRF   QR/IRID       CST     SCOOR
NSM
         9         1       0.0       2.0       1.0       0.0
         0.0
$      TS1       TS2       TT1       TT2
      1.22      1.22      1.17      1.17       0.0       0.0
$
$
$Grade S355 CHS Props-1420 DIA, 23mm thickness
$P2 corner props & P3 horizontal props
$      SID    ELFORM      SHRF   QR/IRID       CST     SCOOR
NSM
        10         1       0.0       2.0       1.0       0.0
         0.0
$      TS1       TS2       TT1       TT2
      1.42      1.42     1.374     1.374       0.0       0.0
$
$
$Grade S355 CHS Props-1520 DIA, 30mm thickness
$P3 corner props
$      SID    ELFORM      SHRF   QR/IRID       CST     SCOOR
NSM
        11         1       0.0       2.0       1.0       0.0
```

```
404          0.0
405  $      TS1       TS2       TT1       TT2
406        1.52      1.52      1.46      1.46       0.0       0.0
407  $
408  $
409  $ Steel props-2No.UB610*305*179kg/m
410  $ P2/P3 girder props at corners next to north box
411           12         2       0.0       2.0       1.0       0.0
              0.0
412  $         a       iss       itt       irr        sa       ist
     (Resultant beam)
413     2.28E-2   1.53E-3  1.141E-4    3.4E-6       0.0       0.0
414  $
415  $
416  $Grade S355 CHS Props-1420 DIA, 25mm thickness
417  $P3 horizontal props
418  $      SID    ELFORM      SHRF   QR/IRID       CST     SCOOR
     NSM
419           13         1       0.0       2.0       1.0       0.0
              0.0
420  $      TS1       TS2       TT1       TT2
421        1.42      1.42      1.37      1.37       0.0       0.0
422  $
423  $
424  $Grade S355 CHS Props-1420 DIA, 40mm thickness
425  $P4 corner props
426  $      SID    ELFORM      SHRF   QR/IRID       CST     SCOOR
     NSM
427           14         1       0.0       2.0       1.0       0.0
              0.0
428  $      TS1       TS2       TT1       TT2
429        1.42      1.42      1.34      1.34       0.0       0.0
430  $
431  $
432  $Grade S355 CHS Props-1220 DIA, 25mm thickness
433  $P2 horizontal props
434  $      SID    ELFORM      SHRF   QR/IRID       CST     SCOOR
     NSM
435           16         1       0.0       2.0       1.0       0.0
              0.0
436  $      TS1       TS2       TT1       TT2
437        0.61      0.61     0.585     0.585       0.0       0.0
438  $
439  $
440  $Grade S355 CHS Props-1220 DIA, 25mm thickness
441  $P2 horizontal props
442  $      SID    ELFORM      SHRF   QR/IRID       CST     SCOOR
     NSM
443           18         1       0.0       2.0       1.0       0.0
              0.0
444  $      TS1       TS2       TT1       TT2
445        0.61      0.61     0.585     0.585       0.0       0.0
446  $
447  $
448  $Grade S355 CHS Props- 1016 DIA, 16mm thickness
449  $P1 horizontal + corner props
450  $      SID    ELFORM      SHRF   QR/IRID       CST     SCOOR
     NSM
451           19         2       0.0       2.0       1.0       0.0
              0.0
452  $      TS1       TS2       TT1       TT2
453     2.28E-2   1.53E-3  1.141E-4    3.4E-6       0.0       0.0
454  $
455           20         1       0.0       2.0       1.0       0.0
              0.0
456        1.42      1.42      1.37      1.37       0.0       0.0
457  $
458           21         1       0.0       2.0       1.0       0.0
              0.0
459        1.42      1.42      1.34      1.34       0.0       0.0
460  $
461  *SECTION_SHELL
```



```
462  $Dwall (1m thick)
463           3         16       0.0          0       0.0       0.0
              0          0
464         1.0        1.0       1.0        1.0       0.0       0.0
            0.0          0
465  $
466  $
467  $Capping Beam (Assumed 1m thick, 1.5m high)
468           4         16       0.0          0       0.0       0.0
              0          0
469         1.0        1.0       1.0        1.0       0.0       0.0
            0.0          0
470  $
471  $
472  $Wailing Beams- Steel beam in 1.66m width from centre of the wall-P1
     level
473  $Thickness based on equivalent EI and EA to real section
474           5         16       0.0          0       0.0       0.0
              0          0
475         1.0        1.0       1.0        1.0       0.0       0.0
            0.0          0
476  $
477  $
478  $Permenant structural slabs- 700mm thick
479           7         16       0.0          0       0.0       0.0
              0          0
480         0.7        0.7       0.7        0.7       0.0       0.0
            0.0          0
481  $
482  *SECTION SOLID
483  $Single integrated soil
484           1          1         0
485  $
486  $
487  $Fully_integrated_soil_solids
488           2          2         0
489  $
490  $
491  $
492  $ ===============
493  $ HOURGLASS cards
494  $ ===============
495  $
496  *HOURGLASS
497           1          4       0.0          0       0.0       0.0
              0.0        0.0
498  $
499  $
500  $ ==========
501  $ PART cards
502  $ ==========
503  $
504  *PART
505  $HMNAME COMPS     101MG
506  $HWCOLOR COMPS     101       3
507  MG
508         101          2         1         0         0         0
              0          0
509  $
510  *PART
511  $HMNAME COMPS     102RTD
512  $HWCOLOR COMPS     102       4
513  RTD
514         102          1         2         0         0         0
              0          0
515  $
516  *PART
517  $HMNAME COMPS     103LC_A3i
518  $HWCOLOR COMPS     103       5
519  LC_A3i
520         103          1         3         0         0         0
              0          0
```

```
$
*PART
$HMNAME COMPS     104LC_A3ii
$HWCOLOR COMPS     104       6
LC_A3ii
         104         1         4         0         0         0
           0         0
$
*PART
$HMNAME COMPS     105LC_A2
$HWCOLOR COMPS     105       7
LC_A2
         105         1         5         0         0         0
           0         0
$
*PART
$HMNAME COMPS     106LG_UMB
$HWCOLOR COMPS     106       8
LG_UMB
         106         1         6         0         0         0
           0         0
$
*PART
$HMNAME COMPS     107LG_LMB
$HWCOLOR COMPS     107       9
LG_LMB
         107         1         7         0         0         0
           0         0
$
*PART
$HMNAME COMPS     108LG_LMB_UF
$HWCOLOR COMPS     108      13
LG_LMB_UF
         108         1         8         0         0         0
           0         0
$
*PART
$HMNAME COMPS     109Ts
$HWCOLOR COMPS     109      17
Ts
         109         1         9         0         0         0
           0         0
$
*PART
$HMNAME COMPS     110S_MG_Ex1
$HWCOLOR COMPS     110      20
S_MG_Ex1
         110         2         1         0         0         0
           0         0
$
*PART
$HMNAME COMPS     112S_RTD_Ex2
$HWCOLOR COMPS     112      24
S_RTD_Ex2
         112         1         2         0         0         0
           0         0
$
*PART
$HMNAME COMPS     113S_LC_A3i_Ex2
$HWCOLOR COMPS     113      25
S_LC_A3i_Ex2
         113         1         3         0         0         0
           0         0
$
*PART
$HMNAME COMPS     114S_LC_A3i_Ex3
$HWCOLOR COMPS     114      28
S_LC_A3i_Ex3
         114         1         3         0         0         0
           0         0
$
*PART
```



```
$HMNAME COMPS     115S_LC_A3i Ex3.1
$HWCOLOR COMPS     115      29
S_LC_A3i Ex3.1
         115         1         3         0         0         0
           0         0
$
*PART
$HMNAME COMPS     116S_LC_A3ii_Ex4
$HWCOLOR COMPS     116      33
S_LC_A3ii Ex4
         116         1         4         0         0         0
           0         0
$
*PART
$HMNAME COMPS     117S_LC_A3ii_Ex5
$HWCOLOR COMPS     117      35
S_LC_A3ii Ex5
         117         1         4         0         0         0
           0         0
$
*PART
$HMNAME COMPS     118S_LC_A2 Ex5
$HWCOLOR COMPS     118      37
S_LC_A2 Ex5
         118         1         5         0         0         0
           0         0
$
*PART
$HMNAME COMPS     119S_LC_A2 Ex6
$HWCOLOR COMPS     119      40
S_LC_A2 Ex6
         119         1         5         0         0         0
           0         0
$
*PART
$HMNAME COMPS     120S_Piles LC_A2
$HWCOLOR COMPS     120      41
S_Piles LC_A2
         120         1         5         0         0         0
           0         0
$
*PART
$HMNAME COMPS     121S_P-Slip LC_A2
$HWCOLOR COMPS     121      44
S_P-Slip LC_A2
         121         1         5         0         0         0
           0         0
$
*PART
$HMNAME COMPS     122S_Piles LG_UMB
$HWCOLOR COMPS     122      48
S_Piles LG_UMB
         122         1         6         0         0         0
           0         0
$
*PART
$HMNAME COMPS     123S_P-Slip LG_UMB
$HWCOLOR COMPS     123      49
S_P-Slip LG_UMB
         123         1         6         0         0         0
           0         0
$
*PART
$HMNAME COMPS     124S_Piles LG_LMB
$HWCOLOR COMPS     124      52
S_Piles LG_LMB
         124         1         7         0         0         0
           0         0
$
*PART
$HMNAME COMPS     125S_P-Slip LG_LMB
$HWCOLOR COMPS     125      53
```

```
S_P-Slip LG_LMB
       125         1         7         0         0         0
         0         0
$
*PART
$HMNAME COMPS     126S_Piles LG_UF
$HWCOLOR COMPS     126      56
S_Piles LG_UF
       126         1         8         0         0         0
         0         0
$
*PART
$HMNAME COMPS     130S_Inner MG_Ex1
$HWCOLOR COMPS     130      60
S_Inner MG_Ex1
       130         2         1         0         0         0
         0         0
$
*PART
$HMNAME COMPS     132S_Outer MG
$HWCOLOR COMPS     132      64
S_Outer MG
       132         2         1         0         0         0
         0         0
$
*PART
$HMNAME COMPS     133S_Inner_RTD_Ex2
$HWCOLOR COMPS     133       3
S_Inner RTD_Ex2
       133         1         2         0         0         0
         0         0
$
*PART
$HMNAME COMPS     134S_Outer_RTD
$HWCOLOR COMPS     134       4
S_Outer RTD
       134         1         2         0         0         0
         0         0
$
*PART
$HMNAME COMPS     135S_Inner_LC_A3i_Ex2
$HWCOLOR COMPS     135       5
S_Inner LC_A3i_Ex2
       135         1         3         0         0         0
         0         0
$
*PART
$HMNAME COMPS     136S_Inner_LC_A3i_Ex3
$HWCOLOR COMPS     136       6
S_Inner LC_A3i_Ex3
       136         1         3         0         0         0
         0         0
$
*PART
$HMNAME COMPS     137S_Inner_LC_A3i_Ex4
$HWCOLOR COMPS     137       7
S_Inner LC_A3i_Ex4
       137         1         3         0         0         0
         0         0
$
*PART
$HMNAME COMPS     138S_Outer_LC_A3i
$HWCOLOR COMPS     138       8
S_Outer LC_A3i
       138         1         3         0         0         0
         0         0
$
*PART
$HMNAME COMPS     139S_Inner_LC_A3ii_Ex4
$HWCOLOR COMPS     139       9
S_Inner LC_A3ii_Ex4
       139         1         4         0         0         0
```



```
         0         0
$
*PART
$HMNAME COMPS     140S_Inner LC_A3ii_Ex5
$HWCOLOR COMPS     140      13
S_Inner LC_A3ii_Ex5
       140         2         4         0         0         0
         0         0
$
*PART
$HMNAME COMPS     141S_Outer A3ii
$HWCOLOR COMPS     141      17
S_Outer A3ii
       141         2         4         0         0         0
         0         0
$
*PART
$HMNAME COMPS     142S_Inner_A2_Ex5
$HWCOLOR COMPS     142      20
S_Inner A2_Ex5
       142         1         5         0         0         0
         0         0
$
*PART
$HMNAME COMPS     143S_Inner_A2_Ex6
$HWCOLOR COMPS     143      29
S_Inner A2_Ex6
       143         1         5         0         0         0
         0         0
$
*PART
$HMNAME COMPS     144S_Outer A2
$HWCOLOR COMPS     144      24
S_Outer A2
       144         1         5         0         0         0
         0         0
$
*PART
$HMNAME COMPS     145S_DSlips LG_UMB
$HWCOLOR COMPS     145      25
S_DSlips LG_UMB
       145         1         6         0         0         0
         0         0
$
*PART
$HMNAME COMPS     146S_DSlips LG_LMB
$HWCOLOR COMPS     146      28
S_DSlips LG_LMB
       146         1         7         0         0         0
         0         0
$
*PART
$HMNAME COMPS     155N_MG_Ex1
$HWCOLOR COMPS     155      29
N_MG_Ex1
       155         2         1         0         0         0
         0         0
$
*PART
$HMNAME COMPS     157N_RTD_Ex2
$HWCOLOR COMPS     157      35
N_RTD_Ex2
       157         1         2         0         0         0
         0         0
$
*PART
$HMNAME COMPS     158N_LC_A3i Ex2
$HWCOLOR COMPS     158      37
N_LC_A3i Ex2
       158         1         3         0         0         0
         0         0
$
```

```
*PART
$HMNAME COMPS     159N_LC_A3i Ex3
$HWCOLOR COMPS     159       40
N_LC_A3i Ex3
       159         1         3         0         0         0
         0         0
$
*PART
$HMNAME COMPS     160S_Piles_LC_A3i
$HWCOLOR COMPS     160       41
S_Piles LC_A3i
       160         1         3         0         0         0
         0         0
$
*PART
$HMNAME COMPS     161S_P-Slip_LC_A3i
$HWCOLOR COMPS     161       44
S_P-Slip LC_A3i
       161         1         3         0         0         0
         0         0
$
*PART
$HMNAME COMPS     162S_Piles LC_A3ii
$HWCOLOR COMPS     162       48
S_Piles LC_A3ii
       162         1         4         0         0         0
         0         0
$
*PART
$HMNAME COMPS     163S_P-Slip LC_A3ii
$HWCOLOR COMPS     163       49
S_P-Slip LC_A3ii
       163         1         4         0         0         0
         0         0
$
*PART
$HMNAME COMPS     164S_Piles LC_A2.1
$HWCOLOR COMPS     164       52
S_Piles LC_A2.1
       164         1         5         0         0         0
         0         0
$
*PART
$HMNAME COMPS     165S_P-Slip LC_A2.1
$HWCOLOR COMPS     165       53
S_P-Slip LC_A2.1
       165         1         5         0         0         0
         0         0
$
*PART
$HMNAME COMPS     166S_Piles LG_UMB.1
$HWCOLOR COMPS     166       56
S_Piles LG_UMB.1
       166         1         6         0         0         0
         0         0
$
*PART
$HMNAME COMPS     167S_P-Slip LG_UMB.1
$HWCOLOR COMPS     167       57
S_P-Slip LG_UMB.1
       167         1         6         0         0         0
         0         0
$
*PART
$HMNAME COMPS     170N_Inner MG_Ex1
$HWCOLOR COMPS     170       60
N_Inner MG_Ex1
       170         2         1         0         0         0
         0         0
$
*PART
$HMNAME COMPS     172N_Outer_MG
```



```
$HWCOLOR COMPS     172       64
N_Outer MG
       172         2         1         0         0         0
         0         0
$
*PART
$HMNAME COMPS     173N_Inner_RTD_Ex2
$HWCOLOR COMPS     173       3
N_Inner_RTD_Ex2
       173         1         2         0         0         0
         0         0
$
*PART
$HMNAME COMPS     174N_Outer_RTD
$HWCOLOR COMPS     174       4
N_Outer_RTD
       174         1         2         0         0         0
         0         0
$
*PART
$HMNAME COMPS     175N_Inner_LC_A3i_Ex2
$HWCOLOR COMPS     175       5
N_Inner LC_A3i_Ex2
       175         1         3         0         0         0
         0         0
$
*PART
$HMNAME COMPS     176N_Outer_LC_A3i
$HWCOLOR COMPS     176       6
N_Outer LC_A3i
       176         1         3         0         0         0
         0         0
$
*PART
$HMNAME COMPS     177N_Inner_LC_A3i_Ex3
$HWCOLOR COMPS     177       7
N_Inner LC_A3i_Ex3
       177         1         3         0         0         0
         0         0
$
*PART
$HMNAME COMPS     178N_DSlips LC_A3ii
$HWCOLOR COMPS     178       8
N_DSlips LC_A3ii
       178         1         4         0         0         0
         0         0
$
*PART
$HMNAME COMPS     200D_Wall
D_Wall
       200         3        11         0         0         0
         0         0
$
*PART
$HMNAME COMPS     201Dividing Wall
Dividing Wall
       201         3        11         0         0         0
         0         0
$
*PART
$HMNAME COMPS     202Capping Beam
Capping Beam
       202         4        12         0         0         0
         0         0
$
*PART
$HMNAME COMPS     203Pile-Concrete
$HWCOLOR COMPS     203       11
Pile-Concrete
       203         2        10         0         0         0
         0         0
$
```

```
*PART
$HMNAME COMPS     204S_Base Slab_Concrete
$HWCOLOR COMPS     204       15
S_Base Slab_Concrete
         204         2        10         0         0         0
         0         0
$
*PART
$HMNAME COMPS     205N_Base Slab_Concrete
$HWCOLOR COMPS     205       32
N_Base Slab_Concrete
         205         2        10         0         0         0
         0         0
$
*PART
$HMNAME COMPS     300S_Wailer_P1
S_Wailer P1
         300         5        21         0         0         0
         0         0
$
*PART
$HMNAME COMPS     301S_Beams_P1
S_Beams P1
         301         6        25         0         0         0
         0         0
$
*PART
$HMNAME COMPS     303S_Beams_P2 _girder
S_Beams P2 _girder
         303        12        29         0         0         0
         0         0
$
*PART
$HMNAME COMPS     304S_Wailer_P2_horizontal
S_Wailer P2_horizontal
         304         5        26         0         0         0
         0         0
$
*PART
$HMNAME COMPS     305S_Beam_P2_H
S_Beam_P2 H
         305         9        24         0         0         0
         0         0
$
*PART
$HMNAME COMPS     307S_Beam_P2_corner
S_Beam_P2 corner
         307        10        27         0         0         0
         0         0
$
*PART
$HMNAME COMPS     308S_Wailer_P3
S_Wailer P3
         308         5        26         0         0         0
         0         0
$
*PART
$HMNAME COMPS     309S_Beams_P3_H
S_Beams P3_H
         309        13        32         0         0         0
         0         0
$
*PART
$HMNAME COMPS     310S_Wailer_P4
S_Wailer P4
         310         5        26         0         0         0
         0         0
$
*PART
$HMNAME COMPS     311S_Beams_P4_Corner
S_Beams P4_Corner
         311        14        33         0         0         0
```



```
         0         0
$
*PART
$HMNAME COMPS     320North Propping P1_Wailer
North Propping P1_Wailer
         320         5        21         0         0         0
         0         0
$
*PART
$HMNAME COMPS     321North Propping P1_Beams
North Propping P1_Beams
         321         6        22         0         0         0
         0         0
$
*PART
$HMNAME COMPS     322North Propping P2_Wailer
North Propping P2_Wailer
         322         5        21         0         0         0
         0         0
$
*PART
$HMNAME COMPS     324North Propping P2_Beams
North Propping P2_Beams
         324         6        22         0         0         0
         0         0
$
*PART
$HMNAME COMPS     350Slab Level -3
Slab Level -3
         350         7        23         0         0         0
         0         0
$
*PART
$HMNAME COMPS     352Slab Level -4
Slab Level -4
         352         7        23         0         0         0
         0         0
$
*PART
$HMNAME COMPS     353Slab Level -2
Slab Level -2
         353         7        23         0         0         0
         0         0
$
*PART
$HMNAME COMPS     354Slab Level -1
Slab Level -1
         354         7        23         0         0         0
         0         0
$
*PART
$HMNAME COMPS     355Roof Slab Level 0
Roof Slab Level 0
         355         7        23         0         0         0
         0         0
$
*PART
$HMNAME COMPS     400MC_S_P-Slip_LC_A2
$HWCOLOR COMPS     400       29
MC_S_P-Slip_LC_A2
         400         1        17         0         0         0
         0         0
$
*PART
$HMNAME COMPS     401MC_S_P-Slip_LG_UMB
$HWCOLOR COMPS     401       53
MC_S_P-Slip_LG_UMB
         401         1        18         0         0         0
         0         0
$
*PART
$HMNAME COMPS     402MC_S_P-Slip_LG_LMB
```

```
$HWCOLOR COMPS     402      45
MC_S_P-Slip_LG_LMB
        402         1        19         0         0         0
        0         0
$
*PART
$HMNAME COMPS     403MC_S_Pile Slip_LC_A2_Base Slab_Ex
$HWCOLOR COMPS     403      37
MC_S_Pile Slip_LC_A2_Base Slab_Ex
        403         1        17         0         0         0
        0         0
$
*PART
$HMNAME COMPS     404MC_N_P-Slip_LC_A3i
$HWCOLOR COMPS     404      26
MC_N_P-Slip_LC_A3i
        404         1        15         0         0         0
        0         0
$
*PART
$HMNAME COMPS     405MC_N_P-Slip_LC_A3ii
$HWCOLOR COMPS     405      31
MC_N_P-Slip_LC_A3ii
        405         1        16         0         0         0
        0         0
$
*PART
$HMNAME COMPS     406MC_N_P-Slip_LC_A2
$HWCOLOR COMPS     406      38
MC_N_P-Slip_LC_A2
        406         1        17         0         0         0
        0         0
$
*PART
$HMNAME COMPS     407MC_N_P-Slip_LG-UMB
$HWCOLOR COMPS     407      46
MC_N_P-Slip_LG-UMB
        407         1        18         0         0         0
        0         0
$
*PART
$HMNAME COMPS     410MC_S_Inner_MG_Ex1
$HWCOLOR COMPS     410      57
MC_S_Inner_MG_Ex1
        410         2        13         0         0         0
        0         0
$
*PART
$HMNAME COMPS     412MC_S_Outer_MG
$HWCOLOR COMPS     412      59
MC_S_Outer_MG
        412         2        13         0         0         0
        0         0
$
*PART
$HMNAME COMPS     413MC_S_Inner_RTD_Ex2
$HWCOLOR COMPS     413      49
MC_S_Inner_RTD_Ex2
        413         1        14         0         0         0
        0         0
$
*PART
$HMNAME COMPS     414MC_S_Outer_RTD
$HWCOLOR COMPS     414      51
MC_S_Outer_RTD
        414         1        14         0         0         0
        0         0
$
*PART
$HMNAME COMPS     415MC_S_Inner_LC_A3i_Ex2
$HWCOLOR COMPS     415      41
MC_S_Inner_LC_A3i_Ex2
```



```
        415         1        15         0         0         0
        0         0
$
*PART
$HMNAME COMPS     416MC_S_Inner_LC_A3i_Ex3
$HWCOLOR COMPS     416      43
MC_S_Inner_LC_A3i_Ex3
        416         1        15         0         0         0
        0         0
$
*PART
$HMNAME COMPS     417MC_S_Inner_LC_A3i_Ex4
$HWCOLOR COMPS     417      33
MC_S_Inner_LC_A3i_Ex4
        417         1        15         0         0         0
        0         0
$
*PART
$HMNAME COMPS     418MC_S_Outer_LC_A3i
$HWCOLOR COMPS     418      35
MC_S_Outer_LC_A3i
        418         1        15         0         0         0
        0         0
$
*PART
$HMNAME COMPS     419MC_S_Inner_LC_A3ii_Ex4
$HWCOLOR COMPS     419      25
MC_S_Inner_LC_A3ii_Ex4
        419         1        16         0         0         0
        0         0
$
*PART
$HMNAME COMPS     420MC_S_Inner_LC_A3ii_Ex5
$HWCOLOR COMPS     420      27
MC_S_Inner_LC_A3ii_Ex5
        420         2        16         0         0         0
        0         0
$
*PART
$HMNAME COMPS     421MC_S_Outer_LC_A3ii
$HWCOLOR COMPS     421      17
MC_S_Outer_LC_A3ii
        421         2        16         0         0         0
        0         0
$
*PART
$HMNAME COMPS     422MC_S_Inner_LC_A2_Ex5
$HWCOLOR COMPS     422       9
MC_S_Inner_LC_A2_Ex5
        422         1        17         0         0         0
        0         0
$
*PART
$HMNAME COMPS     423MC_S_Inner_LC_A2_Ex6
$HWCOLOR COMPS     423      12
MC_S_Inner_LC_A2_Ex6
        423         1        17         0         0         0
        0         0
$
*PART
$HMNAME COMPS     424MC_S_Outer_LC_A2
$HWCOLOR COMPS     424      21
MC_S_Outer_LC_A2
        424         1        17         0         0         0
        0         0
$
*PART
$HMNAME COMPS     425MC_S_DSlip_LG_UMB
$HWCOLOR COMPS     425      29
MC_S_DSlip_LG_UMB
        425         1        18         0         0         0
        0         0
```

```
$
*PART
$HMNAME COMPS     426MC_S_DSlip_LG_LMB
$HWCOLOR COMPS     426       31
MC_S_DSlip_LG_LMB
        426         1        19         0         0         0
        0         0
$
*PART
$HMNAME COMPS     427MC_N_Inner_MG_Ex1
$HWCOLOR COMPS     427       57
MC_N_Inner_MG_Ex1
        427         2         1         0         0         0
        0         0
$
*PART
$HMNAME COMPS     429MC_N_Outer_MG
$HWCOLOR COMPS     429       61
MC_N_Outer_MG
        429         2        13         0         0         0
        0         0
$
*PART
$HMNAME COMPS     430MC_N_Inner_RTD_Ex2
$HWCOLOR COMPS     430       49
MC_N_Inner_RTD_Ex2
        430         1        14         0         0         0
        0         0
$
*PART
$HMNAME COMPS     431MC_N_Outer_RTD
$HWCOLOR COMPS     431       29
MC_N_Outer_RTD
        431         1        14         0         0         0
        0         0
$
*PART
$HMNAME COMPS     432MC_N_Inner_LC_A3i_Ex2
$HWCOLOR COMPS     432       50
MC_N_Inner_LC_A3i_Ex2
        432         1        15         0         0         0
        0         0
$
*PART
$HMNAME COMPS     434MC_N_Outer_LC_A3i
$HWCOLOR COMPS     434       42
MC_N_Outer_LC_A3i
        434         1        15         0         0         0
        0         0
$
*PART
$HMNAME COMPS     435MC_N_Inner_LC_A3i_Ex3
$HWCOLOR COMPS     435       34
MC_N_Inner_LC_A3i_Ex3
        435         1        15         0         0         0
        0         0
$
*PART
$HMNAME COMPS     436MC_N_DSlip_LC_A3ii
$HWCOLOR COMPS     436       26
MC_N_DSlip_LC_A3ii
        436         1        16         0         0         0
        0         0
$
*PART
$HMNAME COMPS    1191S_LC_A2 Ex7_base slab
$HWCOLOR COMPS    1191       30
S_LC_A2 Ex7_base slab
       1191         1         5         0         0         0
        0         0
$
*PART
```



```
$HMNAME COMPS    1431S_Inner A2_Ex7_base slab
$HWCOLOR COMPS    1431       37
S_Inner A2_Ex7_base slab
       1431         1         5         0         0         0
        0         0
$
*PART
$HMNAME COMPS    1591N_LC_A3i Ex4_base slab
$HWCOLOR COMPS    1591       50
N_LC_A3i Ex4_base slab
       1591         1         3         0         0         0
        0         0
$
*PART
$HMNAME COMPS    2011Dividing Wall_Ex
Dividing Wall_Ex
       2011         3        11         0         0         0
        0         0
$
*PART
$HMNAME COMPS    4231MC_S_Inner_LC_A2_Ex7_base slab
$HWCOLOR COMPS    4231       37
MC_S_Inner_LC_A2_Ex7_base slab
       4231         1        17         0         0         0
        0         0
$
*PART
$HMNAME COMPS    4351MC_N_Inner_LC_A3i_Ex4_base slab
$HWCOLOR COMPS    4351       61
MC_N_Inner_LC_A3i_Ex4_base slab
       4351         1        15         0         0         0
        0         0
$
*PART
$HMNAME COMPS    4352S_Beams_P1_girder
S_Beams P1_girder
       4352         8        22         0         0         0
        0         0
$
*PART
$HMNAME COMPS    4353S_Wailer_P1_Corner
S_Wailer P1_Corner
       4353         5        21         0         0         0
        0         0
$
*PART
$HMNAME COMPS    4354S_Beam_P3_Corner
S_Beam P3 Corner
       4354        11        31         0         0         0
        0         0
$
*PART
$HMNAME COMPS    4355S_Beam_P3_girder
S_Beam P3 girder
       4355        12        29         0         0         0
        0         0
$
*PART
$HMNAME COMPS    4356S_Beam_P4_H
S_Beam P4 H
       4356        10        27         0         0         0
        0         0
$
*PART
$HMNAME COMPS    4357S_Wailer_P2_corner_1
S_Wailer P2_corner
       4357         5        26         0         0         0
        0         0
$
*PART
$HMNAME COMPS    4358S_Beams_P3_H_end
S_Beams_P3_H-end
```

```
1258        4358         9        24         0         0         0
            0         0
1259  $
1260  $
1261  $
1262  $ ============
1263  $ DEFINE cards
1264  $ ============
1265  $
1266  $
1267  *DEFINE_CURVE
1268  $
1269  $: Cross-reference summary for Load-curve 22
1270  $: ------------------------------------------------
1271  $
1272  $: Loading definition <No label>: Factor vs time
1273  $: X axis : Time                        (Units: Time)
1274  $: Y axis : Factor                      (Units: Scalar, no units)
1275  $:    :
1276  $: (To a total of 26 unlabelled Loading definition entries)
1277  $
1278  $: Usage: Transient analysis
1279  $
1280  $
1281  $ Load Gravity Curve
1282          22         0       0.0       0.0       0.0       0.0
             0         0
1283                  0.0                 0.0
1284             1.0000000           1.0000000
1285             100.00000           1.0000000
1286  $
1287  $
1288  *DEFINE_CURVE
1289  $
1290  $: Cross-reference summary for Load-curve 111
1291  $: ------------------------------------------------
1292  $
1293  $: Control card <No label>: Limiting timestep size vs time
1294  $: X axis : Time                        (Units: Time)
1295  $: Y axis : Limiting timestep           (Units: Time)
1296  $
1297  $: Usage: Transient analysis
1298  $
1299         111         0       0.0       0.0       0.0       0.0
             0         0
1300                  0.0        1.9999999E-4
1301             100.00000        1.9999999E-4
1302  $
1303  $
1304  *DEFINE_CURVE
1305  $
1306  $: Cross-reference summary for Load-curve 400
1307  $: ------------------------------------------------
1308  $
1309  $: Global damping <No label>: Global nodal damping vs time
1310  $: X axis : Time                        (Units: Time)
1311  $: Y axis : Global nodal mass-weighted damping  (Units: Mass damping)
1312  $
1313  $: Usage: Transient analysis
1314  $
1315  $
1316  $load curve for viscous damping
1317         400         0       0.0       0.0       0.0       0.0
             0         0
1318                  0.0           10.000000
1319             1.0000000          10.000000
1320             1.1000000          10.000000
1321             100.00000          10.000000
1322  $
1323  $
1324  *DEFINE_CURVE
1325  $
```



```
1326  $: Cross-reference summary for Load-curve 880
1327  $: ------------------------------------------------
1328  $
1329  $: Boundary condition <No label>: Analysis type vs. time
1330  $: X axis : Time                        (Units: Time)
1331  $: Y axis : Analysis type               (Units: Scalar, no units)
1332  $:    :
1333  $: (To a total of 71 unlabelled Boundary condition entries)
1334  $
1335  $: Usage: Transient analysis
1336  $
1337         880         0       0.0       0.0       0.0       0.0
               0         0
1338                     0.0           2.0000000
1339                1.0000000          2.0000000
1340                1.1000000          1.0000000
1341                8.0000000          1.0000000
1342                100.00000          1.0000000
1343  $
1344  *DEFINE_CONSTRUCTION_STAGES
1345  $    STAGE      START        END       RAMP  RL_START    RL_END
1346            1        0.0        1.0        0.1        0.0        1.0
                  0
1347            2        1.0        2.0        0.1        1.0        2.0
                  0
1348            3        2.0        3.0        0.1        2.0        3.0
                  0
1349            4        3.0        4.0        0.1        3.0        4.0
                  0
1350            5        4.0        5.0        0.1        4.0        5.0
                  0
1351            6        5.0        6.0        0.1        5.0        6.0
                  0
1352            7        6.0        7.0        0.1        6.0        7.0
                  0
1353            8        7.0        8.0        0.1        7.0        8.0
                  0
1354            9        8.0        9.0        0.1        8.0        9.0
                  0
1355           10        9.0       10.0        0.1        9.0       10.0
                  0
1356           11       10.0       11.0        0.1       10.0       11.0
                  0
1357           12       11.0       12.0        0.1       11.0       12.0
                  0
1358           13       12.0       13.0        0.1       12.0       13.0
                  0
1359           14       13.0       14.0        0.1       13.0       14.0
                  0
1360           15       14.0       15.0        0.1       14.0       15.0
                  0
1361           16       15.0       16.0        0.1       15.0       16.0
                  0
1362           17       16.0       17.0        0.1       16.0       17.0
                  0
1363           18       17.0       18.0        0.1       17.0       18.0
                  0
1364           19       18.0       19.0        0.1       18.0       19.0
                  0
1365           20       19.0       20.0        0.1       19.0       20.0
                  0
1366           21       20.0       21.0        0.1       20.0       21.0
                  0
1367           22       21.0       22.0        0.1       21.0       22.0
                  0
1368           23       22.0       23.0        0.1       22.0       23.0
                  0
1369           24       23.0       24.0        0.1       23.0       24.0
                  0
1370           25       24.0       25.0        0.1       24.0       25.0
                  0
1371  *DEFINE_STAGED_CONSTRUCTION_PART
```

```
$
$      PID       ADD    REMOVE
$Stratigraphy
         101         0         0
         102         0         0
         103         0         0
         104         0         0
         105         0         0
         106         0         0
         107         0         0
         108         0         0
         109         0         0
$South Box Soil
         110         0         3
         112         0         4
         113         0         4
         114         0         5
         115         0         5
         116         0         6
         117         0         7
         118         0         7
         119         0         8
        1191         0         9
$South Box Piles (soil) & slips
         120         0         2
         121         0         2
         122         0         2
         123         0         2
         124         0         2
         125         0         2
         126         0         2
$South Box DWall Slips
         130         0         2
         132         0         2
         133         0         2
         134         0         2
         135         0         2
         136         0         2
         137         0         2
         138         0         2
         139         0         2
         140         0         2
         141         0         2
         142         0         2
         143         0         2
        1431         0         2
         144         0         2
         145         0         2
         146         0         2
$North Box Soil
         155         0        15
         157         0        17
         158         0        17
         159         0        18
        1591         0        19
$North Box Piles (soil) & slips
         160         0         2
         161         0         2
         162         0         2
         163         0         2
         164         0         2
         165         0         2
         166         0         2
         167         0         2
$North Box DWall Slips
         170         0         2
         172         0         2
         173         0         2
         174         0         2
         175         0         2
         176         0         2
         177         0         2
```



```
         178         0         2
$Dwall
         200         2         0
$Dividing Wall
         201         2         0
        2011         2        18
$Capping Beam
         202         2         0
$Concrete Piles
         203         2         0
$South Box base slab
         204         9         0
$North Base Slab
         205        19         0
$M-C Pile Slips
         403         2         9
         400         2         0
         401         2         0
         402         2         0
         404         2        19
         405         2         0
         406         2         0
         407         2         0
$M-C South Box DWall Slips
         410         2         3
         412         2         0
         413         2         4
         414         2         0
         415         2         4
         416         2         5
         417         2         6
         418         2         0
         419         2         6
         420         2         7
         421         2         0
         422         2         7
         423         2         8
        4231         2         9
         424         2         0
         425         2         0
         426         2         0
$M-C North Box DWall Slips
         427         2        15
         429         2         0
         430         2        17
         431         2         0
         432         2        17
         434         2         0
         435         2        18
        4351         2        19
         436         2         0
$Propping P1
         300         4        22
        4353         4        22
         301         4        22
        4352         4        22
$Propping P2
        4357         5        20
         304         5        20
         303         5        20
         305         5        20
         307         5        20
$Propping P3
         308         6        13
         309         6        13
        4354         6        13
        4355         6        13
        4358         6        13
$Propping P4
         310         7        11
         311         7        11
        4356         7        11
```

```
$Slab Level -3
        350        12          0
$Slab Level -4
        352        14          0
$Slab Level -2
        353        14          0
$North Propping P1
        320        17         22
        321        17         22
$North Propping P2
        322        18         20
        324        18         20
$North Base Slab******
$       205        19          0
$Slab Level -1
        354        21          0
$Roof Slab Level 0
        355        23          0
$
$
$ =============
$ DAMPING cards
$ =============
$
*DAMPING_GLOBAL
        400       0.0       0.0       0.0       0.0       0.0
        0.0       0.0
$
$
$ ==============
$ BOUNDARY cards
$ ==============
$
*BOUNDARY_PORE_FLUID_PART
$
$Geology
        101       0.0       0.0         2       0.0         0
        0       0.0
        102       0.0       0.0         2       0.0         0
        0       0.0
        103       0.0       0.0         2       0.0       880
        0     100.0
        104       0.0       0.0         2       0.0       880
        0     100.0
        105       0.0       0.0         2       0.0       880
        0     100.0
        106       0.0       0.0         2       0.0       880
        0     100.0
        107       0.0       0.0         2       0.0       880
        0     100.0
        108       0.0       0.0         2       0.0         0
        0       0.0
        109       0.0       0.0         2       0.0         0
        0       0.0
$South Box Soil
        110       0.0       0.0         2       0.0         0
        0       0.0
        112       0.0       0.0         2       0.0         0
        0       0.0
        113       0.0       0.0         2       0.0       880
        0     100.0
        114       0.0       0.0         2       0.0       880
        0     100.0
        115       0.0       0.0         2       0.0       880
        0     100.0
        116       0.0       0.0         2       0.0       880
        0     100.0
        117       0.0       0.0         2       0.0       880
        0     100.0
        118       0.0       0.0         2       0.0       880
        0     100.0
        119       0.0       0.0         2       0.0       880
```



```
        0     100.0
       1191       0.0       0.0         2       0.0       880
        0     100.0
$South Box Piles Initial
        120       0.0       0.0         2       0.0       880
        0     100.0
        121       0.0       0.0         2       0.0       880
        0     100.0
        122       0.0       0.0         2       0.0       880
        0     100.0
        123       0.0       0.0         2       0.0       880
        0     100.0
        124       0.0       0.0         2       0.0       880
        0     100.0
        125       0.0       0.0         2       0.0       880
        0     100.0
        126       0.0       0.0         2       0.0         0
        0       0.0
$South Box DWall Slips
        130       0.0       0.0         2       0.0         0
        0       0.0
        132       0.0       0.0         2       0.0         0
        0       0.0
        133       0.0       0.0         2       0.0         0
        0       0.0
        134       0.0       0.0         2       0.0         0
        0       0.0
        135       0.0       0.0         2       0.0       880
        0     100.0
        136       0.0       0.0         2       0.0       880
        0     100.0
        137       0.0       0.0         2       0.0       880
        0     100.0
        138       0.0       0.0         2       0.0       880
        0     100.0
        139       0.0       0.0         2       0.0       880
        0     100.0
        140       0.0       0.0         2       0.0       880
        0     100.0
        141       0.0       0.0         2       0.0       880
        0     100.0
        142       0.0       0.0         2       0.0       880
        0     100.0
        143       0.0       0.0         2       0.0       880
        0     100.0
       1431       0.0       0.0         2       0.0       880
        0     100.0
        144       0.0       0.0         2       0.0       880
        0     100.0
        145       0.0       0.0         2       0.0       880
        0     100.0
        146       0.0       0.0         2       0.0       880
        0     100.0
$North Box Soil
        155       0.0       0.0         2       0.0         0
        0       0.0
        157       0.0       0.0         2       0.0         0
        0       0.0
        158       0.0       0.0         2       0.0       880
        0     100.0
        159       0.0       0.0         2       0.0       880
        0     100.0
       1591       0.0       0.0         2       0.0       880
        0     100.0
$North Box Piles Initial
        160       0.0       0.0         2       0.0       880
        0     100.0
        161       0.0       0.0         2       0.0       880
        0     100.0
        162       0.0       0.0         2       0.0       880
        0     100.0
        163       0.0       0.0         2       0.0       880
```

```
1607         0     100.0
1608       164       0.0       0.0         2       0.0       880
             0     100.0
1609       165       0.0       0.0         2       0.0       880
             0     100.0
1610       166       0.0       0.0         2       0.0       880
             0     100.0
1611       167       0.0       0.0         2       0.0       880
             0     100.0
1612  $North Box DWall Slips
1613       170       0.0       0.0         2       0.0         0
             0       0.0
1614       172       0.0       0.0         2       0.0         0
             0       0.0
1615       173       0.0       0.0         2       0.0         0
             0       0.0
1616       174       0.0       0.0         2       0.0         0
             0       0.0
1617       175       0.0       0.0         2       0.0       880
             0     100.0
1618       176       0.0       0.0         2       0.0       880
             0     100.0
1619       177       0.0       0.0         2       0.0       880
             0     100.0
1620       178       0.0       0.0         2       0.0       880
             0     100.0
1621  $M-C Pile Slips
1622       400       0.0       0.0         2       0.0       880
             0     100.0
1623       401       0.0       0.0         2       0.0       880
             0     100.0
1624       402       0.0       0.0         2       0.0       880
             0     100.0
1625       403       0.0       0.0         2       0.0       880
             0     100.0
1626       404       0.0       0.0         2       0.0       880
             0     100.0
1627       405       0.0       0.0         2       0.0       880
             0     100.0
1628       406       0.0       0.0         2       0.0       880
             0     100.0
1629  $M-C DWall Slips
1630       410       0.0       0.0         2       0.0         0
             0       0.0
1631       412       0.0       0.0         2       0.0         0
             0       0.0
1632       413       0.0       0.0         2       0.0         0
             0       0.0
1633       414       0.0       0.0         2       0.0         0
             0       0.0
1634       415       0.0       0.0         2       0.0       880
             0     100.0
1635       416       0.0       0.0         2       0.0       880
             0     100.0
1636       417       0.0       0.0         2       0.0       880
             0     100.0
1637       418       0.0       0.0         2       0.0       880
             0     100.0
1638       419       0.0       0.0         2       0.0       880
             0     100.0
1639       420       0.0       0.0         2       0.0       880
             0     100.0
1640       421       0.0       0.0         2       0.0       880
             0     100.0
1641       422       0.0       0.0         2       0.0       880
             0     100.0
1642       423       0.0       0.0         2       0.0       880
             0     100.0
1643      4231       0.0       0.0         2       0.0       880
            0     100.0
1644       424       0.0       0.0         2       0.0       880
             0     100.0
```



```
1645       425       0.0       0.0         2       0.0       880
             0     100.0
1646       426       0.0       0.0         2       0.0         0
             0       0.0
1647       427       0.0       0.0         2       0.0         0
             0       0.0
1648       429       0.0       0.0         2       0.0         0
             0       0.0
1649       430       0.0       0.0         2       0.0         0
             0       0.0
1650       431       0.0       0.0         2       0.0         0
             0       0.0
1651       432       0.0       0.0         2       0.0       880
             0     100.0
1652       434       0.0       0.0         2       0.0       880
             0     100.0
1653       435       0.0       0.0         2       0.0       880
             0     100.0
1654      4351       0.0       0.0         2       0.0       880
            0     100.0
1655       436       0.0       0.0         2       0.0       880
             0     100.0
1656  $
1657  $
1658  $ ==========
1659  $ LOAD cards
1660  $ ==========
1661  $
1662  *LOAD_GRAVITY_PART
1663  $
1664  $       PID       DOF        LC     ACCEL      LCDR      STGA
      STGR
1665  $
1666       300         3        22   1.0E-20         0         0
             0
1667       301         3        22   1.0E-20         0         0
             0
1668      4352         3        22   1.0E-20         0         0
            0
1669      4353         3        22   1.0E-20         0         0
             0
1670      4357         3        22   1.0E-20         0         0
             0
1671       303         3        22   1.0E-20         0         0
             0
1672       304         3        22   1.0E-20         0         0
             0
1673       305         3        22   1.0E-20         0         0
             0
1674       307         3        22   1.0E-20         0         0
             0
1675       308         3        22   1.0E-20         0         0
             0
1676       309         3        22   1.0E-20         0         0
             0
1677      4354         3        22   1.0E-20         0         0
            0
1678      4355         3        22   1.0E-20         0         0
            0
1679      4358         3        22   1.0E-20         0         0
            0
1680       310         3        22   1.0E-20         0         0
             0
1681       311         3        22   1.0E-20         0         0
             0
1682      4356         3        22   1.0E-20         0         0
            0
1683       320         3        22   1.0E-20         0         0
             0
1684       321         3        22   1.0E-20         0         0
             0
1685       322         3        22   1.0E-20         0         0
```

```
1685         0
1686         324         3         22   1.0E-20         0         0
             0
1687         350         3         22   1.0E-20         0         0
             0
1688         352         3         22   1.0E-20         0         0
             0
1689         353         3         22   1.0E-20         0         0
             0
1690         354         3         22   1.0E-20         0         0
             0
1691         355         3         22   1.0E-20         0         0
             0
1692  $
1693  *TITLE
1694  TCR_west_SB1
1695  $
1696  $
1697  *END
1698  $
1699  $ ==============
1700  $ Assembly cards
1701  $ ==============
1702  $
1703  *SUBSET
1704  South Box Propping
1705  $
1706
```

Initial_Stresses_V2.txt

```
*KEYWORD
$> Include file: C:\Analysis\TCR\INC\Initial Stresses_V2.txt
$> (Used by master file: C:\Analysis\TCR\Mohr-C.key)
$>
$> Primer14.0 created on: Thu Oct 19 10:45:16 2017
$> LS-DYNA version: R9.0
$>
$INITIAL CONDITIONS
$
$Initial Stress Profile-------------------------------------------------
$K0 values not explicit - stress curves defined for horizontal stresses
$
$      PID      R0_G    ZDATUM     KFACT    LCURVE       LCH
$Stratigraphy
$South Box Soil
$South Box Piles
$South Box DWall Sl
$North Box Soil
$North Box Piles
$North Box DWall Slips
$
$Two curves for imposing Ko
$
$ Vertical effective stress
$       ELEVATION(m)       Sigma-v'(kPa)
$
$
$ Horizontal effective stress
$       ELEVATION(m)       Sigma-h'(kPa)
$
$
$Pore water pressure proflies-----------------------------------------
$
$      PID        LC
$Stratigraphy
$South Box Soil
$South Box Piles
$South Box DWall Slips
$North Box Soil
$North Box Piles
$North Box DWall Slips
$
$Under-drainage Profile
$Input from XR vertical PWP profile as supplied on 01/03/2011
$               z(m)             Head(m)
$
$
$
$> end_saved_comments
$
$
$
$ ============
$ DEFINE cards
$ ============
$
$
*DEFINE_CURVE
$
$: Cross-reference summary for Load-curve 666
$: ---------------------------------------------
$
$: Initial conditions <No label>: PWP head vs. Z coord
$: X axis : Z coord                    (Units: Length)
$: Y axis : PWP head                   (Units: Length)
$:    :
$: (To a total of 64 unlabelled Initial conditions entries)
$
$: Usage: Transient analysis
$
```



```
       666         0       0.0       0.0       0.0       0.0         0
       0
            70.000000                 0.0
            74.000000                 0.0
            75.000000                 0.0
            76.000000          0.60000002
            77.099998           1.3000000
            78.099998           1.9000000
            79.099998           2.5000000
            80.099998           3.0999999
            81.000000           3.7000000
            82.000000           4.3000002
            83.000000           4.9000001
            84.000000           5.5999999
            85.000000           6.1999998
            86.000000           6.8000002
            87.000000           7.4000001
            88.000000           7.8000002
            89.000000           8.1999998
            90.000000           8.6000004
            91.000000           8.8000002
            92.000000           9.0000000
            93.000000           9.1999998
            94.000000           9.3000002
            95.000000           9.1000004
            96.000000           9.1000004
            97.000000           9.1000004
            98.000000           9.3000002
            99.000000           9.6000004
            100.00000           10.000000
            101.00000           9.8999996
            102.00000           9.6999998
            103.00000           9.5000000
            104.00000           9.3000002
            105.00000           9.1000004
            106.00000           9.0000000
            106.90000           8.6000004
            108.10000           8.1999998
            109.00000           7.9000001
            110.00000           7.5999999
            111.10000           7.1999998
            112.00000           6.9000001
            113.10000           6.3000002
            114.10000           5.5000000
            115.10000           4.6999998
            116.10000           3.8000000
            117.00000           2.9000001
            118.10000           1.9000000
            119.90000          0.10000000
            120.00000                 0.0
            121.00000                 0.0
            125.00000                 0.0
$
$
*DEFINE_CURVE
$
$: Cross-reference summary for Load-curve 777
$: ---------------------------------------------
$
$: Initial conditions <No label>: Stress vs. Z coord
$: X axis : Z coord                    (Units: Length)
$: Y axis : Stress                     (Units: Stress)
$:    :
$: (To a total of 64 unlabelled Initial conditions entries)
$
$: Usage: Transient analysis
$
       777         0       0.0       0.0       0.0       0.0         0
       0
            70.000000          -1097.2000
            74.000000          -1013.2000
            75.000000          -992.20001
```

```
             76.000000          -965.29999
             77.099998          -935.40002
             78.099998          -908.50000
             79.099998          -881.59998
             80.099998          -854.70001
             81.000000          -827.79999
             82.000000          -801.90002
             83.000000          -776.00000
             84.000000          -750.09998
             85.000000          -724.20001
             86.000000          -698.29999
             87.000000          -671.59998
             88.000000          -647.90002
             89.000000          -622.90002
             90.000000          -600.50000
             91.000000          -577.00000
             92.000000          -555.79999
             93.000000          -533.40002
             94.000000          -513.20001
             95.000000          -494.29999
             96.000000          -474.60001
             97.000000          -455.10001
             98.000000          -433.10001
             99.000000          -409.60001
             100.00000          -385.60001
             101.00000          -367.10001
             102.00000          -348.60001
             103.00000          -331.10001
             104.00000          -312.60001
             105.00000          -294.00000
             106.00000          -276.60001
             106.90000          -261.70001
             108.10000          -241.80000
             109.00000          -226.80000
             110.00000          -209.89999
             111.10000          -192.00000
             112.00000          -177.10001
             113.10000          -162.30000
             114.10000          -150.00000
             115.10000          -138.39999
             116.10000          -127.20000
             117.00000          -116.70000
             118.10000          -106.00000
             119.90000          -90.699997
             120.00000          -90.199997
             121.00000          -72.000000
             125.00000                 0.0
$
$
*DEFINE_CURVE
$
$: Cross-reference summary for Load-curve 888
$: ---------------------------------------------
$
$: Initial conditions <No label>: Horizontal stress vs. Z coord
$: X axis : Z coord                    (Units: Length)
$: Y axis : Horiz. stress              (Units: Stress)
$:    :
$: (To a total of 64 unlabelled Initial conditions entries)
$
$: Usage: Transient analysis
$
       888         0       0.0       0.0       0.0       0.0         0
         0
             70.000000          -1097.2000
             74.000000          -1013.2000
             75.000000          -992.20001
             76.000000          -965.29999
             77.099998          -935.40002
             78.099998          -908.50000
             79.099998          -881.59998
             80.099998          -854.70001
```



```
             81.000000          -827.79999
             82.000000          -801.90002
             83.000000          -776.00000
             84.000000          -750.09998
             85.000000          -724.20001
             86.000000          -698.29999
             87.000000          -671.59998
             88.000000          -647.90002
             89.000000          -622.90002
             90.000000          -600.50000
             91.000000          -577.00000
             92.000000          -555.79999
             93.000000          -533.40002
             94.000000          -513.20001
             95.000000          -494.29999
             96.000000          -474.60001
             97.000000          -455.10001
             98.000000          -433.10001
             99.000000          -409.60001
             100.00000          -385.60001
             101.00000          -367.10001
             102.00000          -348.60001
             103.00000          -331.10001
             104.00000          -312.60001
             105.00000          -294.00000
             106.00000          -331.89999
             106.90000          -314.00000
             108.10000          -290.10001
             109.00000          -272.20001
             110.00000          -251.89999
             111.10000          -230.39999
             112.00000          -212.50000
             113.10000          -194.70000
             114.10000          -180.10001
             115.10000          -166.10001
             116.10000          -152.60001
             117.00000          -140.00000
             118.10000          -53.000000
             119.90000          -45.400002
             120.00000          -45.099998
             121.00000          -36.000000
             125.00000                 0.0
$
$
$
$ =============
$ INITIAL cards
$ =============
$
*INITIAL_PWP_DEPTH
         101       666
         102       666
         103       666
         104       666
         105       666
         106       666
         107       666
         108       666
         109       666
         110       666
         112       666
         113       666
         114       666
         115       666
         116       666
         117       666
         118       666
         119       666
        1191       666
         120       666
         121       666
         122       666
```

```
284         123       666
285         124       666
286         125       666
287         126       666
288         130       666
289         132       666
290         133       666
291         134       666
292         135       666
293         136       666
294         137       666
295         138       666
296         139       666
297         140       666
298         141       666
299         142       666
300         143       666
301        1431       666
302         144       666
303         145       666
304         146       666
305         155       666
306         157       666
307         158       666
308         159       666
309        1591       666
310         160       666
311         161       666
312         162       666
313         163       666
314         164       666
315         165       666
316         166       666
317         167       666
318         170       666
319         172       666
320         173       666
321         174       666
322         175       666
323         176       666
324         177       666
325         178       666
326  *INITIAL STRESS_DEPTH
327         101       0.0       0.0       0.5       777       888         0
328         102       0.0       0.0       0.5       777       888         0
329         103       0.0       0.0       1.2       777       888         0
330         104       0.0       0.0       1.2       777       888         0
331         105       0.0       0.0       1.0       777       888         0
332         106       0.0       0.0       1.0       777       888         0
333         107       0.0       0.0       1.0       777       888         0
334         108       0.0       0.0       1.0       777       888         0
335         109       0.0       0.0       1.0       777       888         0
336         110       0.0       0.0       0.5       777       888         0
337         112       0.0       0.0       0.5       777       888         0
338         113       0.0       0.0       1.0       777       888         0
339         114       0.0       0.0       1.0       777       888         0
340         115       0.0       0.0       1.0       777       888         0
341         116       0.0       0.0       1.0       777       888         0
342         117       0.0       0.0       1.0       777       888         0
343         118       0.0       0.0       1.0       777       888         0
344         119       0.0       0.0       1.0       777       888         0
345        1191       0.0       0.0       1.0       777       888         0
346         120       0.0       0.0       1.0       777       888         0
347         121       0.0       0.0       1.0       777       888         0
348         122       0.0       0.0       1.0       777       888         0
349         123       0.0       0.0       1.0       777       888         0
350         124       0.0       0.0       1.0       777       888         0
351         125       0.0       0.0       1.0       777       888         0
352         126       0.0       0.0       1.0       777       888         0
353         130       0.0       0.0       0.5       777       888         0
354         132       0.0       0.0       0.5       777       888         0
355         133       0.0       0.0       0.5       777       888         0
```



```
356         134       0.0       0.0       0.5       777       888         0
357         135       0.0       0.0       1.2       777       888         0
358         136       0.0       0.0       1.2       777       888         0
359         137       0.0       0.0       1.2       777       888         0
360         138       0.0       0.0       1.2       777       888         0
361         139       0.0       0.0       1.2       777       888         0
362         140       0.0       0.0       1.2       777       888         0
363         141       0.0       0.0       1.2       777       888         0
364         142       0.0       0.0       1.0       777       888         0
365         143       0.0       0.0       1.0       777       888         0
366        1431       0.0       0.0       1.0       777       888         0
367         144       0.0       0.0       1.0       777       888         0
368         145       0.0       0.0       1.0       777       888         0
369         146       0.0       0.0       1.0       777       888         0
370         155       0.0       0.0       0.5       777       888         0
371         157       0.0       0.0       0.5       777       888         0
372         158       0.0       0.0       0.5       777       888         0
373         159       0.0       0.0       1.2       777       888         0
374        1591       0.0       0.0       1.2       777       888         0
375         160       0.0       0.0       1.2       777       888         0
376         161       0.0       0.0       1.2       777       888         0
377         162       0.0       0.0       1.2       777       888         0
378         163       0.0       0.0       1.2       777       888         0
379         164       0.0       0.0       1.0       777       888         0
380         165       0.0       0.0       1.0       777       888         0
381         166       0.0       0.0       1.0       777       888         0
382         167       0.0       0.0       1.0       777       888         0
383         170       0.0       0.0       0.5       777       888         0
384         172       0.0       0.0       0.5       777       888         0
385         173       0.0       0.0       0.5       777       888         0
386         174       0.0       0.0       0.5       777       888         0
387         175       0.0       0.0       1.2       777       888         0
388         176       0.0       0.0       1.2       777       888         0
389         177       0.0       0.0       1.2       777       888         0
390         178       0.0       0.0       1.2       777       888         0
391  $
392  *END
393
```

Dewater.txt

```
*KEYWORD
$
$TCR_WTH_deep box (South box)_Mohr-Coulomb model
$
$PWP tables for dewatering drained materials (MG and RTD) inside
excavation
$Applicable to all soil and slips within perimeter wall
$
$Deep box - South Box Soil
*BOUNDARY_PWP_TABLE
       110                1.0
                 0                101
*BOUNDARY_PWP_TABLE
       112                1.0
                 0                101
$Inner South Box D-Wall Slips (M-C Material)
*BOUNDARY_PWP_TABLE
       410                1.0
                 0                101
*BOUNDARY_PWP_TABLE
       413                1.0
                 0                101
$North Box Soil
*BOUNDARY_PWP_TABLE
       155                1.0
                 0                110
*BOUNDARY_PWP_TABLE
       157                1.0
                 0                110
$Inner North Box D-Wall Slips (M-C Material)
*BOUNDARY_PWP_TABLE
       427                1.0
                 0                110
*BOUNDARY_PWP_TABLE
       430                1.0
                 0                110
$
$pwp table for excavation (South Box)
*DEFINE_TABLE
       101       0.0       0.0
$
                 0.0
                 2.0
                 2.1
               100.0
$
*DEFINE_CURVE
$ 1 - Under-drainage Profile inside excavation
       671
                 117                2.9
                 120               0.00
                 121               0.00
                 125               0.00
*DEFINE_CURVE
$ 2 - Under-drainage Profile inside excavation before excavation
       672
                 117                2.9
                 120               0.00
                 121               0.00
                 125               0.00
*DEFINE_CURVE
$ 3 - Under-drainage Profile inside excavation during excavation
       673
                 117               0.00
                 120               0.00
                 121               0.00
                 125               0.00
*DEFINE_CURVE
$ 4 - Under-drainage Profile inside excavation at end of construction
       674
                 117               0.00
                 120               0.00
```



```
                 121               0.00
                 125               0.00
$pwp table for excavation (North Box)
*DEFINE_TABLE
       110       0.0       0.0
$
                 0.0
                14.0
                14.1
               100.0
$
*DEFINE_CURVE
$ 1 - Under-drainage Profile inside excavation
       675
                 117                2.9
                 120               0.00
                 121               0.00
                 125               0.00
*DEFINE_CURVE
$ 2 - Under-drainage Profile inside excavation before excavation
       676
                 117                2.9
                 120               0.00
                 121               0.00
                 125               0.00
*DEFINE_CURVE
$ 3 - Under-drainage Profile inside excavation during excavation
       677
                 117               0.00
                 120               0.00
                 121               0.00
                 125               0.00
*DEFINE_CURVE
$ 4 - Under-drainage Profile inside excavation at end of construction
       678
                 117               0.00
                 120               0.00
                 121               0.00
                 125               0.00
$
*END
```

BRICK_I4.key

```
*KEYWORD 200000000
$>
$> Primer14.0 created on: Fri Oct 20 09:48:35 2017
$> LS-DYNA version: R9.0
$>
$> model title: TCR_WTH_deep box (South box)_BRICK model_Iteration4
$>
$
$CONSTRUCTION SEQUENCE
$ 1 - Initialisation with under-drained pwp profile
$ 2 - Construct DWalls & capping beam & wish in place 1.8mDIA piles
$ 3 - S/Box: Ex1 to 121.6mATD
$ 4 - S/Box: Install P1 at 122.4mATD and Ex2 to 115.975mATD
$ 5 - S/Box: Install P2 at 118.7mATD (corner) and 117.2mATD and Exc3 to 111.1mATD
$ 6 - S/Box: Install P3 at 112.0mATD and Exc4 to 107.84mATD
$ 7 - S/Box: Install P4 at 109.1mATD and Exc5 to 101.2mATD
$ 8 - S/Box: (INSTALL P5 AT 102.0MATD - NOT APPLIED) Exc6 to 97.0mATD
$
$---------------------------------------------------------------------------------------------
$ 9 - S/Box: Excavate to +96.3mATD(bottom of the base slab), and construct Base slab (S/Box: top level 98.27mATD)
$10 - S/Box: (Install Level -5 raking props and remove horizontal propping at P5 - NOT APPLIED)
$11 - S/Box: Remove P4
$12 - S/Box: (Remove raking props at Level -5 - NOT APPLIED) Install slab Level -3 at 109.1mATD
$13 - S/Box: Remove P3
$14 - S/Box: Install slab Level -2 at 114.4mATD and Level -4 at 102.0mATD
$
$---------------------------------------------------------------------------------------------
$15 - N/Box: Ex1 to 121.6mATD
$16 - S/Box: Remove P2 at 118.7mATD (corner) and install horizontal P2 at 117.2mATD
$17 - N/Box: Install P1 at 122.4mATD and Ex2 to +116.4mATD
$18 - N/Box: Cut down dividing DWall to 113.87mATD, install P2 at 117.2mATD and Ex3 to 112.7mATD
$19 - N/Box: Excavate to +112.0mATD (bottom of the base slab), and construct Level -2 slab at +114.4mATD(S/Box), Base slab (N/Box: top level 113.8mATD)
$20 - Remove P2
$21 - Install slab Level -1 at 119.7mATD
$22 - Remove P1
$23 - Install roof slab Level 0 at 125.0mATD
$
$
$ ASSUMPTIONS
$ South base slab = 1.97m (top at +98.27 and bottom at +96.3) and North base slab = 1.8m (top at +113.87 and bottom at +112)
$ 3D model is based on the As-built record
$ Temporaray propping is confirmed as the As-built information (4 levels of props for the S/Box)
$ Levels are as rounded to 1dp or nearest whole number to simplify the mesh
$ THE EXISTING BUILDINGS AND TUNNELS AROUND AND UNDER THIS SITE HAVE NOT BEEN MODELLED. NO SURCHARGES HAVE BEEN APPLIED - TBC ?
$ The top of the perimeter capping beam has been assumed to be at ground level, 125.0mATD.
$ No capping beam on the dividing wall.
$ Capping beam modelled as a 1m wide and 1.5m high continuous element, with isotropic stiffness.
$ No installation effects considered
$ Young's modulus of the 1m thick diaphragm wall: Ey = Ez = 33 GPa and Ex= 5.6 GPa (in-plane axis), mu=0.2
$ No lining walls modelled
$ Internal slabs modelled as 700mm thick continuous shell elements without internal openings (50% stiffness of structural concrete), assumed weightless
$ Bottom slabs modelled as solid elements.
```



```
$ Top slab level is at +124.4mATD
$ Temporary props modelled as beam elements; thrust blocks as nodal restraints.
$ Waling beams are to be modelled as shell elements with appropriate stiffness.
$ 50mm slip elements adjacent to the perimeter walls and around the piles account for the disturbance effects during installation of structural elements
$ Undrained conditions during construction have been modelled with unlimited suction.
$ Long term drained conditions have not been modelled.
$
$ GENERAL COMMENTS
$ Mohr-Coloumb Model parametes are applied for MG/RTD/TS
$ Maximum overburden level for LC is assumed as 200m above strata level
$ Maximum overburden level for LG is assumed as 300m above strata level
$ BRICK THEORY 4 for K0
$
$
$ =============
$ INCLUDE cards
$ =============
$
*INCLUDE
C:\Analysis\Ying\TCR\A2\1\INC\ne.k
$
*INCLUDE
C:\Analysis\Ying\TCR\A2\1\INC\Dewater.txt
$
*INCLUDE
C:\Analysis\Ying\TCR\A2\1\INC\Initial_Stresses_V2.txt
$
$
$
$ =============
$ CONTROL cards
$ =============
$
*CONTROL_OUTPUT
         1         3         0         0       0.0         0
         0         0
*CONTROL PORE FLUID
$water table at 120.0mOD
         2       0.0     120.0       1.0      10.0 2200000.0
         1       1.0
       0.0       0.0       0.0       0.0       0.0       0.0
       0.0       0.0
*CONTROL_SOLID
         1         0         0         0         0       0.0
         0
*CONTROL_STAGED_CONSTRUCTION
$                STGS      STGE      GRAV      FACT
       0.0         1         9      10.0    1.0E-6         0
         0         0
*CONTROL TIMESTEP
       0.0       0.8         0       0.0   -2.5E-4       111
         0         0
$
$
$ ==============
$ DATABASE cards
$ ==============
$
*DATABASE RCFORC
    5.0E-4         0         0         0
*DATABASE_BINARY_D3PLOT
       0.5         0         0         0         0
*DATABASE_BINARY_D3THDT
    5.0E-4         0
*DATABASE_EXTENT_BINARY
```

```
$additional history variables (PWP is Solid Extra 2)
         1         0         0         1         0         0
         0         0
         0         1         0         0         0         0
         0         0
         0         0       0.0         0         0         0
         0         0         0
*DATABASE_FORMAT
         0         1
$
$
$ ====================
$ MAT (Material) cards
$ ====================
$
*MAT_MOHR_COULOMB
$Mohr-Coulomb material - Made Ground(Drained) - phi=27, E'=46000
$top @ +125mATD, bottom at +121.6mATD
$      MID        RO      GMOD       RNU     BLANK       PHI
CVAL       PSI
         1       2.0   18400.0      0.25              0.4712
         1.0E-3       0.0
$    Blank   NPLANES     BLANK    LCCPDR     LCCPT    LCCJDR
LCCJT    LCSFAC
         0         0                   0         0         0
         0         0
$   GMODDP    GMODGR    LCGMEP   LCPHIEP   LCPSIEP    LCGMST
CVALGR     ANISO
      125.0       0.0         0         0         0       0.0
      0.0       0.0
$
*MAT MOHR COULOMB
$Mohr-Coulomb material - River Terrace Deposits - phi=42,E'=101000
$top @ +121.6mATD, bottom at +117.2mATD
$      MID        RO      GMOD       RNU     BLANK       PHI
CVAL       PSI
         2       2.1   40400.0      0.25               0.733
         1.0E-3       0.0
$    Blank   NPLANES     BLANK    LCCPDR     LCCPT    LCCJDR
LCCJT    LCSFAC
         0         0                   0         0         0
         0         0
$   GMODDP    GMODGR    LCGMEP   LCPHIEP   LCPSIEP    LCGMST
CVALGR     ANISO
      121.6       0.0         0         0         0       0.0
      0.0       0.0
$
*MAT SOIL BRICK
$BRICK material - I4, THEORY 4 to limit K0 - London Clay Layer A3i
$top @ +117.2mATD, bottom at +112mATD
$      MID        R0    RLAMDA    RKAPPA     RIOTA    RBETA1
RBETA2        RMU
         3       2.0       0.1    1.0E-2    1.5E-3       5.0
         5.0       1.3
$      RNU     RLCID       TOL       PGCL   SUB-INC       BLK
GRAV    THEORY
        0.2         2       0.0     317.2    5.0E-3  100000.0
        10.0         4
$    RVHHH   XSICRIT     ALPHA       RVH     RNU21   ANISO_4
        0.5       0.0       0.0       0.0       0.0       0.0
$
*MAT SOIL BRICK
$BRICK material - I4, THEORY 4 to limit K0 - London Clay Layer A3ii
$top @ +112mATD, bottom at +106mATD
$      MID        R0    RLAMDA    RKAPPA     RIOTA    RBETA1
RBETA2        RMU
         4       2.0       0.1    1.0E-2    1.5E-3       5.0
         5.0       1.3
$      RNU     RLCID       TOL       PGCL   SUB-INC       BLK
GRAV    THEORY
        0.2         2       0.0     312.0    5.0E-3  100000.0
        10.0         4
```



```
$    RVHHH   XSICRIT     ALPHA       RVH     RNU21   ANISO_4
        0.5       0.0       0.0       0.0       0.0       0.0
$
*MAT SOIL BRICK
$BRICK material - I4, THEORY 4 to limit K0 - London Clay Layer A2
$top @ +106ATD, bottom at +94.5mATD
$      MID        R0    RLAMDA    RKAPPA     RIOTA    RBETA1
RBETA2        RMU
         5       2.1       0.1    1.0E-2    1.5E-3       5.0
         5.0       1.3
$      RNU     RLCID       TOL       PGCL   SUB-INC       BLK
GRAV    THEORY
        0.2         2       0.0     306.0    5.0E-3  100000.0
        10.0         4
$    RVHHH   XSICRIT     ALPHA       RVH     RNU21   ANISO_4
        0.5       0.0       0.0       0.0       0.0       0.0
$
*MAT SOIL BRICK
$BRICK material - I4, THEORY 4 to limit K0 - Lambeth Group Layer UMB
$top @ +94.5ATD, bottom at +86mATD
$      MID        R0    RLAMDA    RKAPPA     RIOTA    RBETA1
RBETA2        RMU
         6       2.1       0.1    1.0E-2    1.5E-3       5.0
         5.0       1.3
$      RNU     RLCID       TOL       PGCL   SUB-INC       BLK
GRAV    THEORY
        0.2         2       0.0     594.5    5.0E-3  100000.0
        10.0         4
$    RVHHH   XSICRIT     ALPHA       RVH     RNU21   ANISO_4
        0.5       0.0       0.0       0.0       0.0       0.0
$
*MAT SOIL BRICK
$BRICK material - I4, THEORY 4 to limit K0 - Lambeth Group Layer LMB
$top @ +86ATD, bottom at +78mATD
$      MID        R0    RLAMDA    RKAPPA     RIOTA    RBETA1
RBETA2        RMU
         7       2.1       0.1    1.0E-2    1.5E-3       5.0
         5.0       1.3
$      RNU     RLCID       TOL       PGCL   SUB-INC       BLK
GRAV    THEORY
        0.2         2       0.0     586.0    5.0E-3  100000.0
        10.0         4
$    RVHHH   XSICRIT     ALPHA       RVH     RNU21   ANISO_4
        0.5       0.0       0.0       0.0       0.0       0.0
$
*MAT SOIL BRICK
$BRICK material - I4, THEORY 4 to limit K0 - Lambeth Group Layer UF
$top @ +78ATD, bottom at +75mATD
$      MID        R0    RLAMDA    RKAPPA     RIOTA    RBETA1
RBETA2        RMU
         8       2.1       0.1    1.0E-2    1.5E-3       5.0
         5.0       1.3
$      RNU     RLCID       TOL       PGCL   SUB-INC       BLK
GRAV    THEORY
        0.2         2       0.0     578.0    5.0E-3  100000.0
        10.0         4
$    RVHHH   XSICRIT     ALPHA       RVH     RNU21   ANISO_4
        0.5       0.0       0.0       0.0       0.0       0.0
$
*MAT_MOHR_COULOMB
$
$Mohr-Coulmb material - Lambeth Group Layer UF(Drained),phi'=33, E'=
196800+4320
$top @ +75ATD, bottom at +70mATD
$      MID        RO      GMOD       RNU     BLANK       PHI
CVAL       PSI
         9       1.9   83300.0       0.2              0.6632
         1.0E-3       0.0
$    Blank   NPLANES     BLANK    LCCPDR     LCCPT    LCCJDR
LCCJT    LCSFAC
         0         0                   0         0         0
         0         0
```

```
$   GMODDP    GMODGR    LCGMEP   LCPHIEP   LCPSIEP    LCGMST
CVALGR     ANISO
      75.0       0.0         0         0         0       0.0
       0.0       0.0
$
*MAT ELASTIC
$Concrete (Bearing Piles & solid base slab)
         10       2.4     2.8E7       0.2       0.0       0.0
          0.0
$
*MAT ORTHOTROPIC ELASTIC
$Linear Elastic - D-wall
$       MID        RO        EA        EB        EC      PRBA
PRCA       PRCB
         11       2.4 6600000.0     3.3E7     3.3E7       0.2
          0.2       0.2
$       GAB       GBC       GCA      AOPT         G      SIGF
    1.32E7    1.32E7 2600000.0       3.0    1000.0       1.0
          0.0       0.0       0.0       0.0       0.0       0.0
          0       0.0
          0.0       0.0       1.0       0.0       0.0       0.0
          0.0       0.0
$
*MAT ELASTIC
$Capping beam
         12       2.4     3.3E7       0.2       0.0       0.0
          0.0
$
*MAT MOHR COULOMB
$Slip MG (Drained), phi=27, E'=46000
$Reduce strength to tan.phi'/ 2 (in Rads)
$       MID        RO      GMOD       RNU     BLANK       PHI
CVAL       PSI
         13       2.0   18400.0      0.25              0.2495
         1.0E-3       0.0
$    Blank   NPLANES     BLANK    LCCPDR     LCCPT    LCCJDR
LCCJT    LCSFAC
          0         0                   0         0         0
          0         0
$   GMODDP    GMODGR    LCGMEP   LCPHIEP   LCPSIEP    LCGMST
CVALGR     ANISO
         0.0       0.0         0         0         0       0.0
         0.0       0.0
$
*MAT_MOHR_COULOMB
$Slip RTD (Drained), phi=42,E'=101000
$Reduce strength to tan.phi'/ 2 (in Rads)
$       MID        RO      GMOD       RNU     BLANK       PHI
CVAL       PSI
         14       2.1   40400.0      0.25               0.423
         1.0E-3       0.0
$    Blank   NPLANES     BLANK    LCCPDR     LCCPT    LCCJDR
LCCJT    LCSFAC
          0         0                   0         0         0
          0         0
$   GMODDP    GMODGR    LCGMEP   LCPHIEP   LCPSIEP    LCGMST
CVALGR     ANISO
         0.0       0.0         0         0         0       0.0
         0.0       0.0
$
*MAT_MOHR_COULOMB
$Slip LC A3i (Undrained) Cu= 75+16.6, Eu=1600 Cu
$Reduce strength to 0.5Cu
$Strata 5m thick, top @ 117mATD
$       MID        RO      GMOD       RNU     BLANK       PHI
CVAL       PSI
         15       2.0   21900.0       0.2              1.0E-3
         37.5       0.0
$    Blank   NPLANES     BLANK    LCCPDR     LCCPT    LCCJDR
LCCJT    LCSFAC
          0         0                   0         0         0
          0         0
```



```
$   GMODDP    GMODGR    LCGMEP   LCPHIEP   LCPSIEP    LCGMST
CVALGR     ANISO
      117.2   -4841.7         0         0         0       0.0
       -8.3       0.0
$
*MAT MOHR COULOMB
$Slip LC A3ii (Undrained), Cu= 161.3+16.6, Eu=1600 Cu
$Reduce strength to 0.5Cu
$Strata 6m thick, top @ 112mATD
$       MID        RO      GMOD       RNU     BLANK       PHI
CVAL       PSI
         16       2.0   47100.0       0.2              1.0E-3
         80.66       0.0
$    Blank   NPLANES     BLANK    LCCPDR     LCCPT    LCCJDR
LCCJT    LCSFAC
          0         0                   0         0         0
          0         0
$   GMODDP    GMODGR    LCGMEP   LCPHIEP   LCPSIEP    LCGMST
CVALGR     ANISO
      112.0   -4841.7         0         0         0       0.0
       -8.3       0.0
$
*MAT MOHR COULOMB
$Slip LC A2 (Undrained), Cu= 210+17.3, Eu=1600 Cu
$Reduce strength to 0.5Cu
$Strata 12m thick, top @ 106mATD
$       MID        RO      GMOD       RNU     BLANK       PHI
CVAL       PSI
         17       2.1   70000.0       0.2              1.0E-3
         105.0       0.0
$    Blank   NPLANES     BLANK    LCCPDR     LCCPT    LCCJDR
LCCJT    LCSFAC
          0         0                   0         0         0
          0         0
$   GMODDP    GMODGR    LCGMEP   LCPHIEP   LCPSIEP    LCGMST
CVALGR     ANISO
      106.0   -5766.7         0         0         0       0.0
       -8.65       0.0
$
*MAT MOHR COULOMB
$Slip LG UMB (Undrained),Cu= 280+17.3kPa, Eu=2500 Cu
$Reduce strength to 0.5Cu
$       MID        RO      GMOD       RNU     BLANK       PHI
CVAL       PSI
         18       2.1  117000.0       0.2              1.0E-3
         140.0       0.0
$    Blank   NPLANES     BLANK    LCCPDR     LCCPT    LCCJDR
LCCJT    LCSFAC
          0         0                   0         0         0
          0         0
$   GMODDP    GMODGR    LCGMEP   LCPHIEP   LCPSIEP    LCGMST
CVALGR     ANISO
       94.5   -2666.7         0         0         0       0.0
       -3.2       0.0
$
*MAT MOHR COULOMB
$Slip LG LMB (Undrained), Cu= 350kPa, Eu=2500 Cu
$Reduce strength to 0.5Cu
$       MID        RO      GMOD       RNU     BLANK       PHI
CVAL       PSI
         19       2.1  146000.0       0.2              1.0E-3
         175.0       0.0
$    Blank   NPLANES     BLANK    LCCPDR     LCCPT    LCCJDR
LCCJT    LCSFAC
          0         0                   0         0         0
          0         0
$   GMODDP    GMODGR    LCGMEP   LCPHIEP   LCPSIEP    LCGMST
CVALGR     ANISO
        0.0       0.0         0         0         0       0.0
        0.0       0.0
$
*MAT_MOHR_COULOMB
```

```
$Slip LG UF (Drained), E'=196800, Phi'=33 deg
$Reduce strength to tan.phi'/ 2 (in Rads)
$       MID         RO       GMOD       RNU      BLANK        PHI
    CVAL        PSI
          20        2.0   82000.0        0.2                0.314
          1.0E-2        0.0
$    Blank   NPLANES      BLANK    LCCPDR     LCCPT    LCCJDR
    LCCJT    LCSFAC
           0         0                  0         0         0
           0         0
$   GMODDP    GMODGR    LCGMEP   LCPHIEP   LCPSIEP    LCGMST
    CVALGR     ANISO
         78.0   -1800.0         0         0         0       0.0
         0.0       0.0
$
*MAT_ELASTIC
$Steel (Wailing beam 2No.UB686*254*170kg/m, P1 level)
          21    0.3335    1.07E8        0.2       0.0       0.0
          0.0
$
*MAT ELASTIC
$Steel (Girder Props 2NoUB533*210*109kg/m, P1 level)
          22    0.2139     2.1E8        0.2       0.0       0.0
          0.0
$
*MAT ELASTIC
$Concrete slabs- weightless and 50% stiffness of concrete (28e6 kPa)
          23       2.4     1.4E7        0.2       0.0       0.0
          0.0
$
*MAT ELASTIC
$Steel (CHS 1220, t=25, P2-horizontal)
          24    0.7228     2.1E8        0.2       0.0       0.0
          0.0
$
*MAT ELASTIC
$Steel (CHS 1067, t=16, P1)
          25    0.4068     2.1E8        0.2       0.0       0.0
          0.0
$
*MAT ELASTIC
$Steel (Wailing beam 2No.UB914*419*343kg/m, P2/P3/P4 level)
          26     0.673    1.76E8        0.2       0.0       0.0
          0.0
$
*MAT ELASTIC
$Steel (CHS 1420, T=23, P2-Corner)
          27    0.7773     2.1E8        0.2       0.0       0.0
          0.0
$
*MAT ELASTIC
$Steel (NONE)
          28      1.35     2.1E8        0.2       0.0       0.0
          0.0
$
*MAT ELASTIC
$Steel (Girder Props 2NoUB610*305*179kg/m, P2/P3level)
          29    0.3512     2.1E8        0.2       0.0       0.0
          0.0
$
*MAT_ELASTIC
$Steel (NONE)
          30    0.7228     2.1E8        0.2       0.0       0.0
          0.0
$
*MAT ELASTIC
$Steel (CHS 1520, t=30, P3-Corner)
          31    1.0814     2.1E8        0.2       0.0       0.0
          0.0
$
*MAT ELASTIC
$Steel (CHS 1420, t=25, P3-Horizontal near the shallow box)
```



```
          32    0.8437     2.1E8        0.2       0.0       0.0
          0.0
$
*MAT ELASTIC
$Steel (CHS 1420, t=40, P4-Corner)
          33    1.3354     2.1E8        0.2       0.0       0.0
          0.0
$
$
$
$ =============
$ SECTION cards
$ =============
$
*SECTION BEAM
$Grade S355 CHS Props-1016 DIA, 16mm thickness
$P1 horizontal + corner props
$       SID     ELFORM       SHRF    QR/IRID       CST     SCOOR
    NSM
           6          1       0.0       2.0       1.0       0.0
           0.0
$       TS1        TS2        TT1        TT2
      1.067      1.067      1.035      1.035       0.0       0.0
$
$
$ Steel props - 2No.UB 533*210*109kg/m, P1 level
$ P1 girder props at corners next to north box
           8          2       0.0       2.0       1.0       0.0
           0.0
$         a        iss        itt        irr         sa        ist
    (Resultant beam)
    1.39E-2   6.682E-4   2.943E-5   1.78E-6       0.0       0.0
$
$
$Grade S355 CHS Props-1220 DIA, 25mm thickness
$P2 horizontal props
$       SID     ELFORM       SHRF    QR/IRID       CST     SCOOR
    NSM
           9          1       0.0       2.0       1.0       0.0
           0.0
$       TS1        TS2        TT1        TT2
      1.22       1.22       1.17       1.17       0.0       0.0
$
$
$Grade S355 CHS Props-1420 DIA, 23mm thickness
$P2 corner props & P3 horizontal props
$       SID     ELFORM       SHRF    QR/IRID       CST     SCOOR
    NSM
          10          1       0.0       2.0       1.0       0.0
           0.0
$       TS1        TS2        TT1        TT2
      1.42       1.42      1.374      1.374       0.0       0.0
$
$
$Grade S355 CHS Props-1520 DIA, 30mm thickness
$P3 corner props
$       SID     ELFORM       SHRF    QR/IRID       CST     SCOOR
    NSM
          11          1       0.0       2.0       1.0       0.0
           0.0
$       TS1        TS2        TT1        TT2
      1.52       1.52       1.46       1.46       0.0       0.0
$
$
$ Steel props-2No.UB610*305*179kg/m
$ P2/P3 girder props at corners next to north box
          12          2       0.0       2.0       1.0       0.0
           0.0
$         a        iss        itt        irr         sa        ist
    (Resultant beam)
    2.28E-2   1.53E-3  1.141E-4    3.4E-6       0.0       0.0
$
```

```
$
$Grade S355 CHS Props-1420 DIA, 25mm thickness
$P3 horizontal props
$       SID     ELFORM       SHRF    QR/IRID        CST      SCOOR
NSM
          13          1        0.0        2.0        1.0        0.0
           0.0
$       TS1        TS2        TT1        TT2
       1.42       1.42       1.37       1.37        0.0        0.0
$
$
$Grade S355 CHS Props-1420 DIA, 40mm thickness
$P4 corner props
$       SID     ELFORM       SHRF    QR/IRID        CST      SCOOR
NSM
          14          1        0.0        2.0        1.0        0.0
           0.0
$       TS1        TS2        TT1        TT2
       1.42       1.42       1.34       1.34        0.0        0.0
$
$
$Grade S355 CHS Props-1220 DIA, 25mm thickness
$P2 horizontal props
$       SID     ELFORM       SHRF    QR/IRID        CST      SCOOR
NSM
          16          1        0.0        2.0        1.0        0.0
           0.0
$       TS1        TS2        TT1        TT2
       0.61       0.61     0.585      0.585        0.0        0.0
$
$
$Grade S355 CHS Props-1220 DIA, 25mm thickness
$P2 horizontal props
$       SID     ELFORM       SHRF    QR/IRID        CST      SCOOR
NSM
          18          1        0.0        2.0        1.0        0.0
           0.0
$       TS1        TS2        TT1        TT2
       0.61       0.61     0.585      0.585        0.0        0.0
$
$
$Grade S355 CHS Props- 1016 DIA, 16mm thickness
$P1 horizontal + corner props
$       SID     ELFORM       SHRF    QR/IRID        CST      SCOOR
NSM
          19          2        0.0        2.0        1.0        0.0
           0.0
$       TS1        TS2        TT1        TT2
   2.28E-2   1.53E-3  1.141E-4    3.4E-6        0.0        0.0
$
          20          1        0.0        2.0        1.0        0.0
           0.0
       1.42       1.42       1.37       1.37        0.0        0.0
$
          21          1        0.0        2.0        1.0        0.0
           0.0
       1.42       1.42       1.34       1.34        0.0        0.0
$
*SECTION_SHELL
$Dwall (1m thick)
           3         16        0.0          0        0.0        0.0
           0          0
         1.0        1.0        1.0        1.0        0.0        0.0
         0.0          0
$
$
$Capping Beam (Assumed 1m thick, 1.5m high)
           4         16        0.0          0        0.0        0.0
           0          0
         1.0        1.0        1.0        1.0        0.0        0.0
         0.0          0
$
```



```
$
$Wailing Beams- Steel beam in 1.66m width from centre of the wall-P1
level
$Thickness based on equivalent EI and EA to real section
           5         16        0.0          0        0.0        0.0
           0          0
         1.0        1.0        1.0        1.0        0.0        0.0
         0.0          0
$
$
$Permenant structural slabs- 700mm thick
           7         16        0.0          0        0.0        0.0
           0          0
         0.7        0.7        0.7        0.7        0.0        0.0
         0.0          0
$
*SECTION_SOLID
$Single integrated soil
           1          1          0
$
$
$Fully_integrated_soil_solids
           2          2          0
$
$
$
$ ===============
$ HOURGLASS cards
$ ===============
$
*HOURGLASS
           1          4        0.0          0        0.0        0.0
           0.0        0.0
$
$
$ ==========
$ PART cards
$ ==========
$
*PART
$HMNAME COMPS      101MG
$HWCOLOR COMPS      101        3
MG
         101          2          1          0          0          0
           0          0
$
*PART
$HMNAME COMPS      102RTD
$HWCOLOR COMPS      102        4
RTD
         102          1          2          0          0          0
           0          0
$
*PART
$HMNAME COMPS      103LC_A3i
$HWCOLOR COMPS      103        5
LC_A3i
         103          1          3          0          0          0
           0          0
$
*PART
$HMNAME COMPS      104LC_A3ii
$HWCOLOR COMPS      104        6
LC_A3ii
         104          1          4          0          0          0
           0          0
$
*PART
$HMNAME COMPS      105LC_A2
$HWCOLOR COMPS      105        7
LC_A2
         105          1          5          0          0          0
```

```
535         0         0
536  $
537  *PART
538  $HMNAME COMPS     106LG_UMB
539  $HWCOLOR COMPS     106       8
540  LG_UMB
541         106         1         6         0         0         0
            0         0
542  $
543  *PART
544  $HMNAME COMPS     107LG_LMB
545  $HWCOLOR COMPS     107       9
546  LG_LMB
547         107         1         7         0         0         0
            0         0
548  $
549  *PART
550  $HMNAME COMPS     108LG_LMB_UF
551  $HWCOLOR COMPS     108      13
552  LG_LMB_UF
553         108         1         8         0         0         0
            0         0
554  $
555  *PART
556  $HMNAME COMPS     109Ts
557  $HWCOLOR COMPS     109      17
558  Ts
559         109         1         9         0         0         0
            0         0
560  $
561  *PART
562  $HMNAME COMPS     110S_MG_Ex1
563  $HWCOLOR COMPS     110      20
564  S_MG_Ex1
565         110         2         1         0         0         0
            0         0
566  $
567  *PART
568  $HMNAME COMPS     112S_RTD_Ex2
569  $HWCOLOR COMPS     112      24
570  S_RTD_Ex2
571         112         1         2         0         0         0
            0         0
572  $
573  *PART
574  $HMNAME COMPS     113S_LC_A3i Ex2
575  $HWCOLOR COMPS     113      25
576  S_LC_A3i Ex2
577         113         1         3         0         0         0
            0         0
578  $
579  *PART
580  $HMNAME COMPS     114S_LC_A3i Ex3
581  $HWCOLOR COMPS     114      28
582  S_LC_A3i Ex3
583         114         1         3         0         0         0
            0         0
584  $
585  *PART
586  $HMNAME COMPS     115S_LC_A3i Ex3.1
587  $HWCOLOR COMPS     115      29
588  S_LC_A3i Ex3.1
589         115         1         3         0         0         0
            0         0
590  $
591  *PART
592  $HMNAME COMPS     116S_LC_A3ii_Ex4
593  $HWCOLOR COMPS     116      33
594  S_LC_A3ii Ex4
595         116         1         4         0         0         0
            0         0
596  $
```



```
597  *PART
598  $HMNAME COMPS     117S_LC_A3ii_Ex5
599  $HWCOLOR COMPS     117      35
600  S_LC_A3ii Ex5
601         117         1         4         0         0         0
            0         0
602  $
603  *PART
604  $HMNAME COMPS     118S_LC_A2 Ex5
605  $HWCOLOR COMPS     118      37
606  S_LC_A2 Ex5
607         118         1         5         0         0         0
            0         0
608  $
609  *PART
610  $HMNAME COMPS     119S_LC_A2 Ex6
611  $HWCOLOR COMPS     119      40
612  S_LC_A2 Ex6
613         119         1         5         0         0         0
            0         0
614  $
615  *PART
616  $HMNAME COMPS     120S_Piles LC_A2
617  $HWCOLOR COMPS     120      41
618  S_Piles LC_A2
619         120         1         5         0         0         0
            0         0
620  $
621  *PART
622  $HMNAME COMPS     121S_P-Slip LC_A2
623  $HWCOLOR COMPS     121      44
624  S_P-Slip LC_A2
625         121         1         5         0         0         0
            0         0
626  $
627  *PART
628  $HMNAME COMPS     122S_Piles LG_UMB
629  $HWCOLOR COMPS     122      48
630  S_Piles LG_UMB
631         122         1         6         0         0         0
            0         0
632  $
633  *PART
634  $HMNAME COMPS     123S_P-Slip LG_UMB
635  $HWCOLOR COMPS     123      49
636  S_P-Slip LG_UMB
637         123         1         6         0         0         0
            0         0
638  $
639  *PART
640  $HMNAME COMPS     124S_Piles LG_LMB
641  $HWCOLOR COMPS     124      52
642  S_Piles LG_LMB
643         124         1         7         0         0         0
            0         0
644  $
645  *PART
646  $HMNAME COMPS     125S_P-Slip LG_LMB
647  $HWCOLOR COMPS     125      53
648  S_P-Slip LG_LMB
649         125         1         7         0         0         0
            0         0
650  $
651  *PART
652  $HMNAME COMPS     126S_Piles LG_UF
653  $HWCOLOR COMPS     126      56
654  S_Piles LG_UF
655         126         1         8         0         0         0
            0         0
656  $
657  *PART
658  $HMNAME COMPS     130S_Inner_MG_Ex1
```

```
$HWCOLOR COMPS     130      60
S_Inner MG_Ex1
        130         2         1         0         0         0
        0         0
$
*PART
$HMNAME COMPS     132S_Outer_MG
$HWCOLOR COMPS     132      64
S_Outer_MG
        132         2         1         0         0         0
        0         0
$
*PART
$HMNAME COMPS     133S_Inner_RTD_Ex2
$HWCOLOR COMPS     133       3
S_Inner_RTD_Ex2
        133         1         2         0         0         0
        0         0
$
*PART
$HMNAME COMPS     134S_Outer_RTD
$HWCOLOR COMPS     134       4
S_Outer_RTD
        134         1         2         0         0         0
        0         0
$
*PART
$HMNAME COMPS     135S_Inner_LC_A3i_Ex2
$HWCOLOR COMPS     135       5
S_Inner LC_A3i_Ex2
        135         1         3         0         0         0
        0         0
$
*PART
$HMNAME COMPS     136S_Inner_LC_A3i_Ex3
$HWCOLOR COMPS     136       6
S_Inner LC_A3i_Ex3
        136         1         3         0         0         0
        0         0
$
*PART
$HMNAME COMPS     137S_Inner_LC_A3i_Ex4
$HWCOLOR COMPS     137       7
S_Inner LC_A3i_Ex4
        137         1         3         0         0         0
        0         0
$
*PART
$HMNAME COMPS     138S_Outer_LC_A3i
$HWCOLOR COMPS     138       8
S_Outer LC_A3i
        138         1         3         0         0         0
        0         0
$
*PART
$HMNAME COMPS     139S_Inner_LC_A3ii_Ex4
$HWCOLOR COMPS     139       9
S_Inner LC_A3ii_Ex4
        139         1         4         0         0         0
        0         0
$
*PART
$HMNAME COMPS     140S_Inner LC_A3ii_Ex5
$HWCOLOR COMPS     140      13
S_Inner LC_A3ii_Ex5
        140         2         4         0         0         0
        0         0
$
*PART
$HMNAME COMPS     141S_Outer_A3ii
$HWCOLOR COMPS     141      17
S_Outer_A3ii
```



```
        141         2         4         0         0         0
        0         0
$
*PART
$HMNAME COMPS     142S_Inner A2_Ex5
$HWCOLOR COMPS     142      20
S_Inner A2_Ex5
        142         1         5         0         0         0
        0         0
$
*PART
$HMNAME COMPS     143S_Inner A2_Ex6
$HWCOLOR COMPS     143      29
S_Inner A2_Ex6
        143         1         5         0         0         0
        0         0
$
*PART
$HMNAME COMPS     144S_Outer A2
$HWCOLOR COMPS     144      24
S_Outer A2
        144         1         5         0         0         0
        0         0
$
*PART
$HMNAME COMPS     145S_DSlips LG_UMB
$HWCOLOR COMPS     145      25
S_DSlips LG_UMB
        145         1         6         0         0         0
        0         0
$
*PART
$HMNAME COMPS     146S_DSlips LG_LMB
$HWCOLOR COMPS     146      28
S_DSlips LG_LMB
        146         1         7         0         0         0
        0         0
$
*PART
$HMNAME COMPS     155N_MG_Ex1
$HWCOLOR COMPS     155      29
N_MG_Ex1
        155         2         1         0         0         0
        0         0
$
*PART
$HMNAME COMPS     157N_RTD_Ex2
$HWCOLOR COMPS     157      35
N_RTD_Ex2
        157         1         2         0         0         0
        0         0
$
*PART
$HMNAME COMPS     158N_LC_A3i Ex2
$HWCOLOR COMPS     158      37
N_LC_A3i Ex2
        158         1         3         0         0         0
        0         0
$
*PART
$HMNAME COMPS     159N_LC_A3i Ex3
$HWCOLOR COMPS     159      40
N_LC_A3i Ex3
        159         1         3         0         0         0
        0         0
$
*PART
$HMNAME COMPS     160S_Piles LC_A3i
$HWCOLOR COMPS     160      41
S_Piles LC_A3i
        160         1         3         0         0         0
        0         0
```

```
$
*PART
$HMNAME COMPS     161S_P-Slip LC_A3i
$HWCOLOR COMPS     161      44
S_P-Slip LC_A3i
       161         1         3         0         0         0
       0         0
$
*PART
$HMNAME COMPS     162S_Piles LC_A3ii
$HWCOLOR COMPS     162      48
S_Piles LC_A3ii
       162         1         4         0         0         0
       0         0
$
*PART
$HMNAME COMPS     163S_P-Slip LC_A3ii
$HWCOLOR COMPS     163      49
S_P-Slip LC_A3ii
       163         1         4         0         0         0
       0         0
$
*PART
$HMNAME COMPS     164S_Piles LC_A2.1
$HWCOLOR COMPS     164      52
S_Piles LC_A2.1
       164         1         5         0         0         0
       0         0
$
*PART
$HMNAME COMPS     165S_P-Slip LC_A2.1
$HWCOLOR COMPS     165      53
S_P-Slip LC_A2.1
       165         1         5         0         0         0
       0         0
$
*PART
$HMNAME COMPS     166S_Piles LG_UMB.1
$HWCOLOR COMPS     166      56
S_Piles LG_UMB.1
       166         1         6         0         0         0
       0         0
$
*PART
$HMNAME COMPS     167S_P-Slip LG_UMB.1
$HWCOLOR COMPS     167      57
S_P-Slip LG_UMB.1
       167         1         6         0         0         0
       0         0
$
*PART
$HMNAME COMPS     170N_Inner MG_Ex1
$HWCOLOR COMPS     170      60
N_Inner MG_Ex1
       170         2         1         0         0         0
       0         0
$
*PART
$HMNAME COMPS     172N_Outer MG
$HWCOLOR COMPS     172      64
N_Outer MG
       172         2         1         0         0         0
       0         0
$
*PART
$HMNAME COMPS     173N_Inner_RTD_Ex2
$HWCOLOR COMPS     173      3
N_Inner_RTD_Ex2
       173         1         2         0         0         0
       0         0
$
*PART
```



```
$HMNAME COMPS     174N_Outer_RTD
$HWCOLOR COMPS     174      4
N_Outer RTD
       174         1         2         0         0         0
       0         0
$
*PART
$HMNAME COMPS     175N_Inner_LC_A3i_Ex2
$HWCOLOR COMPS     175      5
N_Inner LC_A3i_Ex2
       175         1         3         0         0         0
       0         0
$
*PART
$HMNAME COMPS     176N_Outer_LC_A3i
$HWCOLOR COMPS     176      6
N_Outer LC_A3i
       176         1         3         0         0         0
       0         0
$
*PART
$HMNAME COMPS     177N_Inner_LC_A3i_Ex3
$HWCOLOR COMPS     177      7
N_Inner LC_A3i_Ex3
       177         1         3         0         0         0
       0         0
$
*PART
$HMNAME COMPS     178N_DSlips LC_A3ii
$HWCOLOR COMPS     178      8
N_DSlips LC_A3ii
       178         1         4         0         0         0
       0         0
$
*PART
$HMNAME COMPS     200D_Wall
D_Wall
       200         3        11         0         0         0
       0         0
$
*PART
$HMNAME COMPS     201Dividing Wall
Dividing Wall
       201         3        11         0         0         0
       0         0
$
*PART
$HMNAME COMPS     202Capping Beam
Capping Beam
       202         4        12         0         0         0
       0         0
$
*PART
$HMNAME COMPS     203Pile-Concrete
$HWCOLOR COMPS     203      11
Pile-Concrete
       203         2        10         0         0         0
       0         0
$
*PART
$HMNAME COMPS     204S_Base Slab_Concrete
$HWCOLOR COMPS     204      15
S_Base Slab_Concrete
       204         2        10         0         0         0
       0         0
$
*PART
$HMNAME COMPS     205N_Base Slab_Concrete
$HWCOLOR COMPS     205      32
N_Base Slab_Concrete
       205         2        10         0         0         0
       0         0
```

```
$
*PART
$HMNAME COMPS     300S_Wailer_P1
S_Wailer P1
         300         5        21         0         0         0
         0         0
$
*PART
$HMNAME COMPS     301S_Beams_P1
S_Beams P1
         301         6        25         0         0         0
         0         0
$
*PART
$HMNAME COMPS     303S_Beams_P2 _girder
S_Beams P2 _girder
         303        12        29         0         0         0
         0         0
$
*PART
$HMNAME COMPS     304S_Wailer_P2_horizontal
S_Wailer P2_horizontal
         304         5        26         0         0         0
         0         0
$
*PART
$HMNAME COMPS     305S_Beam_P2_H
S_Beam_P2 H
         305         9        24         0         0         0
         0         0
$
*PART
$HMNAME COMPS     307S_Beam_P2_corner
S_Beam_P2_corner
         307        10        27         0         0         0
         0         0
$
*PART
$HMNAME COMPS     308S_Wailer_P3
S_Wailer P3
         308         5        26         0         0         0
         0         0
$
*PART
$HMNAME COMPS     309S_Beams_P3_H
S_Beams P3_H
         309        13        32         0         0         0
         0         0
$
*PART
$HMNAME COMPS     310S_Wailer_P4
S_Wailer P4
         310         5        26         0         0         0
         0         0
$
*PART
$HMNAME COMPS     311S_Beams_P4_Corner
S_Beams P4_Corner
         311        14        33         0         0         0
         0         0
$
*PART
$HMNAME COMPS     320North Propping P1_Wailer
North Propping P1_Wailer
         320         5        21         0         0         0
         0         0
$
*PART
$HMNAME COMPS     321North Propping P1_Beams
North Propping P1_Beams
         321         6        22         0         0         0
         0         0
```



```
$
*PART
$HMNAME COMPS     322North Propping P2_Wailer
North Propping P2_Wailer
         322         5        21         0         0         0
         0         0
$
*PART
$HMNAME COMPS     324North Propping P2_Beams
North Propping P2_Beams
         324         6        22         0         0         0
         0         0
$
*PART
$HMNAME COMPS     350Slab Level -3
Slab Level -3
         350         7        23         0         0         0
         0         0
$
*PART
$HMNAME COMPS     352Slab Level -4
Slab Level -4
         352         7        23         0         0         0
         0         0
$
*PART
$HMNAME COMPS     353Slab Level -2
Slab Level -2
         353         7        23         0         0         0
         0         0
$
*PART
$HMNAME COMPS     354Slab Level -1
Slab Level -1
         354         7        23         0         0         0
         0         0
$
*PART
$HMNAME COMPS     355Roof Slab Level 0
Roof Slab Level 0
         355         7        23         0         0         0
         0         0
$
*PART
$HMNAME COMPS     400MC_S_P-Slip_LC_A2
$HWCOLOR COMPS     400       29
MC_S_P-Slip_LC_A2
         400         1        17         0         0         0
         0         0
$
*PART
$HMNAME COMPS     401MC_S_P-Slip_LG_UMB
$HWCOLOR COMPS     401       53
MC_S_P-Slip_LG_UMB
         401         1        18         0         0         0
         0         0
$
*PART
$HMNAME COMPS     402MC_S_P-Slip_LG_LMB
$HWCOLOR COMPS     402       45
MC_S_P-Slip_LG_LMB
         402         1        19         0         0         0
         0         0
$
*PART
$HMNAME COMPS     403MC_S_Pile Slip_LC_A2_Base Slab_Ex
$HWCOLOR COMPS     403       37
MC_S_Pile Slip_LC_A2_Base Slab_Ex
         403         1        17         0         0         0
         0         0
$
*PART
```

```
$HMNAME COMPS     404MC_N_P-Slip_LC_A3i
$HWCOLOR COMPS     404       26
MC_N_P-Slip_LC_A3i
        404         1        15         0         0         0
        0         0
$
*PART
$HMNAME COMPS     405MC_N_P-Slip_LC_A3ii
$HWCOLOR COMPS     405       31
MC_N_P-Slip_LC_A3ii
        405         1        16         0         0         0
        0         0
$
*PART
$HMNAME COMPS     406MC_N_P-Slip_LC_A2
$HWCOLOR COMPS     406       38
MC_N_P-Slip_LC_A2
        406         1        17         0         0         0
        0         0
$
*PART
$HMNAME COMPS     407MC_N_P-Slip_LG-UMB
$HWCOLOR COMPS     407       46
MC_N_P-Slip_LG-UMB
        407         1        18         0         0         0
        0         0
$
*PART
$HMNAME COMPS     410MC_S_Inner_MG_Ex1
$HWCOLOR COMPS     410       57
MC_S_Inner_MG_Ex1
        410         2        13         0         0         0
        0         0
$
*PART
$HMNAME COMPS     412MC_S_Outer_MG
$HWCOLOR COMPS     412       59
MC_S_Outer_MG
        412         2        13         0         0         0
        0         0
$
*PART
$HMNAME COMPS     413MC_S_Inner_RTD_Ex2
$HWCOLOR COMPS     413       49
MC_S_Inner_RTD_Ex2
        413         1        14         0         0         0
        0         0
$
*PART
$HMNAME COMPS     414MC_S_Outer_RTD
$HWCOLOR COMPS     414       51
MC_S_Outer_RTD
        414         1        14         0         0         0
        0         0
$
*PART
$HMNAME COMPS     415MC_S_Inner_LC_A3i_Ex2
$HWCOLOR COMPS     415       41
MC_S_Inner_LC_A3i_Ex2
        415         1        15         0         0         0
        0         0
$
*PART
$HMNAME COMPS     416MC_S_Inner_LC_A3i_Ex3
$HWCOLOR COMPS     416       43
MC_S_Inner_LC_A3i_Ex3
        416         1        15         0         0         0
        0         0
$
*PART
$HMNAME COMPS     417MC_S_Inner_LC_A3i_Ex4
$HWCOLOR COMPS     417       33
```



```
MC_S_Inner_LC_A3i_Ex4
        417         1        15         0         0         0
        0         0
$
*PART
$HMNAME COMPS     418MC_S_Outer_LC_A3i
$HWCOLOR COMPS     418       35
MC_S_Outer_LC_A3i
        418         1        15         0         0         0
        0         0
$
*PART
$HMNAME COMPS     419MC_S_Inner_LC_A3ii_Ex4
$HWCOLOR COMPS     419       25
MC_S_Inner_LC_A3ii_Ex4
        419         1        16         0         0         0
        0         0
$
*PART
$HMNAME COMPS     420MC_S_Inner_LC_A3ii_Ex5
$HWCOLOR COMPS     420       27
MC_S_Inner_LC_A3ii_Ex5
        420         2        16         0         0         0
        0         0
$
*PART
$HMNAME COMPS     421MC_S_Outer_LC_A3ii
$HWCOLOR COMPS     421       17
MC_S_Outer_LC_A3ii
        421         2        16         0         0         0
        0         0
$
*PART
$HMNAME COMPS     422MC_S_Inner_LC_A2_Ex5
$HWCOLOR COMPS     422        9
MC_S_Inner_LC_A2_Ex5
        422         1        17         0         0         0
        0         0
$
*PART
$HMNAME COMPS     423MC_S_Inner_LC_A2_Ex6
$HWCOLOR COMPS     423       12
MC_S_Inner_LC_A2_Ex6
        423         1        17         0         0         0
        0         0
$
*PART
$HMNAME COMPS     424MC_S_Outer_LC_A2
$HWCOLOR COMPS     424       21
MC_S_Outer_LC_A2
        424         1        17         0         0         0
        0         0
$
*PART
$HMNAME COMPS     425MC_S_DSlip_LG_UMB
$HWCOLOR COMPS     425       29
MC_S_DSlip_LG_UMB
        425         1        18         0         0         0
        0         0
$
*PART
$HMNAME COMPS     426MC_S_DSlip_LG_LMB
$HWCOLOR COMPS     426       31
MC_S_DSlip_LG_LMB
        426         1        19         0         0         0
        0         0
$
*PART
$HMNAME COMPS     427MC_N_Inner_MG_Ex1
$HWCOLOR COMPS     427       57
MC_N_Inner_MG_Ex1
        427         2        13         0         0         0
```

```
1149         0         0
1150  $
1151  *PART
1152  $HMNAME COMPS     429MC_N_Outer_MG
1153  $HWCOLOR COMPS     429       61
1154  MC_N_Outer_MG
1155         429         2        13         0         0         0
              0         0
1156  $
1157  *PART
1158  $HMNAME COMPS     430MC_N_Inner_RTD_Ex2
1159  $HWCOLOR COMPS     430       49
1160  MC_N_Inner_RTD_Ex2
1161         430         1        14         0         0         0
              0         0
1162  $
1163  *PART
1164  $HMNAME COMPS     431MC_N_Outer_RTD
1165  $HWCOLOR COMPS     431       29
1166  MC_N_Outer_RTD
1167         431         1        14         0         0         0
              0         0
1168  $
1169  *PART
1170  $HMNAME COMPS     432MC_N_Inner_LC_A3i_Ex2
1171  $HWCOLOR COMPS     432       50
1172  MC_N_Inner_LC_A3i_Ex2
1173         432         1        15         0         0         0
              0         0
1174  $
1175  *PART
1176  $HMNAME COMPS     434MC_N_Outer_LC_A3i
1177  $HWCOLOR COMPS     434       42
1178  MC_N_Outer_LC_A3i
1179         434         1        15         0         0         0
              0         0
1180  $
1181  *PART
1182  $HMNAME COMPS     435MC_N_Inner_LC_A3i_Ex3
1183  $HWCOLOR COMPS     435       34
1184  MC_N_Inner_LC_A3i_Ex3
1185         435         1        15         0         0         0
              0         0
1186  $
1187  *PART
1188  $HMNAME COMPS     436MC_N_DSlip_LC_A3ii
1189  $HWCOLOR COMPS     436       26
1190  MC_N_DSlip_LC_A3ii
1191         436         1        16         0         0         0
              0         0
1192  $
1193  *PART
1194  $HMNAME COMPS    1191S_LC_A2 Ex7_base slab
1195  $HWCOLOR COMPS    1191       30
1196  S_LC_A2 Ex7_base slab
1197        1191         1         5         0         0         0
              0         0
1198  $
1199  *PART
1200  $HMNAME COMPS    1431S_Inner A2_Ex7_base slab
1201  $HWCOLOR COMPS    1431       37
1202  S_Inner A2_Ex7_base slab
1203        1431         1         5         0         0         0
              0         0
1204  $
1205  *PART
1206  $HMNAME COMPS    1591N_LC_A3i Ex4_base slab
1207  $HWCOLOR COMPS    1591       50
1208  N_LC_A3i Ex4_base slab
1209        1591         1         3         0         0         0
              0         0
1210  $
```



```
1211  *PART
1212  $HMNAME COMPS    2011Dividing Wall_Ex
1213  Dividing Wall_Ex
1214         2011         3        11         0         0         0
              0         0
1215  $
1216  *PART
1217  $HMNAME COMPS    4231MC_S_Inner_LC_A2_Ex7_base slab
1218  $HWCOLOR COMPS    4231       37
1219  MC_S_Inner_LC_A2_Ex7_base slab
1220         4231         1        17         0         0         0
              0         0
1221  $
1222  *PART
1223  $HMNAME COMPS    4351MC_N_Inner_LC_A3i_Ex4_base slab
1224  $HWCOLOR COMPS    4351       61
1225  MC_N_Inner_LC_A3i_Ex4_base slab
1226         4351         1        15         0         0         0
              0         0
1227  $
1228  *PART
1229  $HMNAME COMPS    4352S_Beams_P1_girder
1230  S_Beams P1_girder
1231         4352         8        22         0         0         0
              0         0
1232  $
1233  *PART
1234  $HMNAME COMPS    4353S_Wailer_P1_Corner
1235  S_Wailer P1_Corner
1236         4353         5        21         0         0         0
              0         0
1237  $
1238  *PART
1239  $HMNAME COMPS    4354S_Beam_P3_Corner
1240  S_Beam P3 Corner
1241         4354        11        31         0         0         0
              0         0
1242  $
1243  *PART
1244  $HMNAME COMPS    4355S_Beam_P3_girder
1245  S_Beam P3 girder
1246         4355        12        29         0         0         0
              0         0
1247  $
1248  *PART
1249  $HMNAME COMPS    4356S_Beam_P4_H
1250  S_Beam P4 H
1251         4356        10        27         0         0         0
              0         0
1252  $
1253  *PART
1254  $HMNAME COMPS    4357S_Wailer_P2_corner_1
1255  S_Wailer P2_corner
1256         4357         5        26         0         0         0
              0         0
1257  $
1258  *PART
1259  $HMNAME COMPS    4358S_Beams_P3_H_end
1260  S_Beams P3_H-end
1261         4358         9        24         0         0         0
              0         0
1262  $
1263  $
1264  $
1265  $ ============
1266  $ DEFINE cards
1267  $ ============
1268  $
1269  $
1270  *DEFINE_CURVE
1271  $
1272  $: Cross-reference summary for Load-curve 2
```

```
$: ------------------------------------------------
$
$: Structural material 3 : G/Gmax vs String lengths
$: X axis : String lengths              (Units: Position)
$: Y axis : G/Gmax                      (Units: Scalar, no units)
$
$: Structural material 4 : G/Gmax vs String lengths
$: X axis : String lengths              (Units: Position)
$: Y axis : G/Gmax                      (Units: Scalar, no units)
$
$: Structural material 5 : G/Gmax vs String lengths
$: X axis : String lengths              (Units: Position)
$: Y axis : G/Gmax                      (Units: Scalar, no units)
$
$: Structural material 6 : G/Gmax vs String lengths
$: X axis : String lengths              (Units: Position)
$: Y axis : G/Gmax                      (Units: Scalar, no units)
$
$: Structural material 7 : G/Gmax vs String lengths
$: X axis : String lengths              (Units: Position)
$: Y axis : G/Gmax                      (Units: Scalar, no units)
$
$: Structural material 8 : G/Gmax vs String lengths
$: X axis : String lengths              (Units: Position)
$: Y axis : G/Gmax                      (Units: Scalar, no units)
$
$: Usage: Transient analysis
$
$
$$Brick strings (most probable)
          2         0       0.0       0.0       0.0       0.0
          0         0
         2.9999999E-5          0.92000002
         7.5000004E-5          0.75000000
         1.5000001E-4          0.60000002
         2.5000001E-4          0.50000000
         5.0000002E-4          0.34999999
         1.0000000E-3          0.25000000
         1.5000000E-3          0.15000001
         2.0000001E-3        5.0000001E-2
         3.3000000E-3        9.9999998E-3
         3.9999999E-2                 0.0
$
$
*DEFINE_CURVE
$
$: Cross-reference summary for Load-curve 22
$: ------------------------------------------------
$
$: Loading definition <No label>: Factor vs time
$: X axis : Time                        (Units: Time)
$: Y axis : Factor                      (Units: Scalar, no units)
$:    :
$: (To a total of 26 unlabelled Loading definition entries)
$
$: Usage: Transient analysis
$
$
$ Load Gravity Curve
         22         0       0.0       0.0       0.0       0.0
         0         0
                  0.0                 0.0
            1.0000000           1.0000000
            100.00000           1.0000000
$
$
*DEFINE_CURVE
$
$: Cross-reference summary for Load-curve 111
$: ------------------------------------------------
$
$: Control card <No label>: Limiting timestep size vs time
```



```
$: X axis : Time                        (Units: Time)
$: Y axis : Limiting timestep           (Units: Time)
$
$: Usage: Transient analysis
$
       111         0       0.0       0.0       0.0       0.0
         0         0
                   0.0        1.9999999E-4
            100.00000        1.9999999E-4
$
$
*DEFINE_CURVE
$
$: Cross-reference summary for Load-curve 400
$: ------------------------------------------------
$
$: Global damping <No label>: Global nodal damping vs time
$: X axis : Time                        (Units: Time)
$: Y axis : Global nodal mass-weighted damping  (Units: Mass damping)
$
$: Usage: Transient analysis
$
$
$load curve for viscous damping
       400         0       0.0       0.0       0.0       0.0
         0         0
                   0.0           10.000000
            1.0000000           10.000000
            1.1000000           10.000000
            100.00000           10.000000
$
$
*DEFINE_CURVE
$
$: Cross-reference summary for Load-curve 880
$: ------------------------------------------------
$
$: Boundary condition <No label>: Analysis type vs. time
$: X axis : Time                        (Units: Time)
$: Y axis : Analysis type               (Units: Scalar, no units)
$:    :
$: (To a total of 71 unlabelled Boundary condition entries)
$
$: Usage: Transient analysis
$
       880         0       0.0       0.0       0.0       0.0
         0         0
                   0.0           2.0000000
            1.0000000           2.0000000
            1.1000000           1.0000000
            8.0000000           1.0000000
            100.00000           1.0000000
$
*DEFINE_CONSTRUCTION_STAGES
$    STAGE     START       END      RAMP  RL_START    RL_END
         1       0.0       1.0       0.1       0.0       1.0
         0
         2       1.0       2.0       0.1       1.0       2.0
         0
         3       2.0       3.0       0.1       2.0       3.0
         0
         4       3.0       4.0       0.1       3.0       4.0
         0
         5       4.0       5.0       0.1       4.0       5.0
         0
         6       5.0       6.0       0.1       5.0       6.0
         0
         7       6.0       7.0       0.1       6.0       7.0
         0
         8       7.0       8.0       0.1       7.0       8.0
         0
         9       8.0       9.0       0.1       8.0       9.0
```

```
1403           0
1404          10       9.0      10.0       0.1       9.0      10.0
              0
1405          11      10.0      11.0       0.1      10.0      11.0
              0
1406          12      11.0      12.0       0.1      11.0      12.0
              0
1407          13      12.0      13.0       0.1      12.0      13.0
              0
1408          14      13.0      14.0       0.1      13.0      14.0
              0
1409          15      14.0      15.0       0.1      14.0      15.0
              0
1410          16      15.0      16.0       0.1      15.0      16.0
              0
1411          17      16.0      17.0       0.1      16.0      17.0
              0
1412          18      17.0      18.0       0.1      17.0      18.0
              0
1413          19      18.0      19.0       0.1      18.0      19.0
              0
1414          20      19.0      20.0       0.1      19.0      20.0
              0
1415          21      20.0      21.0       0.1      20.0      21.0
              0
1416          22      21.0      22.0       0.1      21.0      22.0
              0
1417          23      22.0      23.0       0.1      22.0      23.0
              0
1418          24      23.0      24.0       0.1      23.0      24.0
              0
1419          25      24.0      25.0       0.1      24.0      25.0
              0
1420  *DEFINE_STAGED_CONSTRUCTION_PART
1421  $
1422  $       PID       ADD    REMOVE
1423  $Stratigraphy
1424          101         0         0
1425          102         0         0
1426          103         0         0
1427          104         0         0
1428          105         0         0
1429          106         0         0
1430          107         0         0
1431          108         0         0
1432          109         0         0
1433  $South Box Soil
1434          110         0         3
1435          112         0         4
1436          113         0         4
1437          114         0         5
1438          115         0         5
1439          116         0         6
1440          117         0         7
1441          118         0         7
1442          119         0         8
1443         1191         0         9
1444  $South Box Piles (soil) & slips
1445          120         0         2
1446          121         0         2
1447          122         0         2
1448          123         0         2
1449          124         0         2
1450          125         0         2
1451          126         0         2
1452  $South Box DWall Slips
1453          130         0         2
1454          132         0         2
1455          133         0         2
1456          134         0         2
1457          135         0         2
1458          136         0         2
```



```
1459          137         0         2
1460          138         0         2
1461          139         0         2
1462          140         0         2
1463          141         0         2
1464          142         0         2
1465          143         0         2
1466         1431         0         2
1467          144         0         2
1468          145         0         2
1469          146         0         2
1470  $North Box Soil
1471          155         0        15
1472          157         0        17
1473          158         0        17
1474          159         0        18
1475         1591         0        19
1476  $North Box Piles (soil) & slips
1477          160         0         2
1478          161         0         2
1479          162         0         2
1480          163         0         2
1481          164         0         2
1482          165         0         2
1483          166         0         2
1484          167         0         2
1485  $North Box DWall Slips
1486          170         0         2
1487          172         0         2
1488          173         0         2
1489          174         0         2
1490          175         0         2
1491          176         0         2
1492          177         0         2
1493          178         0         2
1494  $Dwall
1495          200         2         0
1496  $Dividing Wall
1497          201         2         0
1498         2011         2        18
1499  $Capping Beam
1500          202         2         0
1501  $Concrete Piles
1502          203         2         0
1503  $South Box base slab
1504          204         9         0
1505  $North Base Slab
1506          205        19         0
1507  $M-C Pile Slips
1508          403         2         9
1509          400         2         0
1510          401         2         0
1511          402         2         0
1512          404         2        19
1513          405         2         0
1514          406         2         0
1515          407         2         0
1516  $M-C South Box DWall Slips
1517          410         2         3
1518          412         2         0
1519          413         2         4
1520          414         2         0
1521          415         2         4
1522          416         2         5
1523          417         2         6
1524          418         2         0
1525          419         2         6
1526          420         2         7
1527          421         2         0
1528          422         2         7
1529          423         2         8
1530         4231         2         9
```

```
1531         424         2          0
1532         425         2          0
1533         426         2          0
1534  $M-C North Box DWall Slips
1535         427         2         15
1536         429         2          0
1537         430         2         17
1538         431         2          0
1539         432         2         17
1540         434         2          0
1541         435         2         18
1542        4351         2         19
1543         436         2          0
1544  $Propping P1
1545         300         4         22
1546        4353         4         22
1547         301         4         22
1548        4352         4         22
1549  $Propping P2
1550        4357         5         20
1551         304         5         20
1552         303         5         20
1553         305         5         20
1554         307         5         20
1555  $Propping P3
1556         308         6         13
1557         309         6         13
1558        4354         6         13
1559        4355         6         13
1560        4358         6         13
1561  $Propping P4
1562         310         7         11
1563         311         7         11
1564        4356         7         11
1565  $Slab Level -3
1566         350        12          0
1567  $Slab Level -4
1568         352        14          0
1569  $Slab Level -2
1570         353        14          0
1571  $North Propping P1
1572         320        17         22
1573         321        17         22
1574  $North Propping P2
1575         322        18         20
1576         324        18         20
1577  $North Base Slab******
1578  $       205        19          0
1579  $Slab Level -1
1580         354        21          0
1581  $Roof Slab Level 0
1582         355        23          0
1583  $
1584  $
1585  $ =============
1586  $ DAMPING cards
1587  $ =============
1588  $
1589  *DAMPING GLOBAL
1590         400       0.0       0.0       0.0       0.0       0.0
              0.0       0.0
1591  $
1592  $
1593  $ ==============
1594  $ BOUNDARY cards
1595  $ ==============
1596  $
1597  *BOUNDARY_PORE_FLUID_PART
1598  $
1599  $Geology
1600         101       0.0       0.0         2       0.0         0
               0       0.0
```



```
1601         102       0.0       0.0         2       0.0         0
               0       0.0
1602         103       0.0       0.0         2       0.0       880
               0     100.0
1603         104       0.0       0.0         2       0.0       880
               0     100.0
1604         105       0.0       0.0         2       0.0       880
               0     100.0
1605         106       0.0       0.0         2       0.0       880
               0     100.0
1606         107       0.0       0.0         2       0.0       880
               0     100.0
1607         108       0.0       0.0         2       0.0         0
               0       0.0
1608         109       0.0       0.0         2       0.0         0
               0       0.0
1609  $South Box Soil
1610         110       0.0       0.0         2       0.0         0
               0       0.0
1611         112       0.0       0.0         2       0.0         0
               0       0.0
1612         113       0.0       0.0         2       0.0       880
               0     100.0
1613         114       0.0       0.0         2       0.0       880
               0     100.0
1614         115       0.0       0.0         2       0.0       880
               0     100.0
1615         116       0.0       0.0         2       0.0       880
               0     100.0
1616         117       0.0       0.0         2       0.0       880
               0     100.0
1617         118       0.0       0.0         2       0.0       880
               0     100.0
1618         119       0.0       0.0         2       0.0       880
               0     100.0
1619        1191       0.0       0.0         2       0.0       880
              0     100.0
1620  $South Box Piles Initial
1621         120       0.0       0.0         2       0.0       880
               0     100.0
1622         121       0.0       0.0         2       0.0       880
               0     100.0
1623         122       0.0       0.0         2       0.0       880
               0     100.0
1624         123       0.0       0.0         2       0.0       880
               0     100.0
1625         124       0.0       0.0         2       0.0       880
               0     100.0
1626         125       0.0       0.0         2       0.0       880
               0     100.0
1627         126       0.0       0.0         2       0.0         0
               0       0.0
1628  $South Box DWall Slips
1629         130       0.0       0.0         2       0.0         0
               0       0.0
1630         132       0.0       0.0         2       0.0         0
               0       0.0
1631         133       0.0       0.0         2       0.0         0
               0       0.0
1632         134       0.0       0.0         2       0.0         0
               0       0.0
1633         135       0.0       0.0         2       0.0       880
               0     100.0
1634         136       0.0       0.0         2       0.0       880
               0     100.0
1635         137       0.0       0.0         2       0.0       880
               0     100.0
1636         138       0.0       0.0         2       0.0       880
               0     100.0
1637         139       0.0       0.0         2       0.0       880
               0     100.0
1638         140       0.0       0.0         2       0.0       880
```

```
0     100.0
141       0.0       0.0         2       0.0       880
0     100.0
142       0.0       0.0         2       0.0       880
0     100.0
143       0.0       0.0         2       0.0       880
0     100.0
1431      0.0       0.0         2       0.0       880
0     100.0
144       0.0       0.0         2       0.0       880
0     100.0
145       0.0       0.0         2       0.0       880
0     100.0
146       0.0       0.0         2       0.0       880
0     100.0
$North Box Soil
155       0.0       0.0         2       0.0         0
0       0.0
157       0.0       0.0         2       0.0         0
0       0.0
158       0.0       0.0         2       0.0       880
0     100.0
159       0.0       0.0         2       0.0       880
0     100.0
1591      0.0       0.0         2       0.0       880
0     100.0
$North Box Piles Initial
160       0.0       0.0         2       0.0       880
0     100.0
161       0.0       0.0         2       0.0       880
0     100.0
162       0.0       0.0         2       0.0       880
0     100.0
163       0.0       0.0         2       0.0       880
0     100.0
164       0.0       0.0         2       0.0       880
0     100.0
165       0.0       0.0         2       0.0       880
0     100.0
166       0.0       0.0         2       0.0       880
0     100.0
167       0.0       0.0         2       0.0       880
0     100.0
$North Box DWall Slips
170       0.0       0.0         2       0.0         0
0       0.0
172       0.0       0.0         2       0.0         0
0       0.0
173       0.0       0.0         2       0.0         0
0       0.0
174       0.0       0.0         2       0.0         0
0       0.0
175       0.0       0.0         2       0.0       880
0     100.0
176       0.0       0.0         2       0.0       880
0     100.0
177       0.0       0.0         2       0.0       880
0     100.0
178       0.0       0.0         2       0.0       880
0     100.0
$M-C Pile Slips
400       0.0       0.0         2       0.0       880
0     100.0
401       0.0       0.0         2       0.0       880
0     100.0
402       0.0       0.0         2       0.0       880
0     100.0
403       0.0       0.0         2       0.0       880
0     100.0
404       0.0       0.0         2       0.0       880
0     100.0
405       0.0       0.0         2       0.0       880
```



```
0     100.0
406       0.0       0.0         2       0.0       880
0     100.0
$M-C DWall Slips
410       0.0       0.0         2       0.0         0
0       0.0
412       0.0       0.0         2       0.0         0
0       0.0
413       0.0       0.0         2       0.0         0
0       0.0
414       0.0       0.0         2       0.0         0
0       0.0
415       0.0       0.0         2       0.0       880
0     100.0
416       0.0       0.0         2       0.0       880
0     100.0
417       0.0       0.0         2       0.0       880
0     100.0
418       0.0       0.0         2       0.0       880
0     100.0
419       0.0       0.0         2       0.0       880
0     100.0
420       0.0       0.0         2       0.0       880
0     100.0
421       0.0       0.0         2       0.0       880
0     100.0
422       0.0       0.0         2       0.0       880
0     100.0
423       0.0       0.0         2       0.0       880
0     100.0
4231      0.0       0.0         2       0.0       880
0     100.0
424       0.0       0.0         2       0.0       880
0     100.0
425       0.0       0.0         2       0.0       880
0     100.0
426       0.0       0.0         2       0.0         0
0       0.0
427       0.0       0.0         2       0.0         0
0       0.0
429       0.0       0.0         2       0.0         0
0       0.0
430       0.0       0.0         2       0.0         0
0       0.0
431       0.0       0.0         2       0.0         0
0       0.0
432       0.0       0.0         2       0.0       880
0     100.0
434       0.0       0.0         2       0.0       880
0     100.0
435       0.0       0.0         2       0.0       880
0     100.0
4351      0.0       0.0         2       0.0       880
0     100.0
436       0.0       0.0         2       0.0       880
0     100.0
$
$
$ ==========
$ LOAD cards
$ ==========
$
*LOAD_GRAVITY_PART
$
$       PID       DOF        LC     ACCEL      LCDR      STGA
STGR
$
300         3        22   1.0E-20         0         0
0
301         3        22   1.0E-20         0         0
0
4352        3        22   1.0E-20         0         0
```

```
1717         0
1718        4353         3        22   1.0E-20         0         0
            0
1719        4357         3        22   1.0E-20         0         0
            0
1720         303         3        22   1.0E-20         0         0
             0
1721         304         3        22   1.0E-20         0         0
             0
1722         305         3        22   1.0E-20         0         0
             0
1723         307         3        22   1.0E-20         0         0
             0
1724         308         3        22   1.0E-20         0         0
             0
1725         309         3        22   1.0E-20         0         0
             0
1726        4354         3        22   1.0E-20         0         0
            0
1727        4355         3        22   1.0E-20         0         0
            0
1728        4358         3        22   1.0E-20         0         0
            0
1729         310         3        22   1.0E-20         0         0
             0
1730         311         3        22   1.0E-20         0         0
             0
1731        4356         3        22   1.0E-20         0         0
            0
1732         320         3        22   1.0E-20         0         0
             0
1733         321         3        22   1.0E-20         0         0
             0
1734         322         3        22   1.0E-20         0         0
             0
1735         324         3        22   1.0E-20         0         0
             0
1736         350         3        22   1.0E-20         0         0
             0
1737         352         3        22   1.0E-20         0         0
             0
1738         353         3        22   1.0E-20         0         0
             0
1739         354         3        22   1.0E-20         0         0
             0
1740         355         3        22   1.0E-20         0         0
             0
1741  $
1742  *TITLE
1743  TCR_west_SB1
1744  $
1745  $
1746  *END
1747  $
1748  $ ==============
1749  $ Assembly cards
1750  $ ==============
1751  $
1752  *SUBSET
1753  South Box Propping
1754  $
1755
```